

124

DNA 4377P-1

AD A U 48798

**PROCEEDINGS OF THE  
DICE THROW SYMPOSIUM  
21-23 JUNE 1977**

**Volume 1**

General Electric Company—TEMPO  
DASIAC  
816 State Street  
Santa Barbara, California 93102

July 1977

Proceedings

CONTRACT No. DNA 001-75-C-0023

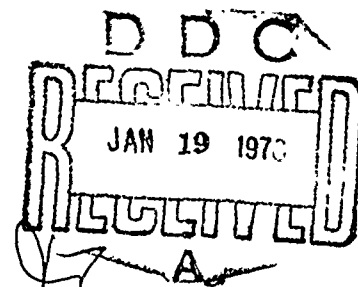
THIS WORK SPONSORED BY THE DEFENSE NUCLEAR AGENCY  
UNDER RDT&E RMSS CODE B337075464P99QAXDC00803H2590D

APPROVED FOR PUBL C RELEASE; DISTRIBUTION UNLIMITED

Prepared for

Director  
DEFENSE NUCLEAR AGENCY  
Washington, D.C. 20305

AD No. —  
DDC FILE COPY



UNCLASSIFIED

SECURITY CLASSIFICATION OF THIS PAGE (When Data Entered)

REPORT DOCUMENTATION PAGE		READ INSTRUCTIONS BEFORE COMPLETING FORM
1. REPORT NUMBER DNA 4377P-1, AE-E391177	2. GOVT ACCESSION NO. 16 1111, 3EIE	3. RECIPIENT'S CATALOG NUMBER
4. TITLE (and Subtitle) PROCEEDINGS OF THE DICE THROW SYMPOSIUM / 21-23 JUNE 1977, VOLUME 1		5. TYPE OF REPORT & PERIOD COVERED Proceedings
7. AUTHOR(s)		6. PERFORMING ORG. REPORT NUMBER
9. PERFORMING ORGANIZATION NAME AND ADDRESS General Electric Company - TEMPO DASIAC 816 State St., Santa Barbara, Ca, 93102		8. CONTRACT OR GRANT NUMBER(s) DNA 001-75-C-0023
11. CONTROLLING OFFICE NAME AND ADDRESS Director Defense Nuclear Agency Washington, D C 20305		10. PROGRAM ELEMENT PROJECT, TASK AREA & WORK UNIT NUMBERS P99QAXDC00803
14. MONITORING AGENCY NAME & ADDRESS (if different from Controlling Office)		12. REPORT DATE July 1977
		13. NUMBER OF PAGES
		15. SECURITY CLASS (of this report) Unclassified
		15a. DECLASSIFICATION/DOWNGRADING SCHEDULE
16. DISTRIBUTION STATEMENT (of this Report)  Approved for public release; distribution unlimited.		
17. DISTRIBUTION STATEMENT (of the abstract entered in Block 20, if different from Report)		
18. SUPPLEMENTARY NOTES		
19. KEY WORDS (Continue on reverse side if necessary and identify by block number) Airblast                      High Explosive Ammonium Nitrate Fuel Oil      Nuclear Weapons Effects Dice Throw                      Simulation Ground Motion		
20. ABSTRACT (Continue on reverse side if necessary and identify by block number) This report contains the proceedings of the DICE THROW Symposium held 21-23 June at the Ballistic Research Laboratory, Aberdeen Proving Ground, Maryland. The presentations contained herein describe the experiments conducted, instrumentation used, and results obtained by the various participating projects from detonation of the 600-ton ANFO HE test 6 October 1976 at the White Sands Missile Range, N.M. The DICE THROW Event was sponsored by the Defense Nuclear Agency		

## FOREWORD

This report contains the proceedings of the DICE THROW Symposium held 21-23 June 1977 at the Ballistic Research Laboratory (BRL), Aberdeen Proving Ground, Maryland. The report is divided into four volumes. Volumes 1 through 3 contain the unclassified presentations and Volume 4 contains the classified presentations.

The DICE THROW Event, which was conducted near the Giant Patriot site on the White Sands Missile Range (WSMR), 6 October 1976, was the final test of the DICE THROW Program. The charge for this test was composed of approximately 628 tons (570 metric tons) of ammonium nitrate fuel oil (ANFO). The charge configuration was a right-circular-cylinder base tangent to the surface with a hemispherical top, the same configuration as the second event in the Pre-DICE THROW II Series. The primary objectives of this test were to provide a simulated nuclear blast and shock environment for target response experiments that are vitally needed by the military services and defense agencies concerned with nuclear weapons effects, and to confirm empirical predictions and theoretical calculations for shock response of military structures, equipment, and weapon systems.

A complement of 33 experimenters and support agencies (including foreign governments) participated in Event DICE THROW. For details pertaining to the as-built experiment configurations, site and charge descriptions, and fielding requirements in support of this program, refer to the DICE THROW Test Execution Report, POR 6965.

PRECEDING PAGE BLANK

iii

ACCESSION for	
NTIS	White Section <input checked="" type="checkbox"/>
DDC	Buff Section <input type="checkbox"/>
UNANNOUNCED	<input type="checkbox"/>
JUSTIFICATION.....	
.....	
BY .....	
DISTRIBUTION/AVAILABILITY CODES	
Dist.	AVAIL. and/or SPECIAL
<i>A</i>	

## TABLE OF CONTENTS ;

### VOLUME 1

1. > ANFO CHARGE DEVELOPMENT PROGRAM & PROGRAM SUMMARY, -  
Capt. Thomas Y. Edwards, SAMSO.
2. DICE THROW OVERVIEW, -LCDR J.D. Strode, Jr., CEC, USN, DNA Field  
Command.
3. CHARGE/DETONATION SYSTEM, (DNA PROJECT 975) - M.M. Swisdak, Jr.,  
Naval Surface Weapons Center, Explosion Dynamics Branch.
4. DICE THROW MAIN EVENT - EXPLOSIVE DIAGNOSTICS, - Bernard Hayes  
and Ronald Boat, Lawrence Livermore Laboratory.
5. TECHNICAL PHOTOGRAPHY, FROM DICE THROW EVENT - John Wisotski,  
Denver Research Institute.
6. INSTRUMENTATION NOISE PROBLEMS, ENCOUNTERED ON DICE THROW  
Noel Gantick, DNA Field Command.
7. FREE - FIELD AIRBLAST DEFINITION, - EVENT DICE THROW - George  
D. Teel, Ballistic Research Laboratory
8. DICE THROW PROJECT OFFICER'S REPORT - THEORETICAL AIR BLAST  
CALCULATIONS, - C.E. Needham, Air Force Weapons Laboratory.
9. BLAST EFFECTS ON HELICOPTER, - EVENT DICE THROW - Robert Mayerhofer,  
Ballistic Research Laboratory.
10. EVENT DICE THROW MOBILITY EXPERIMENTS, - C.E. Green, U.S. Army  
Engineer Waterways Experiment Station.

### VOLUME 2

11. BLAST EFFECTS ON THE CREWS OF U.S. ARMY TACTICAL EQUIPMENT  
D.R. Richmond, J.T. Yelverton, E.R. Fletcher, W. Hicks, K. Saunders, and A  
Trujillo, Lovelace Biomedical and Environmental Research Institute, Inc
12. DICE THROW OFF-SITE BLAST PREDICTIONS AND MEASUREMENTS  
Jack W. Reed, Sandia Laboratories, Environmental Research Division.
13. EVENT DICE THROW - INDUSTRIAL EQUIPMENT SURVIVAL/RECOVERY  
FEASIBILITY PROGRAM - Edwin N. York, The Boeing Aerospace Company.
14. FEDERAL REPUBLIC OF GERMANY STRUCTURES TEST PROGRAM -  
EVENT DICE THROW - James M. Watt, Jr., Major Gerhard Zahlmann, and  
Robert A. Cole, U.S. Army Engineer Waterways Experiment Station.
15. AIRCRAFT SHELTER TESTS IN THE DICE THROW EVENT - Capt Harry  
T. Webster, Air Force Weapons Laboratory, Civil Engineering Research Division



16. GROUP HELMET ARMY PERSONNEL SHELTERS—Golden E. Lane, Jr., Civil Engineering Research Facility.
17. PROJECT C-4, FREE-FLIGHT MEASUREMENT OF THE DRAG FORCES ON CYLINDERS - EVENT DICE THROW—A.W.M. Gibb and D.A. Hill, Defence Research Establishment Suffield.
18. PROJECT C-2, BLAST RESPONSE OF UHF POLEMAST ANTENNA - EVENT DICE THROW—C.G. Coffey and G.V. Price, Defence Research Establishment Suffield.
19. BLAST RESPONSE OF LATTICE MAST - EVENT DICE THROW—B.G. Laidlaw, Defence Research Establishment Suffield.
20. BLAST RESPONSE OF 35-FT FIBERGLASS WHIP ANTENNA - EVENT DICE THROW—G.V. Price and C.G. Coffey, Defence Research Establishment Suffield.
21. PROJECT C-5, CANADIAN AIR BLAST MEASUREMENTS - EVENT DICE THROW—F.H. Winfield, Defence Research Establishment Suffield.
22. UHF/SHF TRANSMISSION EXPERIMENT—Alan A. Burns, SRI International.
23. DICE THROW DUST CLOUD CALCULATIONS—Major Gary P. Ganong, Susan E. Check, and Charles E. Needham, Air Force Weapons Laboratory.
24. DICE THROW SEISMIC MEASUREMENTS—Laurence S. Melzer, Air Force Weapons Laboratory.
25. ARMY PERSONNEL SHELTERS - DNA PROJECT NO. 329—William L. Huff, U.S. Army Engineer Waterways Experiment Station.

### VOLUME 3

26. NORWEGIAN BLAST DOOR—Golden E. Lane, Jr., Civil Engineering Research Facility.
27. BLAST TESTS OF EXPEDIENT SHELTERS IN THE DICE THROW EVENT—C.H. Kearny, Oak Ridge National Laboratory.
28. EXPERIMENTAL STUDY OF AIRCRAFT STRUCTURAL RESPONSE TO BLAST - DICE THROW PROJECT NO. 118—Rudolf Friedberg and Peter Hughes, Naval Weapons Evaluation Facility.
29. BLAST DISPLACEMENT IN FIELD FORTIFICATIONS—E.R. Fletcher, D.R. Richmond, R.O. Clark, and J.T. Yelverton, Lovelace Biomedical and Environmental Research Institute, Inc.
30. DYNAMIC RESPONSE OF TWO TYPES OF GERMAN HOUSE CONSTRUCTION—C.K. Wiehle, J.R. Rempel, and J.E. Beck, Stanford Research Institute.
31. TEST SUMMARY - NBDS OPTICAL MEASUREMENTS—M. Oberst, Sandia Laboratory Albuquerque.

32. RESULTS OF THE SPECIAL FORCES COMMUNICATIONS EXPERIMENT AT THE DICE THROW MAIN EVENT—Capt. Alexander F. Wojcicki, SOC, USAOCCS.
33. CRATER AND EJECTA ENHANCEMENT STUDIES—R.W. Henny, Air Force Weapons Laboratory and G.D. Jones, Civil Engineering Research Facility.

## LIST OF ATTENDEES

ABRAHAMSSON, Eddy - Sweden  
ALLISON, W. Don - BRL  
ALTER, MAJ William A. - DNA  
ALVAREZ, CPT Vicen A. - FCDNA  
ATKINS, Marvin C. - DNA  
AXELSSON, Hakan - Sweden  
BACHMANN, Eberhard - Germany  
BALLARD, James - WES  
BALSARA, Jimmy P. - WES  
BASPANT, MAJ Ronald W. - HQSAC  
BELLIVEAU, Louis - HDL  
BEZEMER, Ole R. - Canada  
BRADSHAW, 1LT Joel C. - AFWL  
BREAZEAL, Norman - Sandia Labs  
BROWN, Larry L. - DRI  
BRUEGMANN, LTC Dieter - Germany  
BRYANT, Edward - GE-TEMPO  
BURNS, Alan A. - SRI  
BUTALA, Edward - NSA  
CARLSON, Roland - Boeing  
CAULIFIELD, Eugene - USASCA  
CHAN, Warren - GE-TEMPO

CHAPYAK, Edward - RDA  
CHECK, Susan - AFWL  
CLARK, Robert O. - Lovelace  
COFFEY, Clayton - Canada  
COOPER, Henry - RDA  
CRISCIONE, Emanuel - Kaman Avidyne  
CRONK, Richard - KOA  
DeBOY, William - NSA  
DELANY, W. D. - ASWE  
DeRAAD, CPT Robert G. - FCDNA  
DYSART, Richard - WSMR  
EDGERTON, LCDR E. W. - NSSC  
EDWARDS, CPT Thomas - SAMSO  
ERLEMANN, COL Rudolf - Germany  
ETHRIDGE, Noel - BRL  
FLATHAU, William - WES  
FLETCHER, E. Royce - Lovelace  
FLUGER, Alvin - ARRADCOM  
FREIBERG, Robert - USAECOM  
FRIEDBERG, RUDOLF - NWEF  
GANTICK, Noel - FCDNA  
GIBB, Allan W. M. - Canada  
GOMEZ, COL Robert - BRL  
GRANT, G. A. - Canada  
GREEN, Dale W. - WSMR

GUNBY, MAJ E. Neal - DNA  
GUPTA, Aaron - BRL  
GURKE, Gerhard - Germany  
HAYES, Bernard - LLL  
HEGGIE, R. M. - Canada  
HEINTZEL, COL Hans-H. - Germany  
HUFF, William L. - WES  
HUGHES, Peter - NWEF  
JACOBSON, John - BRL  
JONES, Glen - CERF  
KAUFMANN, LTC Ronald - WES/Germany  
KEARNY, Cresson - ORNL  
KEEFER, John - BRL  
KELSO, Jack - GE-TEMPO  
KENNEDY, Tom - DNA  
KING, Vincent - BRL  
KINGERY, Charles - BRL  
KLIMMEK, LT Charles - FCDNA  
KNOWLES, Cyrus - RDA  
LANE, Golden - CERF  
LAIDLAW, Bryan - Canada  
LIND, MAJ Alan - USANA  
MAYERHOFER, Robert - BRL  
McDONNELL, Michael - SAI  
MELZER, Steve - AFWL  
MESZAROS, Julius J. - BRL

MUELLER, MAJ Edmund - HQCNA  
NEEDHAM, Charles - AFWL  
NOREN, Brig Gen Gunnar - Sweden  
OLIVER, Lawrence - NWEF  
PACHUTA, Michael A. - DCPA  
PAHL, LTC Hermonn - Germany  
PARKER, Hassel - MIG  
PASMAN, H. J. - Netherlands  
PEARSON, Richard - BRL  
PECKHAM, Phillip - NSWC/WOL  
PERRY, Gerald - GE-TEMPO  
PETERSON, Robert L. - BRL  
PICKETT, Stephen - CERF  
PETES, Joseph - NSWC/WOL  
PFRENGLE, Herman - Germany  
PLAMONDON, Maynard A. - AFWL  
PYLE, Jay C. - Boeing  
QUIGLEY, Ennis - BRL  
RALEY, Robert J. - BRL  
RAVOTTO, Martin - ARRADCOM  
REED, Jack - SLA  
REICHENBACH, Heinz - Germany  
REISLER, Ralph E. - BRL  
ROECKER, Eugene - BRL  
RICHMOND, Donald - Lovelace  
RIGOTTI, David L. - BRL

RULA, Adam A. - WES  
SCHILLING, Robert - Germany  
SCHUMACHER, Robert - BRL  
SCHUMAN, William J. - BRL  
SHELTON, Russell - BRL  
SKJELTORP, Arne - Norway  
SMITH, Ross - Chrysler  
STILL, LTC Edwin T. - DNA  
STRODE, LCDR J. D. - FCDNA  
SULLIVAN, John - BRL  
SWISDAK, Michael - NSWC/WOL  
TAYLOR, William - BRL  
TEEL, George - BRL  
UECKE, MAJ John - USANA  
VAULT, William - HDL  
VAN KUEREN, E. - RCA  
WARD, Robert - EG&G  
WARREN, LIC James - AFWL  
WATSON, George - BRL  
WATT, James - WES  
WAXLER, Daniel - ARRADCOM  
WEBSTER, Harry - AFWL  
WIEHLE, Carl - SRI  
WIHERLE, Matthew - BRL  
WISOTSKI, John - DRI  
WOJCICKI, Alexander - USAOCCS

YORK, Edwin - Boeing

ZAKER, Thomas - ODES



**1. ANFO CHARGE DEVELOPMENT PROGRAM -  
PROGRAM SUMMARY**

by  
Capt. Thomas Y. Edwards  
SAMSO

## CONTENTS

	Page
ABSTRACT . . . . .	v
ILLUSTRATIONS . . . . .	vi
TABLES . . . . .	viii
SECTION	
I PROGRAM DESCRIPTION . . . . .	3
A. Phase 1 . . . . .	7
B. Phase 2 . . . . .	10
C. Phase 3 . . . . .	11
D. Phase 4 . . . . .	21
II CONCLUSIONS . . . . .	39
III RECOMMENDATIONS. . . . .	42
REFERENCES. . . . .	43

### ABSTRACT

This paper briefly summarizes the need, objectives, results, conclusions and recommendations of the DNA-sponsored ANFO Charge Development Program (Pre-DICE THROW), conducted in January through September 1975. Detailed discussion of specific programs can be found in the references.

The author gratefully acknowledges the support received in preparing and reviewing this brief overview of the ANFO Charge Development Program.

## ILLUSTRATIONS

Figure		Page
1	General Charge Configurations for the ANFO Charge Development Program	8
2	Pre-DICE THROW I Vertical Particle Velocities at 1.5-Foot Depth	13
3	Pre-DICE THROW I Horizontal Particle Velocities at 1.5-Foot Depth	14
4	Phase 3, Event 1 (PDTI-1) Crater Profile	15
5	Phase 3, Event 2 (PDTI-2) Crater Profile	16
6	Phase 3, Event 3 (PDTI-3) Crater Profile	17
7	Phase 3, Event 4 (PDTI-4) Crater Profile	18
8	Peak Shock Overpressure Versus Ground Range, Phase 3, Events 1 through 4	20
9	Peak Shock Overpressure Versus Ground Range, Pre-DICE THROW II, Event 1, BRL Data	23
10	Overpressure Impulse Versus Ground Range, Pre-DICE THROW II, Event 1, BRL Data	24
11	Peak Shock Overpressure Versus Ground Range, Pre-DICE THROW II, Event 2, BRL Data	25
12	Overpressure Impulse Versus Ground Range, Pre-DICE THROW II, Event 2, BRL Data	26
13	Peak Vertical and Horizontal Velocity Versus Range, Pre-DICE THROW II, Events 1 and 2, WES Data	28
14	Peak Horizontal and Vertical Displacement Versus Range, Pre-DICE THROW II, Events 1 and 2, WES Data	29
15	WES Vertical Velocity Waveforms, at 80-Foot Range, Pre-DICE THROW II, Events 1 and 2	30

(Continued)

# ILLUSTRATIONS (cont'd)

Figure		Page
16	Horizontal Velocity Waveforms at 80-Foot Range, Pre-DICE THROW II, Events 1 and 2, WES Data	31
17	WES Vertical Velocity Waveform at 400-Foot Range, Pre-DICE THROW II, Events 1 and 2	32
18	Horizontal Velocity Waveforms at 400-Foot Range, Pre-DICE THROW II, Events 1 and 2, WES Data	33
19	SSS Measured Peak Stress Versus Range, Pre-DICE THROW II, Event 1	34
20	SSS Measured Peak Stress Versus Range, Pre-DICE THROW II, Event 2	35
21	SRI Recorded Stress-Time Profiles, Pre-DICE THROW II, Events 1 and 2	36
22	Summary of Velocity Data, Pre-DICE THROW II, Event 2, AFWL Data	37
23	Comparison of Pre-DICE THROW II, Apparent Craters, AFWL/CERF Data	38
24	Generalized Crater Cross-Section, Pre-DICE THROW II, Event 1, USGS Data	40
25	Generalized Crater Cross-Section, Pre-DICE THROW II, Event 2, USGS Data	41

## TABLES

Table		Page
1	ANFO Charge Development Program Participants	5
2	Phase 1 Experimental Test Program	9
3	Phase 2 Experimental Test Program	10
4	Phase 3 Experimental Test Program	12
5	Phase 4 Experimental Test Program	22

## ANFO CHARGE DEVELOPMENT PROGRAM

### I. INTRODUCTION

In January 1975, under the direction of the Defense Nuclear Agency (DNA), an intensive program was initiated to develop an alternate high-explosive (HE) source for use on large-scale nuclear weapons effects (NWE) testing programs. Several factors contributed to the need for an alternate explosive source. Among these were the dwindling reserves of TNT (trinitrotoluene), which had been salvaged from munitions, and mounting costs for remolding TNT into a suitable size and shape for charge construction. In addition, TNT detonations commonly exhibited a large number of "explosive jets" or airshock anomalies, resulting in perturbed dynamic pressures in some regions of the test bed which adversely affected the desired uniform airshock expansion in a highly unpredictable manner. The net effect was that 20 to 30 percent of the surface airblast targets could be subjected to a shock environment for which they were not designed, resulting in loss of valuable experimental data.

The objectives of the charge development program were to develop a less expensive HE source that would preserve the general phenomenological effects of a surface tangent sphere (STS) of TNT and to develop and characterize an improved HE airblast source.

Several potential HE sources were examined before the program was formally initiated. Three explosive candidates which appeared to be compatible with portions of the program objectives were: detonable gas mixtures, nitromethane and ammonium nitrate with fuel oil (ANFO).

Preliminary investigations indicated that detonable gas detonations produce clean and fairly predictable airshock expansions. However, detonable gas mixtures were extremely hazardous, difficult to field and, although the gas mixtures themselves were fairly inexpensive, the cost and size of a container (e.g., desensitized balloon) for a 500-ton equivalent source was prohibitive. In addition, detonable gas experiments were often unreliable, and insufficient pressures were available from the detonations to reproduce conventional HE cratering phenomenon. Detonable gases were thus considered an unsuitable explosive source to meet the program objectives.

Another potential HE source was nitromethane. Its cost was approximately one-third that of reprocessed TNT and was readily available. Nitromethane is in liquid form, however, and considerable complications were experienced in attempting to minimally contain the material for an above-ground STS detonation.<sup>(1)</sup> A prior program involving the use of nitromethane demonstrated that extensive explosive jetting was produced in a 100-ton STS detonation.<sup>(1)</sup> Nitromethane, therefore, was considered to be a less than optimum source alternative to TNT, and its development was not attempted.

Ammonium nitrate with fuel oil (ANFO) was the third HE candidate considered. There was some experience with ANFO detonations from other agencies, including the Bureau of Mines, the Naval Surface Weapons Center (NSWC, formerly NOL), and the Defence Research Establishment at Suffield (DRES), which indicated that explosive jetting effects appeared minimal. The cost of ANFO, a class 4 explosive (blasting agent), is approximately one-tenth that of reprocessed TNT, and from a safety and ease-of-handling standpoint, it appeared to have desirable characteristics. Thus ANFO was selected as the prime replacement HE source for TNT.

There were, however, some reservations concerning the utility of ANFO. Of particular concern was the ability to scale ANFO equivalency to TNT and explosive parameters in a manner consistent with those of TNT. The ability to scale explosive effects appeared questionable due to observed ANFO reaction rates and resulting time-dependent energy-release rates which were not comparable to TNT detonations. These effects were manifested in one's ability to under- or over-drive ANFO detonations and experience in reliably detonating small ANFO charges.

Although ANFO has been used in the mining industry for years, there was little explosive characterization work done to support its use. Programs were required, therefore, to examine limitations for ANFO usage and to identify detonation parameters. Program schedules dictated that an assumption regarding explosive equivalency to TNT was required before the explosive characterization program was complete. Review of available air-blast data from ANFO events indicated that between static overpressure levels of 1 to 25 psi, an equivalency of 1.2 pounds of ANFO to 1.0 pound of TNT was reasonable.<sup>(2)</sup> Other available explosive information did not appear to contradict this estimate, and an equivalency factor of 1.2 was used throughout the Pre-DICE THROW program.



## II. PROGRAM DESCRIPTION

The objective of the charge development program was to develop a less expensive HE source that could produce cratering and ground-shock phenomenological effects comparable to a surface tangent sphere (STS) TNT event while minimizing undesirable airshock anomalies which are produced by explosive jetting. An additional objective of the program was to characterize the explosive performance of large-scale ANFO detonations.

The program approach was to establish STS TNT baseline parameters in a given media, then to conduct variations in HE configuration, source nature, and charge construction and initiation techniques to address the program objectives.

The ANFO charge development program, as it is referred to hereafter, was broken into four experimental phases: (1) one-pound, (2) 1000-pound, (3) 5-ton, and (4) 100-ton series. In addition, a laboratory program to characterize the detonation parameters of ANFO, and a calculational effort to predict ANFO airblast performance were undertaken.<sup>(3,4)</sup>

The degree of success of the program was measured by the comparability of cratering and ground-motion environments between an ANFO event (120-ton) and an equivalent-yield STS TNT event (100-ton) in a common media. Photographic and recorded air-pressure records were compared to identify explosive jetting and to quantify its effects. Predictions of airblast performance were compared with gage records for different scaled ANFO events to insure yield scalability.

Phase 1 of the program consisted of a series of one-pound events to examine cratering and fireball effects due to explosive configuration and charge initiation technique variations in a highly controlled test medium. A common explosive material, Composition 4 (C4), was used in all the events.

Phase 2 was a series of 1000-pound equivalent events to gain preliminary experience with ANFO and to examine cratering and fireball effects in a common media using both TNT and ANFO explosive charges. The equivalency is relative to TNT (1000 pounds), and the 1.2 multiplicative factor was used to determine the ANFO explosive weight (1200 pounds).

Phase 3 consisted of a series of 5-ton-equivalent events which were lightly instrumented. The objective of this phase was to identify the most likely ANFO source configuration which would meet the stated program objectives in a "real earth" media.

The fourth and final phase of the program (Phase 4) consisted of two 100-ton-equivalent events in a geology of Air Force interest to verify program compliance with the stated objectives and to provide detailed data to support charge-performance characterization of a 500-ton-equivalent event.

A large number of agencies were involved in different facets of the development program. Probably most notable were the efforts conducted in the first three phases of the program by the Air Force Weapons Laboratory (AFWL), under the direction of R. W. Henny, and the Civil Engineering Research Facility (CERF), under the direction of G. D. Jones. A brief summary of the charge-development projects and agencies involved is shown in Table 1

TABLE 1. ANFO Charge Development Program Participants

<u>Agency</u>	<u>Program Phase</u>	<u>Participation</u>
Air Force Weapons Laboratory (AFWL)	1, 2, 3, 4	Crater and Debris Measurements Technical Inputs Phases 1, 2, 3 Technical Supervision Seismic Measurements Ground-Motion Predictions Airblast Calculations Technical Photography
Ballistics Research Laboratory (BRL)	1, 2, 3, 4	Technical Consultation Airblast Measurements Airblast Predictions
University of New Mexico Civil Engineering Research Facility (CERF)	1, 2, 3, 4	Phases 1, 2, 3 Technical Supervision ANFO Charge Construction Crater and Debris Measurements Ground-Motion Measurements Airblast Measurements ANFO Detonation Diagnostics
General Electric Company TEMPO (DASIAC)	1, 2, 3, 4	Program Reporting Environmental Impact Assessment
Defence Research Establishment Suffield (DRES)	4	TNT Charge Construction Detonation Diagnostics
Denver Research Institute (DRI)	3, 4	Technical Photography
Defense Nuclear Agency (DNA)	1, 2, 3, 4	Program Supervision and Coordination
Lawrence Livermore Laboratory (LLL)	4	ANFO Detonation Characterization ANFO Detonation Diagnostics
Naval Surface Weapons Center (NSWC)	4	Technical Inputs Consultant on ANFO Use ANFO Quality Control Booster Manufacturer for ANFO (including Testing)
R&D Associates (RDA)	1, 2, 3, 4	Technical Consultant
Stanford Research Institute (SRI)	4	Stress Measurements
Science Systems & Software (SSS)	4	Stress Measurements Airblast Measurements

(Continued)

TABLE 1. ANFO Charge Development Program Participants (cont'd)

<u>Agency</u>	<u>Program Phase</u>	<u>Participation</u>
U. S. Geological Survey (USGS)	4	Aerial Technical Photography Cratering Consultant
Waterways Experiment Station (WES)	4	Ground-Motion Measurements Cratering Measurements Soil Sampling and Testing Timing and Firing
White Sands Missile Range (WSMR)	3, 4	Construction Support Program Coordination Technical Photography
Williams Aircraft Company	4	Aerial Technical Photography

#### A. Phase 1

There were 19 events in the one-pound program. These events were conducted in a highly controlled, moist-sand test bed at the Civil Engineering Research Facility (CERF) at Kirtland Air Force Base (KAFB) from January to March 1975. Each of the one-pound charges was molded from C4. The explosive configurations tested were spheres, hemispheres, cylinders and hemispherically capped cylinders. (See Figure 1.) Several events were repeated to examine arguments on cratering reproducibility or to verify unexpected trends. A list of the one-pound events conducted in Phase 1 is shown in Table 2. A more detailed description of the events conducted in the Phase 1, 2, and 3 efforts can be found in reference (5).

Several significant observations were made in Phase 1. Cratering measurements indicated that cratering efficiency was directly proportional to the amount of explosive in contact with the test bed surface, and a tangent-above circular cylinder of C4 could reproduce cratering phenomenon of the STS of a like explosive (C4) in a moist-sand media. It was determined that detonation products expand more uniformly when a hemispherical cap is emplaced on a cylindrical charge and the charge is multiply initiated along its center axis. This was emphasized when large explosive jets were observed whenever the predicted shock-front-expansion contour within the explosive charge did not match the contour of the charge/free surface interface.

At the completion of the one-pound series, it was determined that for C4 charges a multiply-initiated, tangent-above, right circular cylinder with length-to-diameter ratio of .84 (measured on the cylindrical section) with hemispherical cap appeared to best meet the desired cratering and fireball shock-expansion program objectives. In addition, it was observed that apparent crater volumes exhibited a  $\pm 10$ -percent variation in reproducibility in a well-controlled test bed. Based on other field data, it is believed that this variation may be as large as 20 percent in a natural geologic medium. A nominal 20-percent variation in apparent crater volume was accepted as the uncertainty in determining cratering agreement for the remainder of the program.

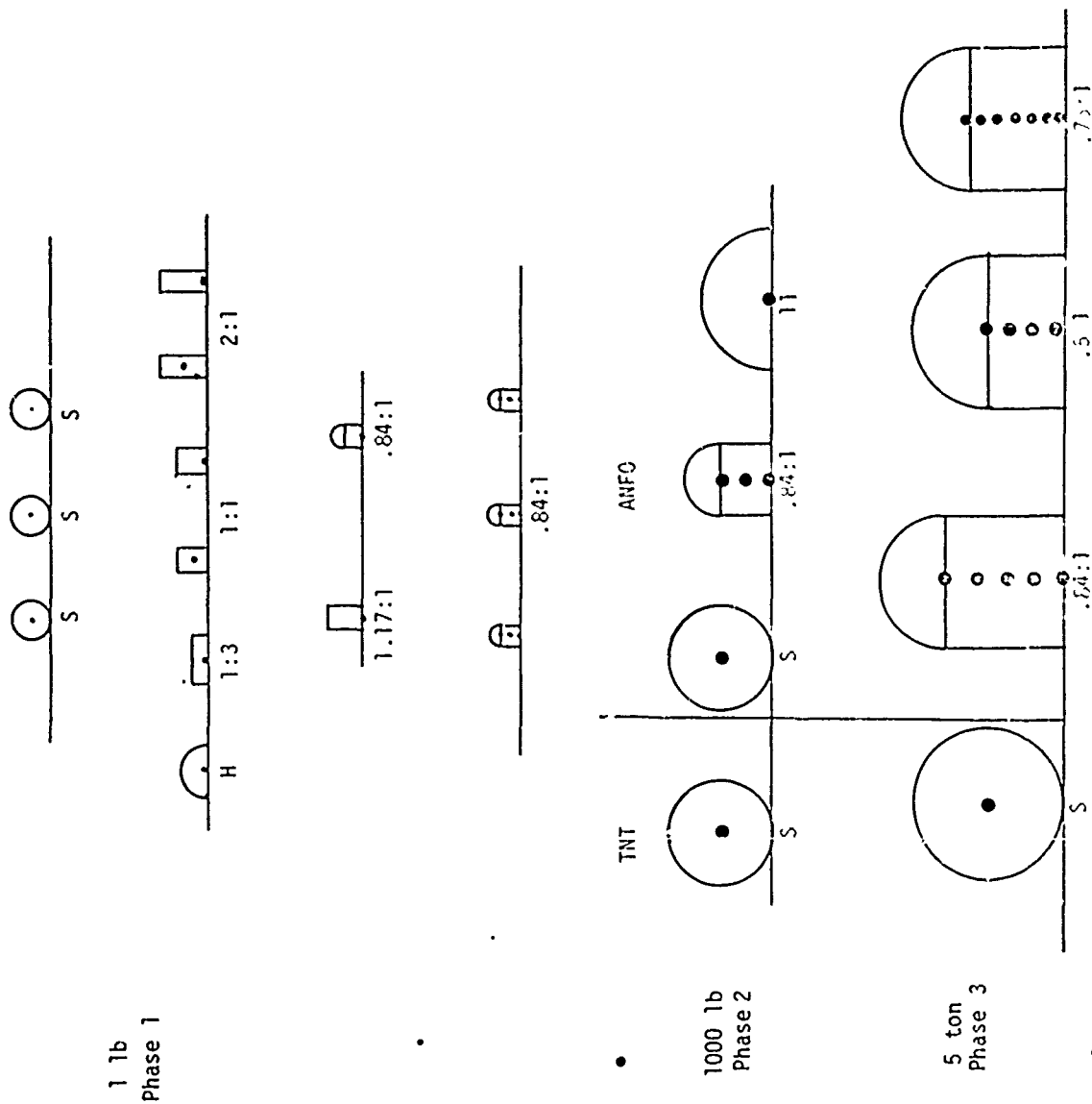


Figure 1. General Charge Configurations for the ANFO Charge Development Program

TABLE 2. Phase 1 Experimental Test Program

Event	Configuration	Charge Dimensions (in.)			Apparent Crater Dimensions		
		radius or L/D	Length	Diameter	R <sub>a</sub> (ft)	D <sub>a</sub> (ft)	V <sub>a</sub> (ft <sup>3</sup> )
1	Sphere	1.61	N/A	3.22	1.18	0.65	1.24
2	Sphere	1.61	N/A	3.22	1.15	0.60	1.02
3	Sphere	1.61	N/A	3.22	1.14	0.74	1.17
4	Cylinder 1:1	1/1	2.81	2.81	1.27	0.73	1.32
5	Hemisphere	2.03	N/A	4.06	1.49	1.01	2.66
6	Cylinder 2:1	2/1	4.46	2.23	1.03	0.64	0.756
7	Cylinder 2:1	2/1	4.46	2.23	1.08	0.68	0.865
8	Cylinder 1:1	1/1	2.81	2.81	1.28	0.81	1.49
9	Cylinder 2:1	2/1	4.46	2.23	0.97	0.57	0.57
10	Cylinder 1:3	1/3	1.35	4.05	1.38	0.92	2.29
11	Cylinder 1.17:1	1.17/1	3.12	2.67	1.26	0.63	1.21
12	Cylinder with cap	.84/1	2.23	2.67	1.27	0.72	1.34
13	Cylinder with cap, Mult. Simultaneous	.84/1	2.23	2.67	1.17	0.73	1.15
14	Cylinder with cap, Mult. Simultaneous	.84/1	2.23	2.67	1.22	0.76	1.27
15	Cylinder with cap, Mult. Simultaneous	.84/1	2.23	2.67	1.27	0.66	1.30
16	Cylinder with cap	.5/1	1.49	2.98	1.32	0.85	1.76
17	Cylinder with cap, Mult. Simultaneous	.5/1	1.49	2.98	1.31	0.66	1.31
18	Cylinder with cap	.75/1	2.05	2.73	1.15	0.62	0.901
19	Cylinder with cap, Mult. Simultaneous	.75/1	2.05	2.73	1.23	0.68	1.26

Notes: (1) 1.0 pound of C4 is equivalent to 1.34 pounds of TNT.  
 (2) Length and diameter dimensions are measured on cylindrical portion of charge.  
 (3) Shots 16, 17, 18, and 19 were done after the 5-ton series conducted at WSMR.

## B. Phase 2

Upon completion of Phase 1, Phase 2 of the ANFO charge-development program was initiated. Four 1000-pound-equivalent events were conducted at the PICK AXE site on KAFB in March 1975. The events, which are described in Table 3, were conducted to gain preliminary experience with ANFO and to attempt to verify trends observed in Phase 1. The 1.2 explosive equivalency factor was employed in this and the following phases of the study. The significant observations from these experiments were that ANFO can be reliably detonated at the 1200-pound level. The cratering trends, as a function of charge geometry observed in the 1000-pound series, supported the observations from the Phase 1 program. Differences were observed in the fireball behavior in the ANFO and the TNT detonations, which are believed to be attributable to the nearly oxygen-balanced ANFO reaction, as compared to the oxygen deficiencies of TNT detonations. As a result, explosive jetting is more difficult to identify in ANFO detonations. The Phase 2 effort was completed in March 1975, and the ANFO charge-development program was moved to the White Sands Missile Range (WSMR) in New Mexico.

Table 3. Phase 2 Experimental Test Program

Event	Configuration	Charge Dimensions (ft)	Explosive	Apparent Crater Dimensions		
				R <sub>a</sub> (ft)	D <sub>a</sub> (ft)	V <sub>a</sub> (ft <sup>3</sup> )
1	Sphere, Surface Tangent	R=1.33	TNT	7.2	2.5	179
2	Sphere, Surface Tangent	R=1.75	ANFO	5.2	1.8	71
3	Cylinder, Hemispher. Cap L/D = 0.84	L=2.43 D=2.90	ANFO	6.6	2.6	135
4	Hemisphere	R=2.2	ANFO	8.8	3.0	346

Note: Explosive weights were:

- 1 - 1000 pounds
- 2 - 1216 pounds
- 3 - 1197 pounds
- 4 - 1240 pounds



### C. Phase 3

Phase 3 was conducted in April through July 1975, at a dry, fine-grained alluvial site near QUEEN 15 on White Sands Missile Range. The series consisted of four events, as described in Table 4. The intent was to select an ANFO charge which appeared to best meet the program objectives by using lightly instrumented and well photographed events.

Approximately 30 channels of ground-motion and airblast instrumentation were recorded on each of the first three events, and six channels of airblast data were recorded on the fourth event. Each event was photographically recorded with high-speed cameras from three azimuths, and measurements of the craters and ejecta were taken.

Velocity-attenuation plots from events 1, 2, and 3 are shown in Figures 2 and 3. The STS TNT baseline data was produced on the first event, entitled PDTI-1. No data trends are apparent in the figures that would enable identification of one event from another. An insufficient number of gage records were available to quantify the data uncertainties; however, prior experience from HE detonations indicates that the measured motions from the three detonations fall within normal reproducibility bands for any single event. There were some effects observed on displacement waveforms which appeared to correlate to crater volume. The correlation of larger recorded displacements, at comparable ranges with increasing crater volume, is consistent with expected trends. The effect is thought to be the result of energy directly coupled through the cratering mechanisms. It appeared that events 2 and 3 bounded the waveform generated from the TNT baseline event. No ground-motion measurements were taken on event 4.

Cratering measurements from the four Phase 3 events are listed in Table 4, and crater profiles shown in Figures 4 through 7. The fourth event, entitled PDTI-4, was identified as the candidate ANFO source selected to replace its STS TNT counterpart. The crater produced by the PDTI-4 event was 28 percent larger than that produced by the STS TNT event (PDTI-1). Although the crater volume variation

TABLE 4. Phase 3 Experimental Test Program

Event	Configuration	Charge Dimensions		Explosive	Apparent Crater Dimensions		
		L (ft)	D (ft)		R <sub>a</sub> (ft)	D <sub>a</sub> (ft)	V <sub>a</sub> (ft <sup>3</sup> )
PDTI-1	Sphere, Surface Tangent		5.66	TNT	14.1	5.8	1640
PDTI-2	Cylinder, Hemis. Cap L/D=0.84	5.09	6.06	ANFO	13.4	4.0	1109
PDTI-3	Cylinder, Hemis. Cap L/D=0.56	3.41	6.82	ANFO	16.2	7.0	2630
PDTI-4	Cylinder, Hemis. Cap L/D=0.75	4.72	6.28	ANFO	14.6	7.0	2036

Note: Explosive weights were:  
PDTI-1 - 9,300 pounds  
PDTI-2 - 11,230 pounds  
PDTI-3 - 11,630 pounds  
PDTI-4 - 11,242 pounds

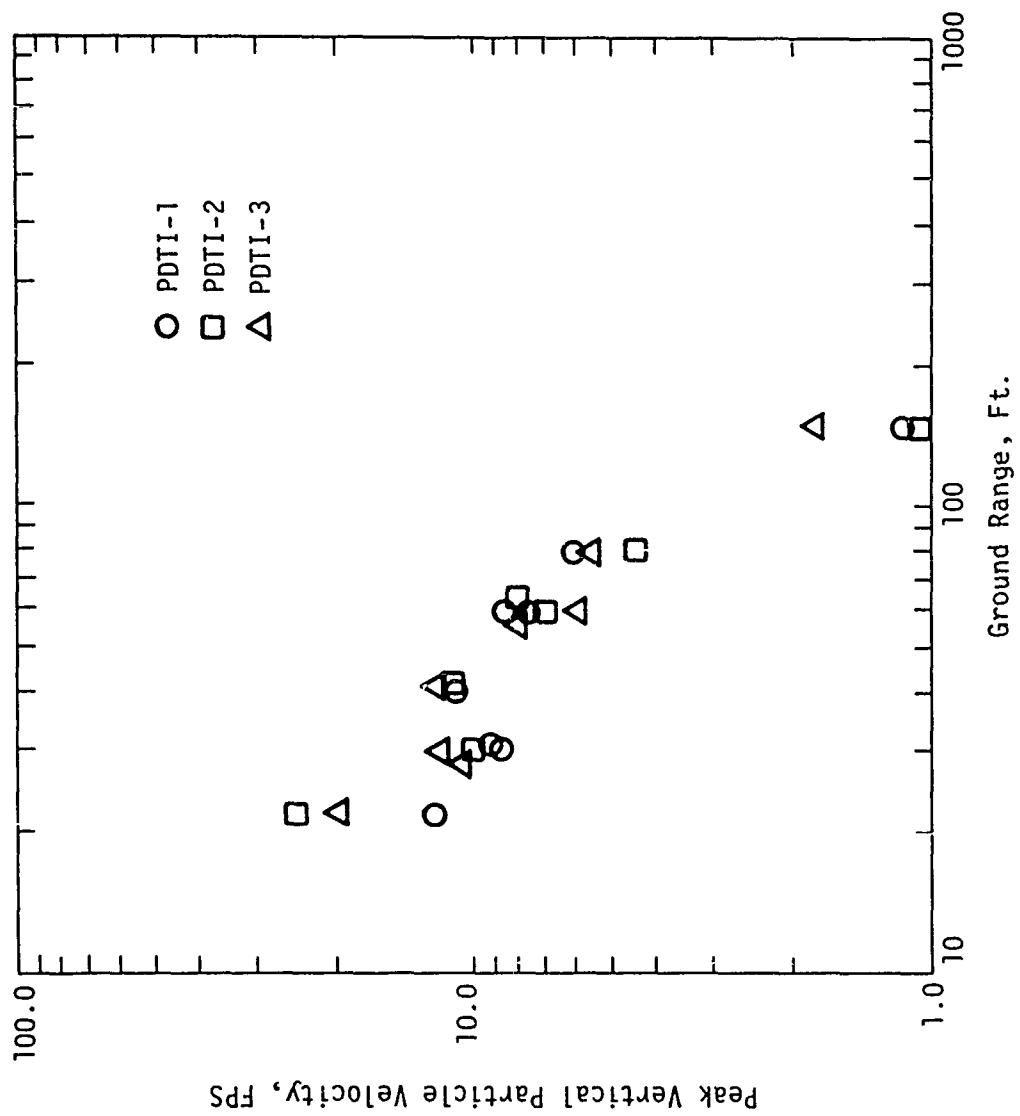


Figure 2. Pre-DICE THROW I Vertical Particle Velocities at 1.5-Foot Depth

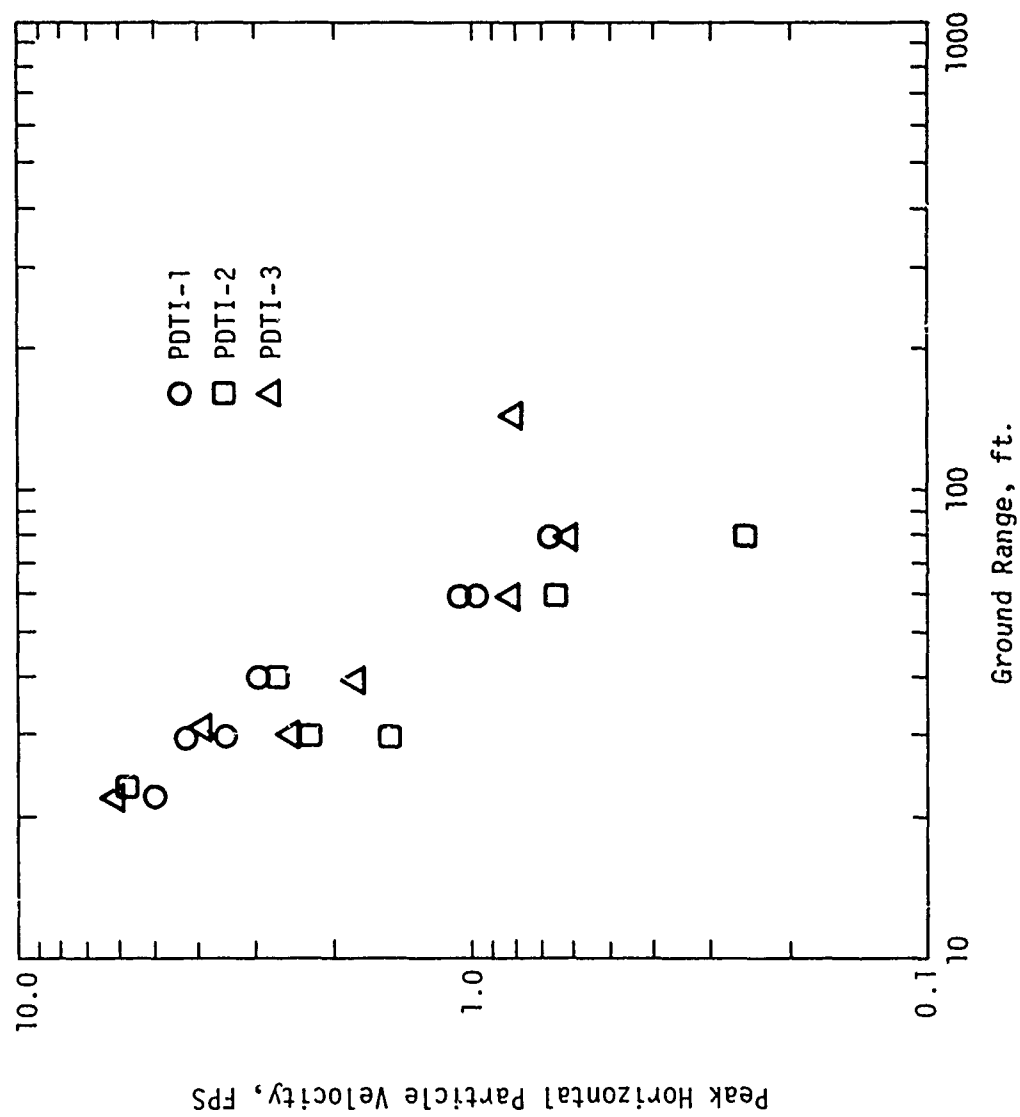


Figure 3. Pre-DICE THROW I Horizontal Particle Velocities at 1.5-Foot Depth

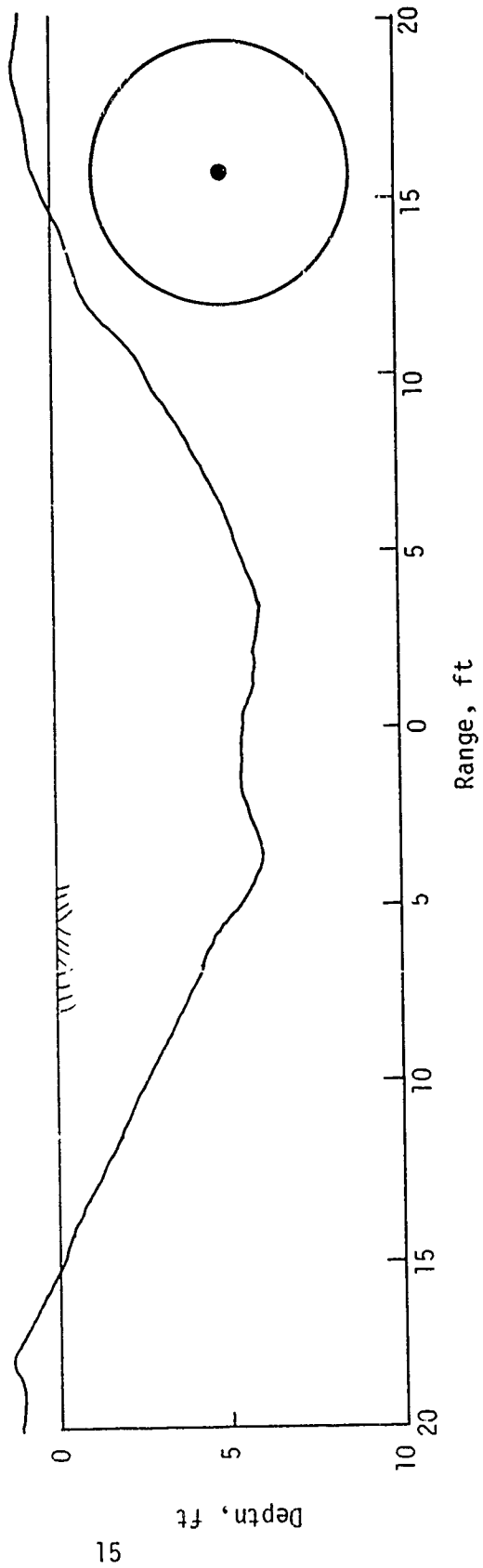


Figure 4. Phase 3, Event 1 (PDTI-1) Crater Profile

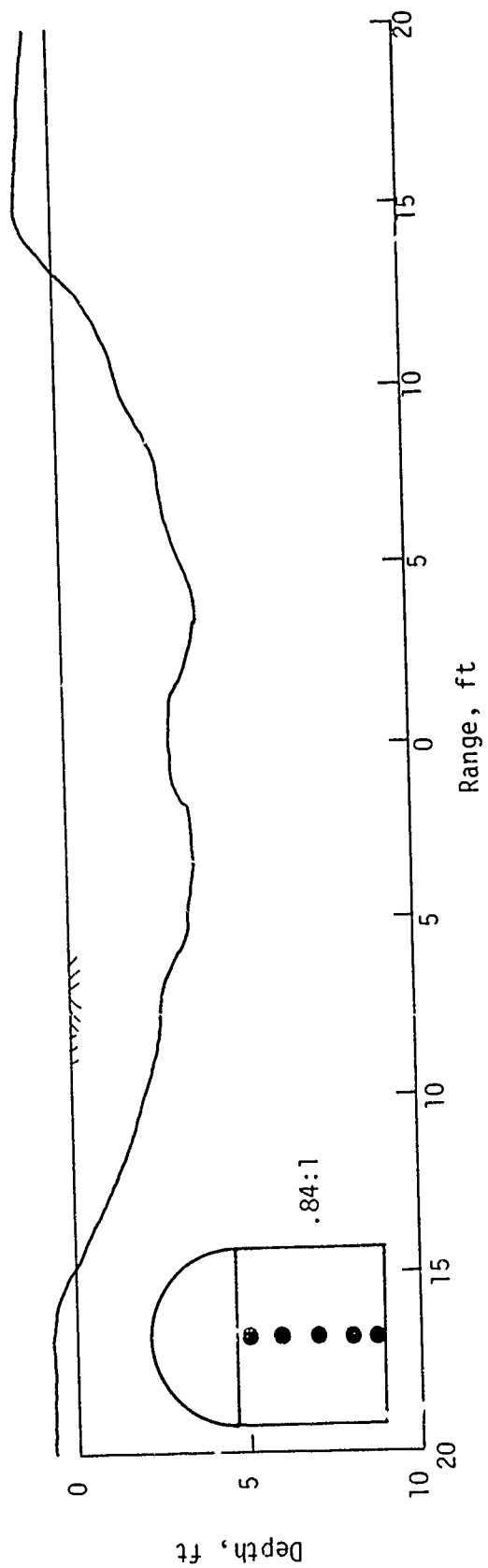


Figure 5. Phase 3, Event 2 (PDTI-2) Crater Profile

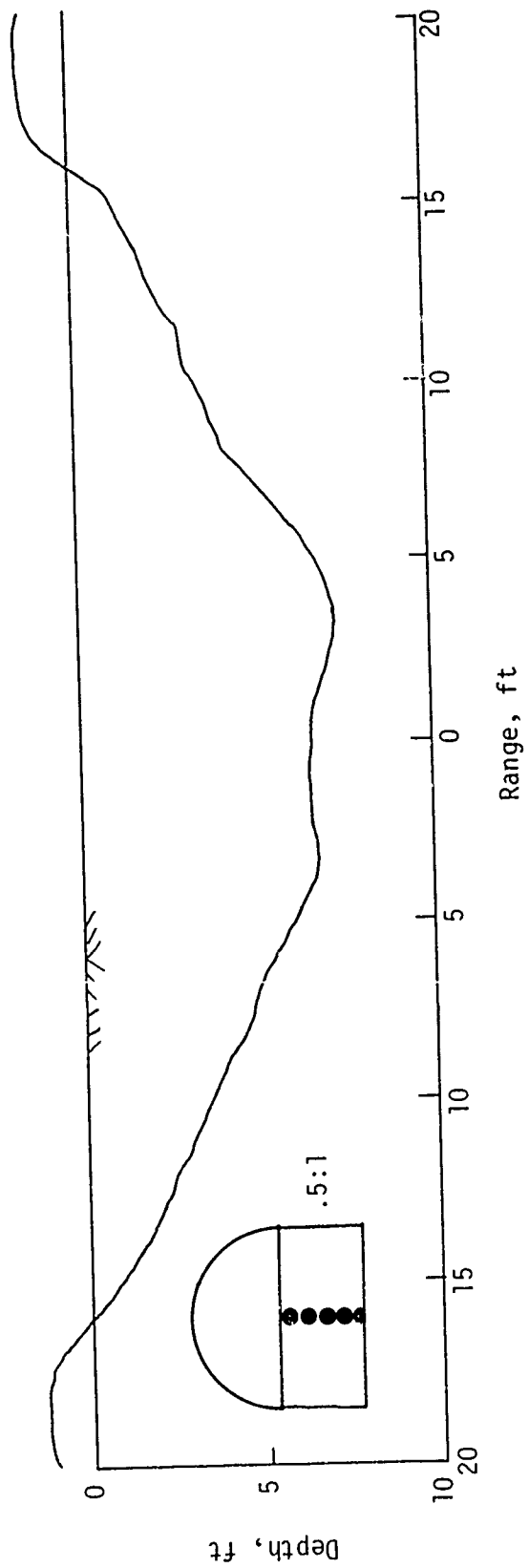


Figure 6. Phase 3, Event 3 (PDTI-3) Crater Profile

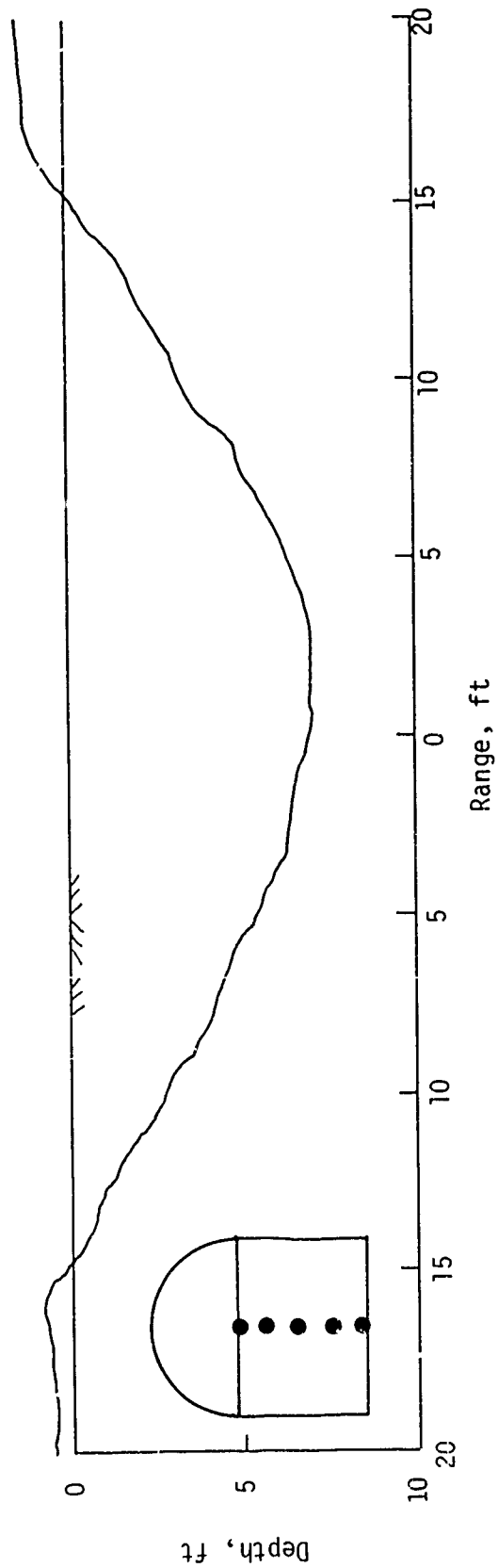


Figure 7. Phase 3, Event 4 (PDTI-4) Crater Profile



was not within expected 20-percent bounds, the crater profiles, as shown in Figures 4 through 7, exhibited general agreement. There was considerably less agreement between the TNT and other ANFO events.

The recorded airblast peak pressures for the Phase 3 events are shown in Figure 8. No unexpected trends were noted in the attenuation character, and it was concluded that, at the relative ranges examined, no one of the 5-ton-equivalent events were identifiable from another.

The high-speed photographic data, however, indicated that severe explosive jetting was produced on the first two ANFO events (PDTI-2 and PDTI-3), which significantly perturbed portions of the shock front. In addition, the point of shockwave separation from the detonation products was observed to occur at a point closer to the charge in the ANFO detonations than for the TNT event, and there were perceptable variations in the dust-cloud character between the ANFO and TNT events noted. The variation in the point of shockwave separation from the detonation products is believed to be attributable to the differences in oxygen balance for the two explosives, and dust-cloud variations are possibly attributable to detonation performance and/or variations in charge configuration. A portion of the calculational program <sup>(4)</sup> appeared to support arguments concerning effects from the charge configuration, but no conclusive tests were conducted to support either postulate.

The results of the first three events in Phase 3 indicated that the objective of matching basic phenomenological effects of TNT and ANFO detonations was obtainable; however, ANFO did not produce a cleaner airblast environment than TNT in the PDTI-2 and PDTI-3 detonations. A fourth ANFO event (PDTI-4) was executed in an attempt to reduce anomalous explosive jetting. Arguments for number, shape and size of boosters, charge configuration and containment methods were reviewed and an ANFO charge was designed to incorporate all reasonable changes. Among the changes incorporated were: the use of a seven cylindrical booster-initiation system in place of a larger five-point system; a charge constructed of bagged ANFO in place of a container filled with loose ANFO; a redundant firing system; and an adjustment

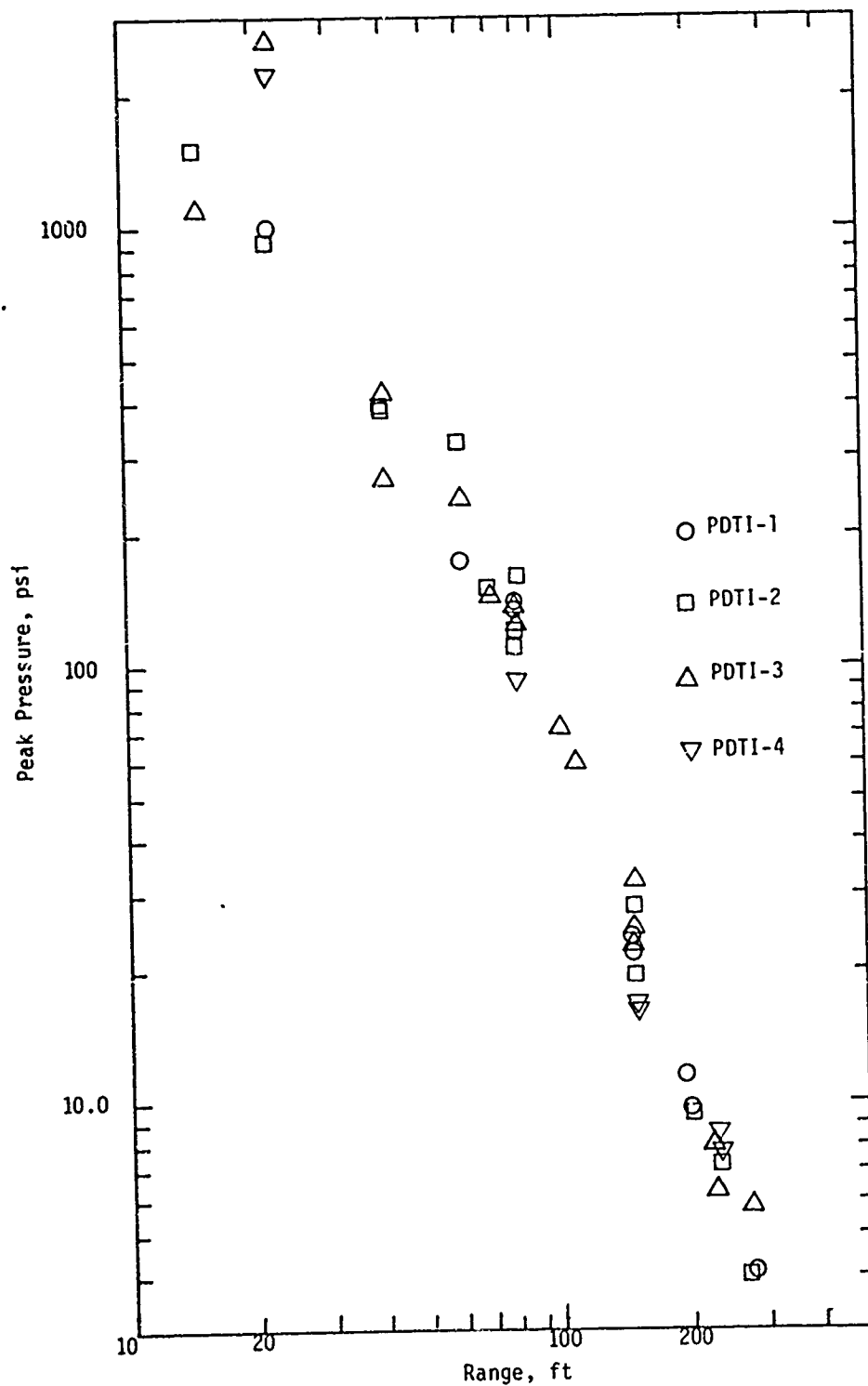


Figure 8. Peak Shock Overpressure Versus Ground Range, Phase 3, Events 1 through 4

to the charge configuration to improve cratering correlations with the TNT baseline data. The event designated as PDTI-4 produced a shock environment with no perceptible explosive jets.

The results of Phase 3 thus indicated some marked variations between ANFO and TNT detonations, although the primary objectives of the program were met if proper care were taken with charge construction and initiation techniques.

#### D. Phase 4

Phase 4 was a 100-ton-equivalent program entitled Pre-DICE THROW II (PDTII) which consisted of (1) a 100-ton STS TNT charge (PDTII-1) to provide baseline phenomenological nuclear weapons effects (NWE) simulation data, and (2) a 120-ton ANFO charge (PDTII-2). The intent of the PDTII-2 event was to verify that the selected ANFO source met the stated program objectives and to characterize the ANFO airblast performance of the main DICE THROW event. A brief description of Phase 4 events can be found in Table 5.

The site selected for the Phase 4 program was within 10,000 feet of the Phase 3 test area and was of interest to the Air Force in support of the MX program. The site was examined for uniformity and the earth materials categorized and modeled<sup>(6,7)</sup> for a calculational program. The PDTII-1 event was conducted in August 1975, and the PDTII-2 event in September 1975. Detailed program descriptions and results can be found in references (8) through (16). A substantial effort was undertaken to quantify what differences might occur between the TNT and ANFO detonations. The measurements that were made for comparison include airblast, ground motion and stress, cratering and technical photography.

Results of the TNT event airblast measurement program are shown in Figures 9 and 10. The ANFO event results are shown in Figures 11 and 12. Comparisons of the overpressure attenuation plots (Figures 9 and 11) for the two events indicate that, although both events agree fairly well with each other and with predictions, the ANFO event exhibits a smaller degree of data spread, possibly indicating a cleaner airshock environment. This observation is reinforced by ground-level

TABLE 5. Phase 4 Experimental Test Program

Event	Configuration	Dimensions (ft)	Explosive	Apparent Crater Dimensions		
				$R_a$ (ft)	$D_a$ (ft)	$V_a$ (ft <sup>3</sup> )
PDTII-1	Sphere, Surface Tangent	R= 7.87	TNT	75.0	13.9	152,000
PDTII-2	Cylinder, Hemis. Cap L/D=0.75	L=12.97 D=17.48	ANFO	85.6	9.6	166,000

Note: Explosive weights were:  
 PDTII-1 - 200,102 pounds  
 PDTII-2 - 244,898 pounds

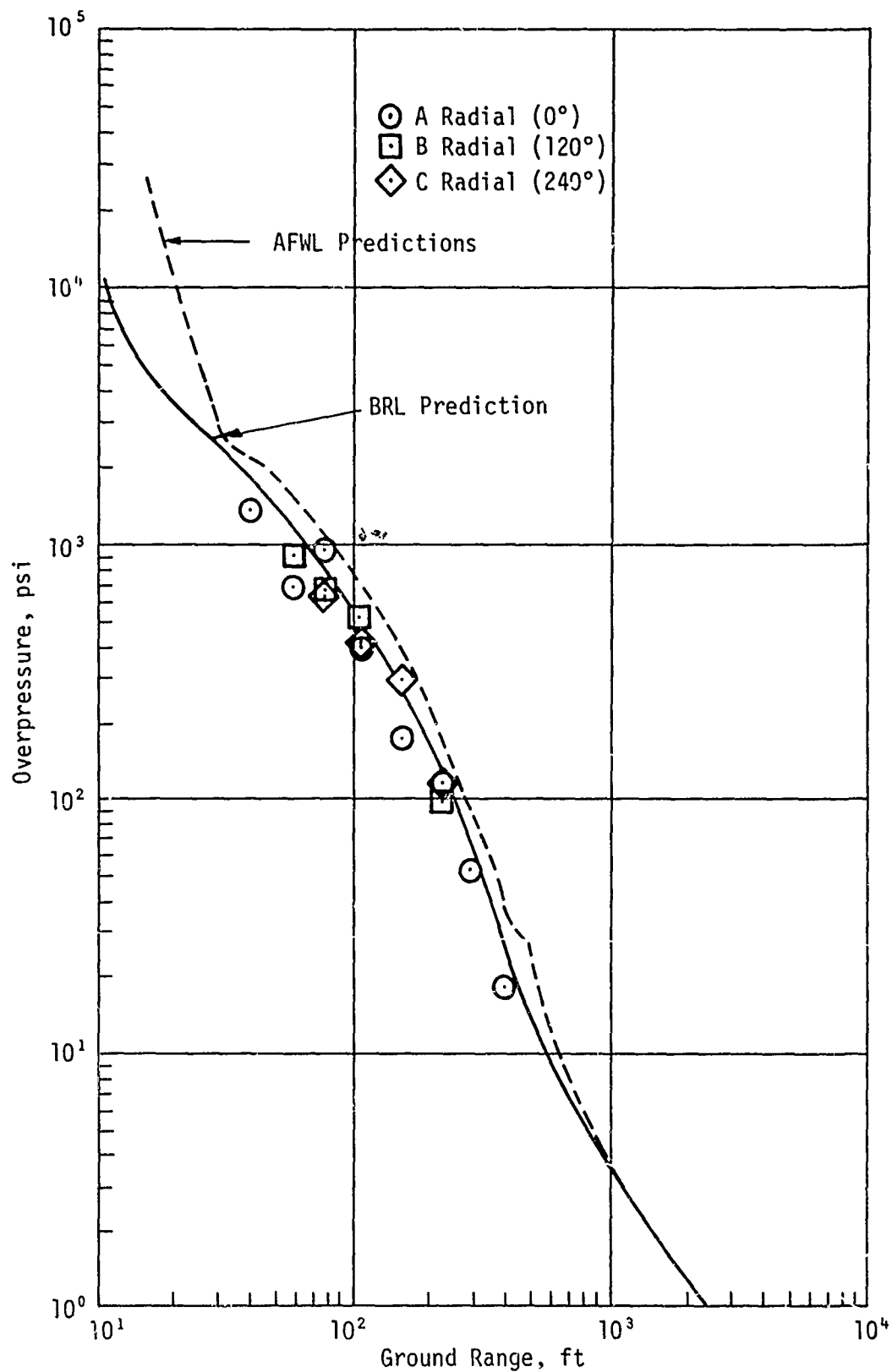


Figure 9. Peak Shock Overpressure Versus Ground Range, Pre-DICE THROW II, Event 1, BRL Data

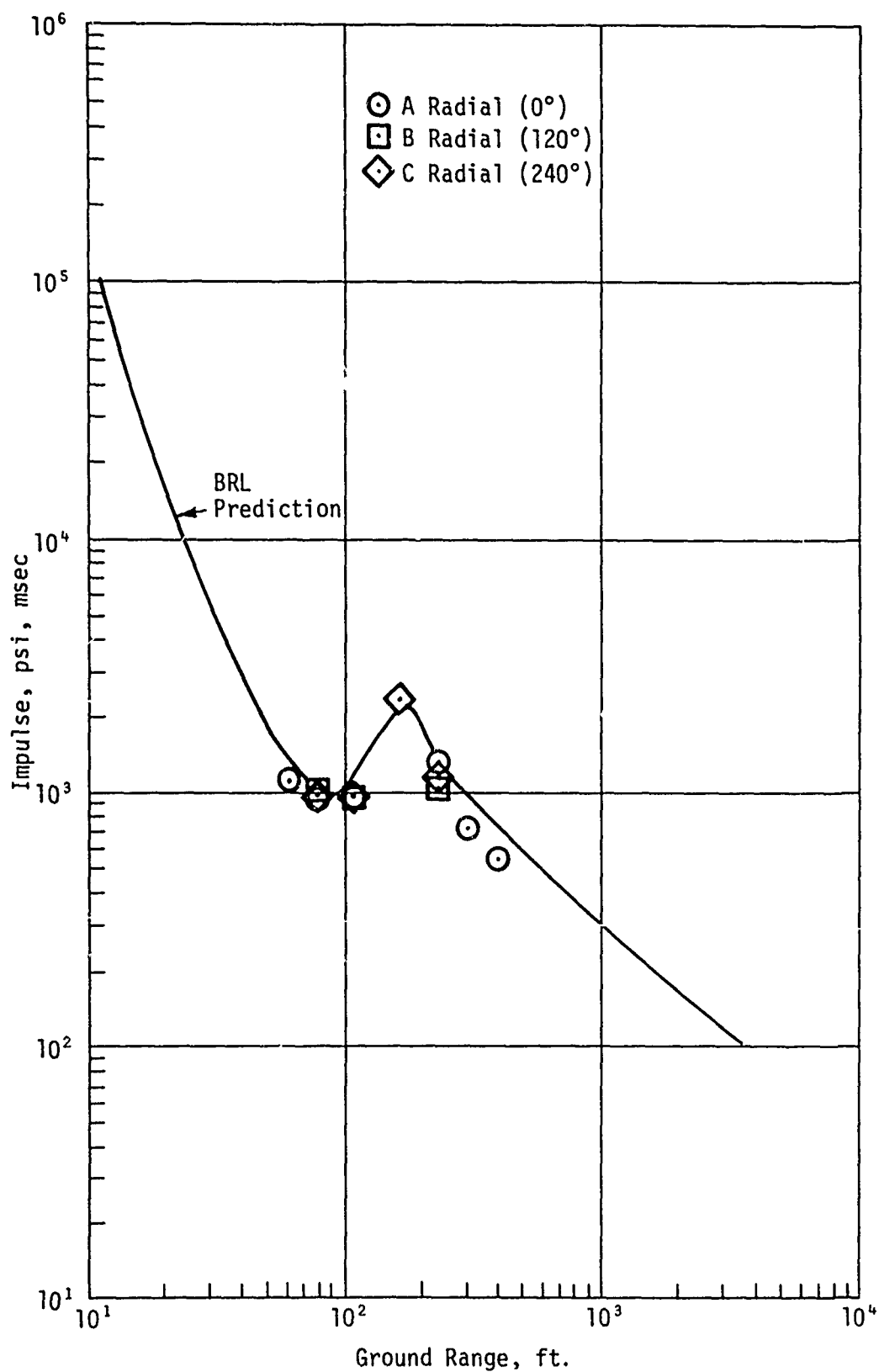


Figure 10. Overpressure Impulse Versus Ground Range,  
Pre-DICE THROW II, Event 1, BRL Data

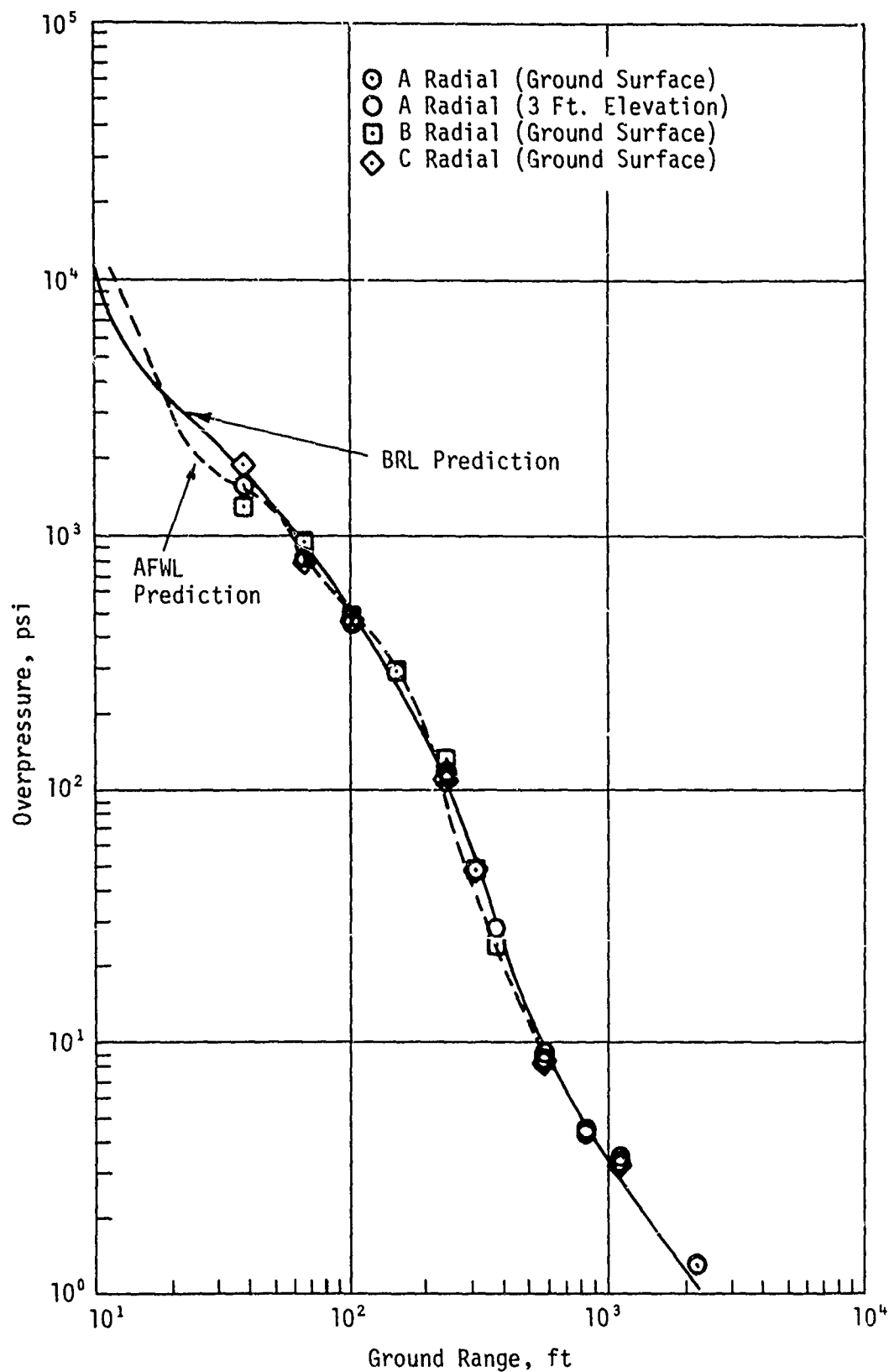


Figure 11. Peak Shock Overpressure Versus Ground Range, Pre-DICE THROW II, Event 2, BRL Data

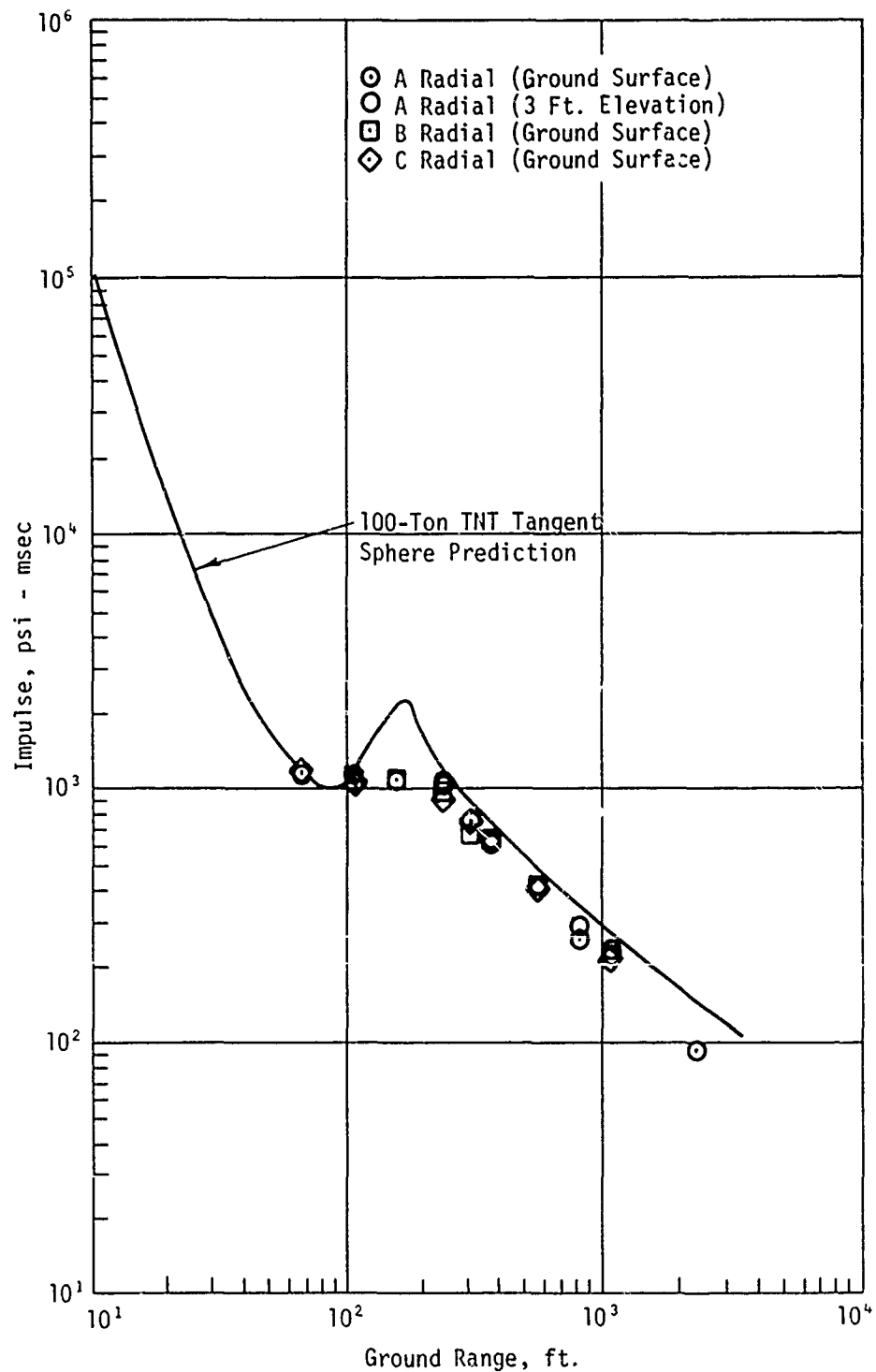


Figure 12. Overpressure Impulse Versus Ground Range, Pre-DICE THROW II, Event 2, BRL Data



and airborne photography. The comparison of impulse attenuation rates (Figures 10 and 12) demonstrates good agreement between events except at the 180-foot range. The inflection point common to impulse-attenuation plots of TNT airblast experiments was not observed on the ANFO event. The apparent absence of this effect is not well understood at this time. The overpressure impulse curves appear less sensitive to the degree of explosive jetting.

Comparison of the ground motions recorded on the two events are shown in Figures 13 through 18. Data for vertical and horizontal attenuation rates for recorded velocity and displacement measurements (Figures 13 and 14) overlap, and the data trends appear to be consistent with the scatter of the data. Examples of horizontal and vertical ground-motion waveforms for both the superseismic and outrunning conditions are shown in Figures 15 through 18. Overall, the data from TNT and ANFO events are quite consistent. Measured stress attenuation rates taken from a region which was dominated by direct-induced motions on the two events are shown in Figures 19 and 20. Reasonable agreement between events was observed. Stress waveforms measured from the two events are shown in Figure 21. The stress-wave character from the two events agree quite well, supporting similarity arguments in shock-coupling effects.

There was, however, a potential discrepancy noted in particle velocity measurements made directly beneath the ANFO charge. Results of the interpreted records are shown in Figure 22. The peculiarity is the second recorded peak in particle velocity. This effect may result from an explosive shock front which has a cylindrical rather than spherical character. The effect is not apparent in the recorded stress records taken at a somewhat greater range, indicating the effect to be short-lived.

Cratering measurements taken from the two events are shown in Table 5. The ANFO crater volume is approximately 10 percent larger than the TNT crater. The ANFO crater is, however, significantly broader and shallower than the comparable STS TNT crater, as shown in the comparison of the representative crater profiles of Figure 23. Geologic profiles of the crater regions for the two events are shown

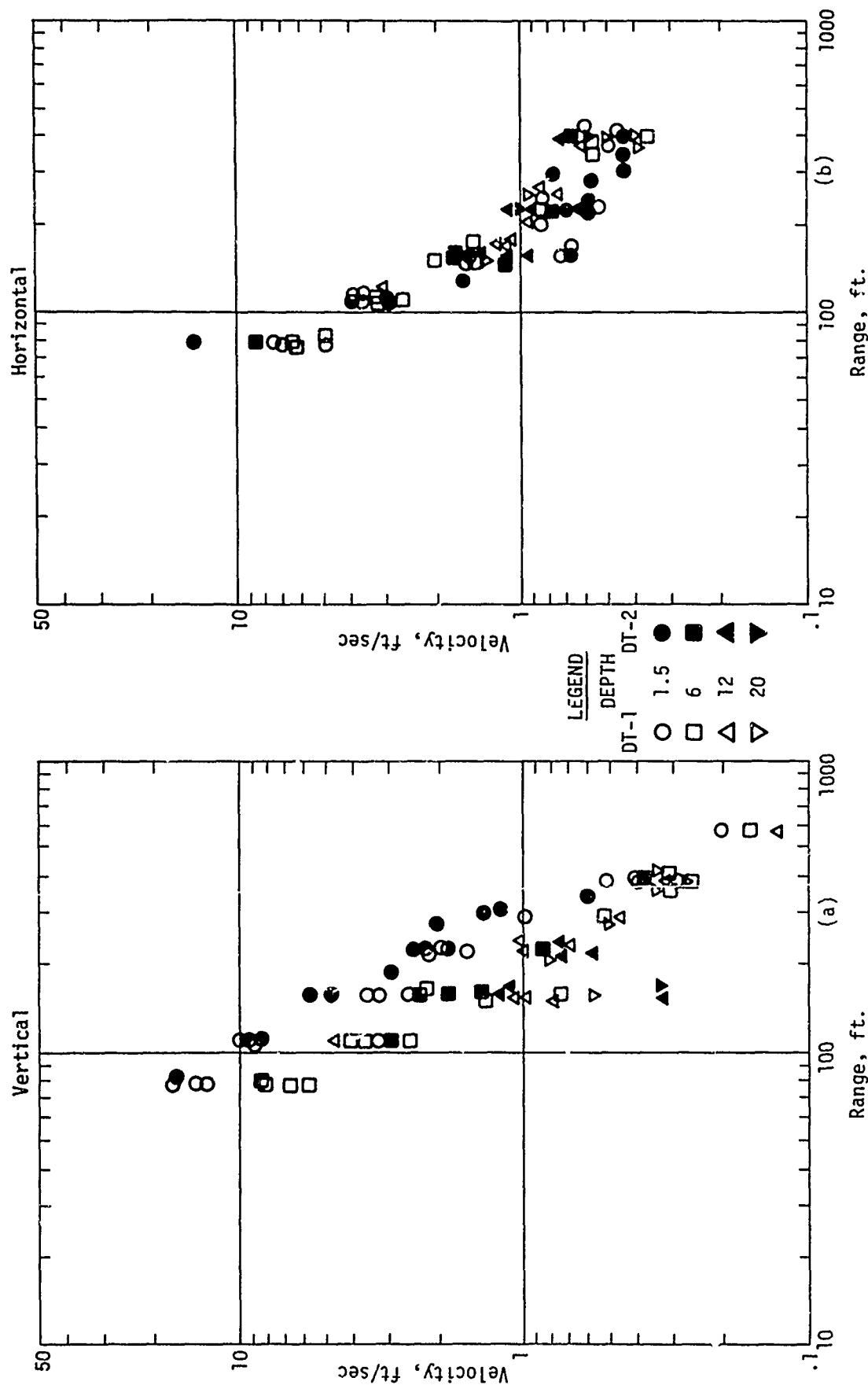


Figure 13. Peak Vertical and Horizontal Velocity versus Range, Pre-DICE THROW II, Events 1 and 2, WES Data

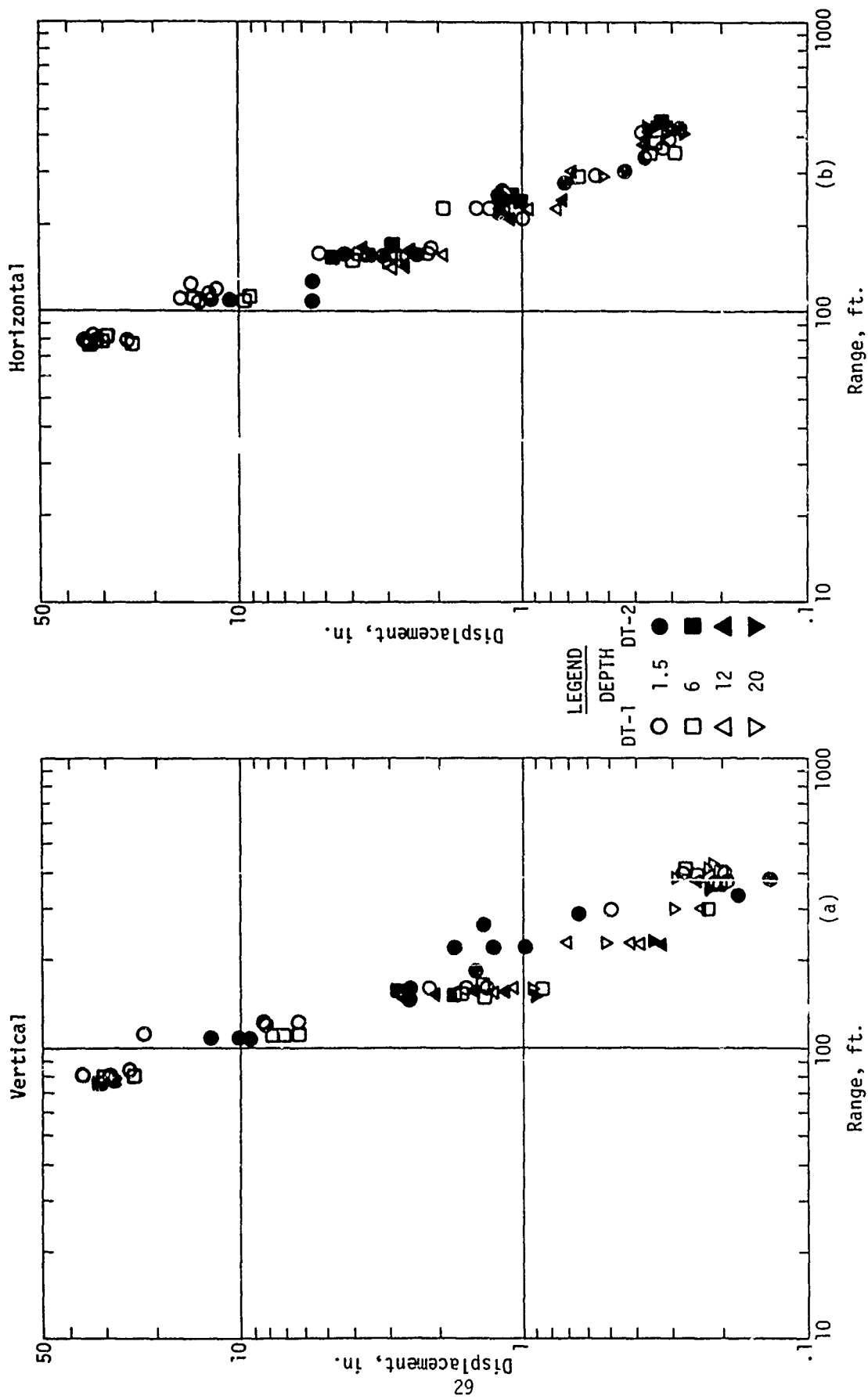
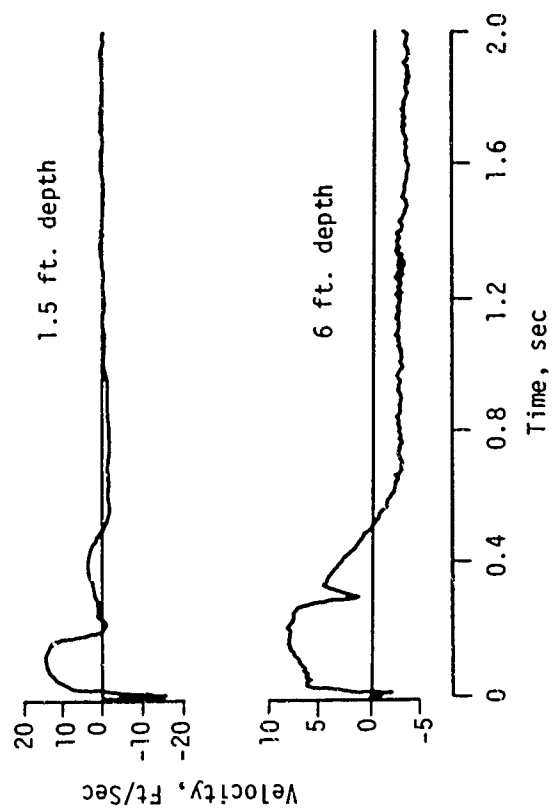


Figure 14. Peak Horizontal and Vertical Displacement Versus Range, Pre-DICE THROW II, Events 1 and 2, WES Data

Event 2



Event 1

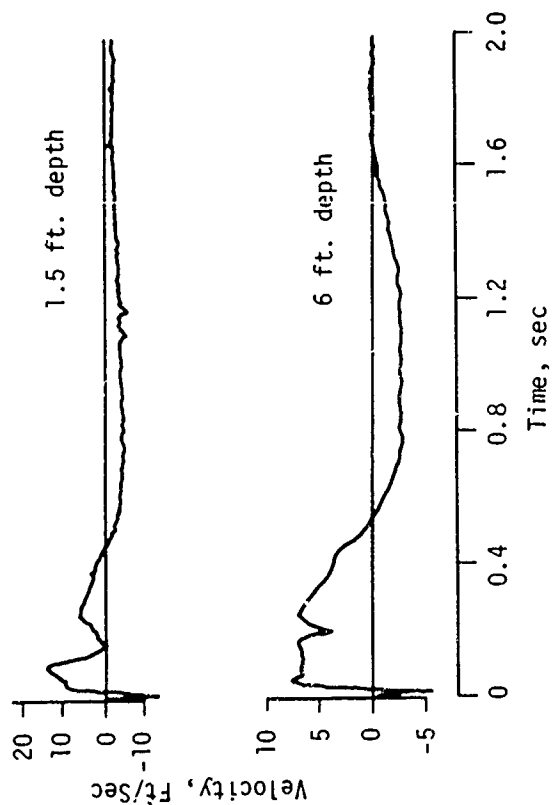


Figure 15. WES Vertical Velocity Waveforms, at 80-Foot Range,  
Pre-DICE THROW II, Events 1 and 2

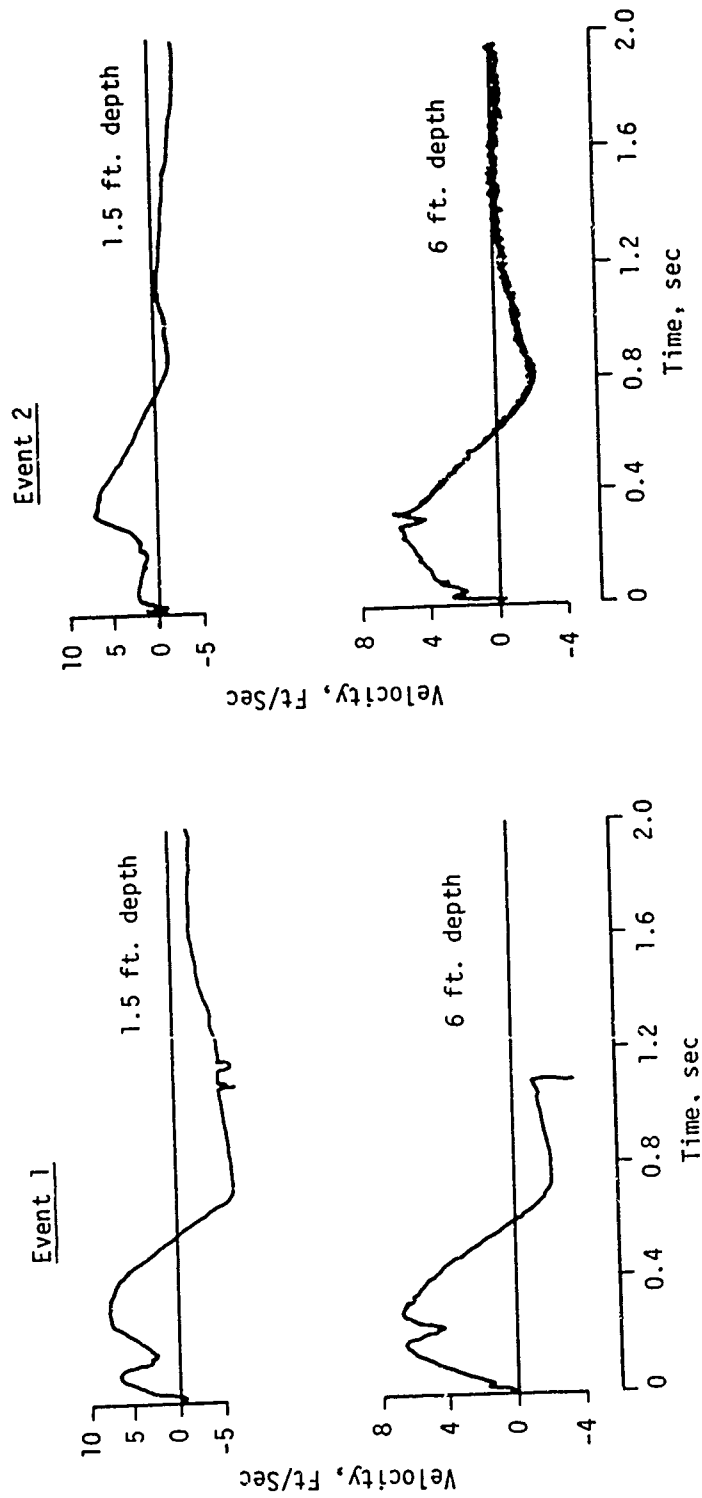


Figure 16. Horizontal Velocity Waveforms at 80-Foot Range, Pre-DICE THROW II, Events 1 and 2, WES Data

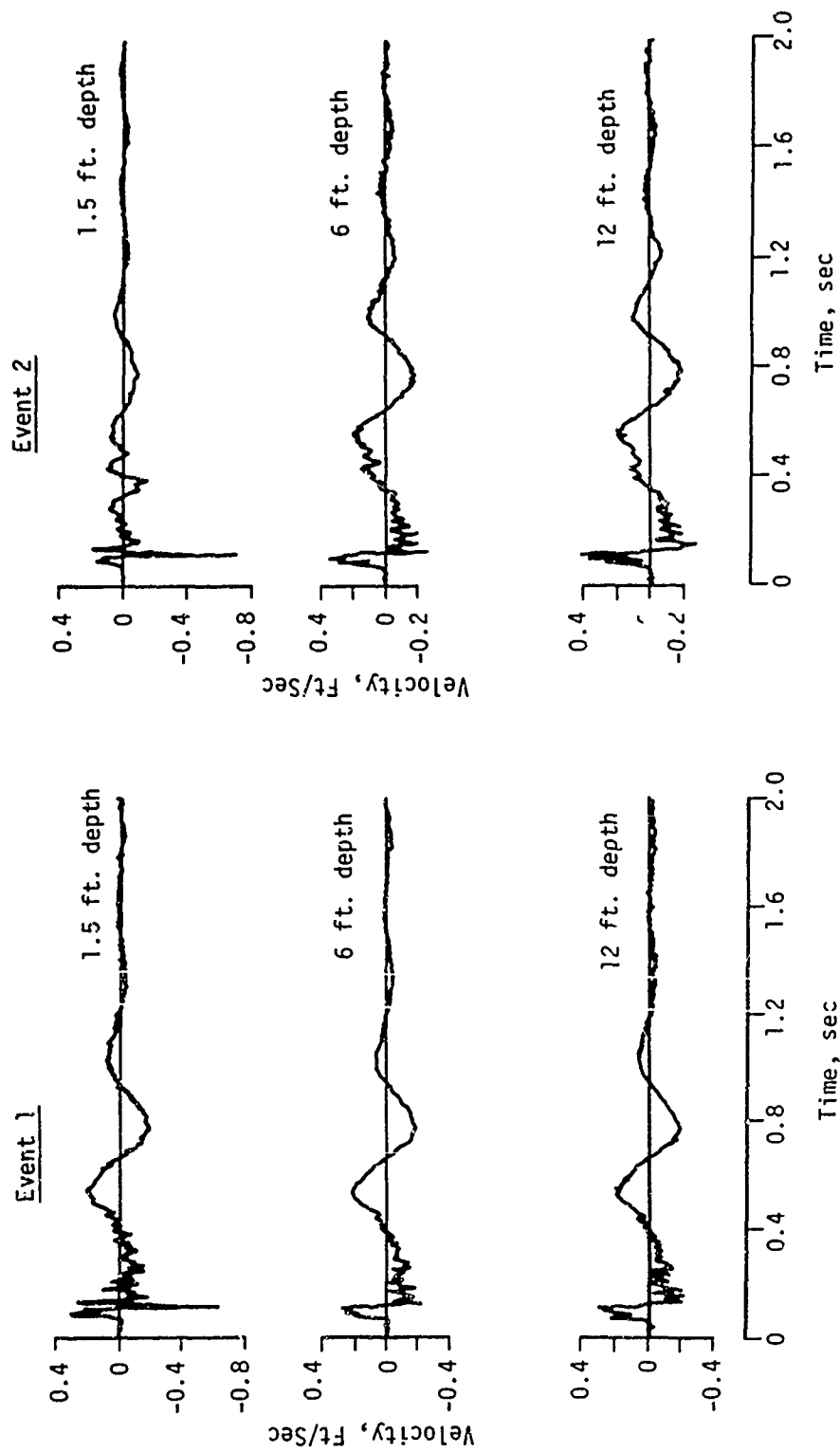


Figure 17. WES Vertical Velocity Waveform at 400-Foot Range, Pre-DICE THROW II, Events 1 and 2

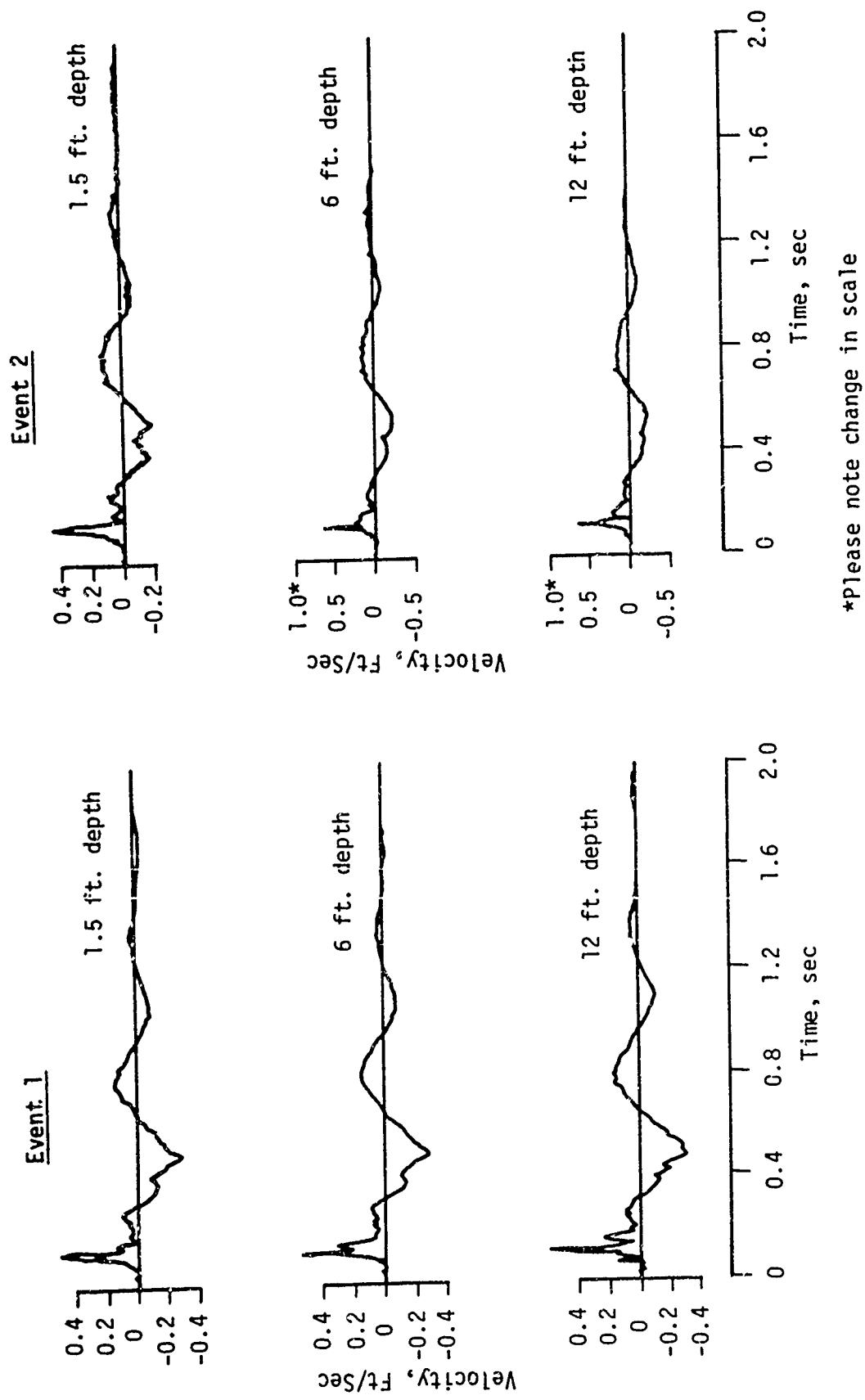


Figure 18. Horizontal Velocity Waveforms at 400-Foot Range, Pre-DICE THROW II, Events 1 and 2, WES Data

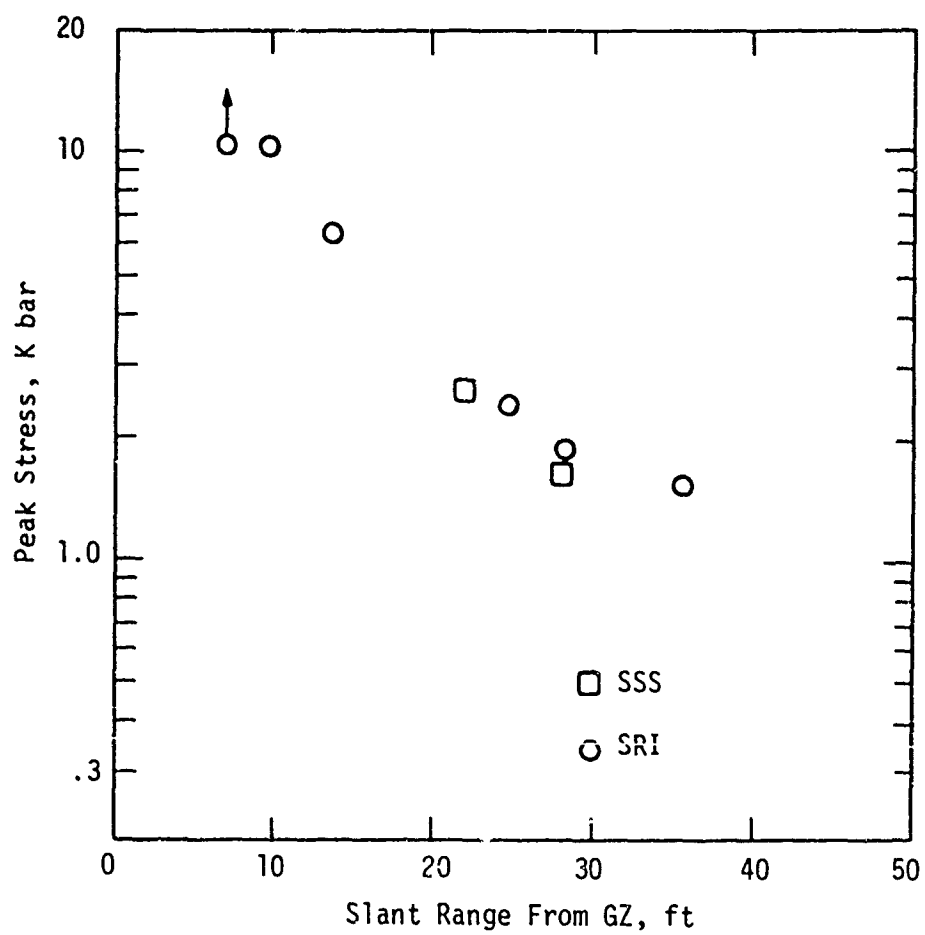


Figure 19. SSS Measured Peak Stress Versus Range, Pre-DICE THROW II, Event 1



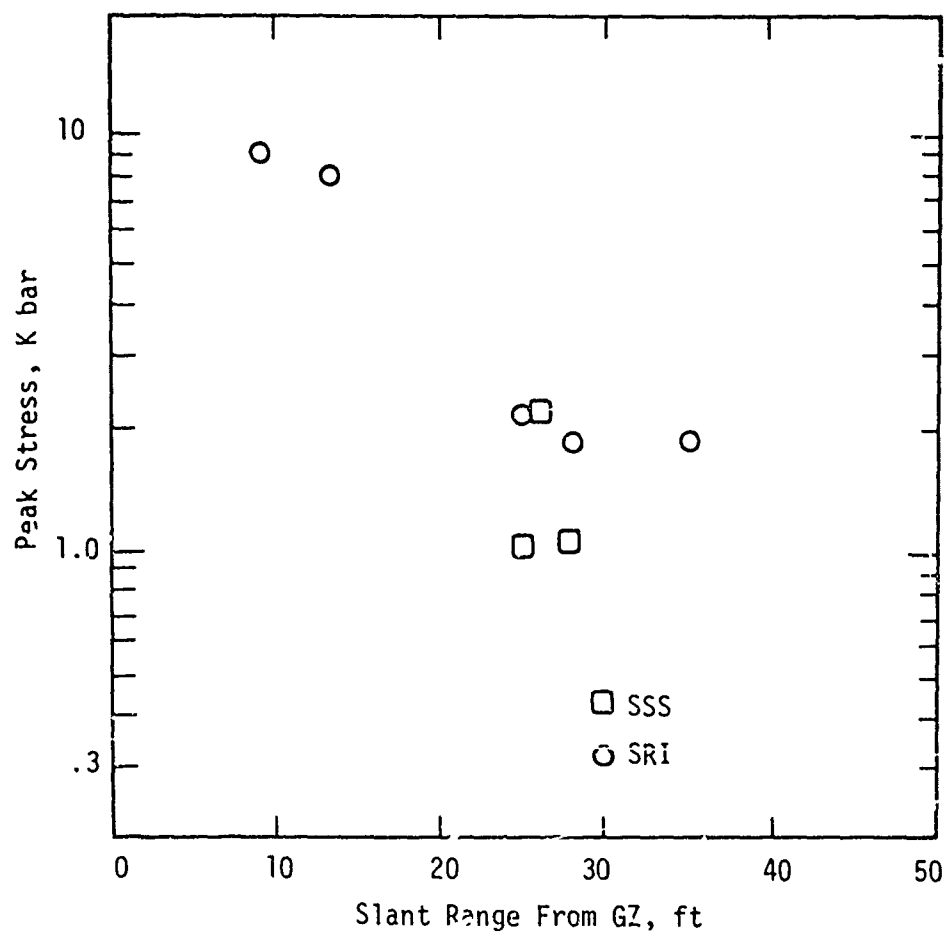


Figure 20. SSS Measured Peak Stress Versus Range, Pre-DICE THROW II, Event 2

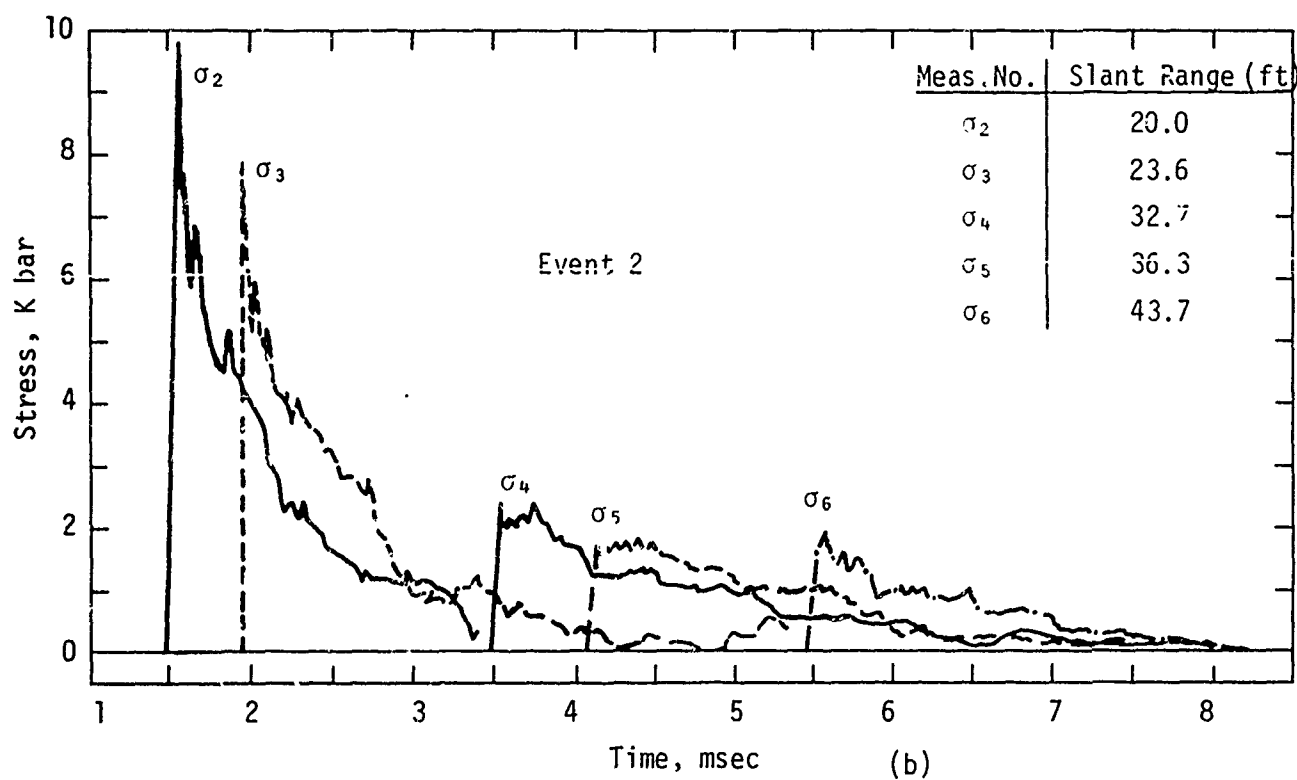
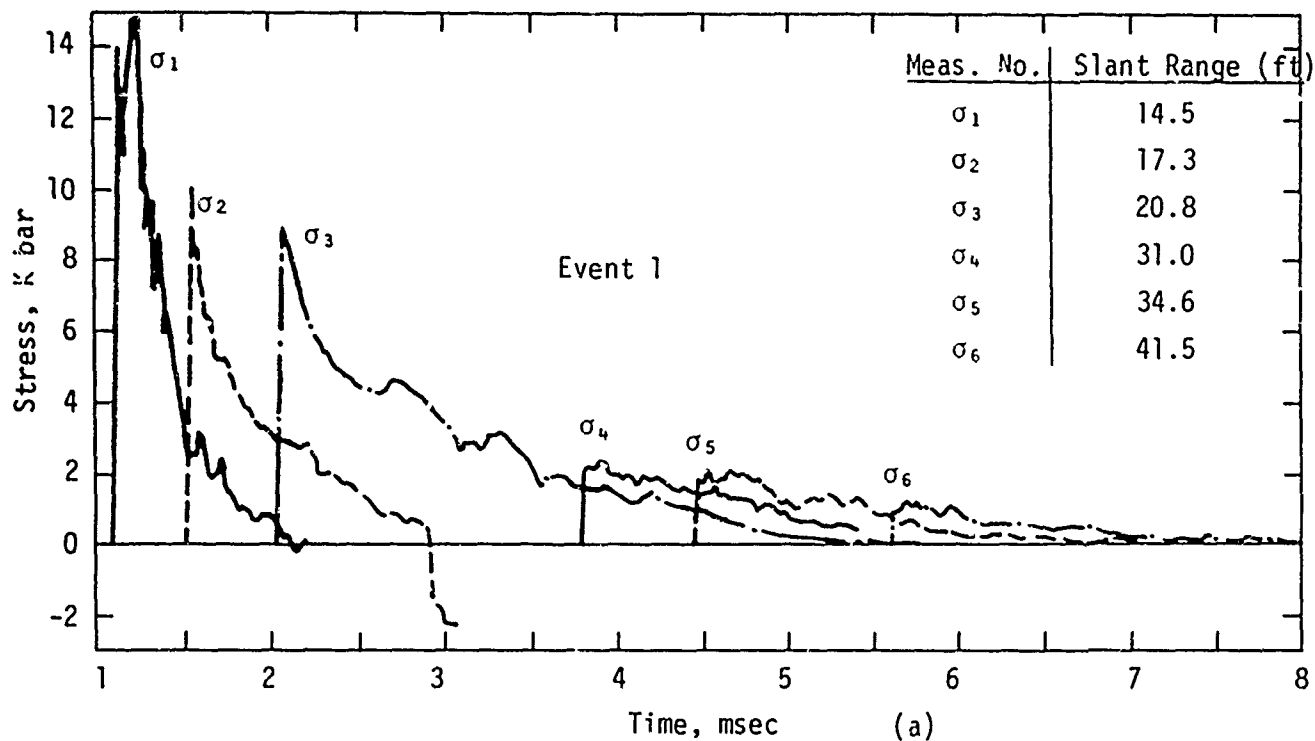


Figure 21. SRI Recorded Stress-Time Profiles, Pre-DICE THROW II, Events 1 and 2

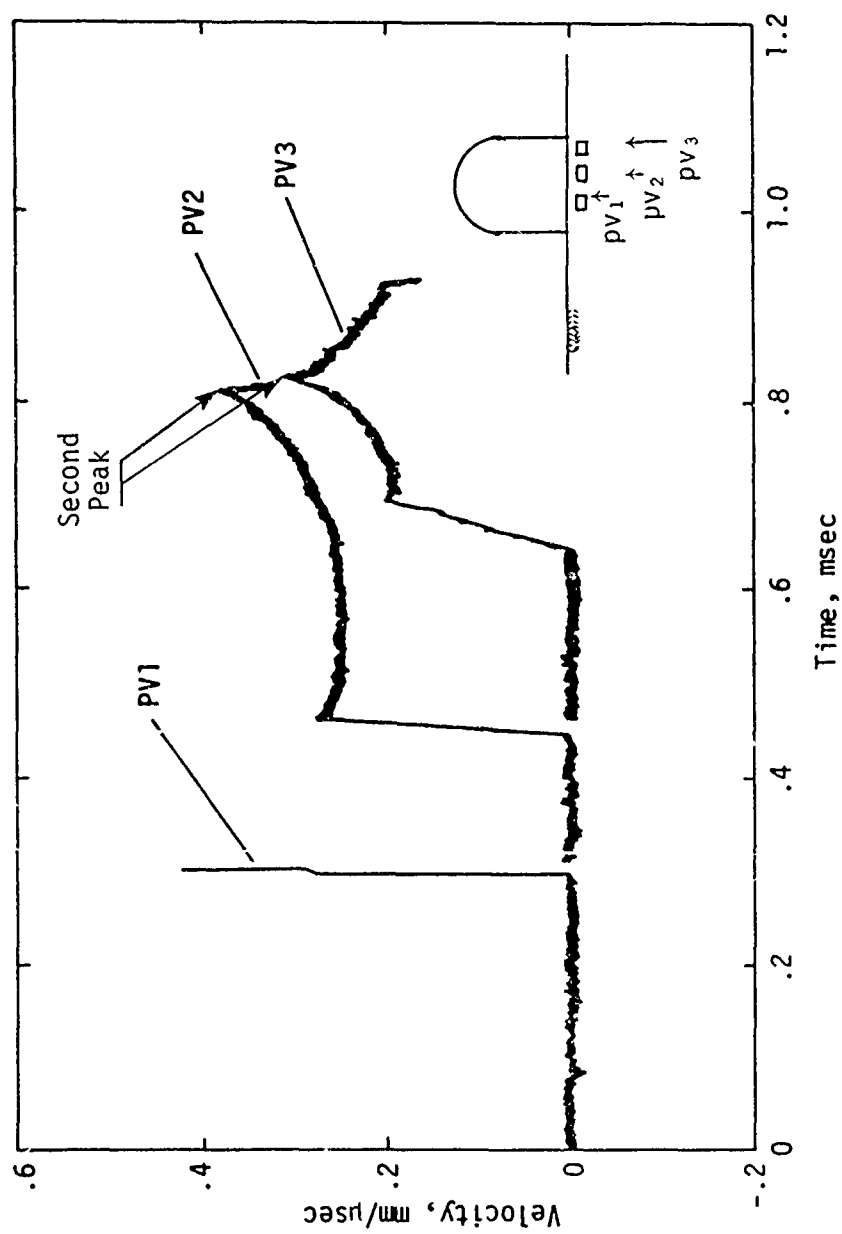


Figure 22. Summary of Velocity Data, Pre-DICE THROW II, Event 2, AFWL Data

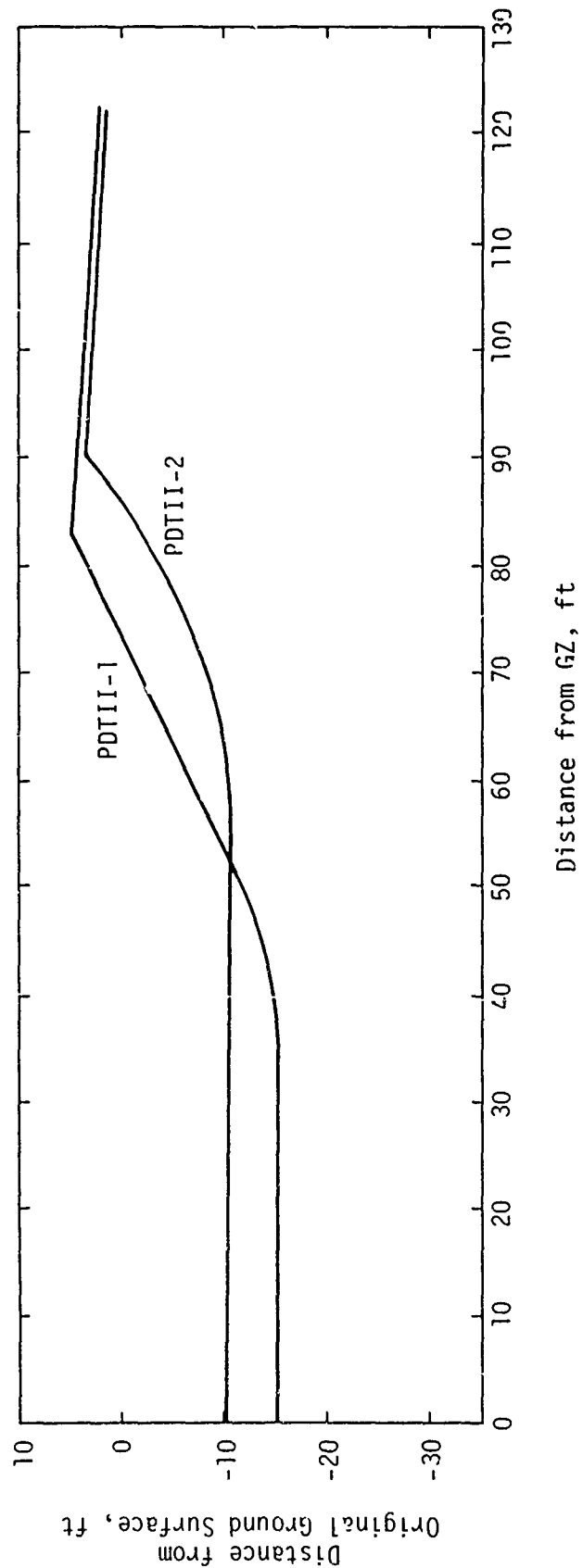


Figure 23. Comparison of Pre-DICE THROW II Apparent Craters, AFWL/CERF Data

in Figures 24 and 25. The crater reconstruction profiles indicate that similar cratering phenomenon occurred in both events, and further indicate differences in materials in the cratered region. It has not been conclusively demonstrated whether the large difference in the observed crater shapes is due to source nature or to geologic variations, or both. However, the measured 10-percent variation in crater volume appears to be well within the reproducibility bounds of cratering experiments.

High-speed photographic measurements verified the improved air-shock environment recorded on the ANFO event. Once again, observable differences in the dust-cloud formation processes were observed in the TNT and ANFO detonations. The possible causes of this phenomenon were discussed in the Phase 3 results.

Results of the Phase 4 effort confirmed the successful completion of the ANFO Charge Development Program. Cratering, airblast, ground-motion and stress behavior from a TNT detonation were successfully reproduced from a comparable-size ANFO source, and significantly fewer airblast anomalies were observed in the ANFO detonation. In addition, the explosive-equivalency factor of 1.2 by weight between ANFO and TNT was shown to be reasonable in correlating phenomenological effects.

### III. CONCLUSIONS

The results of the ANFO Charge Development Program indicate that ANFO, when properly configured and initiated, is a suitable replacement explosive source for conventional nuclear weapons effects (NWE) testing, and that the degree of explosive jetting can be reduced when using ANFO, provided that proper care is exercised when constructing and initiating the charge. The airblast environment is well-behaved, adequately characterized, and appears to be scalable with yield. It is expected, however, that there are some limitations on the minimum yield of ANFO detonations which will reproduce STS TNT phenomenology, particularly for the explosive-equivalency factor selected for this program. The utility of ANFO for charge yields of less than five tons requires further research.

With the distinct advantages of ANFO, as described in the Introduction, there are some reservations for its use. Among these are: sensitivity

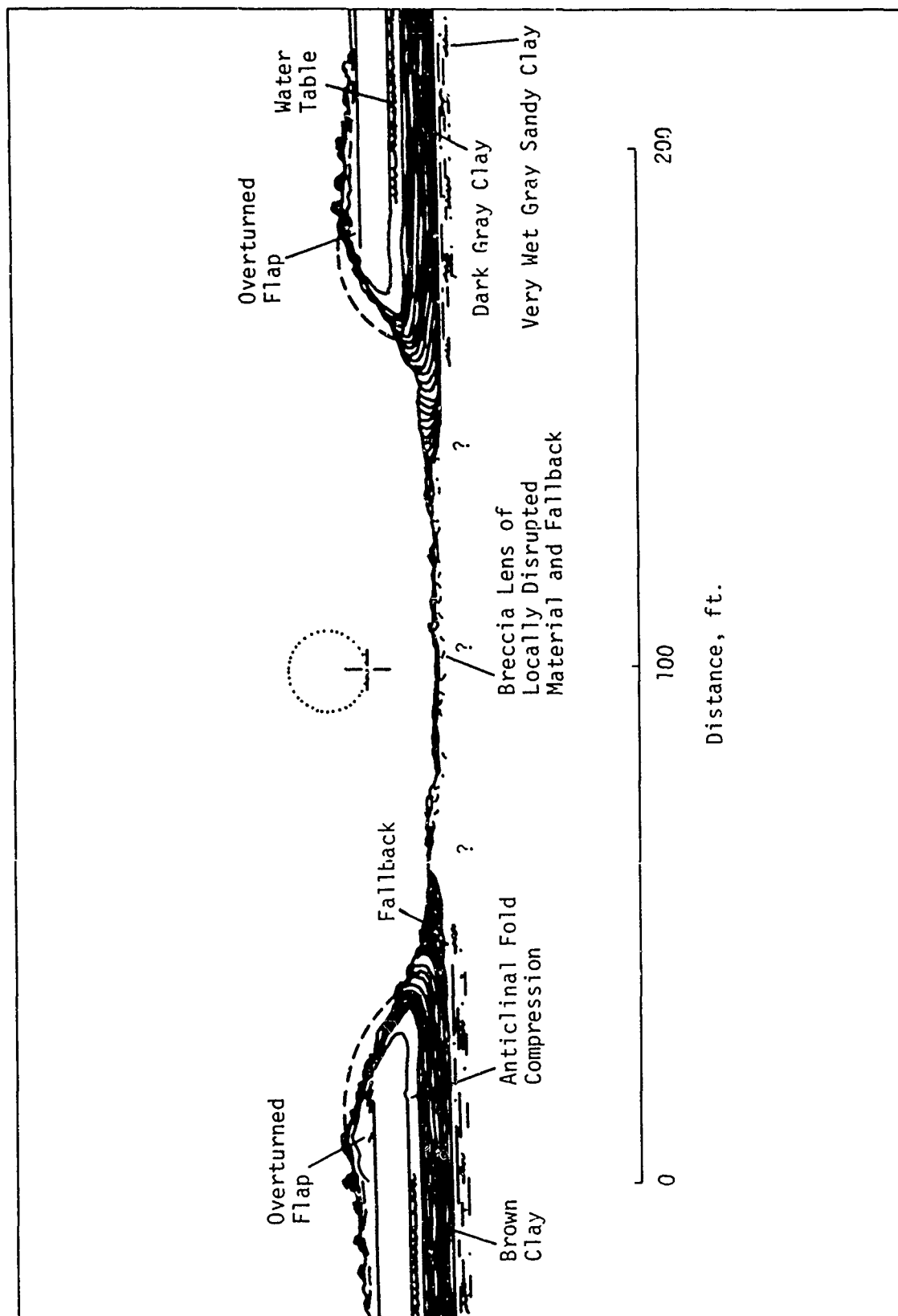


Figure 24. Generalized Crater Cross-Section, Pre-DICE THROW II, Event 1, USGS Data

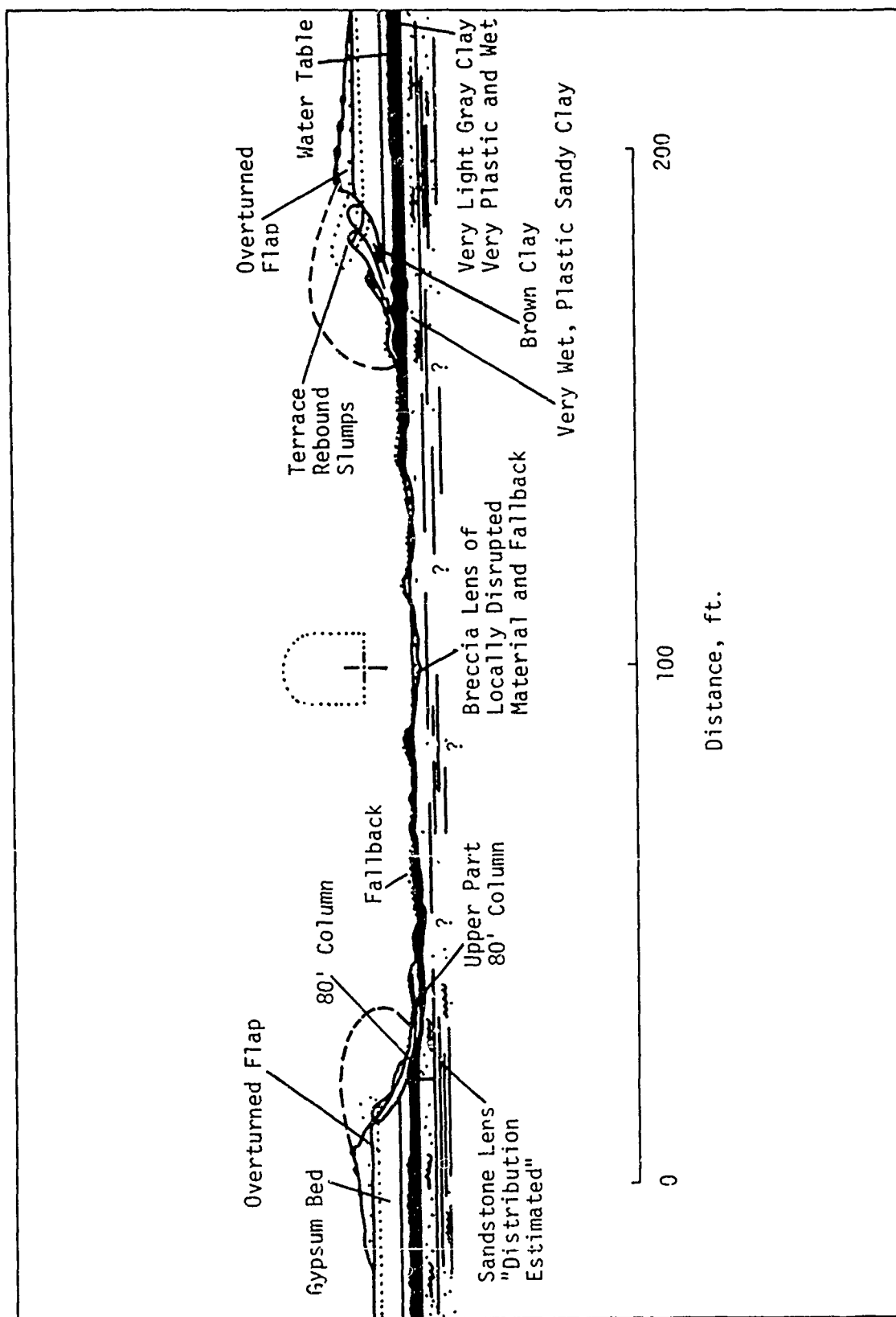


Figure 25. Generalized Crater Cross-Section, Pre-DICE THROW II, Event 2, USGS Data

to moisture and extreme heat, physical limitations on ability to stack the conventional bagged explosives, density variations within the stack due to both static stresses and manufacturing variations, and the effects of these variations on the detonation parameters. In addition, the initiation techniques employed in the ANFO detonations, which were required to produce a clean airshock environment, produce stringent demands on conventional firing systems when exploding bridgewire detonators (EBW) are used. Finally, the effects of reaction zone dependencies of ANFO may limit its use on small-scale events.

With these reservations held in balance, it appears that ANFO can meet or exceed current NWE testing requirements.

#### IV. RECOMMENDATIONS

It is recommended that the phenomenon governing the cloud formation process be closely studied and tested before the dust cloud produced by the candidate ANFO charge is used as a NWE simulation. In addition, the use of ANFO in small (<5-ton) or large (>500-ton) source simulations should be carefully examined before the source is utilized in NWE testing. It would also be advisable to attempt to better quantify the ANFO reaction zone and to examine its effects on small-scale detonations, as well as to examine explosive performance variations from different ammonium nitrate manufacturing sources. Finally, a program to examine what causes explosive jetting, and what measures are required to minimize it, is needed if ANFO or any other HE source is to be developed as a long-term NWE simulation source.



## REFERENCES

1. Sauer, F., Middle North Series, Pre-MINE THROW IV; Technical Director's Summary Report, POR 6828, Defense Nuclear Agency, 1977.
2. Sadwin, L., and Pittman, J., Airblast Characterization of ANFO, Phase I, TR 69-82, Naval Ordnance Laboratory, 1969.
3. Helm, F., et al, High Explosive Characterization for the DICE THROW Event, UCRL-52042, Lawrence Radiation Laboratory, 1976.
4. Needham, C., Theoretical Calculations of Airblast from ANFO Detonations, POR 6914, Defense Nuclear Agency, 1977.
5. Henny, R., and Jones, G., ANFO Charge Configuration Development Program—Pre-DICE THROW, POR 6905, Defense Nuclear Agency, unpub.
6. Jackson, A., Jr., Ballard, R., Jr., and Curro, J., Jr., Material Property Investigation for Pre-DICE THROW I and II: Results from the Subsurface Exploration Programs, U. S. Army Engineer Waterways Experiment Station, 1976.
7. Jackson, A., Jr., and Peterson, R., Material Property Investigation for Pre-DICE THROW I and II: Results from the Laboratory Testing Programs, U.S. Army Engineer Waterways Experiment Station, 1976.
8. Edwards, T., and Perry, G., Middle North Series, Pre-DICE THROW II Events; Preliminary Results Report, POR 6904, Defense Nuclear Agency, 1976.
9. Murri, W., Stress Gage Measurements on Pre-DICE THROW II, POR 6908, Defense Nuclear Agency, 1977.
10. Gaffney, E., Close-in Measurements of Airblast and Ground Shock, POR 6909, Defense Nuclear Agency, 1977.
11. Meyer, J., Crater and Permanent Displacement Study, POR 6912, Defense Nuclear Agency, 1977.
12. Naylor, R., Detonation Velocity of Pre-DICE THROW II, POR 6913, Defense Nuclear Agency, 1977.
13. Teel, G., Freefield Airblast Definition of TNT and ANFO Detonations, POR 6915, Defense Nuclear Agency, 1977.
14. Renick, J., Near Source Ground Motion Measurements, POR 6918, Defense Nuclear Agency, 1977.
15. Wisotski, J., Middle North Series, Pre-DICE THROW I and II Events; Technical Photography, POR 6917, Defense Nuclear Agency, 1976.
16. Murrell, D., Pre-DICE THROW II, Events 1 and 2, Ground Motion Measurements, POR 6910, Defense Nuclear Agency, 1977.

## **2. DICE THROW OVERVIEW**

by

**LCDR J.D. Strobe**  
**DNA Field Command**

## TABLE OF CONTENTS

<u>Section</u>	<u>Page</u>
1. Introduction.....	1
2. Objectives.....	1
3. DNA Responsibilities.....	1
4. Test Site.....	2
5. Test Bed.....	3
6. Instrumentation/Timing & Firing/Technical Photography	5
7. Construction.....	6
8. Explosive Charge/Detonation.....	8
9. Test Site Cleanup.....	10

PRECEDING PAGE BLANK

## ILLUSTRATIONS

<u>Figure</u>		<u>Page</u>
1	Test Group Staff Organizational Chart.....	11
2	Site Location WSMR, NM.....	12
3	Test Site Layout (Engineering Drawing).....	13
4	Test Bed Layout (Engineering Drawing).....	14
5	Test Bed (Aerial View).....	15
6	Test Bed (Aerial View).....	16
7	Instrumentation Trailer Park.....	17
8	Airblast Gages and Mounts .....	18
9	Airblast Gage and Mount.....	19
10	T&F Van (Interior).....	20
11	DRI Camera Station No. 2 .....	21
12	Aligning Cameras on Mounts.....	22
13	Administration Trailer Park/Test Control.....	23
14	Construction Schedule.....	24
15	FRG/WES Structure (Excavated).....	25
16	FRG/WES Structure (Forming).....	26
17	UK/ASWE Slatted Antenna Foundation.....	27
18	UK/ASWE Slatted Antenna.....	28
19	AFWL Underground Aircraft Shelter.....	29
20	SRI German Wall Structure.....	30
21	SRI German Wall Structure (Completed).....	31

PRECEDING PAGE BLANK

### ILLUSTRATIONS (Cont'd)

<u>Figure</u>		<u>Page</u>
22	ANFO Stack (Completed) .....	32
23	ANFO Stack (Cutaway) .....	33
24	ANFO Stack Base/Circular Forms .....	34
25	ANFO Stack (Spreading Bulk ANFO) .....	35
26	ANFO Stack (Installing Booster) .....	36
27	ANFO Stack (Conveyor System) .....	37
28	ANFO Stack (Dismantling the Circular Forms) ..	38
29	ANFO Stack (Completed) .....	39
30	Test Bed (Aerial View) .....	40
31	ANFO Stack Detonation .....	41
32	Dust Cloud .....	42
33	Crater .....	43
34	Test Bed (Post Event Aerial) .....	44
35	Test Bed (After Clean-up) .....	45

## DICE THROW OVERVIEW

BY

LCDR J. D. STRODE, JR. CEC, USN

FIELD COMMAND, DNA

### 1. INTRODUCTION

DICE THROW WAS THE FIFTH IN A SERIES OF 500 TON HIGH EXPLOSIVE EVENTS CONDUCTED BY THE DEFENSE NUCLEAR AGENCY (DNA) FOR THE DEPARTMENT OF DEFENSE. THIS EVENT WAS DESIGNED TO PROVIDE A BLAST AND SHOCK ENVIRONMENT COMPARABLE TO A 1 KILOTON NUCLEAR SOURCE USING ONLY CONVENTIONAL EXPLOSIVES. THE BLAST AND SHOCK ENVIRONMENT IS USED TO INCREASE OUR UNDERSTANDING OF NUCLEAR WEAPONS EFFECTS.

### 2. OBJECTIVES

THE PRIMARY OBJECTIVES OF THIS TEST WERE TO PROVIDE A SIMULATED NUCLEAR BLAST AND SHOCK ENVIRONMENT FOR TARGET RESPONSE EXPERIMENTS THAT ARE VITALLY NEEDED BY THE MILITARY SERVICES AND DEFENSE AGENCIES; AND TO CONFIRM EMPIRICAL PREDICTIONS AND THEORETICAL CALCULATIONS FOR BLAST RESPONSE OF MILITARY STRUCTURES, EQUIPMENT, AND WEAPONS SYSTEMS.

RECORD BLAST AND SHOCK ENVIRONMENT

RECORD DAMAGE TO WEAPONS, SHELTERS, AND SYSTEMS

INCREASE WEAPONS EFFECTS DATA BASE

### 3. DNA RESPONSIBILITIES

FIELD COMMAND, DEFENSE NUCLEAR AGENCY (FCDNA), UNDER THE COMMAND OF BRIGIDER GENERAL THOMAS LACY, WAS RESPONSIBLE FOR (IN ADDITION TO THE PLANNING, COORDINATING, AND DIRECTING DICE THROW) PROVIDING THE ENERGY

SOURCE; T&F SUPPORT; FREE FIELD AIRBLAST ENVIRONMENT MEASUREMENTS; AIRBLAST AND AIRBLAST DAMAGE PREDICTIONS; METEOROLOGY; DETONATION DIAGNOSTIC MEASUREMENTS, INCLUDING TECHNICAL PHOTOGRAPHY; AERIAL AND DOCUMENTARY PHOTOGRAPHY; ENGINEERING AND CONSTRUCTION SUPPORT; TRUNK LINE SIGNAL AND T&F CABLING; FIRE AND SECURITY PROTECTION; AND PROGRAM DOCUMENTATION. TO BE RESPONSIVE IN THESE AREAS, A TEST GROUP STAFF WAS ESTABLISHED. THE STAFF, UNDER THE DIRECTION OF THE TEST GROUP DIRECTOR, WAS MADE-UP OF SIX COMMISSIONED OFFICERS, TWO NCO'S, AND FOUR CIVILIANS (SEE FIGURE 1).

#### 4. TEST SITE

THE DICE THROW EVENT WAS CONDUCTED ON THE WSMR, NM AT THE GIANT PATRIOT SITE, WHICH IS LOCATED 12 MILES SOUTHEAST OF THE STALLION RANGE CENTER IN THE NORTHERN PORTION OF THE RANGE, AND APPROXIMATELY 100 MILES NORTH OF THE MAIN POST AREA. THE SITE IS AT AN ELEVATION OF 4730 FEET ABOVE SEA LEVEL. THE NEAREST MOUNTAINS ARE EIGHT MILES TO THE EAST. THE WATERTABLE IS VARIABLE IN THE AREA, 80 FEET AND GREATER. BEDROCK AT THE SITE IS DEEPER THAN 200 FEET BELOW THE SURFACE. THE TWO MOST ABUNDANT VEGETATION ASSOCIATIONS ON THE TEST SITE ARE CATEGORIZED AS A GYPSUM GRASSLANDS NEAR A SAND GRASSLANDS AND DUNES ASSOCIATION. THE IMMEDIATE AREA OF THE TEST SITE IS LARGELY CHAMISA, GRASSES, AND ISOLATED YUCCA. (SEE FIGURE 2) OF HISTORICAL NOTE, THE SITE IS WITHIN VIEW OF TRINITY, THE LOCATION OF THE FIRST ATMOSPHERIC NUCLEAR DEVICE TEST, IN 1945.

THE TEST SITE, FIGURE 3, WAS LAID OUT WITH THREE INSTRUMENTATION TRAILER PARKS. TRAILER PARK 1 IS LOCATED ON THE 276° RADIAL EMANATING FROM GZ. TRAILER PARK 2 IS ON THE 186° RADIAL AND TRAILER PARK 3 IS ON

THE 076° RADIAL. EACH PARK IS 6000 FEET FROM GZ. THE ADMINISTRATION/TEST CONTROL AREA WAS LOCATED APPROXIMATELY 10,000 FEET SOUTHWEST FROM GZ, AT THE INTERSECTION OF WSMR ROUTES 7 AND 20. DENVER RESEARCH INSTITUTE (DRI) HAS FOUR TECHNICAL PHOTOGRAPHY CAMERA BUNKERS POSITIONED AROUND GZ TO RECORD THE ANFO DETONATION PHENOMENA. THE OLD GIANT PATRIOT TEST STAND IS LOCATED SOUTHEAST OF GZ. THE MAGNITUDE OF THE TEST PROGRAM DICTATED THE CONSTRUCTION OF SEVEN MILES OF ROADS TO SUPPORT THE FIELDING EFFORT. AS PREVIOUSLY INDICATED, STALLION RANGE CENTER IS 12 MILES NORTHWEST OF THE TEST SITE.

#### 5. TEST BED

FIGURE 4, IS THE ENGINEERING DRAWING OF THE TEST BED. GZ IS IN THE CENTER OF THE DRAWING, AND THE THREE FREE-FIELD AIRBLAST GAUGE RADIALS EMANATE FROM GZ. THE DICE THROW EXPERIMENTS ARE GENERALLY GROUPED AROUND THESE THREE RADIALS; AND MOST OF THE TARGET RESPONSE EXPERIMENTS ARE IN THE PREDICTED OVERPRESSURE RANGE OF 100 PSI TO 5 PSI. THE MOST CLOSE-IN EXPERIMENT FIELDIED WAS BY THE BOEING AEROSPACE CORP, AT 600 PSI, (APPROXIMATELY 200 FEET FROM GZ). THIRTY-FIVE COMMANDS, AGENCIES, DOD CONTRACTORS, AND FOREIGN GOVERNMENTS PARTICIPATED IN DICE THROW. THIRTY-ONE DIFFERENT EXPERIMENTAL PROGRAMS WERE FIELDIED AND TWELVE SCIENTIFIC SUPPORT FUNCTIONS PERFORMED. THE US MILITARY SERVICES FIELDIED 15 EXPERIMENTAL PROGRAMS, DOD CONTRACTORS FIELDIED 10 EXPERIMENTAL PROGRAMS, AND THE PARTICIPATING FOREIGN COUNTRIES FIELDIED 6 DISTINCT PROGRAMS. THE FOREIGN COUNTRIES ARE THE UNITED KINGDOM, CANADA, NORWAY, SWEDEN, FEDERAL REPUBLIC OF GERMANY, AND THE NETHERLANDS.

FIGURES 5, 6, AND 7 ARE AERIAL PICTURES OF THE TEST BED. THESE PICTURES WERE PROVIDED BY THE WILLIAMSON AIRCRAFT COMPANY, UNDER CONTRACT TO DNA. FIGURE 5 IS A VIEW LOOKING WEST WITH NORTH TO THE RIGHT OF THE



PICTURE. GAUGE LINE 1 IS AT TOP AND GAUGE LINES 2 AND 3 TO THE LEFT AND BOTTOM, RESPECTIVELY. APPROXIMATELY 1500 CHANNELS OF DATA WERE TAKEN ON DICE THROW. DATA GATHERED INCLUDE AIRBLAST MEASUREMENTS, STRESS AND STRAIN MEASUREMENTS, ACCELEROMETER MEASUREMENTS, AND PHOTOGRAPHIC COVERAGE DURING THE AIRBLAST PHASE. WITH THE EXCEPTION OF TRAILER PARK 1, THE INSTRUMENTATION TRAILER PARKS ARE NOT VISIBLE IN FIGURE 5. AS PREVIOUSLY STATED, THE PARKS ARE 6000 FEET FROM GZ.

FIGURE 6 IS ANOTHER VIEW OF THE TEST BED. THE TOP OF THE PICTURE IS NORTHWEST. THE THREE GAUGE LINES AND THE SIMULATED STRATEGIC AIR COMMAND OR (SAC) RUNWAY CAN BE SEEN VERY CLEARLY. THE SIMULATED SAC RUNWAY IS 15° OFF OF GRID NORTH. SEVERAL OF THE LARGER EXPERIMENTS POSITIONED AROUND GZ, COUNTERCLOCKWISE FROM THE TOP OF THE PICTURE ARE: THE FRG STRUCTURES FIELDIED BY THE USA ENGINEER WATERWAYS EXPERIMENT STATION; THE NAVY AIRCRAFT EXPERIMENT FIELDIED BY THE NAVAL WEAPONS EVALUATION FACILITY; AIRCRAFT SHELTERS FIELDIED BY THE AIR FORCE WEAPONS LABORATORY; EXPEDIENT SHELTERS FIELDIED BY THE OAK RIDGE NATIONAL LABORATORY; COMMAND CONTROL COMMUNICATIONS SYSTEMS FIELDIED BY THE BALLISTIC RESEARCH LABORATORY AND US ARMY ELECTRONICS COMMAND; SHIP MASTS, ANTENNAS AND DRAG CYLINDERS FIELDIED BY THE DEFENCE RESEARCH ESTABLISHMENT SUFFIELD, CANADA; SHIP MASTS, ANTENNA, AND RADOMES FIELDIED BY THE ADMIRALTY SURFACE WEAPONS ESTABLISHMENT, UNITED KINGDOM; US ARMY WHEELED VEHICLES FIELDIED BY THE BALLISTIC RESEARCH LABORATORY; US ARMY WEAPONS SYSTEMS FIELDIED BY THE RODMAN LABORATORY AND WHITE SANDS MISSILE RANGE; AND EJECTA COLLECTORS, DISPLACEMENT PINS, AND ARTIFICAL MISSILES FIELDIED BY THE AFWL AND THE CIVIL ENGINEERING RESEARCH FACILITY (CERF), UNIVERSITY OF NEW MEXICO.

## 6. INSTRUMENTATION/TIMING & FIRING/TECHNICAL PHOTOGRAPHY

RECORDING INSTRUMENTATION IS CONTAINED IN TRAILER VANS. THE MAIN SOURCE OF ELECTRICAL POWER TO THE TEST BED WAS PROVIDED BY THE SOCORRO POWER AND ELECTRIC CO-OP, INC. THIS COMMERCIAL POWER WAS USED EXCLUSIVELY IN TRAILER PARKS 1 AND 2, AND THE ADMINISTRATION AREA. DIESEL GENERATORS PROVIDED POWER TO TRAILER PARK 3. THE INSTRUMENTATION TRAILERS REQUIRED BOTH UTILITY AND INSTRUMENTATION POWER. THIS WAS ACCOMPLISHED BY USING MOTOR-GENERATOR SETS (FIGURE 7) RUN FROM COMMERCIAL OR DIESEL GENERATOR SYSTEMS. THE MOTOR-GENERATOR SETS PROVIDE THE ISOLATION NECESSARY BETWEEN THE TWO TYPES OF DEMAND. TWENTY-ONE DIFFERENT TYPES OF CABLE WERE USED FOR ELECTRICAL POWER AND GAGE SIGNAL RECORDING. ALMOST 1.5 MILLION FEET OF SIGNAL CABLE AND 33,450 FEET OF POWER CABLE WERE LAID. MR. BOB WARD, EG&G LAS VEGAS, PROVIDED THE CABLE COORDINATION BETWEEN DNA AND THE EXPERIMENTERS.

GAGES WERE INSTALLED BY THE BALLISTIC RESEARCH LABORATORY TO RECORD THE AIRBLAST PARAMETERS THROUGHOUT THE PRESSURE RANGE OF 5000 PSI TO 0.5 PSI. (FIGURES 8 AND 9). INCIDENT AND TOTAL HEAD OVERPRESSURES WERE RECORDED, BOTH ALONG THE GROUND SURFACE AND AT VARIOUS HEIGHTS ABOVE THE GROUND. A TOTAL OF 83 FREE-FIELD AIRBLAST MEASUREMENTS WERE RECORDED. THE THREE MAIN GAGE LINES REQUIRED 69 OF THESE MEASUREMENTS. MR. GEORGE TEEL WAS THE PROJECT OFFICER.

FIGURE 10 IS AN INTERIOR SCENE OF THE DEFENCE RESEARCH ESTABLISHMENT SUFFIELD, (DRES), CANADA, TIMING AND FIRING VAN. THE TIMING AND MONITORING SYSTEMS WERE PROVIDED BY DRES AND INSTALLED AND OPERATED UNDER THE SUPERVISION OF MR. CHARLES SUTHERLAND OF CANADA. APPROXIMATELY 30 DIFFERENT TIMING SIGNALS WERE DISTRIBUTED TO THE VARIOUS EXPERIMENTERS. THE FIRING SYSTEM USED WAS BUILT AND INSTALLED BY THE LAWRENCE LIVERMORE

LABORATORY (LLL) UNDER THE DIRECTION OF MR. BUD HAYES. LLL WAS RESPONSIBLE FOR (1) MONITORING THE SIMULTANEITY OF THE SEVEN BOOSTER DETONATIONS IN THE EXPLOSIVE STACK BY DETERMINING THE SHOCK ARRIVAL TIME AT THE BOOSTER - ANFO INTERFACE; (2) OBTAINING A DETONATION VELOCITY FOR THE ANFO; (3) MEASURING DETONATION WAVE TRANSIT TIME; AND (4) PROVIDING PRESSURE PROFILES WITHIN THE EXPLOSIVE STACK.

DENVER RESEARCH INSTITUTE (DRI) UNDER THE DIRECTION OF MR. JOHN WISOTSKI WAS RESPONSIBLE FOR THE TECHNICAL PHOTOGRAPHY OF THE DETONATION PHENOMENA. A TOTAL OF 28 CAMERAS AND 4 PHOTOMETRIC DEVICES WERE EMPLOYED AT FOUR LOCATIONS, APPROXIMATELY 4500 FEET FROM GZ. DRI ALSO PROVIDED TECHNICAL PHOTOGRAPHY SUPPORT TO EIGHT OTHER TARGET RESPONSE EXPERIMENTS, UTILIZING SEVENTY-EIGHT CAMERAS (SEE FIGURES 11 AND 12). WHITE SANDS MISSILE RANGE (DYNAELECTRON CORP) PROVIDED ASSISTANCE TO DRI IN THE FORM OF CAMERAS AND TECHNICIANS.

THE DICE THROW ADMIN AREA, FIGURE 13, PROVIDED ADMINISTRATIVE SPACE FOR THE EXPERIMENTER PROJECT OFFICERS AND TEST CONTROL. THE TYPES AND QUANTITIES OF COMMUNICATIONS EQUIPMENT USED ON DICE THROW WAS EXTENSIVE AND VARIED. THEY INCLUDED: TELEPHONES, PORTABLE MOBILE RADIOS AND BASE STATIONS, AND HARDWIRE INTERCOM UNITS. MOST OF THE TELEPHONES WERE LOCATED IN THE ADMIN AREA OFFICE AND SHOP TRAILERS. THE PORTABLE RADIOS WERE USED FOR DIRECT COMMUNICATION BETWEEN TEST CONTROL AND PERSONNEL IN THE TEST AREA. THE INTERCOM UNITS WERE PLACED IN THE OFFICE TRAILERS, INSTRUMENTATION VANS AND SHOP TRAILERS.

#### 7. CONSTRUCTION

SEVERAL OF THE MAJOR MILESTONE DATES ON DICE THROW WERE: THE PROJECT OFFICER MEETING HELD AT FCDNA, 20 THROUGH 22 JANUARY 1976; SITE

PREPARATION BEGINNING IN MARCH 1976, WITH THE FIRST EXPERIMENTER ARRIVING ON SITE IN MAY (MOST OF THE REMAINING EXPERIMENTERS WERE ON-BOARD BY JULY); THE FIRST FULL POWER FULL FREQUENCY (FPFF) WAS HELD ON THE 17TH OF SEPTEMBER; THE FINAL FPFF WAS ON 5 OCTOBER; THE AMMONIUM NITRATE AND FUEL OIL HIGH EXPLOSIVE OR BLASTING AGENT STACKING OPERATION BEGAN ON THE 23RD OF SEPTEMBER AND CONTINUED THROUGH 4 OCTOBER. THE DICE THROW EVENT WAS SUCCESSFULLY EXECUTED BY THE DEFENSE NUCLEAR AGENCY, FIELD COMMAND, AT 0800 HOURS, 6 OCTOBER 1976. FIGURE 14 IS THE AS BUILT FIELDING SCHEDULE.

WSMR FACILITIES ENGINEER PERFORMED MOST OF THE CONSTRUCTION IN SUPPORT OF DICE THROW. FIGURE 15 IS THE EXCAVATION FOR THE CONSTRUCTION OF A FEDERAL REPUBLIC OF GERMANY (FRG) DESIGN OF A SUBSURFACE SHELTER. THERE ARE FOUR SUBSURFACE AND TWO SURFACE SHELTER OF THIS BASIC DESIGN. THE FACILITIES ENGINEER, UNDER THE SUPERVISION OF MR. DALE GREEN, PERFORMED THE CONSTRUCTION. ALL TEST STRUCTURES OF GERMAN DESIGN (TOTALING TWELVE) REQUIRED A TOTAL OF 450 CUBIC YARDS OF CONCRETE (SEE FIGURE 16). CONCRETE WAS PROVIDED BY THE USE OF A CONCRETE BATCH PLANT SET UP NEAR THE TEST BED. THE FIELDING OF THE FRG EXPERIMENTAL TEST PROGRAM WAS BY THE US ARMY ENGINEER WATERWAYS EXPERIMENT STATION (WES). THE PROJECT OFFICER WAS DR. JIM BALSARA. FIELD ASSISTANCE WAS PROVIDED BY MR. JIMMY WATT AND MR. REED CUMMINGS.

THE UNITED KINGDOM (UK) FOUNDATION FOR A SLATTED ANTENNA REQUIRED 100 CUBIC YARDS OF CONCRETE (SEE FIGURE 17 AND 18). TOTAL CONCRETE PLACED IN DICE THROW WAS 1,300 CUBIC YARDS.

THE AIR FORCE WEAPONS LABORATORY (AFWL) CONTRACTED FOR THE CONSTRUCTION OF FOUR SCALED AIRCRAFT SHELTERS. FIGURE 19 IS A PICTURE OF

ONE OF THE SHELTERS, A SCALED, HARDENED UNDERGROUND SHELTER BEING CONSTRUCTED BY A CIVILIAN CONTRACTOR. THERE WAS ONE OTHER CIVILIAN GENERAL-CONTRACTOR WORKING ON THE TEST BED. THAT FIRM WAS UNDER CONTRACT TO FCDNA AND WAS INVOLVED IN THE CONSTRUCTION OF THREE IDENTICAL STRUCTURES, EACH SITED AT A DIFFERENT PREDICTED OVERPRESSURE LEVEL. THE EXPERIMENT WAS TO INVESTIGATE THE DYNAMIC RESPONSE AND COLLAPSE MODES FOR TWO TYPES OF GERMAN RESIDENTIAL CONSTRUCTION. THE EXPERIMENT WAS FIELDIED BY STANFORD RESEARCH INSTITUTE (SRI) AND THE PROJECT OFFICER WAS MR. CARL WIEHLE. NOTE FIGURES 20 AND 21.

#### 8. EXPLOSIVE CHARGE/DETONATION

THE EXPLOSIVE CHARGE CONFIGURATION WAS DESIGNED TO SIMULATE A 1 - KILOTON NUCLEAR WEAPON. THE CHARGE WAS CONSTRUCTED OF 50 POUND BAGS OF AMMONIUM NITRATE AND FUEL OIL MIXTURE, KNOWN AS ANFO. 622 TONS OF BAGGED AND BULK ANFO, PRODUCED A STACK APPROXIMATELY 30 FEET IN DIAMETER AND 37 FEET HIGH. (SEE FIGURE 22.) FIGURE 23, A CUTAWAY VIEW OF THE ANFO CHARGE, DEPICTS THE SEVEN OCTAL DETONATION BOOSTERS. THE EXPLOSIVE CHARGE DESIGN AND ACTUAL STACKING OPERATIONS WERE PERFORMED BY THE CIVIL ENGINEERING RESEARCH FACILITY, UNIVERSITY OF NEW MEXICO. FIELD WORK WAS UNDER THE SUPERVISION OF MR. KEN BELL.

FIGURE 24 IS A PARTIAL VIEW OF THE PLYWOOD BASE AND CIRCULAR FORMS THAT THE ANFO CHARGE WAS STACKED IN. LOOSE ANFO IS USED TO FILL THE VOIDS BETWEEN BAGS IN EACH LAYER OF THE EXPLOSIVE CHARGE (SEE FIGURE 25). THE QUANTITY USED IS BASED ON THE STACK DESIGN. MR. MIKE SWISDAK FROM THE NAVAL SURFACE WEAPONS CENTER WILL PRESENT A PAPER ON THE STACK DESIGN AND DESIGN, FABRICATION, AND INSTALLATION OF THE CHARGE DETONATION SYSTEM.

FIGURE 26 SHOWS THE INSTALLATION OF ONE OF THE SEVEN OCTAL BOOSTERS DURING THE ANFO STACKING OPERATION. THE OCTAL BOOSTER WAS SECURED INTO PLACE AND LOOSE ANFO PRILL IS LATER POURED AROUND IT.

THE 50 POUND BAGS OF ANFO ARE DELIVERED FROM THE SUPPLIER IN TRAILER VANS AND THEN MOVED TO THE STACK BY A CONVEYOR SYSTEM (SEE FIGURE 27). THE CHARGE CONSTRUCTION SCHEDULE DID NOT CALL FOR A CONTINUOUS DAY AND NIGHT STACKING OPERATION; HOWEVER, DUE TO DELAYS ENCOUNTERED, STACKING WAS PERFORMED AT NIGHT. THE STRUCTURE OR SHELTER COVERING THE EXPLOSIVE CHARGE WAS ERECTED PRIMARILY TO PROVIDE PROTECTION FROM THE ELEMENTS. IT WAS DISMANTLED PRIOR TO EXECUTING THE EVENT. ALSO DISMANTLED WAS THE FORM WORK SURROUNDING THE STACK. THIS CIRCULAR FORM OR CONTAINMENT SYSTEM PROVED VERY BENEFICIAL TO THE OPERATION. THE QUALITY CONTROL ON THE STACK CONFIGURATION WAS MAINTAINED BY ENABLING THE STACKING CREW TO BETTER CONTROL THE CHARGE DIAMETER AND KEEPING THE STACK PLUMB. THE FORM SYSTEM ALSO AFFORDED GREATER SAFETY TO THE CREW WORKING ON THE STACK (SEE FIGURE 28). THE EXPLOSIVE CHARGE WAS COMPLETED ON TIME AND MADE READY FOR DETONATION ON SHOT MORNING (SEE FIGURE 29).

FIGURE 30 IS A VIEW OF THE TEST BED THE DAY BEFORE DICE THROW EXECUTION. THIS SCENE IS LOOKING SOUTHEAST. THE SIMULATED SAC RUNWAY IS AT THE BOTTOM LEFT OF THE PICTURE, GAUGE LINE 1 IS OFF TO THE RIGHT, GAUGE LINE 2 AT THE TOP, AND GAUGE LINE 3 OFF TO THE LEFT. DICE THROW WAS SUCCESSFULLY DETONATED AT 0800 HOURS, WEDNESDAY, 6 OCTOBER 1976. (SEE FIGURE 31).

THE DUST CLOUD DEPICTED IN FIGURE 32 WAS TAKEN APPROXIMATELY 45 SECONDS AFTER DETONATION. A TETHERED HELICOPTER, WHICH REMAINED AIRBORNE, CAN BE SEEN AT THE LOWER LEFT, NEAR THE CLOUD STEM. THE CENTRAL PORTION OF THE RESULTANT CRATER WAS A DEEP, STEEPLY WALLED CAVITY, WITH AN

AVERAGE APPARENT DIAMETER OF 145 FEET, AND A MAXIMUM APPARENT DEPTH OF 25 FEET (SEE FIGURE 33). FIGURE 34 IS AN AERIAL VIEW OF THE TEST BED AFTER DETONATION TAKEN FROM THE SAME ATTITUDE AS FIGURE 30, LOOKING SOUTHEAST. GAUGE LINES 1, 2, AND 3 ARE TO THE RIGHT, TOP, AND LEFT RESPECTIVELY.

#### 9. TEST SITE CLEANUP

FIGURE 35 IS A VIEW OF GZ LOOKING NORTH FROM THE OBSERVATION MOUND, SITUATED ON THE TEST BED, AFTER TEST SITE RESTORATION. AS CAN BE SEEN THE CRATER HAS BEEN FILLED. WSMR AGREED TO ALLOW DNA TO LEAVE IN PLACE ANY EXPERIMENTER STRUCTURE OR EQUIPMENT WHICH REMAINED STRUCTURALLY SOUND AND NOT A SAFETY HAZARD AFTER THE TEST. AIRCRAFT SHELTERS REMAIN AND CAN BE SEEN TO THE FAR LEFT OF THE PICTURE. OTHER ITEMS LEFT ON THE TEST BED ARE CONCRETE PERSONNEL SHELTERS, ANTENNAS, MASTS, AND REMAINS FROM THE RESIDENTIAL WALL EXPERIMENT.

DICE THROW WAS CONSIDERED A SUCCESS. ALL TEST OBJECTIVES WERE MET, A SUBSTANTIALLY CLEAN AIRBLAST ENVIRONMENT WAS PROVIDED, AND THERE WAS 95% DATA RECOVERY. JUST HOW SUCCESSFUL WILL BECOME MORE APPARENT AS EXPERIMENT RESULTS ARE PRESENTED DURING THE NEXT THREE DAYS. THIS CONCLUDES MY PRESENTATION. THANK YOU.

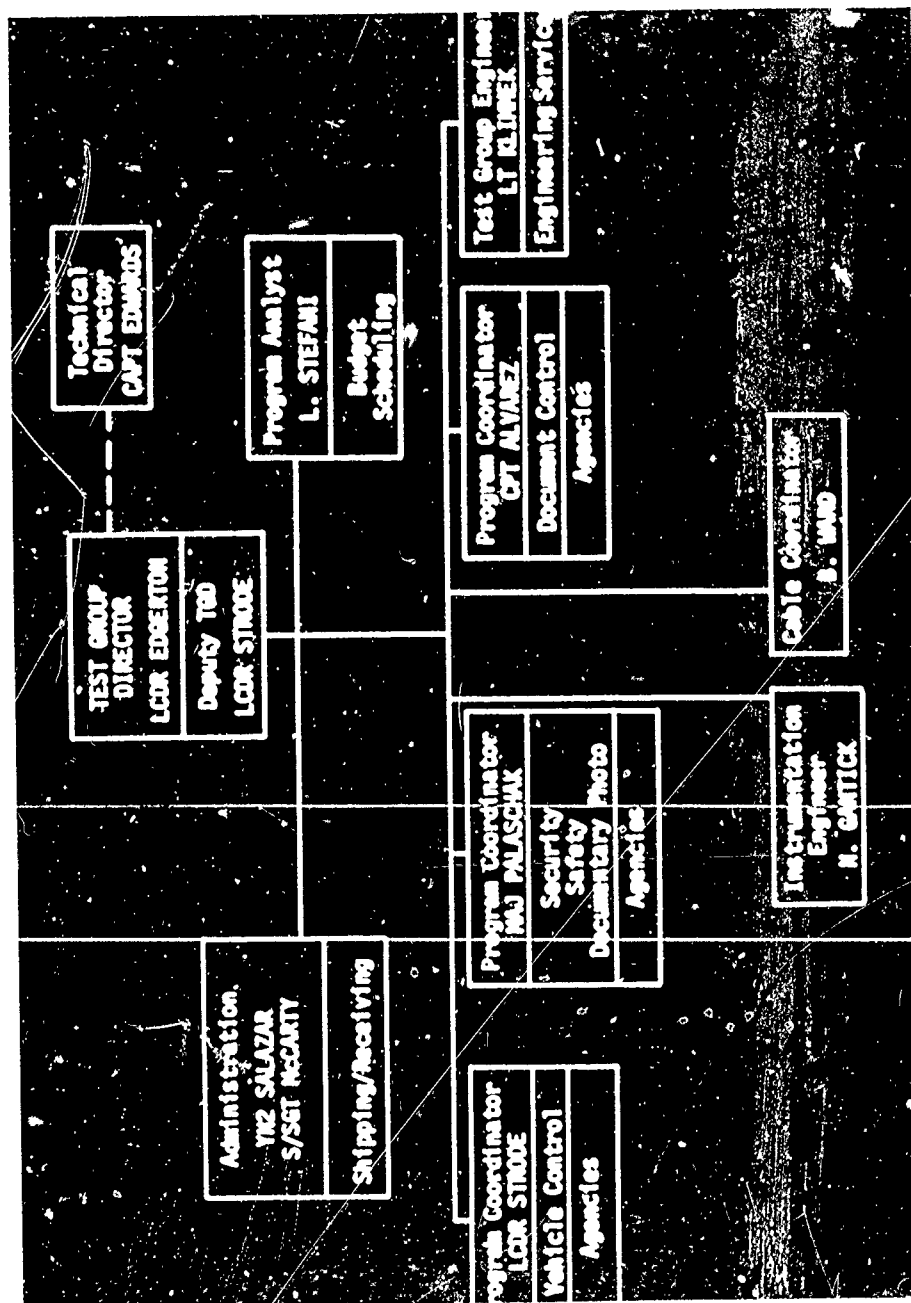


Figure 1. Test Group Staff Organizational Chart.



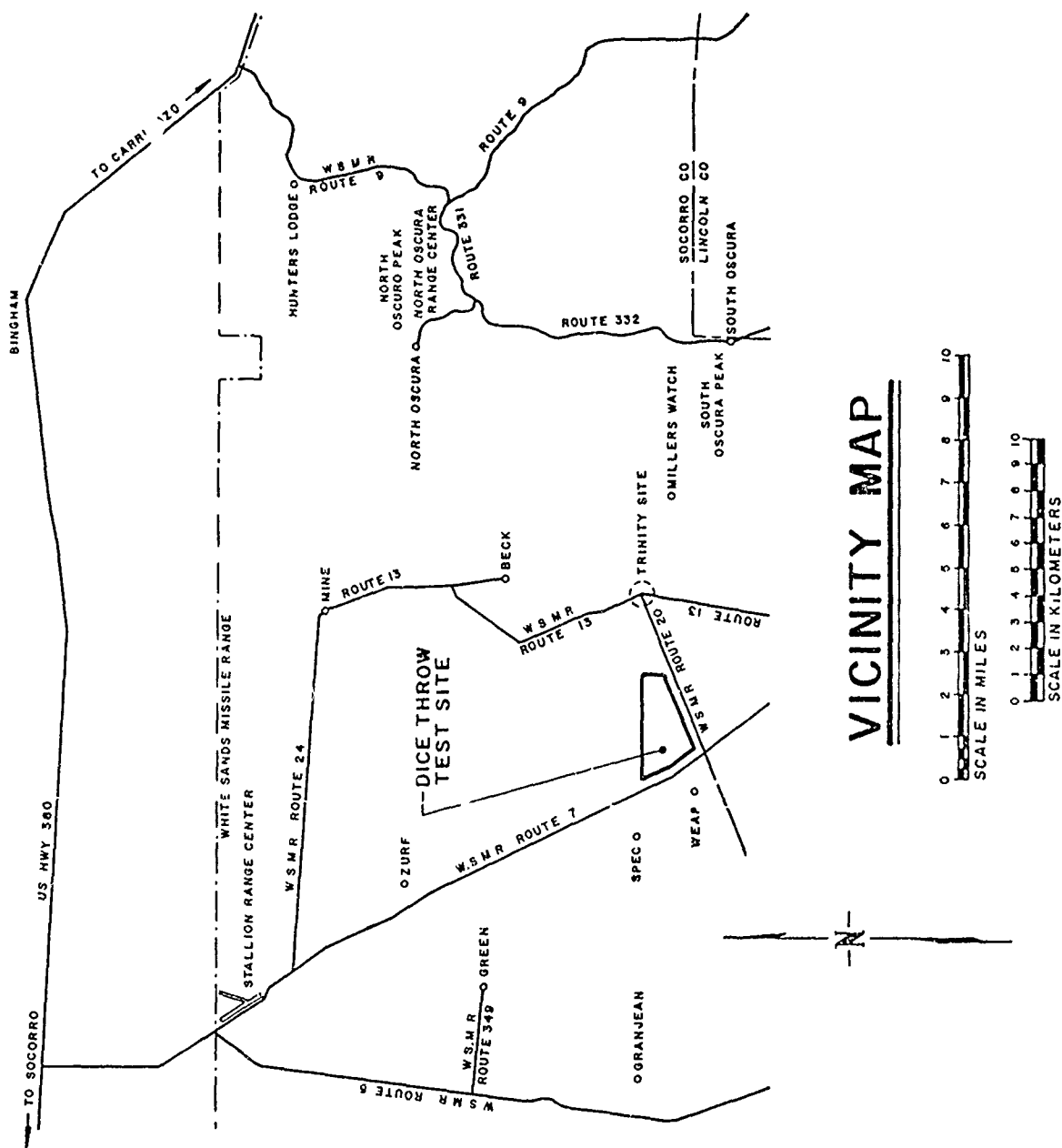


Figure 2. Site Location WSMR, NM.

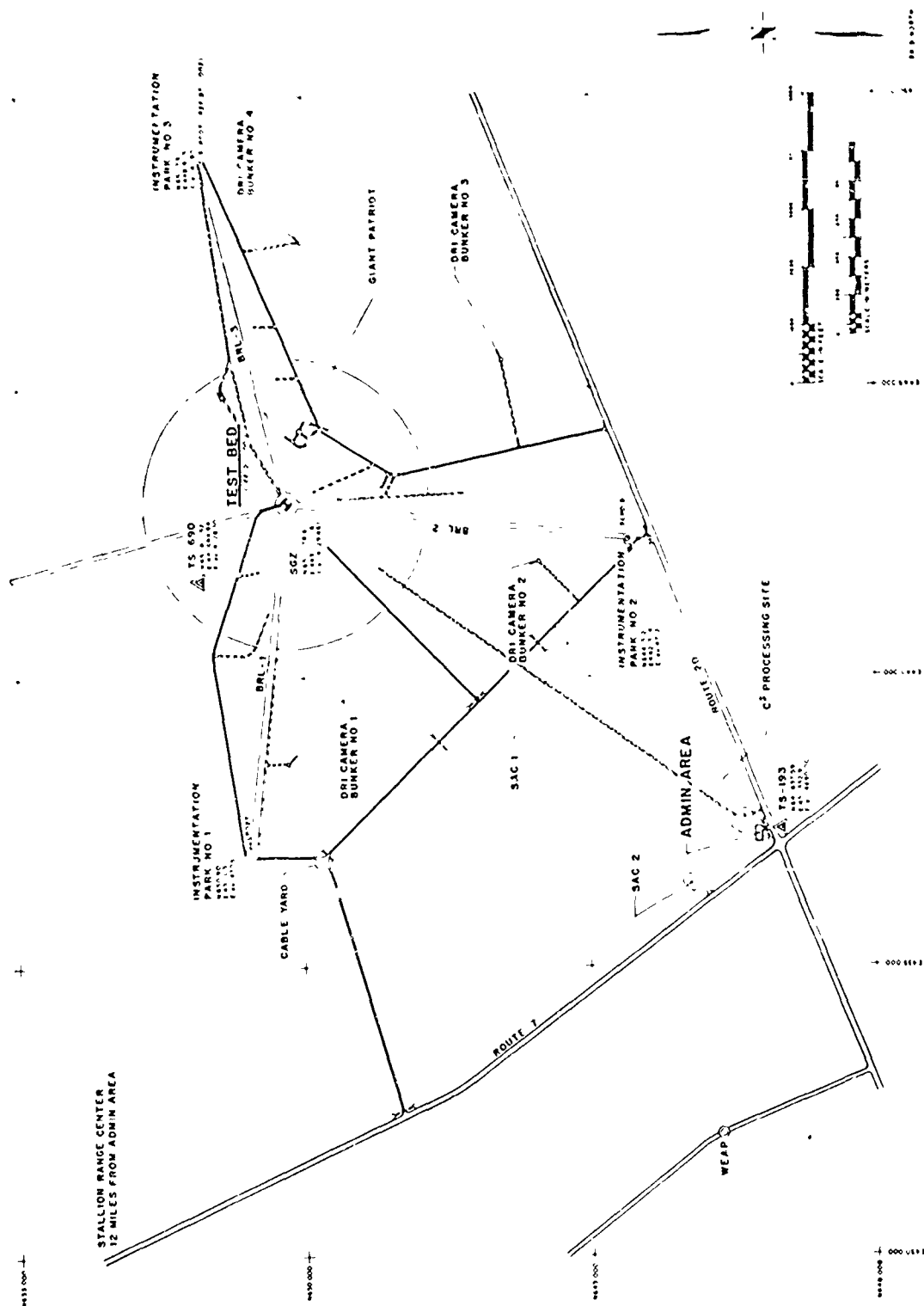


Figure 3, Test Site Layout (Engineering Drawing)



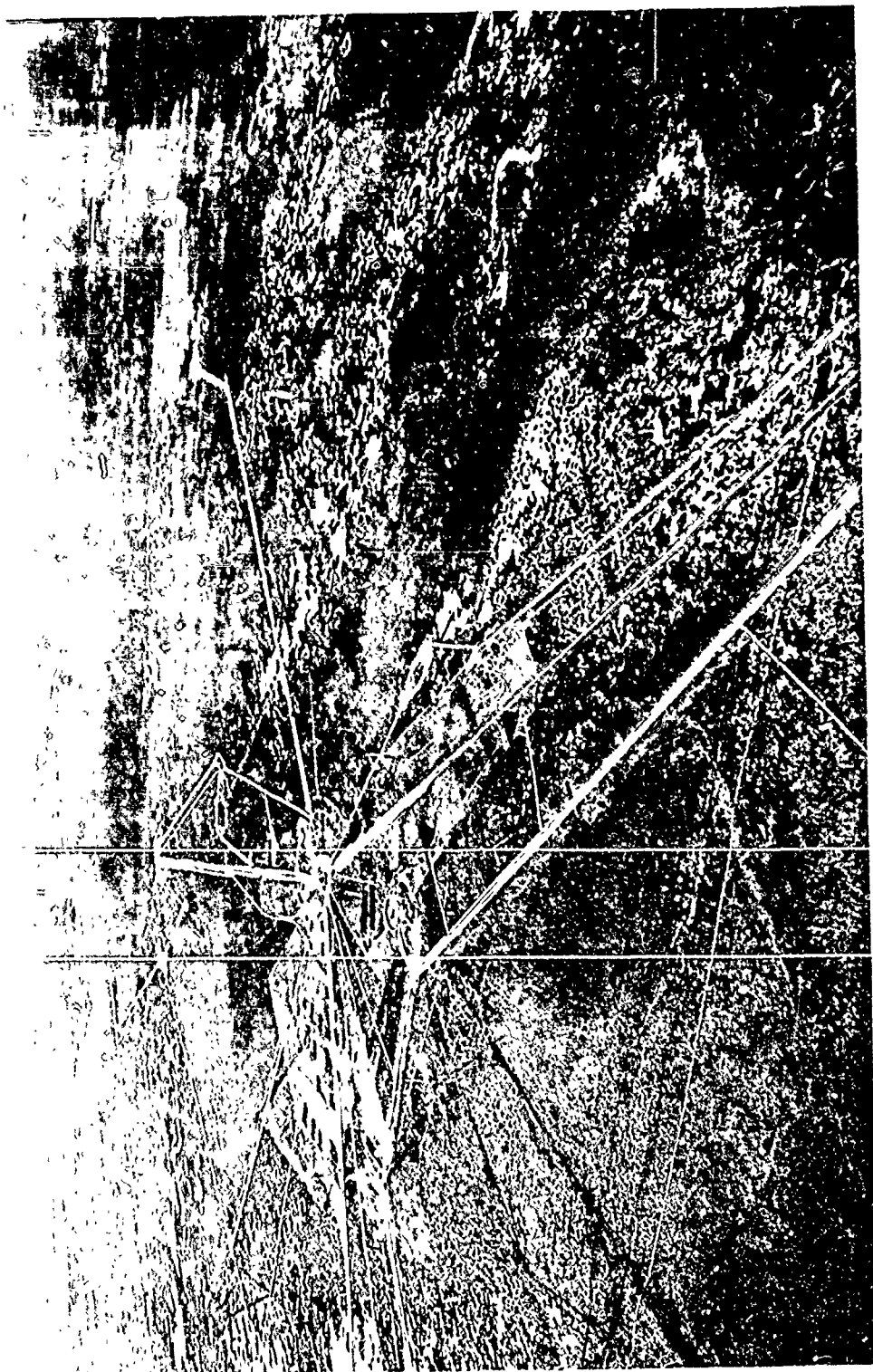


Figure 5. Test Bed (Aerial View).

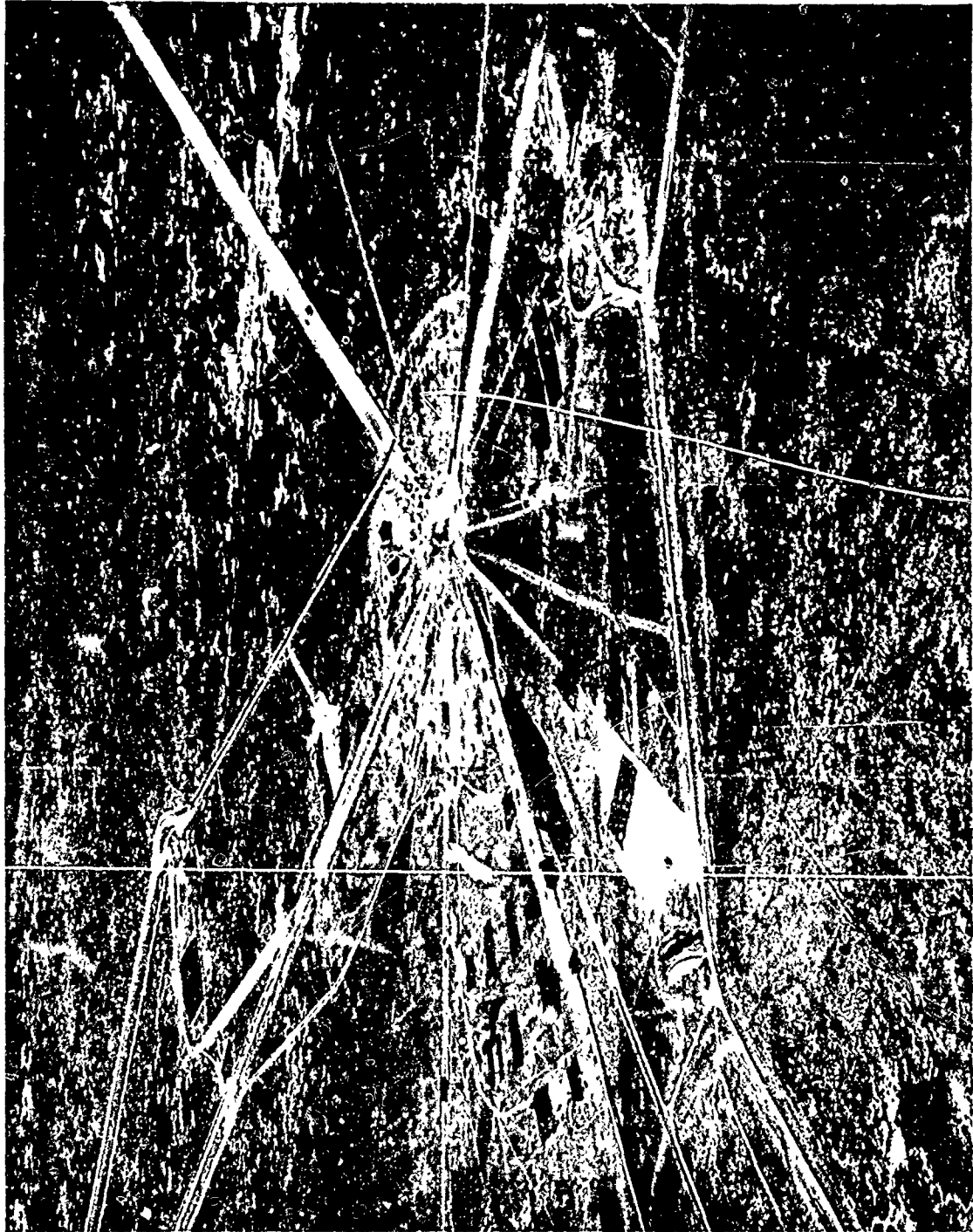


Figure 6. Test Bed (Aerial View).

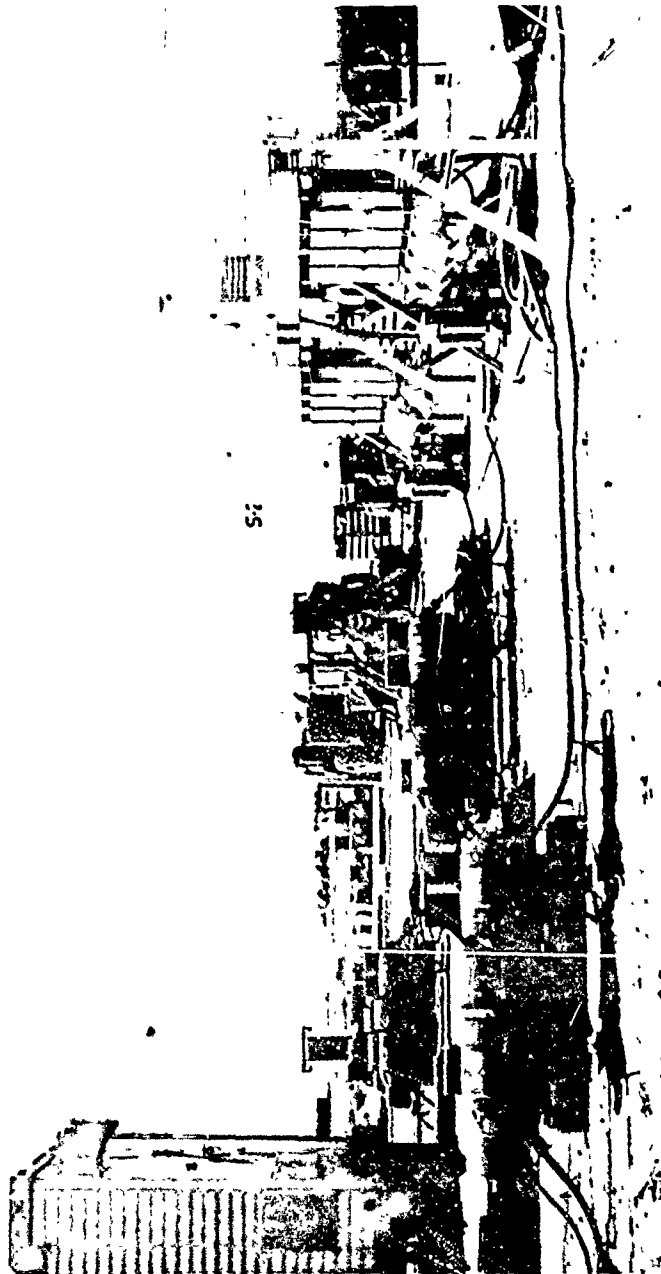


Figure 7. Instrumentation Trailer Park.

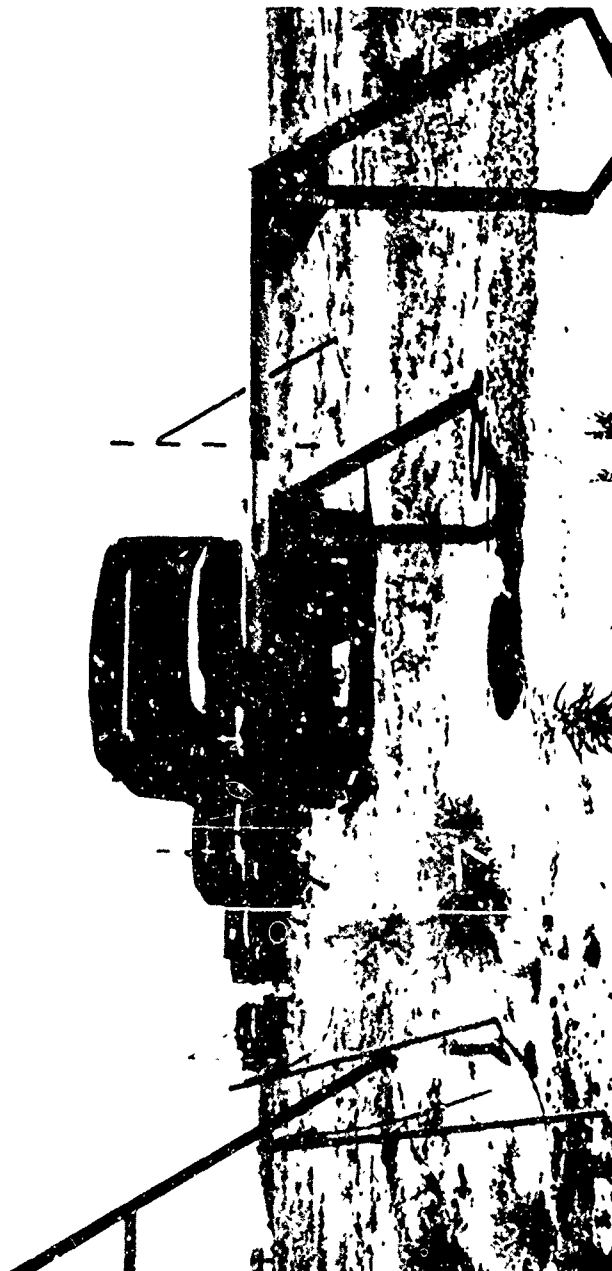


Figure 8. Airblast Gages and Mounts.



Figure 9. Airblast Gage and Mount.



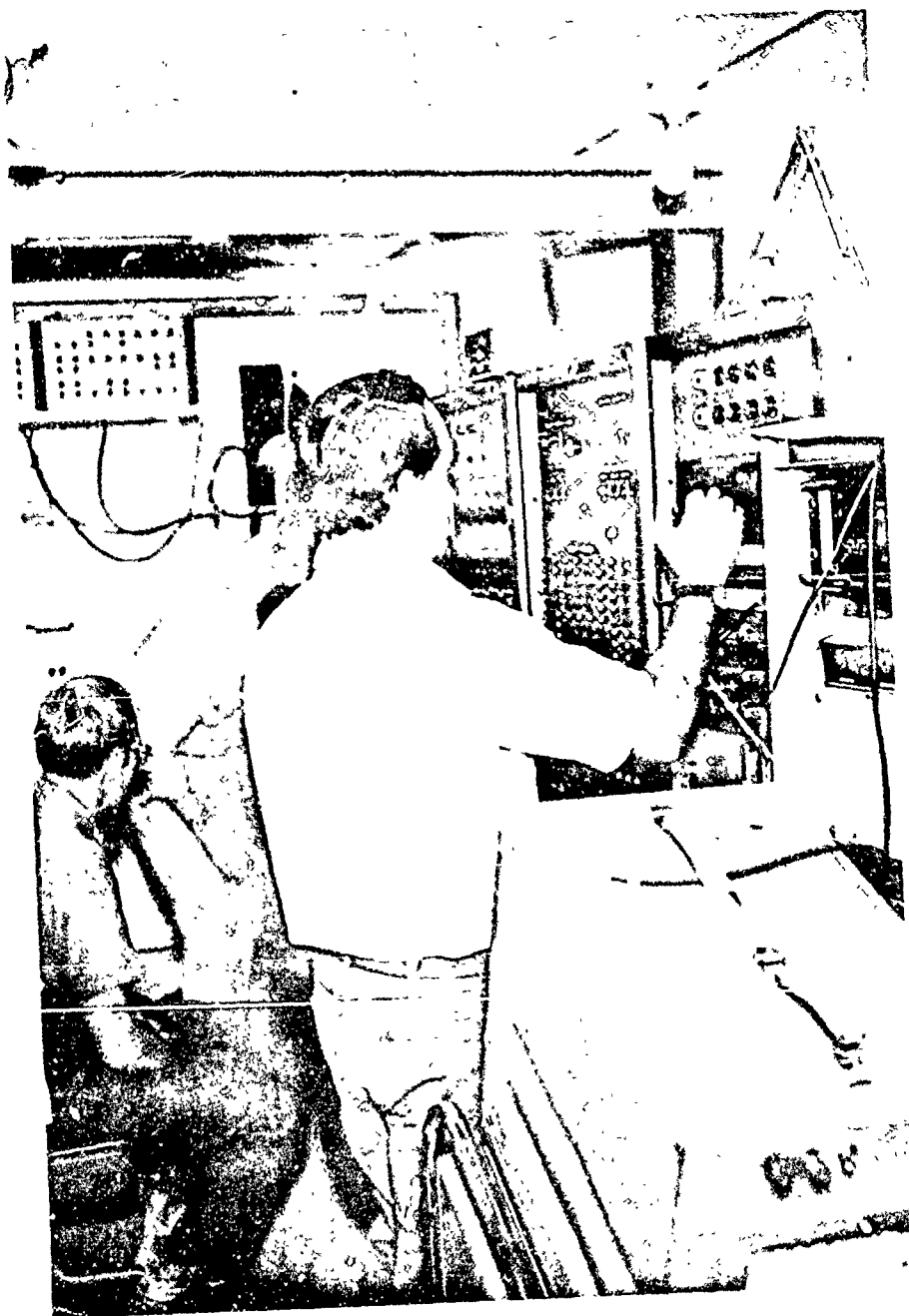
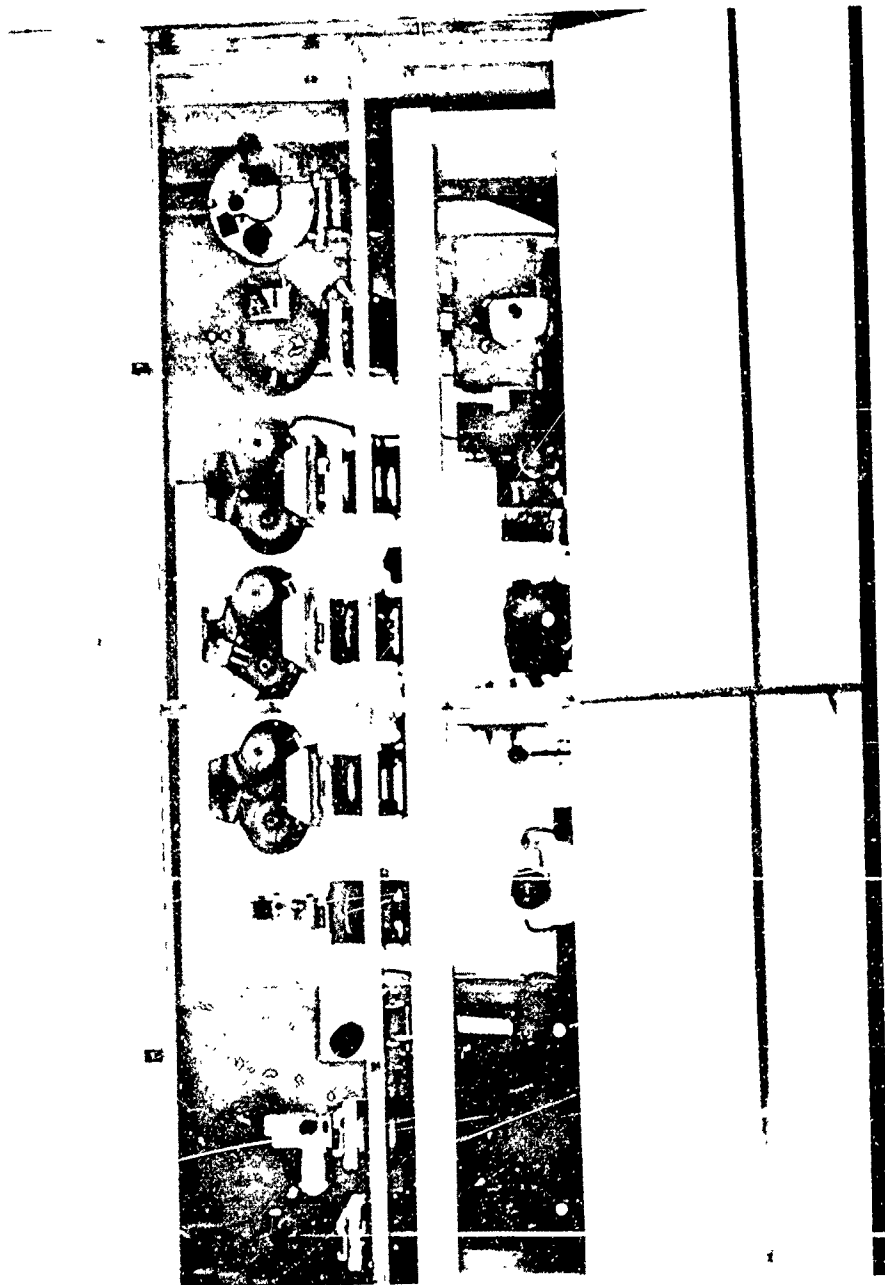


Figure 10. T&F Van (Interior).



F-gure 11. DRI Camera Station No. 2.

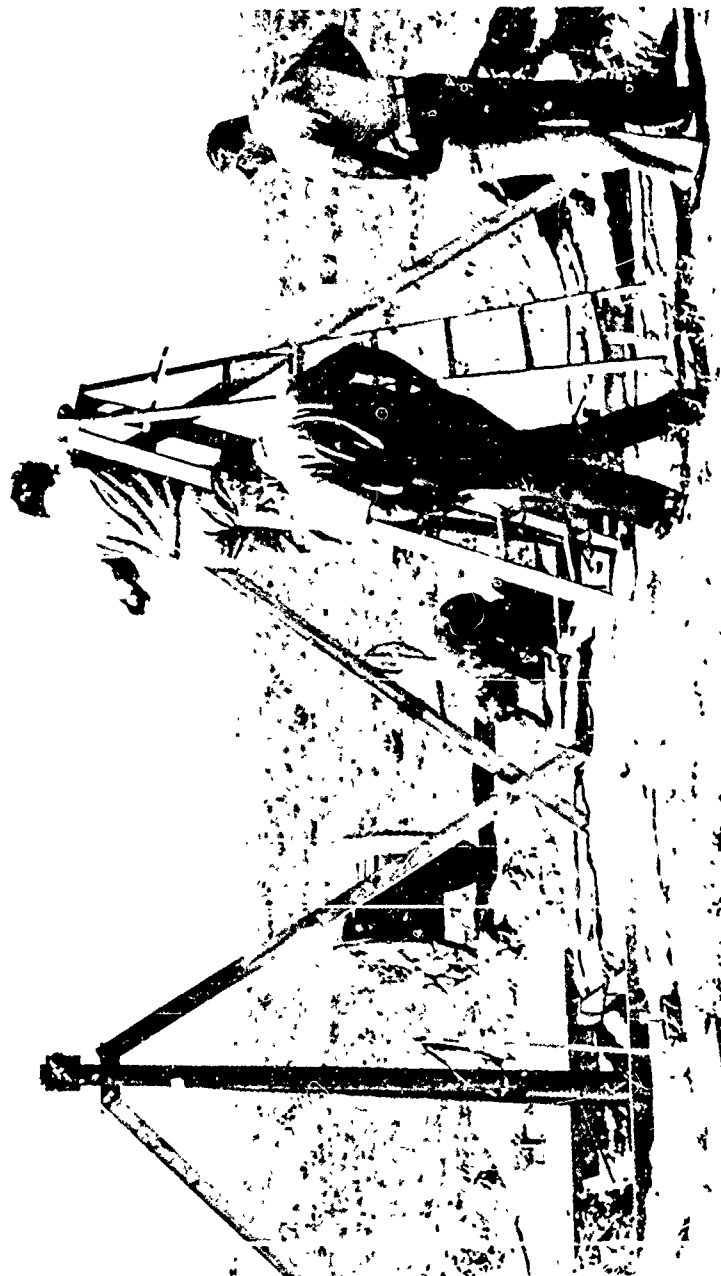


Figure 12. Aligning Cameras on Mounts.

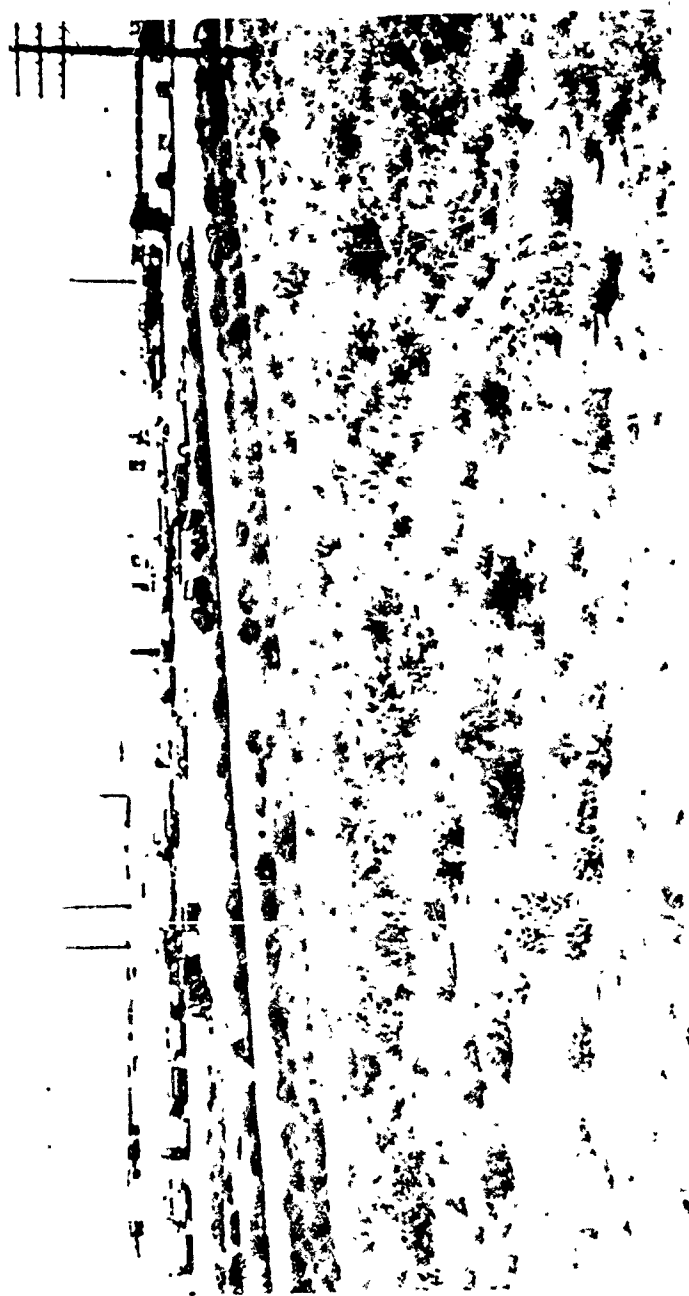


Figure 13. Administration Trailer Park/Test Control.

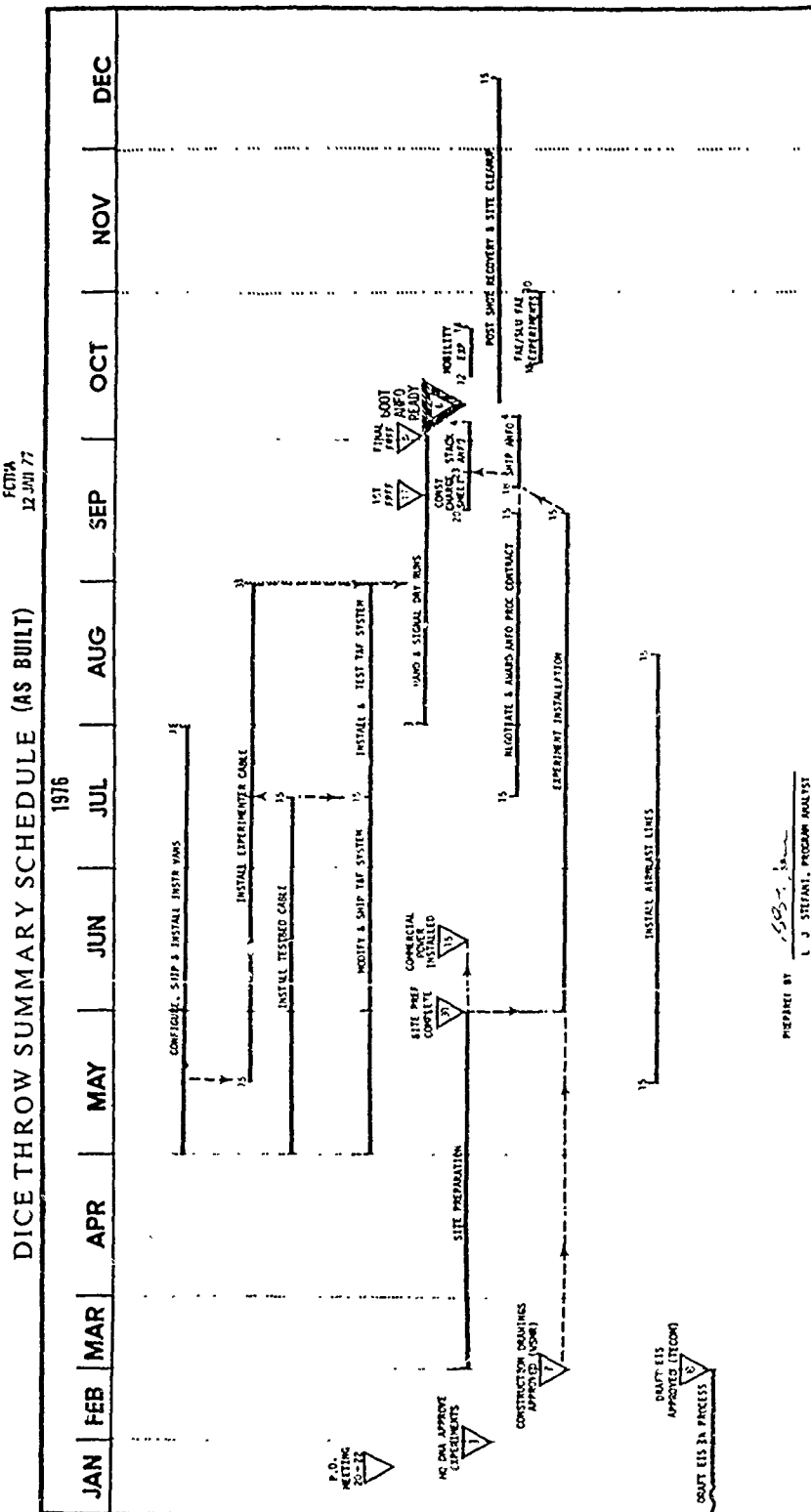


Figure 14. Construction Schedule.

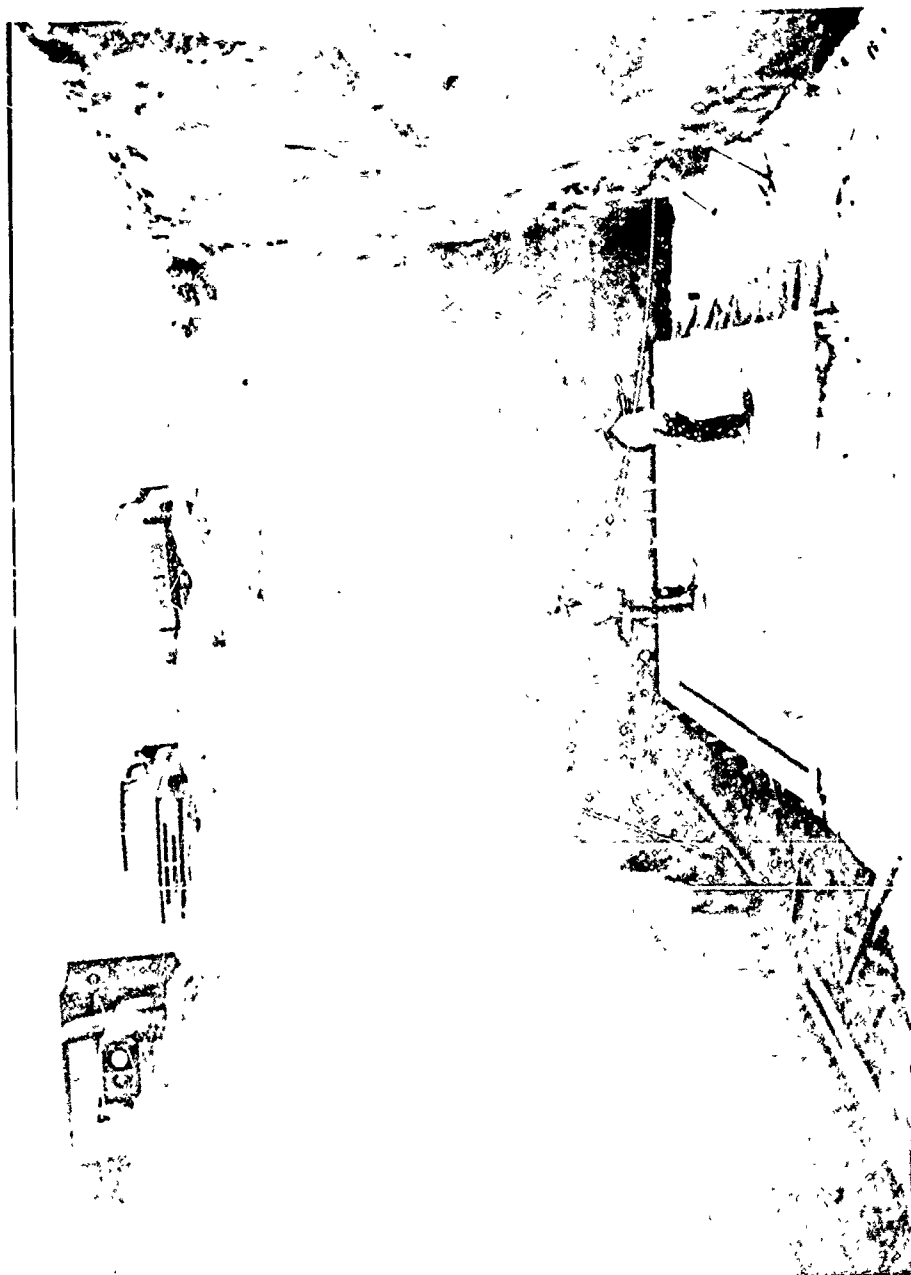


Figure 15. FRG/WES Structure (Excavated).

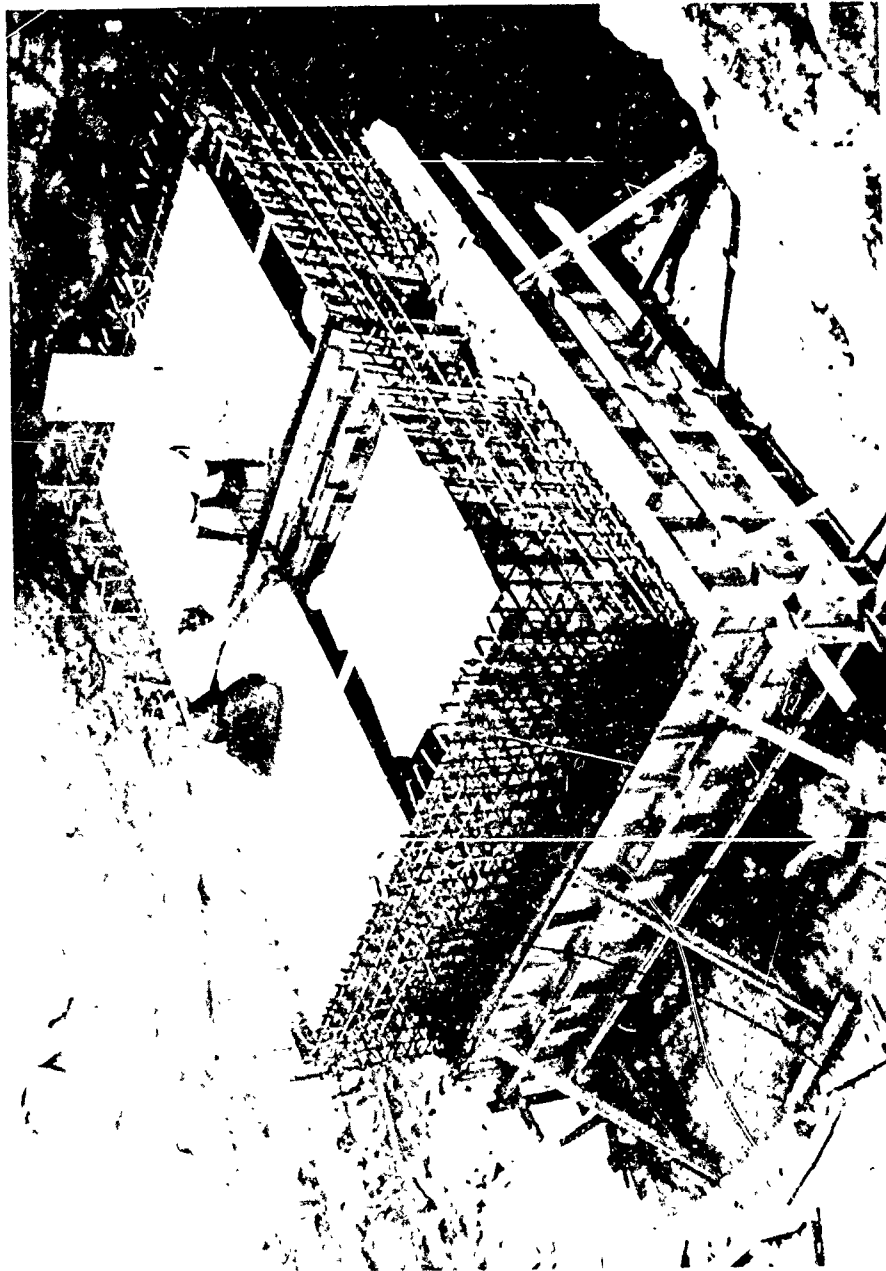


Figure 16. FRG/WES Structure (Forming).

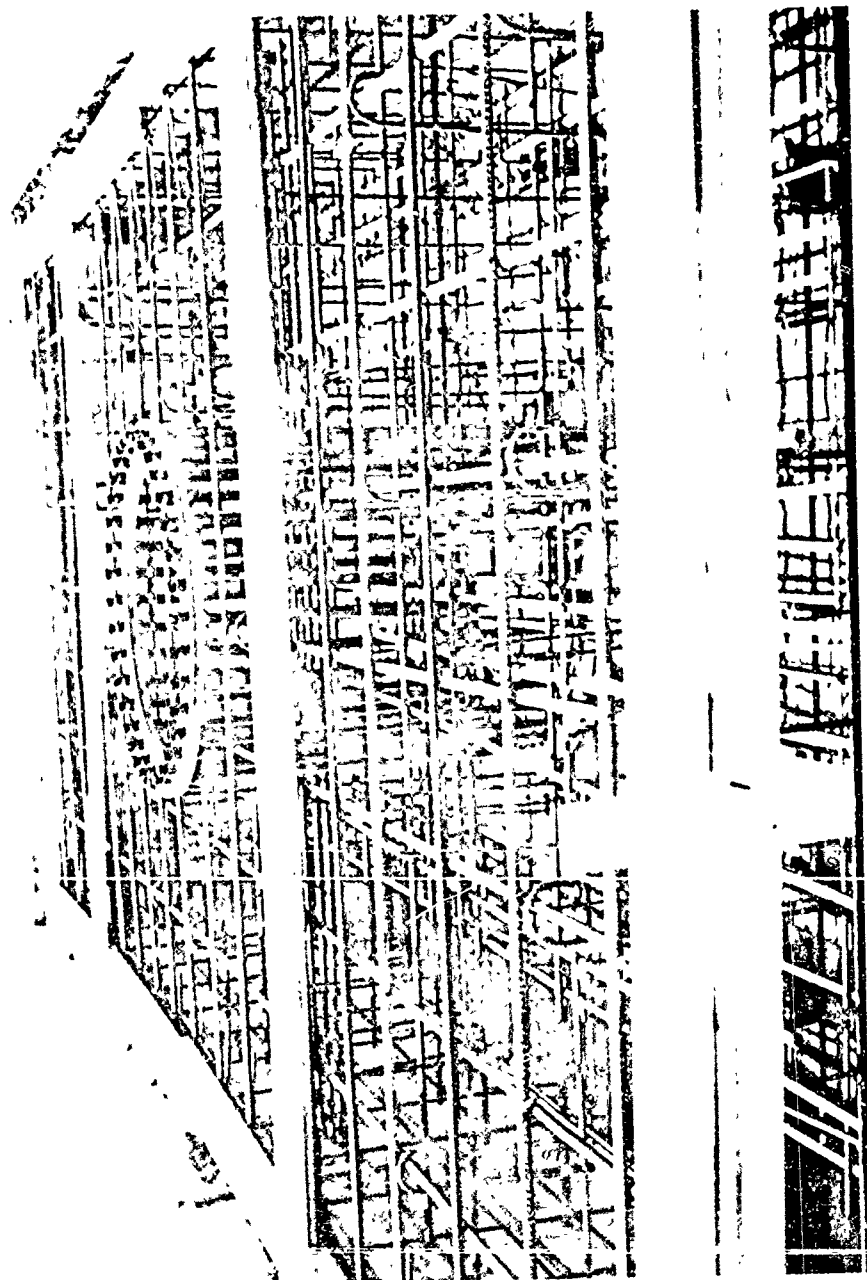


Figure 17. UK/ASWE Slatted Antenna Foundation.





Figure 18. UK/ASWE Slatted Antenna.



Figure 19. AFMIL Underground Aircraft Shelter.



Figure 20, SRI German Wall Structure.

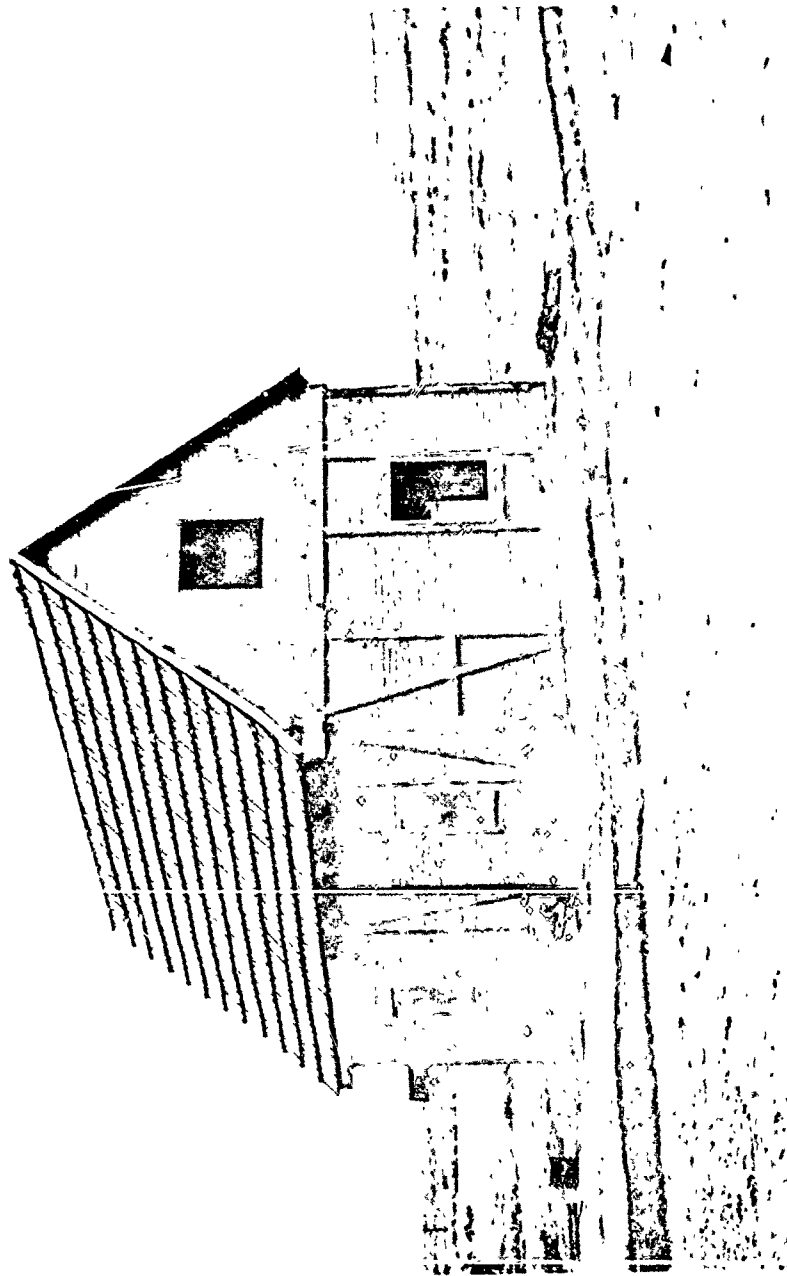


Figure 21. SRI German Wall Structure (Completed).

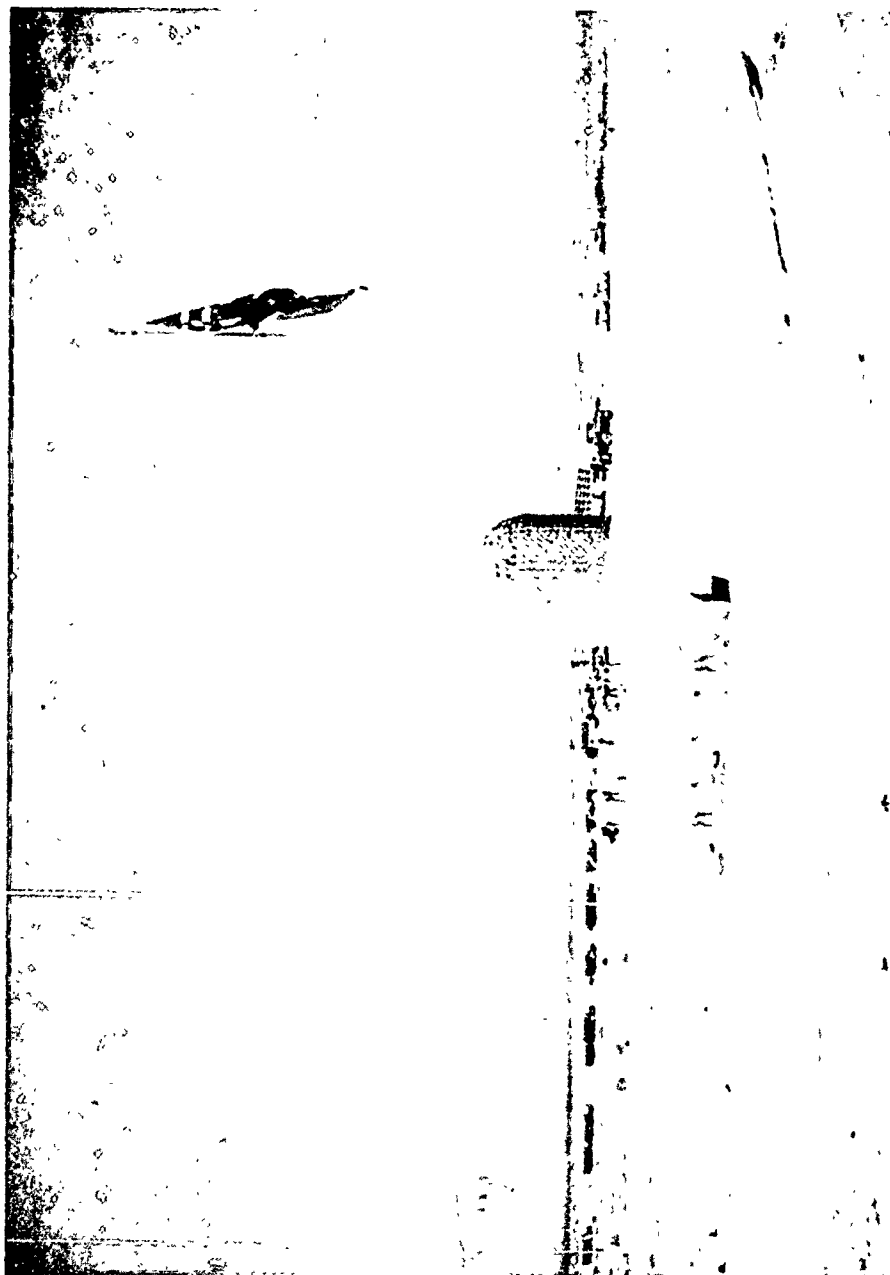


Figure 22. ANFO Stack (Completed)

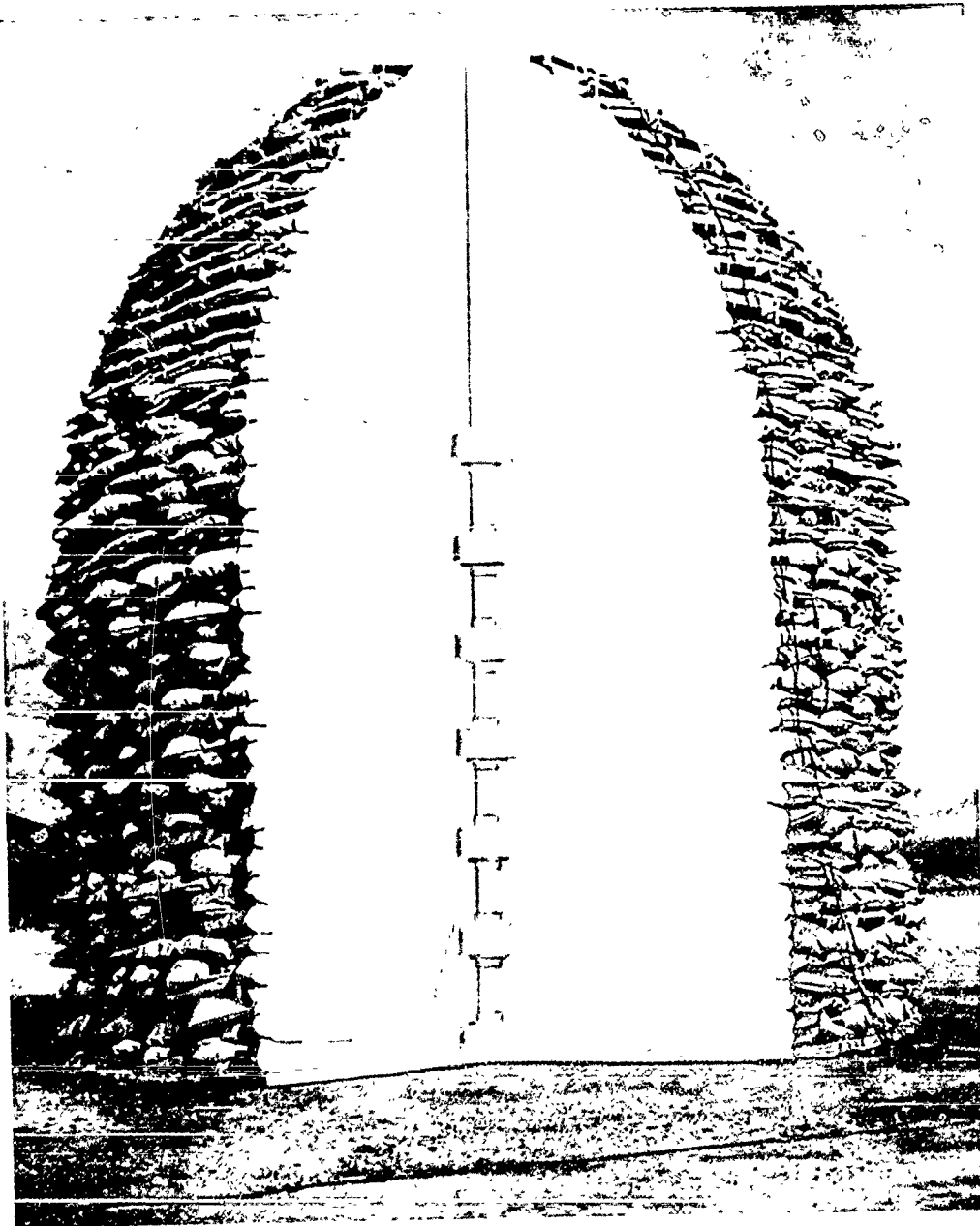


Figure 23. ANFO Stack (Cutaway).

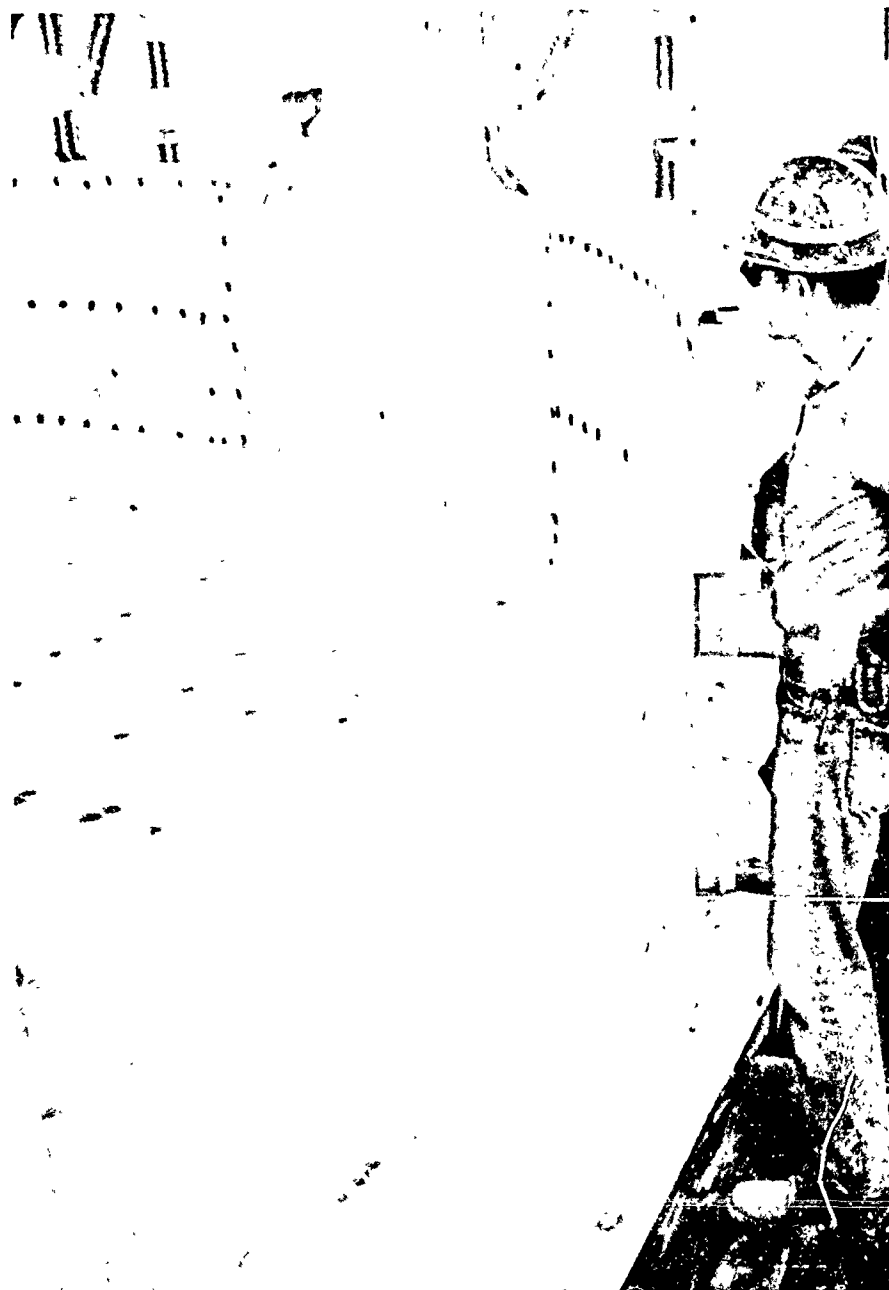


Figure 24. ANFO Stack Base/Circular Forms.



Figure 25. ANFO Stack (Spreading Bulk ANFO).





Figure 26. ANFO Stack (Installing Booster).

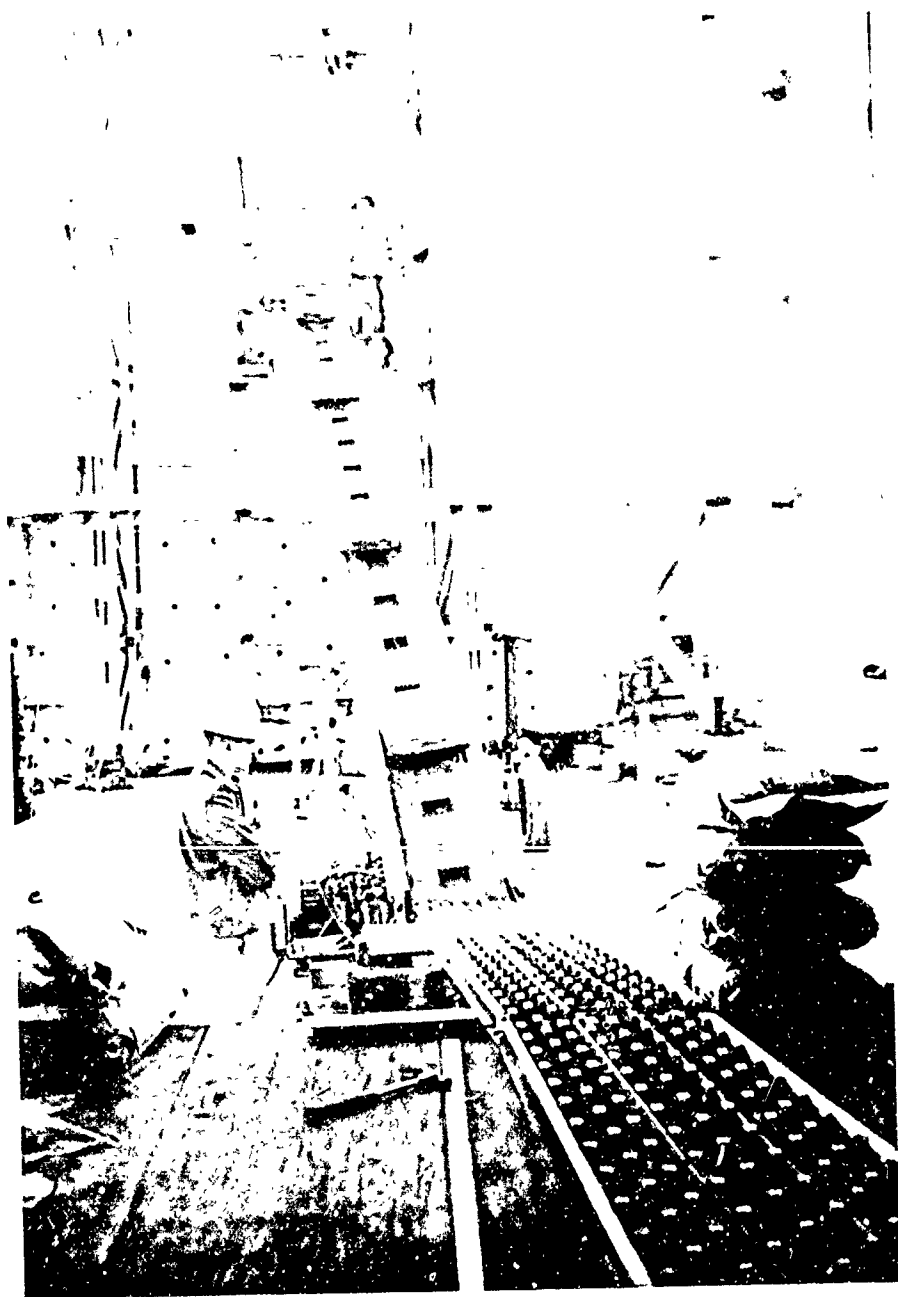


Figure 27. ANFO Stack (Conveyor System).

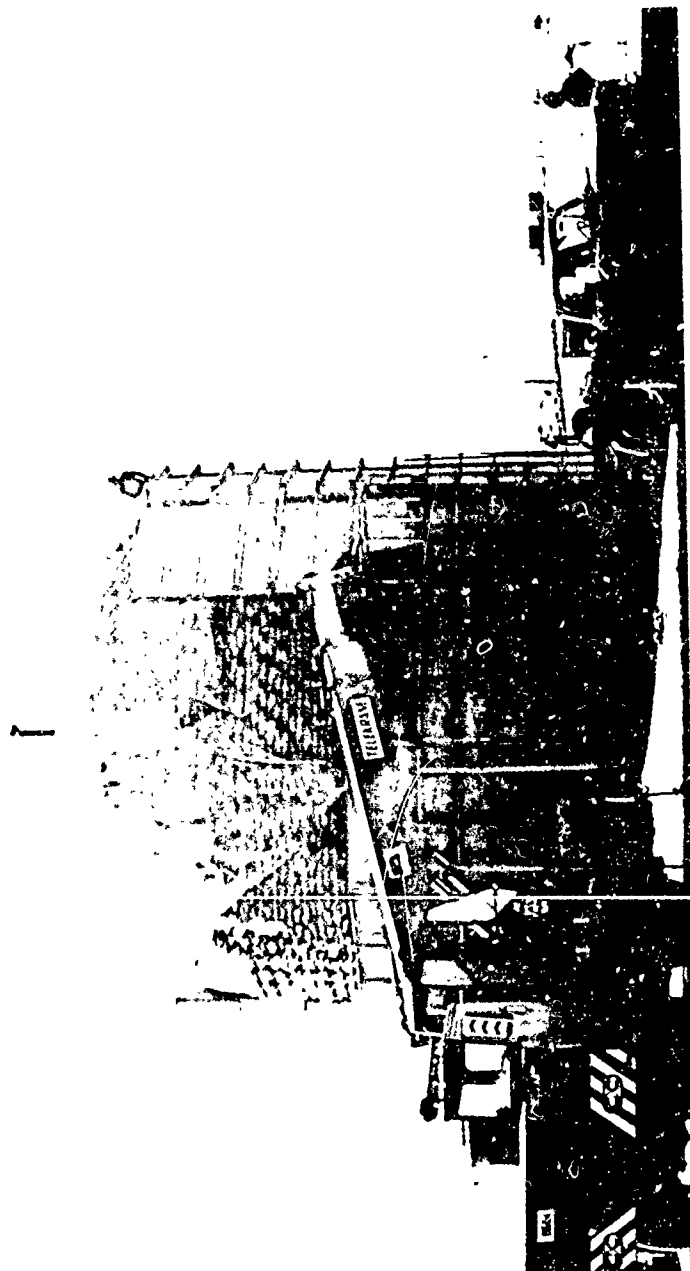


Figure 28. ANFO Stack (Dismantling the Circular Forms).

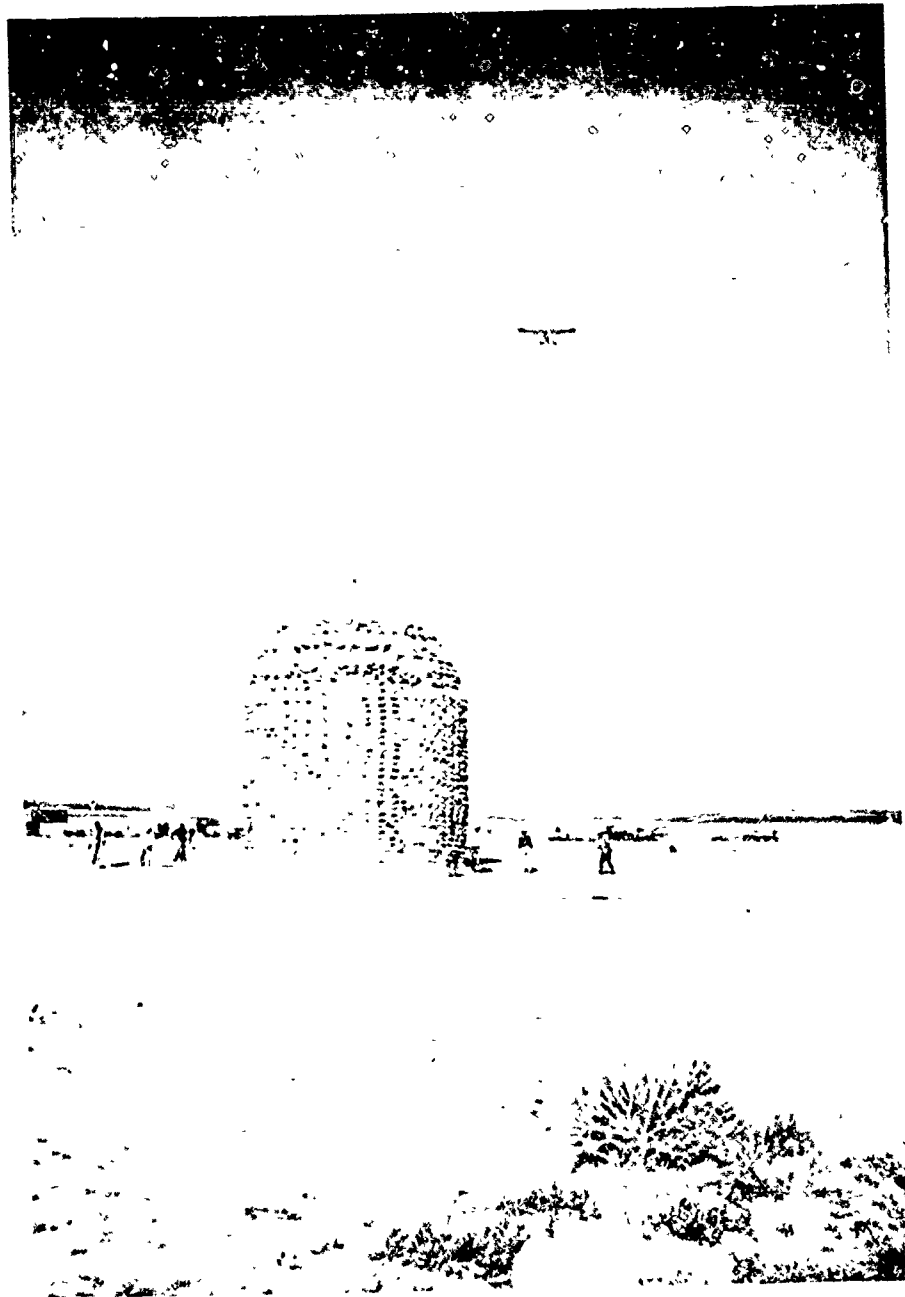


Figure 29. ANFO Stack (Completed).



Figure 30. Test Bed (Aerial View).

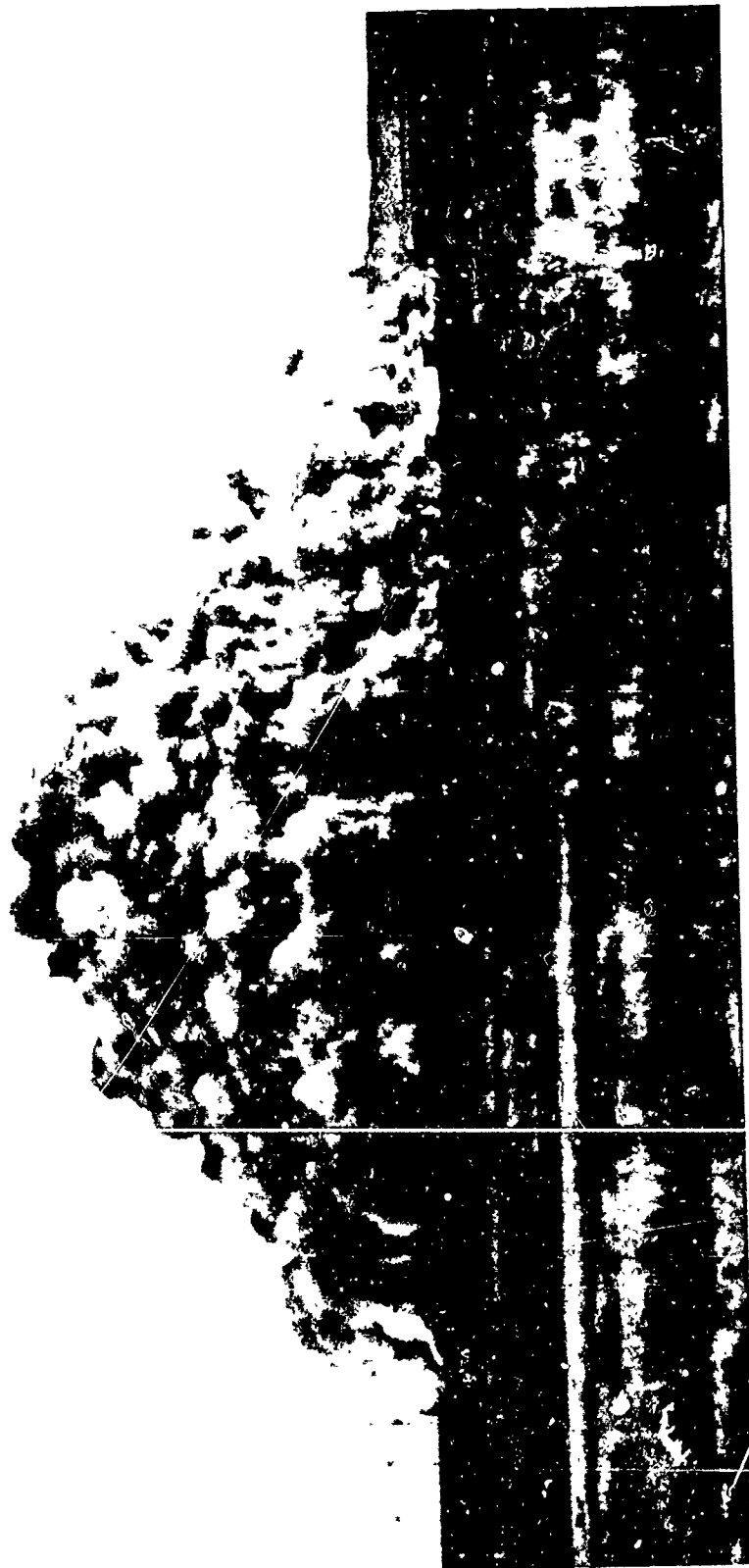


Figure 31. AMFO Stack Detonation.

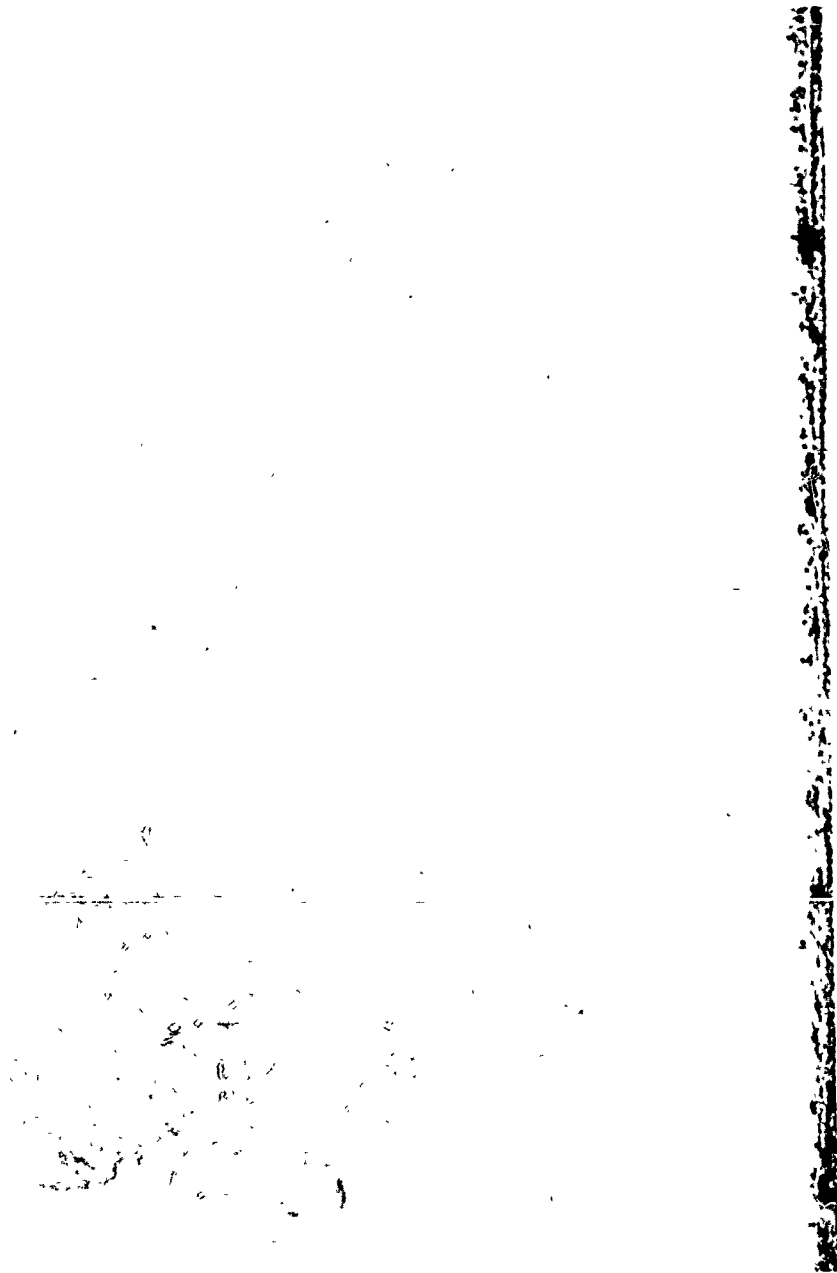


Figure 32. Dust Cloud.



Figure 33. Crater.





Figure 34. Test Bed (Post Event Aerial).

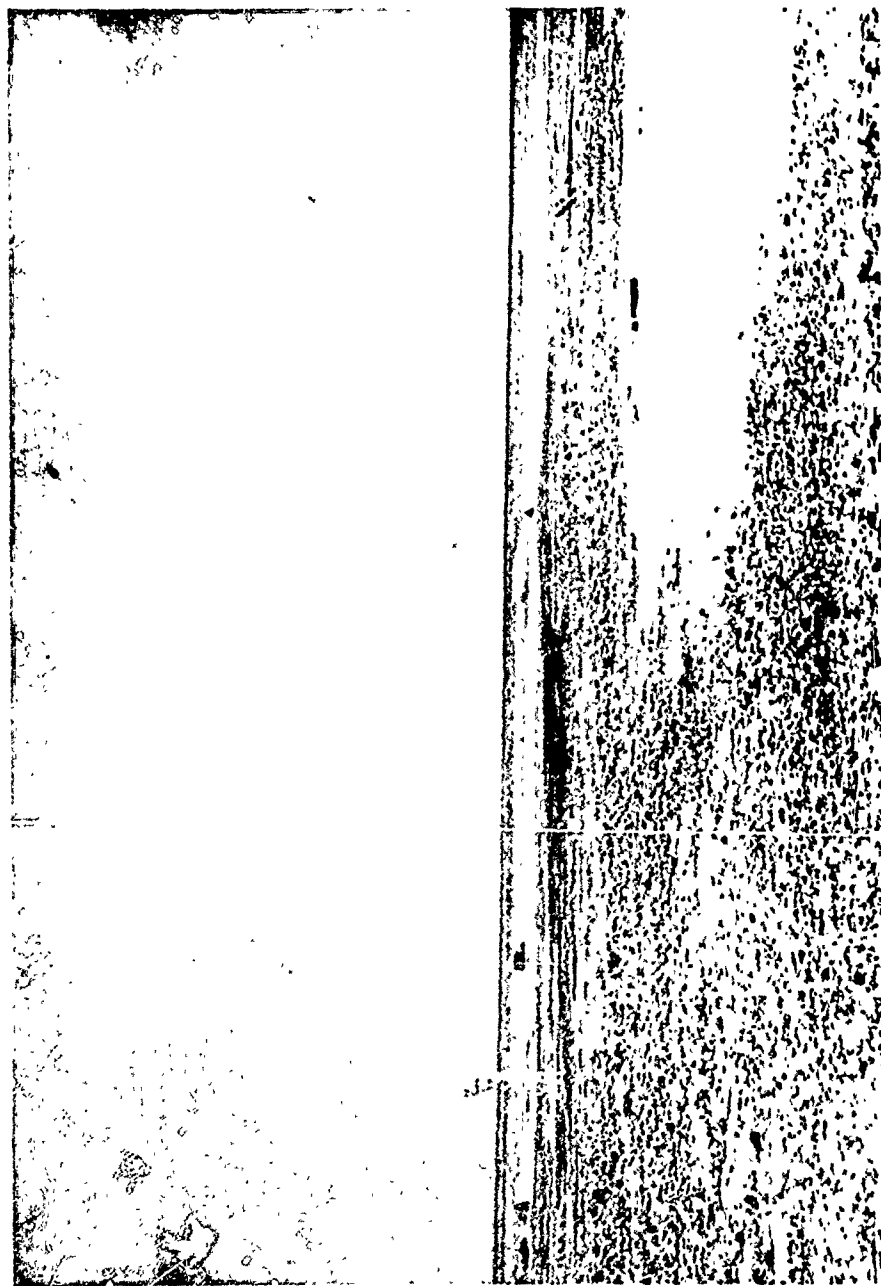


Figure 35. Test Bed (After Clean-up).

**3. CHARGE/DETONATION SYSTEM**  
**(DNA PROJECT 975)**

by  
**M.M. Swisdak, Jr.,**  
**Naval Surface Weapons Center,**  
**Explosion Dynamics Branch**

## CHARGE/DETONATION SYSTEM (DNA PROJECT 975)

by

M. M. Swisdak, Jr.  
Explosion Dynamics Branch  
Naval Surface Weapons Center

### INTRODUCTION

On the basis of a series of small scale tests and the results of the Operation Pre-DICE THROW II shot, the Field Command, Defense Nuclear Agency selected a domed cylinder of ANFO (a 94.5/5.5 percent (by weight) mixture of Ammonium Nitrate (AN) and Number 2 Diesel fuel (FO)) as the main charge for Operation DICE THROW. The charge would be 29.9 feet in diameter, 37.4 feet high, and would weigh 600 tons (based on a bulk ANFO density between 0.85 and 0.90 grams per cubic centimeter).

NSWC/WOL participation was to consist of the following items:

- (1) provide specifications for the ANFO
- (2) design, construct, and emplace the booster system
- (3) monitor the internal temperature of the charge, and
- (4) monitor the fuel oil content and particle size distribution of the ANFO in the charge

### BOOSTER AND INITIATION SYSTEM

The boosting and initiation system was based on the same design as used on the Pre-DICE THROW II Event; i.e., a Main Booster Assembly (MBA) emplaced during the charge construction, and a Booster Initiation System (BIS) lowered into position during Pre-Arming. The details of both the MBA and BIS are provided in references (1) and (2).

### CONSTRUCTION DETAILS

The ANFO was delivered in 25 ton quantities by tractor trailer. The main supplier was located in Carlsbad, New Mexico, with additional material coming from Estancia, New Mexico. Two ten-man stacking crews were utilized during charge construction, with each shift working a nominal 12 hour day. The charge was constructed in 10 working days. The first bag was laid on September 23 and the final bag on 3 October.

A plywood skirt was positioned around the charge to act as a template to guide construction and to ease access to the charge. The skirt was formed from 4 x 8 foot sheets of plywood, bent to the proper curvature and bolted together.

The stacking arrangement of the bags on each layer was quite similar to the design utilized on the 120-ton Pre-DICE THROW II event. A reusable protective shelter was built in which the charge stacking took place. Neither rains nor storms nor winds, of which there were an ample number at the test site, deterred or harmed the stacking task. The housing was designed so that it could be removed easily prior to the shot, be stored, and be ready for use as needed for other charge stacking jobs.

Prior to shot day, both the reuseable shelter and the plywood skirt were removed, leaving a free-standing charge.

The Eric H. Wang Civil Engineering Research Facility supplied the stacking crews, the stacking plan, the plywood skirt, and the reuseable shelter.

#### ANFO QUALITY CHECKS

Both the air temperature and the internal temperature of the explosive stack were monitored with a dual channel thermistor recorder. The stack sensor was located in the sixth layer above the ground, about 9 feet from the edge of the charge. The air temperature sensor was located about 10 feet above the ground, just inside the protective structure. The maximum and minimum air temperatures recorded were 86°F and 55°F, respectively, over the time period between 24 September and 5 October. Over this same time period, the stack temperature varied between 74°F and 78°F.

Samples were taken from each layer of the charge and analyzed for both fuel oil content and particle size distribution. Four samples were taken from the bulk ANFO placed on each layer (if no bulk was used on a layer, bags were cut open to obtain material for the sample). These four samples were then combined and this "combined sample" used in the analyses.

The layer-to-layer variation in the fuel oil content can be seen in the information presented in Table 1. This table also presents other information relevant to each layer -- namely, (1) the number of whole bags, (2) the number of bags of bulk, (3) the total number of bags, (4) the layer radius, (5) the weight of the layer, (6) the average bag weight, and (7) the fuel oil content. Based on this information, the weighted-average fuel oil content was 6.21% for the cylinder, 5.93% for the cap, and 6.12% for the total charge.

Because of production difficulties, two suppliers of ANFO were used during charge construction -- Gulf and Atlas. Thus one would expect two particle size distributions -- corresponding to the two prill manufacturers. This was not the case. Instead, three were found. The Gulf prills were composed of two distinct distributions. The proportion (by weight of the total Gulf material) of these two distributions was approximately 7.5% to 92.5%. All three distributions (Gulf-I, Gulf-II, and Atlas) are shown plotted in Figure 1. Figure 2 presents a comparison of the weighted-average particle size distribution obtained on pre-DICE THROW II with that obtained on DICE THROW.

#### CHARGE SIZE, WEIGHT, AND DENSITY

During charge construction, it became obvious that more material was being packed into each layer than had originally been planned. If the charge shape were not modified, the total charge weight would exceed 650 tons. To reduce the total charge weight, the design was modified as follows: (1) the height of the cylindrical section was reduced from 22.47 feet to 21.36 feet, and (2) the height of the "hemispherical cap" was reduced from 14.93 feet to 14.2 feet. The location of the seventh booster, located on the interface between the cylinder and the hemisphere was also suitably adjusted.

Based on 480 samples (1.9% of the total number of bags contained in the charge), the average ANFO bag weighed 50.43 pounds, with a standard deviation of 1.03 pounds. An empty bag weighed 0.54 pounds. Table 2 presents the total amount of material loaded into the charge -- 628.270 tons.

Upon removal of the skirt from around the charge, it was discovered that the lower portion of the charge had expanded due to hydrostatic pressure. At the base of the charge, the bags were in contact with the skirt -- which had originally been spaced 6 inches from the bags. At the top of the cylindrical section, it did not appear that the bags had expanded. Thus, for the purpose of determining the volume of the cylindrical section, it was assumed that the section was not a cylinder, but rather the frustum of a cone. The radius of the base was taken to be 15.35 feet ( $14.85 + .5$ ), the radius of the top 14.85 feet, and the height 21.36 feet. With these choices and the assumption that the shape was that of the frustum of a cone, the volume is 15,302 cubic feet.

The cap was assumed to be composed of a series of discs -- stacked one upon the other. Each disc was assumed to have a uniform thickness of 0.396 feet. The radius of each layer is presented in Table 1. The total charge height was 35.6 feet. With these assumptions, the volume of the cap was 6705 cubic feet.

Using the volume information just calculated and the weight data presented in Table 2, average densities were computed :

$\rho_{\text{cyl}} = 0.915$  grams/cubic centimeter,  $\rho_{\text{cap}} = 0.912$  grams/cubic centimeter, and  $\rho_{\text{charge}} = 0.914$  grams/cubic centimeter.

Subsequent to charge detonation, it was discovered that the bulk density of the prilled ammonium nitrate supplied by Gulf was of a higher density than had been expected. We had expected a bulk density of between 0.85 and 0.90 grams per cubic centimeter; the supplied material had a bulk density of up to 0.93 grams/cubic centimeter.

#### SUMMARY

The charge for Operation DICE THROW was constructed from 24903 bags of ANFO. The charge consisted of a cylindrical section with a hemispherical cap. The cylindrical section had a density of 0.915 g/cm<sup>3</sup> and an average fuel oil content of 6.21%. The hemispherical cap had a density of 0.912 g/cm<sup>3</sup> and a fuel oil content of 5.93%. The total charge had a weight of 628.27 tons, a density of 0.914 g/cm<sup>3</sup>, and a fuel oil content of 6.12%. These results are summarized in Table 3.

#### REFERENCES

1. NSWC Drawing 76C-1127; NSWC Drawing 76D-1128
2. NSWC Drawing 76D-1123; NSWC Drawing 76D-1129

TABLE 1 STACKING DATA

LAYER NUMBER	LAYER RADIUS	NUMBER OF WHOLE BAGS	NUMBER OF BAGS BULK	TOTAL BAGS	AVERAGE BAG WEIGHT	TOTAL LAYER WEIGHT	AVERAGE FUEL OIL CONTENT
	(ft)				(lb)	(tons)	(%)
1	14.85	298	25	323	50.08	8.081	6.39
2	14.85	291	34	325	49.43	8.023	6.25
3	14.85	299	26	325	50.04	8.124	6.38
4	14.85	291	34	325	50.61	8.215	5.92
5	14.85	287	36	323	50.54	8.152	6.45
6	14.85	285	35	320	50.00	7.991	5.85
7	14.85	298	27	325	49.75	8.077	6.73
8	14.85	296	30	326	50.17	8.170	6.22
9	14.85	294	33	327	50.79	8.295	7.02
10	14.85	299	26	325	50.17	8.146	5.59
11	14.85	308	27	335	50.21	8.403	5.89
12	14.85	303	26	329	49.71	8.170	5.80
13	14.85	295	30	325	50.75	8.239	6.00
14	14.85	300	25	325	50.58	8.213	5.87
15	14.85	300	25	325	50.32	8.170	4.96
16	14.85	297	31	328	51.04	8.362	6.51
17	14.85	303	27	330	50.75	8.366	6.41
18	14.85	306	25	331	50.17	8.296	6.00
19	14.85	307	21	328	51.88	8.503	6.96
20	14.85	300	25	325	50.63	8.221	6.66
21	14.85	307	25	332	50.88	8.439	6.66
22	14.85	305	25	330	50.50	8.326	6.21
23	14.85	306	25	331	50.25	8.310	6.27
24	14.85	298	30	328	50.23	8.230	5.97
25	14.85	304	25	329	50.21	8.253	6.16
26	14.85	301	25	326	50.42	8.212	6.23
27	14.85	300	25	325	50.58	8.213	6.01
28	14.85	301	25	326	50.75	8.266	5.88
29	14.85	304	29	333	50.65	8.425	5.99
30	14.85	297	25	322	50.19	8.074	6.09
31	14.85	305	25	330	50.67	8.354	6.34
32	14.85	306	25	331	50.00	8.268	6.83
33	14.85	304	27	331	50.33	8.322	6.73
34	14.85	298	25	323	50.75	8.189	6.36
35	14.85	297	25	322	51.54	8.291	6.07



TABLE 1 STACKING DATA (CONTINUED)

LAYER NUMBER	LAYER RADIUS	NUMBER OF WHOLE BAGS	NUMBER OF BAGS BULK	TOTAL BAGS	AVERAGE BAG WEIGHT	TOTAL LAYER WEIGHT	AVERAGE FUEL OIL CONTENT
	(ft)				(lb)	(tons)	(%)
36	14.85	300	25	325	50.79	8.247	5.99
37	14.85	305	25	330	52.00	8.573	6.07
38	14.85	300	25	325	49.75	8.078	6.03
39	14.85	299	25	324	51.00	8.255	5.71
40	14.85	298	25	323	50.08	8.081	6.26
41	14.85	298	25	323	49.67	8.015	6.11
42	14.85	297	26	323	50.42	8.136	6.17
43	14.85	309	25	334	50.88	8.490	6.08
44	14.85	304	21	325	51.25	8.322	6.18
45	14.85	304	21	325	52.42	8.513	6.28
46	14.85	302	23	325	50.42	8.187	6.11
47	14.85	310	19	329	52.00	8.549	6.31
48	14.85	307	18	325	51.92	8.432	6.11
49	14.85	303	22	325	50.88	8.262	6.29
50	14.85	298	29	327	51.25	8.372	6.63
51	14.85	296	24	320	52.00	8.314	6.20
52	14.85	297	24	321	48.63	7.799	6.19
53	14.85	304	21	325	49.38	8.019	6.46
TOTAL FOR CYLINDER		15921	1377	17298		437.031	
54	14.85	307	20	327	50.25	8.210	6.12
55	14.85	309	16	325	52.00	8.446	6.47
56	14.85	303	20	323	50.04	8.076	6.81
57	14.85	306	19	325	50.60	8.217	5.76
58	14.85	306	19	325	51.17	8.310	6.62
59	14.69	324	7	331	50.08	8.286	5.50
60	14.69	273	25	298	50.50	7.518	5.25
61	14.69	261	20	281	50.33	7.066	5.71
62	14.45	264	20	284	50.00	7.095	6.00
63	14.34	264	20	284	49.75	7.059	5.80
64	14.21	257	20	277	49.71	6.879	5.49
65	14.21	269	23	292	50.12	7.311	5.94

TABLE 1 STACKING DATA (CONTINUED)

LAYER NUMBER	LAYER RADIUS	NUMBER OF WHOLE BAGS	NUMBER OF BAGS BULK	TOTAL BAGS	AVERAGE BAG WEIGHT	TOTAL LAYER WEIGHT	AVERAGE FUEL OIL CONTENT
	(ft)				(lb)	(tons)	(%)
66	14.08	266	21	287	49.83	7.145	6.04
67	13.92	257	24	281	48.88	6.861	6.18
68	13.76	247	27	274	49.79	6.814	6.02
69	13.58	238	20	258	49.96	6.439	5.92
70	13.38	229	20	249	49.20	6.120	5.75
71	13.16	218	20	238	49.67	5.905	6.11
72	12.93	227	15	242	50.79	6.142	5.99
73	12.67	220	0	220	51.00	5.610	6.03
74	12.40	206	1	207	51.25	5.304	5.99
75	12.11	214	0	214	49.25	5.270	5.09
76	11.79	185	0	185	49.62	4.590	5.19
77	11.45	179	0	179	49.33	4.415	5.90
78	11.08	157	1	158	49.62	3.920	5.44
79	10.68	141	0	141	49.92	3.519	5.54
80	10.24	139	0	139	50.92	3.539	6.24
81	9.77	128	0	128	50.92	3.259	5.89
82	9.26	129	0	129	50.92	3.284	6.02
83	8.69	102	0	102	50.92	2.597	6.19
84	8.06	91	0	91	51.15	2.327	6.03
85	7.36	75	0	75	51.15	1.918	6.13
86	6.54	58	0	58	51.15	1.483	6.37
87	5.58	42	0	42	51.15	1.074	6.12
88	4.38	26	0	26	51.15	.665	5.93
89	2.60	10	0	10	51.15	.256	6.14
TOTAL FOR CAP		7227	378	7605		190.930	
TOTAL FOR CHARGE		23148	1755	24903		627.961	

TABLE 2 CHARGE WEIGHTS

MATERIAL	LOCATION		
	CYLINDER	CAP	CHARGE
ANFO	432.732	188.979	621.711
PAPER BAGS*	4.299	1.951	6.250
BOOSTER	0.109	0	0.109
MISCELLANEOUS**	0.15	0.05	0.20
TOTAL	437.290	190.980	628.270

\*Average weight of bag is 0.54 pounds

\*\*PVC pipe, PVC flanges, and bag glue

NOTE: ALL CHARGE WEIGHTS SHOWN ARE  
IN TONS

TABLE 3 SUMMARY

	CYLINDER	CAP	CHARGE
TOTAL NUMBER OF BAGS	17298	7605	24903
TOTAL WEIGHT(tons)	437.290	190.980	628.270
VOLUME (ft <sup>3</sup> )	15302	6705	22007
DENSITY (g/cm <sup>3</sup> )	0.915	0.912	0.914
AVERAGE FUEL OIL CONTENT (percent by weight)	6.21	5.93	6.12

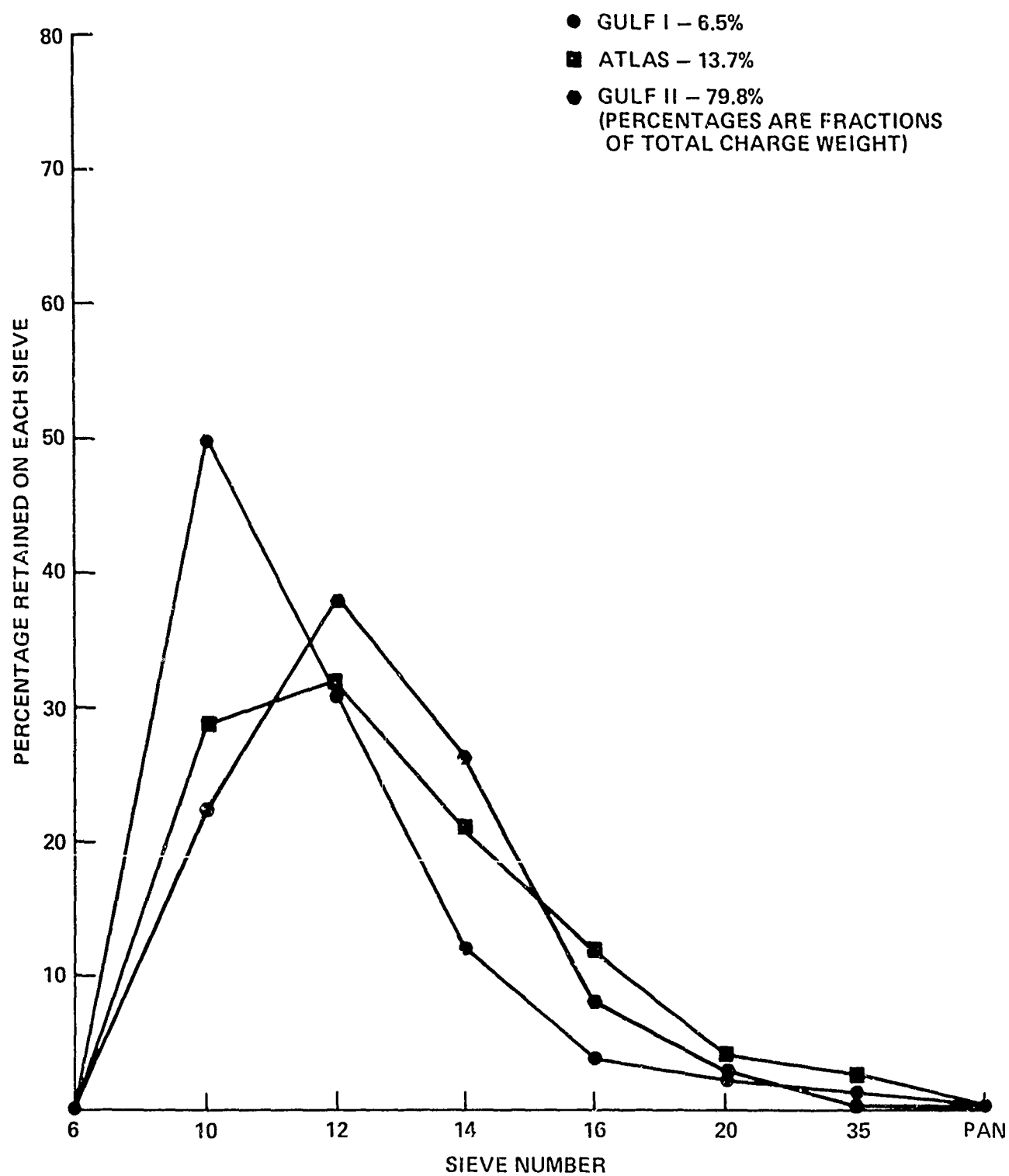


FIG. 1 PARTICLE SIZE DISTRIBUTION IN STACK

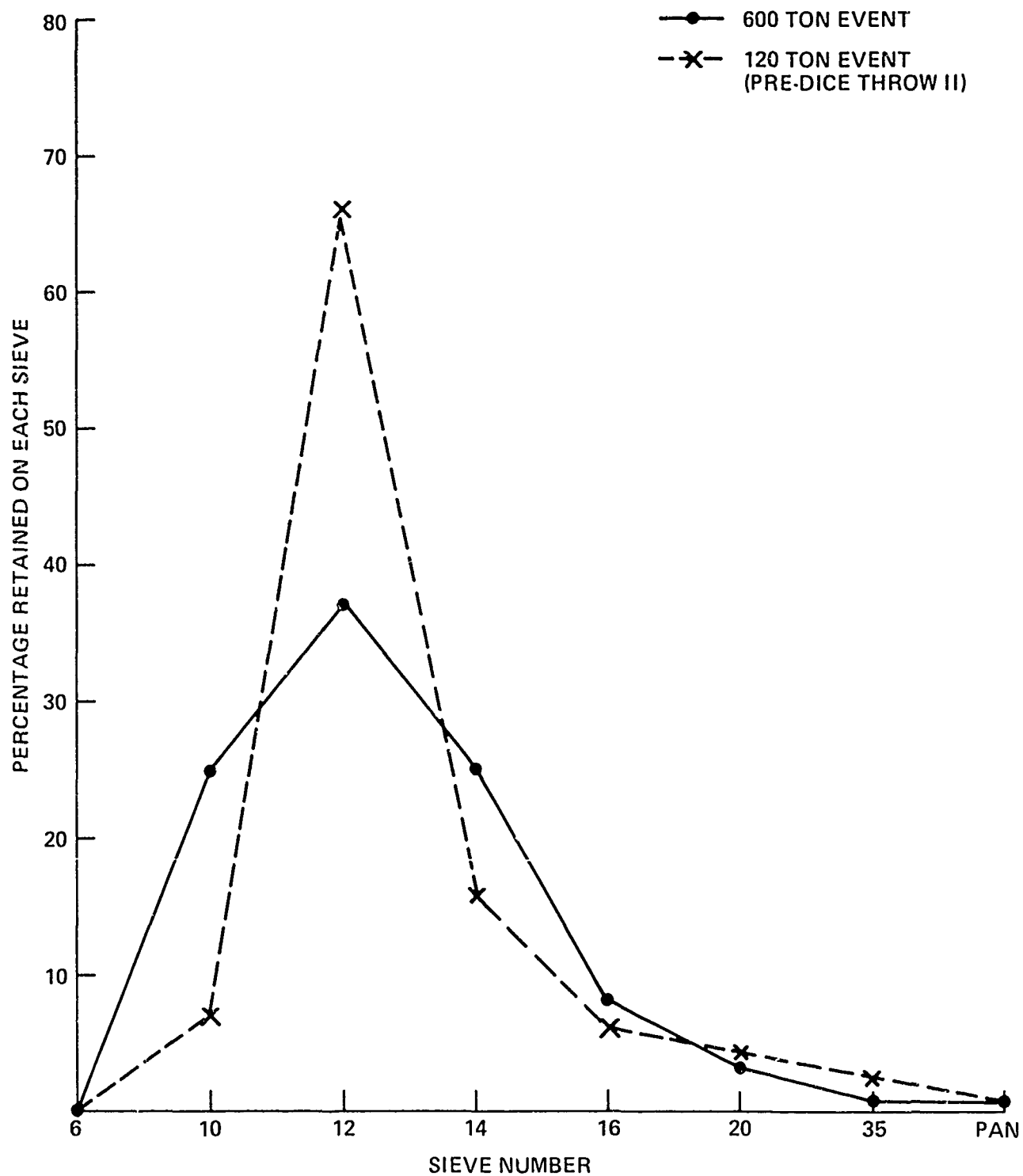


FIG. 2 COMPARISON OF WEIGHTED-AVERAGE PARTICLE SIZE DISTRIBUTIONS: PRE DICE-THROW II AND DICE THROW

**4. DICE THROW MAIN EVENT -  
EXPLOSIVE DIAGNOSTICS**

**by**

**Bernard Hayes and Ronald Boat  
Lawrence Livermore Laboratory**

## EXPLOSIVE DIAGNOSTICS

### Introduction

Personnel from the Lawrence Livermore Laboratory (LLL) participated in the DICE THROW Main Event to provide and monitor a detonator firing system in addition to recording explosion diagnostics from implants in the stacked Ammonium Nitrate Fuel Oil (ANFO) explosive charge. From all indications, the main charge detonated properly but demonstrated performance fluctuations characteristic of density gradients within the stack.

The analysis of the explosion performance is based on seven distinct information sources. These items, their function, and the efficiency of data return, are listed in Table I. The first three items deal exclusively with the detonator system. The last three are concerned with characterizing the main charge. The central item was intended to interface the booster initiation system with the ANFO. The overall response from the diagnostic implants is sufficient to characterize, in a broad sense, the stack performance.

### Firing

The firing system will be discussed first. It comprised four main elements: (1) a high voltage controller with trigger generator, (2) a 1.85-km (6,000-ft) transmission line duplexed for charging and firing, (3) a capacitor discharge unit (CDU), and (4) firing lines and harness to initiate seven detonators in a series string. A duplicate back-up system to provide redundancy functioned 1.5  $\mu$ s after the primary system.

The controllers were located in the timing bunker. THE CDUs were located near ground zero. Charging of the main energy storage capacitors in the CDUs started two minutes before zero time. At zero time according

to the console clock, a fire signal was delivered to the high voltage controllers. In turn, firing pulses were generated and transmitted to the CDUs over separate transmission lines. Part of the primary firing pulse was diverted to the LLL diagnostic trailer to trigger a delay generator. Outputs from the delay generator synchronized three raster oscilloscopes and two relatively fast writing, single sweep oscilloscopes. The former oscilloscopes recorded long rate stick timing information and simultaneity, while the latter were used to record fiducial and detonator current waveforms. A functional diagram of the firing system and its interrelationship to the diagnostic system is shown in Figure 1.

The output from the CDUs fed four parallel firing lines terminating at a firing harness. A reduced and differentiated output from the primary and back-up CDUs was mixed to serve as a fiducial signal for user agencies. The fiducial signal also served to substantiate the time between CDU firing and the quality of the firing discharge. A single current viewing resistor between the firing lines and the firing harness indicated the rate of rise of current in the detonator string bridge wires, the time to bridge wire burst, and the peak burst current. The results are given in Table II. Suffice to say, indications are that a normal full string detonation occurred with no signs of a malfunction.

#### Simultaneity

A total of seven shock sensitive crystal pins were originally butted against the octol booster explosive during stacking. The purpose was to determine the shock arrival time at the booster-ANFO interface. The even booster stations (2, 4, and 6) were mixed for recording on a master-slave raster oscilloscope. The odd booster stations (1, 3, 5, and 7) were mixed



Table I

## INFORMATION SOURCES

<u>Item</u>	<u>Function</u>	<u>Data bits</u>	<u>Lost bits</u>
1	Fire set Controller	1	
2	Discharge Unit Fiducial	2	
3	Detonator Current Viewer	1	
4	Booster Simultaneity Pins	7	5
5	Long Rate Stick	15	1
6	Three Pressure Transducers	3	
7	Three Time Interval Meters	3	—
		32	6

Table II

## DETONATOR FUNCTIONING PARAMETERS

<u>dI/dt</u> <u>amps/<math>\mu</math>s</u>	<u>Bridge burst time</u> <u>tb-<math>\mu</math>s</u>	<u>Burst current</u> <u>I-amps</u>
600	1.10	660

## Firing System

### Lawrence Livermore Laboratory Explosives Diagnostics

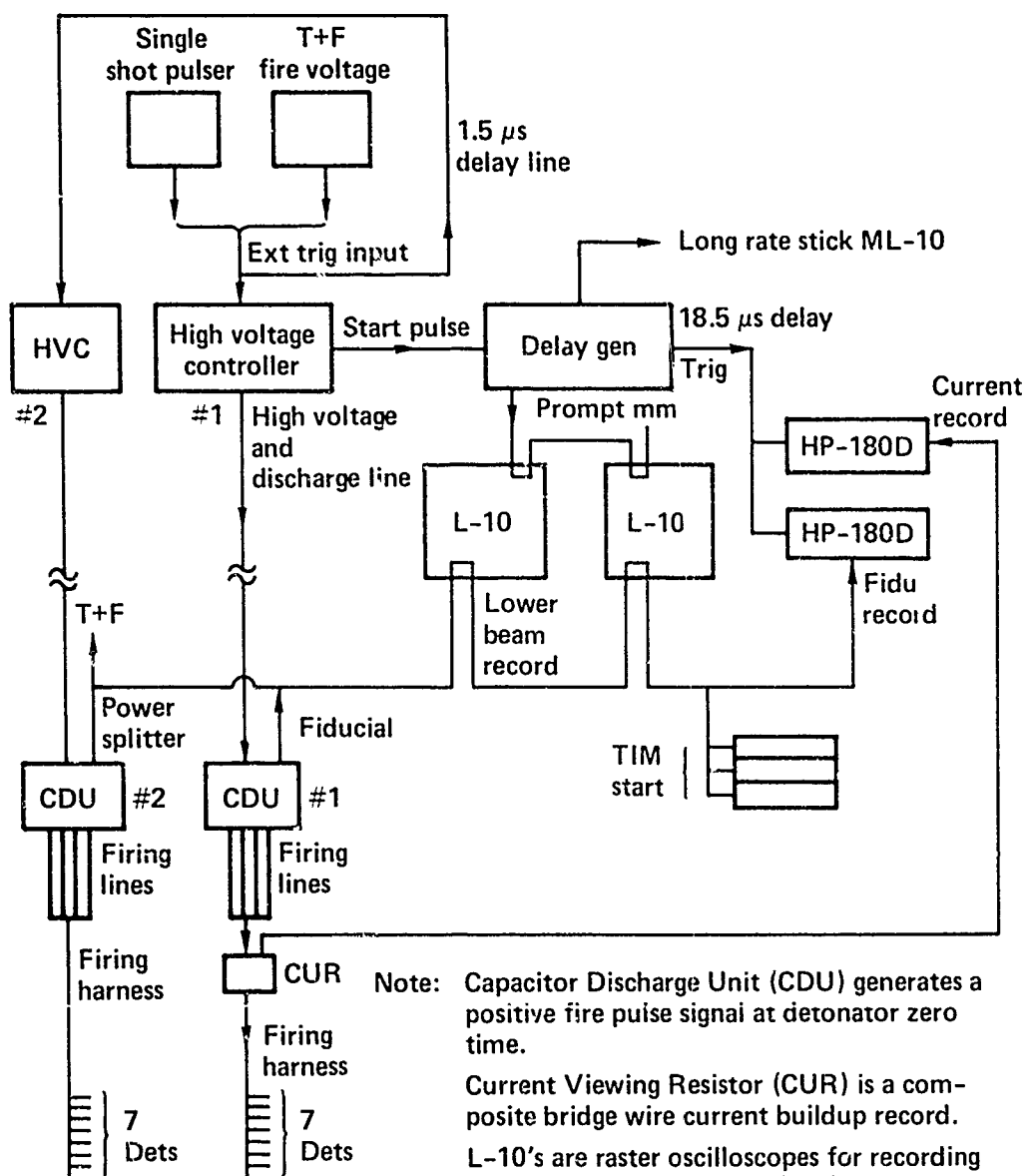


FIGURE 1

for recording on a second raster oscilloscope. Unfortunately, most of these pins did not report.

The simultaneity pins were installed by NSWC personnel, and it is our concerted opinion the frailty of the pins led to their premature demise. Two pins which did report gave a transit time of  $32.5 \mu\text{s}$  from fiducial to booster breakout. This transit time value is quite reasonable when compared to pre-shot test data conducted by NSWC personnel at White Oak, Maryland. Therefore, the measured value is subsequently used for time interval calculations of ANFO detonation velocity.

#### Long Rate Stick

The long rate stick was a phenolic rod 4 m in length with 15 shock sensitive crystal pins arrayed approximately 250 mm apart along one side. The distance between each pin was measured before implanting the stack at the third booster level  $135^\circ$  clockwise from north. All but one station reported. The one station which did not respond neither influences nor affects the results as it was in the middle of the array at the mixer crossover.

The resulting distance-time data was analyzed using linear regression and a quadratic fit to obtain a detonation velocity for the ANFO. The quadratic coefficients give the best fit to the data resulting in a standard deviation of 1.5 mm over a total length of 3582 mm. A summary of results is given in Table III and Figure 2.

The detonation velocities are quite reasonable considering the higher than normal ANFO density which was reported by NSWC. Taking this bit of information into consideration, along with quartz gage measurements reported in the next section, the weight of evidence favors the quadratic fit. In

Table III

## LONG RATE STICK DETONATION VELOCITY

Fit	<u>A</u> <u>mm/<math>\mu</math>S<sup>2</sup></u>	<u>D</u> <u>mm/<math>\mu</math>S</u>	<u>Intercept</u> <u>mm</u>	<u>Mean</u> <u>mm</u>	<u>S.D.</u> <u>mm</u>	<u>Pressure</u> <sup>*</sup> <u>GPa</u>
Linear	0	5.44	-27.7	7.18	4.6	7.75
Quadratic	.0005	5.26	- 5.6	2.24	1.5	7.25

\* Gamma law using an average ANFO density of 0.93 g/cc and a gamma of 2.55.

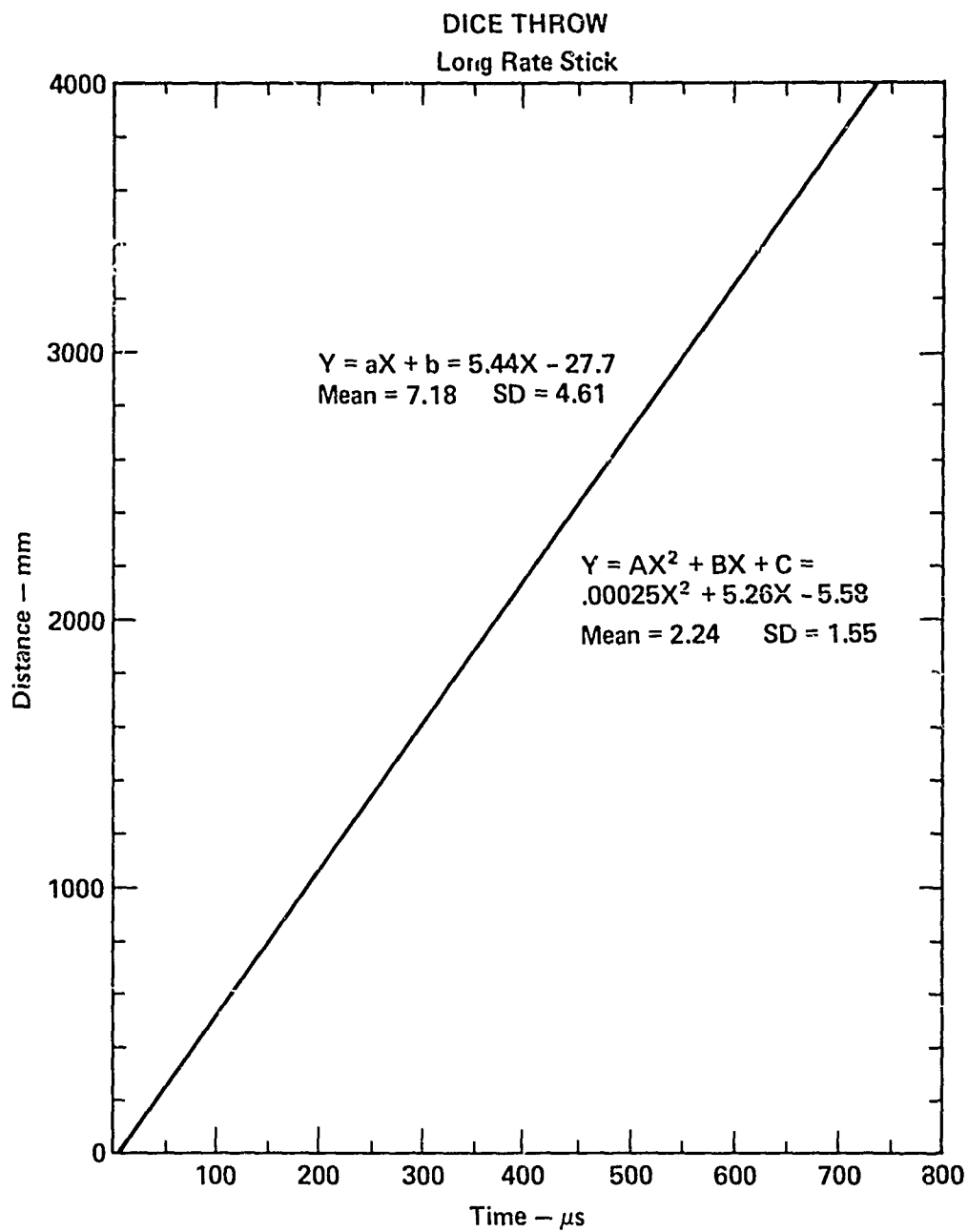


FIGURE 2

addition, the calculated pressure is in closer agreement with the measured peak pressure.

#### Quartz Gages

Impedance-matched quartz gages were implanted opposite booster levels 2, 4, and 6 at 180°, 300°, and 60° respectively clockwise from north. In order, the reduced peak pressures from these gages were 6.11, 7.14, and 6.00 GPa. The pressure values appear reasonable in view of the limited data base available for ANFO with respect to prill size, density, and detonation velocity.

The pressure profiles from the individual gages do demonstrate considerable differences associated with the shock front. In no case is there a classic sharp shock. This fact is consistent with previous measurements by other techniques and may be the reason the slope in the detonation velocity-density plane has such a large value: approximately twice the value of PETN for the same density gradient.

#### Time Interval

Time interval counters started by the fiducial signal and turned off by trigger pins at each quartz gage were employed to measure the detonation wave transit time over a known distance. In effect, they operated as average detonation velocity detectors. A plan view of implants and the data matrix are given in Figure 3. The center circle represents the booster column. The rays depict the detonation path to the different gages. The sequence of number 11, 22, and 33 are along the main diagonal.

Along the main diagonal, the values for the average detonation velocity do not approach the detonation velocity determined from the long rate stick. One of the diagonal values exceeds the long rate stick value indicating asymmetry in the explosion expansion. From the position and direction of the

# TIME INTERVAL MATRIX

Gauge	Distance*	Time	Corrected Time <sup>+</sup>	Dij - mm/μs		
1	863	221.2	188.7	4.57 <sub>11</sub>		
2	1918	415.7	383.2	5.42 <sub>12</sub>	5.01 <sub>22</sub>	
3	3013	681.5	649.0	4.67 <sub>13</sub>	4.12 <sub>23</sub>	4.64 <sub>33</sub>

\*Pin distance from booster explosive in mm.

<sup>+</sup>Counter time minus simultaneity time in microseconds.

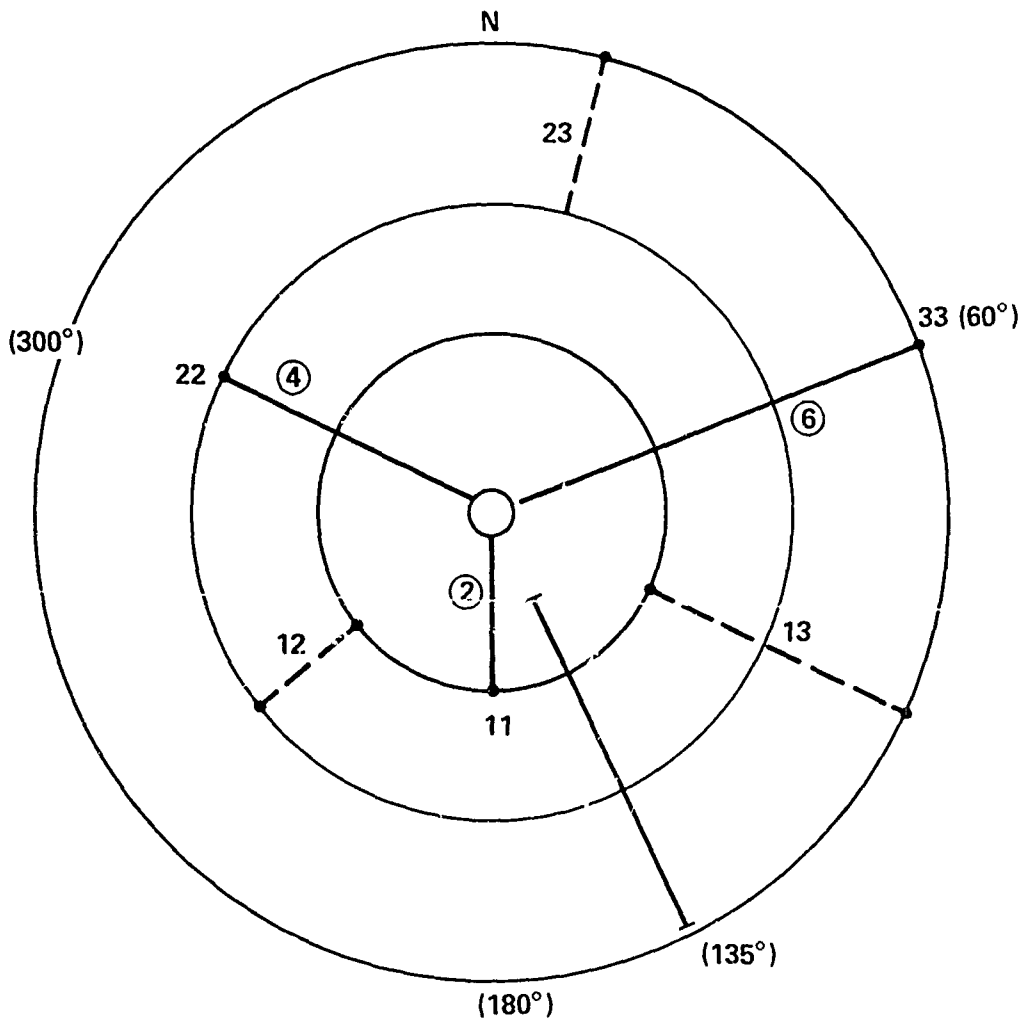


FIGURE 3

higher velocity rays, it would appear stack breakout should have occurred first in the lower southern quadrant.

### Conclusions

The ANFO explosive stack used on the DICE THROW Main Event was successfully initiated and instrumented by LLL personnel. The explosive charge was more energetic than initially planned. The reason for the higher yield was a direct result of the higher than normal average stack density. Detonation velocity and detonation pressure are both a function of density. While the explicit relationship for ANFO is not known, both the measured detonation velocity and pressure confirm there were density gradient regions within the stack. As a consequence, it is not unreasonable to expect hydrodynamic instabilities to develop since the change in detonation velocity with respect to a change in density is like a factor of seven. This effect will lead to considerable internal turbulence which does not smooth out. More probably, cellular disturbances are generated fostering multiple interactions which disrupt the smooth isentropic expansion of the detonation products.



**5. TECHNICAL PHOTOGRAPHY FROM  
DICE THROW EVENT**

**by**

**John Wisotski**

**Denver Research Institute**

## ABSTRACT

Technical information pertaining to the detonation of a 628-ton ammonium nitrate/fuel oil (AN/FO) hemispherical-ended cylindrical charge was obtained photographically and photoelectrically from the DICE THROW (DT) Event. The DT information contains parametric data which were compared to the scaled-up data from the Pre-DICE THROW I and II 6-ton and 120-ton cratering series and to equivalent data procured from trinitrotoluene (TNT) detonations. Comparisons were made on the total light, color temperature, detonation velocities, free-air and surface-surge fireball growth, shockwave separation and arrival times along the air-surface interface, cloud development and rise and dynamic ejecta.

The DT photographic and photoelectric derived data suggest that some aspects of the detonation process scaled well to those derived from PDT I and II while others did not. What differences did exist can be attributed partly to the apparent increase in the DT detonation velocity due to an increase in the AN/FO density and partly to the finer-scaled surface structure of the DT charge. Major differences existed in the total light radiation and color temperature between the DT Event and equivalent TNT detonations.

## TABLE OF CONTENTS

SECTION	PAGE
I. INTRODUCTION . . . . .	1
1.1 OBJECTIVES . . . . .	1
1.2 BACKGROUND AND THEORY . . . . .	2
II. PROCEDURE . . . . .	3
2.1 EXPERIMENTAL SETUP . . . . .	3
2.2 INSTRUMENTATION AND FIELD OPERATION . . . . .	5
III. RESULTS AND DISCUSSION . . . . .	8
3.1 DETONATION VELOCITIES . . . . .	9
3.2 LIGHT RADIATION OUTPUTS . . . . .	19
3.2.1 Total Light Radiation Output . . . . .	20
3.2.2 Unit Light Radiation Output . . . . .	23
3.3 TEMPERATURE TIME . . . . .	24
3.4 TIME-INTEGRATED SPECTRA . . . . .	28
3.5 SURFACE-SURGE SHOCKWAVE SEPARATION DATA . . . . .	30
3.6 SURFACE-SURGE FIREBALL ANOMALIES . . . . .	32
3.7 DUST JETS . . . . .	40
3.8 SHOCKWAVE ARRIVAL TIMES . . . . .	40
3.9 PEAK PRESSURE DATA FROM ARRIVAL TIMES . . . . .	50
3.10 FIREBALL CHARACTERISTICS . . . . .	52
3.11 DYNAMIC EJECTA . . . . .	57
3.12 CLOUD DEVELOPMENT AND RISE . . . . .	58
IV. CONCLUSIONS AND RECOMMENDATIONS . . . . .	60
REFERENCES . . . . .	62

PRECEDING PAGE BLANK

## LIST OF ILLUSTRATIONS

<u>Figure</u>		<u>Page</u>
2.1	DICE THROW 628.3-Ton AN/FO HEC, L/D = 0.71, Support Structures Removed Before Detonation . . . . .	4
2.2	Plan View of DRI Camera Stations Relative to SGZ and BRL Gage Lines . . . . .	7
3.1	Total Light Radiation and Unit Light Radiation Signals. Top to Bottom: TLR (100 mv/cm) and ULR (200 mv/cm) both at 200 $\mu$ /cm, and TLR (100 mv/cm) and ULR (200 mv/cm) both at 2 ms/cm . . . . .	10
3.2	DICE THROW Fireball Sequence, Time Between Frame Approximately 40 $\mu$ s, DRI Station No. 2 . . . . .	11
3.3	Pyl and Mod Pyl Signals at 500 $\mu$ s/cm; Top to Bottom: Band 3 (100 mv/cm), Band 2 (100 mv/cm), ULR (Mod Pyl) (200 mv/cm) and Band 1 (50 mv/cm). . . . .	25
3.4	Time-Integrated DICE THROW Spectrum, Sodium and Mercury Calibration Spectra . . . . .	29
3.5	Fireball and Shockwave From PDT 11-2, 123-Ton AN/FO, HEC, L/D = 0.75 . . . . .	33
3.6	DICE THROW Fireball and Shockwave, DRI Camera Station No. 2 . . . . .	34
3.7	DICE THROW Fireball, Shockwave and Surface-Surge Anomalies (Right 208° & Left 329°) Technical O.P. . . . .	37
3.8	DICE THROW Surface-Surge Anomaly (344°), DRI Camera Station No. 4 . . . . .	38
3.9	Wilson Type Clouds Above DICE THROW Fireball and Surface-Surge Anomalies (208° and 344°), DRI Camera Station No. 4 . . . . .	39
3.10	Aerial Photograph Showing DICE THROW Fireball, Anomalies and Dust Jets at 320 ms . . . . .	41
3.11	Dust Jet Ahead of DICE THROW Shockwave Right of SGZ at 100.7 ms, DRI Station No. 2 . . . . .	42
3.12	DICE THROW Shockwave Arrival Times, Left and Right of SGZ, DRI Station No. 1 . . . . .	43

# LIST OF ILLUSTRATIONS (Continued)

<u>Figure</u>		<u>Page</u>
3.13	DICE THROW Shockwave Arrival Times, Left and Right of SGZ, DRI Station No. 2 . . . . .	44
3.14	DICE THROW Shockwave Arrival Times, Left and Right of SGZ, DRI Station No. 3 . . . . .	45
3.15	DICE THROW Shockwave Arrival Times, Left and Right of SGZ, DRI Station No. 4 . . . . .	46
3.16	DICE THROW Shockwave Arrival Times Along BRL Gage Line 1 and Left of SGZ From DRI Station No. 2 . .	47
3.17	DICE THROW Shockwave Arrival Times Along BRL Gage Line 2 and Right of SGZ From DRI Station No. 1 . .	48
3.18	DICE THROW Shockwave Arrival Times Along BRL Gage Line 3 and Right of SGZ From DRI Station No. 3 . .	49
3.19	DICE THROW Average Shockwave Arrival Times Along BRL Gage Lines 1 and 3 and Pre-DICE THROW 11-2 Average Scaled Arrival Times . . . . .	51

## LIST OF TABLES

<u>Table</u>	<u>Page</u>
2.1 DRI Instrumentation Details . . . . .	6
3.1 Charge Information From DT, PDT 11-2 and PDT 1-4 . . . . .	8
3.2 Tabulation of LLL Pin and Rate Stick Measured, and DRI Photoelectrically Measured and Photographically Interpreted Average Detonation Velocities Through the DT Charge . . . . .	17
3.3 Peak Amplitudes and Times of Total Light Radiation from DT, PDT 11-2, PDT 1-4, PDT 11-1 and PF Scaled to the DT Event . . . . .	21
3.4 The Average Temperature-Time Values From DICE THROW Event . . . . .	26
3.5 The Average Temperature-Time From DICE THROW Event Compared to PRAIRIE FLAT Event . . . . .	27
3.6 DT Times, Distances and Peak Pressure Regions Where the Main Shockwave Passed the Surface-Surge Fireball Expansion . . . . .	31
3.7 DICE THROW Times, Direction, Distance, Peak Pressure Regions Where the Main Shockwave Passed the Surface- Surge Anomalies . . . . .	36
3.8 Arrival Time and Peak Pressure Versus Distance Along BRL Gage Line 1 . . . . .	53
3.9 Arrival Time and Peak Pressure Versus Distance Along BRL Gage Line 2 . . . . .	54
3.10 Arrival Time and Peak Pressure Versus Distance Along BRL Gage Line 3 . . . . .	55
3.11 Fireball Dimensions After Stabilization From PDT 1-4 and 11-2 Scaled to DT . . . . .	56
3.12 Cloud Dimensions From DT Event With Scaled-up Values From PDT 11-2 and PDT 1-4 Events . . . . .	59

## SECTION I

### INTRODUCTION

#### 1.1 OBJECTIVES

The objectives of this project were to record the early-, intermediate-, and late-times detonation phenomenon from the DICE THROW (DT) Event using photographic and photoelectric devices and to analyze and compare the results with similar data obtained from ammonium nitrate/fuel oil (AN/FO) detonations of Pre-DICE THROW I and II (PDT I and II) Series and with data procured electronically from the same DT Event.

The Pre-DICE THROW I Series was a 5-ton trinitrotoluene (TNT) equivalent AN/FO developmental program for the design of the charge configuration for the Pre-DICE THROW II, Event 2 (PDT II-2) 100-ton TNT equivalent AN/FO event, that in turn was the forerunner of the DT Event which is the basis of this report.

#### 1.2 BACKGROUND AND THEORY

The Denver Research Institute (DRI) participated in the events of PDT I and II from which similar information was derived (Refs. 1 and 2). The charge configuration for the AN/FO detonations in PDT I and II programs were hemispherical-ended cylinders (HEC's). The designs were based on cylindrical charge data obtained from pound-size charges (Ref. 3) to which were added simultaneous, multi-initiation schemes on the cylindrical axes. The purpose of the axial initiations was to generate a near vertical shockwave along the air-surface interface void of any perturbations (jets) as those generally created by center-initiated

TNT spheres (Refs. 4 and 5).

Three AN/FO charges in the PDT I Series had length-to-diameter (L/D) ratios for Events 2, 3 and 4 of 0.84, 0.50 and 0.75, respectively with five-point initiations for Events 2 and 3 and seven-point for Event 4. The L/D ratios and initiation schemes were varied until similar cratering and free-field shockwave characteristics were obtained as was procured from the detonation of equivalent TNT spheres. The AN/FO weights were adjusted by a factor of 1.2 times the weight of a center initiated TNT sphere. Event 4 of the PDT I Series (PDT I-4) did produce all the desired shockwave and cratering characteristics; as a result, its charge design was used as a model in the scaled-up event of PDT II-2. Both of these events' detonation parameters will be compared to the output parameters obtained from the DT Event.



## SECTION II

### PROCEDURE

#### 2.1 EXPERIMENTAL SETUP

The DICE THROW Event was a 628-ton AN/F0 HEC charge detonated approximately 12 miles south of the White Sands Missile Range (WSMR) northern boundry on October 6, 1976 at 8:00 AM. The two primary objectives of the experiment were to provide a simulated nuclear blast and shock environment for military targets and to confirm empirical predictions and theoretical calculations for shock response of military structures, equipment, and weapons (Ref. 6).

The charge geometry for DT Event was a HEC constructed from bags of prilled ammonium nitrate with 6 percent No. 2 diesel fuel oil (94/6) weighing approximately 22.7 kilograms (kg) or 50 pounds (lb) apiece. The total weight of explosive, the bags and the seven-point initiation system was 569,967 kg (628.27 tons). The increase in the weight over the anticipated 600-tons was due to compaction. In order to have completed the construction of the hemispherical end (cap) of the charge, it was necessary to add the extra tonage. See Figure 2.1. The wooden support structures in the photograph were being removed by the workmen. Upon removal of the support structures, the whole charge was left free standing in a similar manner as the upper portion of the charge. Loose AN/F0 was placed in the internal voids between the bags during its assembly, none of which is visible in the photograph.

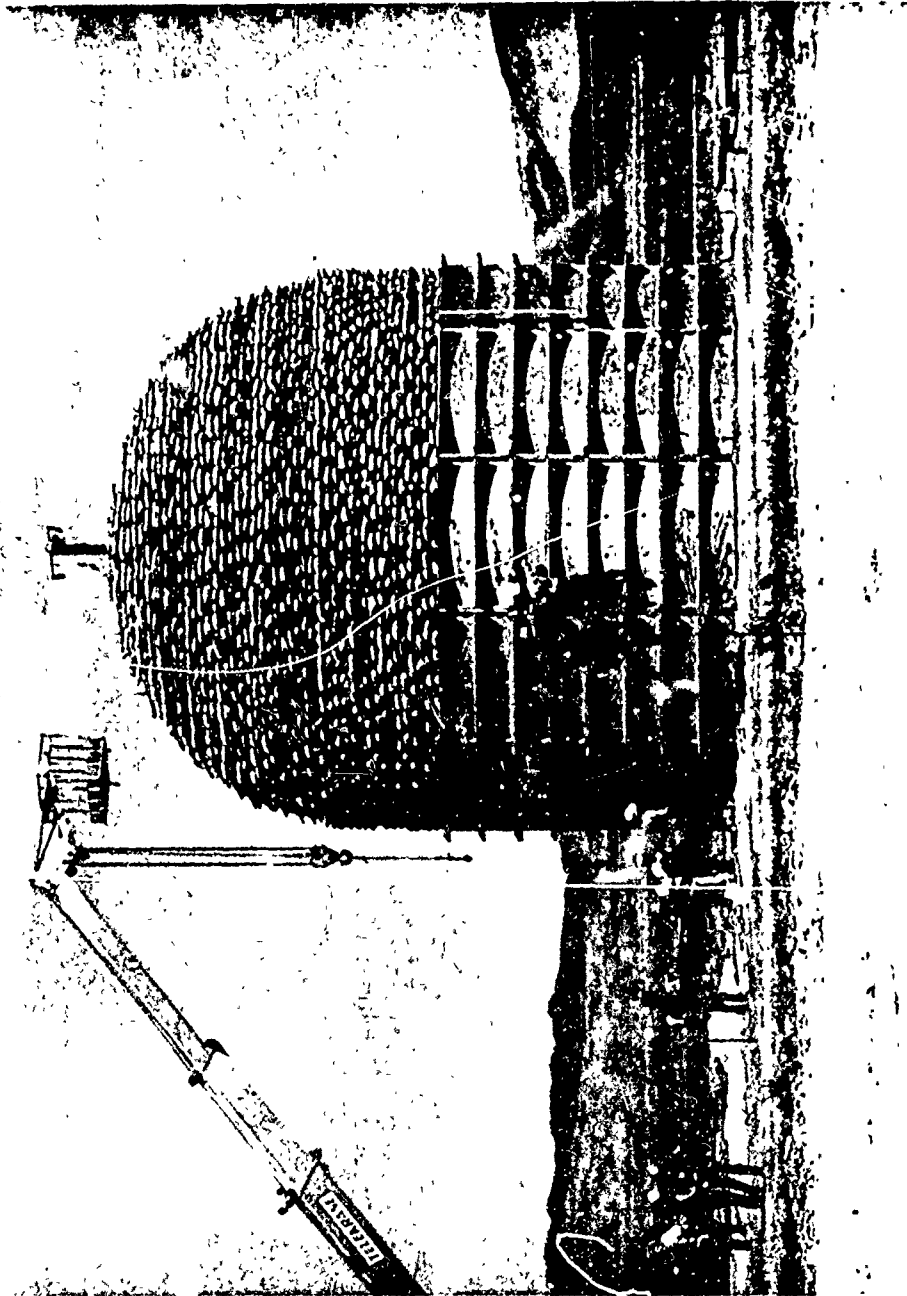


Figure 2.1. DICE THROW 628.3-Ton AN/F0 HEC,  $L/D = 0.71$ , Support Structures Removed Before Detonation.

## 2.2 INSTRUMENTATION AND FIELD OPERATION

The DRI instrumentation for the DT Event consisted of 28 high-speed cameras, whose framing rates ranged from 20 to 26,000 frames per second, one spectrograph and three photoelectric devices. The cameras were located at four stations approximately 1,372 meters (m) or 4,500 feet (ft) from surface ground zero (SGZ) at 270, 192, 138 and 90 degrees from north for stations 1 through 4, respectively. Station 2, which was the main camera station, also housed the spectrographic and photoelectric units. Table 2.1 presents specific information on the instrumentation utilized by DRI. The photoelectric output traces were recorded on three four-beam oscilloscopes. All cameras had LED's and solid-state oscillators for recording timing markers on the films except for the two Dynafax cameras whose framing rates were determined from direct readouts on a counter unit located in a manned bunker near the main camera station. Figure 2.2 presents the DRI camera station positions relative to the Ballistic Research Laboratories (BRL) gage lines. It should be noted each one of the BRL gage lines was near perpendicular to the line-of-sight of one or more of the DRI camera stations.

TABLE 2.1

## DRI Instrumentation Details

No.	Type	Timing (Hz)	Approximate Framing Rate (fr/s)	Lens (mm)	Film**	View***
1	Fastax	1,000	4,500	50	EF	Shockwave Breakout Left SGZ
2	Fastax	1,000	4,500	50	EF	Shockwave Breakout Right SGZ
3	DB Milliken	100	250	25	EF	Fireball/cloud
4	Fastax	1,000	4,500	50	EF	Shockwave Breakout Left SGZ
5	Nova	1,000	4,500	50	EF	Shockwave Breakout Right SGZ
6	Locam	100	500	18	EF	Fireball/cloud
7	Hycam	1,000	24,000	50	EIR	Fireball
8	Hycam <sup>1</sup>	1,000	6,000	35	IR	Fireball
9	Hycam <sup>1</sup>	1,000	6,000	25	IR	Fireball
10	Hulcher	100	20	150	EF	Fireball/cloud
11	Hulcher	100	20	150	SB	Fireball/cloud
12	Hulcher	100	20	150	SB	Left SGZ, Fireball/Ejecta
13	Hulcher	100	20	150	SB	Right SGZ, Fireball/Ejecta
14	DB Milliken	100	128	10	EF	Fireball/cloud
15	Dynafax <sup>2</sup>	-	26,000	240	SB	Fireball
16	Dynafax <sup>2</sup>	-	26,000	150	SB	Fireball
17	Optical Pyrometer (Pyl) <sup>4</sup>	-	Rise Time $\approx 3 \mu\text{sec}$	240	-	Temperature-Time
18	Modified Pyl <sup>4</sup>	-	Rise Time $\approx 3 \mu\text{sec}$	240	-	Unit Radiation - Time
19	Solarcell <sup>4</sup>	-	Rise Time $\approx 3 \mu\text{sec}$	-	-	Total Radiation - Time
20	Spectrograph	-	Time-Integrated	-	SB	Spectra 300 nm to 700 nm
21	Fastax	1,000	4,500	50	EF	Shockwave Breakout Left SGZ
22	Fastax	1,000	4,500	50	EF	Shockwave Breakout Right SGZ
23	DB Milliken <sup>3</sup>	100	200	17	EF	Fireball/cloud
24	Fastax	1,000	4,500	50	EF	Shockwave Breakout Left SGZ
25	Fastax	1,000	4,500	50	EF	Shockwave Breakout Right SGZ
26	DB Milliken	100	400	16	EF	Fireball/cloud
27	Hulcher	100	20	240	SB	Left SGZ, Fireball/Ejecta
28	Hulcher	100	20	240	SB	Left 500 ft., Fireball/Ejecta
29	Hulcher	100	20	240	SB	Right SGZ, Fireball/Ejecta
30	Hulcher	100	20	240	SB	Right 500 ft., Fireball/Ejecta
31	Hulcher	100	20	150	SB	Left SGZ, Fireball/Ejecta
32	Hulcher	100	20	150	SB	Right SGZ, Fireball/Ejecta

<sup>1</sup> Station 1 (1-3), Station 2 (4-20), Station 3 (21-23), Station 4 (24-32)

\*\* Ektachrome EF (EF), Linagraph She'llburst (SB), Ektachrome Infrared (EIR) Infrared (IR)

\*\*\* All views charge centered unless otherwise specified.

<sup>1</sup>Lost Processing

<sup>2</sup>Direct Readout

<sup>3</sup>Out-of-focus

<sup>4</sup>Sensing unit silicone solarcell (SPR-508), manufactured by International Rectifier Company,  
50% points of 525 and 995 nm, peak at 825 nm

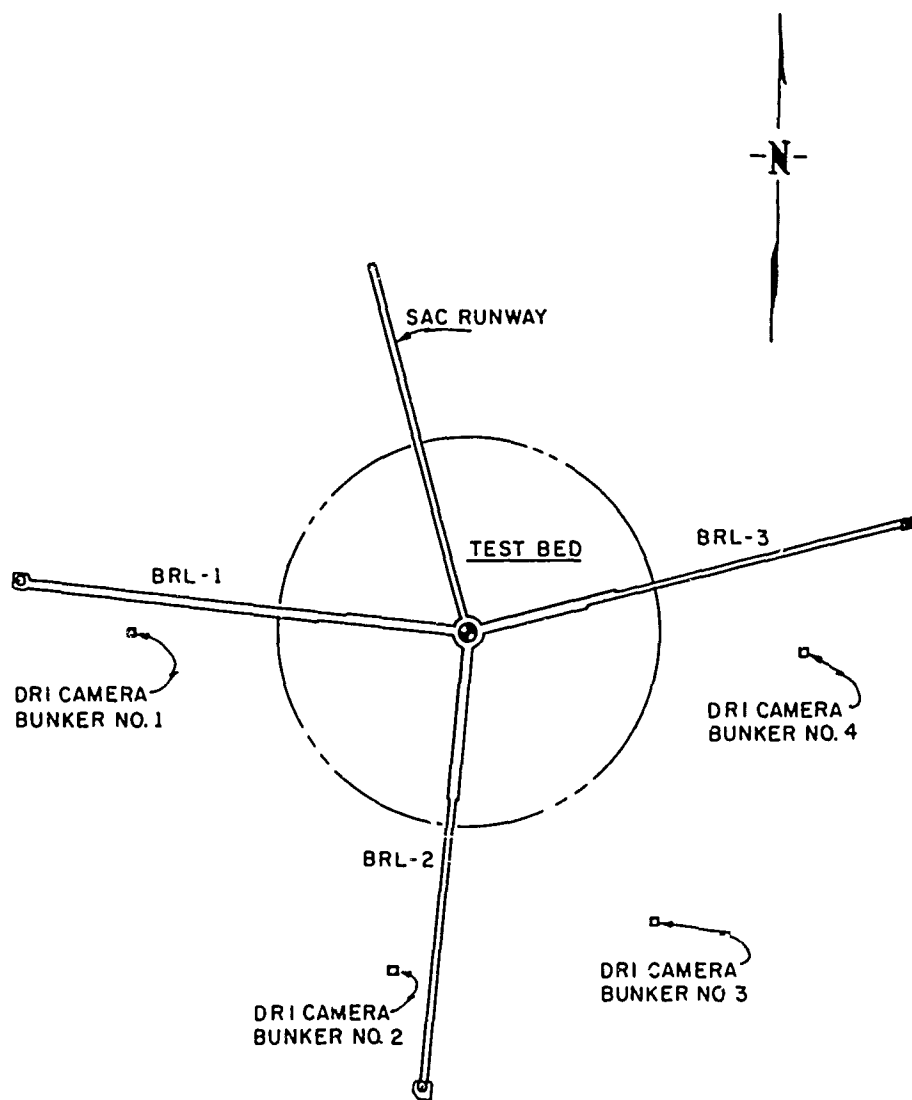


Figure 2.2. Plan View of DRI Camera Stations Relative to SAC and BRL Range Lines.

## SECTION III

### RESULTS AND DISCUSSION

The data presented in this report are based on information obtained from photographic and photoelectric records. Whenever possible these data are compared to similar data procured electronically. In addition, comparisons are made to selected AN/F0 data derived from PDT 11-2 and 1-4 Events for the purpose of substantiating the cube root scaling by weight of the detonation parameters from HEC charges. Charge information on these and the DT Event are presented in Table 3.1. All charges were seven-point initiated HEC's having L/D ratios of approximately 0.75. The scaling factors are based on the DT charge weight.

TABLE 3.1

Charge Information From DT, PDT 11-2 and PDT 1-4

Event	Total Weight		Individual Weight		Radius*		Scaling Factor
	(kg)	(lb)	(kg)	(lb)	(m)	(ft)	
DT	569,954	1,256,540	22.7	50	4.60	15.10	1.000
PDT 11-2	112,148	247,240	22.7	50	2.66	8.74	1.719
PDT 1-4	5,079	11,197	6.8	15	0.96	3.14	4.823

\* Nominal radius - cylinder truncated-base: 4.68 m (15.35 ft)-  
Top: 4.53 m (14.85 ft)

The output parameters associated with the DT Event are presented in the following paragraphs in a sequence which was indicative of the detonation process, i.e., from initiation to cloud development and rise.

### 3.1 DETONATION VELOCITIES

There were three photoelectric devices employed during DT Event whose outputs were recorded on 12 oscilloscope channels with sweep speeds that ranged from 200 microseconds/centimeter ( $\mu\text{s}/\text{cm}$ ) to 2 millisecond/centimeter ( $\text{ms}/\text{cm}$ ). The time between start of the trace and the first indication of a positive rise in the light radiation signal was used in the calculation of the average detonation velocity through the explosive. (Refs. 7 and 8). A (+) 5  $\mu\text{s}$  delay in the line transporting the detonation zero (Det Zero) signal, which started the oscilloscopic traces, was cancelled by a (-) 5  $\mu\text{s}$  light travel time from the charge to the sensors due to approximately the same travel distances involved. Figure 3.1 presents top to bottom: total light radiation (TLR), unit light radiation (ULR) both at sweep speeds of 200  $\mu\text{s}/\text{cm}$ ; and TLR, ULR signals both at 2  $\text{ms}/\text{cm}$ .

A review of Dynafax sequences indicates that the initial light breakout from the charge surface occurred nearly simultaneously at the bottom and top. It took about 80 to 120  $\mu\text{s}$  for the rest of the charge surface to completely detonate. See the Dynafax sequence in Figure 3.2. Due to this condition, the radiation signals produced by DRI's focused devices (Pyl and Mod Pyl) were not used to determine the detonation front average transit time because they were sensing light from a limited surface area at the center of the charge equidistant from its cap and base covering only about half its height. As a result, the average transit times measured from these signals were longer than the time measured from the signal obtained by the TLR device which sensed the initial detonation light breakout.

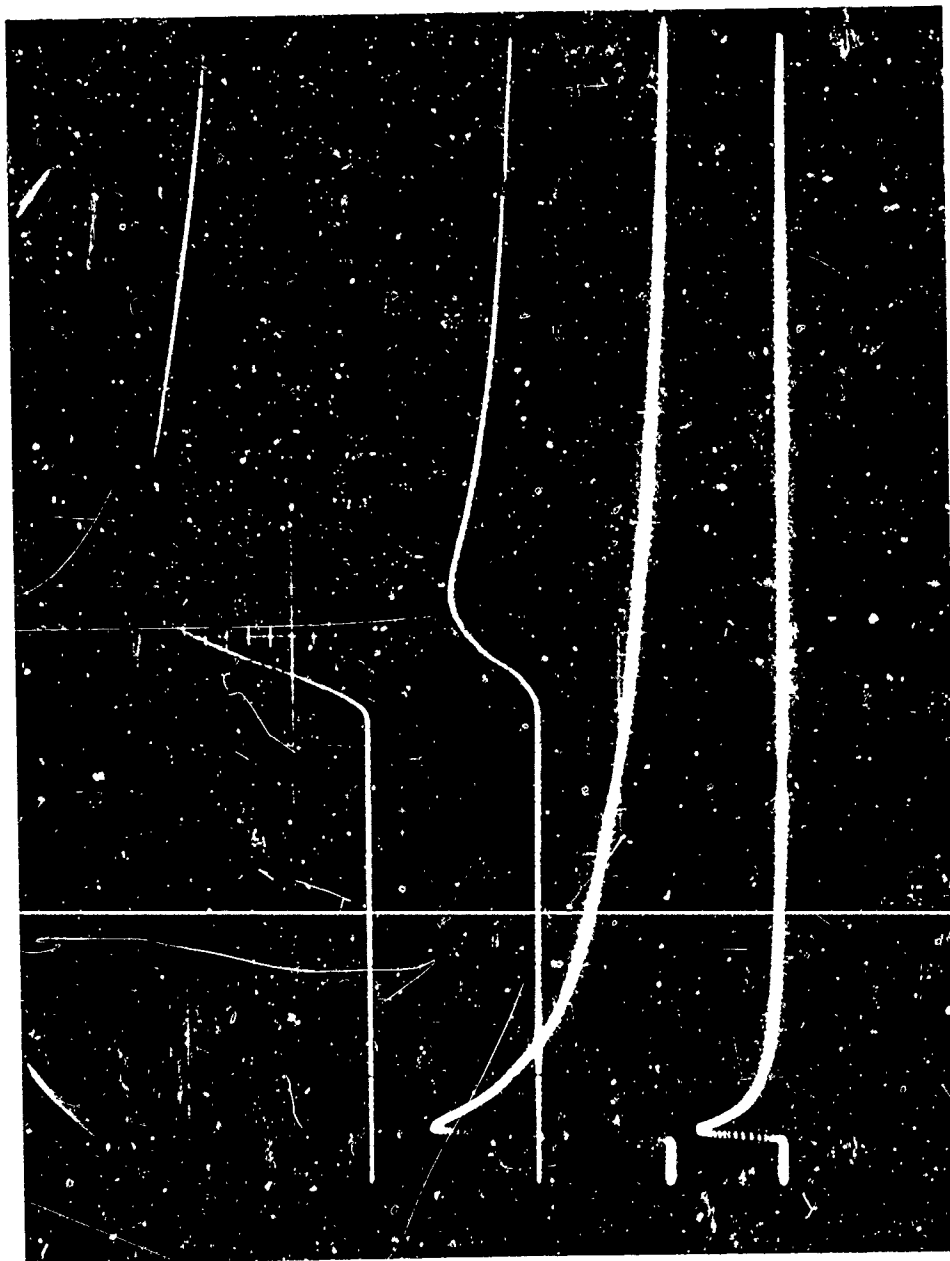
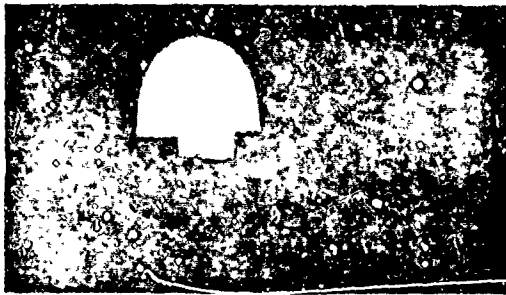


Figure 3.1. Total Light Radiation and Unit Light Radiation Signals.  
Top to Bottom: TLR (100 mv/cm) and ULR (200 mv/cm) both  
at 200  $\mu$ /cm, and TLR (100 mv/cm) and ULR (200 mv/cm)  
both at 2 ms/cm.

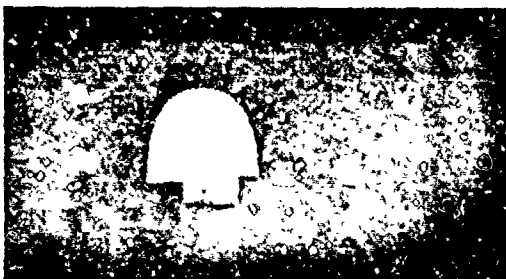




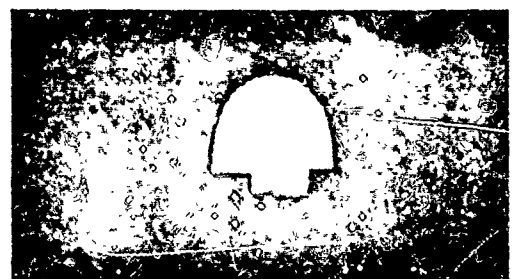
Frame 7



Frame 8



Frame 5



Frame 6



Frame 3



Frame 4

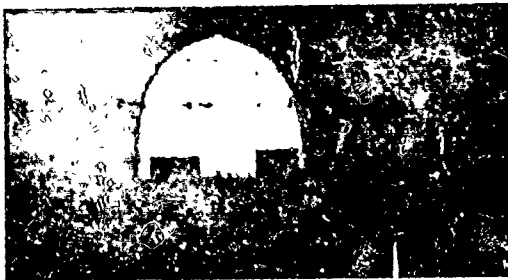


Frame 1

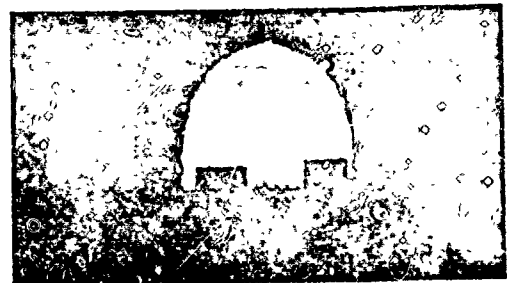


Frame 2

Figure 3.2. DICE THROW Fireball Sequence, Time Between Frame Approximately 40  $\mu$ s, DRI Station No. 2.



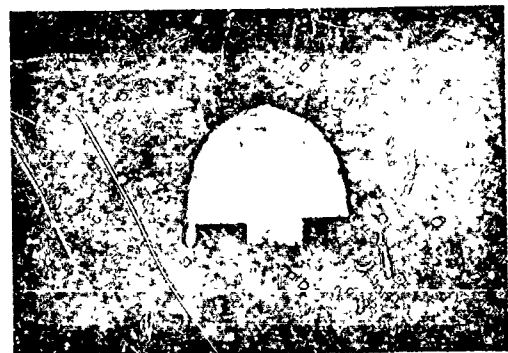
Frame 15



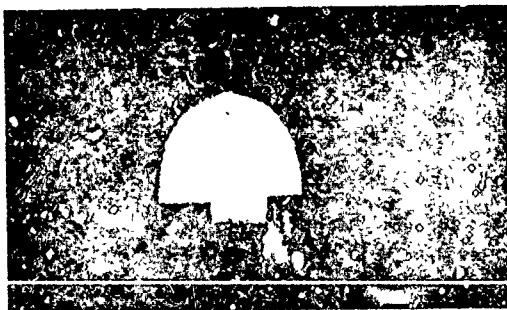
Frame 16



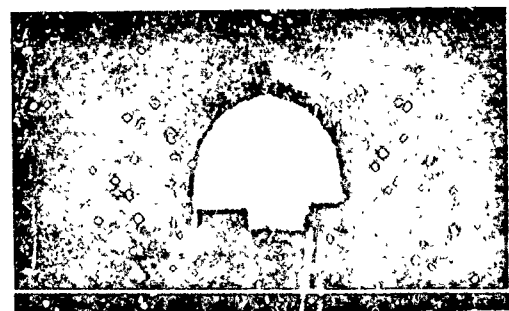
Frame 13



Frame 14



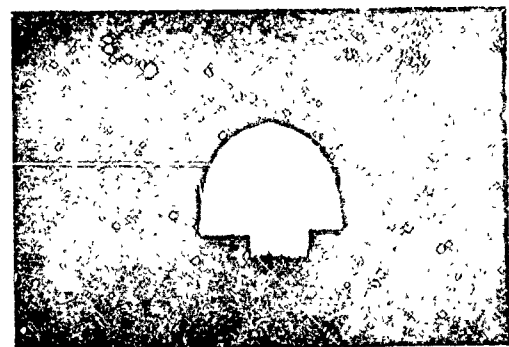
Frame 11



Frame 12

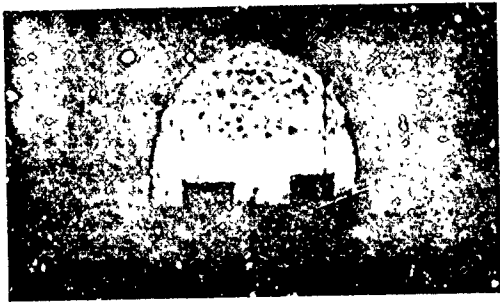


Frame 9

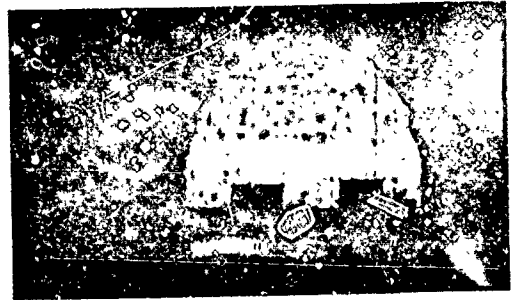


Frame 10

Figure 3.2 (Continued)



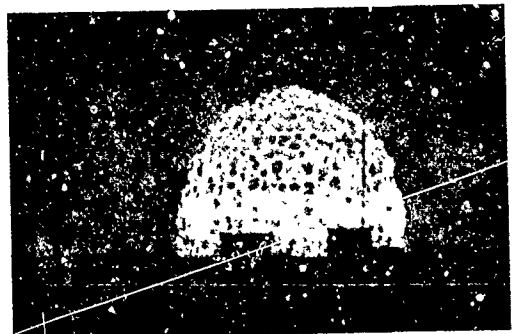
Frame 23



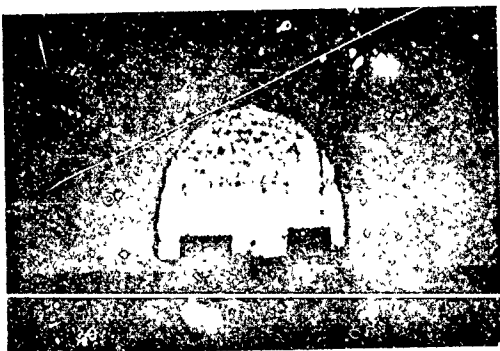
Frame 31



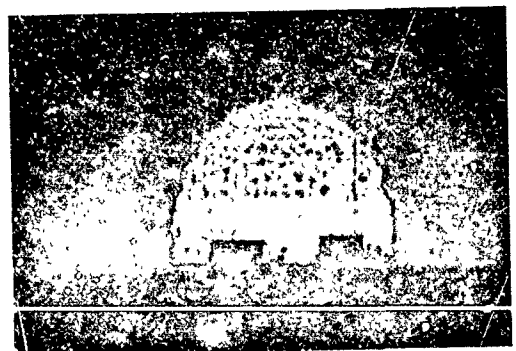
Frame 21



Frame 29



Frame 19



Frame 27



Frame 17

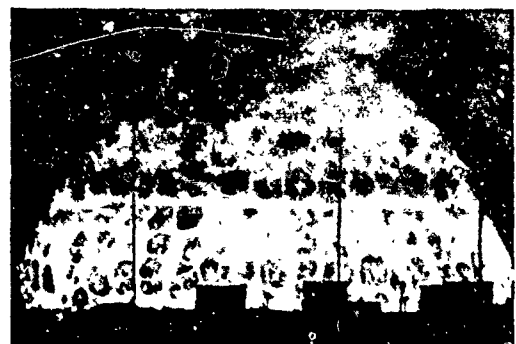


Frame 25

Figure 3.2 (Continued)



Frame 101



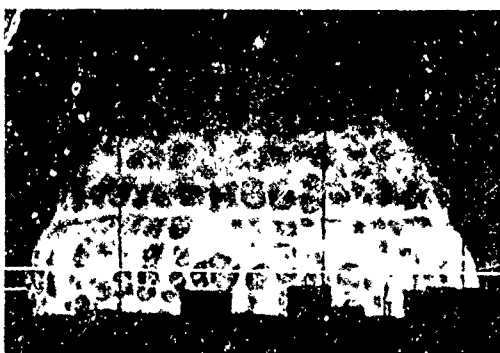
Frame 111



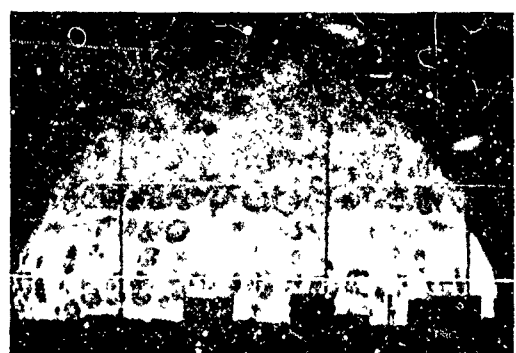
Frame 99



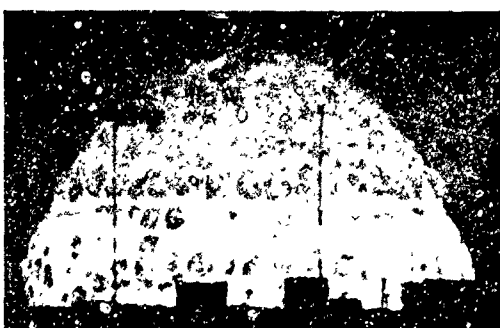
Frame 109



Frame 97



Frame 107



Frame 95



Frame 105

Figure 3.2 (Continued)

The average transit time obtained from the upper TLR trace in Figure 3.1 was 836  $\mu$ sec. Since the radius of the top of the charge (cap) was foreshortened 4.34 m (14.24 ft) and the highest booster placed higher than expected 0.38 m (1.25 ft) with respect to the top of the cylinder, the nominal distance from the booster to the center of the outer surface of the cap was 3.96 m (12.99 ft). Inasmuch as the Dynafax sequence indicated that the cap and the bottom of the charge appeared to produce detonation light at about the same instant, the TLR transit time of 836  $\mu$ s was used in the calculations of average detonation velocities for these two regions. The upper part of the stack had a calculated average velocity as low as 4,740 m/s (15,540 ft/s) while the bottom had a value as high as 5,600 m/s (18,360 ft/s) based on a radius of 4.68 m (15.35 ft) used in its calculation. These values compare to 4,750 m/s (15,570 ft/s) at the cap and 5,170 m/s (16,940 ft/s) at the base for the 120-ton AN/F0 HEC detonation of PDT 11-2 obtained from photoelectric readings and photographic interpretations. Variations in the detonation velocities from the base to the cap of a large AN/F0 HEC charge are plausible because of the density gradient within the stack (Ref. 9).

Electronic measurements of the detonation front arrival times through the AN/F0 stacks of the PDT 11-2 and DT events were made by the Lawrence Livermore Laboratory (LLL) using a long rate-sticks and a number of trigger pins (Ref. 2 and 9). The DT rate stick was 3.58 m (11.75 ft) long and was situated in a plane opposite the number 3 booster (numbered bottom to top), whose center was approximately 2.30 m (7.54 ft) from the base of the charge. The rate stick was positioned

starting near the outer surface of the charge in line with the booster center at an angle from north of  $135^{\circ}$  clockwise. Its arrival-time values gave an average detonation velocity of 5,260 m/s (17,250 ft/s) in this region of the charge (Ref. 9).

In addition to the rate stick, trigger pins were located at three radial distances: 0.86 m (2.82 ft), 1.92 m (6.30 ft) and 3.01 m (9.87 ft) opposite boosters 2 [height = 1.15 m (3.78 ft)], 4 [height = 3.45 m (11.33 ft)] and 6 [height = 5.75 m (18.88 ft)] and at azimuths of  $180^{\circ}$ ,  $240^{\circ}$  and  $60^{\circ}$ , respectively. The average detonation velocities obtained by LLL from the pin-recorded, arrival-time signals are given in Table 3.2 along with the DRI photoelectrically measured and photographically interpreted average detonation velocities. The DRI average detonation velocities listed between the two previously presented values for the charge's bottom and cap were determined by linear interpolation based on actual booster center positions.

The line-of-sight of the Dynafax camera, whose sequence is presented in Figure 3.2, was at approximately  $192^{\circ}$  so that LLL arrival-time radials at  $180^{\circ}$  and  $135^{\circ}$  were in its direction-of-view. The photographic sequences indicate light breakout from the bottom to the top of the cylindrical portion of the charge while in the cap it was from the top to the bottom where the greater cap radius existed.

The LLL rate-stick average velocity in the  $135^{\circ}$  direction (booster 3) appears to compare well with the DRI linear interpolated value to within 50 m/s. The only LLL value which appears to differ by a great amount from the DRI interpolated values is the  $180^{\circ}$  determination

TABLE 3.2  
Tabulation of LLL Pin and Rate Stick Measured, and DRI Photoelectrically  
Measured and Photographically Interpreted Average Detonation  
Velocities Through the DT Charge

Booster Number	Booster Center From Ground Surface (m)	Booster Center (ft)	LLL Average		DRI Average	
			Detonation Velocity (m/s)	Detonation Velocity (ft/s)	Detonation Velocity (m/s)	Detonation Velocity (ft/s)
1	0.06	0.21	-	-	5,600 <sup>4</sup>	18,360
2	1.15	3.80	4,570 <sup>1</sup>	14,990	5,450 <sup>5</sup>	17,880
3	2.30	7.54	5,260	17,250	5,310	17,410
4	3.44	11.28	5,010 <sup>2</sup>	16,430	5,160	16,940
5	4.56	14.97	-	-	5,020	16,470
6	5.76	18.88	4,640 <sup>3</sup>	15,220	4,870	15,980
7	6.89	22.61	-	-	4,740	15,540

<sup>1</sup> Reasonable for a short increment of 0.86 m (2.83 ft) - compares well to an AN/F0 average detonation velocity of 4,670 m/s (15,310 ft/s) obtained from PDT 1-2, 3 and 4 over an average increment of 0.97 m (3.19 ft) and to a rate stick value of 4,380 m/s (14,370 ft/s) over a distance of 0.15 m (0.5 ft) to 0.56 m (1.83 ft) from the booster (2) surface of PDT 11-2.

<sup>2</sup> Possibility that an increment of 1.92 m (6.24 ft) is not long enough to procure a true average as would be obtained over an increment out to the charge surface so that 5,010 m/s (16,430 ft/s) is a reasonable value over an increment equal to 41% of the charge radius

<sup>3</sup> Similarly as under (2) an increment of 3.01 m (9.87 ft) also may not be long enough to attain the average detonation velocity as would be obtained out to the charge surface.

<sup>4</sup> DRI photoelectrically measured and photographically interpreted values opposite boosters 1 and 7.

<sup>5</sup> Linear interpolation values opposite booster 2 through 6.

opposite booster 2 of 4,570 m/s (14,990 ft/s). Even though, this average detonation velocity is plausible since it was obtained over a relatively short distance of 0.86 m (2.82 ft) from the booster surface (Ref. 10). The average detonation velocity obtained from the PDT I AN/F0 Events, whose average charge radius was slightly greater at 0.97 m (3.19 ft), was 4,670 m/s (15,310 ft/s). In addition, the rate stick average detonation velocity from PDT II-2 opposite booster 2 at a distance from the booster surface of 0.15 m (0.5 ft) to 0.56 m (1.83 ft) was 4,380 m/s (14,370 ft/s) (Ref. 2). From all these values, it appears that the average velocity of an AN/F0 detonation over approximately the first meter from a booster, in the charge configurations used in PDT I, II and DT, are of the order of 4,500 m/s (14,760 ft/s). Considering an average detonation velocity of this value over the first meter opposite booster 2 for the DT Event, it is plausible for the detonated AN/F0 to have produced an average velocity greater than 5,400 m/s (17,710 ft/s) over the remaining charge radius of approximately 3.65 m (12 ft). The rate stick procured detonation velocity opposite booster 3 at a height = 1.14 m (3.74 ft) above booster 2 was 5,260 m/s (17,250 ft/s) which substantiates this assumption along with the photographic sequence in Figure 3.2, Frames 1 and 2.

As was mentioned previously, it appears from the Dynafax photographs that it took between 80 to 120  $\mu$ s (100  $\mu$ s average) for the charge surface to completely detonate from the base to the bottom of the cap. Considering a linear variation in the detonation front arrivals from the base, where it took 836  $\mu$ s for the detonation front to penetrate the



surface, to the surface opposite booster 6 in an assumed time of  $836 + 100 \mu s$  ( $936 \mu s$ ), the average detonation velocity at this portion of the charge would have been at least  $4,850 \text{ m/s}$  ( $15,920 \text{ ft/s}$ ) for a charge radius of  $4.54 \text{ m}$  ( $14.91 \text{ ft}$ ). This value compares very well to the DRI interpolated value and close to the LLL calculated value whose incremental time was measured over a  $3.01 \text{ m}$  ( $9.87 \text{ ft}$ ) distance from the surface of booster 6.

The surface region between booster 6 and 7 appears to have detonated last. The Dynafax photographs show this region to be brighter (Frames 6 thru 17) after detonation than the areas above and below. At a little later time period (Frames 17 thru 111) this region develops into a symmetrical bulge with a thin bright ring below the bulged region (Frames 95 thru 111). Comparable conditions existed during the PDT I-2 Event (6-ton AN/F0 HEC,  $L/D = 0.84$ ) which indicated a similar anomalous fireball feature (Ref. 1). This type of fireball perturbation was not photographed during any of the other PDT I and II Events.

### 3.2 LIGHT RADIATION OUTPUTS

Due to an unrealized breakage in the sensing element of the modified time-resolved optical pyrometer (Mod Pyl) prior to the PDT I and II Events and its subsequent repair and remodification with a new sensing element prior to the DT Event, no effort will be made here to compare the ULR signal obtained from the DT Event with this repaired and remodified unit to previous TNT and AN/F0 detonations from which ULR signals were obtained with the original unit. Direct comparisons of the DT ULR data will be deferred until further TNT and AN/F0 data are obtained with the repaired and remodified unit. Even though, a

qualitative comparison between the DT ULR and the DT TRL signals will be made. The TLR signal was recorded directly with a solarcell\* unit. Both the Pyl (time-resolved optical pyrometer), used in the temperature-time recording, and Mod Pyl employed similar solarcell elements as used in the TLR device.

Because of the utilization of a low number of recording channels and the utilization of the malfunctioning Mod Pyl unit during the PDT I and II Series, comparisons of their light radiation signals to the DT light radiation signals are only limited to the early stages of development in the TLR signal. Even though, a comparison of the later stages of development in the DT TLR signal will be made to TLR signals obtained from equivalent TNT detonations.

### 3.2.1 Total Light Radiation Output

The top and second from the bottom traces in Figure 3.1 present the TLR signal at different sweep speeds. The peak value of this signal is compared to those obtained from PDT II-2 and I-4 which are given in Table 3.3. The actual measured TLR peak amplitudes were adjusted by both the cube-root and inverse-square laws whenever the recording device was not located at the correct scaled distances for the size of charges used to produce the TLR signals. Since the DT Event is used as the standard for scaling purposes in this report, the solarcell distance to SGZ and the charge weight for this event determined the adjustment factors which were applied to the actual measured amplitudes. As an example, DT Event weight and distance were 569,954 kg (1,256,540 lb)

---

\*Silicone Solarcell (SPR-508) manufactured by International Rectifier Co.; 50% points 525 and 995 nm, peak at 825 nm.

TABLE 3.3

Peak Amplitudes and Times of Total Light Radiation from DT,  
PDT 11-2, PDT 1-4, PDT 11-1 and PF Scaled to the DT Event

Event	Scaling Factor	Device Distance		Amplitude		Time	
		(m)	(ft)	Actual (mv)	Scaled (mv)	Actual ( $\mu$ s)	Scaled ( $\mu$ s)
DT	1.000	1369	4490	212	212	298	298
PDT 11-2	1.719	1363	4471	75	220	221	380
PDT 1-4	4.823	521	1710	56	189	101	487
PDT 11-1*	1.736	1383	4537	55	170	302	524
PF*	1.000	828	2715	510	186	530	530

\*Center initiated TNT spheres

and 1,369 m (4,490 ft), respectively, while PDT 11-2 weight and distance were 112,145 kg (247,240 lb) and 1,363 m (4,471 ft), respectively. The cube-root scale factor is therefore 1.719. This value indicates that the solarcell should have been placed at  $1,369/1.719$  or 796 m (2,612 ft). Since the device for PDT 11-2 was at 1,363 m the actual measured peak value of 75 millivolts (mv) is adjusted by  $(1,363/796)^2$  to give the scaled value of 220 mv present in Table 3.3. The same procedure was used on the other actual peak amplitude values to obtain their scaled-up values.

There are excellent agreements of the TLR peak amplitudes between DT and PDT 11-2. PDT 1-4 TLR peak amplitude is down by about 13% from the average value from these two events. There is no apparent reason for the TLR to be lower since all three geometries were nearly similar. The only recognizable, minor differences between the 6-ton event and the larger events was that weight per bag was less and the bags were all plastic instead of paper with plastic liners. The adjusted TLR peak amplitude from the 100-ton TNT detonation of PDT 11-1 was 170 mv (Ref. 1); whereas, the PRAIRIE FLAT (PF) 500-ton detonation produced a TLR peak amplitude of 186 mv. (Ref. 7). Both of these values are less than the value obtained from the DT Event.

The actual times of the TLR peaks were scaled-up by multiplying their values by the scaling factors. There is an unexpected large decrease in time with an increase in charge weight. TNT spheres did not exhibit these types of changes (Refs. 1, 7 and 8). A factor which may have had a bearing on the time of formation of the TLR peak was the

average detonation velocities which increased with an increase in charge size and weight as was mentioned previously. A TLR signal signature is effected by the decay in the fireball surface temperature and its expansion rate (Ref. 8). The DT Event reached its peak between the seventh and eighth frame (280-320  $\mu$ s) of the Dynafax record in Figure 3.2. The TLR peak amplitude from DT Event occurred much sooner than it would have from an equivalent TNT which would have reached its peak at approximately 530  $\mu$ s (Ref. 11). The higher peak and faster rise of light radiation from an AN/F0 detonation may be attributed to a better oxygen balance in the AN/F0 mixture than in an equivalent TNT sphere. There is no afterburning in the AN/F0 detonation. See the second trace from the bottom in Figure 3.1. An equivalent TNT sphere, placed at the same distance from the TLR device as it was during the DT Event, would have produced a broad second peak starting from a first minimum at 1.8 ms of 113 mv to a peak of 151 mv at about 50 ms (Ref. 11).

### 3.2.2 Unit Light Radiation Output

The Mod Pyl is a device which recorded the ULR signal from the DT Event. It is a unit that is focused on a unit area of the surface of the source of radiation. The depth-of-field of the lens system is such as to keep the expanding fireball surface in focus for a relatively long period of time. In this manner the recorded radiation is independent of the total presented fireball area which varies with time. Since this unit was repaired and modified just prior to the DT Event, no comparisons of its ULR signal can be made to previously obtained TNT signals.

The ULR peak amplitude value was 158 mv at 205  $\mu$ s. A ULR amplitude comparison to the TLR amplitude has no meaning because the MOD Pyl signal is independent of distance. The ULR peak radiation occurs much sooner than the TLR peak, i.e., 205  $\mu$ s vs. 298  $\mu$ s which is to be expected since the TLR signal amplitude is dependent on the fireball surface temperature and its expanding surface while ULR signal amplitude is only dependent on the surface temperature.

### 3.3 TEMPERATURE TIME

The color temperature-time history from the DT Event was obtained with a time-resolved optical pyrometer (Pyl)\*. The Pyl is operated as a focused device which records narrow-band, radiation-time output signatures of the types shown in Figure 3.3. It was assumed that the fireball surface radiation had constant emissivity and was that of a gray body during the early stages of detonation. Time integrated spectra, which will be discussed in succeeding paragraphs, substantiates this later assumption.

The Pyl narrow bands, whose DT records are presented in Figure 3.3, had peak responses at 555 nanometers (nm) (Band 1), 625 nm (Band 2) and 725 nm (Band 3). Calibrated temperature values for the three narrow band ratios (3/1, 2/1 and 3/2) were used to determine the average color temperature-time output from the DT Event in a similar manner as described in DISTANT PLAIN (DP) and PRAIRIE FLAT (PF) reports (Ref. 8 and 11, respectively). The temperature-time values calculated from the three narrow band DT signals shown in Figure 3.3 are presented in Table 3.4.

---

\* Kottenstette, J. P., Fast-Response Optical Pyrometer Instrument, Society of America Transactions, Vol. 4, No. 3, July 1965.

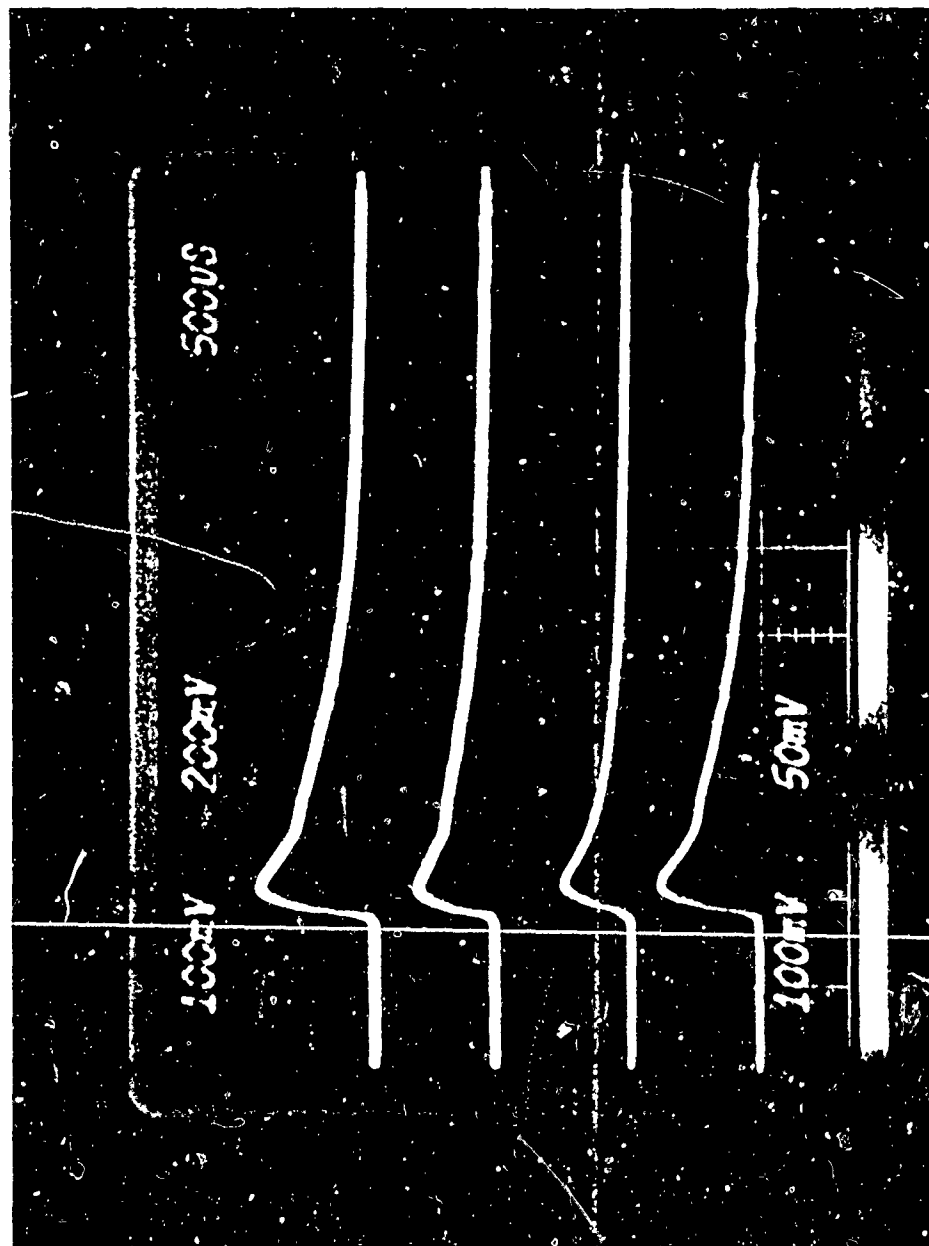


Figure 3.3. Pyl and Mod Pyl Signals at 500 us/cm; Top to Bottom: 725 nm, Band 3 (100 mv/cm); 625 nm, Band 2 (100 mv/cm); ULR, Mod Pyl (200 mv/cm) and 555 nm, Band 1 (50 mv/cm).

TABLE 3.4

The Average Temperature-Time Values From DICE THROW Event

<u>Time (<math>\mu</math>s)</u>	<u>Band Ratio</u>	<u>Ratio Value</u>	<u>Temperature (K<sup>o</sup>)</u>	<u>Average Temperature (K<sup>o</sup>)</u>
167	3/1	2.320	6800	7030
	3/2	1.520	6200	
	2/1	1.520	8100	
367	3/1	2.360	6700	6870
	3/2	1.520	6200	
	2/1	1.540	7700	
567	3/1	2.410	6600	6670
	3/2	1.525	6100	
	2/1	1.570	7300	
767	3/1	2.450	6500	6500
	3/2	1.525	6100	
	2/1	1.600	6900	
967	3/1	2.480	6450	6420
	3/2	1.530	6050	
	2/1	1.630	6750	
1167	3/1	2.530	6300	6320
	3/2	1.530	6050	
	2/1	1.660	6600	
1367	3/1	2.580	6100	6170
	3/2	1.535	6000	
	2/1	1.680	6400	
1567	3/1	2.610	6000	6030
	3/2	1.535	6000	
	2/1	1.700	6100	
1767	3/1	2.640	5900	5900
	3/2	1.540	5900	
	2/1	1.730	5900	
1967	3/1	2.690	5800	5800
	3/2	1.540	5900	
	2/1	1.760	5700	
2167	3/1	2.720	5700	5630
	3/2	1.550	5800	
	2/1	1.790	5400	



In Table 3.5 a comparison of the average temperature-time values from the DT Event is made to the values derived from the PF Event which was a 500-ton TNT sphere detonated tangent to a ground surface (Ref. 11). The comparison of DT AN/F0 detonation with the PF TNT detonation indicates a higher average color temperature of about 800°K within the time period from 100 to 600  $\mu$ s. The temperature difference between the DT and PF Events coincides with the difference in the amplitudes of their TLR signals. Because of the fact that the TLR peaks from these two events do not occur at the same time (298 vs. 530  $\mu$ s) no direct correlation can be made between their amplitudes and their surface temperatures through the application of the Stefan-Boltzman Law as was done in Ref. 8.

TABLE 3.5

The Average Temperature-Time from DICE THROW Event  
Compared to PRAIRIE FLAT Event

Time ( $\mu$ s)	DICE THROW Average Temperature (K°)	PRAIRIE FLAT Average Temperature (K°)
100	-	6200
167	7030	-
200	-	6100
300	-	6050
367	6870	-
400	-	5780
500	-	5500
600	-	5200
767	6500	-

The DT Pyl signals not only had lower ratios (higher temperatures) but their peak amplitudes were higher and their decay rate less over the first few milliseconds than was produced by an equivalent TNT sphere.

### 3.4 TIME-INTEGRATED SPECTRA

A CENCO grating spectrograph (reciprocal dispersion of 1.6 nm per mm) was used to obtain a time-integrated spectral record from the DT Event. The spectrograph looked directly at the charge whose image along its vertical axes was focused upon the entrance slit with a fused-silica lens. This procedure produces, in a sense, a time-resolved effect since a time-related spectral history is obtained as the image of the fireball expands along the slit (Ref. 8). See the DT spectral record in Figure 3.4. The DT spectrum covers the region of 315 nm to 703 nm from left to right. The sodium doublet are the 589.0 and 589.6 nm lines. The second real bright mercury line to the left of the sodium doublet is the 435.8 nm line.

The CENCO slit height was high enough to allow an expansion of the DT fireball image as can be seen by the height of the Na and Hg calibration spectra in Figure 3.4. Note that the DT spectrum height is much less than the height of the calibration lines. This condition indicates that very little spectrum height expansion occurred which is substantiated by the short but intense light duration signals recorded by the TLR and ULR devices. See Figure 3.1.

The DT spectrum contained mostly continuum far different from TNT spectra which consisted of continuum interlaced with molecular and atomic species of  $O_2$ , Na and Ca with some in absorption and some in emission (Ref. 11). The DT continuum without the effects of strong emission or absorption lines collaborates the assumption that the AN/FO radiation is that of a gray body. The DT spectrum also shows a shift



DICE THROW



SODIUM



MERCURY

Figure 3.4. Time-Integrated DICE THROW Spectrum, Sodium and Mercury Calibration Spectra.

toward the blue end of the radiation when compared to the CENCO spectrum produced by an equivalent TNT detonation (Ref. 11). This shift generally indicates a higher temperature which was verified by the DT Pyl temperature-time results when compared to those produced by the equivalent PF TNT Event. See Table 3.5.

### 3.5 SURFACE-SURGE SHOCKWAVE SEPARATION DATA

One of the most important features of a high explosive (HE) detonation at or near a surface is in the generation of a smooth and uniformly-expanding shock front in all directions away from SGZ along the air-surface interface, i.e., no anomalies (jets) along the surface-surge region. It was one of the main purposes of the PDT I developmental program to design an AN/F0 charge that would provide this characteristic. PDT 11-2 and 1-4 Events did generate uniformly expanding shockwaves void of any perturbations, unfortunately, there were anomalies generated during the DT Event whose charge was designed after those used for PDT 11-2 and 1-4 Events.

This section of the report presents data on the normal separation times and distances of the main-surface shockwave independent of the anomalies that may have existed. The information on the DT anomalies will be given in the next section. Table 3.6 presents the normal shock-wave separation data from the DT Event.

Generally, there appeared to be a uniform separation time and distance in the expansion directions indicated in Table 3.6 with the exception of 1R whose data was obtained in the direction of the major jet. The DT average separation time and distance are surprisingly much

TABLE 3.6

DT Times, Distances and Peak Pressure Regions Where the Main Shockwave Passed the Surface-Surge Fireball Expansion

Number <sup>1</sup> View	Azimuth <sup>2</sup> (degrees)	Time (ms)	Distance		Peak Pressure <sup>3</sup>	
			(m)	(ft)	(kPa)	(psi)
1L	270	31.9	90.9	298	1930	280
1R	270	42.9	104.0	341	1450	210
2L	192	40.0	94.2	309	1795	260
2R	192	33.5	87.5	287	2000	290
3L	138	36.9	95.4	313	1760	255
3R	138	32.4	89.0	292	1965	285
4L	90	33.6	92.1	302	1860	270
4R	90	<u>34.8</u>	<u>93.3</u>	<u>306</u>	<u>1825</u>	<u>265</u>
AVG.		35.8	93.3	306	1825	265
PDT 11-2 Scaled		66.1	127.0	418	780	113
PDT 1-4 Scaled		63.1	125.0	409	814	118

<sup>1</sup>Nomenclature: L (left), R (right) of SGZ

<sup>2</sup>Angular position of cameras' lines-of-sight to SGZ;  
view 90°, left or right of SGZ with respect to this value.

<sup>3</sup>Average of all three BRL gage lines (Ref. 12) in this and all succeeding tables.

shorter than the average scaled values from PDT 11-2 and 1-4. There are two conditions which existed that could have contributed to this change: (1) the average detonation velocities from the DT Event were higher due to the AN/F0 density increase in the stack and (2) the size of the individual bags of AN/F0 was not scaled-up from PDT 11-2. This later condition created a more uniform fireball surface expansion than

did PDT 11-2. Compare Figures 3.5 and 3.6 which were taken at approximately the same scaled times.

### 3.6 SURFACE-SURGE FIREBALL ANOMALIES

Ton-size TNT and Nitromethane experiments conducted in the past produced any number of luminous jets (major) and non-luminous jets (minor) (Refs. 5, 7 and 11). Similar anomalies were present during the 100-ton TNT Event of PDT 11.

The character of the anomalies photographed during some of the 6-ton AN/FO HEC events (PDT 1-2 and -3) were very different from those created during previous TNT or Nitromethane detonations. The surface-surge anomalies from the DT Event resembled the ones photographed from these events, especially those from PDT 1-2 (Ref. 1). The AN/FO fireball perturbations from PDT 1-2 and -3 not only originated near the juncture of the charge and the ground but anywhere along the entire surface of the cylindrical portion of the charge. The jets were non-luminous and became translucent as they expanded radially. Their maximum projected scaled\* distances were much greater than the majority recorded from past TNT and Nitromethane detonations. The PDT 1-2 main shockwave healed (formed one shock front) past one of the surface-surge anomalies at a scaled-up (to DT Event) distance of 485 m (1,590 ft) or in a pressure region of 4.3 psi (Ref. 1). The average scaled-up distance where the main shockwave passed five jets from PDT 1-2 was 311 m (1,020 ft); whereas, it was 254 m (834 ft) from six jets of PDT 1-3. The pressure regions for these average distances were 8.8 and 14.8 psi,

---

\*It is not known if anomalies scale. In this and previous DRI reports, they are considered to be scaleable.

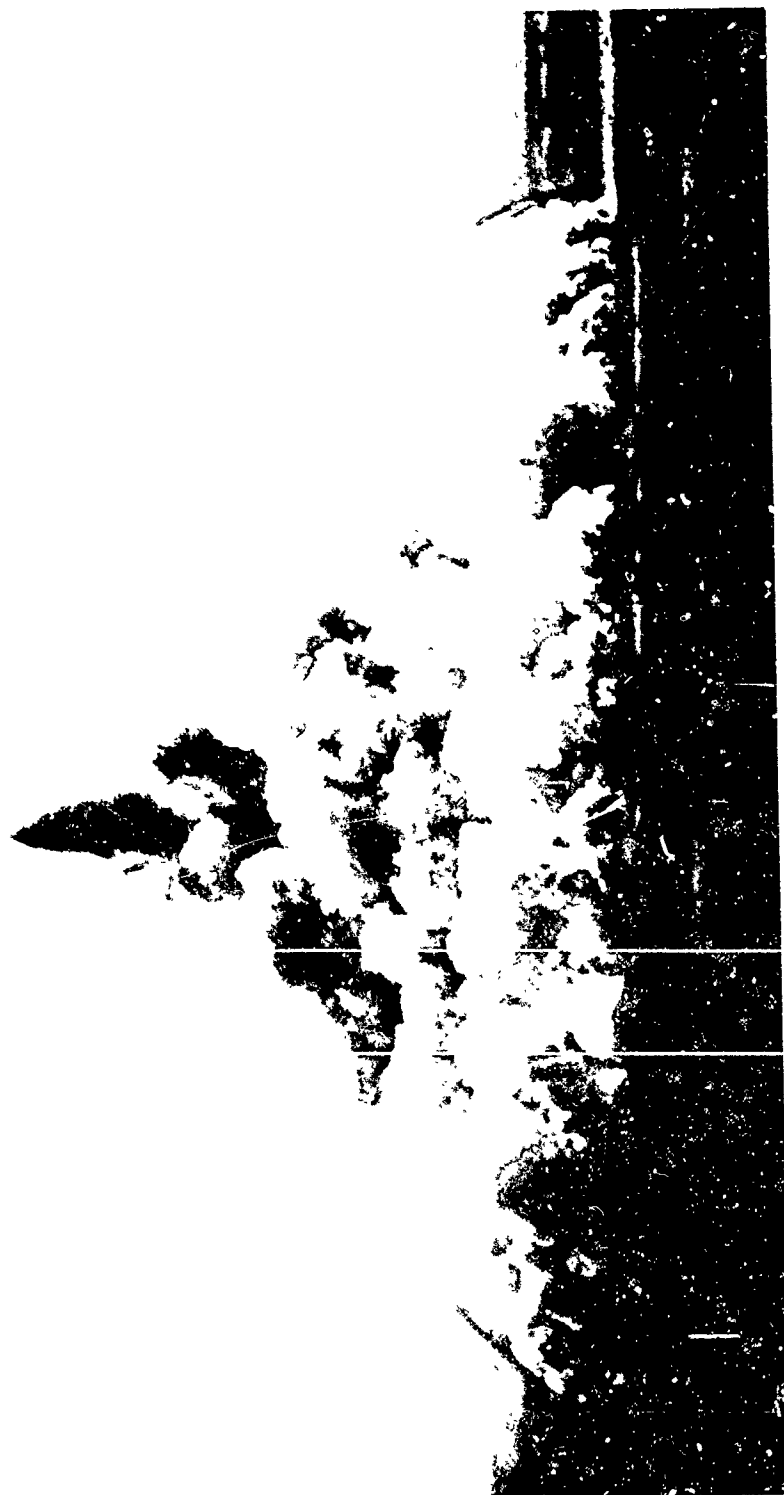


Figure 3.5. Fireball and Shockwave From PDT 11-2, 123-Ton AN/F0, HEC,  $L/D = 0.75$ .

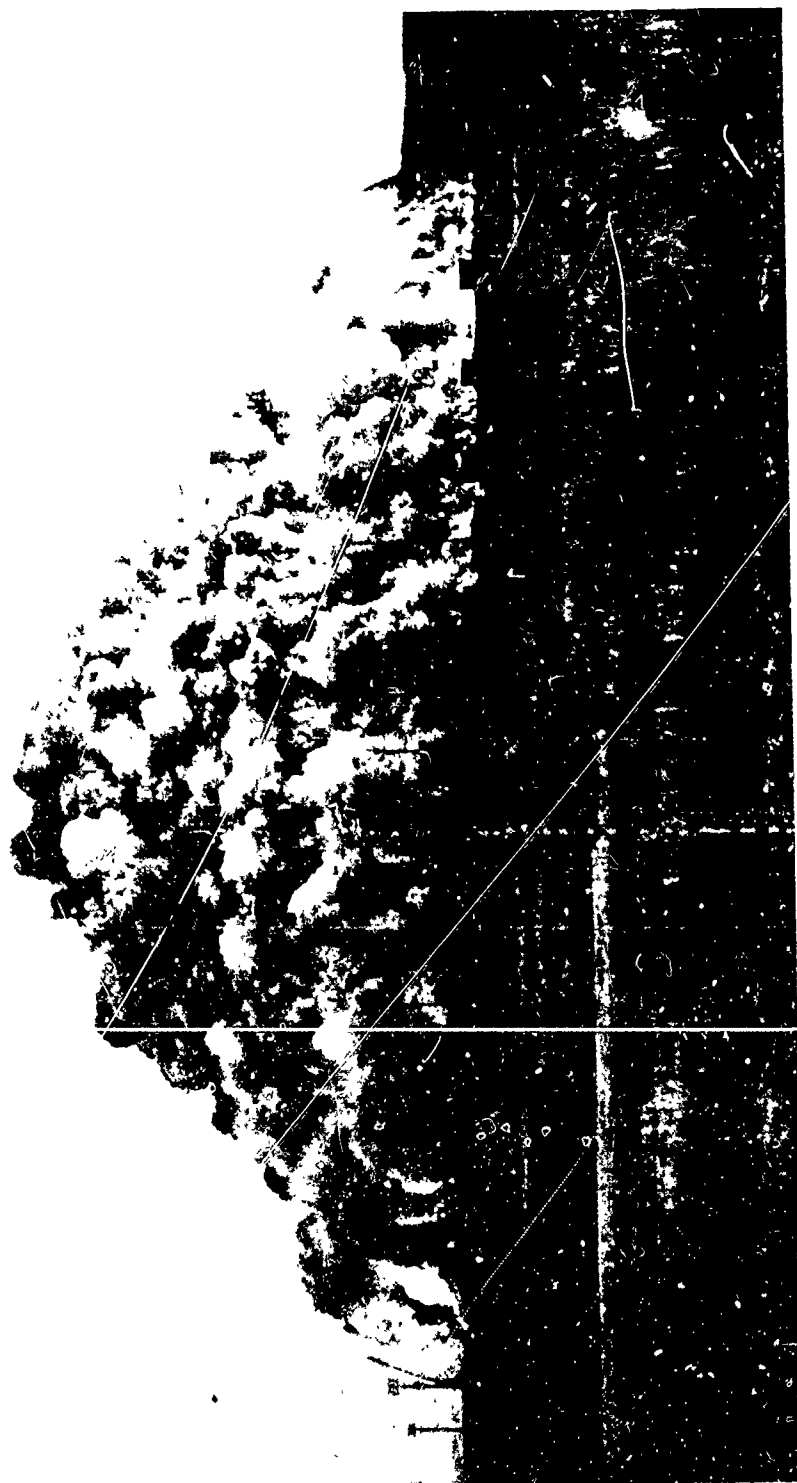


Figure 3.6. DICE THROW Fireball and Shockwave, DRI Camera Station No. 2.



respectively. The longest projected scaled-up distance of any jet from a TNT detonation photographed previously by DRI was from the MINERAL ROCK Event which extended out to 323 m (1,060 ft) or 8.7 psi (Ref. 7). The PF Event, 500-ton TNT tangent sphere, produced jets which propagated out to a maximum of 250 m (820 ft) or 16.1 psi.

The data presented in this section were derived from photographic records obtained from an aircraft station\* as well as DRI ground stations. Since the DT Event was detonated early in the morning and under semi-heavy cloud cover, some of the camera records which relied on ambient light for their spatial resolution were difficult to interpret. As a result, of all the sections presented in this report that relied on photographic information, this section was the most difficult to obtain accurate parametric data for.

Both the aircraft and ground stations' records indicated that there were three major anomalies (jets) produced from the DT Event which had similar features to those created during two of the three PDT 1 AN/F0 Events.

The front of DT jets were very pointed with their apexes approximately 10.5 m (34.4 ft) above the ground. As was mentioned previously, a symmetrical bulge developed during the early stages of the DT fireball expansion similar in character to the one created during PDT 1-2 Event that also produced corresponding jets ahead of the main surface-surge shockwave. The DT symmetrical bulge appeared to form at a height comparable to the heights of the apex of its jets. As these

---

\*Photographic records supplied by Williamson Aircraft, Santa Barbara, California.

jets expanded radially, they were nonluminous and became translucent in a manner similar to the anomalies produced during the PDT 1-2 Event. See Figures 3.7 and 3.8. Table 3.7 presents data on the three anomalies produced during the DT Event.

TABLE 3.7

DICE THROW Times, Direction, Distance, Peak Pressure Regions Where the Main Shockwave Passed the Surface-Surge Anomalies.

Film Record	Times (ms)	Direction (degrees) <sup>1</sup>	Height		Distance		Peak Pressure	
			(m)	(ft)	(m)	(ft)	(kPa)	(psi)
DRI	189	329	10.3	33.7	242	795	110	16.0
DRI	180	344	10.9	35.7	236	774	121	17.5
DRI <sup>2</sup>	168	208	10.3	33.7	221(+)	724(+)	-	-
Aircraft <sup>1</sup>	212	208	-	-	241	792	111	16.1

<sup>1</sup>F. aircraft record - other two jets were translucent during late stages of expansion. It was too difficult under the circumstances to obtain their maximum expansions due to a poor background and low ambient light.

<sup>2</sup>Went out of view of DRI's camera.

A very unusual condition occurred as the anomalies dissipated, i.e., small Wilson type clouds formed slightly above each jet near their maximum radial expansions at about the same time as a large Wilson type cloud formed at approximately the same radial distance immediately above the center of the fireball. See Figure 3.9. There were no physical connections of these small clouds to the main one above the center of the fireball. Wilson type clouds have also formed during other large HE detonations but never near the extreme expansions of anomalies associated with their fireballs.



Figure 3.7. DICE THROW Fireball, Shockwave and Surface-Surge Anomalies (right 208° and left 329°), Technical O.P.



Frame 2.  $T = 81.0$  ms



Frame 3.  $T = 130.7$  ms



Frame 4.  $T = 180.4$  ms

Figure 3.8. DICE THROW Surface-Surge Anomaly ( $344^{\circ}$ ),  
DRI Camera Station No. 4.



Figure 3.9. Wilson Type Clouds Above DICE THROW Fireball and Surface-Surge Anomalies (2080) & (3440), DRI Camera Station No. 4.

There also appeared to be an anomaly which projected in the direction of the free-air fireball expansion. Its effect upon the free-air shock front character cannot be seen; though, its debris was photographed. See Figure 3.9 to the upper left of fireball.

### 3.7 DUST JETS

There were a large number of dust jets formed slightly ahead or behind the DT surface-surge shock front. They invariably developed along radial accesses leading to SGZ. There were at least seven of these jets, many of which extend out to over 305 m (1,000 ft), mostly toward the east and southeast. See Figure 3.10\*. One of these jets, which propagated slightly ahead of the surface-surge shockwave, caused an obscuration effect on military vehicles being photographed at a distance of 229 m (750 ft) from SGZ. See Figure 3.11, right of SGZ. Five of the seven dust jets developed along radial access roads, one along BRL gage line #2, and one along the SAC runway.

### 3.8 SHOCKWAVE ARRIVAL TIMES

Shockwave arrival times were obtained photographically from the four DRI camera stations viewing right and left of SGZ from about 90 m (295 ft) to 190 m (625 ft). Arrival-times curve fits through the DRI photographic derived data are presented in Figures 3.12 thru 3.15. Curve fits procured in the directions of the three BRL gage lines are presented along with the BRL gage data in Figures 3.16 thru 3.18. There was good correlation between DRI 2L (DRI Station #2, left of SGZ) and BRL gage line #1 and DRI 3R and BRL gage line #3; and poor correlation

---

\*Photograph obtained from 16mm sequences supplied by Williamson Aircraft, Santa Barbara, California.

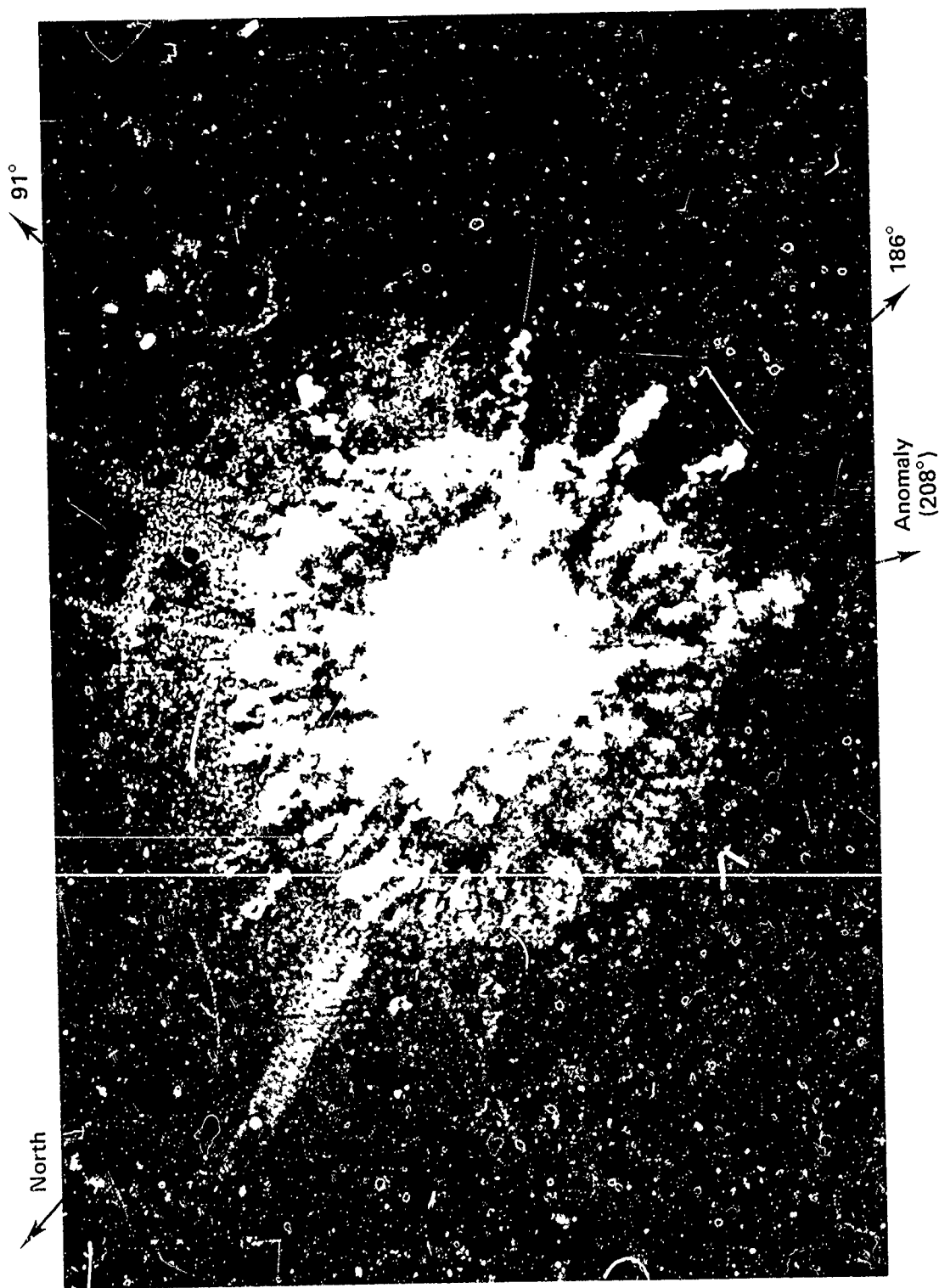


Figure 3.10. Aerial Photograph Showing DICE THROW Fireball, Anomalies and Dust Jets at 320 ms.

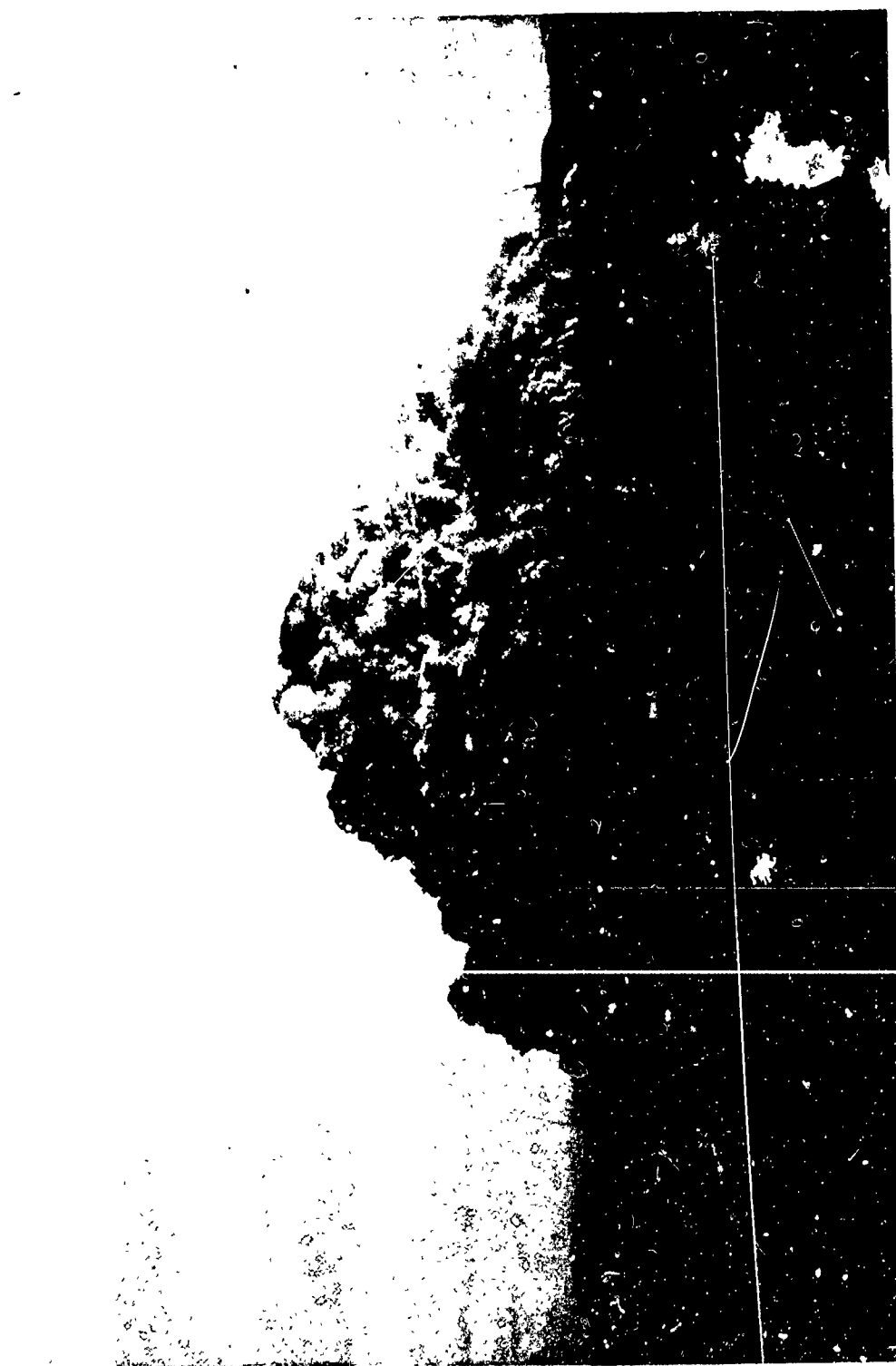


Figure 3.11. Dust Jet Ahead of DICE THROW Shockwave Right of SGZ at 100.7 ms, DRI Station No. 2.



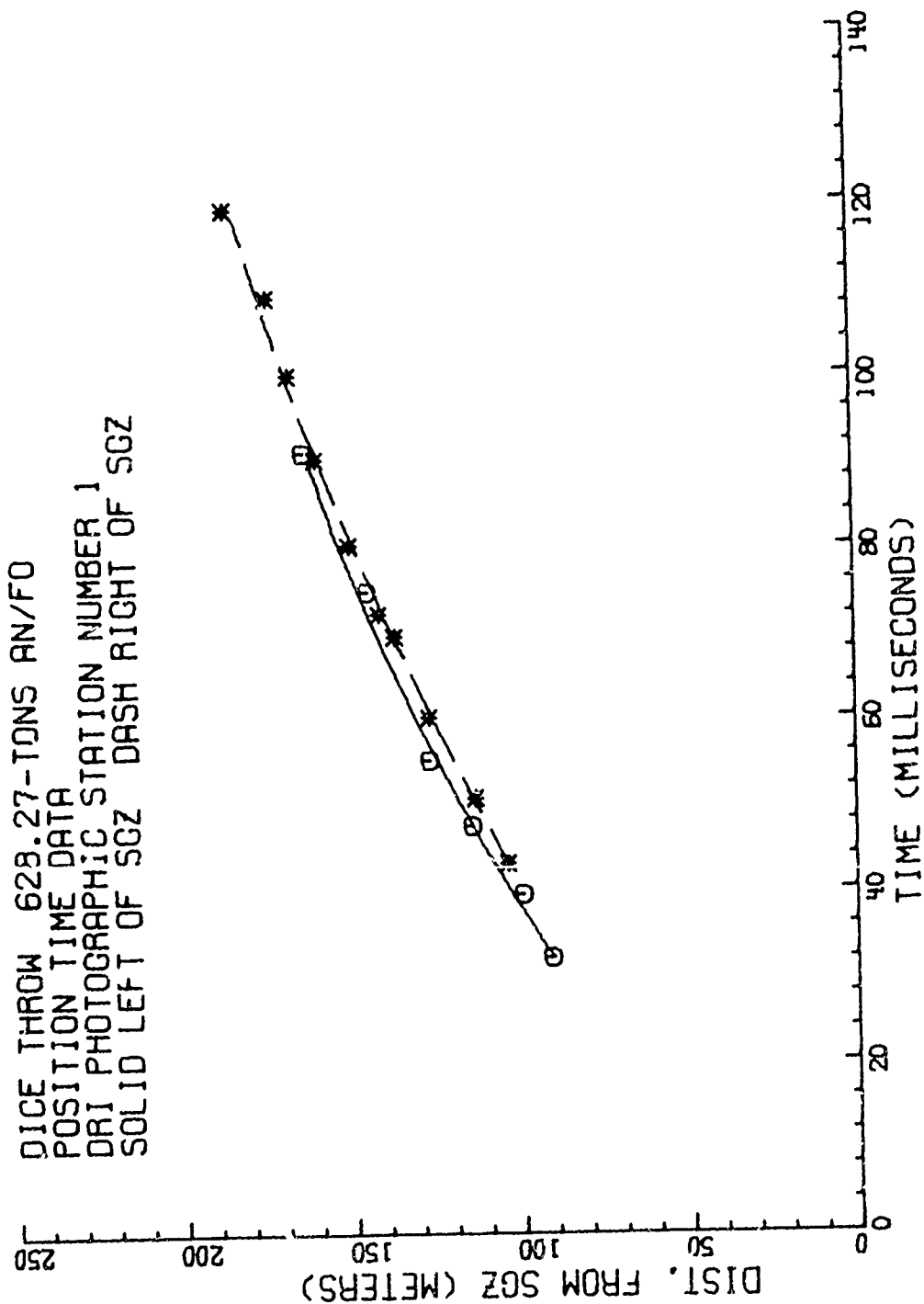


Figure 3.12. DICE THROW Shockwave Arrival Times, Left and Right of SGZ, DRI Station No. 1.

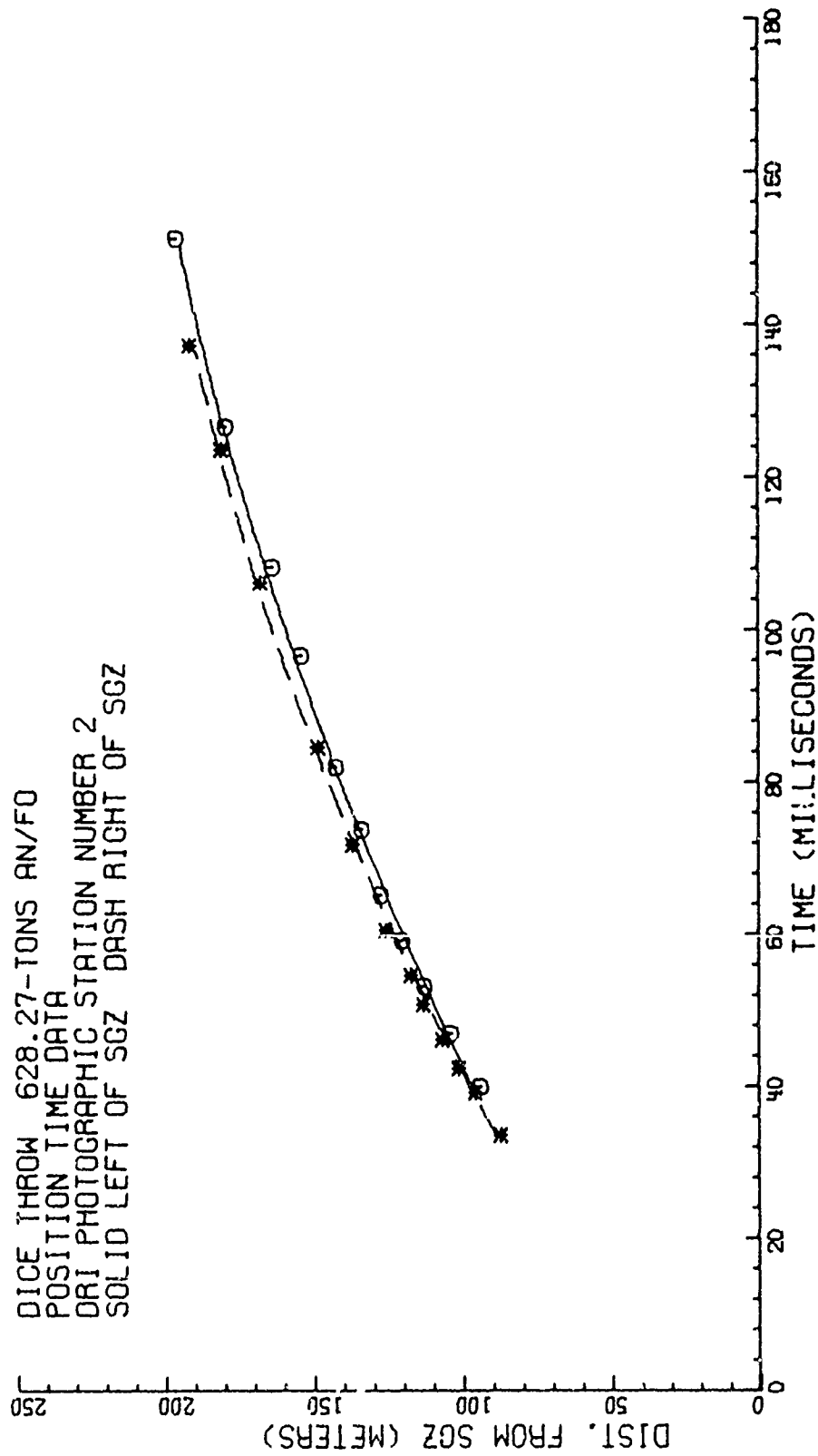


Figure 3.13. DICE THROW Shockwave Arrival Times, Left and Right of SGZ, DRI Station No. 2.

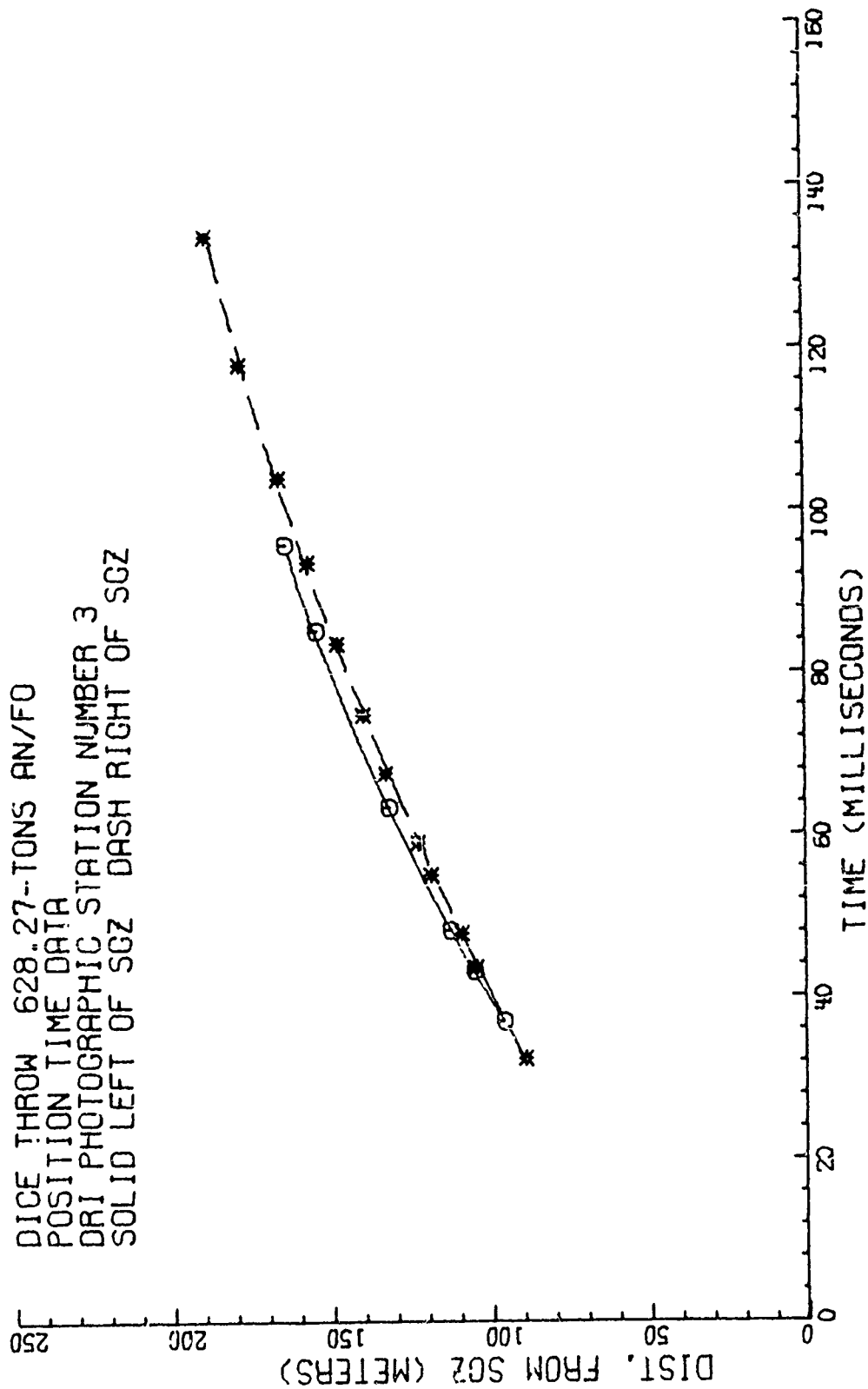


Figure 3.14. DICE THROW Shockwave Arrival Times, Left and Right of SGZ, DRI Station No. 3.

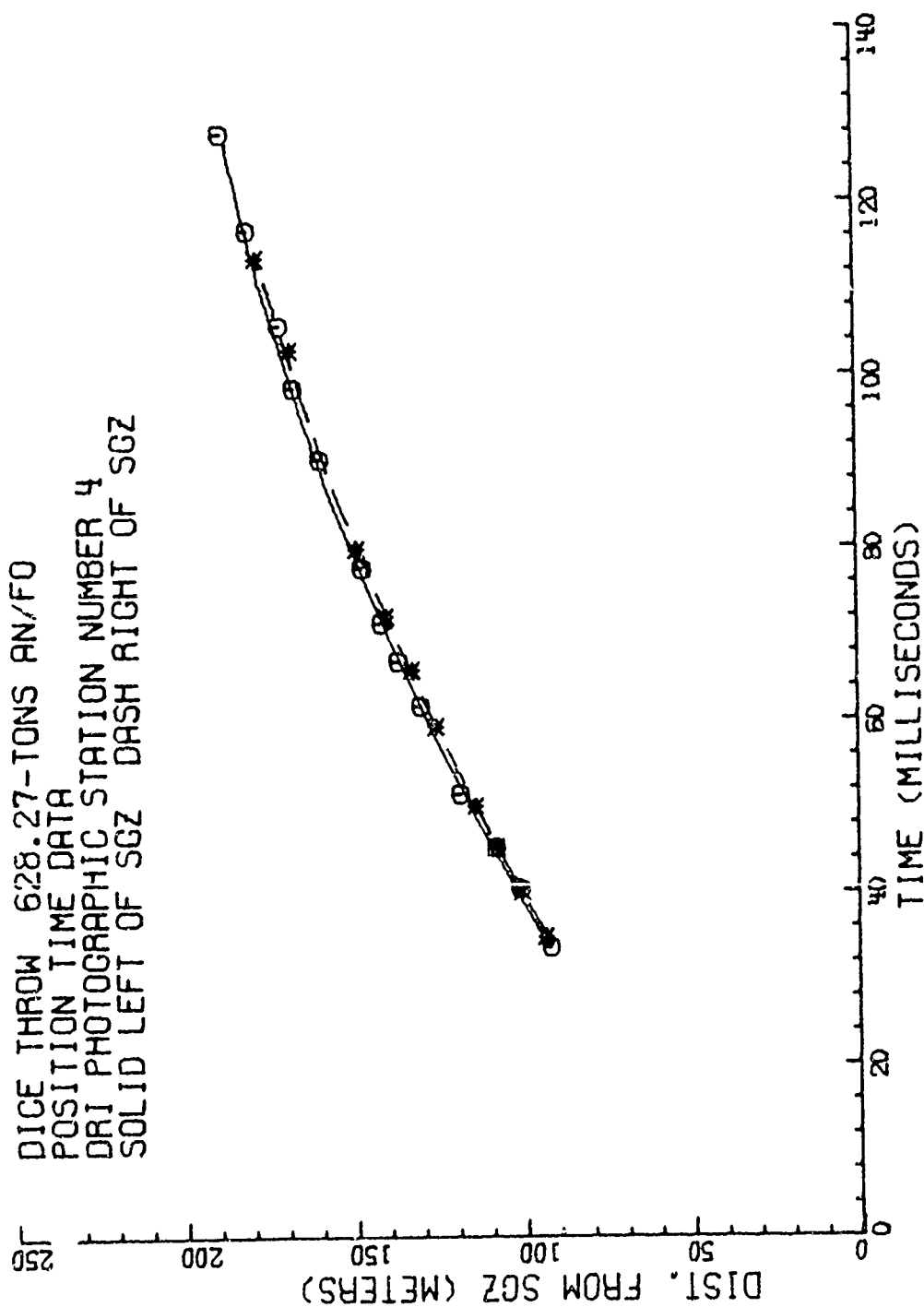


Figure 3.15. DICE THROW Shockwave Arrival Times, Left and Right of SGZ, DRI Station No. 4.

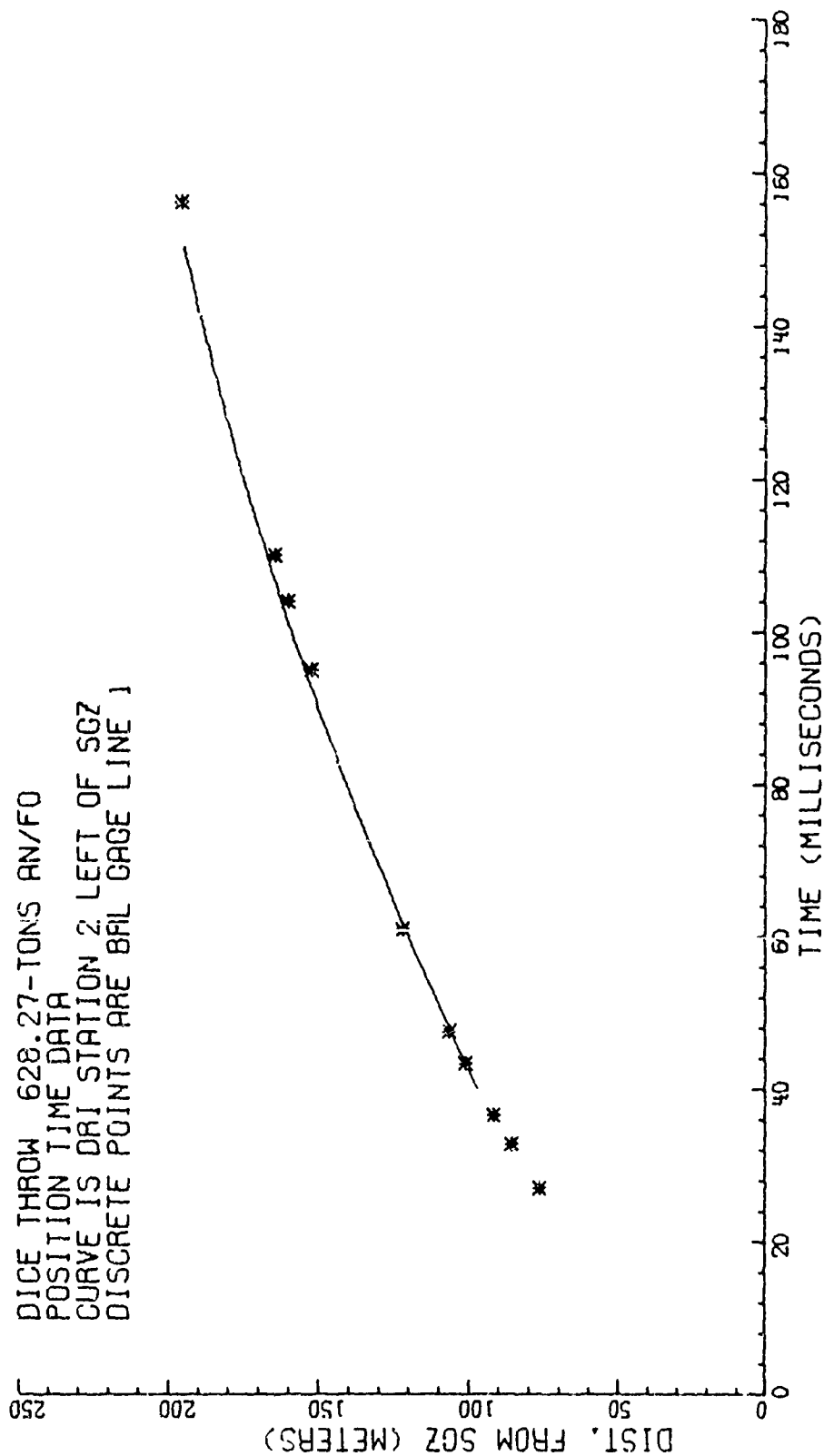


Figure 3.16. DICE THROW Shockwave Arrival Times Along BRL Gage Line 1 and Left of SGZ From DRI Station No. 2.

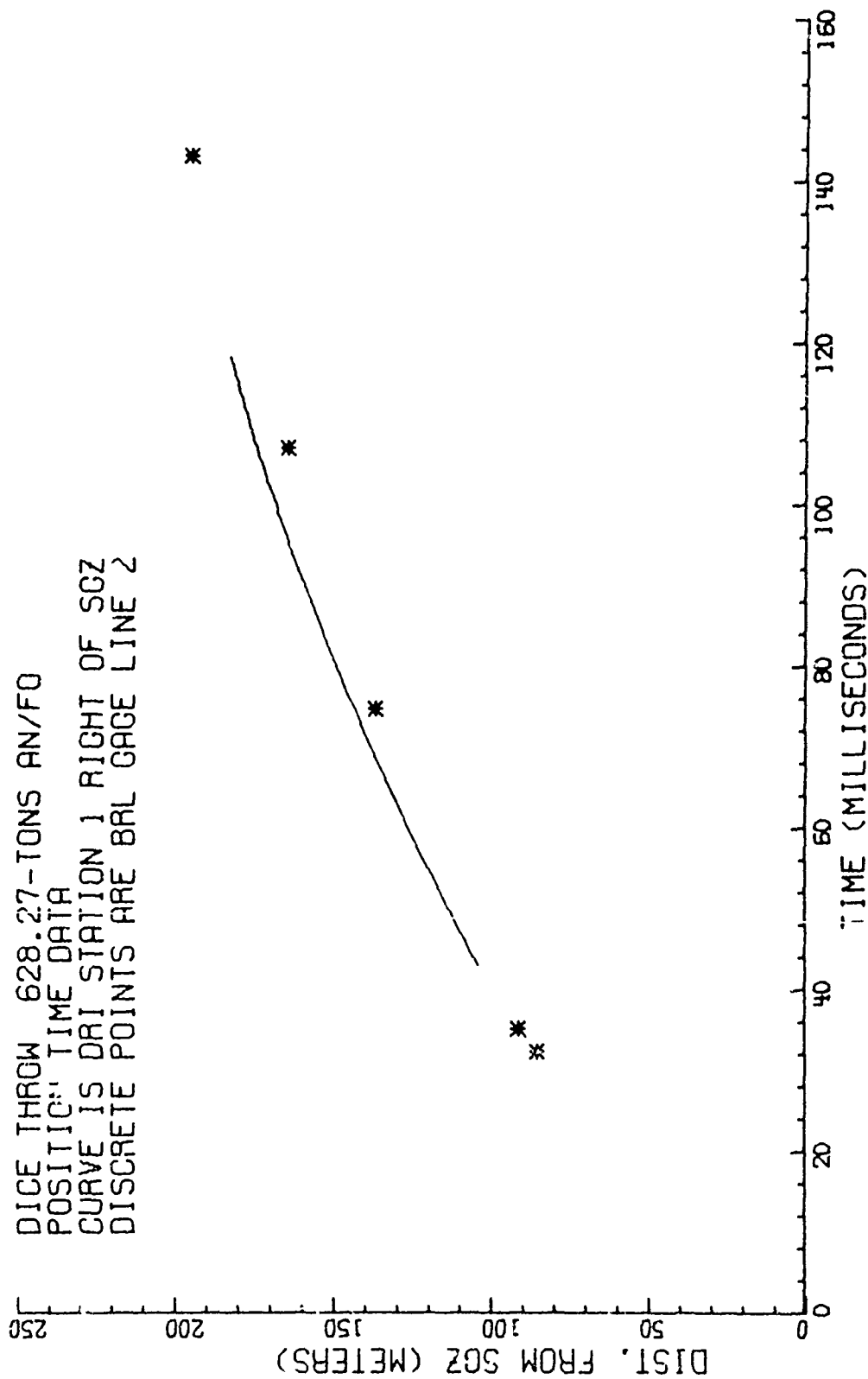


Figure 3.17. DICE THROW Shockwave Arrival Times Along BRL Gage Line 2 and Right of SGZ From DRI Station No. 1.

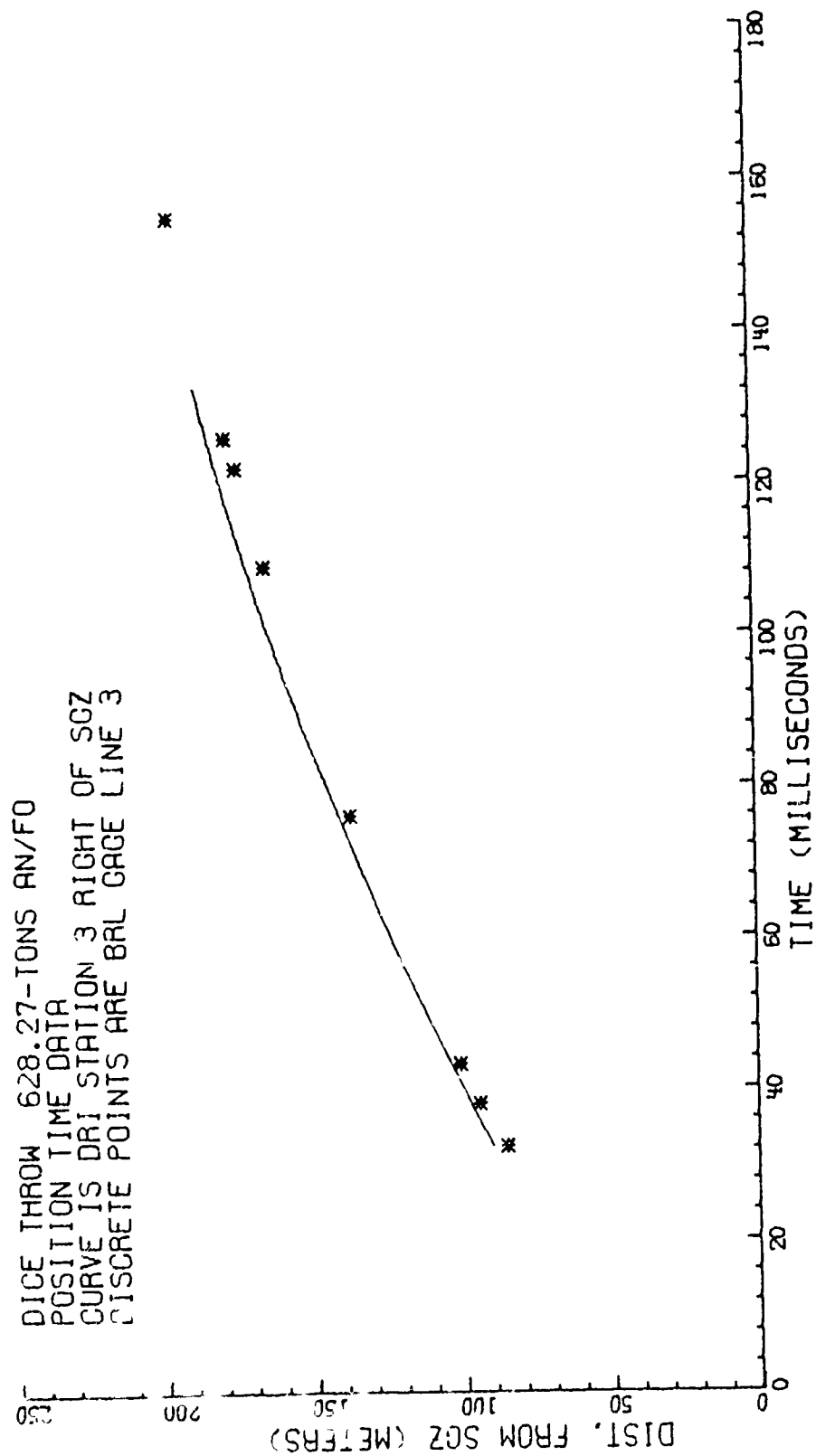


Figure 3.18. DICE THROW Shockwave Arrival Times Along BRL Gage Line 3  
 and Right of SGZ From DRI Station No. 3.

between DRI 1R and BRL gage line #2. DRI 1R and 1L camera records were obtained in the directions of two of the major jets ( $208^{\circ}$  and  $329^{\circ}$ ), respectively. These factors may have had an effect on the accuracies of the readings along with poor spatial resolution due to the direct, dispersed sun light in the background of the cameras' fields-of-view.

Figure 3.19 presents a comparison of the average DRI arrival-time data along BRL gage lines 1 and 3 (line 2 omitted because of questionable data) and the average DRI arrival-time data from PDT 11-2. Note how well the two events compare on a scaled basis.

### 3.9 PEAK PRESSURE DATA FROM ARRIVAL TIMES

Peak pressure values were derived from the shockwave arrival times over the 90 m (295 ft) to 190 m (625 ft) region. Their values were determined by employing the well known Rankine-Hugoniot equation:

$$P = P_0 \left( \frac{2\gamma}{\gamma + 1} \right) \left[ \left( \frac{V}{C} \right)^2 - 1 \right]$$

where

$P$  is the peak overpressure above atmospheric (kPa)

$P_0$  is the atmospheric pressure (kPa)

$\gamma$  is the ratio of specific heats of air

$V$  is the shock velocity

$C$  is the calculated sound velocity at detonation

The value of  $\gamma$  varied with the peak pressure within the range of shockwave velocities photographically recorded during the DT Event. These variations were taken into account in the peak pressure calculations (Ref. 13). Within the peak pressures determined herein,  $\gamma$  varied from 1.368 to 1.402.



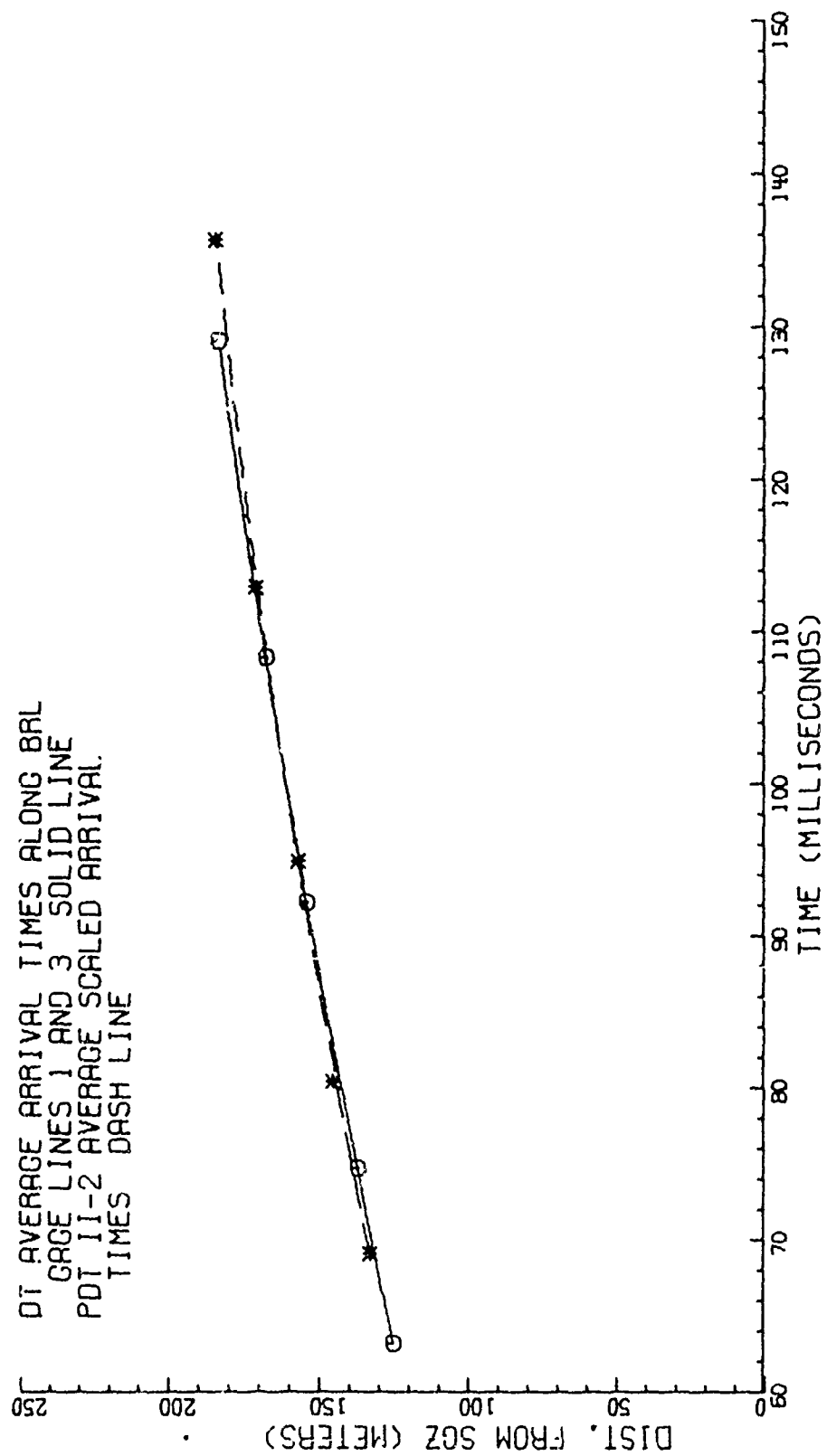


Figure 3.19. DICE THROW Average Shockwave Arrival Times Along BRL Gage  
 Lines 1 and 3 and Pre-DICE THROW 11-2 Average Scaled Arrival Times.

The sonic velocity (C) at the time of detonation was calculated using the expression:

$$C = 331.6 + 0.607t$$

where

C is the sonic velocity (m/s)

t is the ambient temperature (degrees Centigrade)

The ambient temperature and pressure at the time of detonation were 10.4°C, 85.63 kPa (12.42 psi), respectively.

The instantaneous velocities (V's) used in the peak pressure calculations were determined from the slopes along the curve fit to the arrival-time data at the distances presented in Tables 3.8 thru 3.10. Second degree polynomial curve fits were made to the arrival-time data employing the Least Squares method.

The DRI photographically derived values of peak pressure compare fairly well to the BRL gage data along lines 1 and 3. The best comparisons occur at the closer distances, i.e., higher pressures. The DRI peak pressure data along BRL gage line 2 had the largest discrepancies which coincided with the large differences in the arrival times. As was mentioned previously, the large anomaly (208°) could have had an effect on the accuracy of reading in addition to the effects of poor ambient light.

### 3.10 FIREBALL CHARACTERISTICS

The only notable differences in the DT fireball, when compared to those formed during PDT 1-2 and 1-4 Events, were in the formation of

BEST

TABLE 3.2

DICE THIN

BRL GAGE LINE NUMBER 1

TIME OF ARRIVAL/PEAK PRESSURE VERSUS DISTANCE  
FROM DMI PHOTOGRAPHIC RECORDS

CHARGE WEIGHTS 620.27-TONS ANFO

TEMPERATURES: 10.4 (DEG C) 50.7 (DEG F)

AMBIENT PRESSURE: 85.63 (PPA) 12.42 (PSI)

DIST (FT)	ENGLISH UNITS				METRIC UNITS			
	TIME (MSEC)	PEAK PRESS (PSI)	BRL GAGE LINE TIME (MSEC)	VALUES	TIME (MSEC)	PEAK PRESS (KPA)	RRL GAGE LINE TIME (MSEC)	VALUES
450.0								
460.0								
470.0								
480.0								
490.0								
500.0								
510.0								
520.0								
530.0								
540.0								
550.0								
560.0								
570.0								
580.0								
590.0								
600.0								
610.0								
620.0								
630.0								
640.0								
650.0								
660.0								
670.0								
680.0								
690.0								
700.0								
710.0								
720.0								
730.0								
740.0								
750.0								
760.0								
770.0								
780.0								
790.0								
800.0								
810.0								
820.0								
830.0								
840.0								
850.0								
860.0								
870.0								
880.0								
890.0								
900.0								
910.0								
920.0								
930.0								
940.0								
950.0								
960.0								
970.0								
980.0								
990.0								
1000.0								
1010.0								
1020.0								
1030.0								
1040.0								
1050.0								
1060.0								
1070.0								
1080.0								
1090.0								
1100.0								
1110.0								
1120.0								
1130.0								
1140.0								
1150.0								
1160.0								
1170.0								
1180.0								
1190.0								
1200.0								
1210.0								
1220.0								
1230.0								
1240.0								
1250.0								
1260.0								
1270.0								
1280.0								
1290.0								
1300.0								
1310.0								
1320.0								
1330.0								
1340.0								
1350.0								
1360.0								
1370.0								
1380.0								
1390.0								
1400.0								
1410.0								
1420.0								
1430.0								
1440.0								
1450.0								
1460.0								
1470.0								
1480.0								
1490.0								
1500.0								
1510.0								
1520.0								
1530.0								
1540.0								
1550.0								
1560.0								
1570.0								
1580.0								
1590.0								
1600.0								
1610.0								
1620.0								
1630.0								
1640.0								
1650.0								
1660.0								
1670.0								
1680.0								
1690.0								
1700.0								
1710.0								
1720.0								
1730.0								
1740.0								
1750.0								
1760.0								
1770.0								
1780.0								
1790.0								
1800.0								
1810.0								
1820.0								
1830.0								
1840.0								
1850.0								
1860.0								
1870.0								
1880.0								
1890.0								
1900.0								
1910.0								
1920.0								
1930.0								
1940.0								
1950.0								
1960.0								
1970.0								
1980.0								
1990.0								
2000.0								

BEST

TABLE 3.9

DICE INKROW  
HRL GAGE LINE NUMBER 2

TIME (F ARRIVAL/PEAK PRESSURE VERSUS DISTANCE  
FROM ORI PHOTOGRAPHIC RECORDS

CHANGE WEIGHT: 628.27-TONS AW/FU

TEMPERATURE: 10.4 (DEG C) 50.7 (DEG F)

AMPLITUDE PRESSURE: 85.6J (KPA) 12.42 (PSI)

DIST (FT)	ENGLISH UNITS			METRIC UNITS			DIST (METERS)
	ORI PHOTOGRAPHIC RECORD	TIME (MS/L)	PEAK PRESS (PSI)	ORI PHOTOGRAPHIC RECORD	TIME (MS/L)	PEAK PRESS (KPA)	
281.0	11	11	11	11	11	11	11
300.0	11	11	11	11	11	11	11
345.0	11	11	11	11	11	11	11
350.0	11	11	11	11	11	11	11
355.0	11	11	11	11	11	11	11
360.0	11	11	11	11	11	11	11
365.0	11	11	11	11	11	11	11
370.0	11	11	11	11	11	11	11
375.0	11	11	11	11	11	11	11
380.0	11	11	11	11	11	11	11
385.0	11	11	11	11	11	11	11
390.0	11	11	11	11	11	11	11
395.0	11	11	11	11	11	11	11
400.0	11	11	11	11	11	11	11
405.0	11	11	11	11	11	11	11
410.0	11	11	11	11	11	11	11
415.0	11	11	11	11	11	11	11
420.0	11	11	11	11	11	11	11
425.0	11	11	11	11	11	11	11
430.0	11	11	11	11	11	11	11
435.0	11	11	11	11	11	11	11
440.0	11	11	11	11	11	11	11
445.0	11	11	11	11	11	11	11
450.0	11	11	11	11	11	11	11
455.0	11	11	11	11	11	11	11
460.0	11	11	11	11	11	11	11
465.0	11	11	11	11	11	11	11
470.0	11	11	11	11	11	11	11
475.0	11	11	11	11	11	11	11
480.0	11	11	11	11	11	11	11
485.0	11	11	11	11	11	11	11
490.0	11	11	11	11	11	11	11
495.0	11	11	11	11	11	11	11
500.0	11	11	11	11	11	11	11
505.0	11	11	11	11	11	11	11
510.0	11	11	11	11	11	11	11
515.0	11	11	11	11	11	11	11
520.0	11	11	11	11	11	11	11
525.0	11	11	11	11	11	11	11
530.0	11	11	11	11	11	11	11
535.0	11	11	11	11	11	11	11
540.0	11	11	11	11	11	11	11
545.0	11	11	11	11	11	11	11
550.0	11	11	11	11	11	11	11
555.0	11	11	11	11	11	11	11
560.0	11	11	11	11	11	11	11
565.0	11	11	11	11	11	11	11
570.0	11	11	11	11	11	11	11
575.0	11	11	11	11	11	11	11
580.0	11	11	11	11	11	11	11
585.0	11	11	11	11	11	11	11
590.0	11	11	11	11	11	11	11
595.0	11	11	11	11	11	11	11
600.0	11	11	11	11	11	11	11
605.0	11	11	11	11	11	11	11
610.0	11	11	11	11	11	11	11
615.0	11	11	11	11	11	11	11
620.0	11	11	11	11	11	11	11
625.0	11	11	11	11	11	11	11
630.0	11	11	11	11	11	11	11
635.0	11	11	11	11	11	11	11
640.0	11	11	11	11	11	11	11
645.0	11	11	11	11	11	11	11
650.0	11	11	11	11	11	11	11
655.0	11	11	11	11	11	11	11
660.0	11	11	11	11	11	11	11
665.0	11	11	11	11	11	11	11
670.0	11	11	11	11	11	11	11
675.0	11	11	11	11	11	11	11
680.0	11	11	11	11	11	11	11
685.0	11	11	11	11	11	11	11
690.0	11	11	11	11	11	11	11
695.0	11	11	11	11	11	11	11
700.0	11	11	11	11	11	11	11
705.0	11	11	11	11	11	11	11
710.0	11	11	11	11	11	11	11
715.0	11	11	11	11	11	11	11
720.0	11	11	11	11	11	11	11
725.0	11	11	11	11	11	11	11
730.0	11	11	11	11	11	11	11
735.0	11	11	11	11	11	11	11
740.0	11	11	11	11	11	11	11
745.0	11	11	11	11	11	11	11
750.0	11	11	11	11	11	11	11
755.0	11	11	11	11	11	11	11
760.0	11	11	11	11	11	11	11
765.0	11	11	11	11	11	11	11
770.0	11	11	11	11	11	11	11
775.0	11	11	11	11	11	11	11
780.0	11	11	11	11	11	11	11
785.0	11	11	11	11	11	11	11
790.0	11	11	11	11	11	11	11
795.0	11	11	11	11	11	11	11
800.0	11	11	11	11	11	11	11
805.0	11	11	11	11	11	11	11
810.0	11	11	11	11	11	11	11
815.0	11	11	11	11	11	11	11
820.0	11	11	11	11	11	11	11
825.0	11	11	11	11	11	11	11
830.0	11	11	11	11	11	11	11
835.0	11	11	11	11	11	11	11
840.0	11	11	11	11	11	11	11
845.0	11	11	11	11	11	11	11
850.0	11	11	11	11	11	11	11
855.0	11	11	11	11	11	11	11
860.0	11	11	11	11	11	11	11
865.0	11	11	11	11	11	11	11
870.0	11	11	11	11	11	11	11
875.0	11	11	11	11	11	11	11
880.0	11	11	11	11	11	11	11
885.0	11	11	11	11	11	11	11
890.0	11	11	11	11	11	11	11
895.0	11	11	11	11	11	11	11
900.0	11	11	11	11	11	11	11
905.0	11	11	11	11	11	11	11
910.0	11	11	11	11	11	11	11
915.0	11	11	11	11	11	11	11
920.0	11	11	11	11	11	11	11
925.0	11	11	11	11	11	11	11
930.0	11	11	11	11	11	11	11
935.0	11	11	11	11	11	11	11
940.0	11	11	11	11	11	11	11
945.0	11	11	11	11	11	11	11
950.0	11	11	11	11	11	11	11
955.0	11	11	11	11	11	11	11
960.0	11	11	11	11	11	11	11
965.0	11	11	11	11	11	11	11
970.0	11	11	11	11	11	11	11
975.0	11	11	11	11	11	11	11
980.0	11	11	11	11	11	11	11
985.0	11	11	11	11	11	11	11
990.0	11	11	11	11	11	11	11
995.0	11	11	11	11	11	11	11
1000.0	11	11	11	11	11	11	11

REF / 1000000000

TABLE 3.10

DICE FROM  
BKL GAGE (INF NUMBER 3)

TIME OF ARRIVAL/PEAK PRESSURE VERSUS DISTANCE  
FROM DRI PHOTOGRAPHIC RECORDS

CHARGE WEIGHT: 620.27-TONS AN/10

TEMPERATURE: 10.6 (DEG C) 50.7 (DEG F)

AMBIENT PRESSURE: 85.63 (KPA) 12.42 (PSI)

DIST (FT)	ENGLISH UNITS				METRIC UNITS				DIST (METERS)
	DRI PHOTOGRAPHIC RECORD	ARR GAGE LINE VALUES	PEAK PRESS (PSI)	TIME (MSEC)	DRI PHOTOGRAPHIC RECORD	ARR GAGE LINE VALUES	PEAK PRESS (KPA)	TIME (MSEC)	
281.0	11	11	11	11	11	11	11	11	11
285.0	11	11	11	11	11	11	11	11	11
300.0	11	11	11	11	11	11	11	11	11
305.0	11	11	11	11	11	11	11	11	11
310.0	11	11	11	11	11	11	11	11	11
315.0	11	11	11	11	11	11	11	11	11
320.0	11	11	11	11	11	11	11	11	11
325.0	11	11	11	11	11	11	11	11	11
330.0	11	11	11	11	11	11	11	11	11
335.0	11	11	11	11	11	11	11	11	11
340.0	11	11	11	11	11	11	11	11	11
345.0	11	11	11	11	11	11	11	11	11
350.0	11	11	11	11	11	11	11	11	11
355.0	11	11	11	11	11	11	11	11	11
360.0	11	11	11	11	11	11	11	11	11
365.0	11	11	11	11	11	11	11	11	11
370.0	11	11	11	11	11	11	11	11	11
375.0	11	11	11	11	11	11	11	11	11
380.0	11	11	11	11	11	11	11	11	11
385.0	11	11	11	11	11	11	11	11	11
390.0	11	11	11	11	11	11	11	11	11
395.0	11	11	11	11	11	11	11	11	11
400.0	11	11	11	11	11	11	11	11	11
405.0	11	11	11	11	11	11	11	11	11
410.0	11	11	11	11	11	11	11	11	11
415.0	11	11	11	11	11	11	11	11	11
420.0	11	11	11	11	11	11	11	11	11
425.0	11	11	11	11	11	11	11	11	11
430.0	11	11	11	11	11	11	11	11	11
435.0	11	11	11	11	11	11	11	11	11
440.0	11	11	11	11	11	11	11	11	11
445.0	11	11	11	11	11	11	11	11	11
450.0	11	11	11	11	11	11	11	11	11
455.0	11	11	11	11	11	11	11	11	11
460.0	11	11	11	11	11	11	11	11	11
465.0	11	11	11	11	11	11	11	11	11
470.0	11	11	11	11	11	11	11	11	11
475.0	11	11	11	11	11	11	11	11	11
480.0	11	11	11	11	11	11	11	11	11
485.0	11	11	11	11	11	11	11	11	11
490.0	11	11	11	11	11	11	11	11	11
495.0	11	11	11	11	11	11	11	11	11
500.0	11	11	11	11	11	11	11	11	11
505.0	11	11	11	11	11	11	11	11	11
510.0	11	11	11	11	11	11	11	11	11
515.0	11	11	11	11	11	11	11	11	11
520.0	11	11	11	11	11	11	11	11	11
525.0	11	11	11	11	11	11	11	11	11
530.0	11	11	11	11	11	11	11	11	11
535.0	11	11	11	11	11	11	11	11	11
540.0	11	11	11	11	11	11	11	11	11
545.0	11	11	11	11	11	11	11	11	11
550.0	11	11	11	11	11	11	11	11	11
555.0	11	11	11	11	11	11	11	11	11
560.0	11	11	11	11	11	11	11	11	11
565.0	11	11	11	11	11	11	11	11	11
570.0	11	11	11	11	11	11	11	11	11
575.0	11	11	11	11	11	11	11	11	11
580.0	11	11	11	11	11	11	11	11	11
585.0	11	11	11	11	11	11	11	11	11
590.0	11	11	11	11	11	11	11	11	11
595.0	11	11	11	11	11	11	11	11	11
600.0	11	11	11	11	11	11	11	11	11
605.0	11	11	11	11	11	11	11	11	11
610.0	11	11	11	11	11	11	11	11	11
615.0	11	11	11	11	11	11	11	11	11
620.0	11	11	11	11	11	11	11	11	11
625.0	11	11	11	11	11	11	11	11	11
630.0	11	11	11	11	11	11	11	11	11
635.0	11	11	11	11	11	11	11	11	11
640.0	11	11	11	11	11	11	11	11	11

the three anomalies and in the finer structure of its surface due to the relative size of the AN/F0 bags. See Figures 3.5 and 3.6.

There are major differences in the fireball shape, intensity and apparent density between TNT and AN/F0 detonations due to the charge geometry and the explosive composition. For the same equivalent output, the AN/F0 HEC fireball was smaller and lost its light intensity quickly (Ref. 1). The edges of the fireball debris also appeared to be translucent at relatively early times; whereas, at a much later time, the TNT fireball was radiating and opaque.

Table 3.11 presents the DT fireball average dimensions after its initial stabilization, along with the scaled-up data from PDT 11-2 and 1-4. The surface-surge and free-air average dimensions were measured from SGZ in a plane perpendicular to DRI camera station #2. The outline of the fireball was void of any anomalies (dust jet excluded) which happened to be directed toward ( $203^{\circ}$ ) or away ( $329^{\circ}$  and  $344^{\circ}$ ) from the cameras' line-of-sight ( $192^{\circ}$ ). See Figure 3.11. The presented cross-sectional areas were calculated from measurements made with a planimeter.

TABLE 3.11

Fireball Dimensions After Stabilization  
From PDT 1-4 and 11-2 Scaled to DT

Event	Time (ms)	Surface-Surge		Free-Air		Area	
		(m)	(ft)	(m)	(ft)	(m <sup>2</sup> )	(ft <sup>2</sup> )
DT	282	203	665	123	403	23,020	247,700
PDT 11-2	282	185	609	107	352	22,220	239,100
PDT 1-4	282	224	734	110	364	24,510	263,700

There appeared to be good agreement in the presented cross-sectional areas between the DT Event and the two PDT Events. Its value falls in between the two PDT values.

### 3.11 DYNAMIC EJECTA

There were no photographic crater-related dynamic ejecta which propagated beyond the fireball debris from either the "debris suppression" or undisturbed  $60^\circ$  sectors of the DT crater (Ref. 6). Large artificial missiles (16-pound bowling balls and concrete spheres) were placed in the undisturbed sector and were to be tracked photographically beyond the fireball debris. None of these missiles were apparently photographed with the DRI high-resolution 70mm cameras (0.06 m at a camera distance of 1,370 m); though, non-crater related debris were tracked at low angles starting at very early times of 0.65s to 2s at distances of 220 m (640 ft) to 270 m (890 ft) from SGZ, respectively. The velocities of these non-crater related debris, if considered to have had their origins in the crater at SGZ, would have been 304 m/s (996 ft/s) to 136 m/s (446 ft/s), much greater than would have been expected based on previously recorded dynamic ejecta from detonations of this size. (Ref. 14).

The actual in-flight velocities of the non-crater related particles were from 102 m/s (336 ft/s) at 0.65 s at a distance of 220 m (640 ft) to 35.4 m/s (116 ft/s) at 2 s at a distance of 270 m (890 ft). These particles also had presented areas which ranged from  $0.32 \text{ m}^2$  ( $3.5 \text{ ft}^2$ ) to  $0.4 \text{ m}^2$  ( $4.3 \text{ ft}^2$ ). From these velocities, times and distances, the non-crater related debris must have had their origins outside the crater radius. Also, from their apparent cross-sectional areas, they could have been some of the many ejecta collector plates which were

situated from 16 m (200 ft) to 213 m (700 ft) from SGZ (Ref. 15).

The dynamic ejecta from the DT Event was expected to have velocities of 51.8 m/s (170 ft/s) to 76.2 m/s (250 ft/s) over an impact range of 213 m (700 ft) to 457 m (1500 ft) based on previous crater data. The impact times would have ranged from 7 s to 10 s over these impact distances. The DT fireball/cloud radius was over 253 m (830 ft) at 3.4 s and 267 m (875 ft) at 8.6 s.

From after-the-fact information, only one of the artificial missiles, a 16-pound bowling ball, propagated beyond these distances to a range of 427 m (1,400 ft). Considering no drag and a  $45^{\circ}$  escape angle, it should have taken this bowling ball 9.3 s at a velocity of 64.6 m/s (212 ft/s) to reach this range. No in-flight particles were resolved on any part of the 70mm film record at anywhere near this time. In fact, ground dust had risen to a height which would have had some effect on resolving particles of the size of a bowling ball. These conditions plus the poor ambient light could have easily prevented the film from producing adequate ejecta images for tracking purposes.

A number of low-angle, short range, high-velocity ejection spires were seen in a few frames recorded with the 70mm cameras. The ejection angle from the "debris suppression" region was  $42^{\circ}$  while from an undisturbed  $60^{\circ}$  sector it was  $43^{\circ}$ . These compare to  $30^{\circ}$  to  $36^{\circ}$  for the PDT 11-2 Event.

### 3.12 CLOUD DEVELOPMENT AND RISE

There appeared to be decided differences in the cloud dimensions with time from the 628-ton DT Event when compared to the 123-ton PDT 11-2 Event, as there were between the PDT 11-2 Event and the 5.6 ton PDT 1-4 Event.



Not only were the dimensions different, but there was a stem formed during later-times (25.8 s) which was not present at scaled times during any of the PDT AN/F0 Events. The results are presented in Table 3.12. Part of the differences shown in this table may be attributed to variations in geology from one site to the other as well as variations in relative size of the individual AN/F0 bags from one event to the other and in the average charge density which in turn effected the average detonation velocities in the explosive.

TABLE 3.12

Cloud Dimensions From DT Event With Scaled-Up Values  
From PDT 11-2 and PDT 1-4 Events

Time (s)	DT Height		PDT 11-2* Height		PDT 1-4* Height	
	(m)	(ft)	(m)	(ft)	(m)	(ft)
3.4	149	490	201	660	93	280
8.6	125	410	314	1030	104	340
17.2	223	730	330	1080	140	460
25.8	314	1030	366	1200	174	570
Time (s)	Diameter		Diameter		Diameter	
	(m)	(ft)	(m)	(ft)	(m)	(ft)
3.4	506	1660	384	1260	534	1750
8.6	534	1750	473	1550	555	1820
17.2	567	1860	576	1890	683	2240
25.8	527	1730	735	2310	738	2420
Time (s)	DT Stem Diameter		DT Toroid Thickness			
	(m)	(ft)	(m)	(ft)		
25.8	338	1110	238		780	

\*No stem or toroid formed at scaled time of 25.8 s.

## SECTION IV

### CONCLUSIONS AND RECOMMENDATIONS

The DT photographic and photoelectric derived data suggest that some aspects of the detonation process scaled well to those derived from PDT 11-2 and 1-4 Events while others did not. What differences did exist can be attributed partly to the apparent increase in the DT detonation velocity due to an increase in the AN/FO density and partly to the finer-scaled surface structure of the DT charge.

The temperature-time history from the DT Event denoted higher color temperatures over the first 600  $\mu$ s than were obtained from the fireball surface of the 500-ton TNT PF Event. Total light radiation output over the first 20 ms also indicated that there was no first minimum peak with a rise to a broad secondary peak in its signature as is typical in a TLR signal produced by an equivalent TNT detonation where after burning is present.

It appeared from the DT Dynafax records that the early stages of the fireball development showed a symmetrical perturbation in its upper region. This anomalous behavior may have been the precursor to the three major anomalies whose apexes developed at approximately the same height as the perturbable region.

The dust jets from the DT Events appeared to develop along radial accesses to SGZ. In order to decrease the effects of these dust jets upon peak pressure, pressure-time, and dynamic pressure readings and the obscuration effects upon photographed targets, radial accesses should be reduced. If accesses, such as roads, are necessary they should have

a wide break or wide barrier near SGZ (100 to 200 m from SGZ for a 600-ton AN/F0 detonation), where the natural ground is left undisturbed. Another approach is to limit access to SGZ from a direction which has no effect upon targets or gage readings.

## REFERENCES

1. Wisotski, J., MIDDLE NORTH SERIES Pre-DICE THROW I and II Events Technical Photography, POR 6917, 15 March 1976.
2. Edwards, T. Y., Perry, G.L.E., MIDDLE NORTH SERIES Pre-DICE THROW II Events Preliminary Results Report, POR 6904, September 1976.
3. Wisotski, J., Snyder, W. H., Characteristics of Blast Waves Obtained from Cylindrical High Explosive Charges, DRI 2286, DDC #367-625, November 1965.
4. DNA, Proceedings of the MIXED COMPANY/MIDDLE GUST Results Meeting, 13-15 March 1973, Vol. 1, Sessions 1, 2A and 3A, DNA 3151P1, 1 May 1973.
5. Wisotski, J., Technical Photography From Pre-MINE THROW IV, Event 6, POR 6835, DRI 2560, March 24, 1975.
6. DNA Field Command, MIDDLE NORTH SERIES DICE THROW EVENT TEST PLAN, July 9, 1976.
7. Wisotski, J., Technical Photography of a 100-Ton TNT Detonation on Granite, MINERAL ROCK EVENT, MS 2166, DRI 2543, June 1970.
8. Wisotski, J., Early Explosion Phenomena From Operation DISTANT PLAIN, DRI 2448, October 1968.
9. Harris, B., Summary of Preliminary DICE THROW Main Event Results, December 13, 1976.
10. Condon, J. L., Snodgrass, J. J., Effects of Primer Type and Borehole Diameter on AN/FO Detonation Velocities, Mining Congress Journal, Vol. 60, No. 6, June 1974.
11. Wisotski, J., Technical Photography and Explosion Phenomenology Measurements, Operation PRAIRIE FLAT Symposium Report, Vol. I, Part I, DASA 2377-1 DASIAC SR-92, January 1970.
12. Teel, G. D., DICE THROW Final Free Field Blast Data, Letter FCTMOT, 17 March 1977.
13. Williell, J. E., and Lehto, D. L., Normal Shock (Rankine-Hugoniot) Relationships for Various Altitudes from Sea Level to 300,000 Feet, NAVORD Report 6075, 14 April 1958.
14. Wisotski, J., Dynamic Ejecta Measurements for Selected MIDDLE GUST and PACE Cratering Events, Denver Research Institute, Air Force Weapons Laboratory Report, AFWL TR-75-104, In publication.
15. Jones, E., Preliminary Report of DT Ejecta Studies, Civil Engineering Research Facility, December 1976.

**6. INSTRUMENTATION NOISE PROBLEMS  
ENCOUNTERED ON DICE THROW**

by  
Noel Gantick  
DNA Field Command

## INSTRUMENTATION NOISE PROBLEMS ENCOUNTERED ON DICE THROW

### A. INTRODUCTION

Electrical noise problems encountered on the DICE THROW events consisted of five categories.

- . Equipment Produced Noise
- . Power System Related Noise
- . Local Atmospheric Noise
- . Impulsive Periodic Noise
- . Impulsive Non-Periodic Noise

### B. DISCUSSION OF NOISE

#### 1. Equipment Related Noise:

a. In early August BRL fielding personnel described impulsive noise bursts being encountered in the vans located in all trailer parks. The noise appeared consistent in all vans, was reminiscent of timing signals, and had a nominal repetition rate of 3100 pulses per second. The model QRC 40-4 power supply was found to be the source of this noise. This supply, a unit that had been used for years at NTS with no problems, was in this application a source of inverter switching transients. These switching transients were within the specified limits of the power supply. The solution to the problem was to use a different supply, one whose output was noise free.

#### 2. Power System Related Noise:

a. The second category of noise was power system related and had frequency components to 50 Kilohertz. The appearance was that of impulsive noise synchronized with the frequency of the commercial power. The primary sources of this type noise are light dimmer switches in the vans and other power source controllers employing silicon controlled rectifiers. The solution has been to remove these switches from the instrumentation vans as they are found. A second power system noise problem was produced by a faulty A/C in one of the AFWL vans. This air conditioner had a faulty compressor and revealed itself the morning of the shot as an apparent power failure indication on the Instrumentation park 1 power monitors. This apparent power failure indication was caused by the 200 ampere current pulses produced whenever the air conditioner tried to come on line. A third rather interesting phenomenon was the presence of high level noise currents flowing in soil at park 2. When a pair of pins were driven in the earth separated a distance of 100 feet and connected by means of a current meter, currents in excess of 30 milliamperes were noted. Oscilloscope examination revealed this noise contained commercial power harmonics to a frequency of 1200 Hertz. The action taken

to alleviate this noise was to remove the commercial power ground to a distance of 200 feet from the park. This commercial power neutral ground point was later moved to the intersection of WSMR highways 7 and 20, a distance of one mile from the instrumentation parks. A continuing problem was power pole noise, noise pulses produced whenever power lines are moved by the wind. This situation was particularly severe on DICE THROW since the commercial power was at 24 KV with substations in parks 1 and 2.

### 3. Local Atmospheric Noise:

a. The DICE THROW events were executed during the rainy part of the year at WSMR. Thunder storms occurred daily in view of the sites. Noise monitored on the lines as a result of these local electrical storms exhibited durations of 10's of milliseconds and appeared quite hashy reminiscent of potentiometer or relay wiper noise. This noise was distinctly different from the impulsive non-periodic type. Since the shot would not be executed in an electrical storm this type noise was ignored.

### 4. Impulsive Periodic Noise

a. Impulsive periodic noise was a transitory problem on the Pre-DICE THROW series executed at the Queen 15 site some 20 miles south of the GIANT PATRIOT site. This noise appeared strongest under the range timing system transmission lines parallel to the data lines at Queen 15 but displaced by a mile. The noise resembled digital range timing signals and would occur for hours on end but not every day. The suspicion was that this noise was man-made, originating on the range. After appearing off and on for a few weeks this noise disappeared abruptly at the culmination of an announced test down range and never reappeared. This noise was not present during the main event fielding.

### 5. Impulsive Non-Periodic Noise:

a. The main source of problems during the DICE THROW fielding was non-periodic impulsive noise. This noise was first detected in the BRL vans in all parks. It was later seen in all of the other vans that were storing data with bandwidths greater than 5000 Hertz. It was even monitored in a field wire fence line located between parks 1 and 2. Transient currents in excess of 30 milliamperes were measured in this fence. This noise was present on all conductors on the test bed to varying degrees and was independent of test site activities. It occurred when all commercial power was off within a 10 mile radius from the test bed. The rate of occurrence of the noise pulses was a function of time of day. A very definite minimum was noted in the early morning hours and a peak in the late evening hours.

b. Long duration oscillograph recordings were made to determine if the noise was occurring at some repetition rate or rates as might be expected if the noise source was an energy storage center charging to

static electricity and arcing as some discharge threshold was reached. There was no discernible rate or rates in the duration of evaluation. The assumption therefore was that the noise was random and had a flat distribution in the expected test duration of six seconds. Attempts were made using crude directional antennas to vector to the noise source if one existed. This failed. Help was requested from the area frequency management people to locate and determine the source. The conclusions of the team was that this noise was broadband atmospheric with no particular source. In summary, the noise was seen on all conductors on the test bed and appeared as short, highly damped oscillations with durations of less than one millisecond. The viewed noise appeared characterized by the impulse functions of the circuits being monitored.

c. Figures 1 and 2 are tracings of the monitored noise. The traces on the left in figure 1 are pulses monitored in van 50025 in park 2 while the traces on the right are pulses monitored in trailer 40003 in park 1 about 2 miles away. The duration of these traces is 2 milliseconds and the vertical scale is 10 millivolts per division. In each case the noise was monitored on a twisted shielded pair of conductors terminated by a gage. Figure 2 has a horizontal scale of 200 microseconds and a vertical scale of 100 millivolts per division. These signals were monitored on an unterminated RG-213 coaxial cable running from the firing van in trailer park 2 to the stack. These were by no means the largest noise signals seen on this RG-213 but rather representative samples.

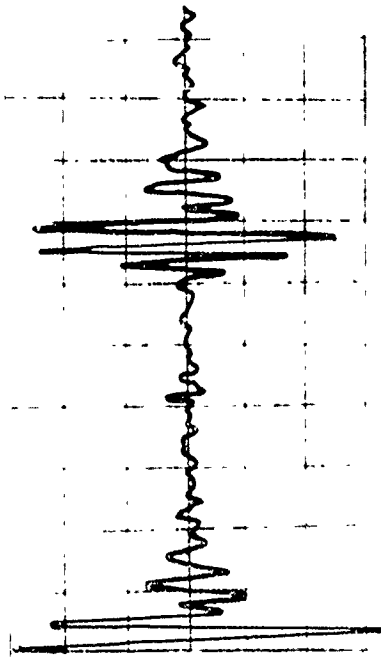
#### 6. Effects of Random Noise on Data:

a. Since the noise appeared less severe in the early morning hours it was felt that the probability of data degradation would be minimized if the shot were executed at this time. To gather information supporting or refuting this premise the noise measurement test set-up in figure 3 was used. A typical data channel in trailer 40003 was connected via a threshold sensitive gate to an event counter. The number of impulses on this data channel exceeding a predetermined level in a fixed time interval of 5 minutes was noted on an hourly basis. The chosen threshold levels were 3.0 millivolts and 7.5 millivolts into the Baylab Model 5503 amplifier that had a gain of 10. The results of this series of tests are shown in the table of figure 4. The noise at 0800 hours was 0.2 that of 1300 hours. These results are shown for two days but were repeated for a week with similar results. Based on this information the decision was to execute the test at approximately 0800 hours.

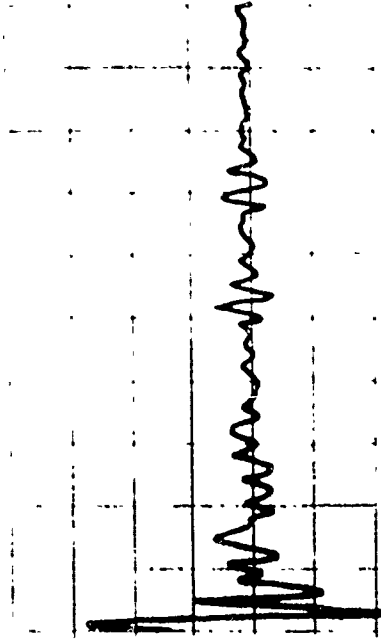
b. A question that is most relevant is "What is the effect of this impulsive noise on the test data"? Would it obscure or degrade the data? If a random impulse noise rate of 4 bursts per minute with a noise duration of 0.5 to 1.5 milliseconds is assumed along with a data duration of 5 to 100 milliseconds in a test of 6 seconds. It is easily shown that the probability of noise overlapping a data ranges from .0003 to .007.



TRAILER 50025



TRAILER 40003



HORIZONTAL SCALE 200 US/DIVISION  
VERTICAL SCALE 10 MILLIVOLTS/DIVISION

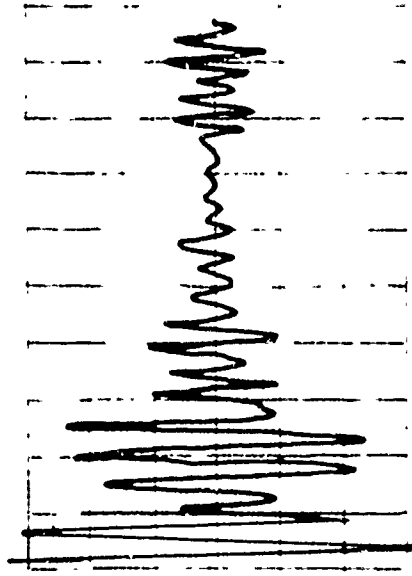
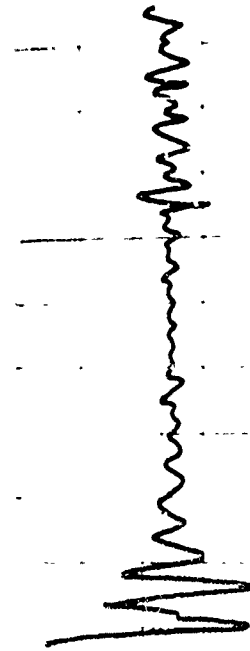
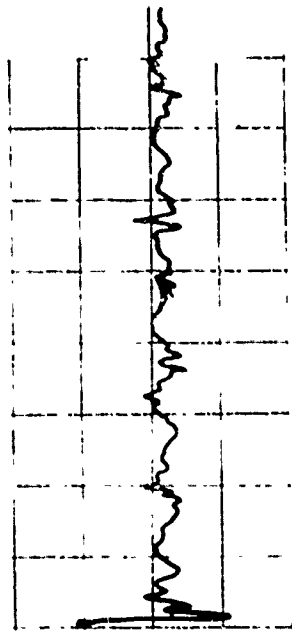
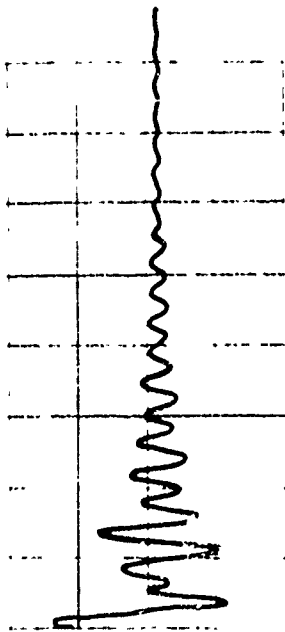


FIGURE 1. IMPULSIVE NON-PERIODIC NOISE WAVEFORMS  
MONITORED IN TRAILERS 40003 AND 50025.



VERTICAL SCALE 100 MILLIVOLTS/DIVISION  
HORIZONTAL SCALE 200 US/DIVISION

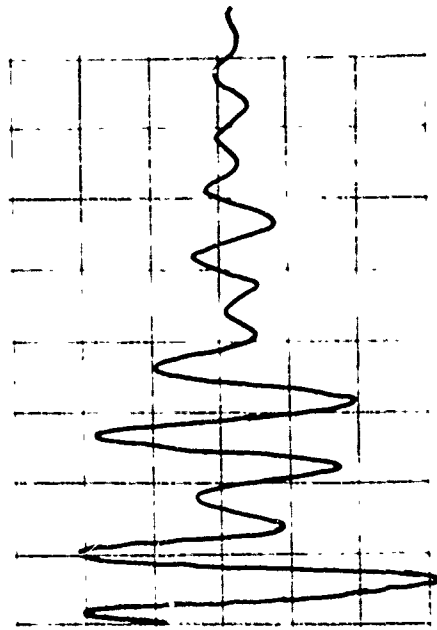
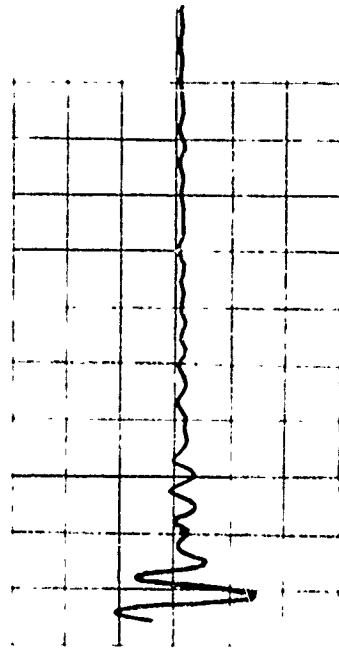


FIGURE 2. IMPULSIVE NON-PERIODIC NOISE  
WAVE FORMS MONITORED IN TRAILER 36016.

# NOISE DISTRIBUTION MEASUREMENT TEST SET-UP

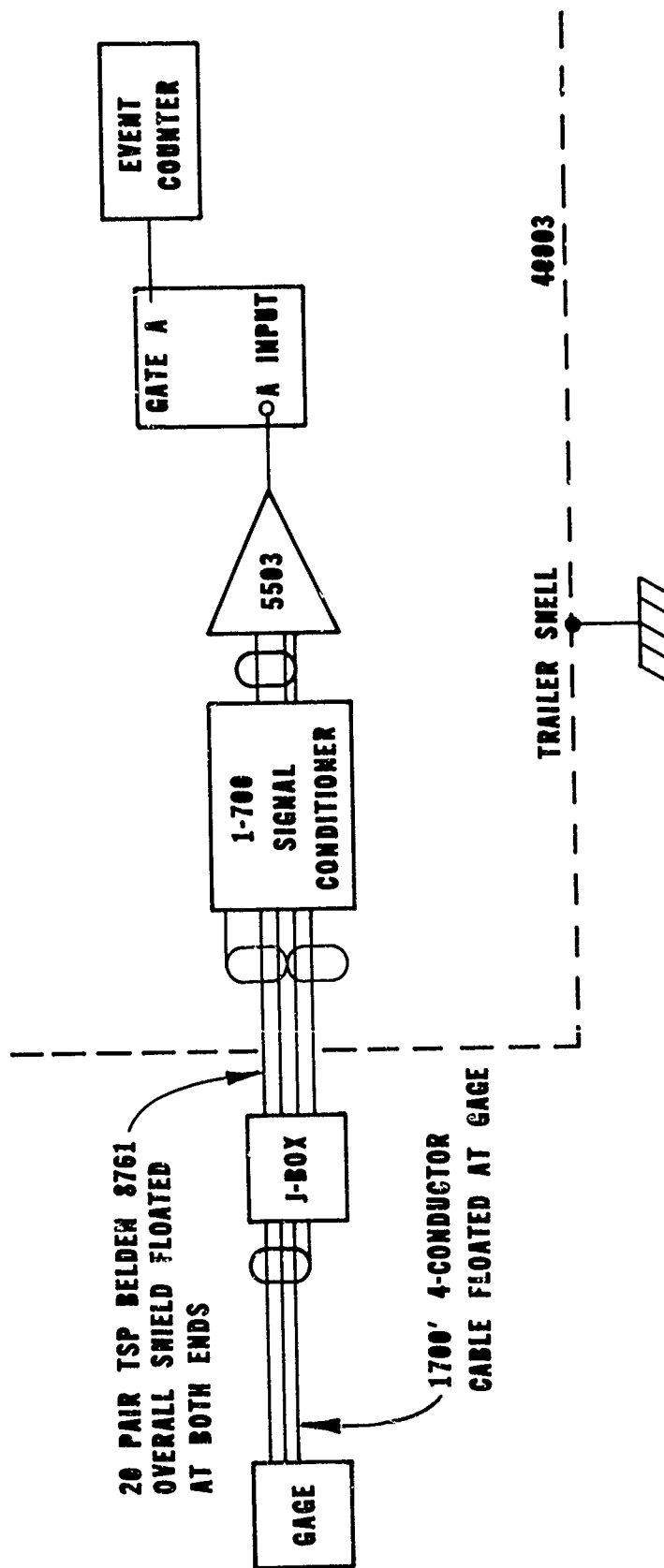


FIGURE 3

TIME OF DAY	19 SEPTEMBER				21 SEPTEMBER			
	COUNTS IN EXCESS OF 30 MILLIVOLTS		COUNTS IN EXCESS OF 75 MILLIVOLTS		COUNTS IN EXCESS OF 30 MV		COUNTS IN EXCESS OF 75MV	
	RAW	NORMAL	RAW	NORMAL	RAW	NORMAL	RAW	NORMAL
0400					*46	.71	*4	.062
0500					65	1.0	3	.046
0600	*19	.047	*0	0	21	.32	5	.071
0700	20	.049	1	.002	2	.031	1	.015
0800	21	.052	15	.037	**2	.031	**1	.015
0900	61	.15	36	.089				
1000	61	.15	50	.12				
1100	92	.23	38	.094				
1200	101	.25	87	.21				
1300	107	.26	64	.16				
1400	110	.27	52	.13				
1500	172	.42	53	.13				
1600	130	.32	100	.25				
1700	291	.72	260	.64				
1800	**406	1.0	**291	1.0				

\*START OF TEST

\*\* END OF TEST

FIGURE 4. TABLE OF IMPULSIVE NON-PERIODIC NOISE DENSITY MEASURED IN 5 MINUTE INTERVALS.

It can also be shown that although the longer duration data have the greatest probability of occurring simultaneously with a noise pulse the probability of degradation is minimal with an independent probability of severe degradation that is less than 0.1. The result is a rather small chance of losing a particular data because of this type of noise. The figure 5 depicts a data degraded by one of these noise impulses (shown in the oval). As is usual the noise pulse is on the order of 1 millisecond and exceeds the data in amplitude. This represents a rather extreme situation where the data is very long relative to the noise but also the condition most likely to occur.

#### C. NON-PERIODIC NOISE MITIGATION TECHNIQUES

The steps taken to eliminate the non-periodic noise were:

1. Trailer grounding was improved. The resistance of the earth electrodes was reduced and lower impedance conductors were used to tie the trailers to earth.
2. Cable shields were connected to the external surface of the vans and to earth.
3. MC-12, a balanced 4-conductor shielded cable was used in place of the DNA supplied 20 pair cable for strain measurements.
4. The event was executed at a time of day when the noise was least severe.

#### D. TRAILER PARK GROUNDS

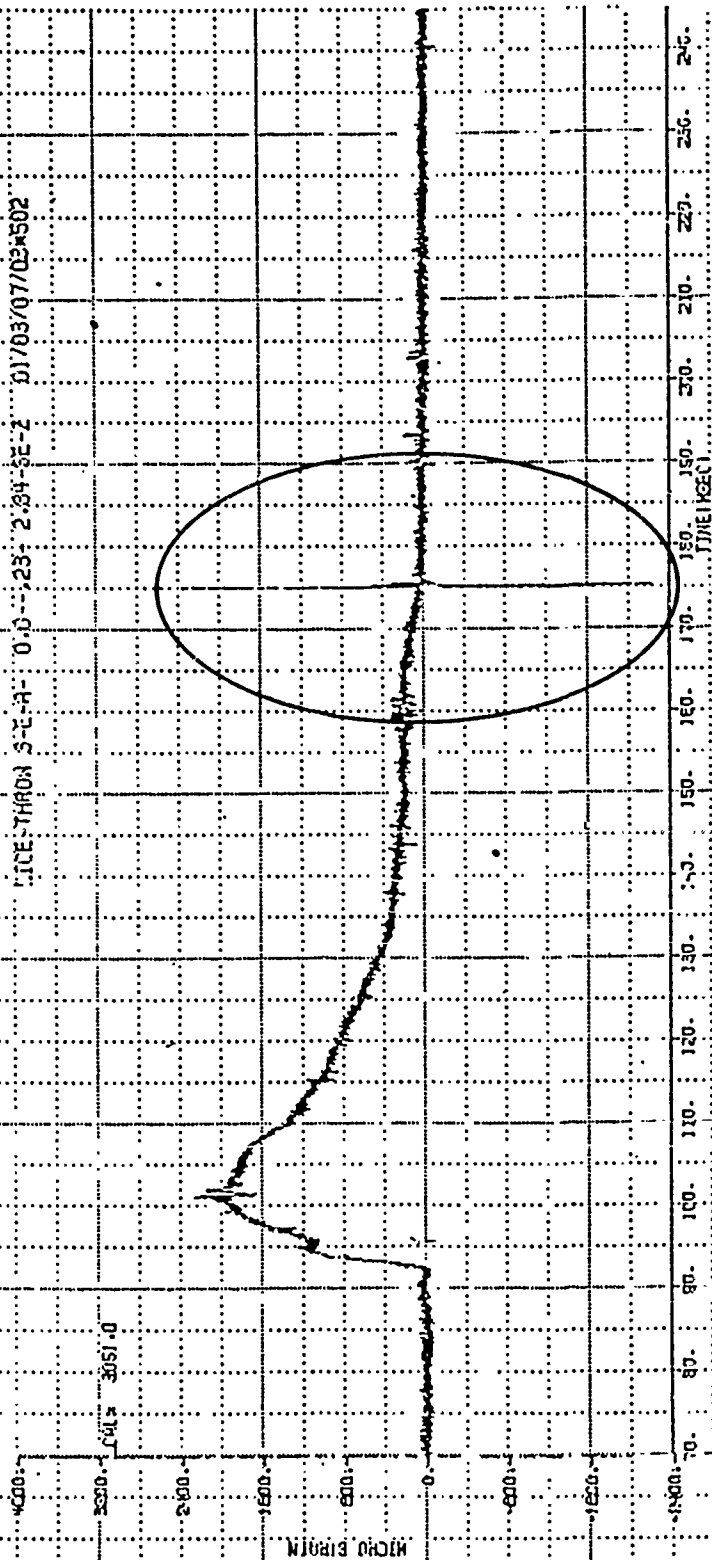
1. Figure 6 presents schematically the results of using a star or single ground point for a trailer park. If any trailer sources noise a current flows thru the electrode-to-earth resistance producing a noise voltage then seen by all the vans in a park. In this way a dimmer switch in one van can effectively disable all the vans in a park. This single point ground is the lowest cost to implement but of little value where low level distributed instrumentation systems are concerned. A preferred trailer grounding scheme is shown in figure 7. Each trailer has its own ground rod located close to each van and a distance  $d$  from the nearest other ground rod. This distance  $d$  is set to at least twice the buried ground rod length thus providing 34 db of isolation between grounds. Note that a separate ground is dedicated for the timing system cable so that noise signals on this shield are grounded prior to entering the park. This system is more costly than the single point ground but is capable of providing the required isolation between vans to insure noise free operations.

FIGURE 5 AMPLIFIED STRAIN GAGE CHANNEL #502

EXPERIMENTER AFWL

BRIDGE OUTPUT AT 2000 MICROSTRAIN 21.1 MV  
AMPLIFIER GAIN 29 LINE LENGTH APPROX 1600 METERS

TIME-THROW SET-A- 0.0--23: 2:34-SE-2 01/03/07/03#502



## PARK 1 EARTHING SCHEMATICS

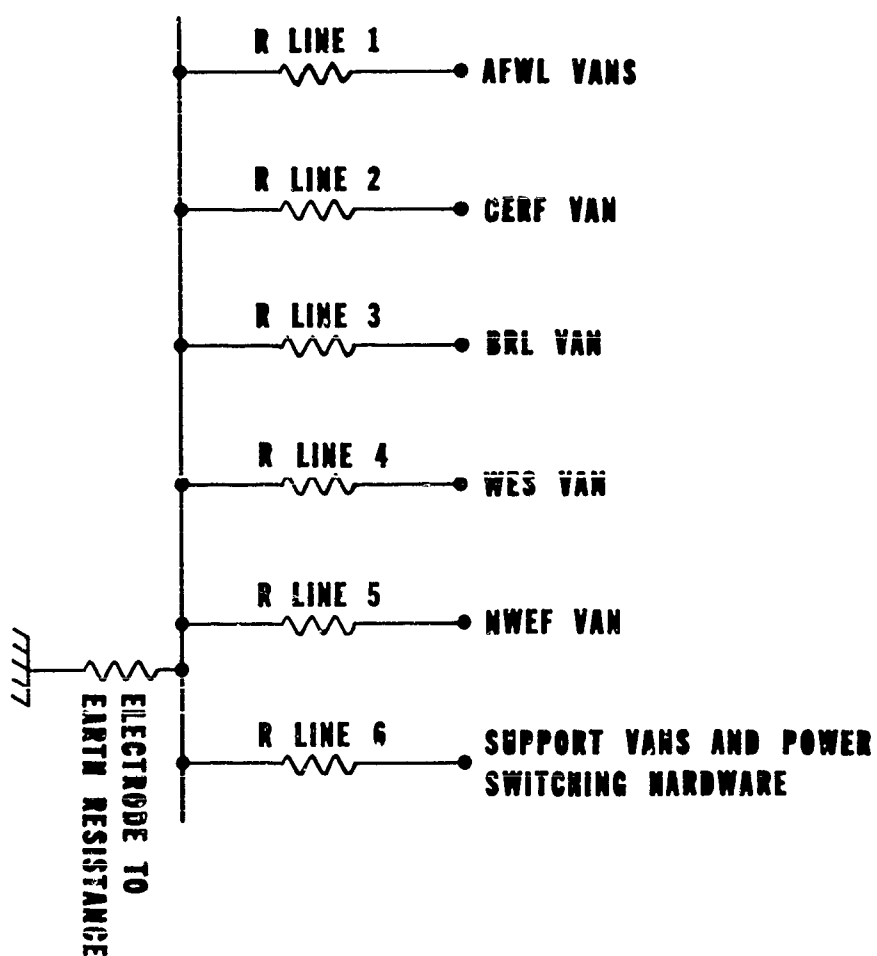


FIGURE 6

# PREFERRED TRAILER GROUNDING

ALL BUNDLE SHIELDS THAT  
ARE ROUTED TO VAN 1

PARK TIMING CABLE  
BUNDLE SHIELDS

THE DISTANCE BETWEEN GROUNDS  
MUST BE GREATER THAN 2X  
BURIED GROUND ROD LENGTH

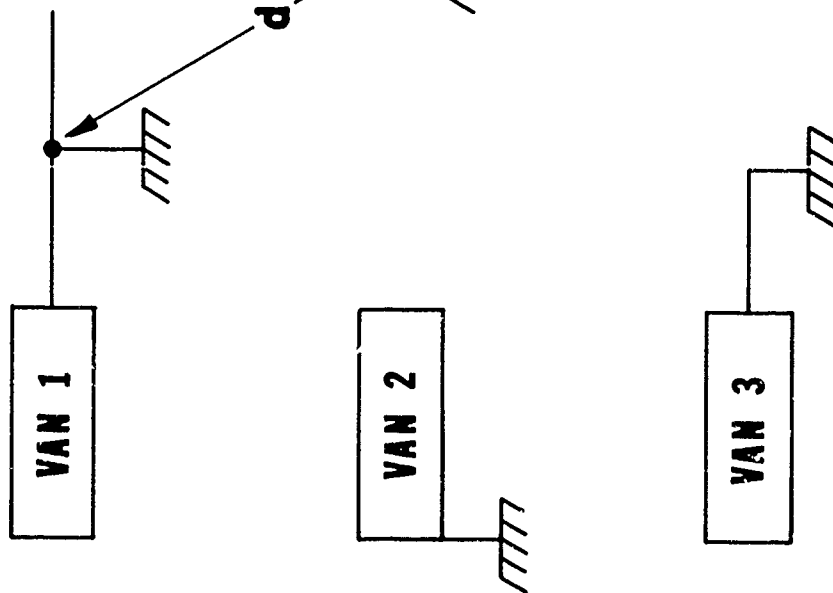


FIGURE 7.



#### E. TREATMENT OF CABLE BUNDLE SHIELDS

1. Figure 8 shows how cable shields were treated at the J-Boxes by some experimenters. Note that the 20 pair cable shield is floating allowing a potential to develop on the cable shield relative to earth. This shield terminated at the van looks like a quarter wave transmission line. This, coupled with the near electromagnetically transparent 1 mil spiral foil wrapped bundle shield on the 20 pair cable, is not desirable from an EMI point of view. A better arrangement is shown in the lower half of Figure 8. The shield now is tied to earth at the J-Box along with the 4-conductor shield assuring that the line must be a half wave transmission line at best. This will double the frequency of coupled noise signals and reduce the effect on data. Again the cost of installing grounds at the J-Boxes is a cost impact item justified by the noise immunity produced.

#### F. CONCLUSIONS

1. These non-periodic noise signals encountered on DICE THROW were unique and not before seen on high explosive tests in the previous five years.

2. The shielding methods employed were not effective.

3. Test equipment for evaluating the noise was not available.

4. Trailer park grounding schemes were not adequate.

5. Unbalanced pre-storage signal conditioning systems are very susceptible to noise.

6. Gage selection should be such as to insure a high level output assuring a high signal-to-noise ratio.

7. The failure to evaluate the noise environment at GIANT PATRIOT prior to fielding was a serious oversight.

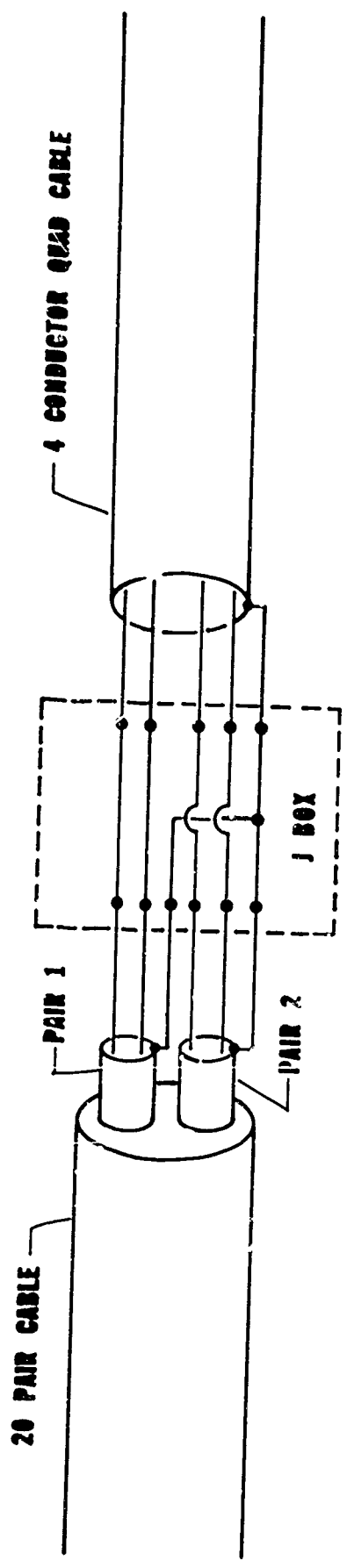
#### G. RECOMMENDATIONS

1. The distributed trailer park earthing scheme described in figure 7 should be adopted.

2. The cable shield treatment described in figure 8 should be followed and particular care should be made to couple shields to earth with low impedance conductors prior to van entry.

3. Pre-fielding evaluation of test site noise conditions is a requirement.

4. Dummy twisted pairs should be dedicated in each cable bundle to obtain a measure of the background noise. With this done, post-test noise cancellation techniques are available which can produce an order of magnitude reduction in noise levels. These techniques are mathematical and readily implemented on tape stored data.



4 CONDUCTOR TO 20 PAIR CABLE INTERFACE AS EMPLOYED ON DICE THROW MAIN EVENT.

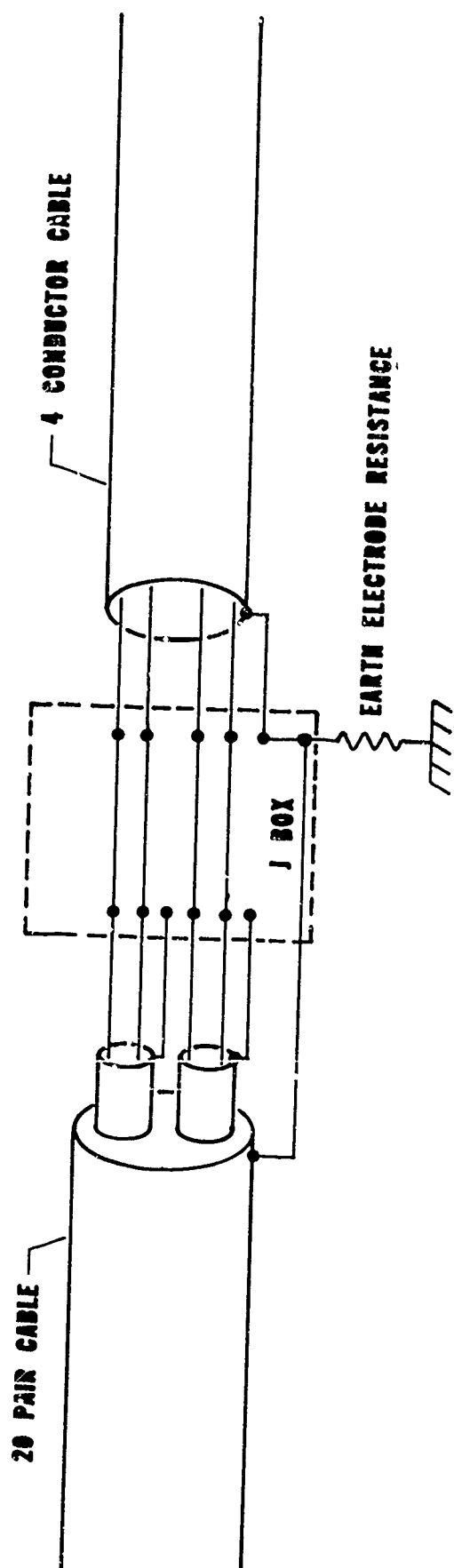


FIGURE 8 RECOMMEND J BOX INTERFACE TREATMENT

**7. FREE-FIELD AIRBLAST DEFINITION -  
EVENT DICE THROW**

**by**

**George D. Teel**

**Ballistic Research Laboratory**

## ABSTRACT

The air blast parameters to be expected on the DICE THROW Event were predicted on the basis of the Lawrence Livermore Laboratory developed equation-of-state for ANFO, the Air Force Weapons Laboratory HULL Code calculation and the Ballistic Research Laboratory data obtained from the Pre-DICE THROW II-2 Event. These predictions were provided to the Defense Nuclear Agency Test Group Staff for distribution to the experimenters. Three blast lines were instrumented in the test area and other instrumentation was placed in specific experiment areas as requested. This instrumentation was to acquire the following air blast parameters; shock wave arrival time, incident shock overpressure, positive phase duration, positive phase impulse, horizontal dynamic pressure, and horizontal dynamic pressure impulse. A very acceptable data return was accomplished. An air blast anomaly in the southwesterly direction influenced some of the measurements taken in the AFWL and BRL areas along Blast Line 2. The data acquired on the DICE THROW Event for arrival time, incident overpressure, dynamic pressure, and dynamic pressure impulse agree well with predictions. The positive phase duration and positive phase impulse data would seem to agree with the observations on Pre DICE THROW II-2 in that the curve inflections due to the shock wave and fireball separation are either reduced or eliminated.

## ACKNOWLEDGEMENTS

An experiment of this magnitude and complexity can never be accomplished by a single individual. The author is indebted to the following persons who contributed to the success of the effort:

Warren Baity, Ballistic Research Laboratory;  
Vincent King, Ballistic Research Laboratory;  
Richard Pearson, Ballistic Research Laboratory;  
Robert Peterson, Ballistic Research Laboratory;  
Burnett Pettit, Ballistic Research Laboratory;  
George Watson, Ballistic Research Laboratory;  
Harry Hassell, Bendix Field Engineering;  
Theodore Maxfield, Bendix Field Engineering;  
Neil Speer, Bendix Field Engineering;  
Frank Stepaniak, Bendix Field Engineering.

Their assistance in the planning, fielding, and data processing for this experiment has been invaluable.

## TABLE OF CONTENTS

	<u>Page</u>
1. Introduction . . . . .	13
2. Objectives . . . . .	16
3. Approach . . . . .	17
4. Instrumentation . . . . .	35
4.1 Transducers . . . . .	35
4.2 Recording Equipment . . . . .	36
4.3 Calibration . . . . .	37
5. Data Reduction . . . . .	40
6. Results . . . . .	43
7. Conclusions and Recommendations . . . . .	75
Appendix A. Incident and Dynamic Pressure-Time Histories - Blast Line 1 . . . . .	77
Appendix B. Incident and Dynamic Pressure-Time Histories - Blast Line 2 . . . . .	121
Appendix C. Incident and Dynamic Pressure-Time Histories - Blast Line 3 . . . . .	165

## LIST OF ILLUSTRATIONS

<u>Figure</u>		<u>Page</u>
1	The ANFO source for DICE THROW . . . . .	14
2	The DICE THROW test site layout . . . . .	15
3	Predicted arrival time versus ground range . . . . .	22
4	Predicted shock overpressure versus ground range . . . . .	23
5	Predicted positive phase duration versus ground range . . . . .	24
6	Predicted positive phase impulse versus ground range . . . . .	25
7	Predicted horizontal dynamic pressure versus ground range . . . . .	26
8	Predicted horizontal dynamic pressure impulse versus ground range . . . . .	27
9	Experiment layout for the Free Field Air Blast Definition experiment . . . . .	28
10	A ground level station to measure incident pressure . . . . .	29
11	A station to measure ground level incident pressure and elevated stagnation pressure . . . . .	30
12	An elevated incident pressure station . . . . .	31
13	A station to measure incident overpressure and stagnation pressure at an elevation of 2.44 meters . . . . .	32
14	A station to measure incident overpressure and stagnation pressure at an elevation of 3.66 meters . . . . .	34
15	Measured arrival time versus ground range - Blast Line 1 . . . . .	48
16	Measured incident shock overpressure versus ground range - Blast Line 1 . . . . .	49
17	Measured positive phase duration versus ground range - Blast Line 1 . . . . .	50
18	Measured positive phase impulse versus ground range - Blast Line 1 . . . . .	51
19	Measured horizontal dynamic pressure versus ground range - Blast Line 1 . . . . .	52
20	Measured horizontal dynamic pressure impulse versus ground range - Blast Line 1 . . . . .	53

# LIST OF ILLUSTRATIONS (Continued)

<u>Figure</u>		<u>Page</u>
21	DICE THROW and Pre-DICE THROW II-2 waveforms showing shock wave formation . . . . .	55
22	Measured arrival time versus ground range - Blast Line 2 . . . . .	56
23	Measured incident shock overpressure versus ground range - Blast Line 2 . . . . .	57
24	Measured positive phase duration versus ground range - Blast Line 2 . . . . .	58
25	Measured positive phase impulse versus ground range - Blast Line 2 . . . . .	59
26	Measured horizontal dynamic pressure versus ground range - Blast Line 2 . . . . .	60
27	Measured horizontal dynamic pressure impulse versus ground range - Blast Line 2 . . . . .	61
28	Measured arrival time versus ground range - Blast Line 3 . . . . .	62
29	Measured incident shock overpressure versus ground range - Blast Line 3 . . . . .	63
30	Measured positive phase duration versus ground range - Blast Line 3 . . . . .	64
31	Measured positive phase impulse versus ground range - Blast Line 3 . . . . .	65
32	Measured horizontal dynamic pressure versus ground range - Blast Line 3 . . . . .	66
33	Measured horizontal dynamic pressure impulse versus ground range - Blast Line 3 . . . . .	67
34	DICE THROW arrival time versus ground range . . . . .	69
35	DICE THROW incident shock overpressure versus ground range . . . . .	70
36	DICE THROW positive phase duration versus ground range . . . . .	71
37	DICE THROW positive phase impulse versus ground range . . . . .	72
38	DICE THROW horizontal dynamic pressure versus ground range . . . . .	73



# LIST OF ILLUSTRATIONS (Continued)

<u>Figure</u>		<u>Page</u>
39	DICE THROW horizontal dynamic pressure impulse versus ground range . . . . .	74
A1	Incident pressure-time history - Station 101-1 . . . . .	78
A2	Incident pressure-time history - Station 101-2 . . . . .	79
A3	Incident pressure-time history - Station 102-1 . . . . .	80
A4	Incident pressure-time history - Station 102-2 . . . . .	81
A5	Incident pressure-time history - Station 103-1 . . . . .	82
A6	Incident pressure-time history - Station 104 . . . . .	83
A7	Incident pressure-time history - Station 105 . . . . .	84
A8	Incident pressure-time history - Station 106 . . . . .	85
A9	Incident pressure-time history - Station 107 . . . . .	86
A10	Incident pressure-time history - Station 109 . . . . .	87
A11	Incident pressure-time history - Station 110 . . . . .	88
A12	Incident pressure-time history - Station 111 . . . . .	89
A13	Incident pressure-time history - Station 112 . . . . .	90
A14	Incident pressure-time history - Station 112-2 . . . . .	91
A15	Incident pressure-time history - Station 113 . . . . .	92
A16	Incident pressure-time history - Station 114 . . . . .	93
A17	Incident pressure-time history - Station 115 . . . . .	94
A18	Incident pressure-time history - Station 116 . . . . .	95
A19	Incident pressure-time history - Station 120 . . . . .	96
A20	Incident pressure-time history - Station 122 . . . . .	97
A21	Incident pressure-time history - Station 123 . . . . .	98
A22	Incident pressure-time history - Station 125 . . . . .	99
A23	Incident pressure-time history - Station 125-2 . . . . .	100
A24	Incident pressure-time history - Station 126 . . . . .	101
A25	Incident pressure-time history - Station 130 . . . . .	102
A26	Incident pressure-time history - Station 131 . . . . .	103
A27	Incident pressure-time history - Station 132-2 . . . . .	104

# LIST OF ILLUSTRATIONS (Continued)

<u>Figure</u>		<u>Page</u>
A28	Incident pressure-time history - Station 134 . . . . .	105
A29	Incident pressure-time history - Station 135 . . . . .	106
A30	Incident pressure-time history - Station 135-2 . . . . .	107
A31	Incident pressure-time history - Station 136 . . . . .	108
A32	Incident pressure-time history - Station 139 . . . . .	109
A33	Incident pressure-time history - Station 139-2 . . . . .	110
A34	Incident pressure-time history - Station 140 . . . . .	111
A35	Dynamic pressure-time history - Station 112 . . . . .	112
A36	Dynamic pressure-time history - Station 112-2 . . . . .	113
A37	Dynamic pressure-time history - Station 113 . . . . .	114
A38	Dynamic pressure-time history - Station 116 . . . . .	115
A39	Dynamic pressure-time history - Station 120 . . . . .	116
A40	Dynamic pressure-time history - Station 126 . . . . .	117
A41	Dynamic pressure-time history - Station 131 . . . . .	118
A42	Dynamic pressure-time history - Station 134 . . . . .	119
A43	Dynamic pressure-time history - Station 136 . . . . .	120
B1	Incident pressure-time history - Station 201 . . . . .	122
B2	Incident pressure-time history - Station 202 . . . . .	123
B3	Incident pressure-time history - Station 203 . . . . .	124
B4	Incident pressure-time history - Station 204 . . . . .	125
B5	Incident pressure-time history - Station 206 . . . . .	126
B6	Incident pressure-time history - Station 207 . . . . .	127
B7	Incident pressure-time history - Station 213 . . . . .	128
B8	Incident pressure-time history - Station 214 . . . . .	129
B9	Incident pressure-time history - Station 214-2 . . . . .	130
B10	Incident pressure-time history - Station 216 . . . . .	131
B11	Incident pressure-time history - Station 219 . . . . .	132
B12	Incident pressure-time history - Station 219-2 . . . . .	133
B13	Incident pressure-time history - Station 220 . . . . .	134

# LIST OF ILLUSTRATIONS (Continued)

<u>Figure</u>		<u>Page</u>
B14	Incident pressure-time history - Station 222 . . . . .	135
B15	Incident pressure-time history - Station 223 . . . . .	136
B16	Incident pressure-time history - Station 225 . . . . .	137
B17	Incident pressure-time history - Station 229 . . . . .	138
B18	Incident pressure-time history - Station 229-2 . . . . .	139
B19	Incident pressure-time history - Station 229-3 . . . . .	140
B20	Incident pressure-time history - Station 232 . . . . .	141
B21	Incident pressure-time history - Station 232-2 . . . . .	142
B22	Incident pressure-time history - Station 232-3 . . . . .	143
B23	Incident pressure-time history - Station 232-4 . . . . .	144
B24	Incident pressure-time history - Station 233 . . . . .	145
B25	Incident pressure-time history - Station 235 . . . . .	146
B26	Incident pressure-time history - Station 235-2 . . . . .	147
B27	Incident pressure-time history - Station 235-3 . . . . .	148
B28	Incident pressure-time history - Station DRES . . . . .	149
B29	Incident pressure-time history - Station DRI . . . . .	150
B30	Incident pressure-time history - Station 239 . . . . .	151
B31	Incident pressure-time history - Station 240 . . . . .	152
B32	Dynamic pressure-time history - Station 214 . . . . .	153
B33	Dynamic pressure-time history - Station 214-2 . . . . .	154
B34	Dynamic pressure-time history - Station 216 . . . . .	155
B35	Dynamic pressure-time history - Station 219 . . . . .	156
B36	Dynamic pressure-time history - Station 219-2 . . . . .	157
B37	Dynamic pressure-time history - Station 223 . . . . .	158
B38	Dynamic pressure-time history - Station 229 . . . . .	159
B39	Dynamic pressure-time history - Station 229-2 . . . . .	160
B40	Dynamic pressure-time history - Station 232 . . . . .	161
B41	Dynamic pressure-time history - Station 232-3 . . . . .	162
B42	Dynamic pressure-time history - Station 235 . . . . .	163

# LIST OF ILLUSTRATIONS (Continued)

<u>Figure</u>		<u>Page</u>
C1	Incident pressure-time history - Station 302 . . . . .	166
C2	Incident pressure-time history - Station 303 . . . . .	167
C3	Incident pressure-time history - Station 304 . . . . .	168
C4	Incident pressure-time history - Station 306 . . . . .	169
C5	Incident pressure-time history - Station 308 . . . . .	170
C6	Incident pressure-time history - Station 309 . . . . .	171
C7	Incident pressure-time history - Station 313 . . . . .	172
C8	Incident pressure-time history - Station 316 . . . . .	173
C9	Incident pressure-time history - Station 317 . . . . .	174
C10	Incident pressure-time history - Station 318 . . . . .	175
C11	Incident pressure-time history - Station 320 . . . . .	176
C12	Incident pressure-time history - Station 320-2 . . . . .	177
C13	Incident pressure-time history - Station 321 . . . . .	178
C14	Incident pressure-time history - Station 321-2 . . . . .	179
C15	Incident pressure-time history - Station 322 . . . . .	180
C16	Incident pressure-time history - Station 322-2 . . . . .	181
C17	Incident pressure-time history - Station 322-3 . . . . .	182
C18	Incident pressure-time history - Station 323 . . . . .	183
C19	Incident pressure-time history - Station 323-2 . . . . .	184
C20	Incident pressure-time history - Station 324 . . . . .	185
C21	Incident pressure-time history - Station 324-2 . . . . .	186
C22	Incident pressure-time history - Station 324-3 . . . . .	187
C23	Incident pressure-time history - Station 325 . . . . .	188
C24	Incident pressure-time history - Station 325-2 . . . . .	189
C25	Incident pressure-time history - Station 327 . . . . .	190
C26	Incident pressure-time history - Station 328 . . . . .	191
C27	Incident pressure-time history - Station 330 . . . . .	192
C28	Incident pressure-time history - Station 330-2 . . . . .	193
C29	Incident pressure-time history - Station 332 . . . . .	194

# LIST OF ILLUSTRATIONS (Continued)

<u>Figure</u>		<u>Page</u>
C30	Incident pressure-time history - Station 332-2 . . . . .	195
C31	Incident pressure-time history - Station 335 . . . . .	196
C32	Incident pressure-time history - Station 335-2 . . . . .	197
C33	Incident pressure-time history - Station 336 . . . . .	198
C34	Incident pressure-time history - Station 338 . . . . .	199
C35	Incident pressure-time history - Station 339 . . . . .	200
C36	Incident pressure-time history - Station 340 . . . . .	201
C37	Dynamic pressure-time history - Station 318 . . . . .	202
C38	Dynamic pressure-time history - Station 320 . . . . .	203
C39	Dynamic pressure-time history - Station 320-2 . . . . .	204
C40	Dynamic pressure-time history - Station 322 . . . . .	205
C41	Dynamic pressure-time history - Station 322-2 . . . . .	206
C42	Dynamic pressure-time history - Station 322-3 . . . . .	207
C43	Dynamic pressure-time history - Station 324-2 . . . . .	208
C44	Dynamic pressure-time history - Station 324-3 . . . . .	209
C45	Dynamic pressure-time history - Station 325 . . . . .	210
C46	Dynamic pressure-time history - Station 330 . . . . .	211
C47	Dynamic pressure-time history - Station 330-2 . . . . .	212
C48	Dynamic pressure-time history - Station 332 . . . . .	213
C49	Dynamic pressure-time history - Station 332-2 . . . . .	214
C50	Dynamic pressure-time history - Station 335 . . . . .	215

## LIST OF TABLES

<u>Table</u>		<u>Page</u>
1	Predicted air blast parameters for DICE THROW Event . . . . .	19
2a	Measured air blast parameters - Blast Line 1 . . . . .	44
2b	Measured air blast parameters - Blast Line 2 . . . . .	45
2c	Measured air blast parameters - Blast Line 3 . . . . .	46

## 1. INTRODUCTION

The U.S. Army Ballistic Research Laboratory conducted the Free Field Air Blast Definition Experiment (Experiment No. 101) on Event DICE THROW of the MIDDLE NORTH Test Series. This event was successfully executed at 0800 hours MST on 6 October 1976 at the Giant Patriot Test Site, White Sands Missile Range, New Mexico. This report presents the results obtained by this experiment.

Event DICE THROW was the detonation of  $5.7 \times 10^5$  kg (628 ton) charge of ANFO (ammonium nitrate and fuel oil mixture). The charge geometry was a hemispherically capped right circular cylinder (see Figure 1). The charge cylinder was placed with its base on the ground surface and had an aspect ratio (L/D) of 0.75. The charge was constructed from 22.7 kg (50-pound) bags of ANFO. A general layout of the test site is shown in Figure 2.

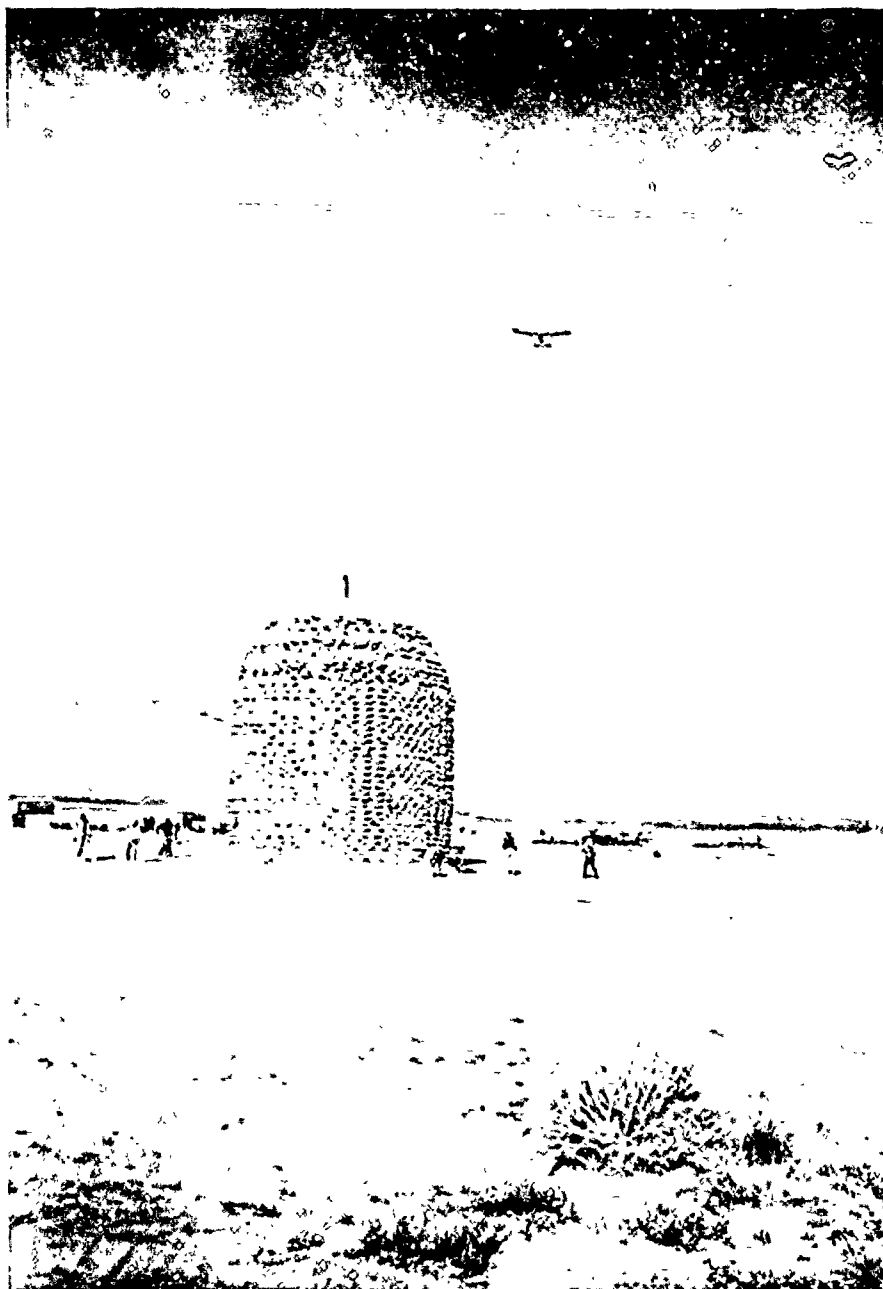


Figure 1. The ANFO source for DICE THROW



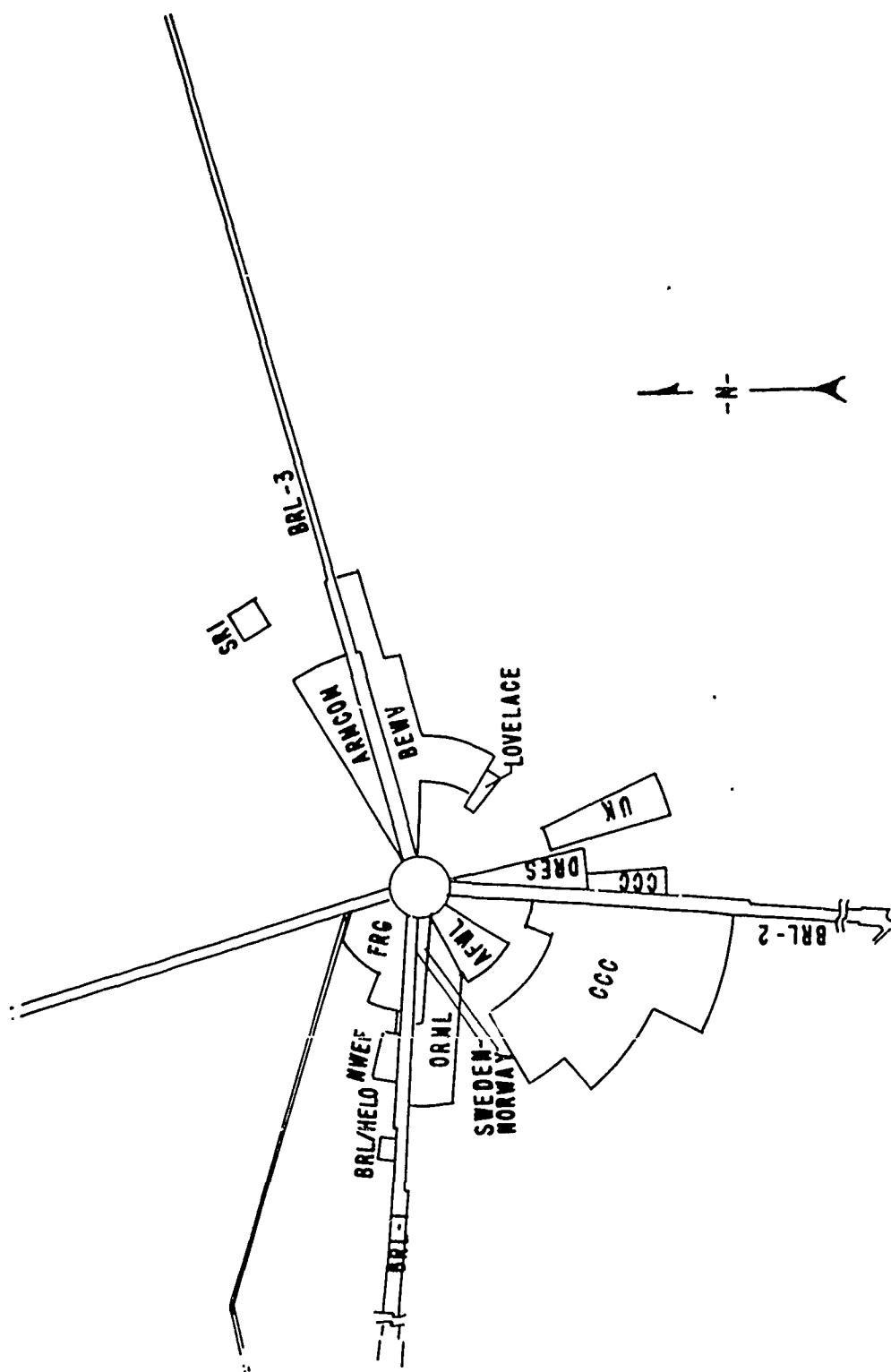


Figure 2. The DICE THROW test site layout

## 2. OBJECTIVES

There were three objectives of the Free Field Air Blast Definition Experiment. The first objective was to prepare pre-test predictions of the air blast environment to be expected on the DICE THROW Event and make these predictions available to the potential experimenters prior to the event so that they might judiciously plan for the placement of their experiments. The second was to place air blast instrumentation in the test layout and acquire air blast data to document the air blast environment from this specific explosive/geometry combination for correlation with pre-test predictions, to provide a record of the environment generated by this event, and to expand the data base for this explosive/geometry combination in the event that this combination might be used for future nuclear weapons effect simulation tests. The final objective was to place additional instrumentation at specific locations in support of other experiments which require the acquisition of the air blast environment at their specific target or location.

### 3. APPROACH

The pre-test blast predictions were prepared and provided to the Defense Nuclear Agency Test Group Staff. These predictions were distributed to the experimenters by the Technical Director for the Test Group Staff on 9 March 1976 and were subsequently published in the DICE THROW Test Plan on 9 July 1976. The predictions were derived from a combination of the results of a HULL Code calculation performed by Mr. C. Needham of the Air Force Weapons Laboratory (AFWL) using the ANFO Equation-of-State developed by the Lawrence Livermore Laboratory (LLL) under the direction of Dr. M. Finger and the results obtained from the Free Field Air Blast Definition Experiment conducted on the Pre-DICE THROW II-2 Event. For the purpose of generating these predictions it was assumed, from an examination of historical weather data in the general test site area, that the temperature and barometric pressure at the time of execution of the DICE THROW Event would be 12°C (53.6°F) and 86.74 kPa (12.58 psi) respectively. The analytical results and the Pre-DICE THROW II-2 experimental data were scaled to these expected ambient atmospheric conditions using the conventional air blast scaling equations\* shown below:

$$P_s = P_s^* (P_1/P_1^*) \quad (1)$$

$$d = d^* W^{1/3} (P_1^*/P_1)^{1/3} \quad (2)$$

$$t = t^* W^{1/3} (P_1^*/P_1)^{1/3} (T_1^*/T_1)^{1/2} \quad (3)$$

$$I = I^* W^{1/3} (P_1/P_1^*)^{2/3} (T_1^*/T_1)^{1/2} \quad (4)$$

\*S. Glasstone, Ed., The Effects of Nuclear Weapons, U.S. Atomic Energy Commission, Rev. Ed., April 1962.

where:

$d$  = distance from explosive center, m (ft);

$t$  = time, milliseconds;

$P_s$  = shock overpressure, kPa (psi);

$P_1$  = atmospheric pressure, kPa (psi);

$T_1$  = ambient temperature, °Kelvin;

$W$  = charge weight, kg (pound);

\* refers to standard conditions.

Following the event the predictions were revised to reflect the actual temperature and barometric pressure at the time of the event, 9.7°C (49.5°F) and 85.01 kPa (12.33 psi) respectively. These revised predictions are listed in Table 1 and the various parameters are plotted versus ground range in Figures 3 through 8.

In order to accomplish the second and third objectives of the experiment, a total of 139 pressure transducers were installed in the test area. The total number of transducers were allocated as 101 to measure side-on or incident overpressure and 38 to measure total head or stagnation overpressure. Transducers were placed at ground ranges from 9.88 meters (32.4 feet) to 2134 meters (7000 feet) and were located at elevations from the ground surface to 12.2 meters (40 feet) above the ground surface. The locations of the free field stations are shown on the layout in Figure 9.

Those stations installed to provide side-on overpressure time histories were emplaced in mounts either flush with the ground surface (Figures 10 and 11) or elevated above the ground surface (Figures 12 and 13). All total head instrumentation was placed above the ground

### Table 1. Predicted Air Blast Parameters for DICE THROW Event

GR	ft	A		PS		PPD msec	OPI		HDP		HDI	
		msec	psi	kPa	psi		kPa	msec	psi	kPa	msec	
9.91	32.5	2.38	4904.	33812.	24.7	188110.	27283.	-----	-----	-----	-----	
11.4	37.5	2.68	2942.	20284.	24.6	116287.	16866.	-----	-----	-----	-----	
15.3	50.1	3.54	14203.	2060.	24.2	54724.	7937.	-----	-----	-----	-----	
30.5	100.	7.69	8115.	1177.	18.4	17375.	2520.	5100.	5100.	212048.	30755.	
34.4	113.	9.31	6764.	981	16.8	14775.	2143.	29075.	4217.	177850.	25795.	
45.7	150.	13.4	4737.	687	11.3	12314.	1786.	21305.	3090.	102608.	14882.	
61.3	201.	20.2	3447.	500.	5.7	12521.	1816.	11831.	1716.	64301	9326.	
63.1	207.	21.3	3378.	490.	6.1	12790.	1855.	10818.	1569.	61563.	8929.	
76.5	251.	28.6	2572.	373.	14.2	15182.	2202.	6019.	873.	45147.	6548.	
86.0	282.	34.4	2027.	294.	101.	24628.	3572.	4330.	628.	39672.	5754.	
91.7	301.	38.0	1827.	265.	97.2	24966.	3621.	3585.	520.	39672.	5754.	
311.	311.	40.0	1689.	245.	93.1	23939.	3472.	3316.	481.	39335.	5705.	
333.	333.	44.5	1420.	206.	89.1	18126.	2629.	2606.	378.	37625.	5457.	
351.	351.	49.1	1248.	181.	87.0	14638.	2123.	2165.	314.	34887.	5060.	
401.	401.	61.7	862.	125.	87.0	11969.	1736.	1303.	189.	23939.	3472.	
441.	441.	73.9	676.	98.1	89.1	11080.	1607.	883.	128.	18126.	2629.	
451.	451.	76.9	609.	88.3	90.1	10604.	1538.	814.	118.	16416.	2381.	
501.	501.	95.1	440.	6.8	93.1	9853.	1429.	494.	71.6	11287.	1637.	
516	516	101.	405.	51.8	96.2	9094.	1319.	433.	62.8	9922.	1439.	
527.	527.	105.	372.	53.9	98.2	9032.	1310.	379.	54.9	9067.	1315.	
552	552	116.	325.	47.1	101.	8481.	1230.	304.	44.1	7522.	1091.	
572	572	125.	304.	44.1	104.	8212.	1191.	253.	36.3	6157.	893.	
582.	582.	130.	270.	39.2	106.	7936.	1151.	223.	32.4	5405.	784.	
602.	602.	139.	243.	35.3	110.	7729.	1121.	190.	27.5	4785.	694.	
607	607	142.	236.	34.3	111.	7660.	1111.	176.	25.5	4585.	665.	
642	642	158.	203.	29.4	115.	7184.	1042.	128.	18.6	3896.	565.	
652	652	166.	190.	27.5	118.	7046.	1022.	115.	16.7	3627.	526.	
682	682	185.	169.	24.5	123.	6771.	982.	90.3	13.1	3075.	446.	
702	702	198.	156.	22.6	128.	6564.	952.	75.8	11.0	2668.	387.	
742	742	223.	135.	19.6	136.	6226.	903.	59.3	8.6	2255.	327.	
752	752	227.	132.	19.1	140.	6157.	893.	55.8	8.1	2158.	313.	
824.	824.	258.	110.	16.0	152.	5743.	833.	40.7	5.9	1710.	248.	
822.	822.	268.	101.	14.7	154.	5612.	814.	35.2	5.1	1606.	233.	
852.	852.	294.	94.5	13.7	162.	5405.	784.	30.3	4.4	1400.	203.	

Table 1. Predicted Air Blast Parameters for DICE THROW Event (Continued)

GR	m	ft	TA		PS		PPD	OPI		HDP		HDPI	
			msec		kPa	psi	msec	kPa-msec	psi-msec	kPa	psi	kPa-msec	psi-msec
275.		903.	324.		82.7	12.0	174.	5103.	744.	23.4	3.4	1165.	169.
290.		953.	354.		72.4	10.5	187.	4854.	704.	18.6	2.7	993.	144.
295.		965.	369.		67.6	9.8	191.	4757.	690.	16.9	2.45	924.	134.
306.		1003.	385.		64.8	9.4	202.	4619.	670.	14.9	2.16	855.	124.
321.		1053.	445.		56.5	8.2	220.	4378.	635.	11.5	1.67	703.	102.
329.		1078.	455.		53.8	7.8	226.	4309.	625.	10.8	1.57	677.	98.2
336.		1103.	466.		53.1	7.7	233.	4240.	615.	10.1	1.47	649.	94.2
340.		1115.	471.		51.0	7.4	235.	4206.	610.	9.65	1.40	629.	91.3
342.		1123.	476.		49.6	7.2	238.	4171.	605.	9.31	1.35	602.	87.3
348.		1143.	496.		47.6	6.9	245.	4102.	595.	8.69	1.26	547.	79.4
367.		1203.	526.		44.1	6.4	259.	3896.	565.	7.45	1.08	513.	74.4
376.		1234.	557.		40.7	5.9	267.	3765.	546.	6.62	.96	452.	65.5
397.		1304.	607.		38.6	5.6	281.	3592.	521.	5.65	.82	403.	58.5
419.		1374.	668.		33.8	4.9	295.	3385.	491.	4.62	.67	328.	47.6
428.		1404.	683.		32.4	4.7	300.	3351.	486.	4.27	.62	308.	44.6
458.		1504.	759.		31.0	4.5	314.	3144.	456.	3.38	.49	250.	36.2
482.		1580.	820.		26.9	3.9	324.	2979.	432.	2.83	.41	209.	30.3
489.		1605.	840.		26.2	3.8	329.	2944.	427.	2.69	.39	199.	28.8
520.		1705.	921.		25.5	3.7	344.	2772.	402.	2.21	.32	164.	23.8
529.		1735.	957.		23.4	3.4	349.	2737.	397.	2.00	.29	154.	22.3
550.		1805.	1012.		22.7	3.29	354.	2634.	382.	1.79	.26	137.	19.8
581.		1906.	1093.		21.6	3.14	369.	2496.	362.	1.52	.22	113.	16.4
611.		2006.	1164.		19.9	2.89	380.	2392.	347.	1.31	.19	97.2	14.1
672.		2206.	1341.		17.6	2.55	400.	2186.	317.	.97	.14	68.9	10.0
734.		2407.	1518.		16.4	2.38	415.	1986.	288.	.69	.10	-----	-----
795.		2608.	1700.		14.3	2.08	430.	1848.	268.	-----	-----	-----	-----
841.		2758.	1842.		13.5	1.96	435.	1744.	253.	-----	-----	-----	-----
856.		2808.	1873.		13.1	1.90	440.	1710.	248.	-----	-----	-----	-----
917.		3009.	2050.		12.2	1.77	450.	1606.	233.	-----	-----	-----	-----
1070.		3510.	2480.		10.0	1.45	476.	1365.	198.	-----	-----	-----	-----
1223.		4012.	2935.		8.5	1.23	486.	1200.	174.	-----	-----	-----	-----
1376.		4513.	3441.		7.4	1.08	-----	-----	-----	-----	-----	-----	-----
1529.		5015.	3846.		6.6	.95	-----	-----	-----	-----	-----	-----	-----

BEST AVAILABLE COPY

Table 1. Predicted Air Blast Parameters for DICE THROW Event (Continued)

	GR		TA msec	P's		PPD msec	OPI		HDP		HDPI	
	m	ft		kPa	psi		kPa-msec	psi-msec	kPa	psi	kPa-msec	psi-msec
1681.		5516.	4352.	5.9	.85	----	----	----	----	----	----	----
1834.		6017.	4757.	6.3	.77	----	----	----	----	----	----	----
1987.		6519.	5263.	4.8	.70	----	----	----	----	----	----	----
2140.		7020.	5668.	4.4	.64	----	----	----	----	----	----	----

	Scale Factors	
	kg, meter	pound, foot
S <sub>p</sub>	1.1922	1.1922
S <sub>d</sub>	.0114	.0087
S <sub>t</sub>	.0113	.0087
S <sub>i</sub>	.0134	.0103

GR-----Ground range, horizontal distance from ground zero; m (ft).  
 AT-----Arrival time, lapsed time from detonation to shock wave arrival; msec.  
 OP-----Shock pressure, maximum shock overpressure; kPa (psi).  
 PPD-----Duration, length of positive overpressure phase; msec.  
 OPI-----Overpressure impulse, integral of positive overpressure phase; kPa-msec (psi-msec).  
 HDP-----Dynamic pressure, maximum horizontal dynamic pressure; kPa (psi).  
 HDPI-----Dynamic pressure impulse, integral of dynamic pressure phase; kPa-msec (psi-msec).

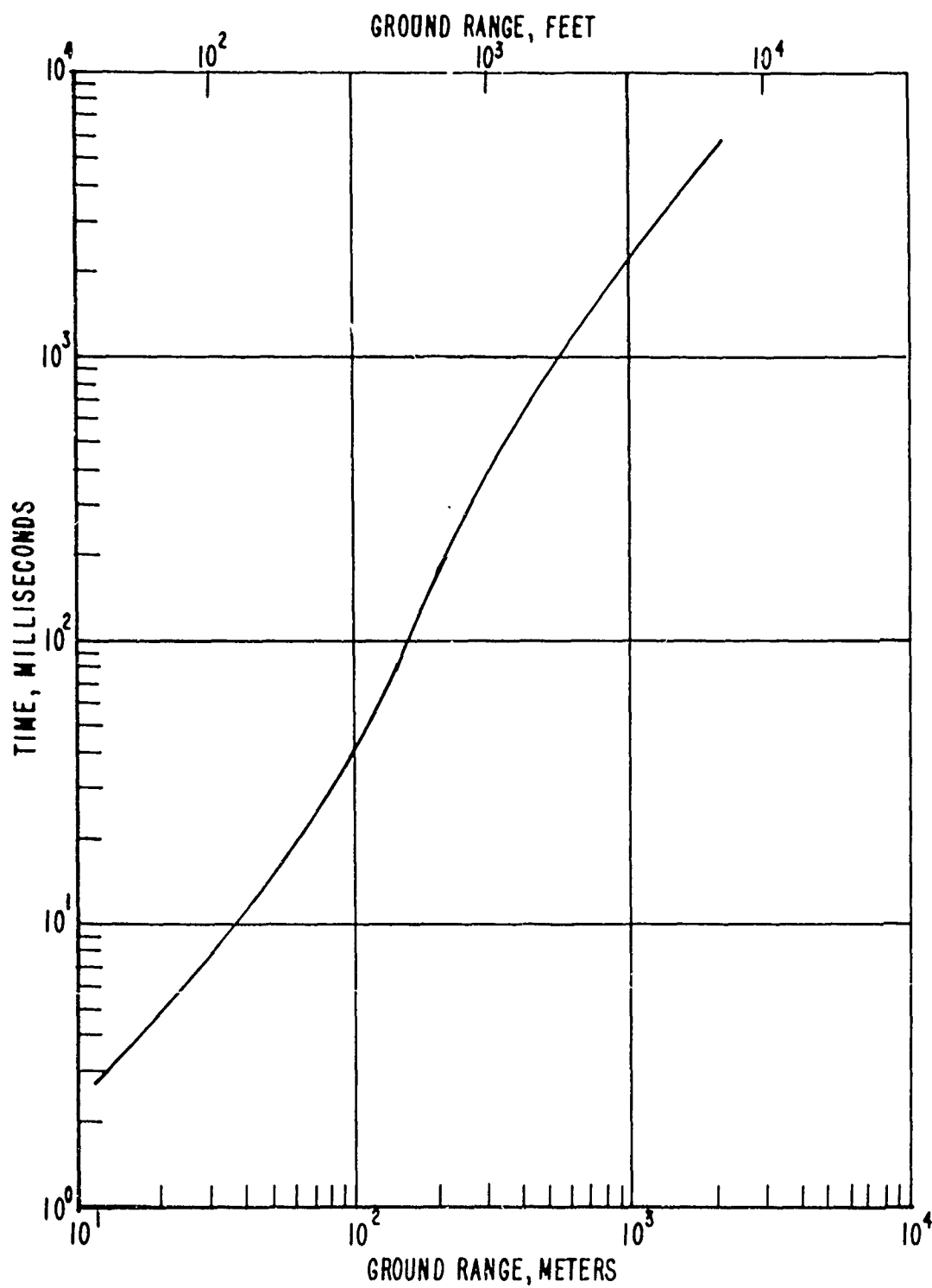


Figure 3. Predicted arrival time versus ground range



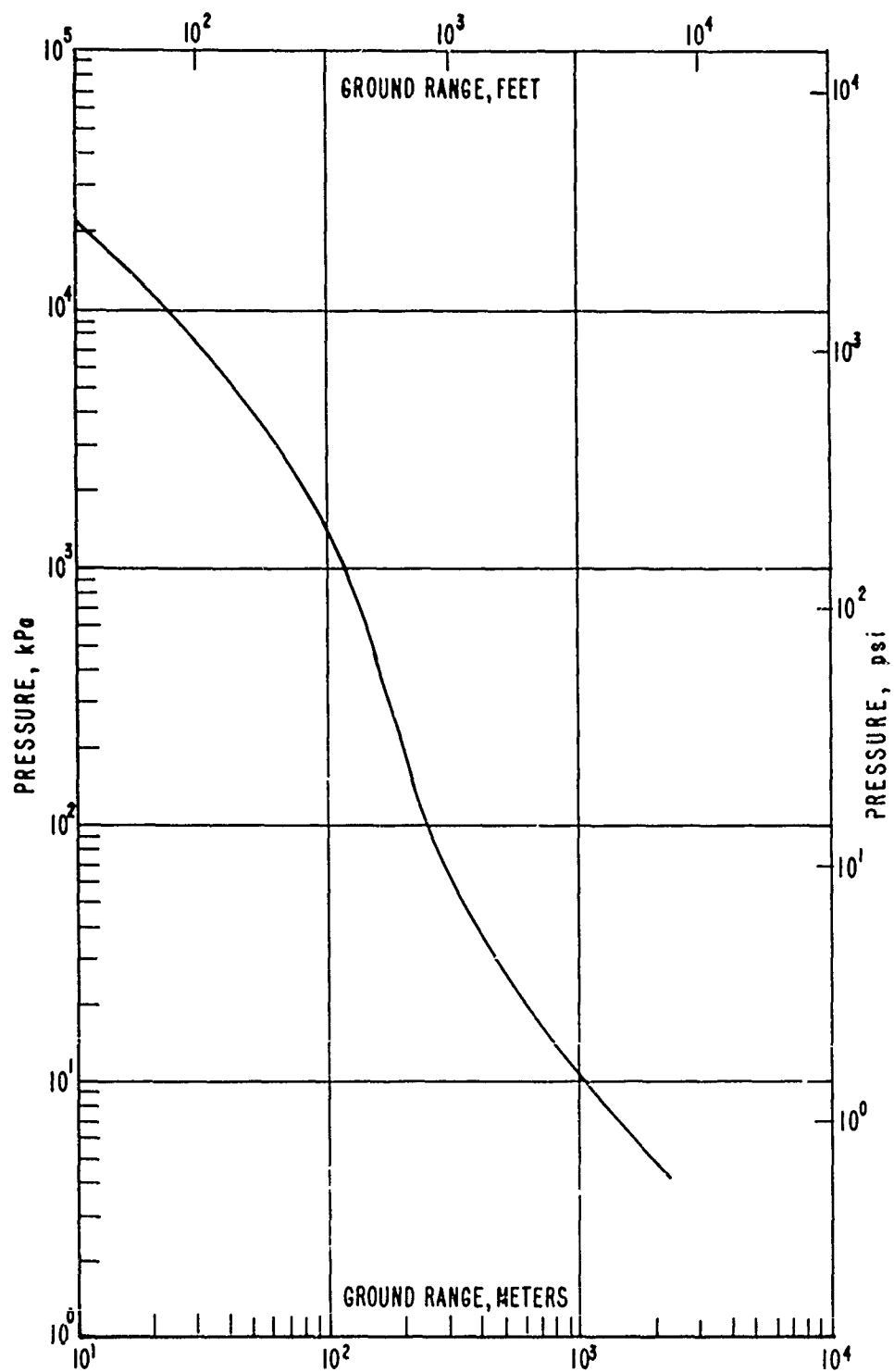


Figure 4. Predicted shock overpressure versus ground range

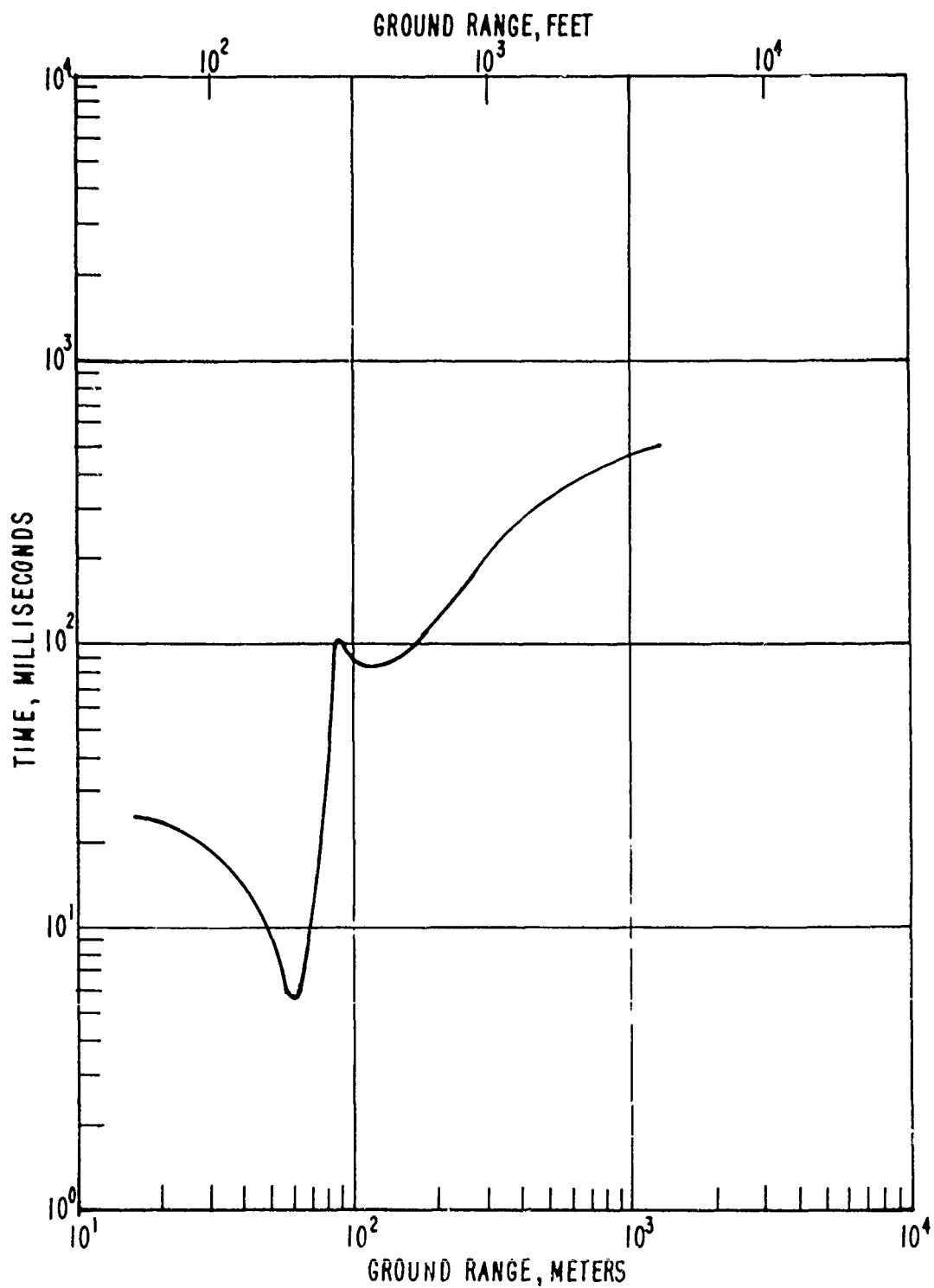


Figure 5. Predicted positive phase duration versus ground range

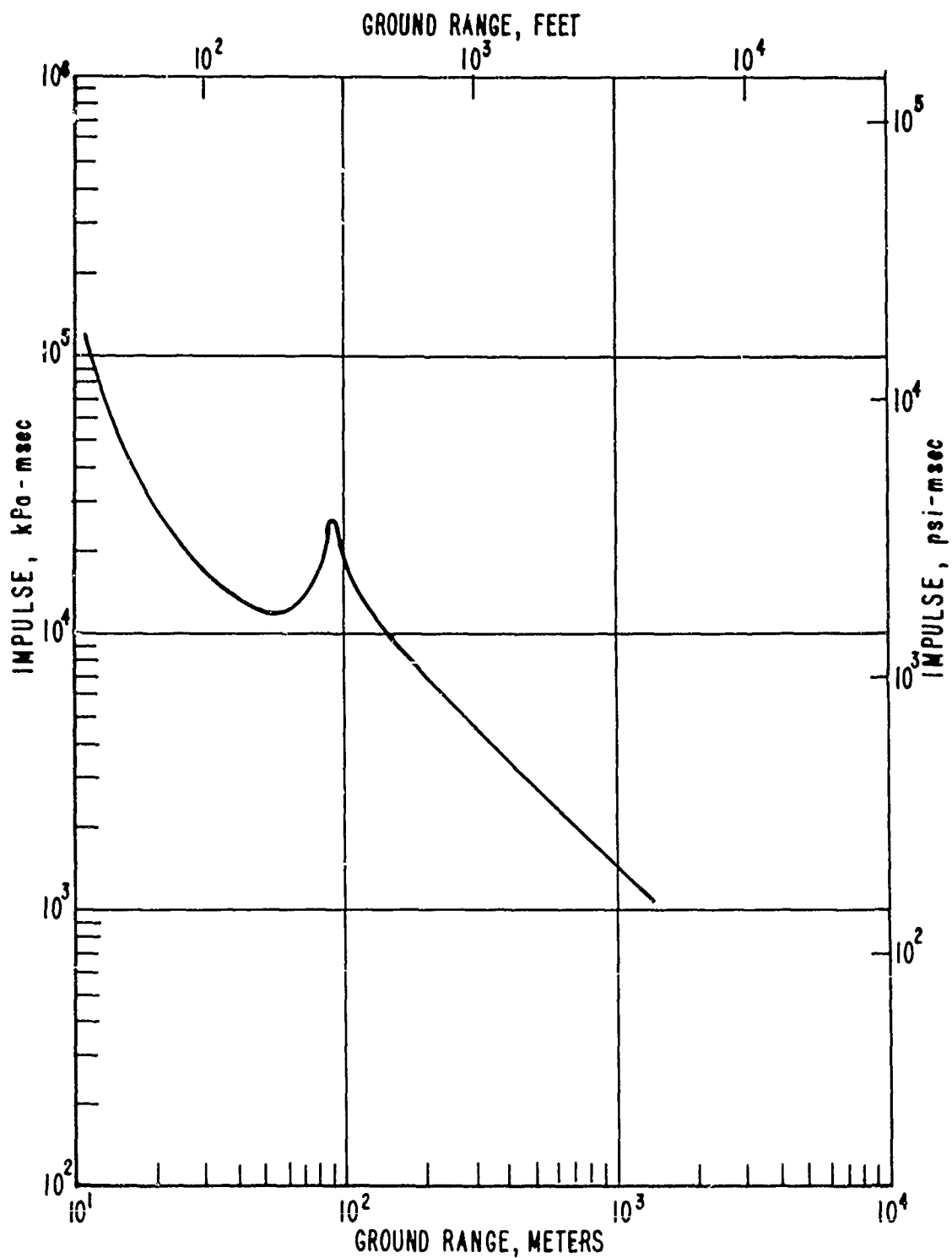


Figure 6. Predicted positive phase impulse versus ground range

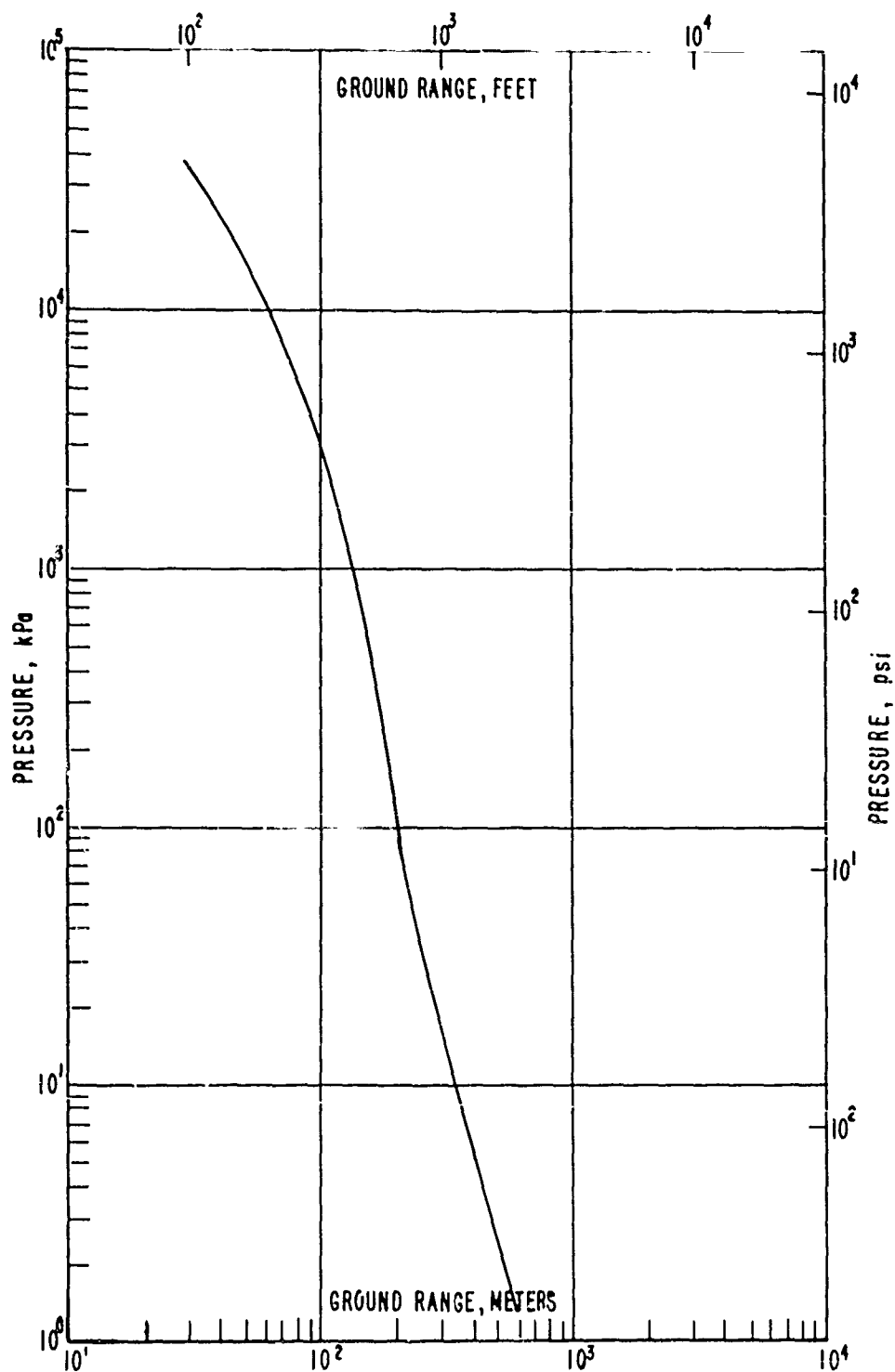


Figure 7. Predicted horizontal dynamic pressure versus ground range

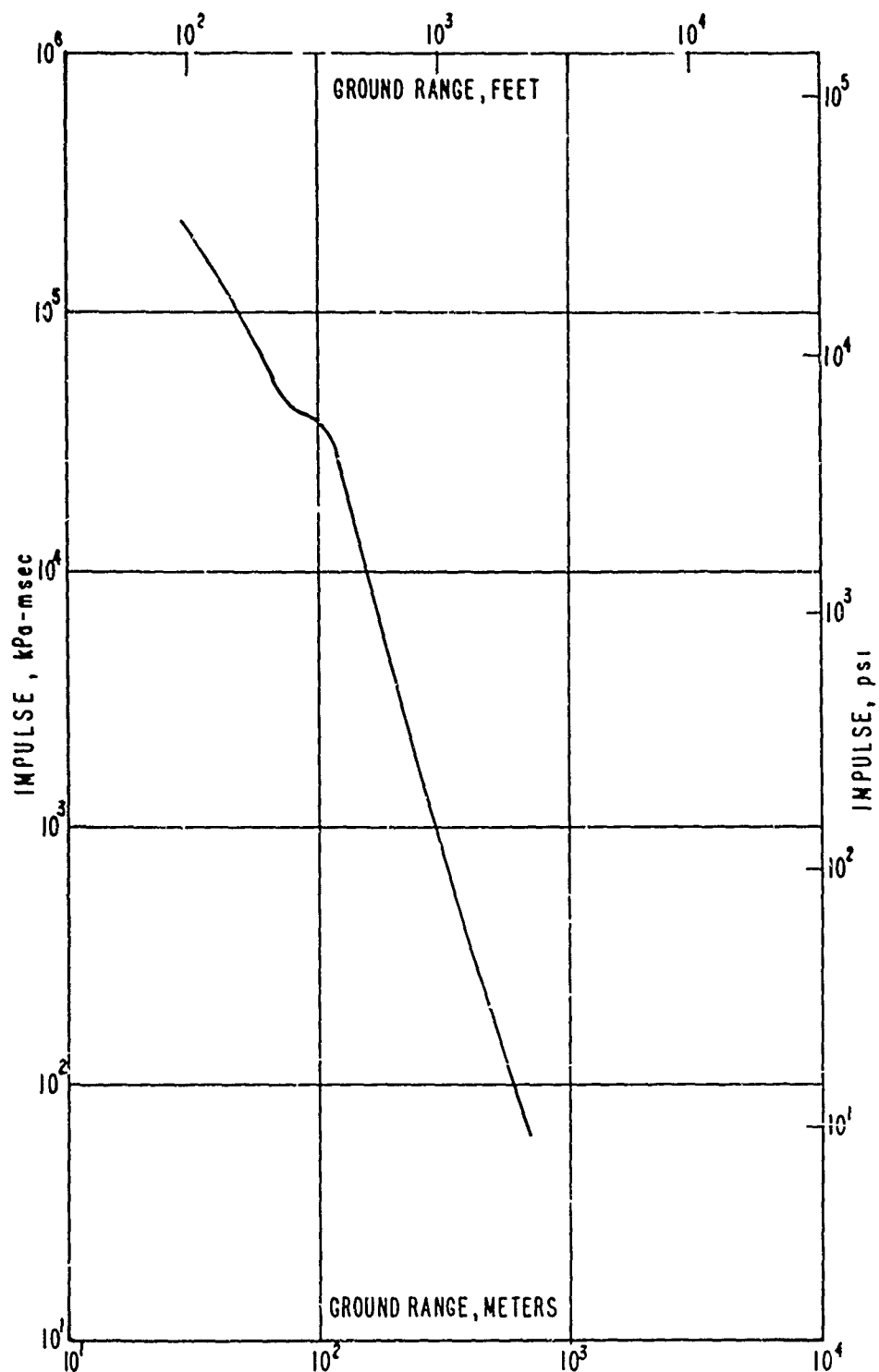


Figure 3. Predicted horizontal dynamic pressure impulse versus ground range

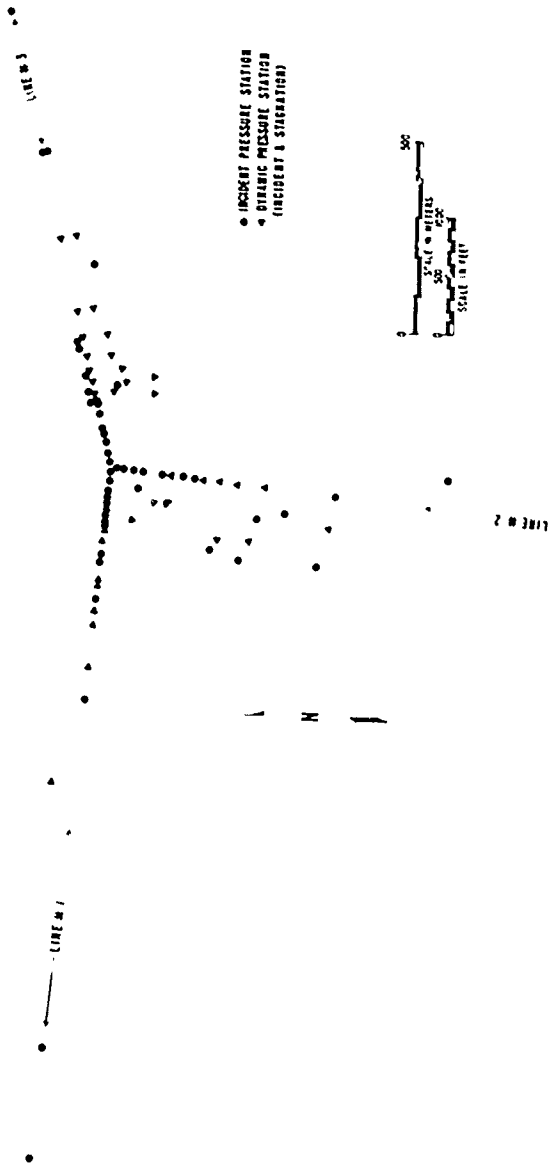


Figure 9. Experiment layout for the Free Field Air Blast Definition experiment

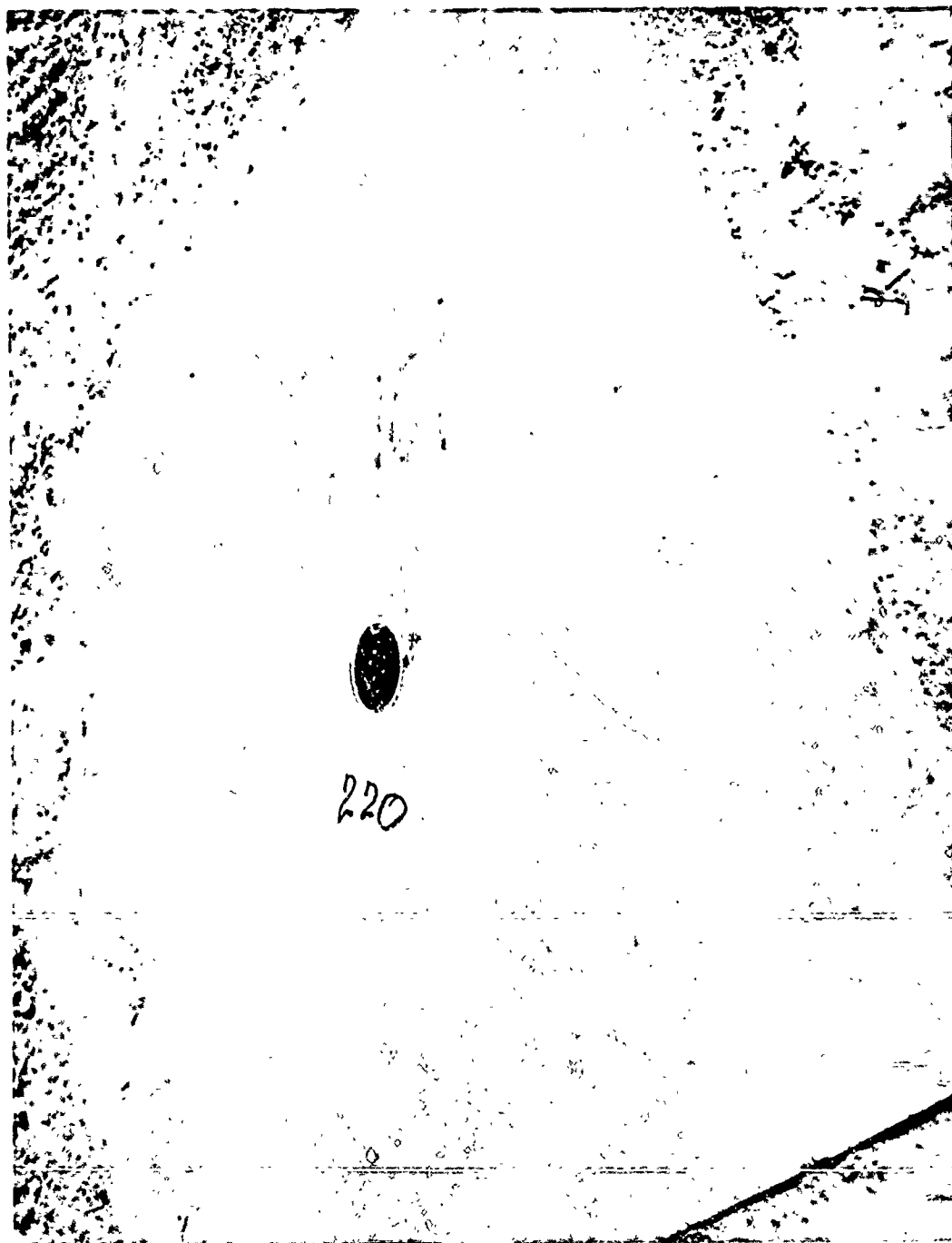


Figure 10. A ground level station to measure incident pressure

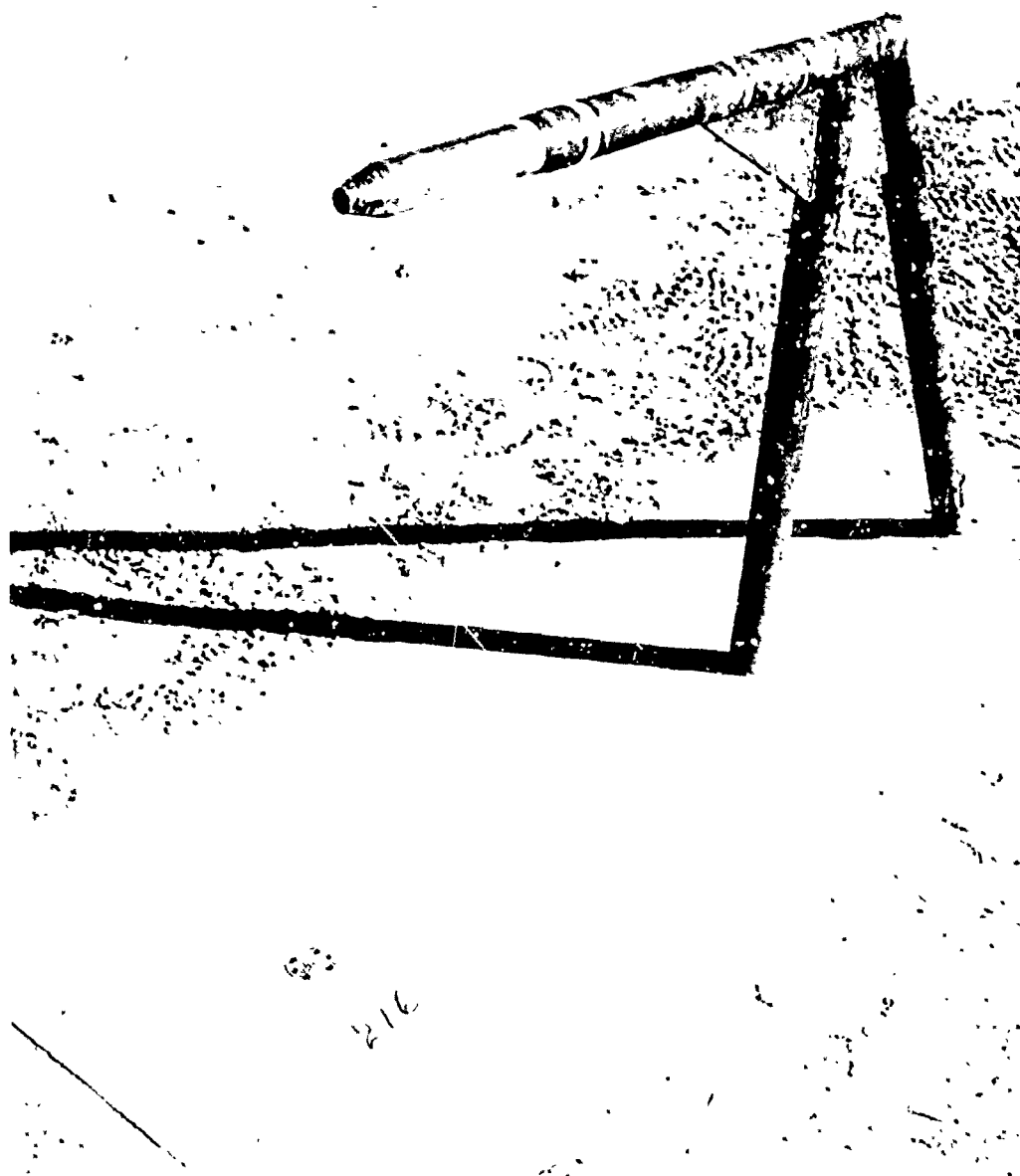


Figure 11. A station to measure ground level incident pressure and elevated stagnation pressure



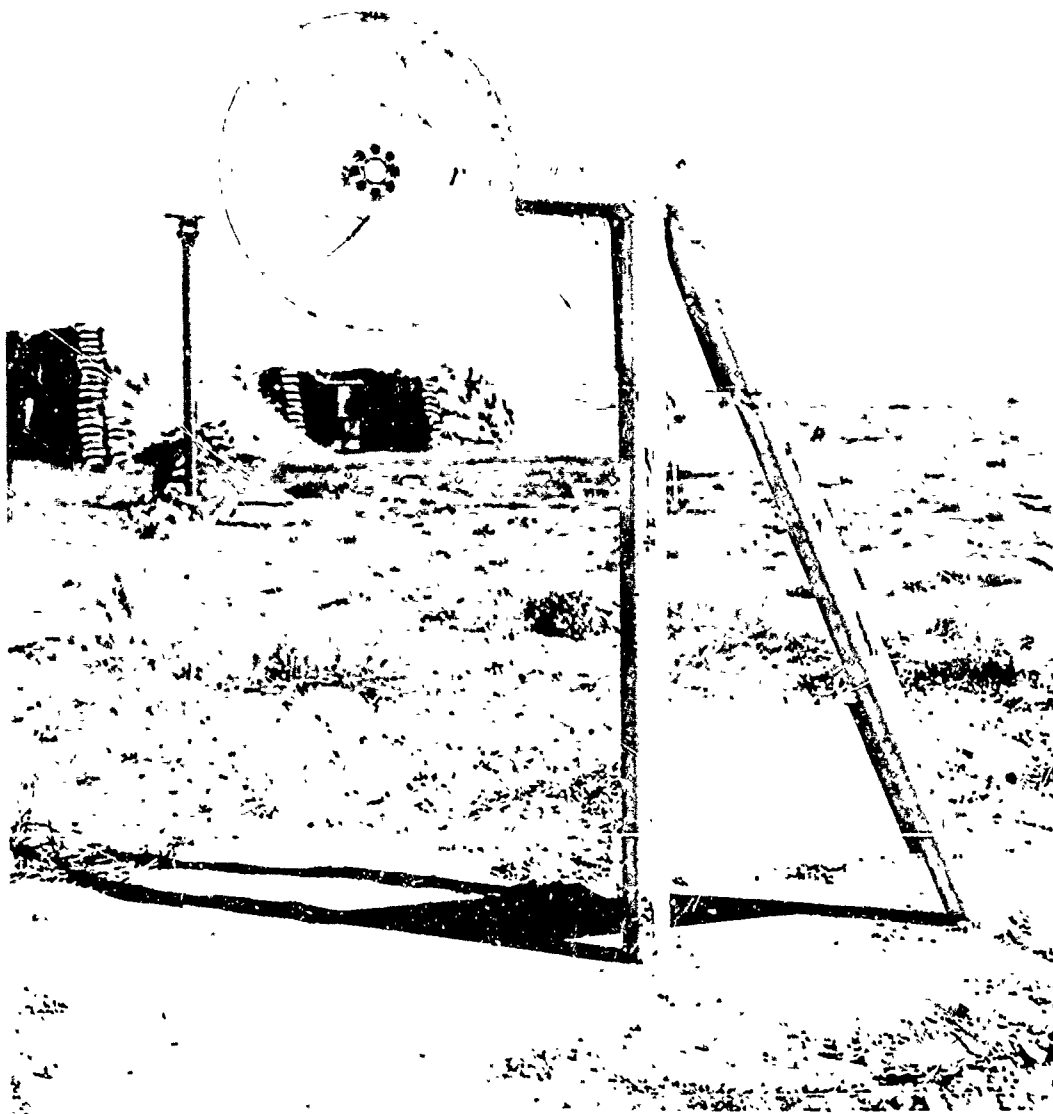


Figure 12. An elevated incident pressure station

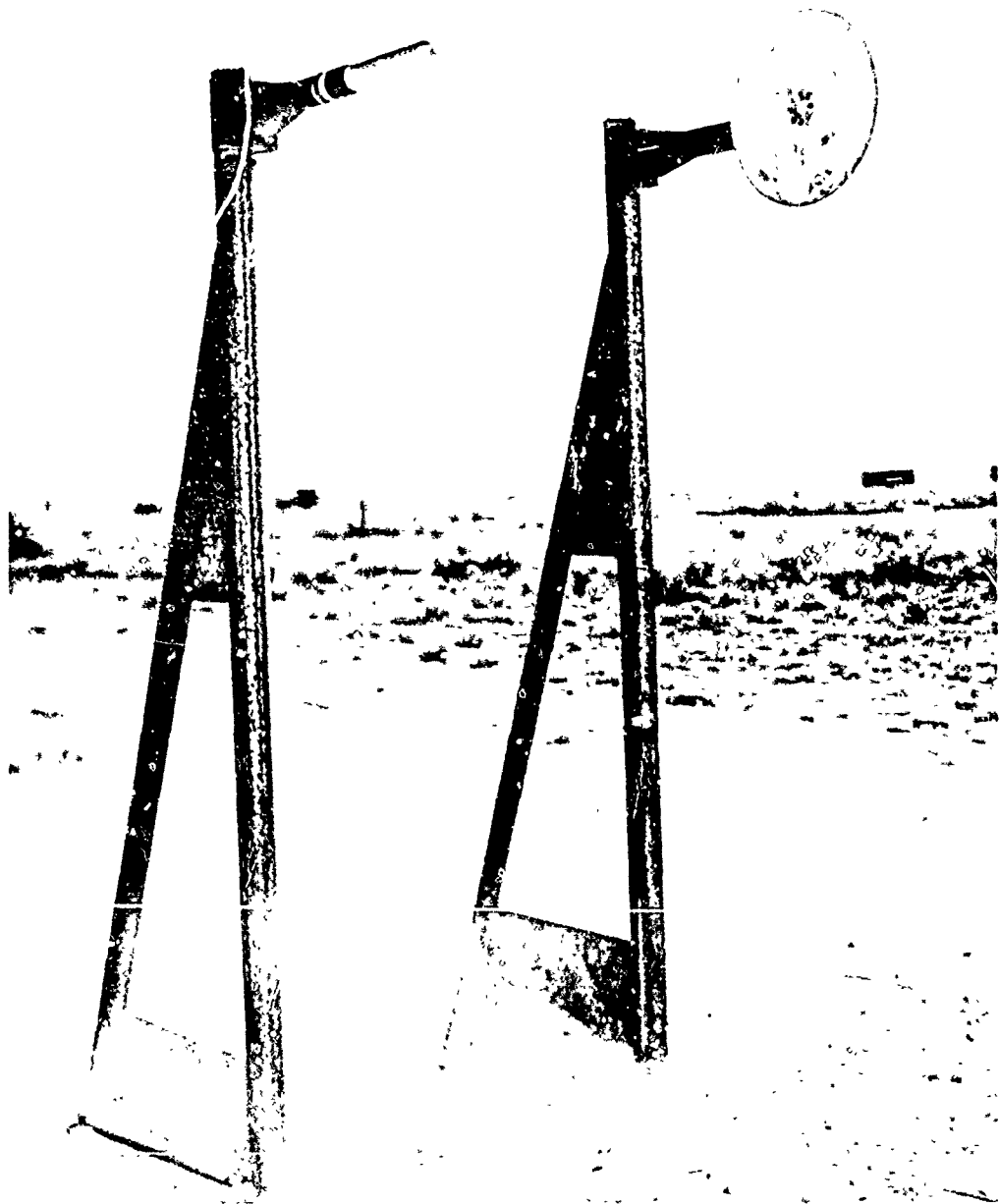


Figure 13. A station to measure incident overpressure and stagnation pressure at an elevation of 2.44 meters

surface with the transducers mounted in probes as shown in Figures 11, 13, and 14.

Those experiments which were directly supported by the Free Field Air Blast Definition Experiment included but were not necessarily limited to:

- Exp. 034 Blast Effects on Wheeled Vehicles;
- Exp. 036 Blast Effects on Army Operationally Oriented Weapon Systems;
- Exp. 103 Vulnerability & Hardening of Command Control and Communication Shelter Systems;
- Exp. 107 Blast Effects on In-Flight Helicopter;
- Exp. 337 Collateral Damage Wall Test;
- Exp. 398 Blast Effects on Blast Door and Shelter;
- Exp. 408 Blast Displacement Effects in Field Fortifications.

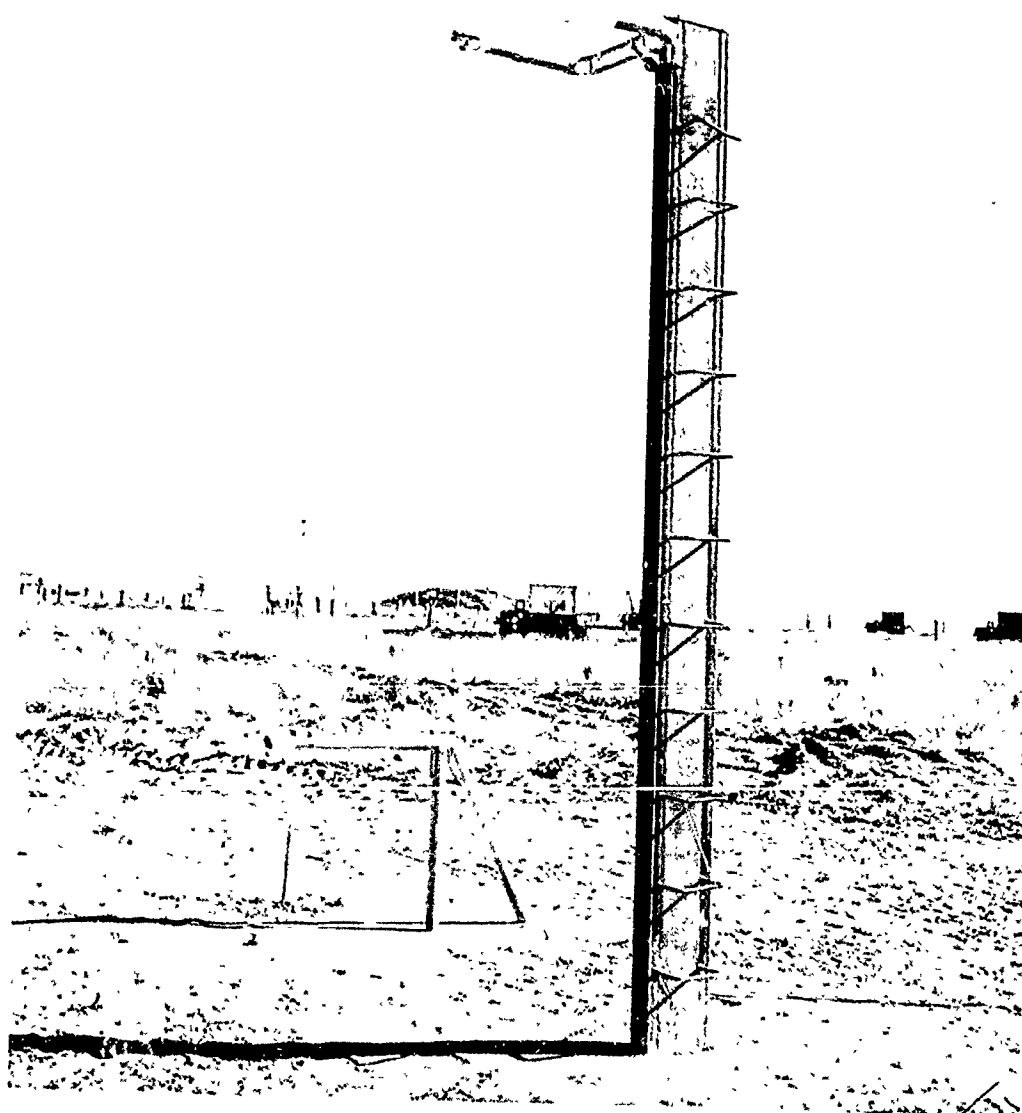


Figure 14. A station to measure incident overpressure and stagnation pressure at an elevation of 3.66 meters

## 4. INSTRUMENTATION

### 4.1 TRANSDUCERS.

Three types of pressure transducers were employed to acquire the free field air blast data for this experiment. The vast majority of the transducers employed were Tyco (Bytrex) Model HFG. This transducer is a 4-arm Wheatstone bridge configuration utilizing semi-conductor strain elements. The transducer has two active arms for sensing and two passive arms for bridge completion and temperature compensation. AC or DC excitation of up to 25 volts may be used and the device has a nominal output of 7 mV/V full scale. The natural frequencies of these transducers vary with the rated pressure range. This varies from approximately 15 kHz for a 103 kPa (15 psi) unit to about 80 kHz for a 13790 kPa (2000 psi) unit.

A second type of transducer employed was the Endevco Model 8510. This transducer employs a silicon diaphragm on which a 4-arm Wheatstone bridge is atomically bonded with a diffusion process. Balancing and compensation elements are contained in the transducer. The transducer can be used with an excitation voltage up to 10 VDC and has a nominal output of 30 mV/V full scale. The natural frequency for a 103 kPa (15 psi) unit is a nominal 65 kHz.

The third transducer type employed was a PCB Model 102. This transducer is a quartz piezo-electric design with a built in amplifier. These devices were employed in the very high pressure region, 6895 kPa (1000 psi) and higher, and the very low pressure region, 6.89 kPa (1 psi) and lower. Both ranges of transducers require a 4 ma constant current excitation. The low pressure unit has an output of 2.9 mV/kPa (20 mV/psi) while the output of the high pressure unit is .07 mV/kPa (.5 mV/psi). The nominal natural frequency for both ranges is 500 kHz with an associated time constant of 1000 seconds for the high pressure range and 1 second for the low pressure range.

The Endevco and PCB transducers were used only in incident pressure applications while the Tyco (Bytrex) transducers were used for both incident and stagnation pressure measurements.

#### 4.2 RECORDING EQUIPMENT.

The data for this experiment were acquired on analog magnetic tape recorders housed in instrumentation trailers located in each of the three instrumentation parks. The tape recorders, associated input/output signal conditioning equipment, ancillary equipment, and instrumentation trailers were supplied from the DNA instrument pool at the Nevada Test Site. Instrumentation configuration was accomplished by the DNA field support contractor as per instructions from the experimenter.

B & F Model 1-700 signal conditioning equipment was used to condition all data signals. These units provide gage excitation, balancing, and calibration functions. For the 4-arm Wheatstone bridge transducers [Tyco (Bytrex) and Endevco] the standard B & F Model 1-700SG signal conditioning card was employed. A specially designed and fabricated card, B & F Model 1-700TC-1A, was used when the piezo-electric transducers (PCB) were employed. Both of these signal conditioning cards are interchangeable and may be intermixed within a recording package.

Baylab Model 5503 data amplifiers were used where required to increase the transducer signal to a level compatible with the tape recorder input requirements. The 5503 amplifier is a high gain differential unit with a data bandwidth of DC to 100 kHz.

Three types of analog magnetic tape recorders were employed to acquire the data for this experiment. The recorders were: (1) Honeywell Model 96; (2) Sangamo Model 4784; and (3) Bell & Howell CEC Model VR-3300. The Honeywell and Bell & Howell recorders were 14 track configurations and the Sangamo recorders were 32 track versions. Two

tracks on each recorder were operated in the direct record mode to record a combined time reference and fiducial signal, one track was operated in the FM mode to record an IRIG time signal (IRIG-A in Instrument Park #2 and IRIG-B in Instrument Parks #1 and #3), and the remaining tracks (11 for the Honeywell and Bell & Howell recorders and 29 for the Sangamo machines) were operated in the FM mode to record the individual pressure-time histories in a channel per track format. A total of nine tape machines were employed all or in part for this experiment.

During the event the recording equipment was operated remotely through the use of timing signals provided via hardwire from the timing and firing system provided and operated by the Defence Research Establishment - Suffield. The timing signals controlled or furnished the following functions: (1) tape recorder start; (2) shunt calibration; (3) fiducial time; and (4) tape recorder hold. In addition, monitor signals were transmitted from the instrumentation trailers to the timing and firing bunker to confirm instrumentation power on, temperature overrides off, and tape recorder operation.

#### 4.3 CALIBRATION.

Two different types of calibration procedures were required for the different types of transducers employed for this experiment. The 4-arm Wheatstone bridge transducers [Tyco (Bytrex) and Endevco] were handled in the following manner. Once the complete data channel (transducer, signal cable, signal conditioner, amplifier, and tape recorder) had been installed and connected together, the calibration was accomplished by statically applying the expected forcing function to the transducer and recording its resultant signal on magnetic tape. The expected forcing function calibration is provided to the transducer through a system of regulators using dry nitrogen as the pressure source and monitoring the applied static pressure with a precision

dial manometer whose calibration is traceable to the National Bureau of Standards. Amplifier and recorder gains are adjusted at this time to yield a pre-determined FM carrier deviation. Concurrently a shunt calibration level is established which is approximately equal to the level of the expected forcing function. Data channel linearity is confirmed at this time by statically applying incremental pressure steps and monitoring the resultant incremental outputs. All measuring equipment used for these purposes (digital voltmeters, frequency counters, etc.) also have calibrations traceable to the National Bureau of Standards. Once the FM carrier deviation has been established, the shunt calibration level set, and the linearity confirmed, the forcing function and shunt calibration levels are recorded on magnetic tape. The shunt calibration level is re-recorded immediately prior to the event (T-1 minute). No gain or shunt resistance adjustments are made between the calibration and the event.

Since the piezo-electric transducers (PCB) do not have DC response, they cannot be calibrated statically in the field and consequently other procedures must be used. These transducers were calibrated in the laboratory using two independent methods. First the transducers were pulse calibrated over a range of pressures to determine their individual sensitivities and to confirm linearity. The pulse calibration is accomplished by connecting the transducer to a known pressure source rapidly, through a quick acting valve, and monitoring the transducer output with a peak reading voltmeter and an oscilloscope. As with the static calibration procedure, all devices used to monitor the pressure source and the transducer output have traceable calibrations. Once the linearity is confirmed and the sensitivity determined the transducer is inserted in a shock tube and tested dynamically. The waveshape is monitored with an oscilloscope and the sensitivity of the transducer is confirmed by relating its output to the actual shock level applied as determined from the shock front velocity versus shock front pressure using the



following Rankine-Hugoniot relation\*:

$$P_s = \frac{7P_1}{6} \left( \frac{u_s^2}{a^2} - 1 \right) \quad (5)$$

where:

$P_s$  = shock overpressure, kPa (psi);

$P_1$  = atmospheric pressure, kPa (psi);

$u_s$  = shock front velocity, m/sec (ft/sec);

$a$  = ambient sound velocity, m/sec (ft/sec).

Calibration levels and recorder carrier deviations for the event are established by using the transducer sensitivity determined in the laboratory and the voltage insertion calibration capabilities of the B & F Model 1-700TC-1A signal conditioner card. The transducer sensitivity and the expected forcing function level are combined to determine the desired calibration voltage which is established with the signal conditioner card and used to set the desired FM carrier deviation. This voltage calibration is then inserted remotely and recorded on the magnetic tape immediately prior (T-1 minute) to the event.

---

\*I. I. Glass, Shock Tubes, Part I: Theory and Performance of Simple Shock Tubes, University of Toronto, Toronto, Ontario, Canada, UTIA Review No. 12, Part I, May 1958

## 5. DATA REDUCTION

The calibrations and data recorded on magnetic analog tape are converted to digital format using an analog to digital (A to D) converter. The resultant digital pressure-time histories are computer processed to convert the information to engineering units referenced to the forcing function calibration with gain corrections, if required, based on the ratio of the two shunt calibration levels.

The real time recorded time references are used as external clocks for the analog to digital conversion thus eliminating the need for electronic tape speed compensation during the data playback. Arrival time information is obtained by initiating the A to D converter at zero time (fiducial mark) and accumulating time based on the reference frequency until shock wave arrival is sensed at each particular transducer location.

Overpressure impulse is obtained by performing a point by point numerical integration of the pressure-time histories. The beginning and ending pressure values for each time (digital sample) interval are averaged and multiplied by the length of the time interval. These incremental areas are accumulated to obtain the impulse-time parameter.

The resultant data, after conversion to engineering units, are displayed in tabular form and are plotted for presentation of the time history waveforms. Specific values of arrival time, overpressure, duration, and impulse are taken from the tabulations and are presented in tabular form. These data are plotted against ground range for comparison with the analytical and empirical pre-test predictions.

An additional step of data processing is required for those combinations of incident and stagnation measurements taken for the purpose of obtaining dynamic pressure information. The dynamic pressure-time history is constructed by performing an additional calculation with

both the incident and stagnation measurements, taken at the same free field station. The digital histories of the time and pressure are aligned with respect to the blast wave arrival time and the pressure values for the stagnation and incident pressures are compared at equal time intervals thereafter.

The absolute ratio of stagnation to incident pressure,  $(P_{stag} + P_1)/(P_s + P_1)$  is determined for each time interval beginning with blast wave arrival time. Using this ratio, the Mach number of the flow is calculated for each time interval using one of the following equations:

$$M^2 = \frac{2}{\gamma-1} \left[ \left( \frac{P_{stag} + P_1}{P_s + P_1} \right)^{(\gamma-1)/\gamma} - 1 \right] \text{ for } M \leq 1; \quad (6)$$

or,

$$M^2 = \frac{2}{\gamma+1} \left[ \left( \frac{P_{stag} + P_1}{P_s + P_1} \right)^{\gamma-1} \left( \frac{2\gamma}{\gamma+1} M^2 - \frac{\gamma-1}{\gamma+1} \right) \right]^{1/\gamma} \text{ for } M > 1; \quad (7)$$

where:

- M = flow Mach number;
- $P_1$  = atmospheric pressure, kPa (psi);
- $P_s$  = incident overpressure, kPa (psi);
- $P_{stag}$  = stagnation overpressure, kPa (psi);
- $\gamma$  = ratio of specific heats\*.

\*C. N. Kingery and B. F. Pannill, Parametric Analysis of the Regular Reflection of Air Blast, Ballistic Research Laboratory, Aberdeen Proving Ground, Maryland, BRL Report 1249, June 1964.

In using the above equations, the following procedure is employed. The ratio of stagnation to incident pressure is first inserted into Equation (6) and a value for  $M$  is determined. If  $M \leq 1$ , the calculation is continued to the next step. If however  $M > 1$ , the ratio is used with Equation (7) in an iteration process to determine the value of  $M$ .

When the values for  $M$  have been obtained in this manner, the value of  $M$  for each time is combined with the corresponding incident pressure value and the dynamic pressure is then calculated from the equation:

$$P_D = \frac{\gamma M^2}{2} (P_s + P_1); \quad (8)$$

where:

$P_D$  = dynamic overpressure, kPa (psi).

When the values of  $P_D$  have been determined for each time value in the time history, the dynamic pressure impulse is determined in the same manner as described previously for the incident pressure impulse.

The results of this calculation are also presented in both tabular and plotted form.

## 6. RESULTS

The results available from the final data reduction indicate that a 91% data return was achieved for the Free Field Air Blast Definition Experiment.

The results of the measurements of arrival time, incident over-pressure, duration, impulse, dynamic pressure, and dynamic pressure impulse are listed in Table 2. The results are listed separately for Blast Lines 1, 2, and 3. Also included in the listing for each particular blast line are those stations located adjacent to the particular lines in support of other experiments.

The results obtained along Blast Line 1 are plotted in Figures 15 through 20. The data points are plotted as a function of ground range and are shown in comparison to the pre-test prediction, the solid line on the figures. The pressure-time histories of the incident pressure measurements and the time histories resulting from the dynamic pressure calculations are found in Appendix A of this report. With the exception of those time histories shown for Station 112, the waveforms along this blast line appear to be classical in nature. Station 112 was located to the South of the blast line in the AFWL area (Exp. 398) and was influenced by the air blast anomaly that traveled through that region.

Figures 17 and 18, the plots of positive phase duration and impulse versus ground range seem to substantiate the conclusions drawn from the Pre-DICE THROW II-2 results\* that the significant inflection points associated with the blast wave separation from the fireball previously observed during TNT detonations either do not exist or are greatly reduced in the environment generated by the ANFO detonation.

*\*G. D. Teel, Pre-DICE THROW II Events: Free Field Air Blast Definition of TNT and AN/FO Detonation, Ballistic Research Laboratory, Aberdeen Proving Ground, Maryland, Defense Nuclear Agency POR 6915, to be released.*

Table 2a. Measured Air Blast Parameters - Blast Line 1

STA #	GR		ELEV		A		PS		PPD		OPI		HDP		HDI	
	m	ft	m	ft	m/sec	ft/sec	kPa	psi	msec	ft/msec	kPa-msec	psi-msec	kPa	psi	kPa-msec	psi-msec
101	9.88	32.4	0	0	1.67	0	19980.	2895.	8.82	89890.	13035.					
102	11.4	37.4	0	0	1.98	0	17910.	2595.	8.57	79780.	11570.					
102	11.4	37.4	0	0	2.00	0	27560.	3995.	-1	-1	-1	-1				
103	34.4	113.	0	0	8.20	0	8520.	1235.	-1	-1	-1	-1				
103	34.4	113.	0	0	8.23	0	-2	-2	-2	-2	-2	-2				
104	62.8	206.	0	0	19.6	0	3355.	487.	21.1	13340.	1935.					
105	76.2	250.	0	0	26.9	0	2255.	327.	28.2	12560.	1820.					
106	85.6	281.	0	0	32.8	0	2335.	339.	-3	-3	-3	-3				
107	91.4	300.	0	0	36.6	0	1850.	268.	-3	-3	-3	-3				
109	101.	332.	0	0	43.4	0	1375.	199.	27.8	13070.	1895.					
110	107.	350.	0	0	47.7	0	1255.	182.	-3	-3	-3	-3				
111	122.	400.	0	0	61.0	0	1095.	159.	-3	-3	-3	-3				
112 <sup>6</sup>	134.	440.	0	0	89.9	0	452.	65.6	67.8	9880.	1435.		600.	87.0	9980.	1445.
112 <sup>6</sup>	134.	440.	3.66	12.0	90.2	0	488.	70.8	55.0	8380.	1215.		591.	85.7	9295.	1350.
113	137.	450.	0	0	77.0	0	553.	80.2	68.3	9900.	1435.		809.	117.	14935.	2165.
114	152.	500.	0	0	95.0	0	487.	70.6	98.4	8045.	1165.					
115	160.	525.	0	0	104.	0	408.	59.2	74.3	8350.	1210.					
116	165.	540.	0	0	110.	0	362.	52.5	119.	8690.	1260.					
120	195.	640.	0	0	156.	0	215.	31.2	122.	6930.	1005.		465.	67.4	16510.	2395.
122	226.	740.	0	0	210.	0	137.	19.9	140.	5655.	820.		147.	21.3	3670.	532.
123	250.	820.	0	0	257.	0	103.	14.9	153.	4855.	704.					
125	294.	965.	0	0	352.	0	60.5	8.8	174.	4045.	587.					
125	294.	965.	0	0	352.	0	75.2	10.9	195.	5110.	741.					
126	311.	1020.	0	0	390.	0	59.4	8.6	220.	4675.	678.		16.5	2.39	969.	141.
130	347.	1140.	0	0	475.	0	46.3	6.7	235.	4240.	615.					
131	375.	1230.	0	0	542.	0	41.9	6.1	240.	3955.	574.		8.07	1.17	565.	81.9
132	418.	1370.	0	0	643.	0	40.0	5.8	249.	3790.	550.					
134	527.	1730.	0	0	910.	0	27.8	4.0	290.	2550.	370.		4.50	.65	45.8	6.65
135	610.	2000.	0	0	1125.	0	23.5	3.4	245.	2150.	312.					
136 <sup>7</sup>	838.	2750.	12.2	40.0	1760.	0	17.3	2.5	350.	1850.	268.		3.54	.51	8.31	1.21
139	1524.	5000.	0	0	3690.	0	9.09	1.3	365.	727.	105.					
139	1524.	5000.	0	0	3690.	0	10.2	1.5	410.	1000.	154.					
140	1829.	6000.	0	0	4510.	0	8.36	1.2	391.	784.	114.					

Table 2b. Measured Air Blast Parameters - Blast Line 2

STA #	GR		ELEV		TA msec	PS		PPD msec	OPI		HDP		HDPI	
	m	ft	m	ft		kPa	psi		kPa-msec	psi-msec	kPa	psi	kPa-msec	psi-msec
201	9.88	32.4	0	0	1.72	20490.	2970.	-1	-1	-1				
202	11.4	37.4	0	0	2.10	16360.	2375.	-1	-1	-1				
203	34.4	113.	0	0	8.33	7935.	1150.	-30.	-19560.	2835.				
204	62.8	206.	0	0	19.4	4220.	612.	14.0	12540.	1820.				
206	85.6	281.	0	0	32.4	2220.	322.	50.5	15070.	2185.				
207	91.4	300.	0	0	35.2	1905.	276.	68.1	14870.	2155.				
213	137.	450.	0	0	74.8	645.	93.5	62.3	9855.	1430.				
214	152.	500.	0	0	84.4	621.	90.1	104.	10590.	1535.	333.	48.3	5820.	844.
214'	152.	500.	3.66	12.0	84.7	630.	91.4	-4	-4	-4	562.	81.5	6790.	985.
216	165.	540.	0	0	107.	342.	49.6	97.3	7895.	1145.	303.	44.0	6335.	919.
213'	184.	605.	0	0	118.	372.	54.0	150.	7310.	1060.	252.	36.6	1630.	237.
219'	184.	605.	3.66	12.0	110	203.	29.4	142.	6925.	1005.	106.	15.4	3385.	491.
220	195.	640.	0	0	143.	203.	29.4	139.	7100.	1030.				
222	226.	740.	0	0	190.	75.6	11.0	177.	5445.	790.				
223	250.	820.	2.44	8.0	247.	75.9	11.0	155.	4430.	643.	72.4	10.5	-3	-3
225	294.	965.	0	0	354.	63.1	9.2	218.	5095.	739.	-2	-2	-2	-2
229	341.	1120.	2.44	8.0	467.	45.7	6.6	243.	3825.	555.	11.0	1.60	1370.	198.
229'	341.	1120.	2.44	8.0	463.	41.5	6.0	241.	4475.	649.	8.31	1.21	566.	82.1
229'	341.	1120.	2.44	8.0	461.	41.0	6.0	177.	3050.	442.				
232	418.	1370.	2.44	8.0	659.	32.2	4.7	236.	3340.	484.	2.64	.38	29.4	4 26
232'	418.	1370.	2.44	8.0	655.	27.8	4.0	248.	3335.	484.				
232'	418.	1370.	2.44	8.0	657.	27.2	4.0	266.	3320.	482.	1.72	.25	95.4	13.8
232'	418.	1370.	2.44	8.0	656.	27.2	4.0	266.	3565.	517.				
233	480.	1575.	1.22	4.0	820.	28.6	4.2	269.	3075.	446.				
235	610.	2000.	2.44	8.0	1170.	19.5	2.8	189.	1470.	213.				
235'	610.	2000.	2.44	8.0	1180.	17.7	2.6	272.	1820.	264.	1.81	.26	289.	41.9
235'	610.	2000.	2.44	8.0	1120.	20.6	3.0	200.	1320.	191.				
235'	610.	2000.	1.22	4.0	1120.	13.6	2.0	386.	1720.	249.				
235'	914.	3000.	0	0	2030.	7.57	1.1	425.	916.	133.				
235'	1369.	4490.	0	0	3330.	7.57	1.1	425.	916.	133.				
239	1524.	5000.	0	0	3780.	5.37	.8	385.	856.	124.				
240	1829.	6000.	0	0	4630.	3.99	.6	435.	875.	127.				

Table 2c. Measured Air Blast Parameters - Blast Line 3

STA #	GR		ELEV		TA msec	PS		PPD msec	OPI		HDP		HDI	
	m	ft	m	ft		kPa	psi		kPa-msec	psi-msec	kPa	psi	kPa-msec	psi-msec
302	11.4	37.4	0	0	1.92	11800.	1710.	-	-	-	-	-	-	-
303	34.4	113.	0	0	8.06	6525.	946.	-	-	-	-	-	-	-
304	62.8	206.	0	0	19.4	3255.	472.	28.6	12985.	1885.	-	-	-	-
306	85.6	281.	0	0	32.3	1535.	223.	47.8	13795.	2000.	-	-	-	-
308	94.5	310.	0	0	38.0	1380.	200.	126.	13984	2030.	-	-	-	-
309	101.	332.	0	0	43.1	1310.	190.	102.	21940.	3180.	-	-	-	-
313	137.	450.	0	0	75.9	680.	98.6	70.1	10440.	1515.	-	-	-	-
316	165.	540.	0	0	109.	393.	57.0	93.4	5090.	738.	-	-	-	-
317	174.	570.	0	0	122.	300.	43.5	119.	10490.	1520.	-	-	-	-
318	177.	580.	0	0	126.	299.	43.4	114.	7985.	1160.	218.	31.6	2515.	365.
320	195.	640.	0	0	155.	219.	31.8	132.	7315.	1060.	139.	20.2	3195.	463.
320 <sup>14</sup>	195.	640.	.91	3.0	157.	212.	30.7	136.	8965.	1300.	111.	16.1	3335.	484.
321	207.	680.	0	0	176.	162.	23.5	144.	6255.	905.	-	-	-	-
321 <sup>13</sup>	207.	680.	0	0	176.	216.	31.3	148.	8320.	1195.	-	-	-	-
322	226.	740.	0	0	208.	147.	21.3	167.	5895.	855.	58.2	8.44	556.	80.6
322 <sup>14</sup>	226.	740.	0	0	211.	151.	21.9	131.	5655.	820.	67.0	9.72	2430.	352.
322 <sup>15</sup>	226.	740.	.91	3.0	210.	149.	21.6	170.	7055.	1025.	62.2	9.02	1745.	253.
323	250.	820.	0	0	259.	87.8	12.7	198.	6080.	882.	-	-	-	-
323 <sup>13</sup>	250.	820.	0	0	258.	103.	15.2	185.	6860.	995.	-	-	-	-
324	259.	850.	0	0	279.	84.6	12.5	190.	5495.	797.	-	-	-	-
324 <sup>14</sup>	259.	850.	.91	3.0	280.	89.2	12.9	141.	4425.	642.	38.0	5.51	2410.	350.
324 <sup>15</sup>	259.	850.	.91	3.0	278.	96.0	13.9	184.	5710.	828.	38.0	5.51	1225.	178.
325	294.	965.	0	0	358.	63.3	9.2	212.	4900.	711.	24.0	3.48	857.	124.
325 <sup>14</sup>	294.	965.	.91	3.0	357.	68.3	9.9	191.	4640.	673.	-	-	-	-
327	320.	1050.	0	0	419.	55.8	8.1	225.	5290.	767.	-	-	-	-
328	339.	1112.	0	0	465.	46.4	6.7	236.	4455.	646.	-	-	-	-
330	347.	1140.	0	0	485.	43.7	6.3	243.	4355.	632.	-	-	-	-
330 <sup>14</sup>	347.	1140.	.91	3.0	484.	46.3	6.7	192.	3810.	553.	7.27	1.05	1240.	180.
332	418.	1370.	0	0	661.	33.6	4.9	238.	3355.	487.	3.86	.56	388.	56.3
332 <sup>14</sup>	418.	1370.	.91	3.0	662.	34.7	5.0	266.	3685.	534.	4.27	.62	287.	41.6
335	610.	2000.	0	0	1170.	22.9	3.3	319.	3235.	482.	-	-	-	-
335 <sup>14</sup>	610.	2000.	.91	3.0	1170.	29.9	4.3	314.	2635.	382.	-	-	-	-
336	838.	2750.	0	0	1805.	17.4	2.5	345.	1900.	276.	-1.5	-.22	124.	18.0



Table 2c. Measured Air Blast Parameters - Blast Line 3 (continued)

STA #	GR		ELEV		TA msec	PS		PPD msec	OPI		HDP		HDP1	
	m	ft	m	ft		kPa	psi		kPa-msec	psi-msec	kPa	psi	kPa-msec	psi-msec
338	1219.	4000.	0	0	2895.	6.88	1.0	281.	1265.	185.				
339	1524.	5000.	0	0	3775.	5.93	.9	319.	792.	115.				
340	1829.	6000.	0	0	4615.	5.00	.7	-.5	-.5	-.5				
341	2134.	7000.	0	0	-.5	-.5	-.5	-.5	-.5	-.5				

1 Transducer failed or cable broke before pressure-time history returned to zero.

2 Transducer failed at shock arrival.

3 Pressure-time history did not return to zero.

4 Mount failed causing cable break before pressure-time history returned to zero.

5 Data lost when power failed in instrumentation van.

6 Station located in AFWL area.

7 Station located in BRL helicopter area.

8 Location 0-2 in C3 area.

9 Location 0-3 in C3 area.

10 Location 0-4 in C3 area.

11 Station adjacent to DRES instrumentation center.

12 Station adjacent to DRI main camera station.

13 Station located adjacent to Lovelace Foundation fighting bunker.

14 Location 0-2 in Wheeled Vehicle area.

15 Location 0-3 in Wheeled Vehicle area.

GR-----Ground range, horizontal distance from ground zero; m (ft).

ELEV---Elevation, vertical height above ground surface; m (ft).

TA-----Arrival time, lapsed time from detonation to shock wave arrival; msec.

PS-----Shock pressure, maximum shock overpressure; kPa (psi).

PPD-----Duration, length of positive overpressure phase; msec.

OPI-----Overpressure impulse, integral of positive overpressure phase; kPa-msec (psi-msec).

HDP-----Dynamic pressure, maximum horizontal dynamic pressure; kPa (psi).

HDP1-----Dynamic pressure impulse, integral of dynamic pressure phase; kPa-msec (psi-msec)

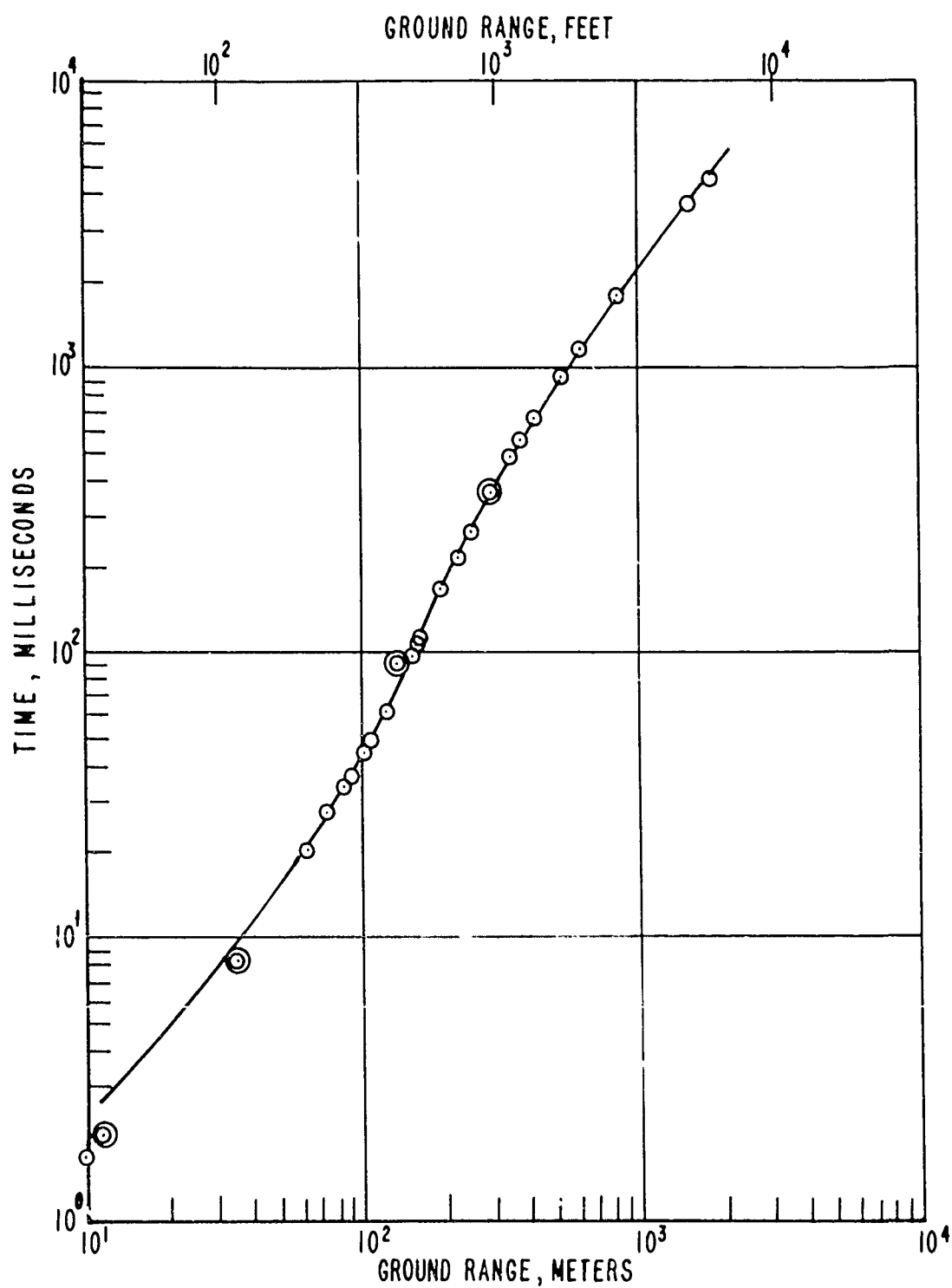
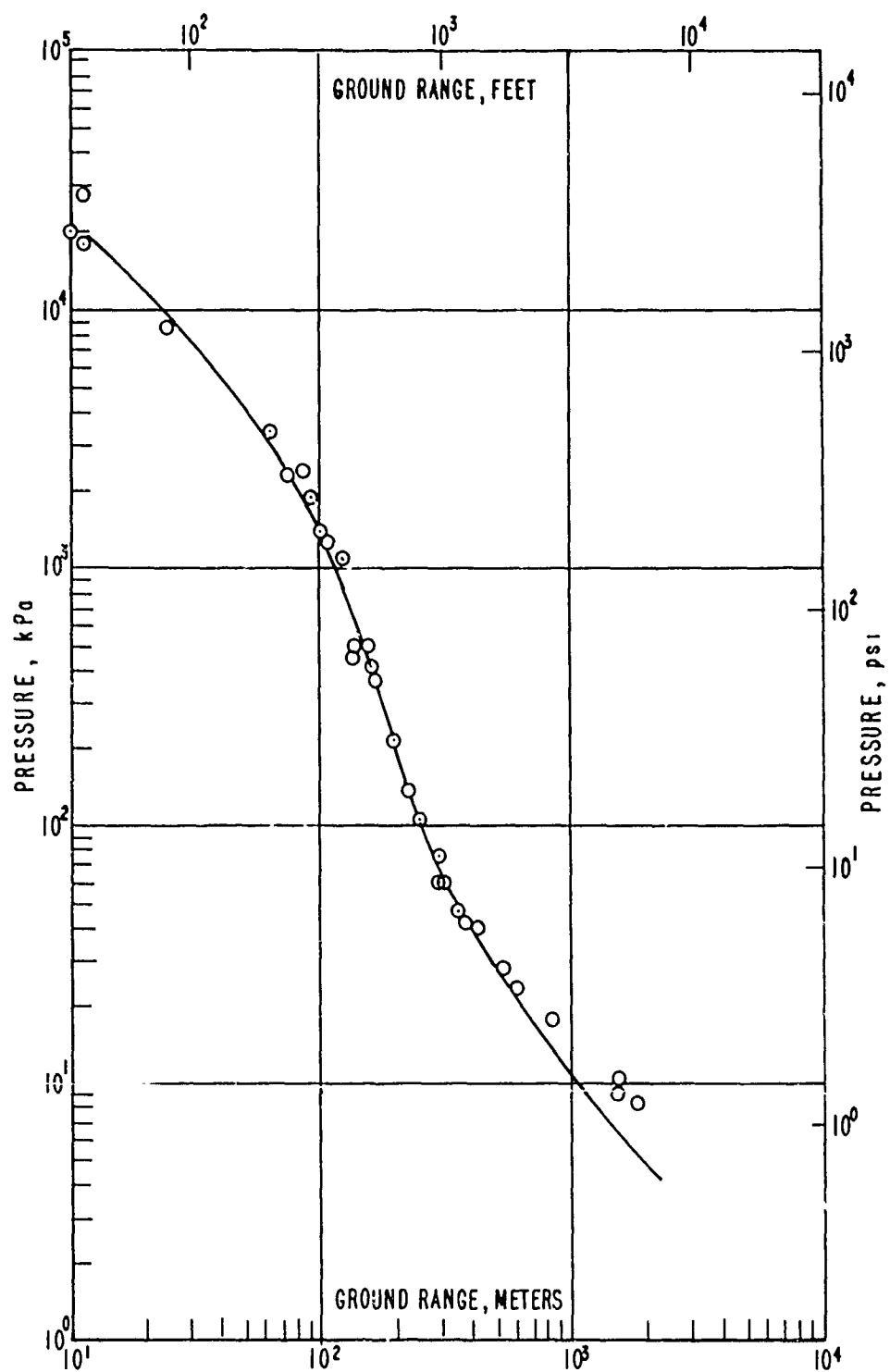


Figure 15. Measured arrival time versus ground range - Blast Line 1



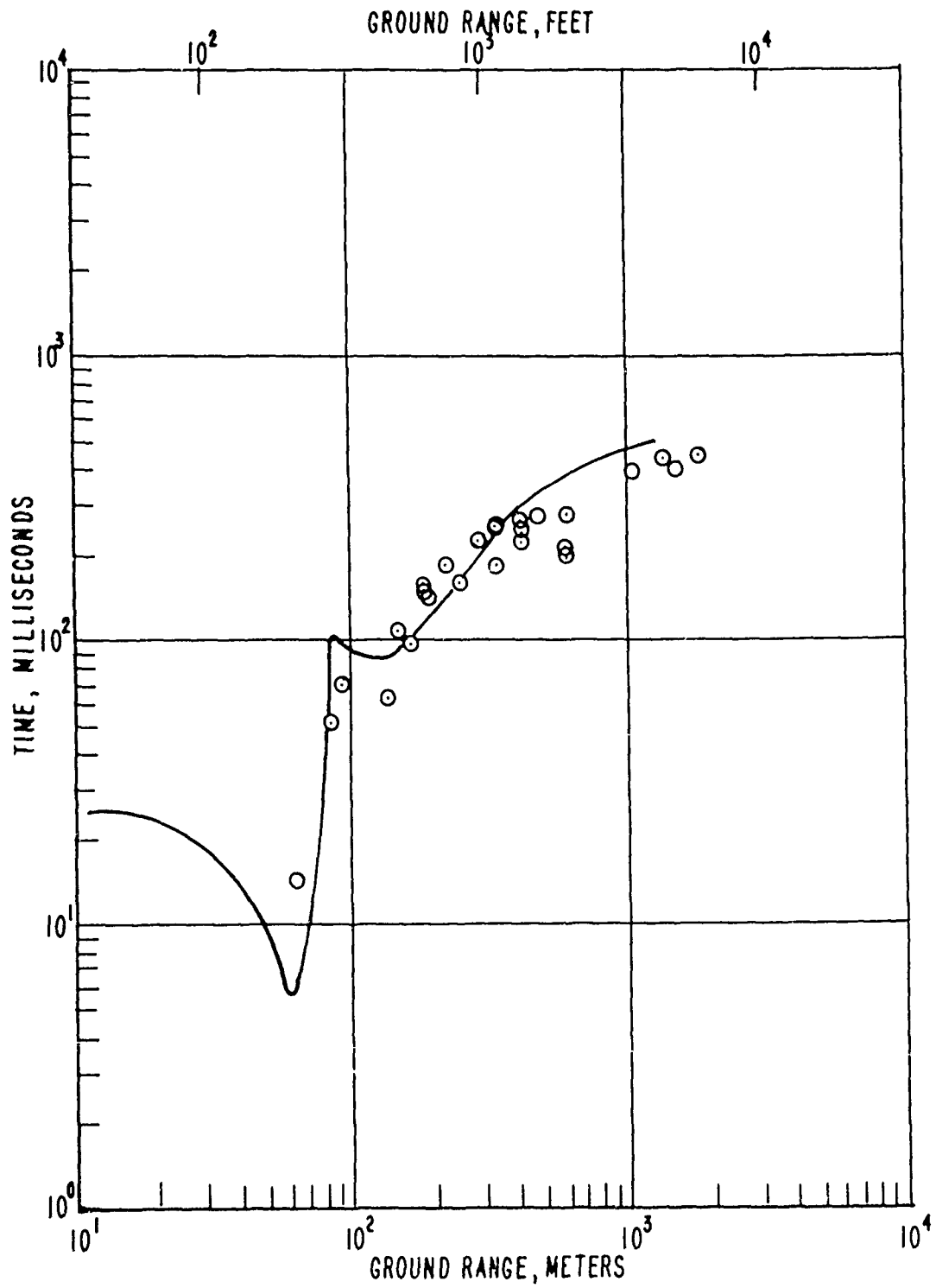


Figure 17. Measured positive phase duration versus ground range - Blast Line 1

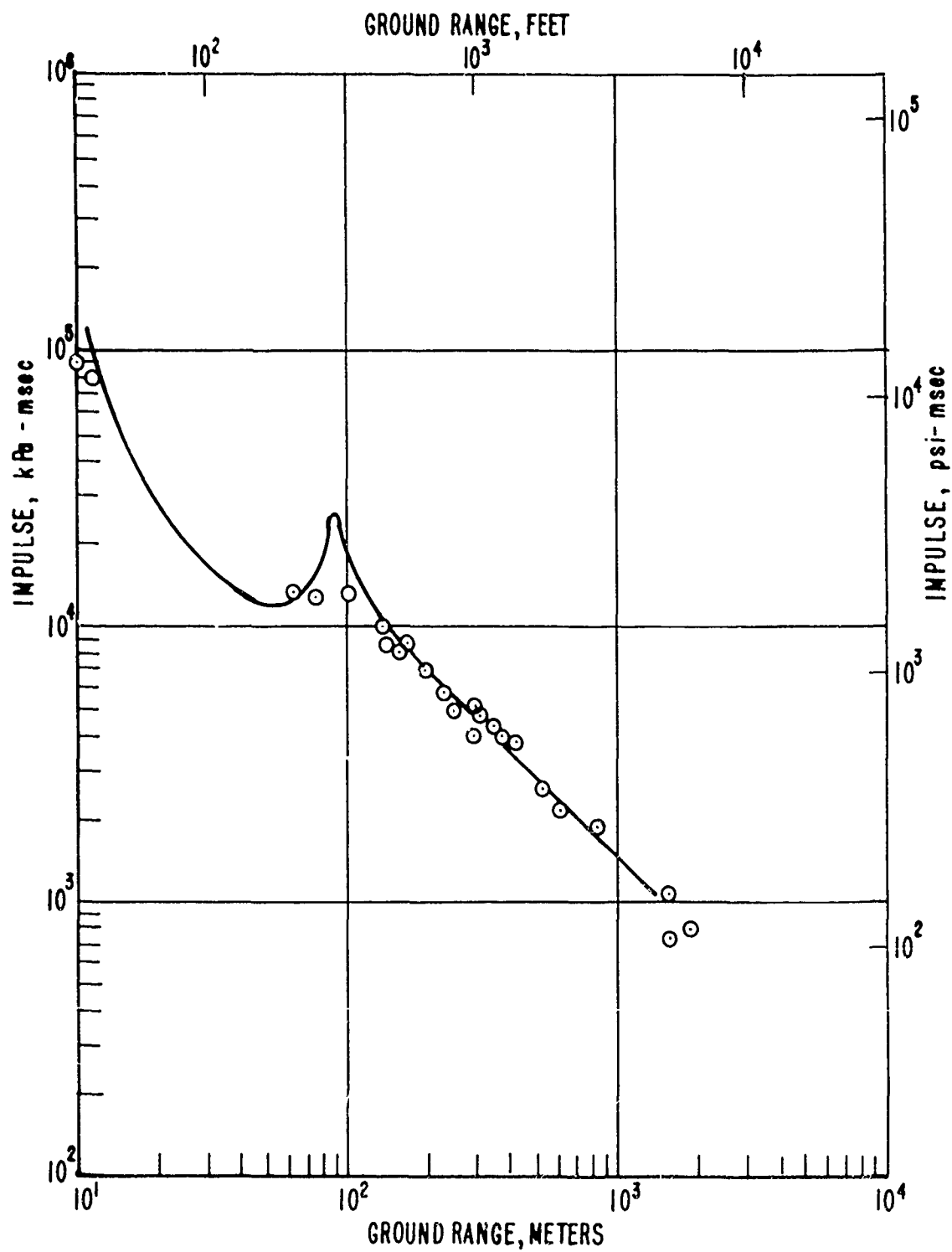


Figure 18. Measured positive phase impulse versus ground range - Blast Line 1

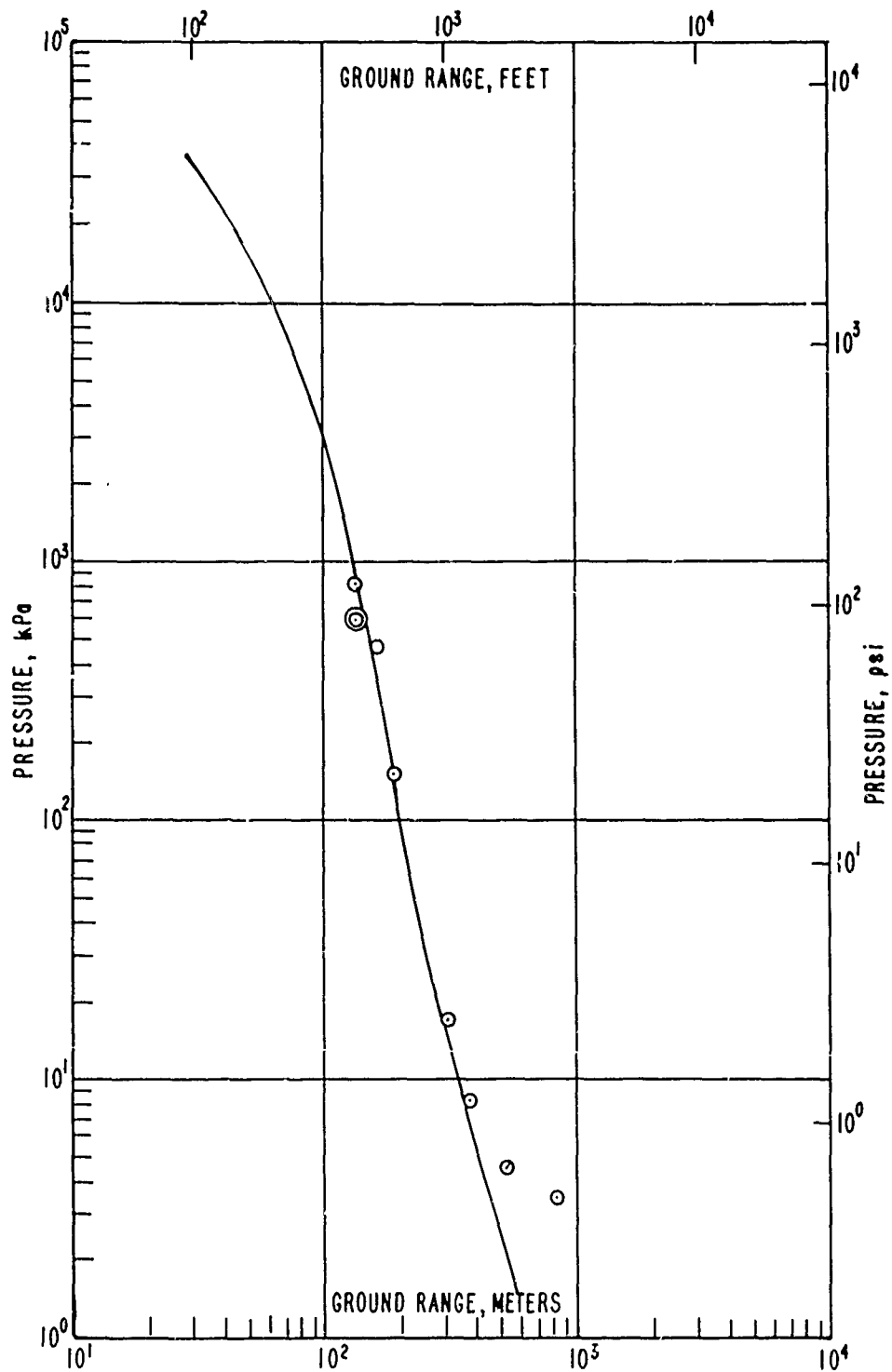


Figure 19. Measured horizontal dynamic pressure versus ground range - Blast Line 1

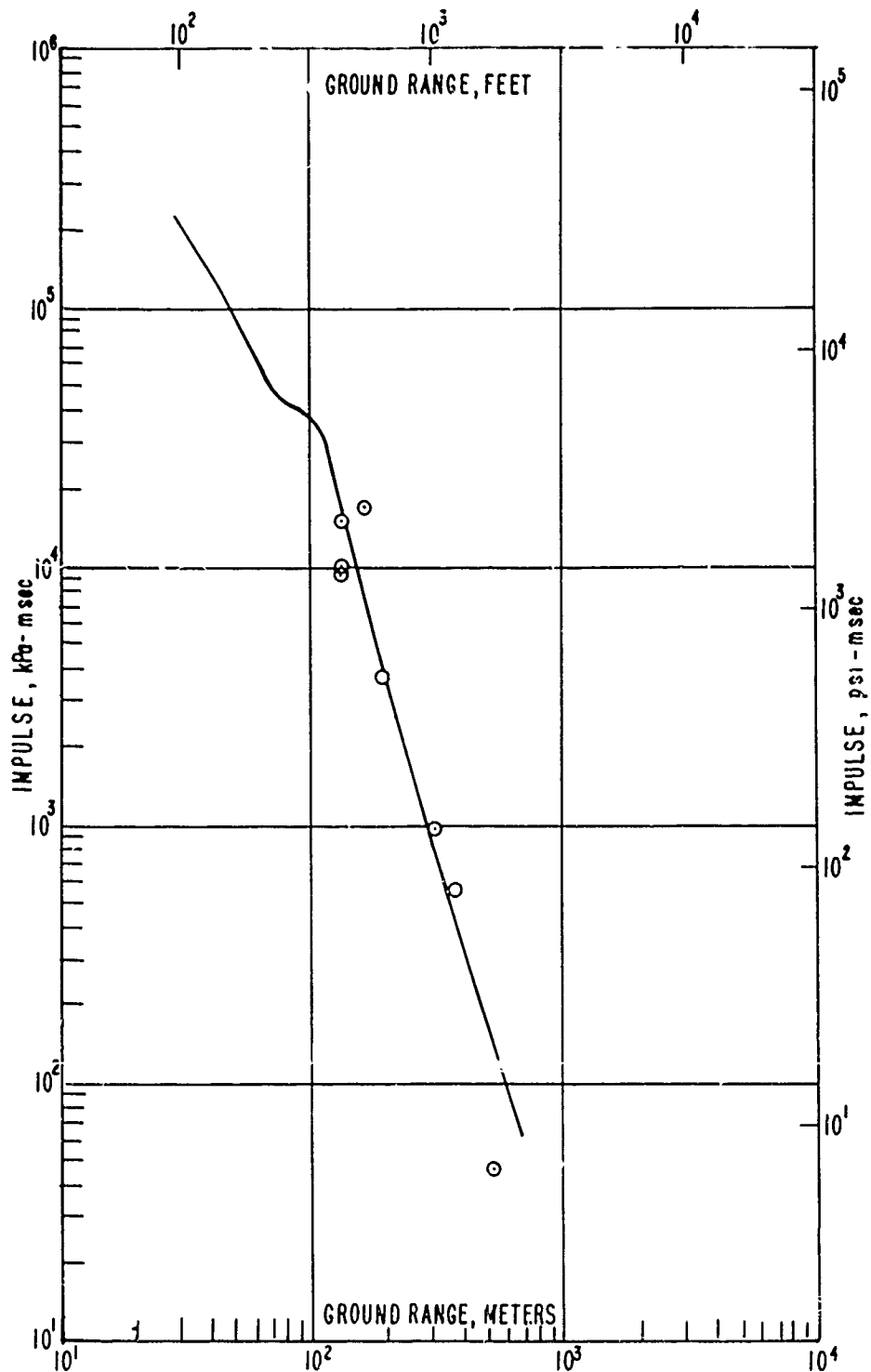


Figure 20. Measured horizontal dynamic pressure impulse versus ground range - Blast Line 1

An additional observation that can be made from a combination of the DICE THROW and Pre-DICE ThROW II-2 data is of the initial shock wave formation. Figure 21 shows the wave shapes obtained from Stations 101, 102, and 103 on DICE THROW and from a station located 12 meters from ground zero on Pre-DICE THROW II-2. When the appropriate distance scaling factors is applied to the Pre-DICE THROW II-2 range it falls between DICE THROW Stations 102 and 103. As the shock wave expands, the shock front steepens and the compressional rise and fall behind the front reduces until the waveform approximates those previously observed from TNT detonations, Station 103.

The plotted results from Blast Line 2 are shown in Figures 22 through 27. The blast wave anomaly in the AFWL area has an influence on a number of the waveforms along this line. This anomaly is particularly noticed on Stations 214 and 219 which were located in the AFWL area and just to the West of the blast line and also at Station 223 which was located on the blast line. Although the data scatter along this sector was somewhat more pronounced than along Blast Line 1, the plots of the duration and impulse would also seem to agree with the premise of the reduced degree of the fireball separation inflection points. The incident and dynamic pressure-time histories recorded on and along Blast Line 2 are presented in Appendix B.

Figures 28 through 33 are the plots of the results obtained along Blast Line 3. As in the case for Blast Line 1 the waveforms appear to be classical and the results are in good agreement with the pre-test predictions. The apparent lessening of the duration and impulse inflection points is not nearly so obvious along this line. No significantly anomalous waveshapes were obtained in this sector. Several of the waveforms do show secondary shocks but these can be traced to reflections generated by a number of massive targets located adjacent to this blast line. The waveforms recorded along Blast Line 3 are contained in Appendix C.



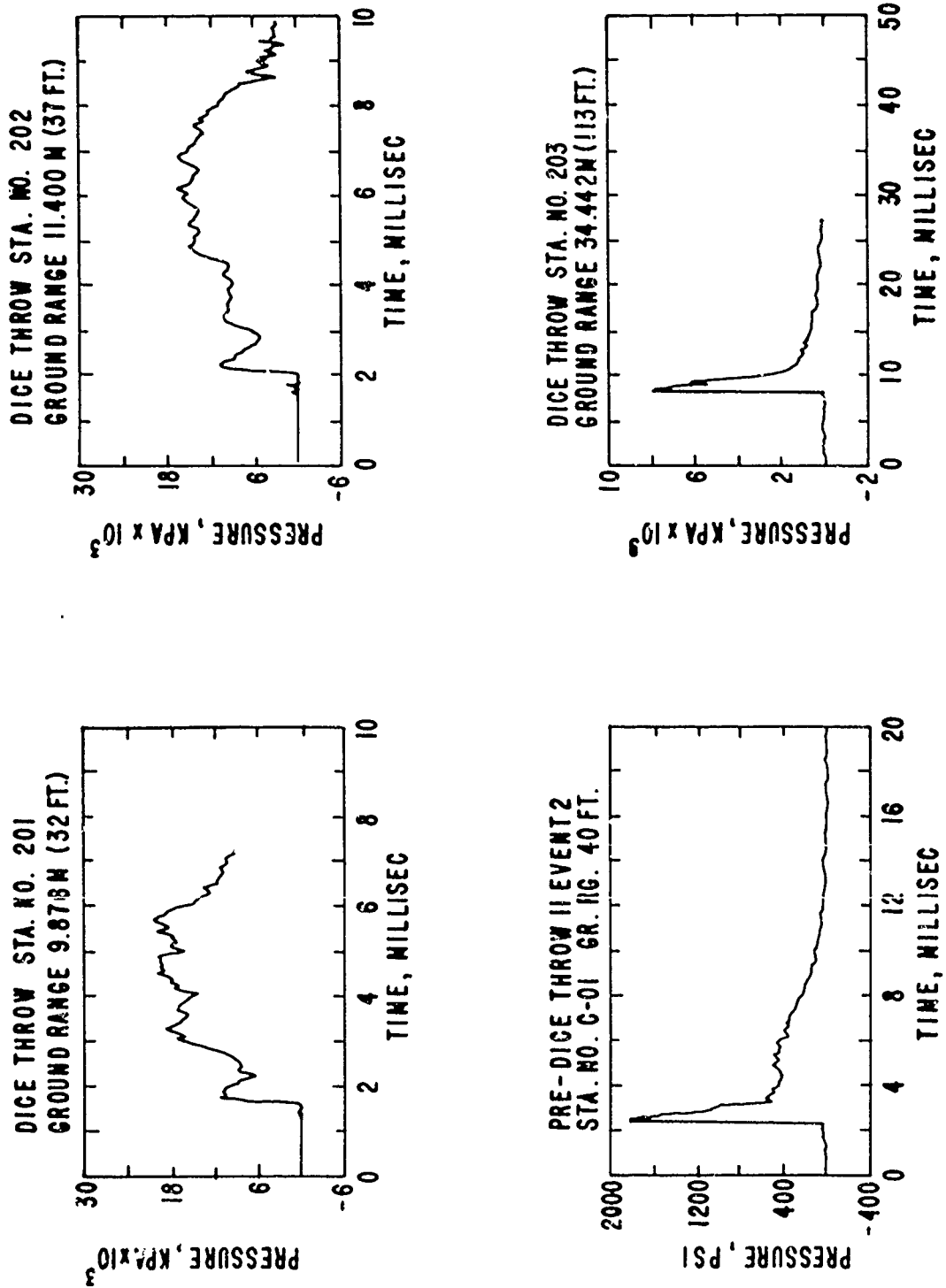


Figure 21. DICE THROW and Pre-DICE THROW II-2 waveforms showing shock wave formation

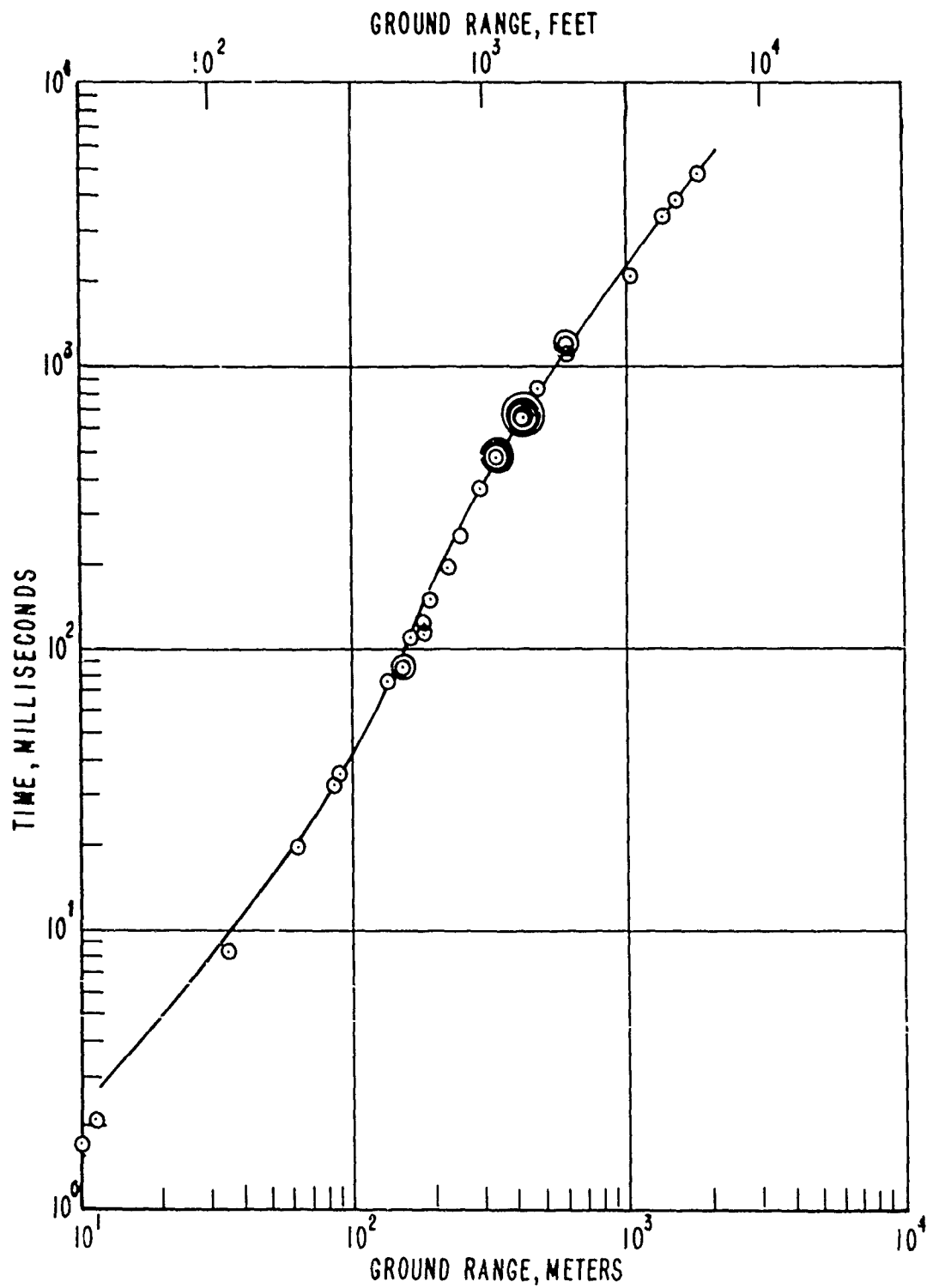


Figure 22. Measured arrival time versus ground range - Blast Line 2

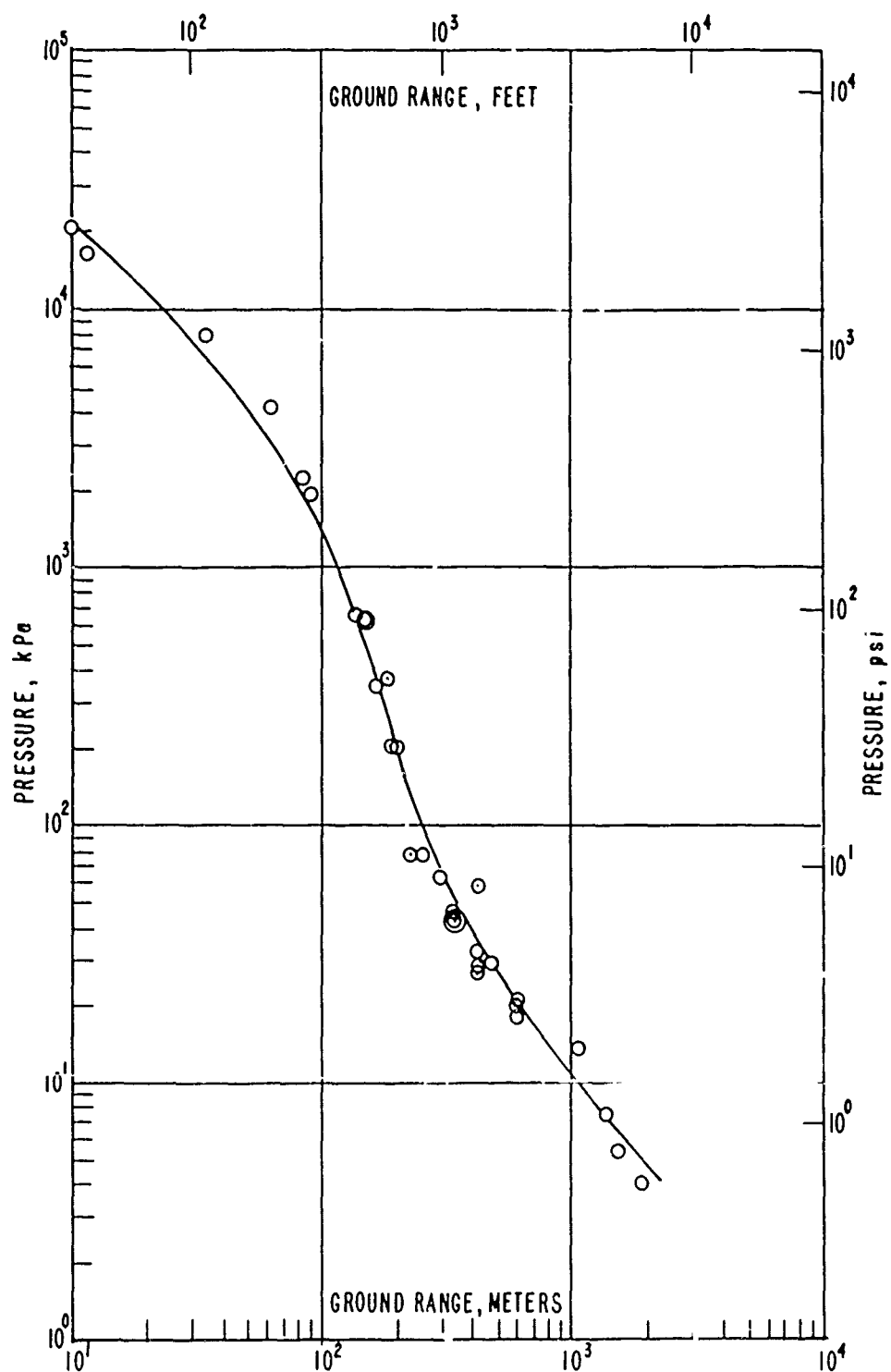


Figure 23. Measured incident shock overpressure versus ground range - Blast Line 2

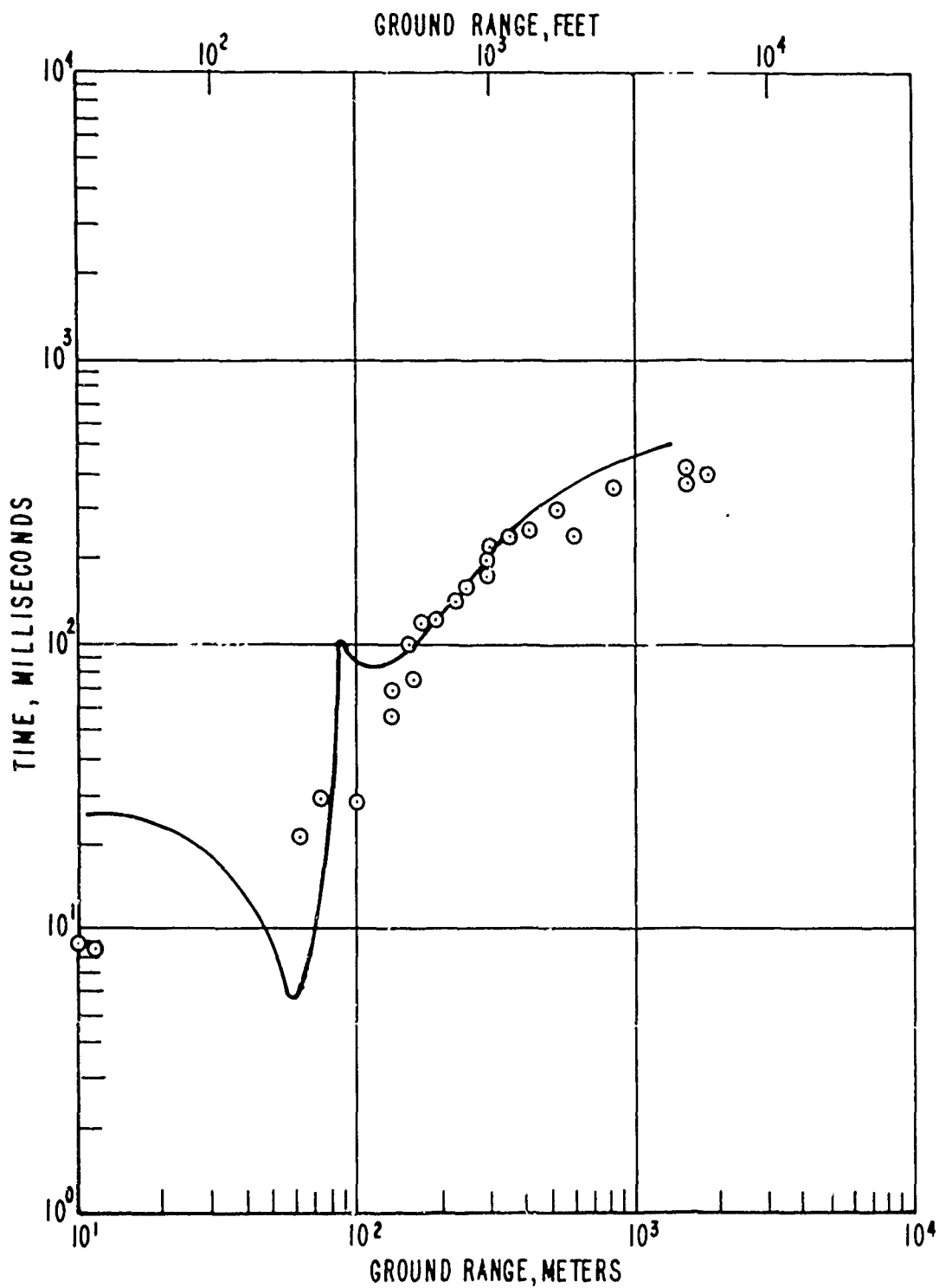


Figure 24. Measured positive phase duration versus ground range - Blast Line 2

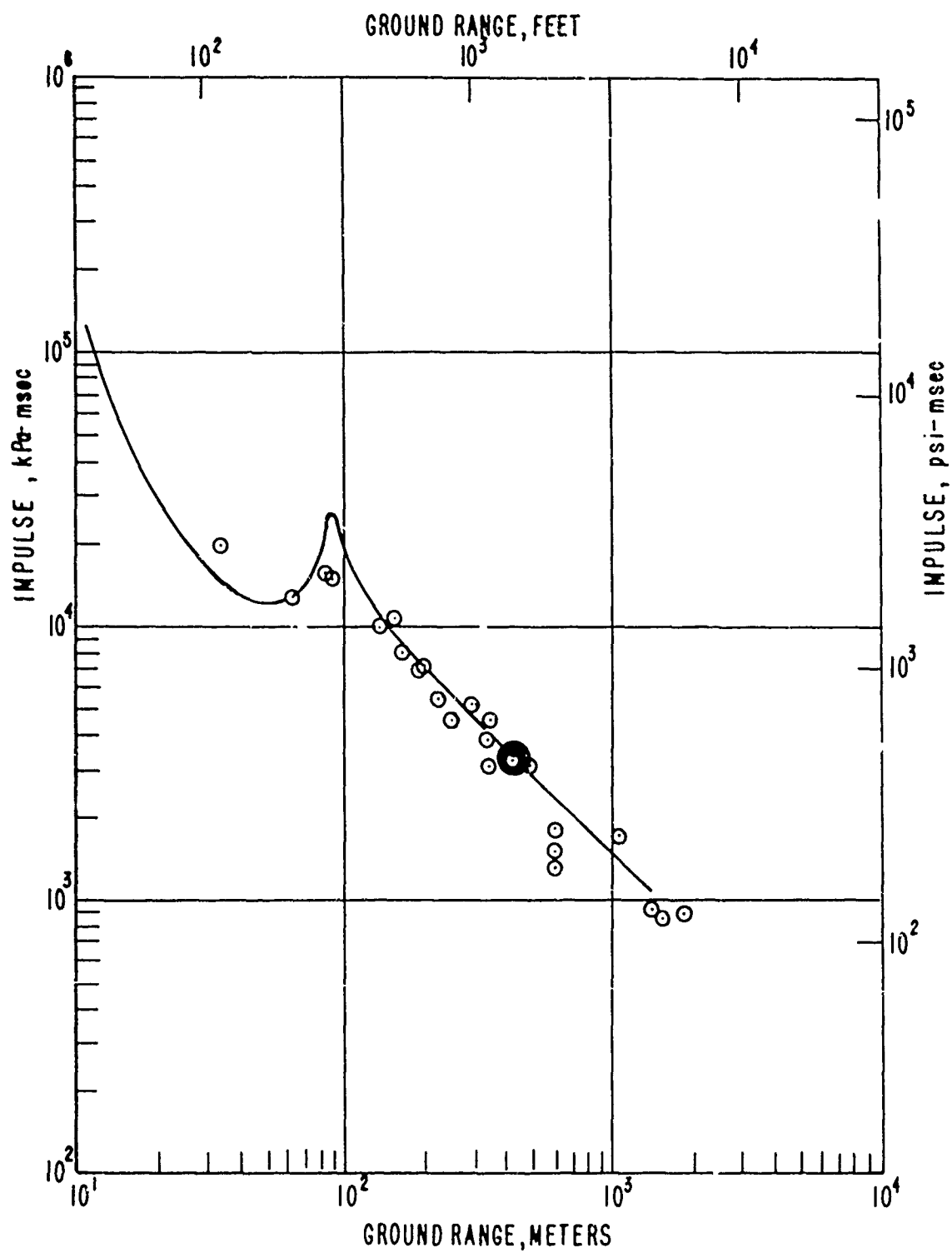


Figure 25. Measured positive phase impulse versus ground range - Blast Line 2

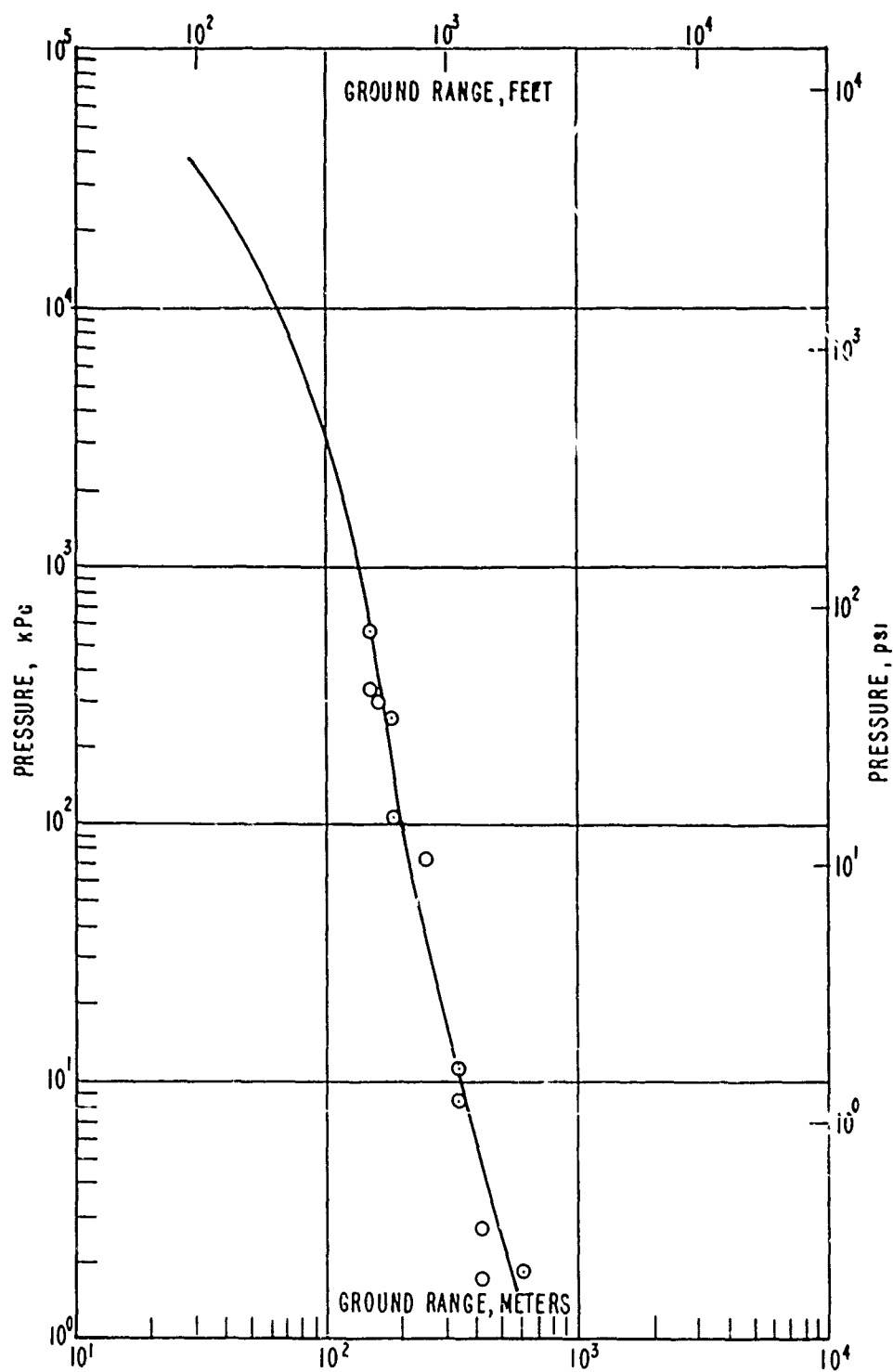


Figure 26. Measured horizontal dynamic pressure versus ground range - Blast Line 2

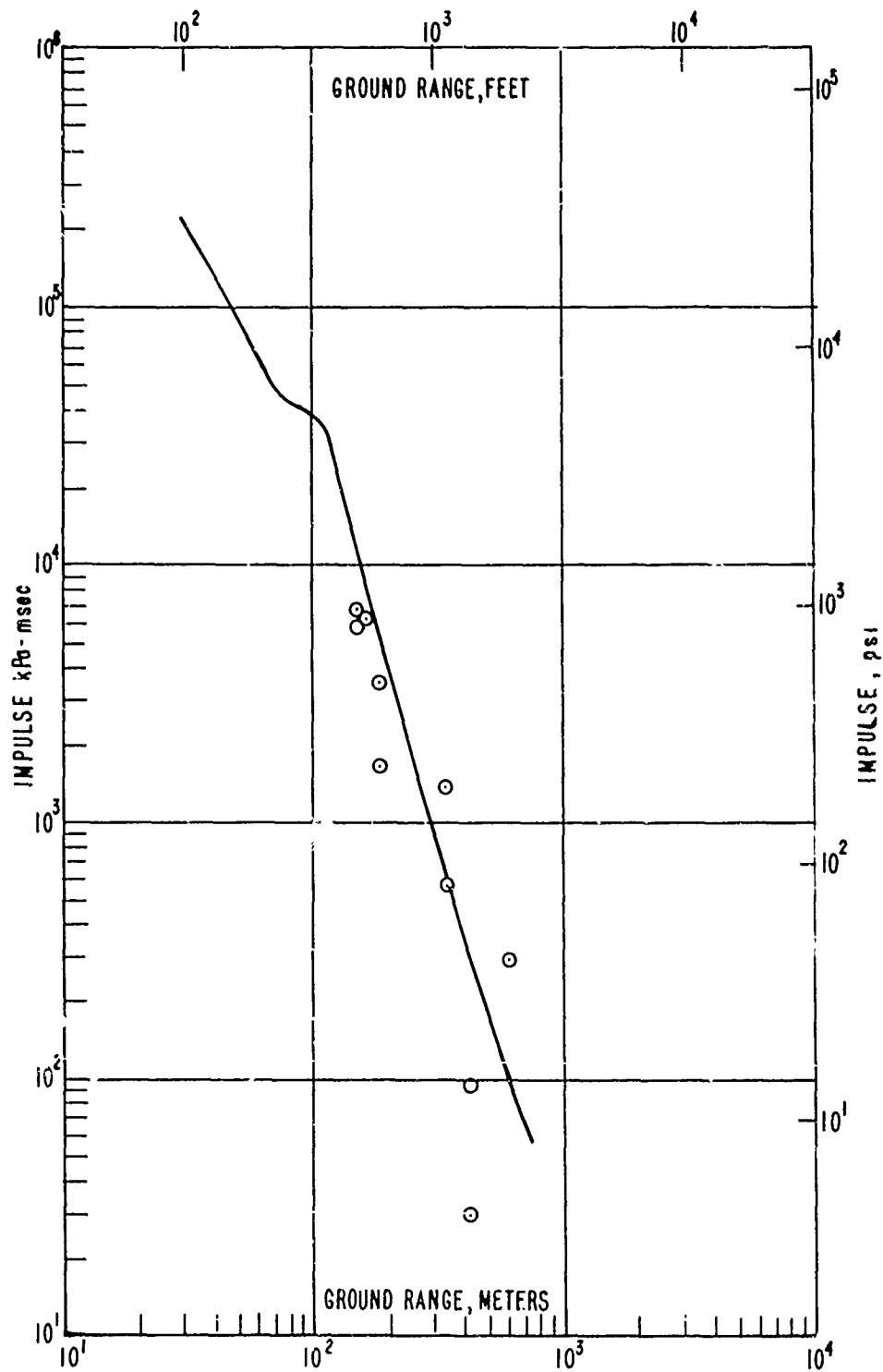


Figure 27. Measured horizontal dynamic pressure impulse versus ground range - Blast Line 2

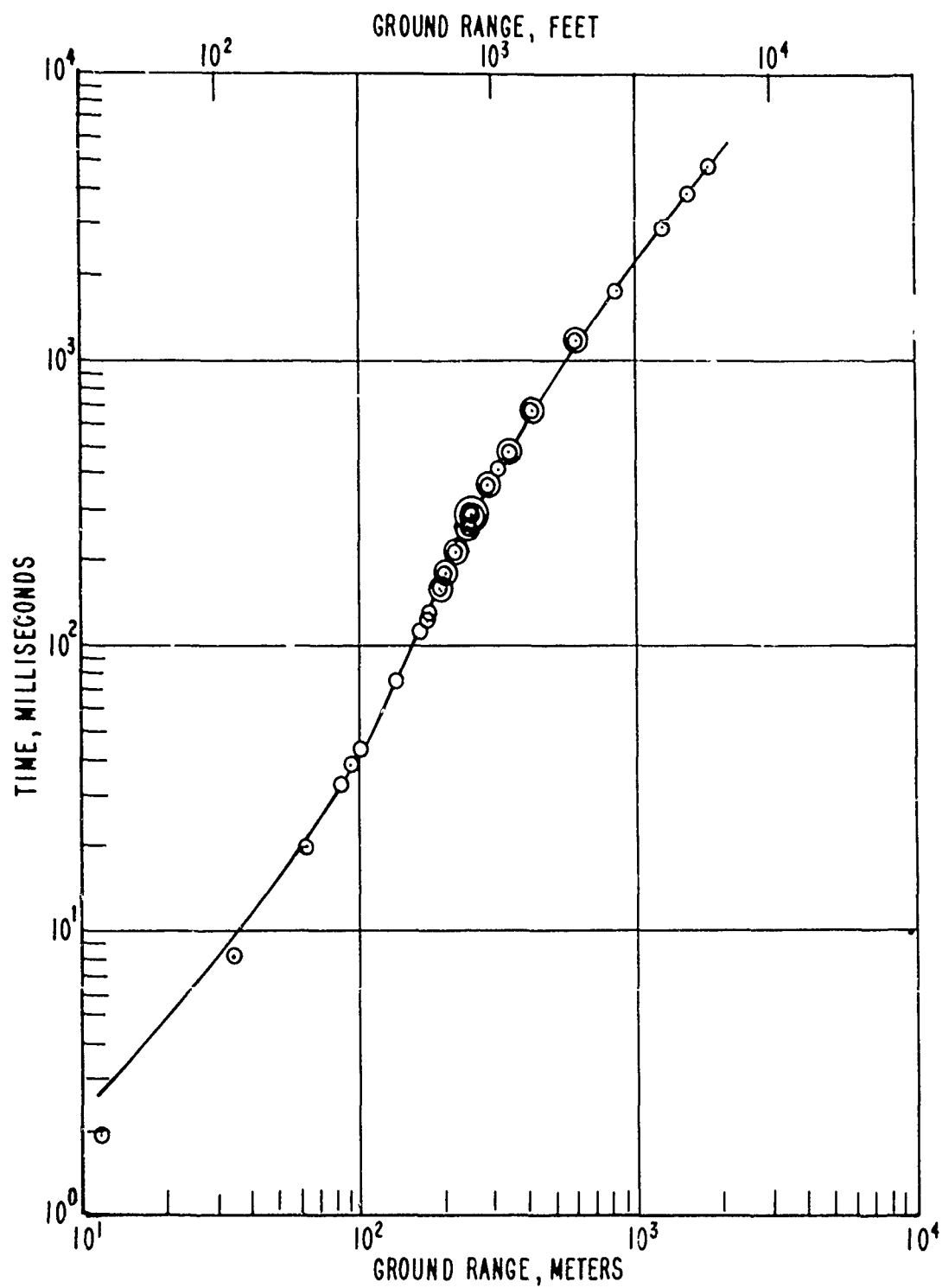


Figure 28. Measured arrival time versus ground range - Blast Line 3



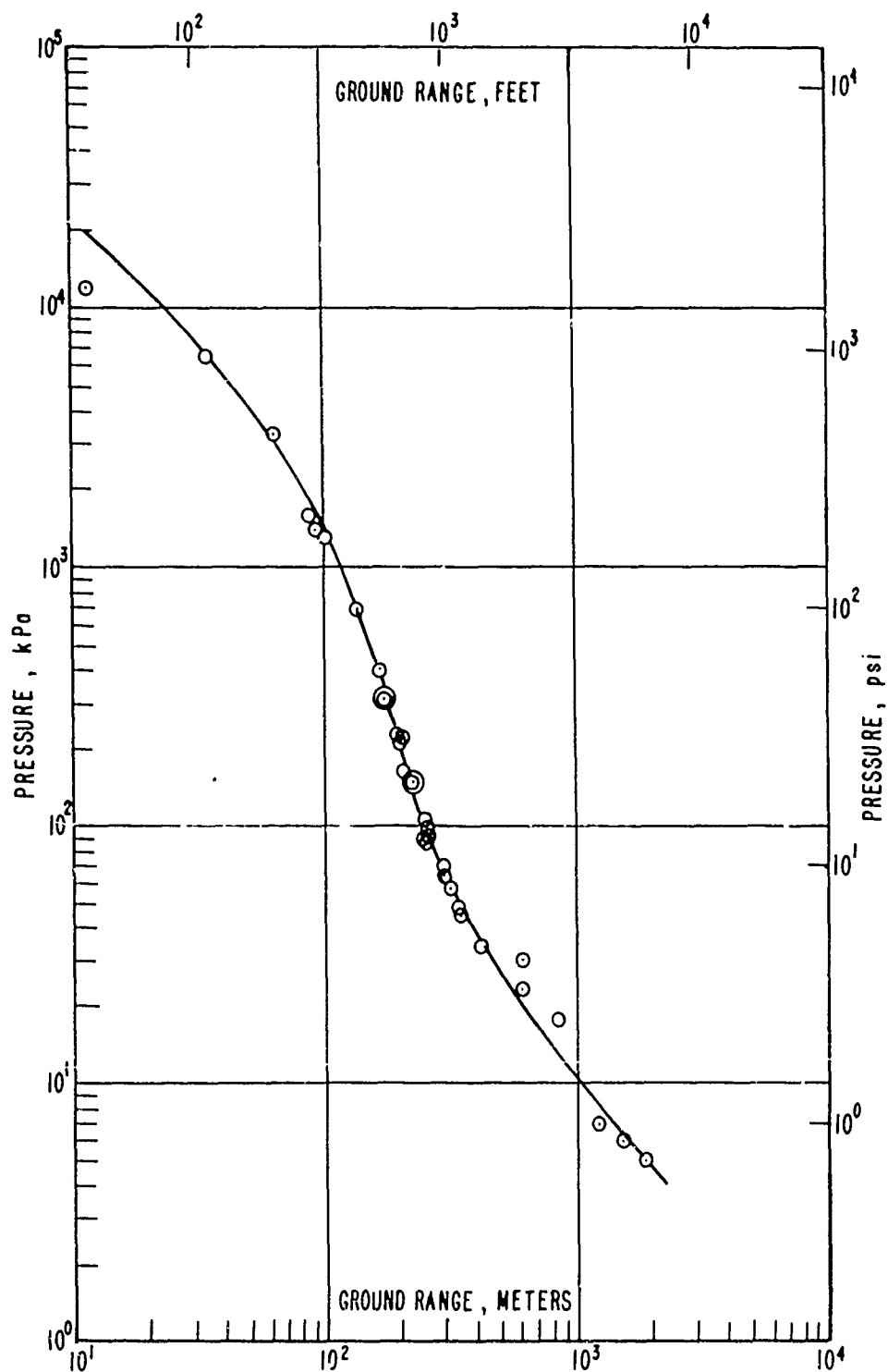


Figure 29. Measured incident shock overpressure versus ground range - Blast Line 3

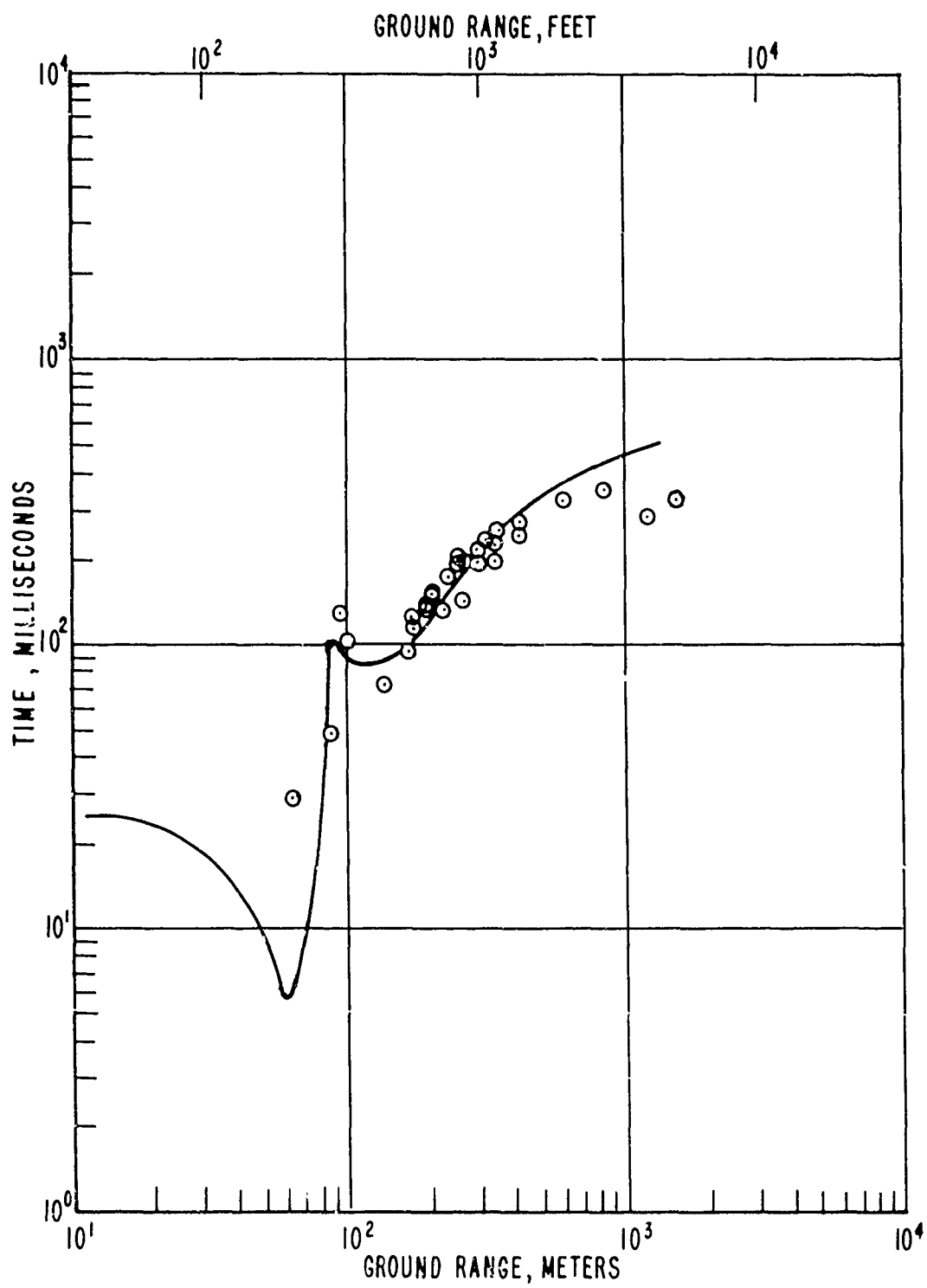


Figure 30. Measured positive phase duration versus ground range - Blast Line 3

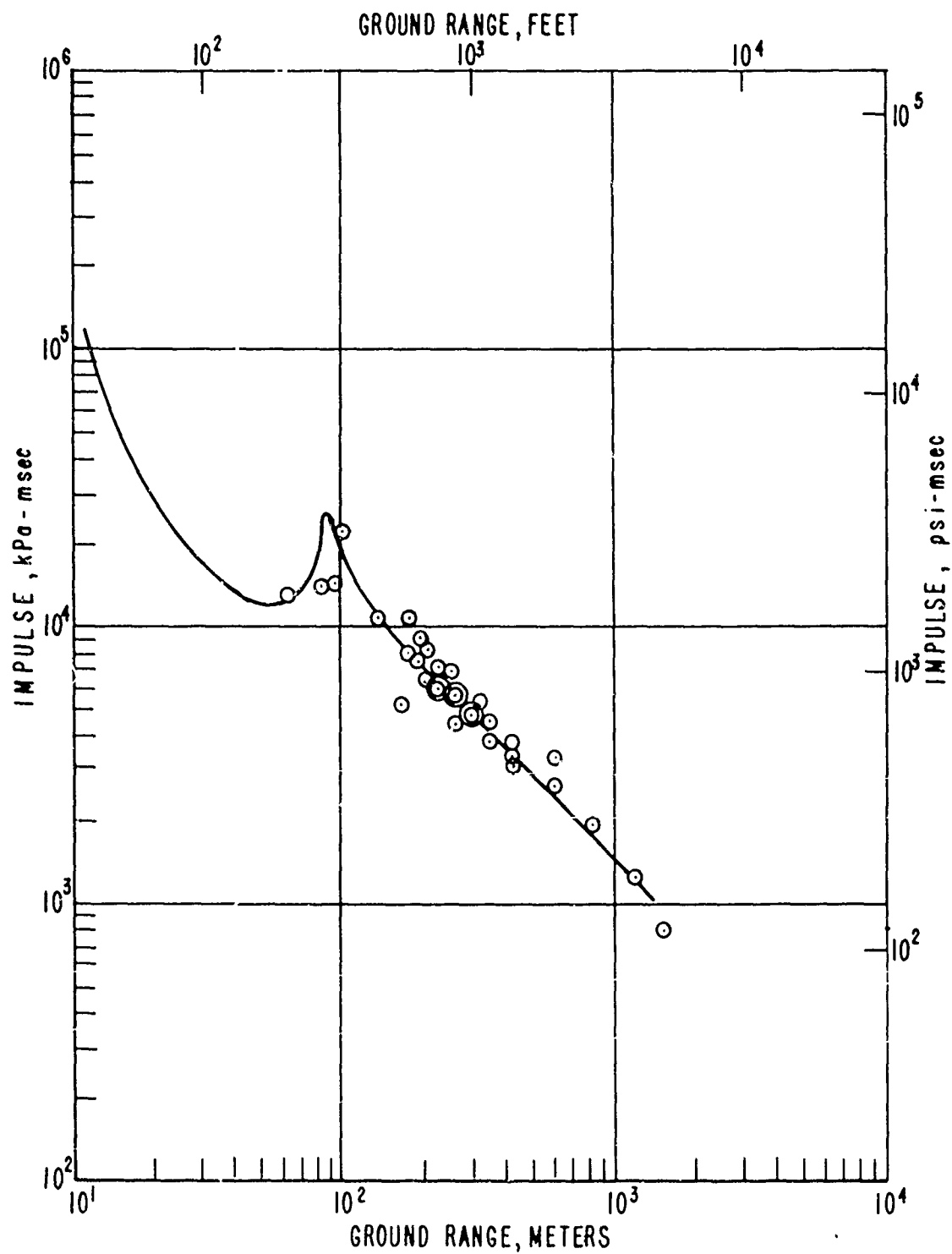


Figure 31. Measured positive phase impulse versus ground range - Blast Line 3

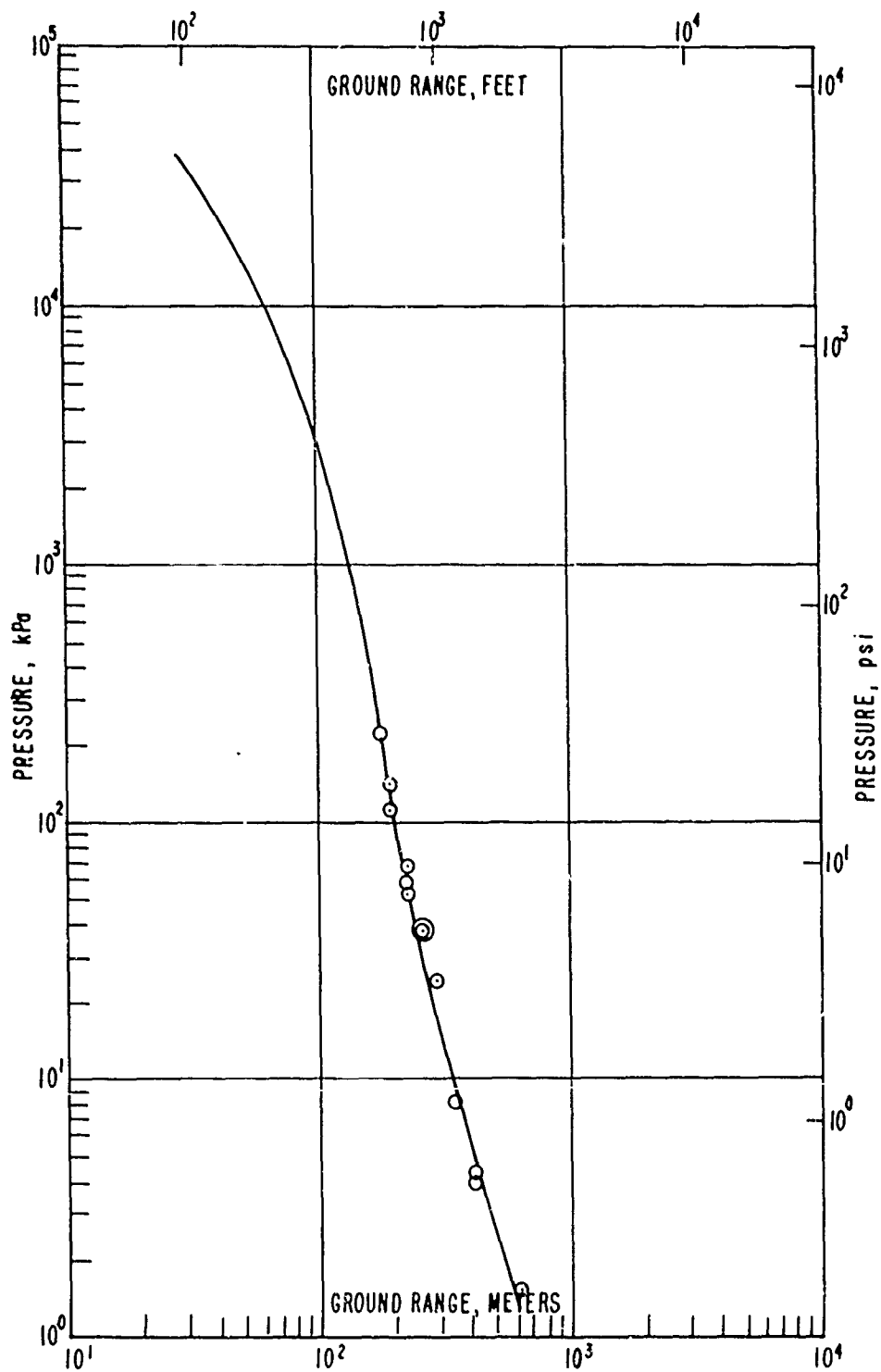


Figure 32. Measured horizontal dynamic pressure versus ground range - Blast Line 3

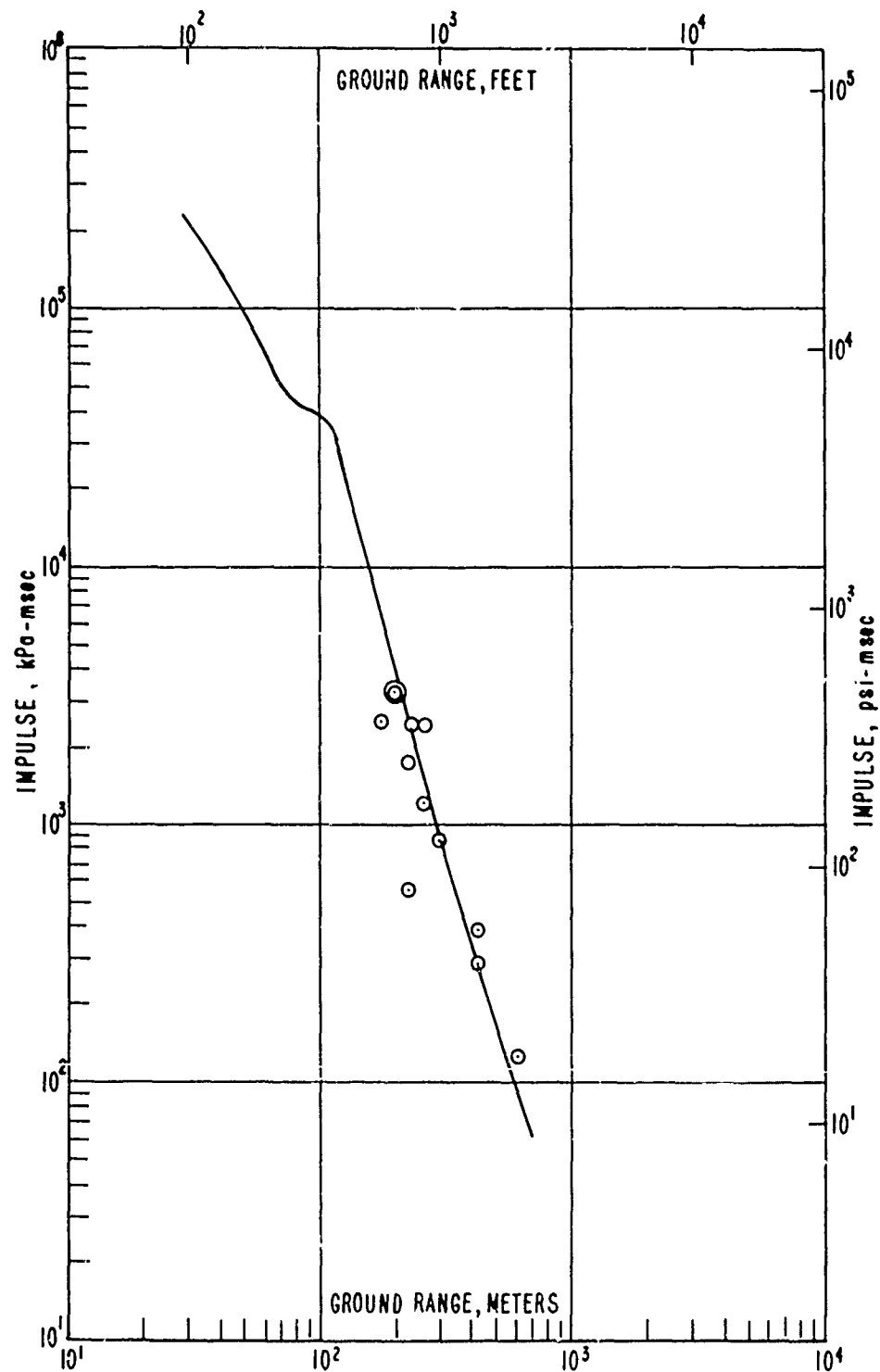
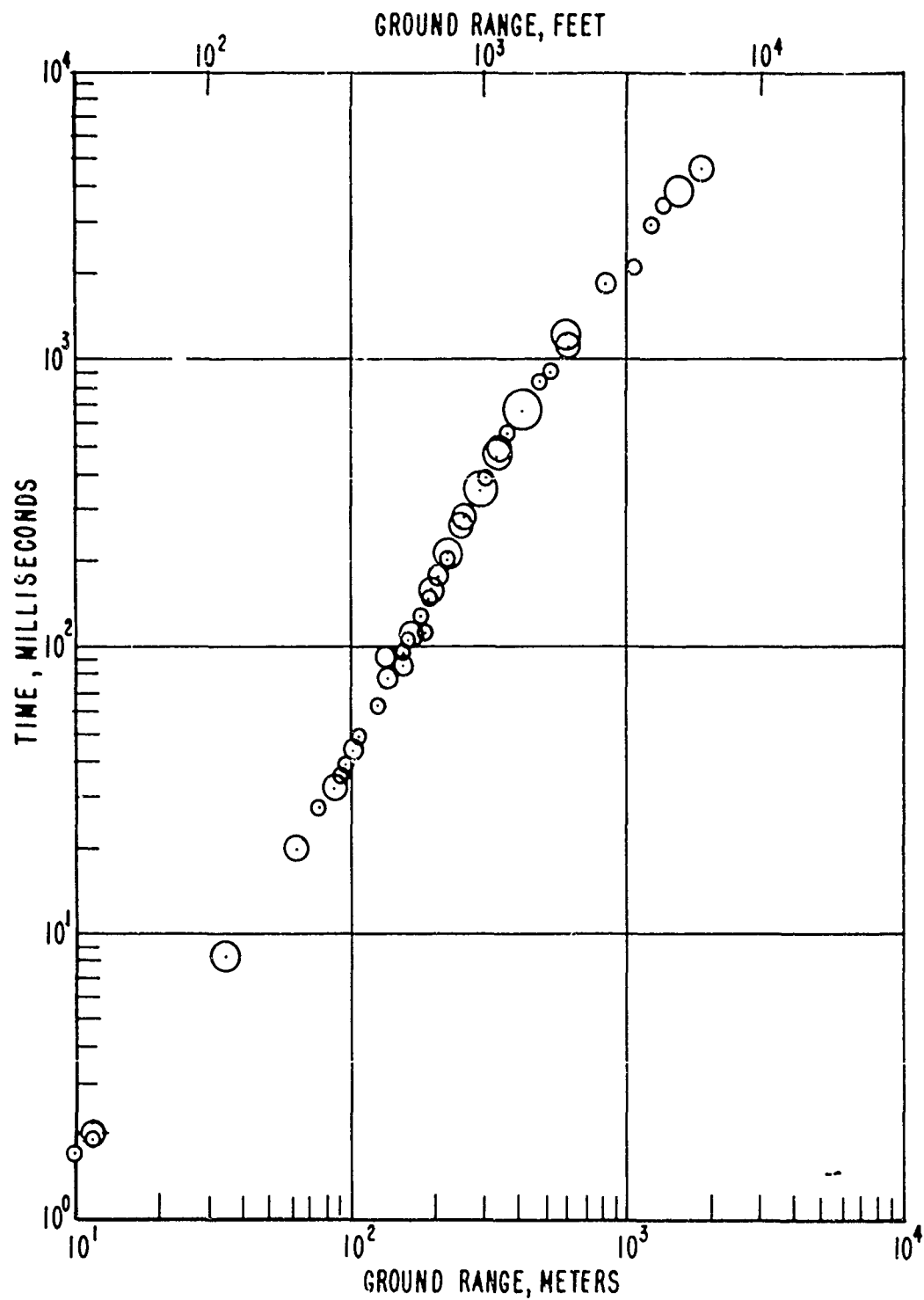


Figure 33. Measured horizontal dynamic pressure impulse versus ground range - Blast Line 3

In order to allow the reader to better interpret the data acquired on the DICE THROW Event only the data points have been plotted versus ground range in Figures 34 through 39. In these figures all of the data have been combined to reflect the average air blast environment around the test site.



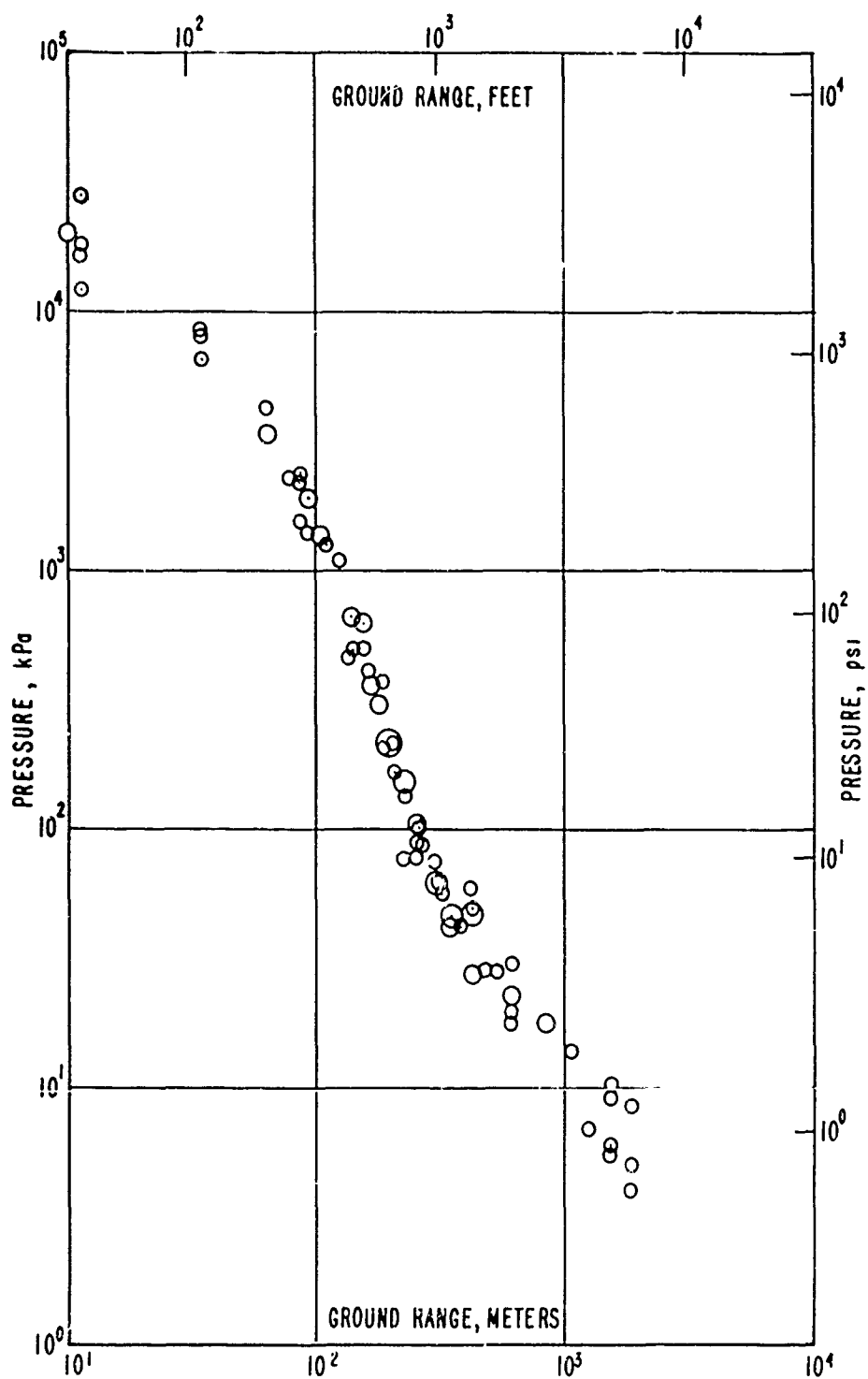
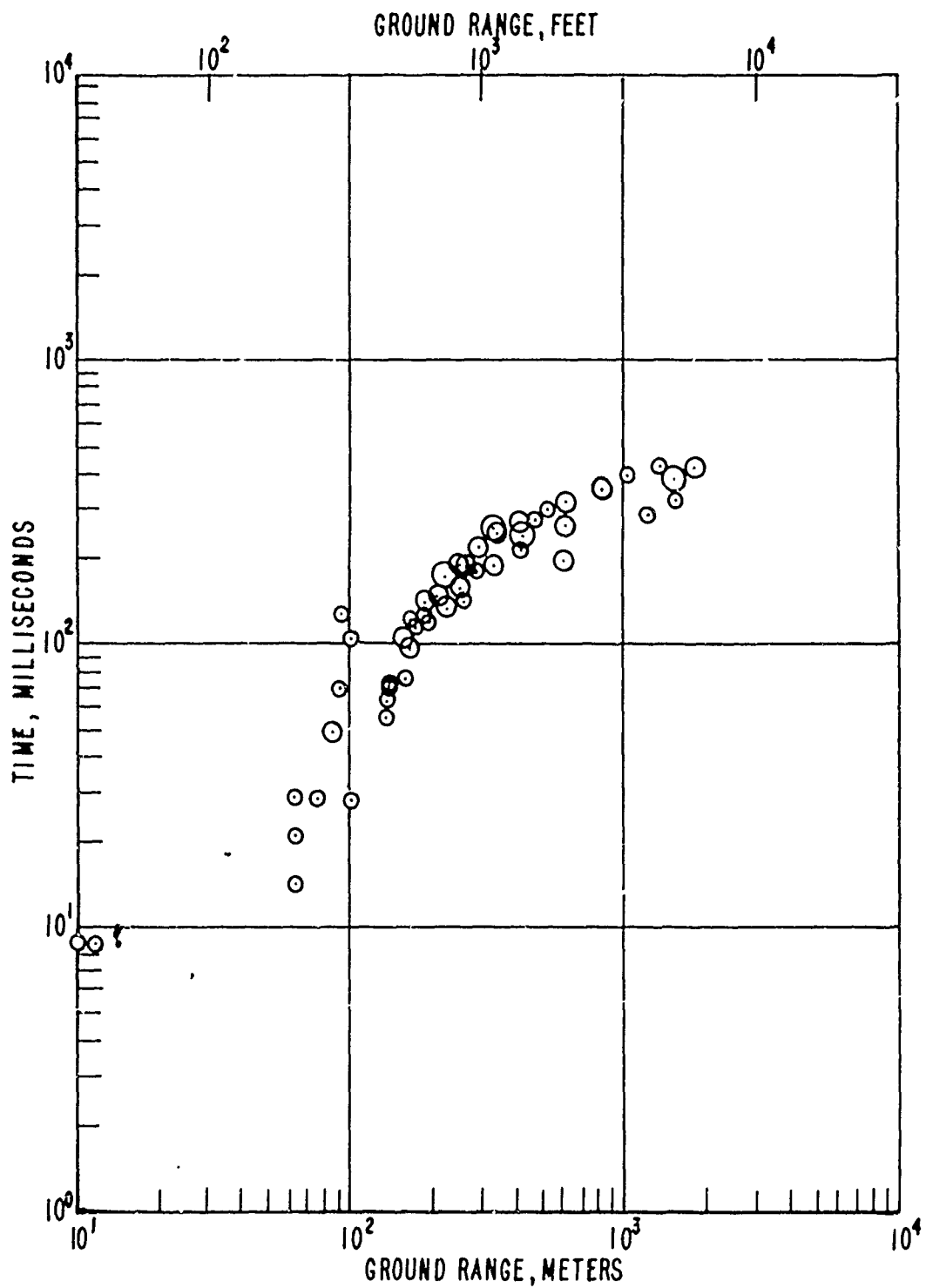


Figure 35. DICE THROW incident shock overpressure versus ground range





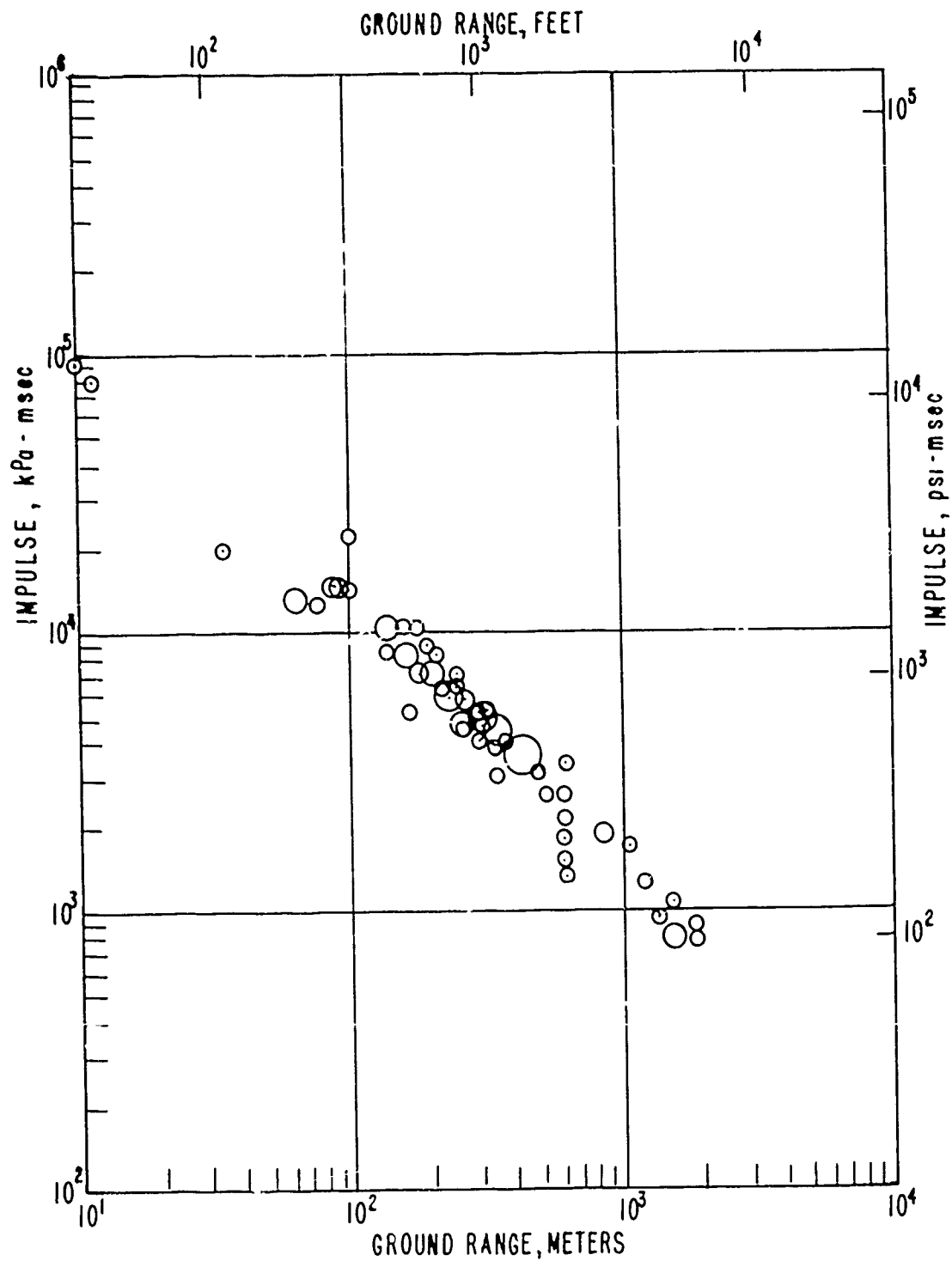


Figure 37. DICE THROW positive phase impulse versus ground range

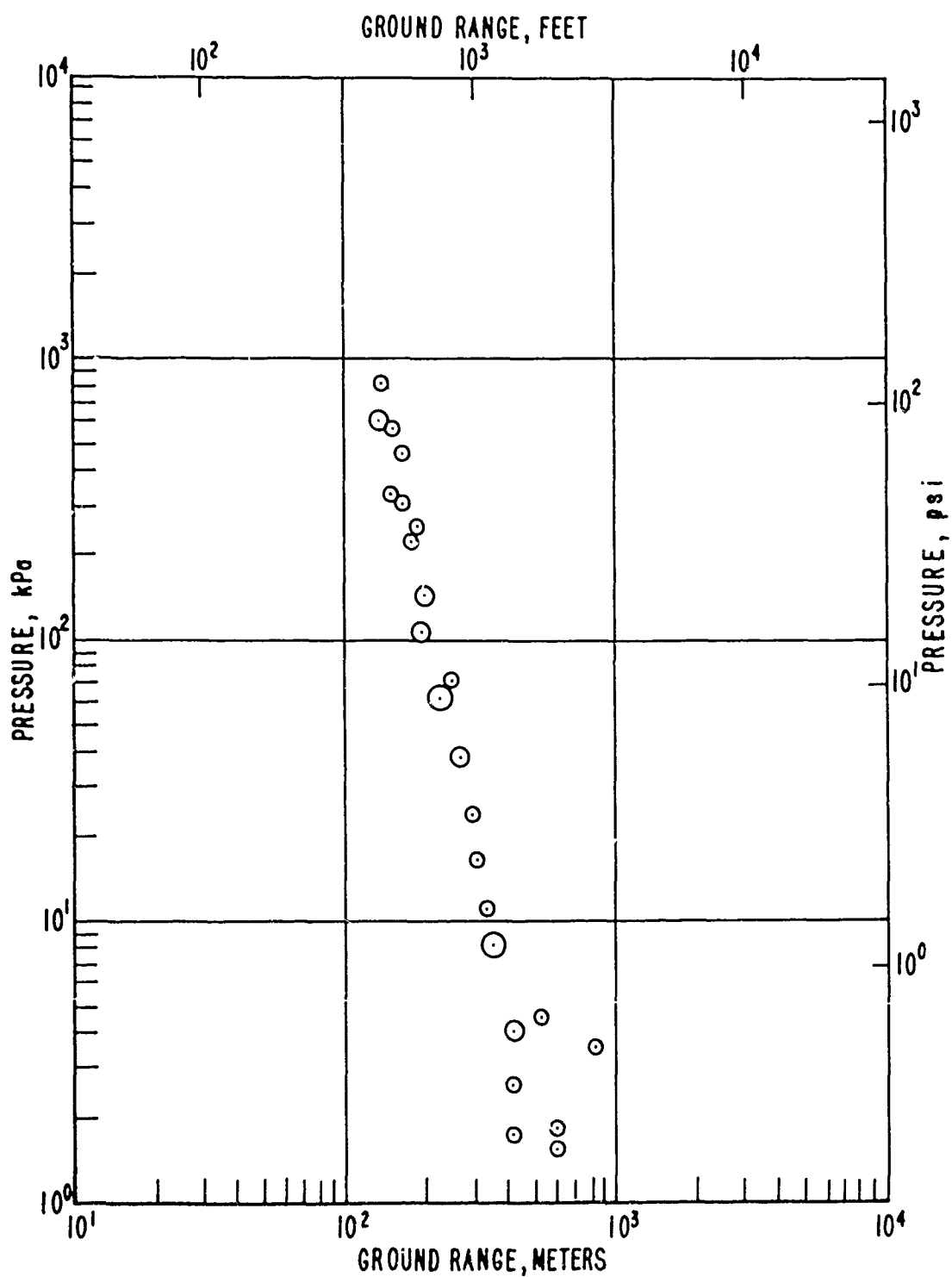


Figure 38. DICE THROW horizontal dynamic pressure versus ground range

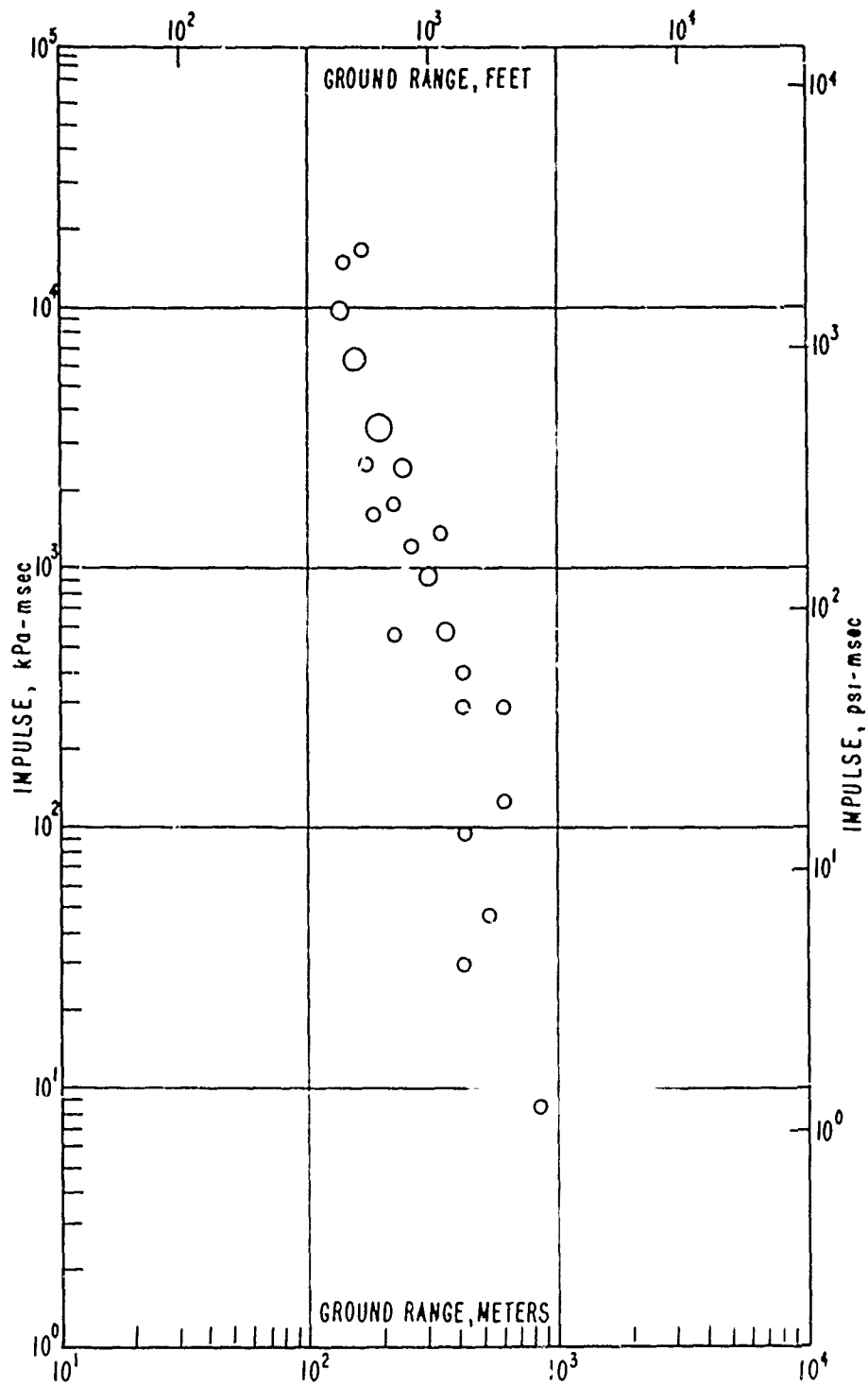


Figure 39. DICE THROW horizontal dynamic pressure impulse versus ground range

## 7. CONCLUSIONS AND RECOMMENDATIONS

The data return for this experiment, 91%, was acceptable. The measured arrival times and incident pressures compared well with the pre-test predictions. While the data do not conclusively show that the inflections in the duration and impulse curves do not exist, it would seem apparent that the ANFO detonation does not result in an environment which accentuates the blast wave fireball separation as in the case of a TNT source.

The use of ANFO as an explosive source does not provide an anomaly free environment as had been expected. Though no blast wave anomalies had been detected on Pre-DICE THROW II-2, at least two significant areas of anomalous behavior were detected on the DICE THROW Event and one of these, to the southwest influenced measurements taken in the AFWL (Exp. 398) and BRL (Exp. 103) areas.

An examination of the results of the measurements and calculations of dynamic pressure re-emphasizes the need for an improved technique for acquiring dynamic pressure-time information in the low pressure regime, below 103 kPa (15 psi) incident overpressure. This region is of particular interest because it is at this level and below where the survivability and vulnerability of many of the tactical military targets is in question or hardening needs to be verified and also where collateral damage effects are of interest. Within this overpressure regime a large number of these potential targets are influenced most significantly by drag forces and it is within this region that dynamic pressure is most difficult to measure using current techniques. This difficulty results primarily from the inability to resolve independent pressure-time histories to the extent required to reduce the dynamic pressure component. Consider for example, the uncertainties involved in making the measurements and calculations to obtain dynamic pressure at the 50 kPa (7.3 psi) incident pressure level which is of particular

concern to the Army's Command, Control, and Communications Systems (Exp. 103). Predictions would indicate that at this 50 kPa (7.3 psi) incident overpressure level that the maximum stagnation pressure should be approximately 60 kPa (8.7 psi). If one assumes that an uncertainty of  $\pm 5\%$  would be applied to each measurement, then the incident pressure range would be 47.5 kPa to 52.5 kPa and the stagnation pressure range would be 57 kPa to 63 kPa. The resulting maximum uncertainty in the calculated dynamic pressure is  $\pm 58\%$ . It is immediately obvious that if target response experiments require dynamic pressure information in these low incident overpressure regions that an effort should be expended to develop a tool which would improve the quality of these measurements.

## APPENDIX A

The free field air blast measurements taken along, and adjacent to, Blast Line 1 have been digitized, computer processed for conversion to engineering units, and machine plotted. The pressure-time histories of the incident and dynamic pressures are presented in this appendix.

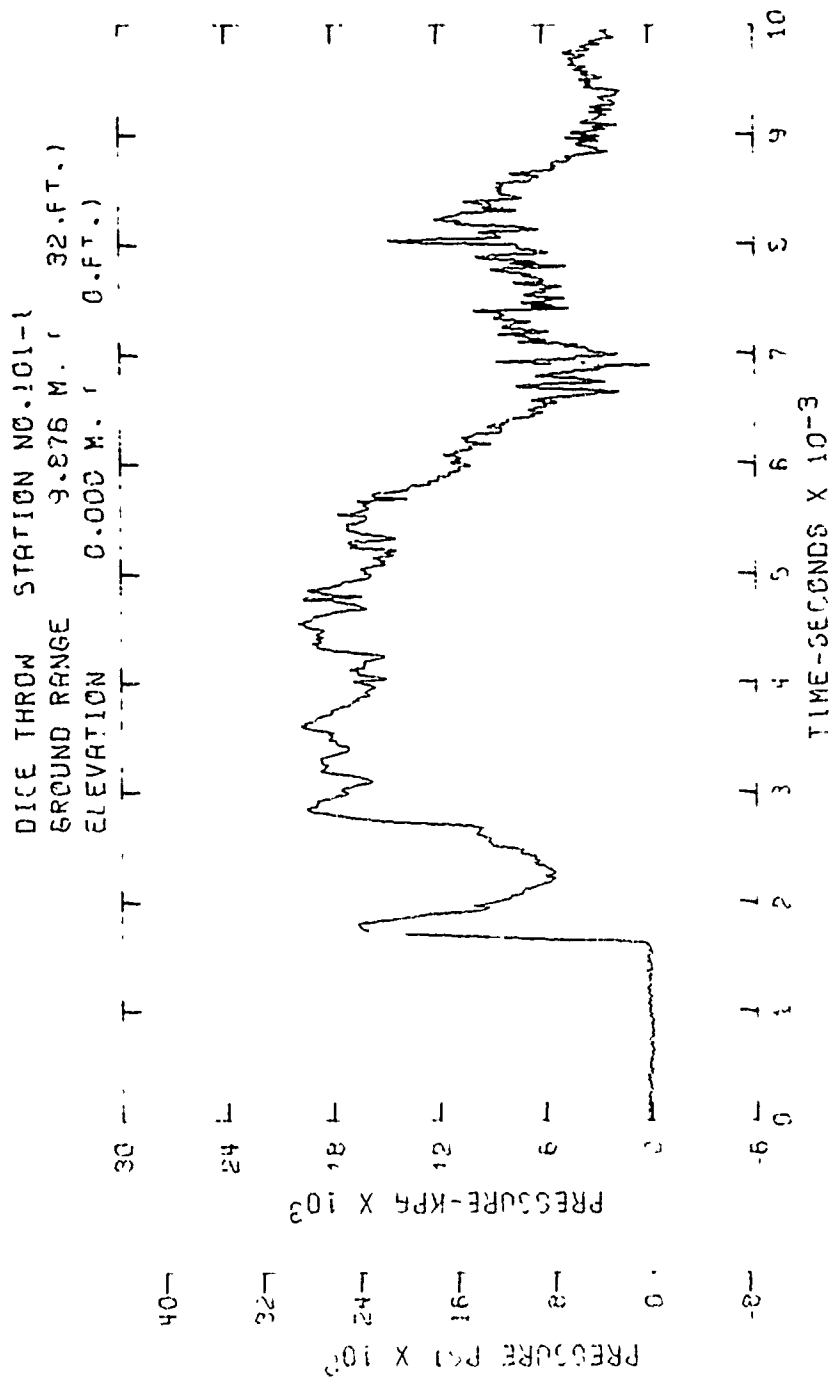


Figure A1. Incident pressure-time history - Station 101-1



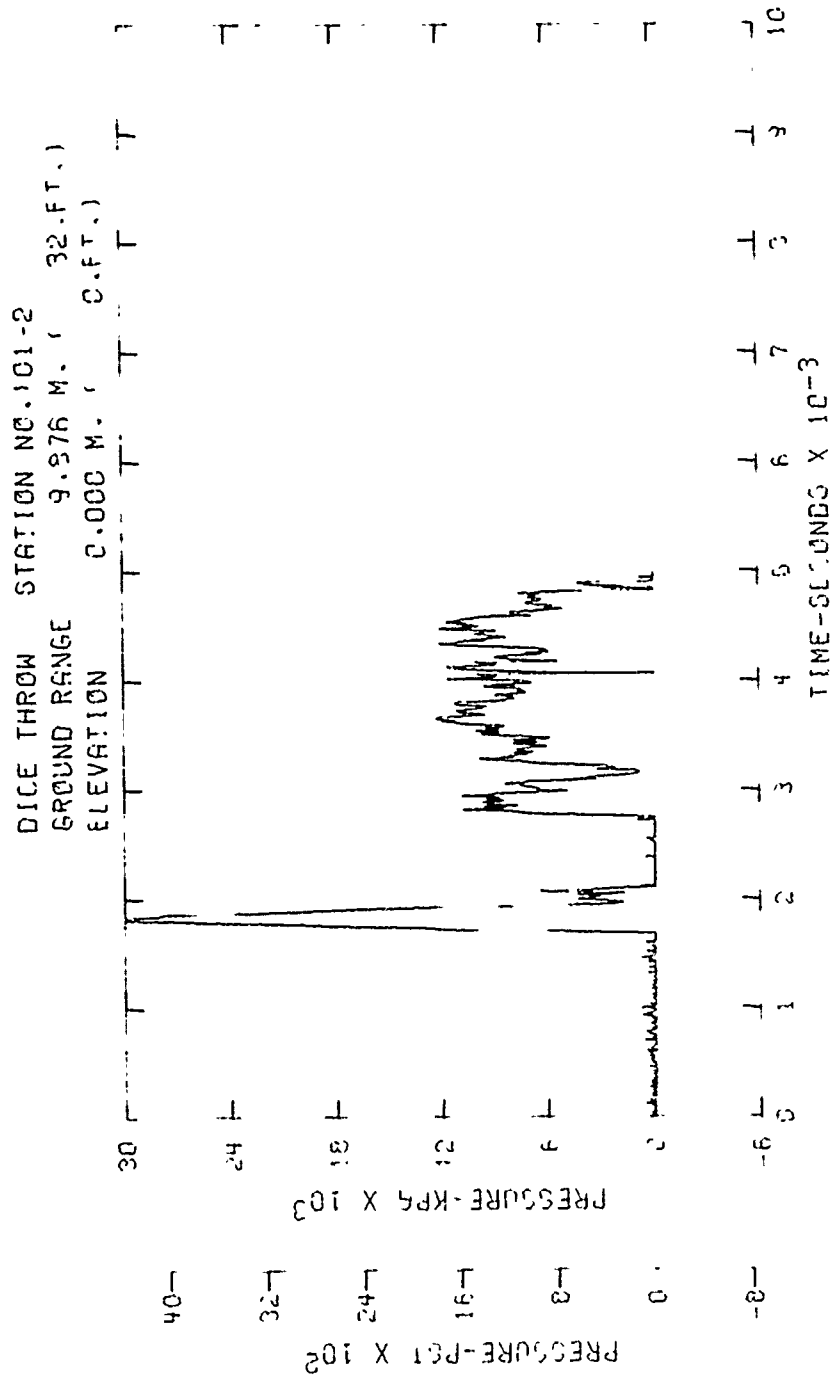


Figure A2. Incident pressure-time history - Station 101-2

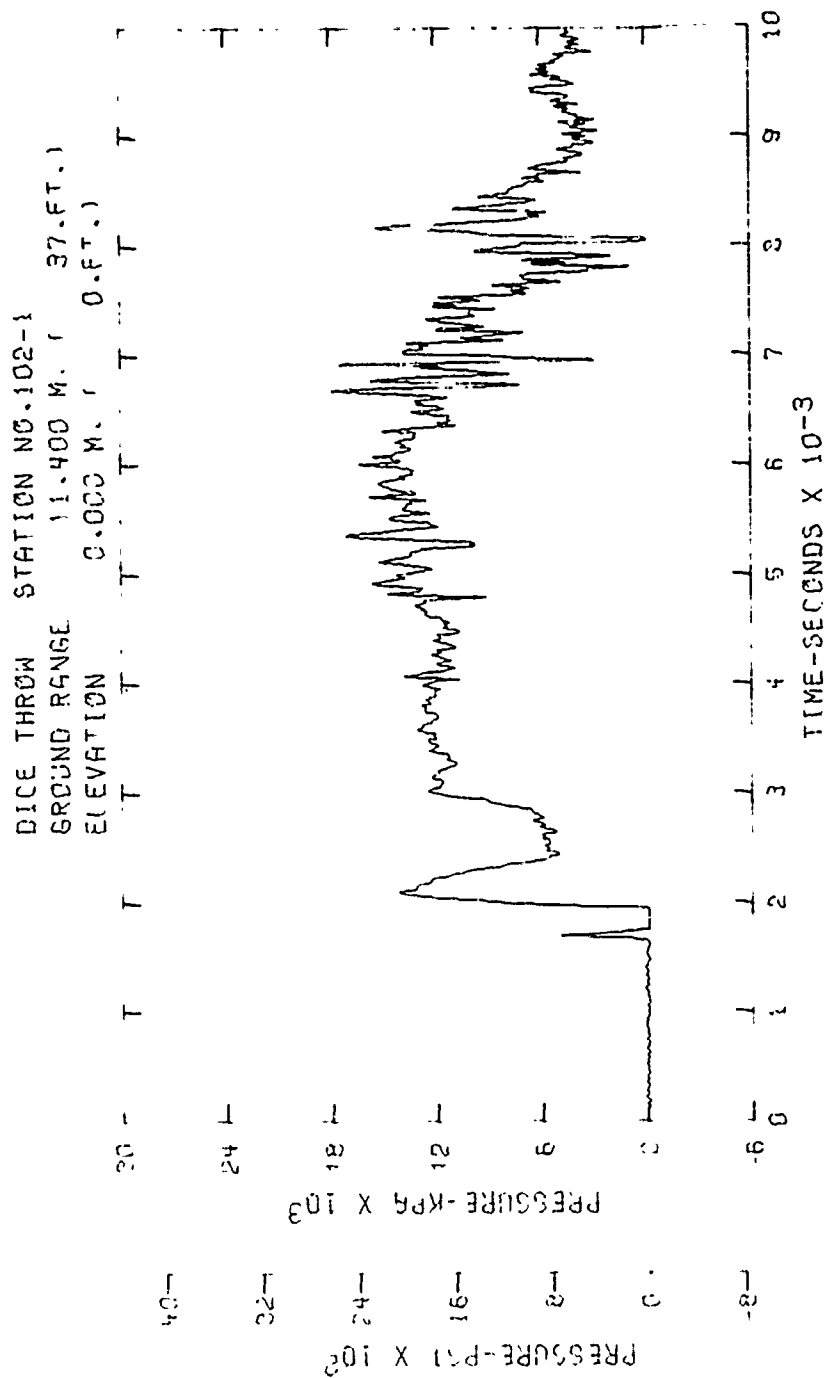


Figure A3. Incident pressure-time history - Station 102-1

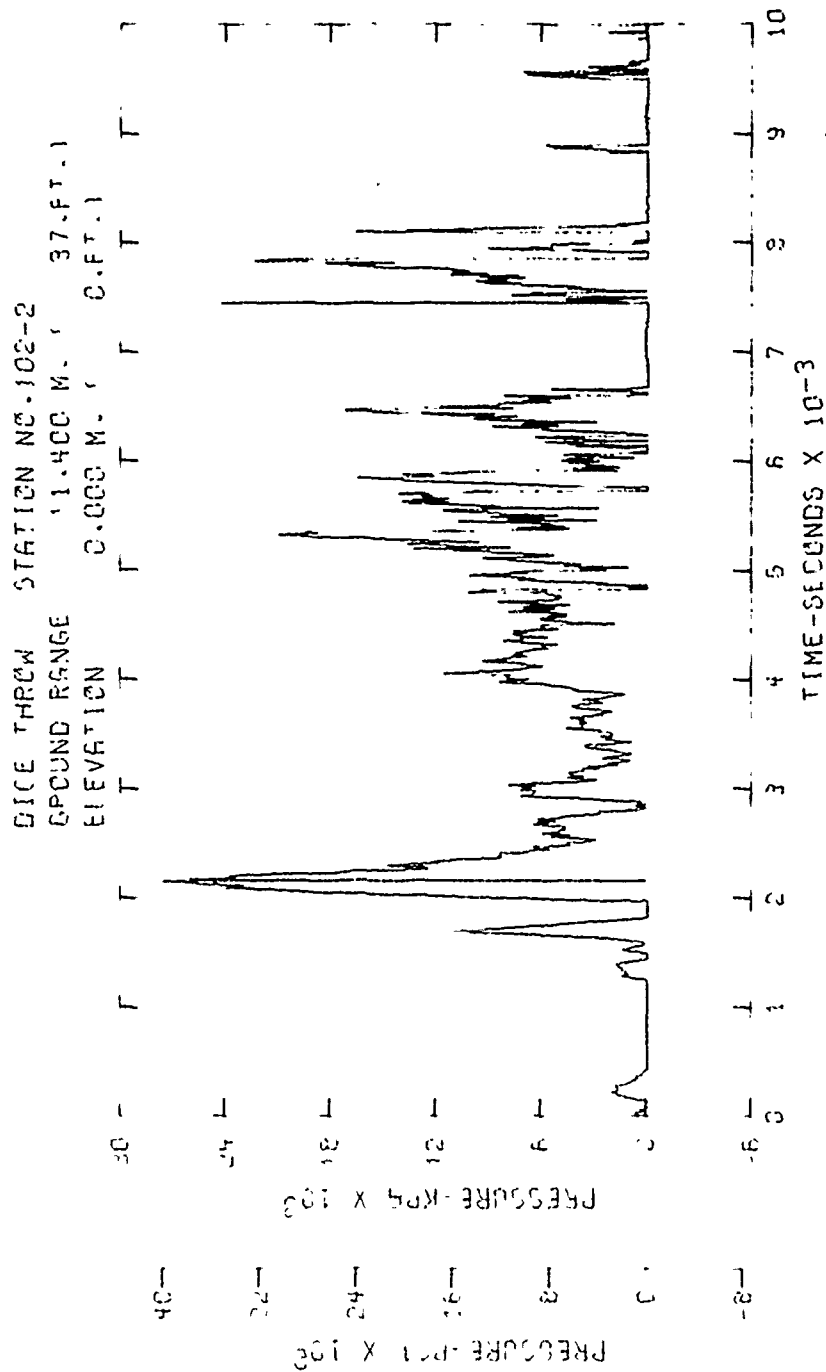


Figure A4. Incident pressure-time history - Station 102-2

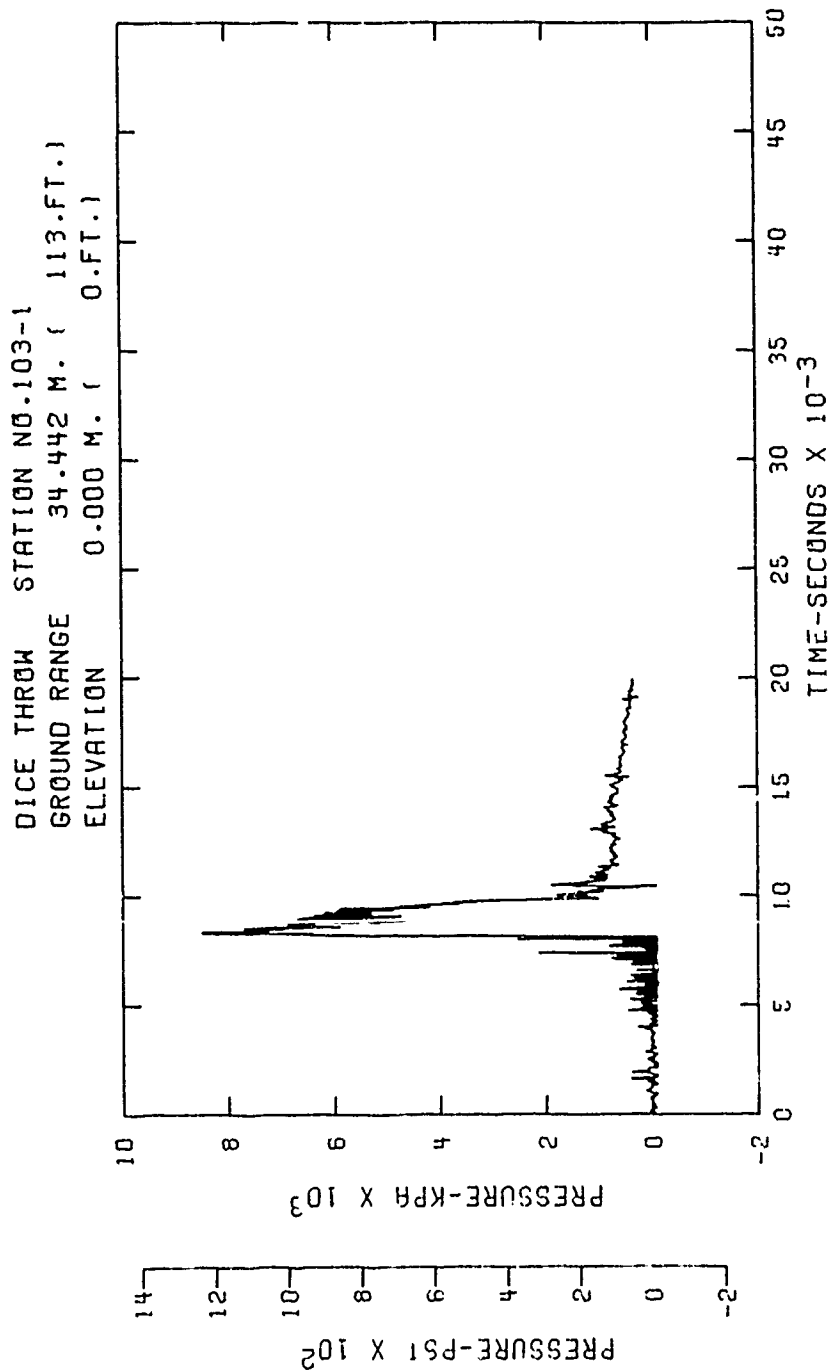


Figure A5. Incident pressure-time history - Station 103-1

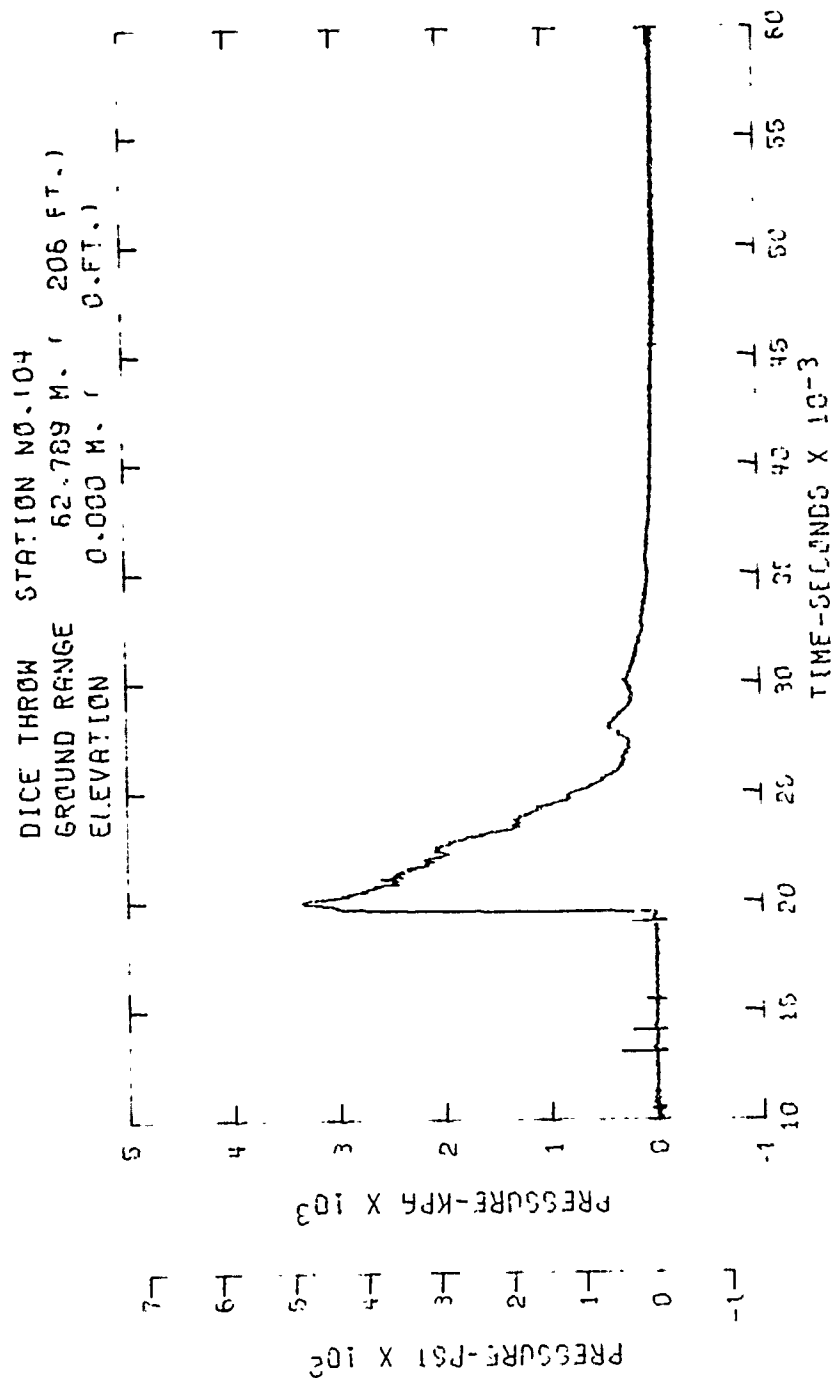


Figure A6. Incident pressure-time history - Station 104

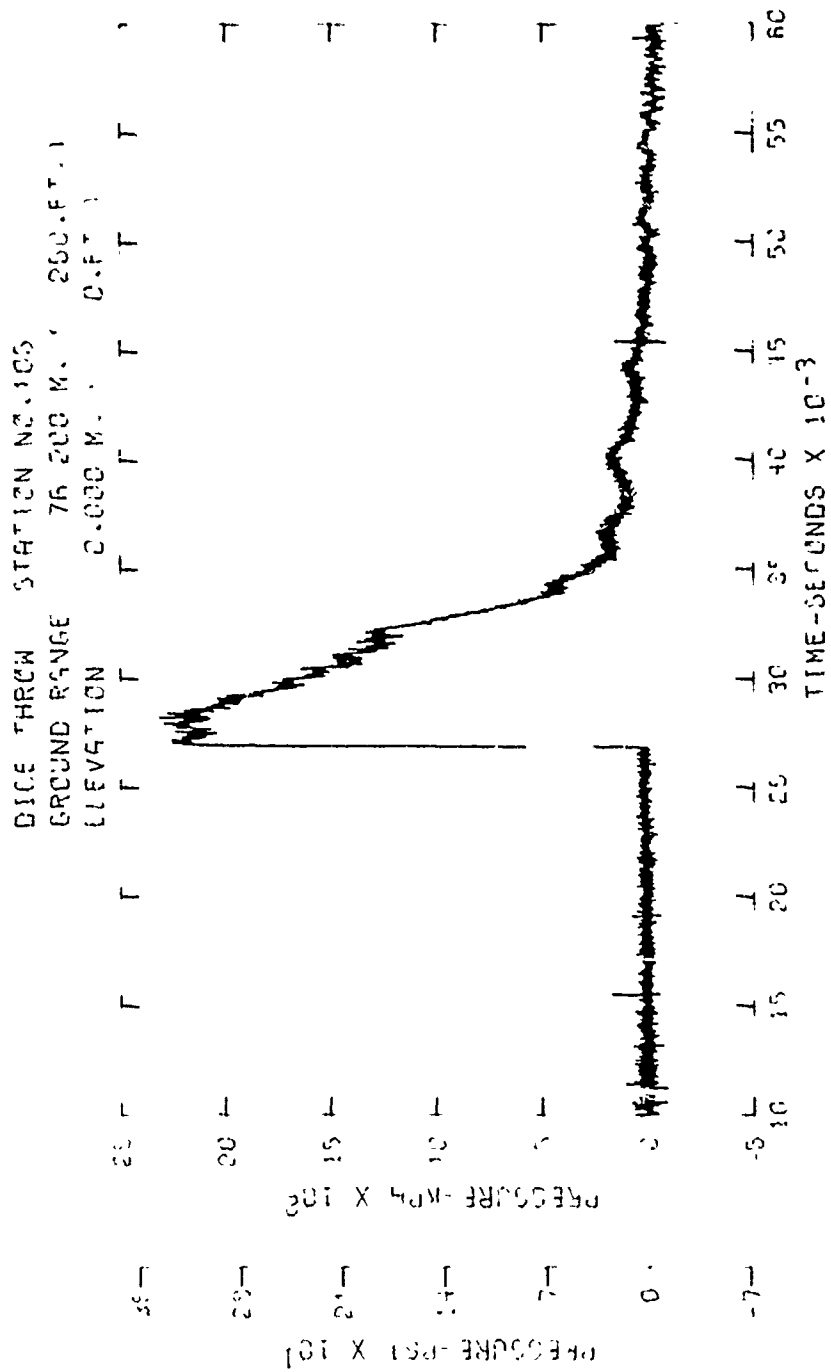


Figure A7. Incident pressure-time history - Station 105

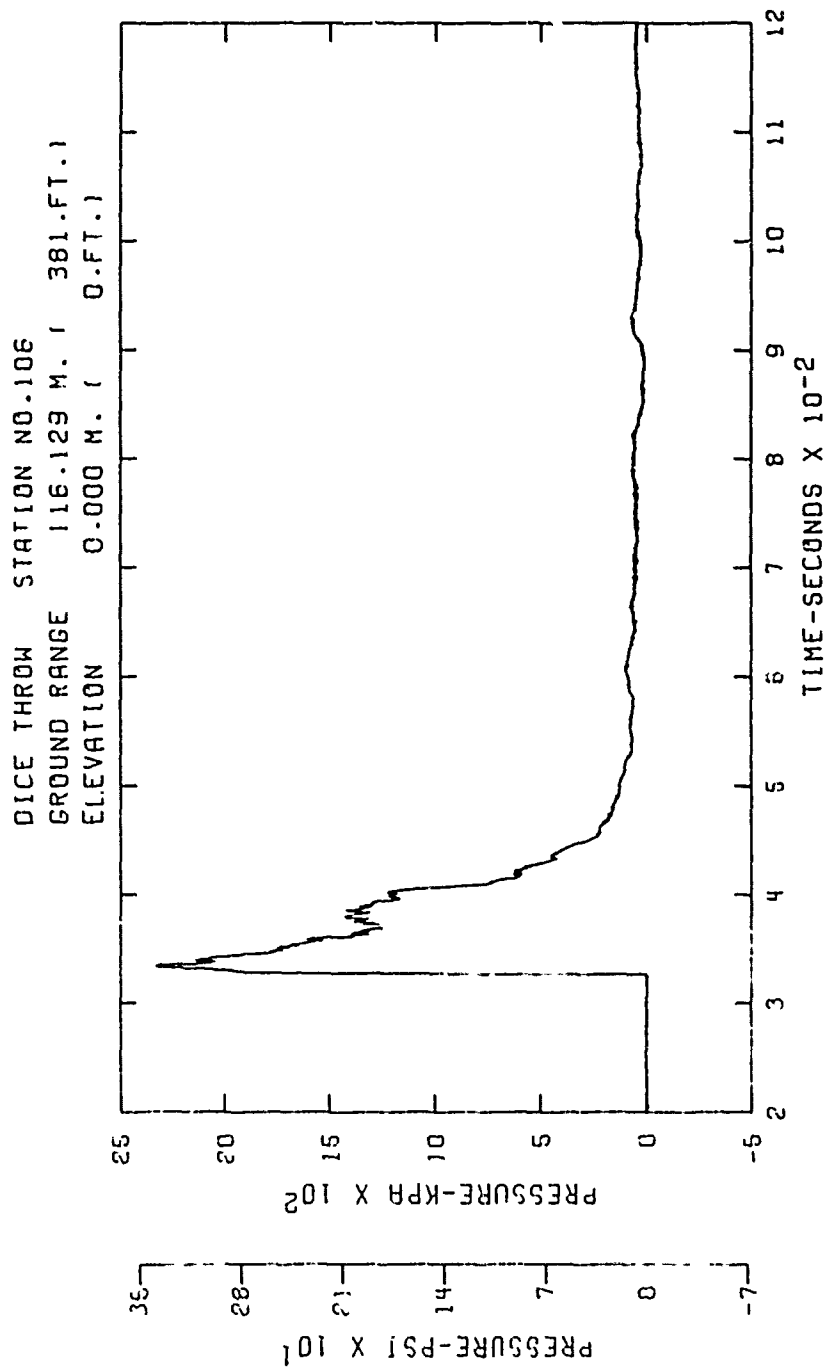


Figure A8. Incident pressure-time history - Station 106

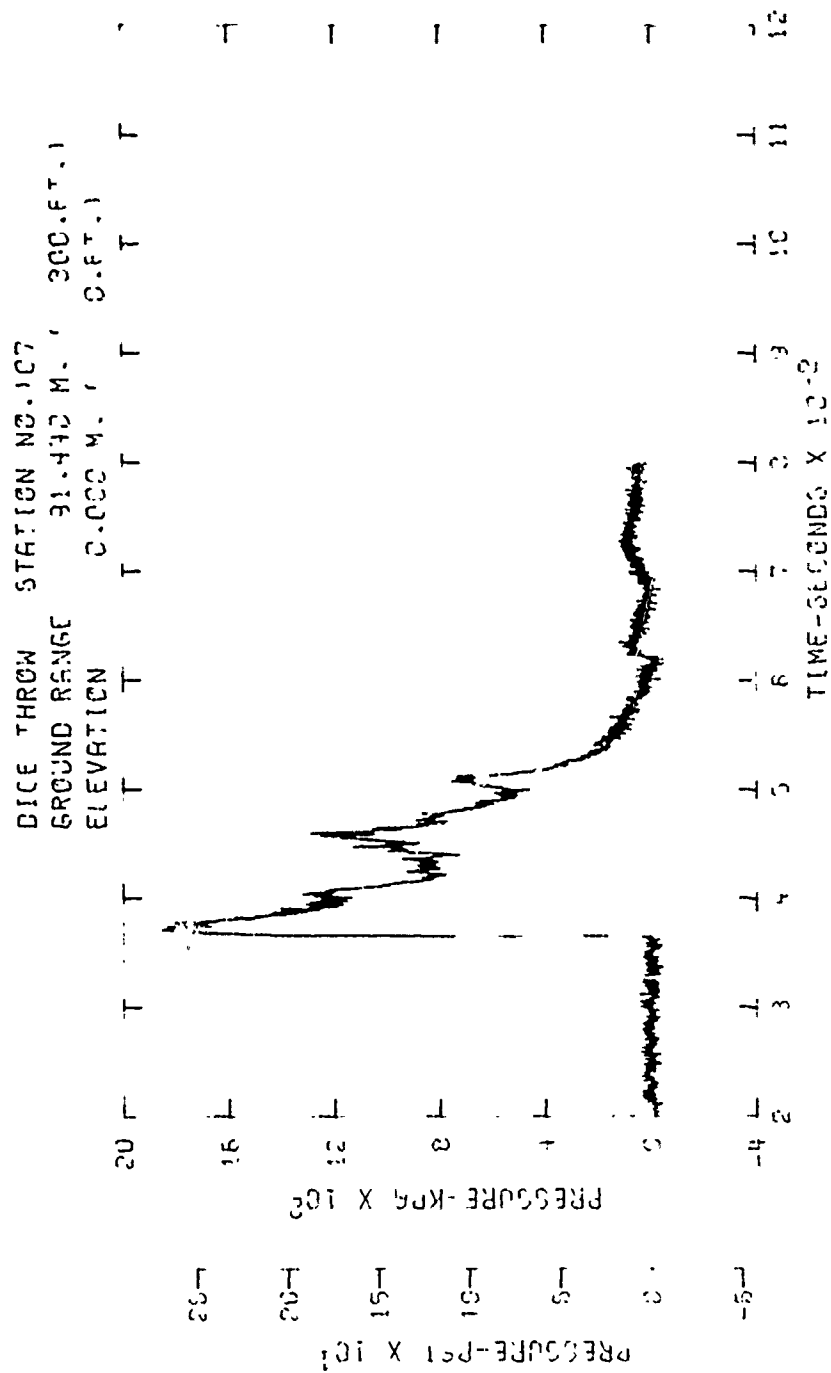


Figure A9. Incident pressure-time history - Station 107



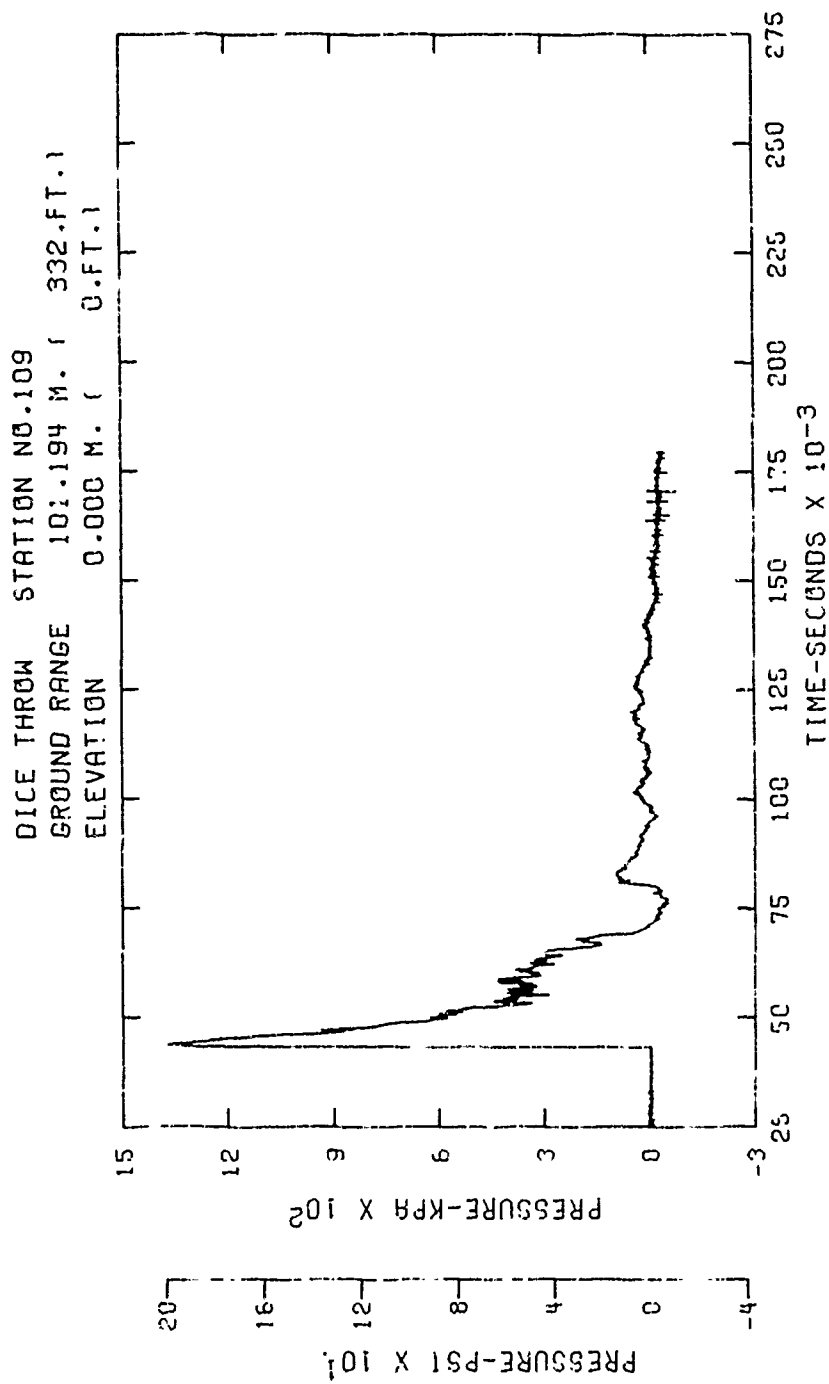


Figure A10. Incident pressure-time history - Station 109

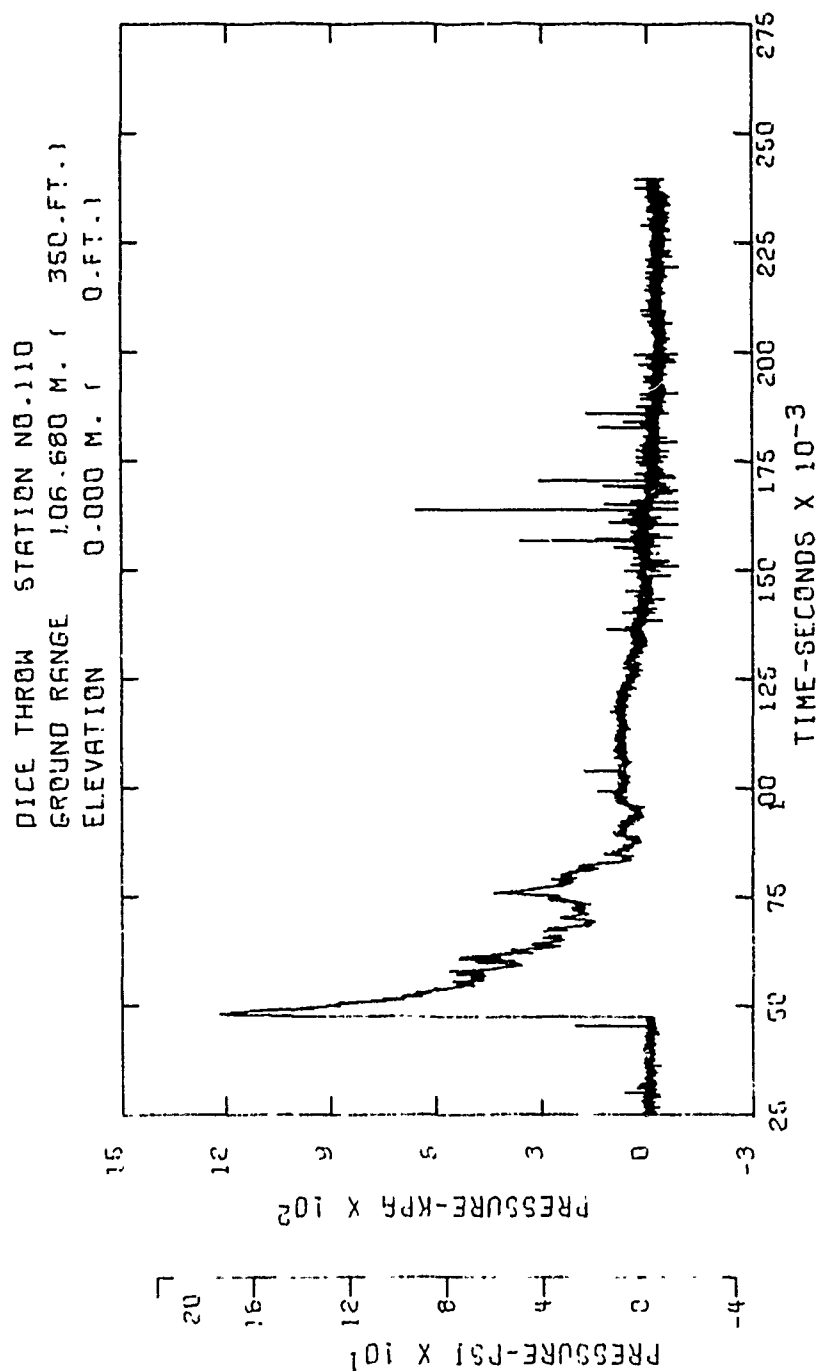


Figure A11. Incident pressure-time history - Station 110

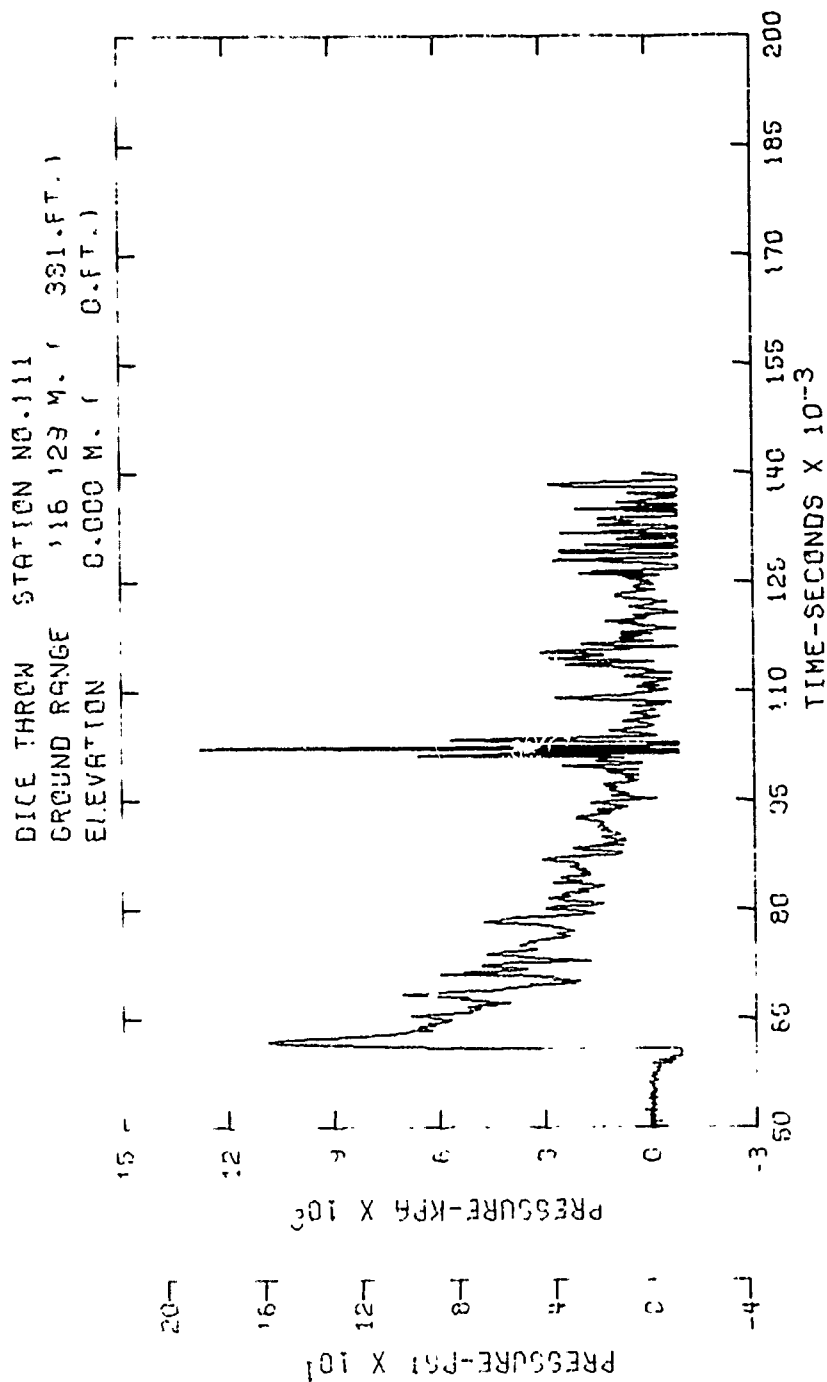


Figure A12. Incident pressure-time history - Station 111

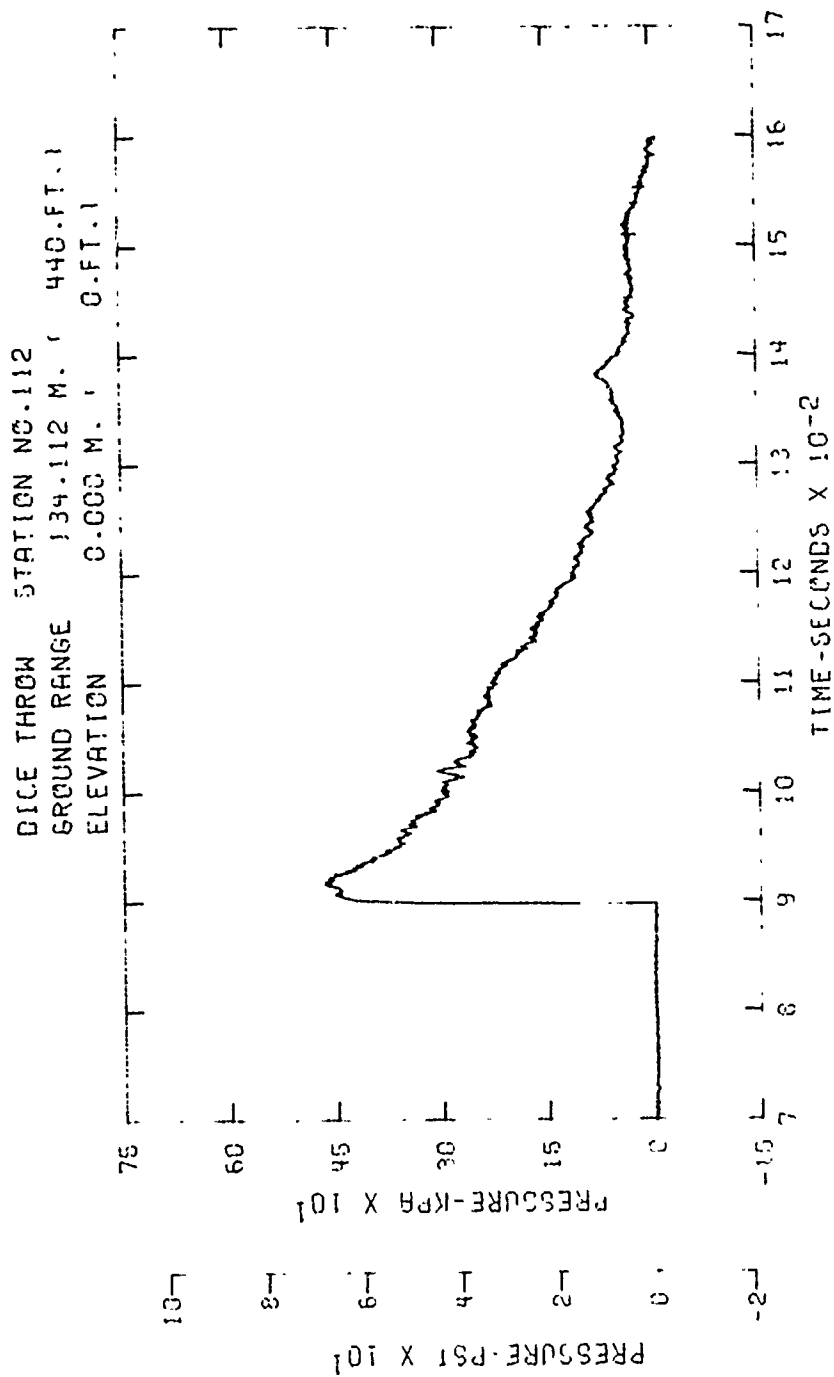


Figure A13. Incident pressure-time history - Station 112

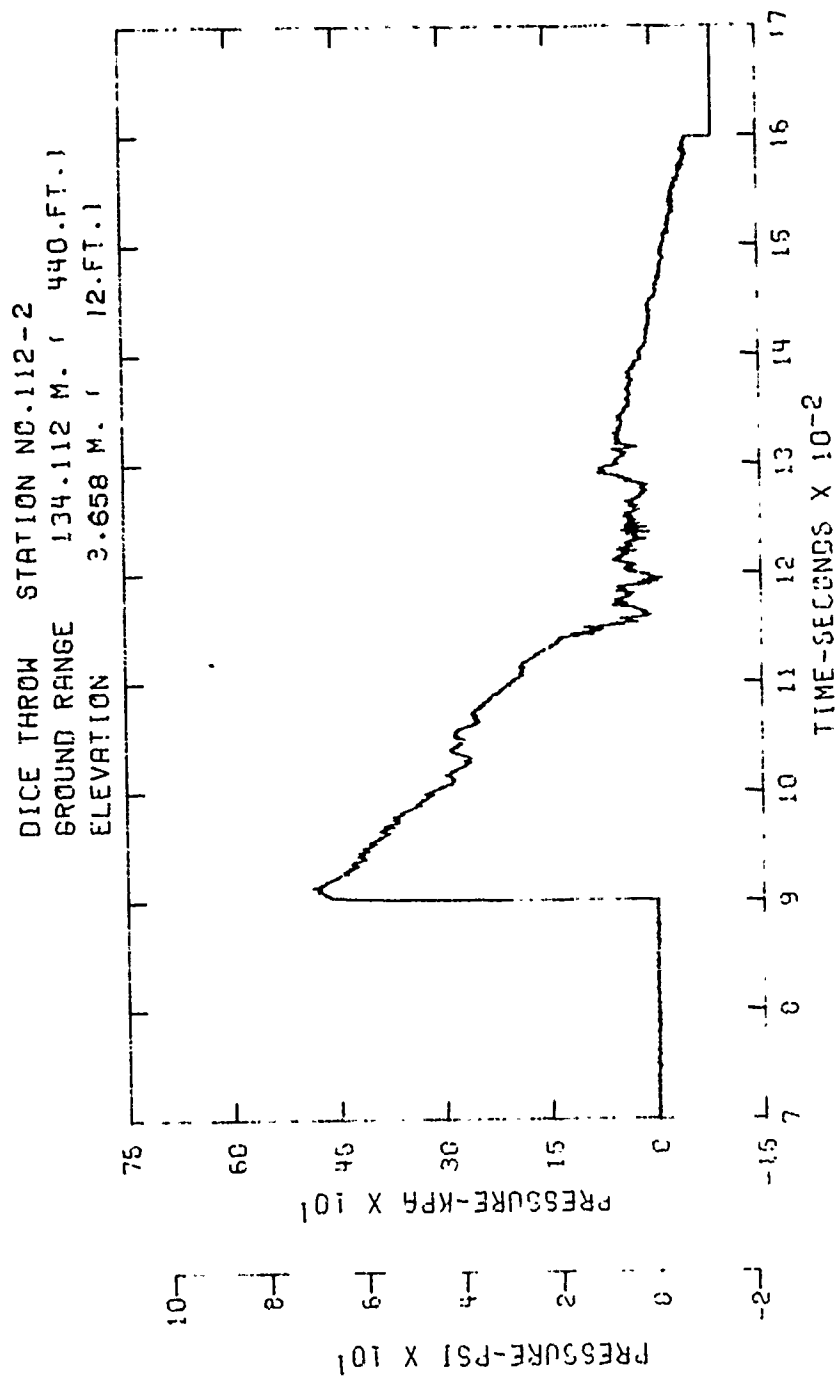


Figure A14. Incident pressure-time history - Station 112-2

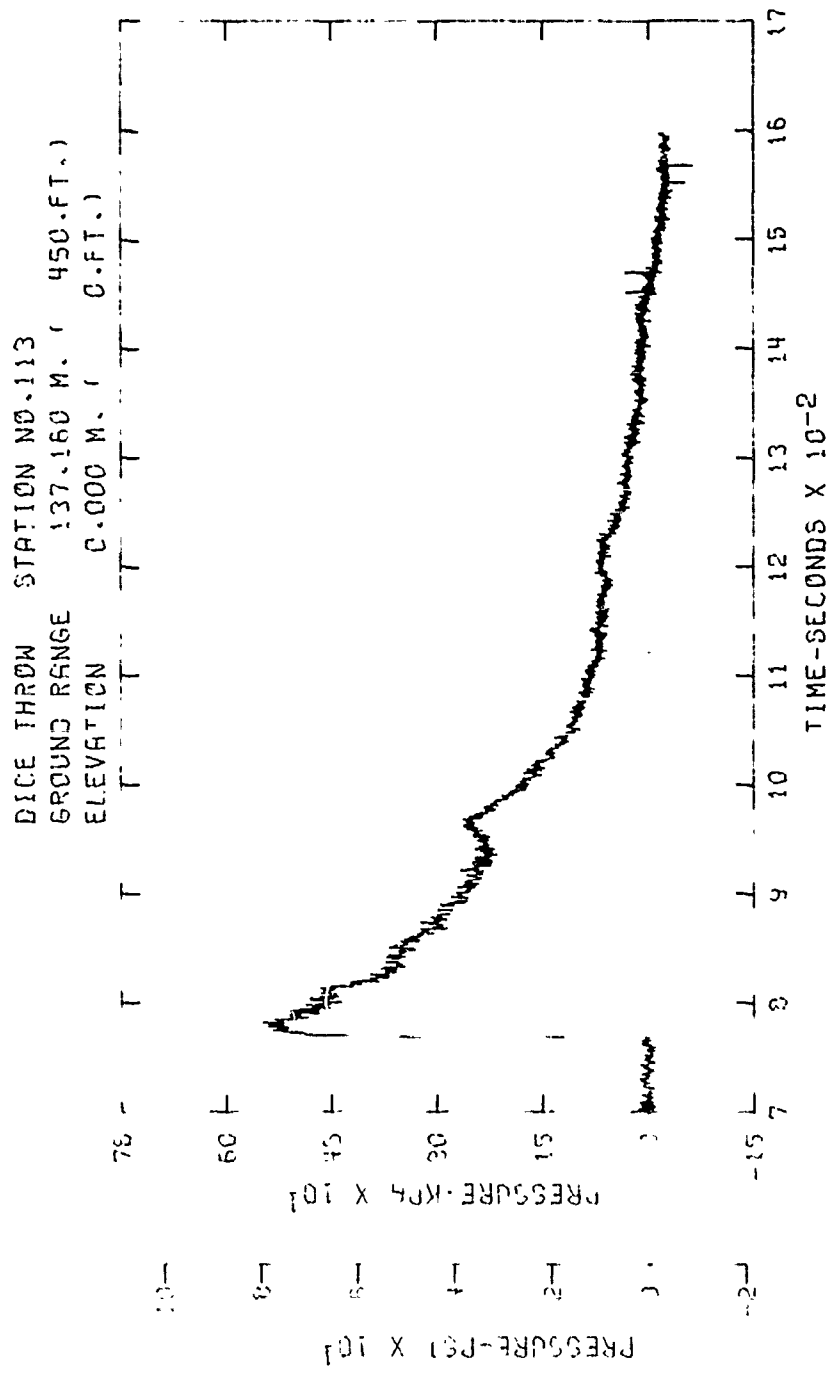


Figure A15. Incident pressure-time history - Station 113

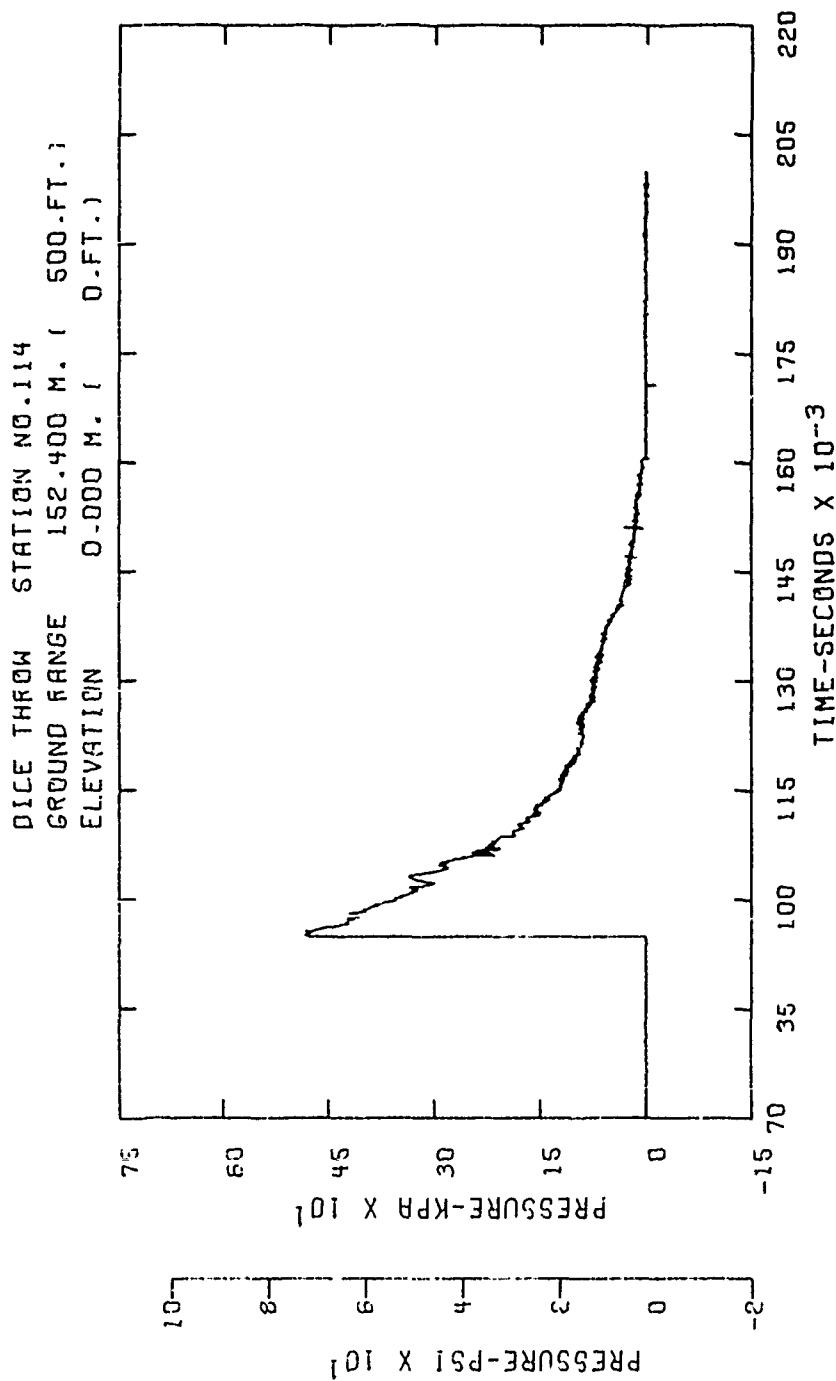


Figure A16. Incident pressure-time history - Station 114

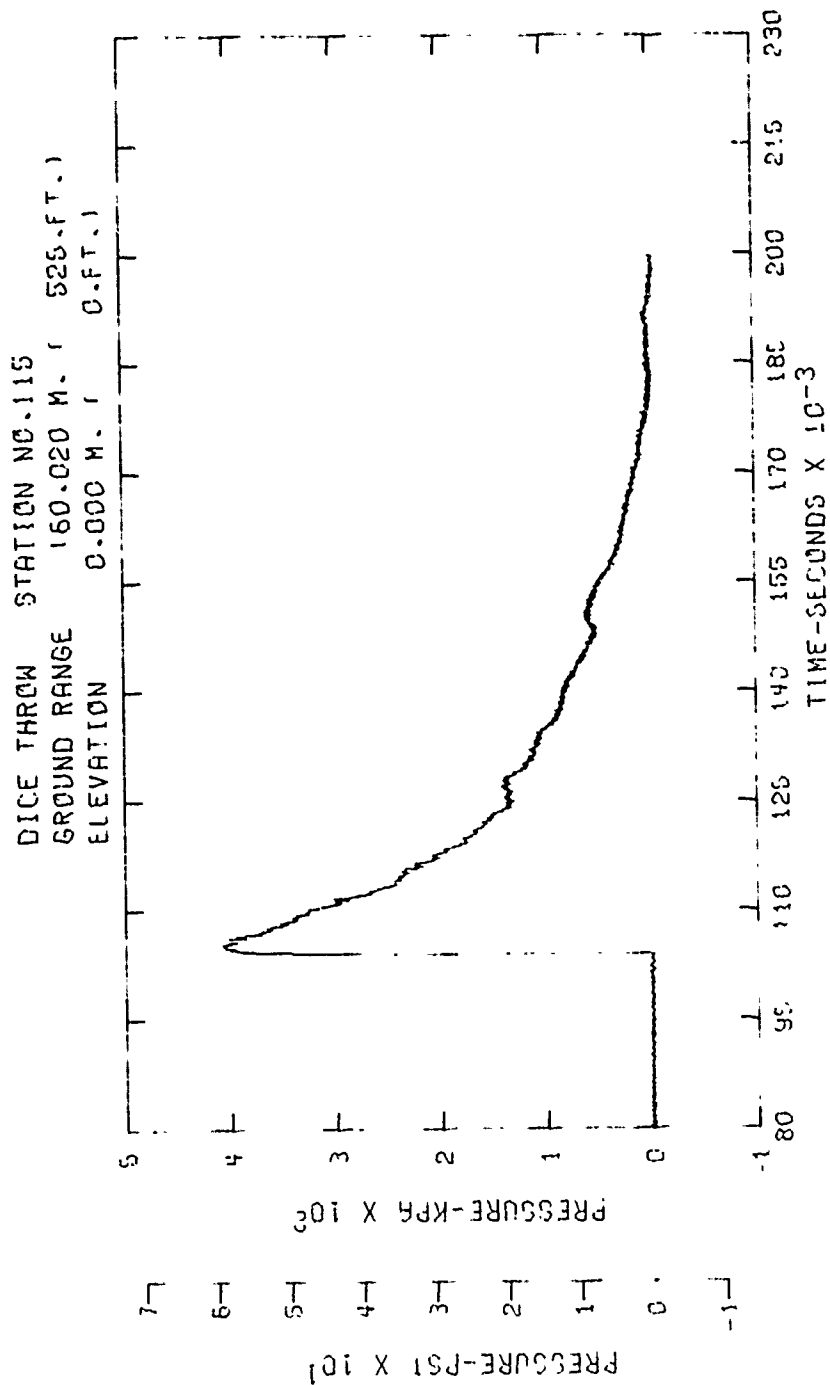


Figure A17. Incident pressure-time history - Station 115



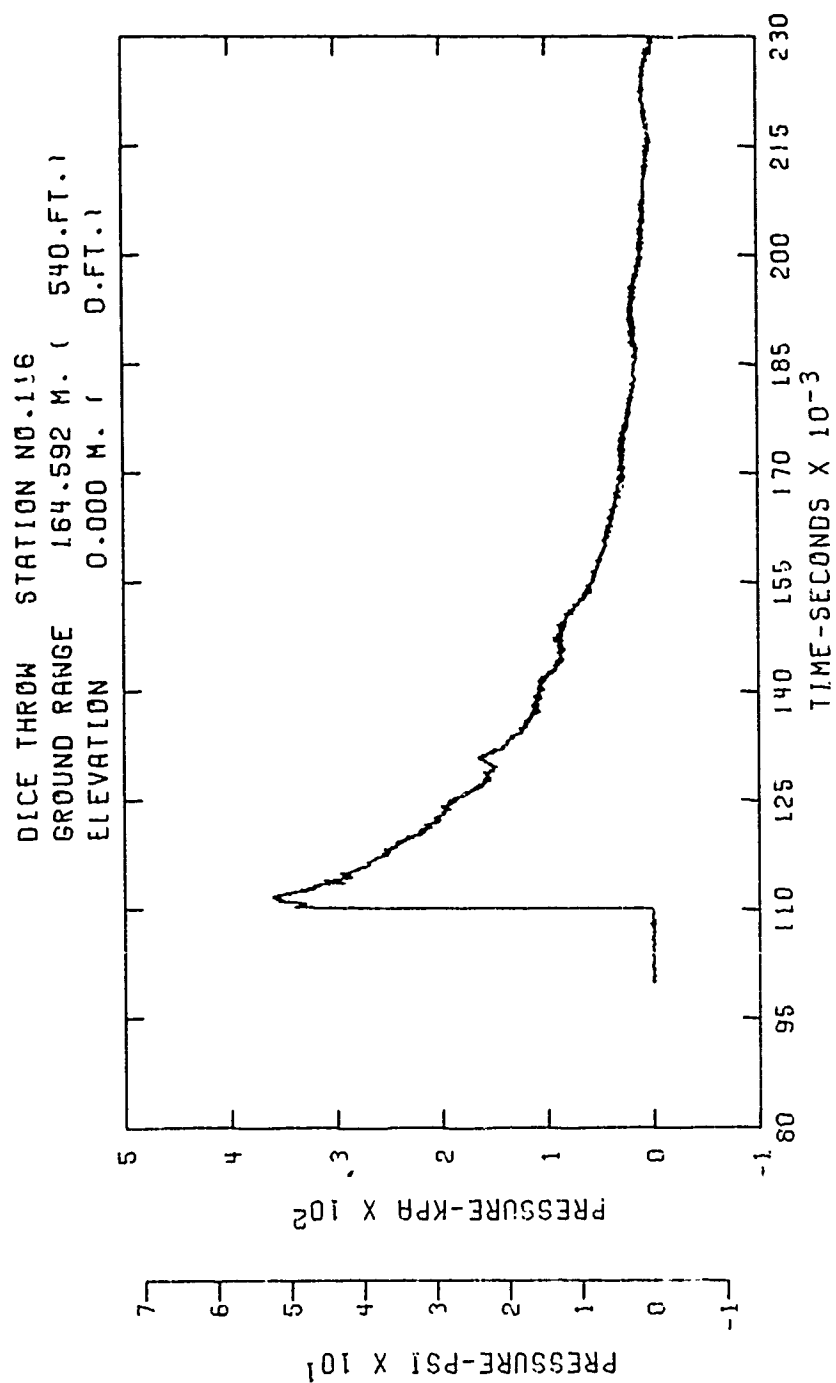


Figure A18. Incident pressure-time history - Station 116

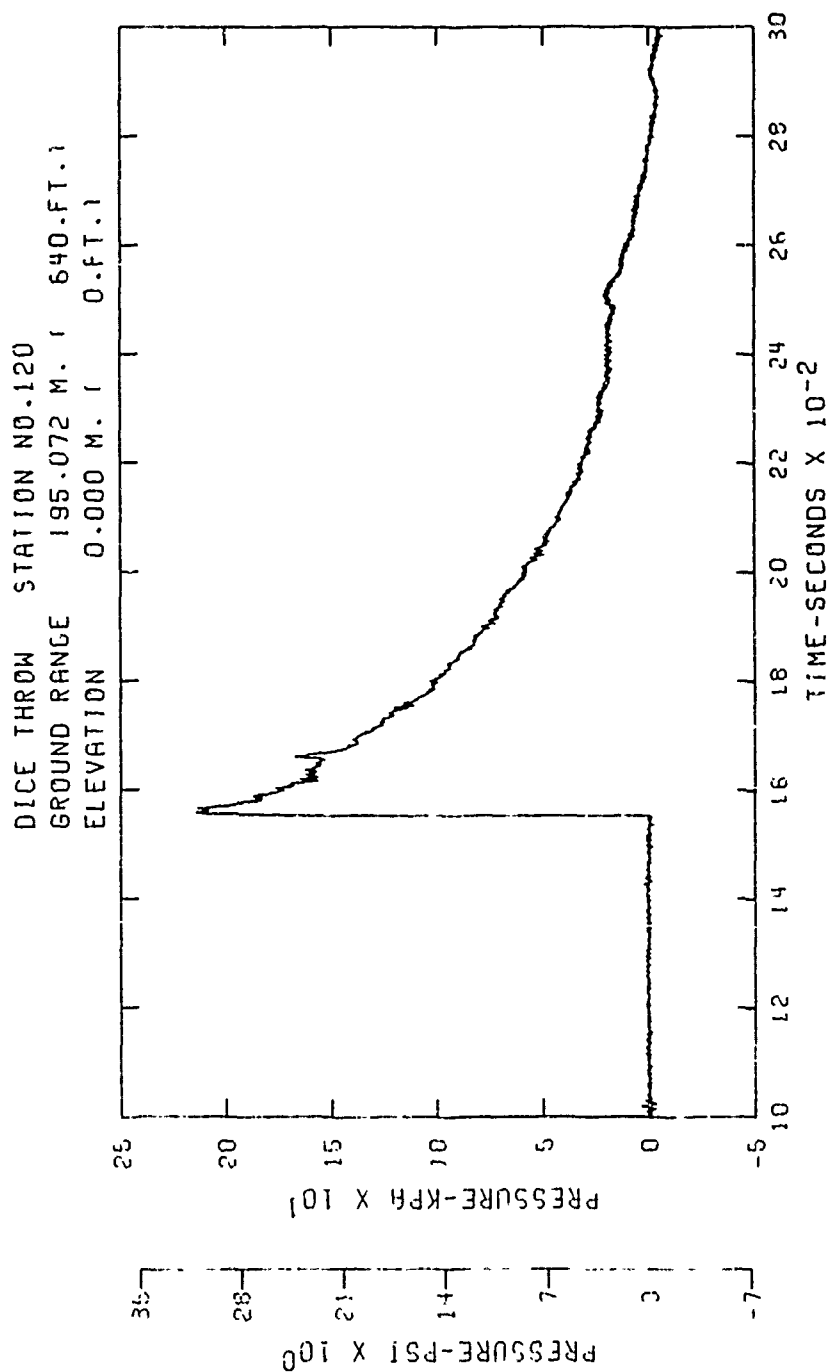


Figure A19. Incident pressure-time history - Station 120

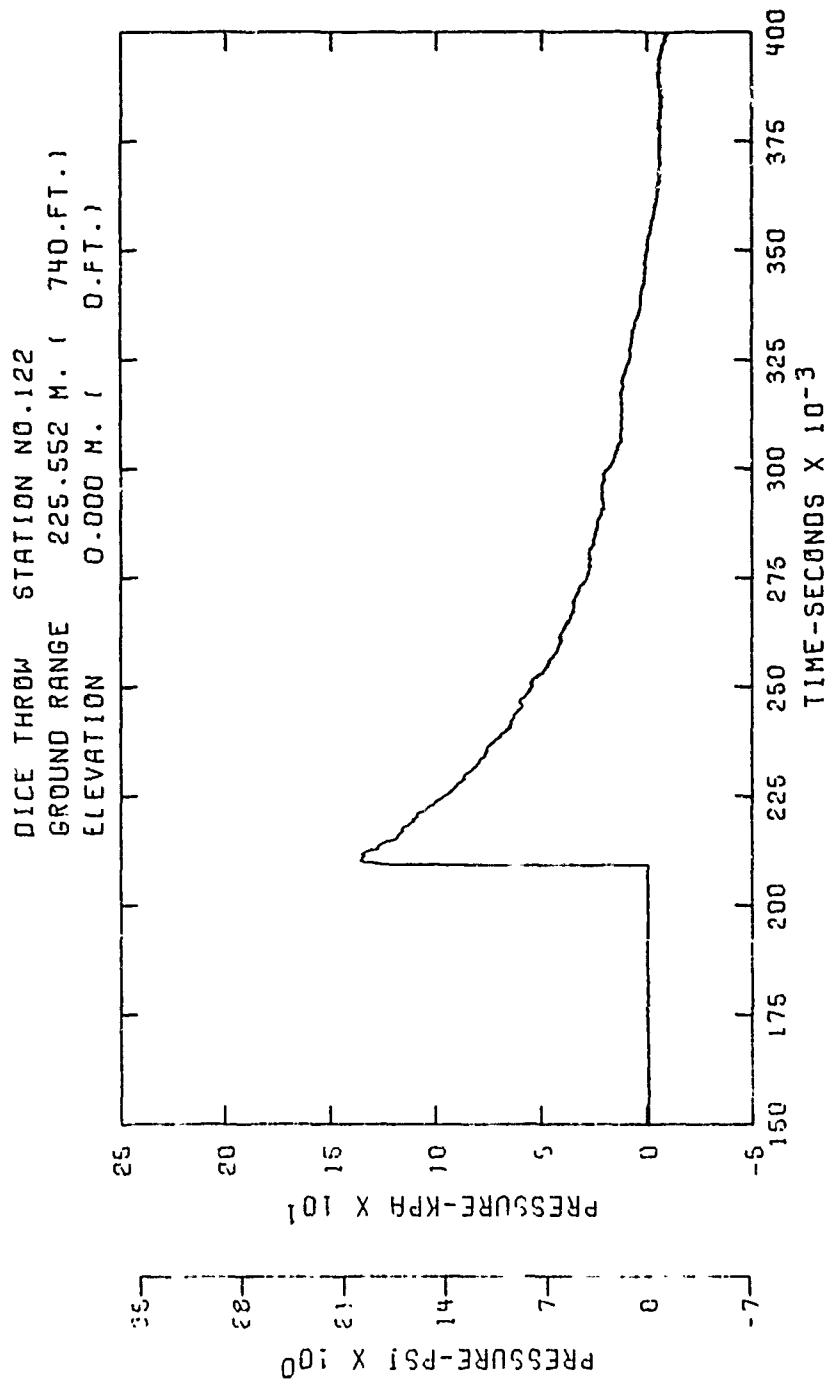


Figure A20. Incident pressure-time history - Station 122

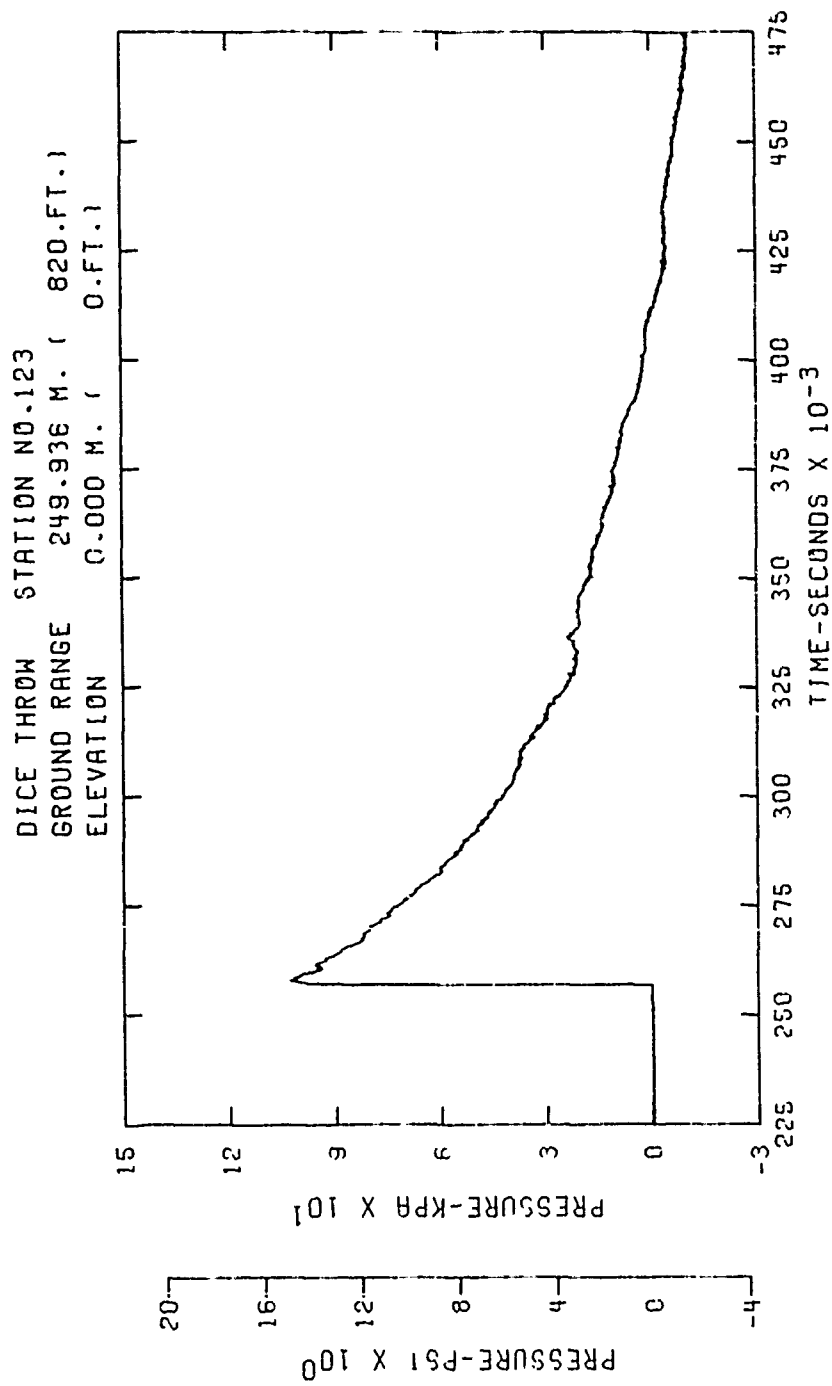


Figure A21. Incident pressure-time history - Station 123

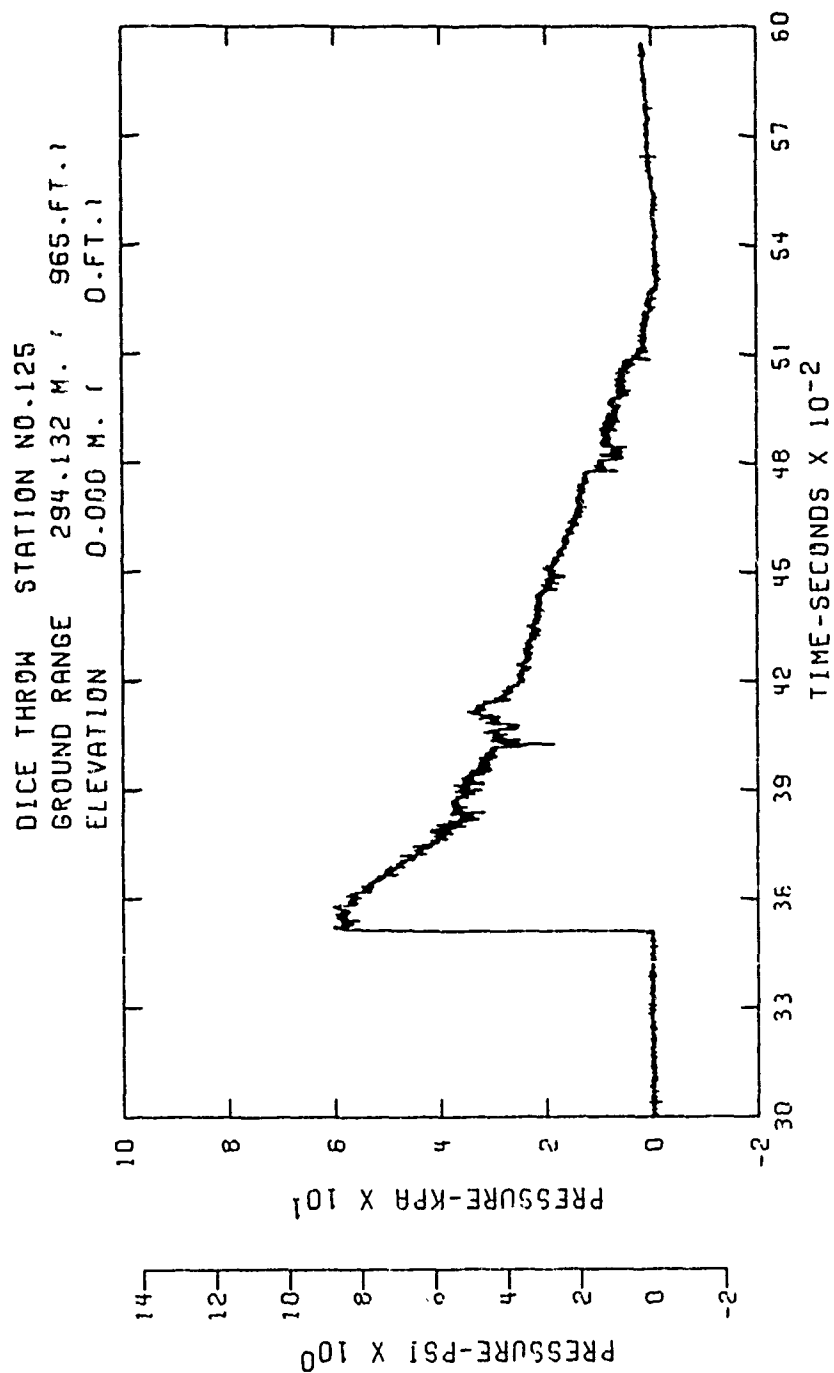


Figure A22. Incident pressure-time history - Station 125

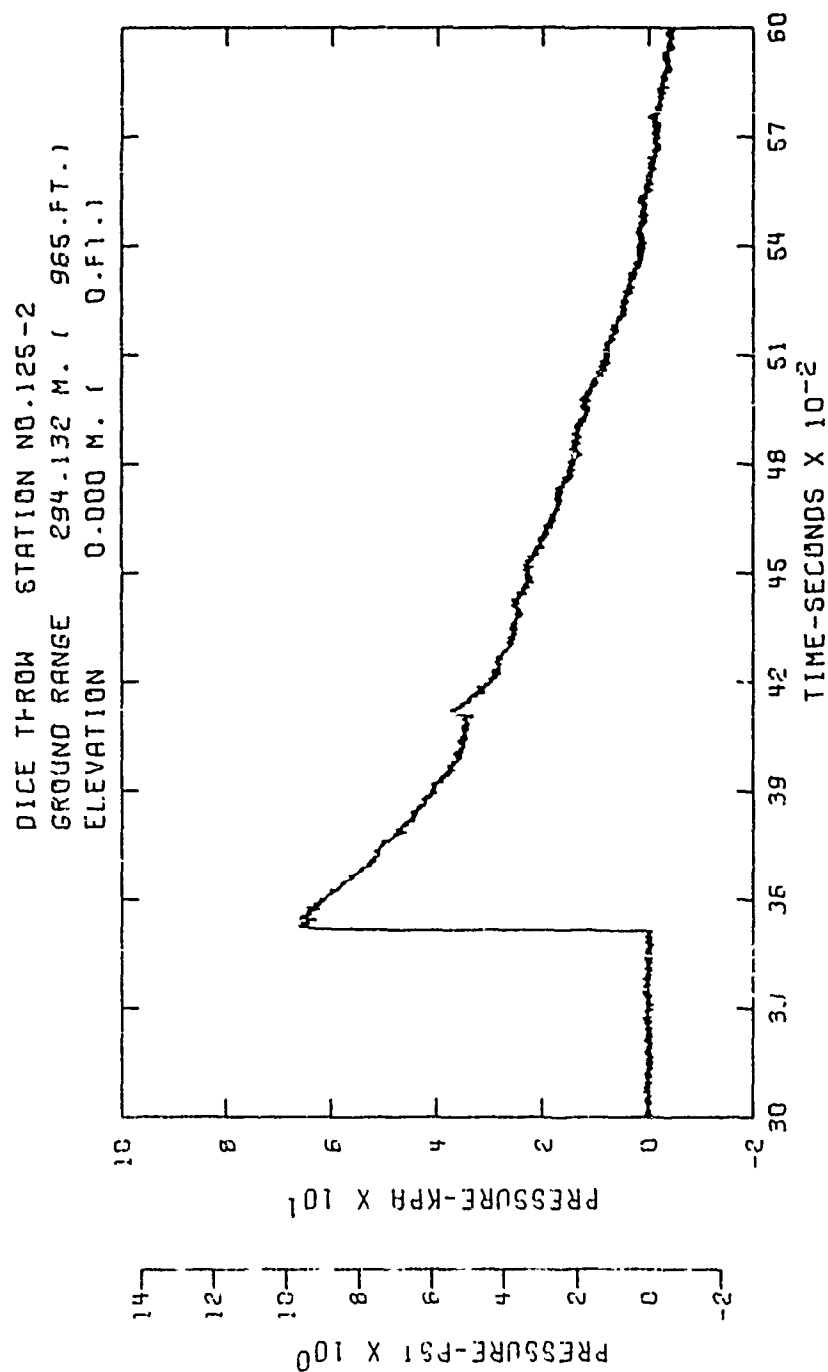


Figure A23. Incident pressure-time history - Station 125-2

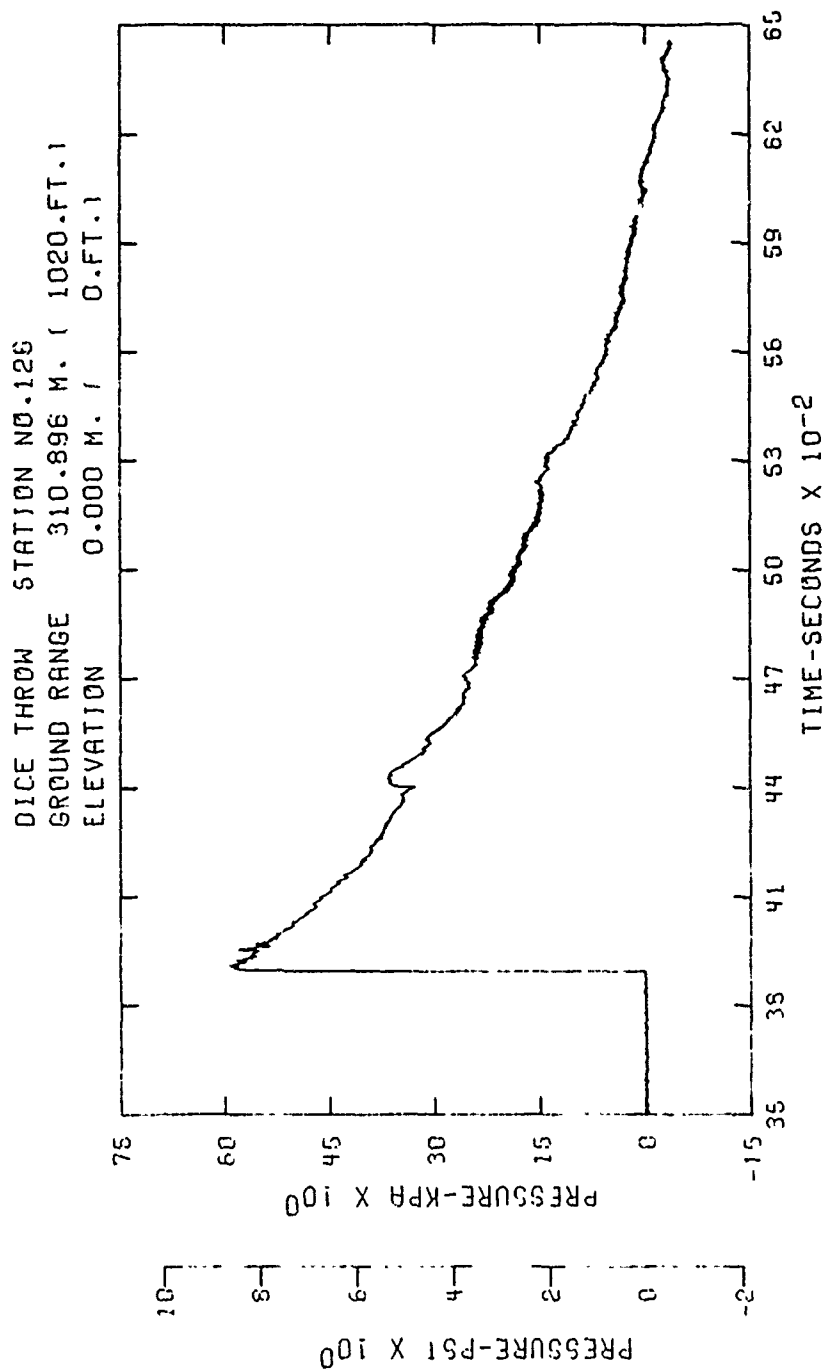


Figure A24. Incident pressure-time history - Station 126

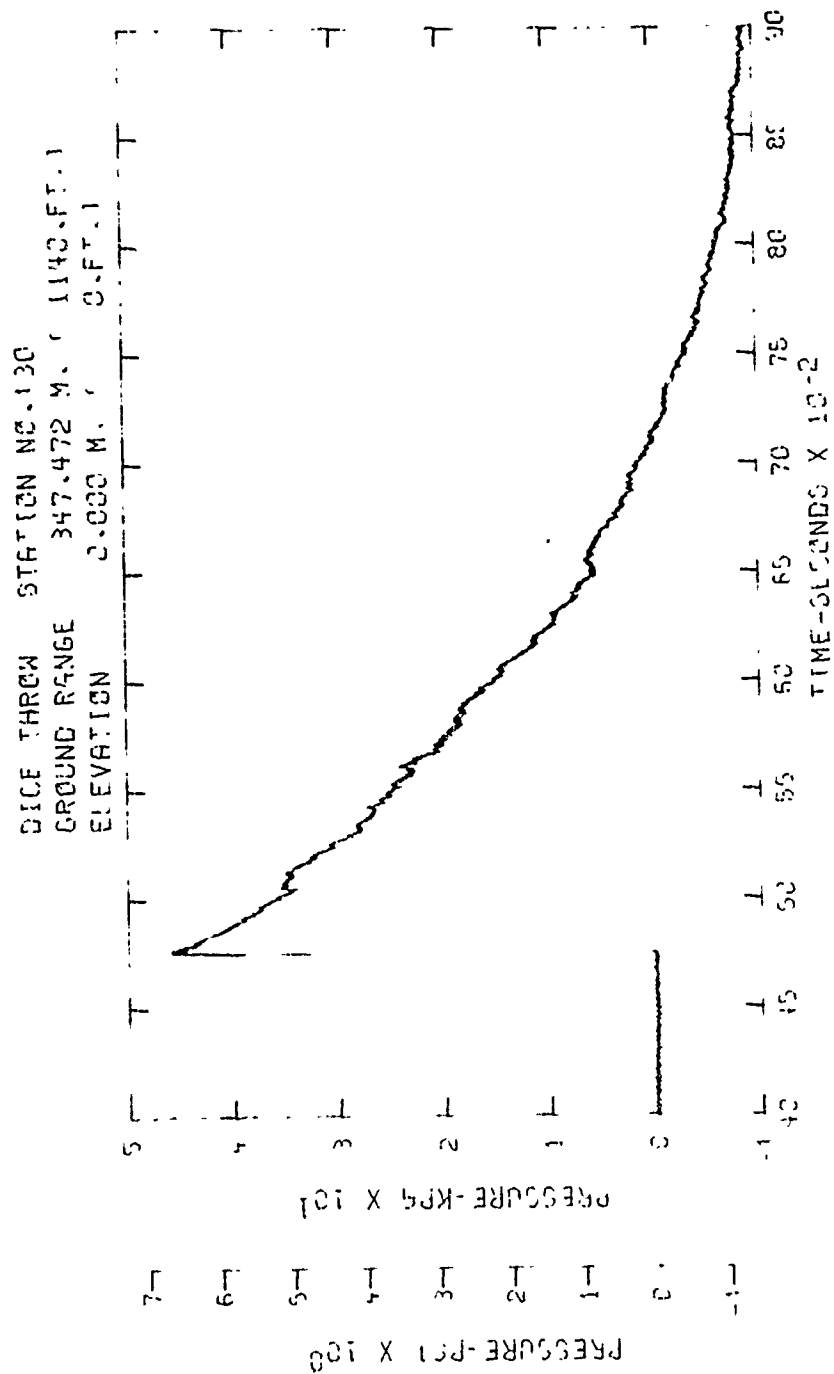


Figure A25. Incident pressure-time history - Station 130



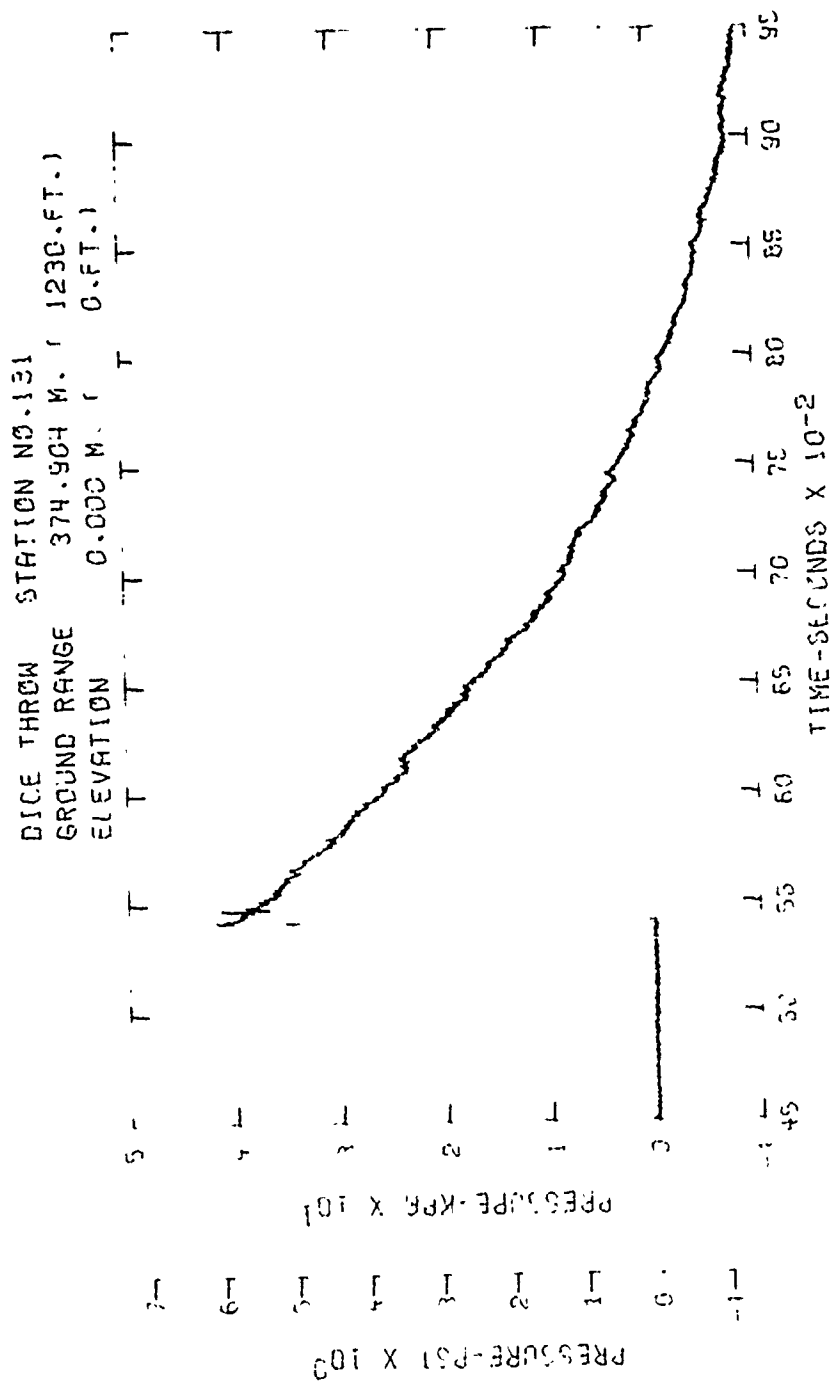


Figure A26. Incident pressure-time history - Station 131

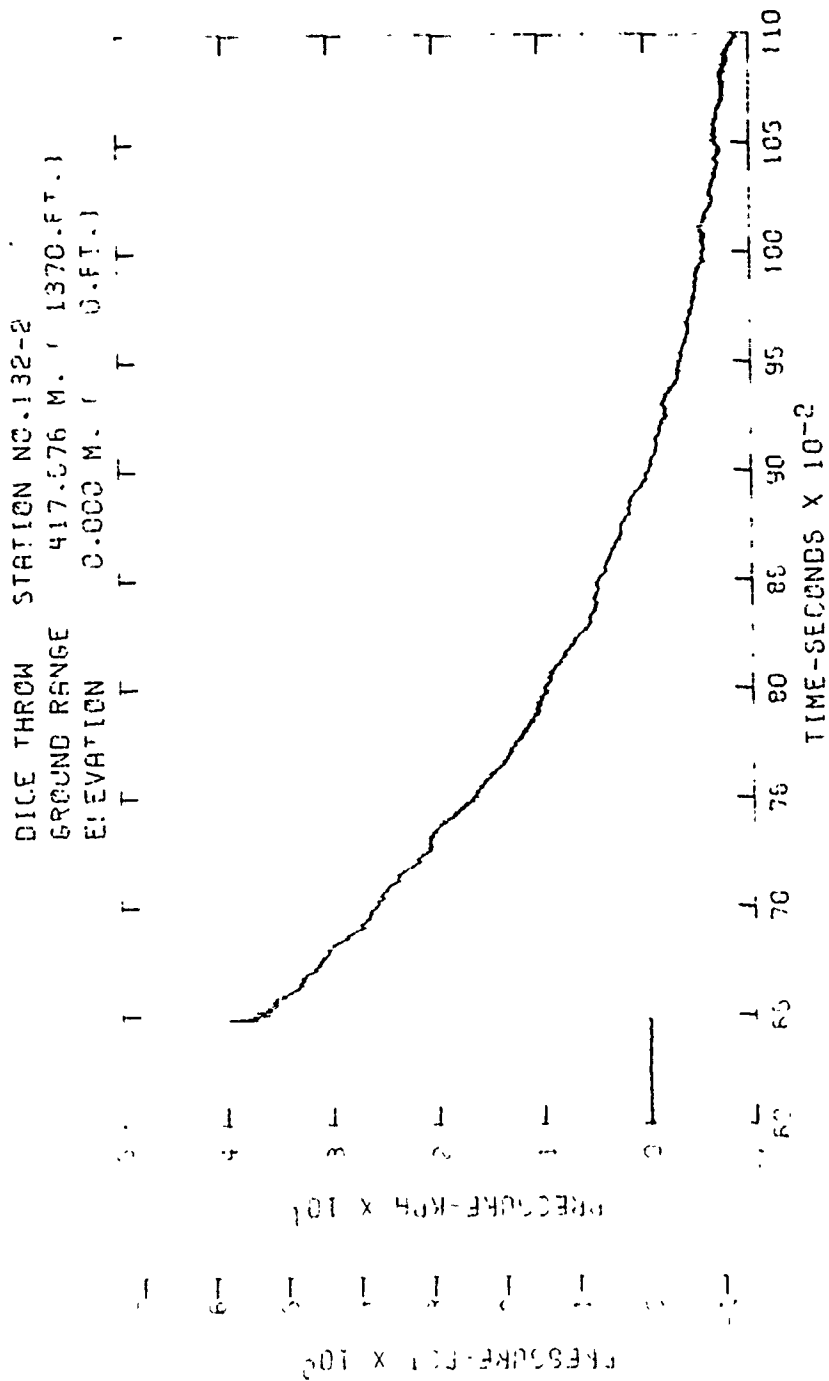


Figure A27. Incident pressure-time history - Station 132-2

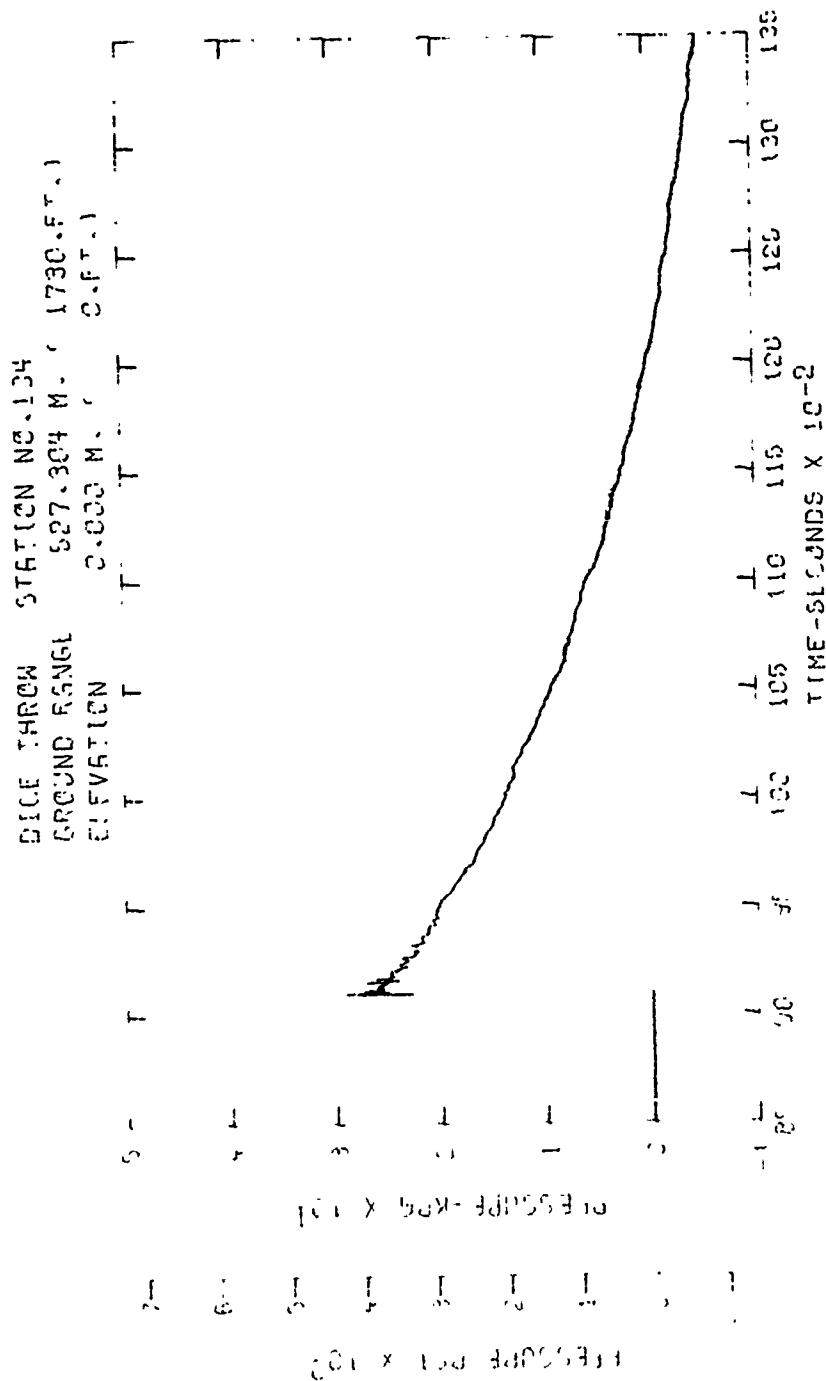


Figure A28. Incident pressure-time history - Station 134

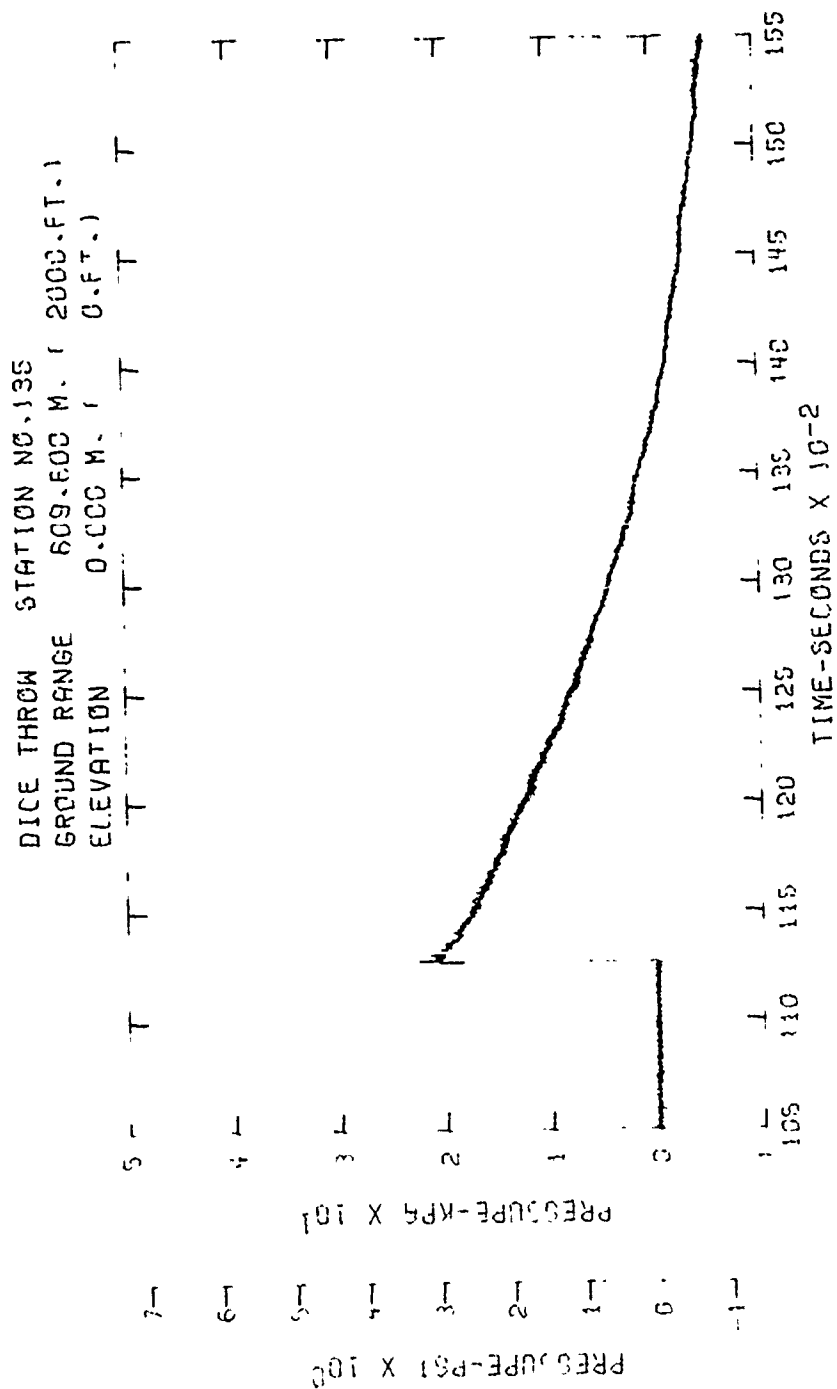


Figure A29. Incident pressure-time history - Station 135

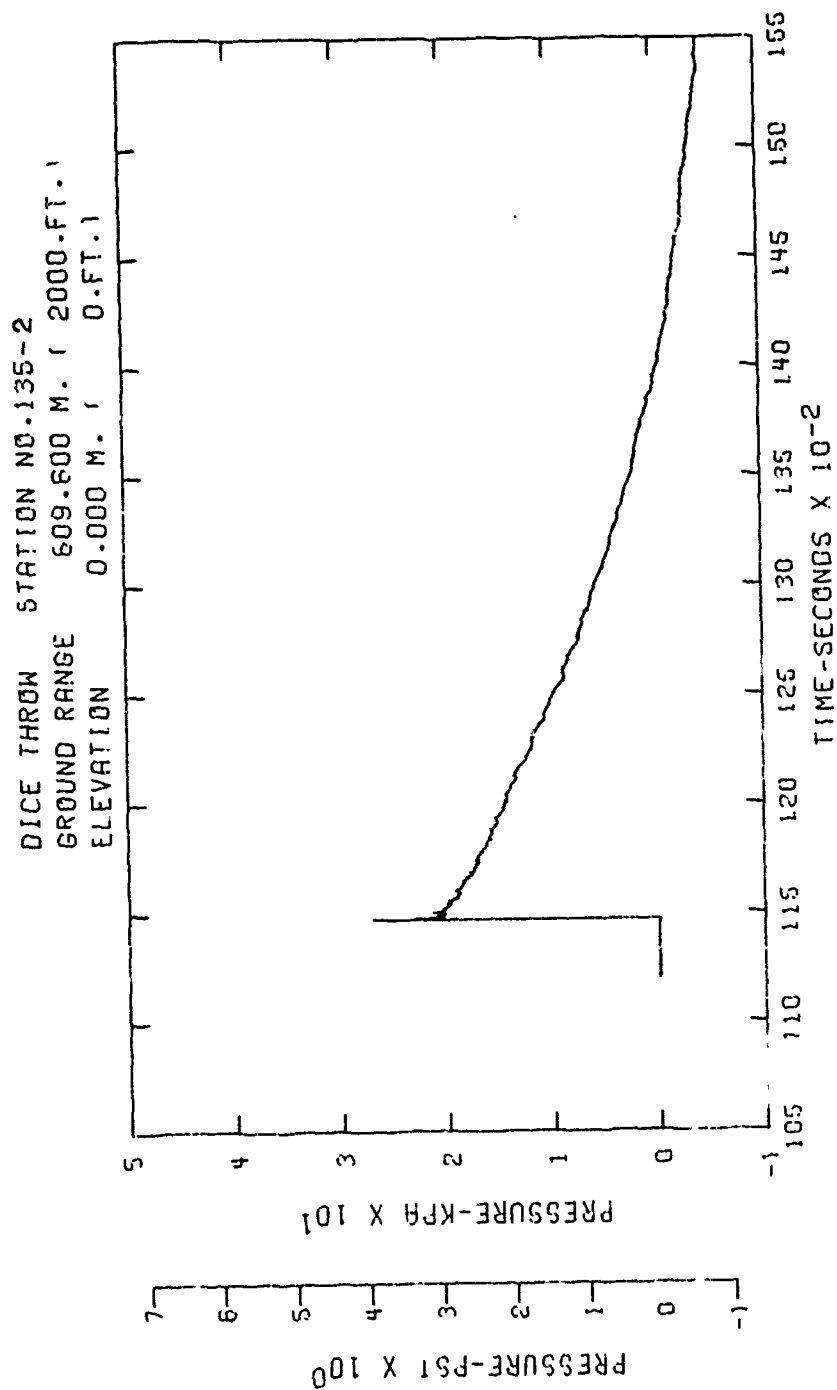


Figure A30. Incident pressure-time history - Station 135-2

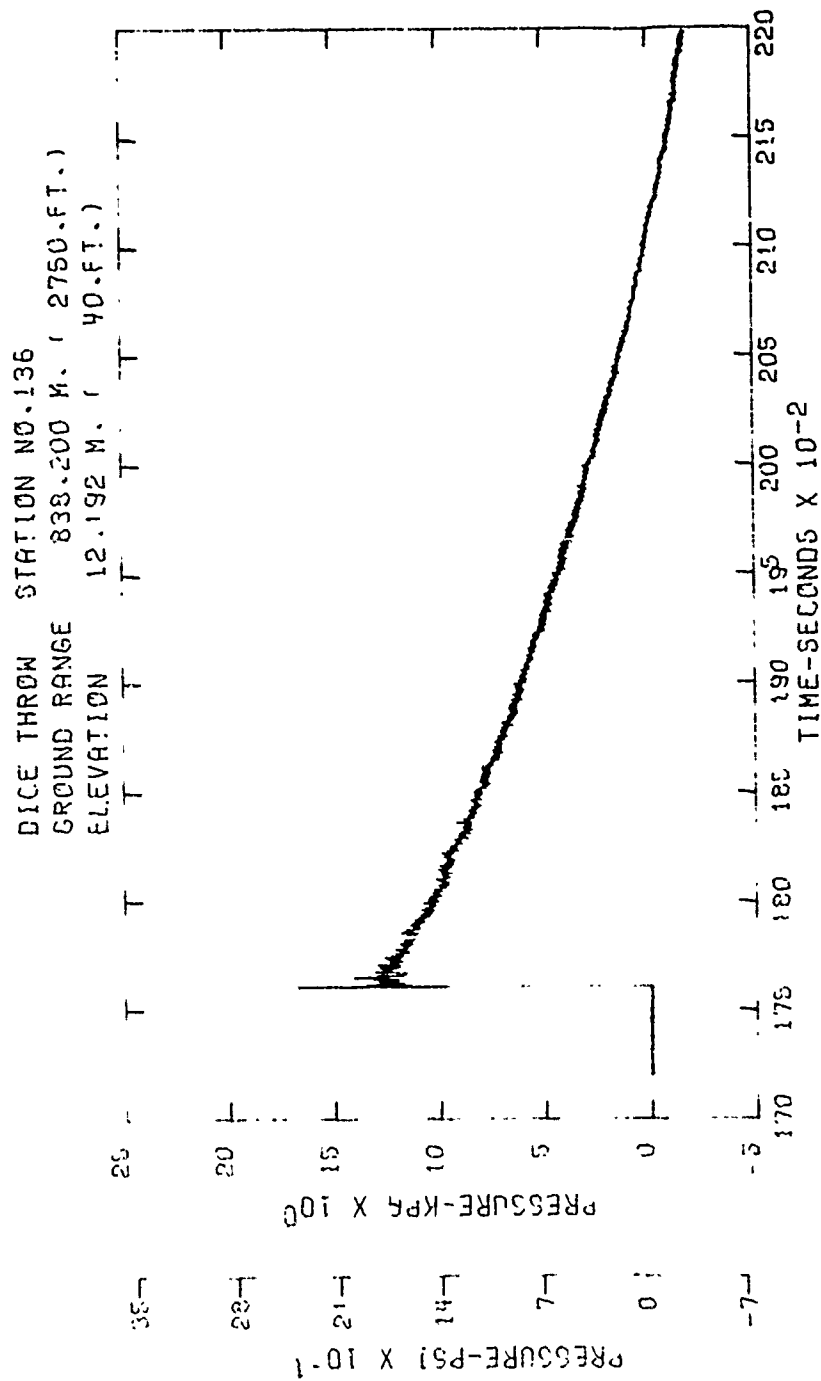


Figure A31. Incident pressure-time history - Station 136

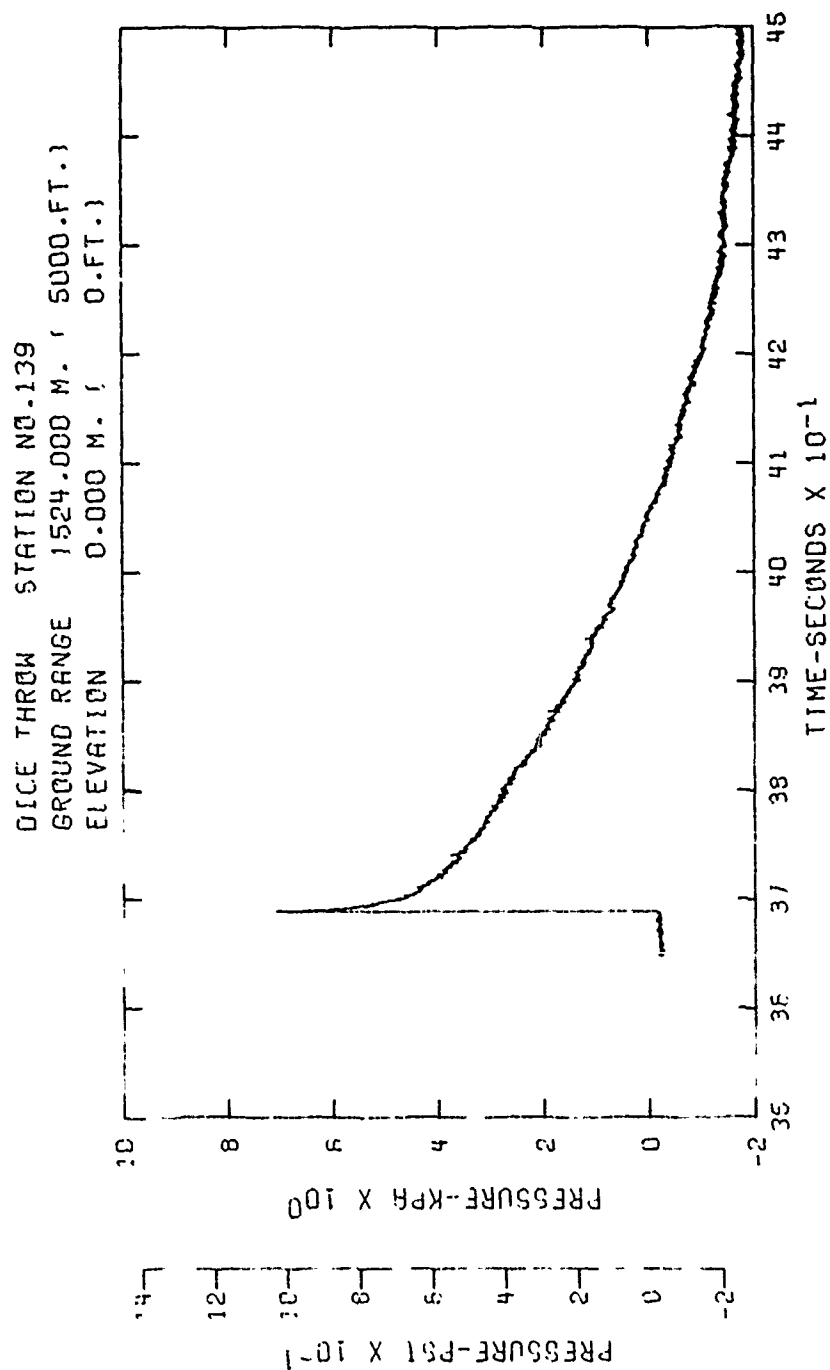


Figure A32. Incident pressure-time history - Station 139

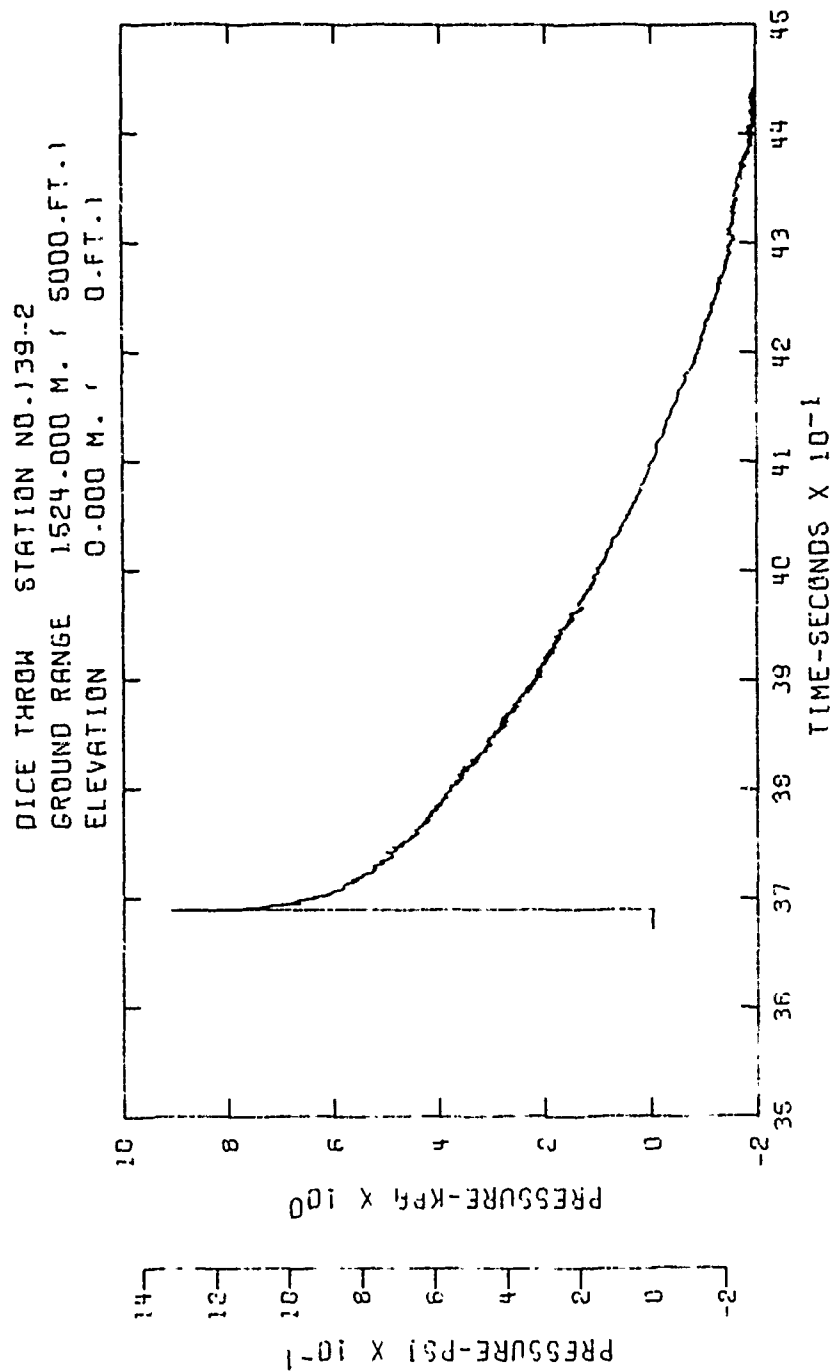


Figure A33. Incident pressure-time history - Station 139-2



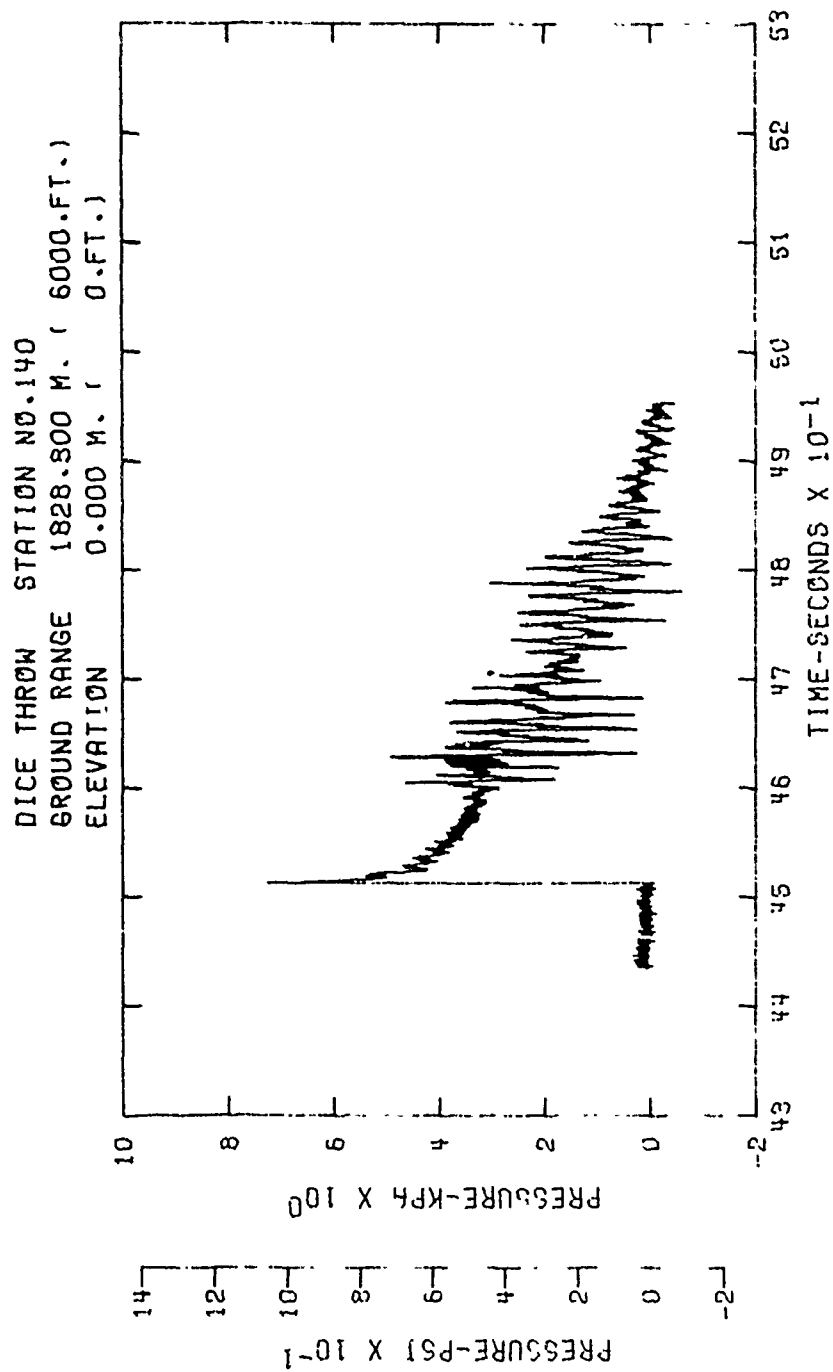


Figure A34. Incident pressure-time history - Station 140

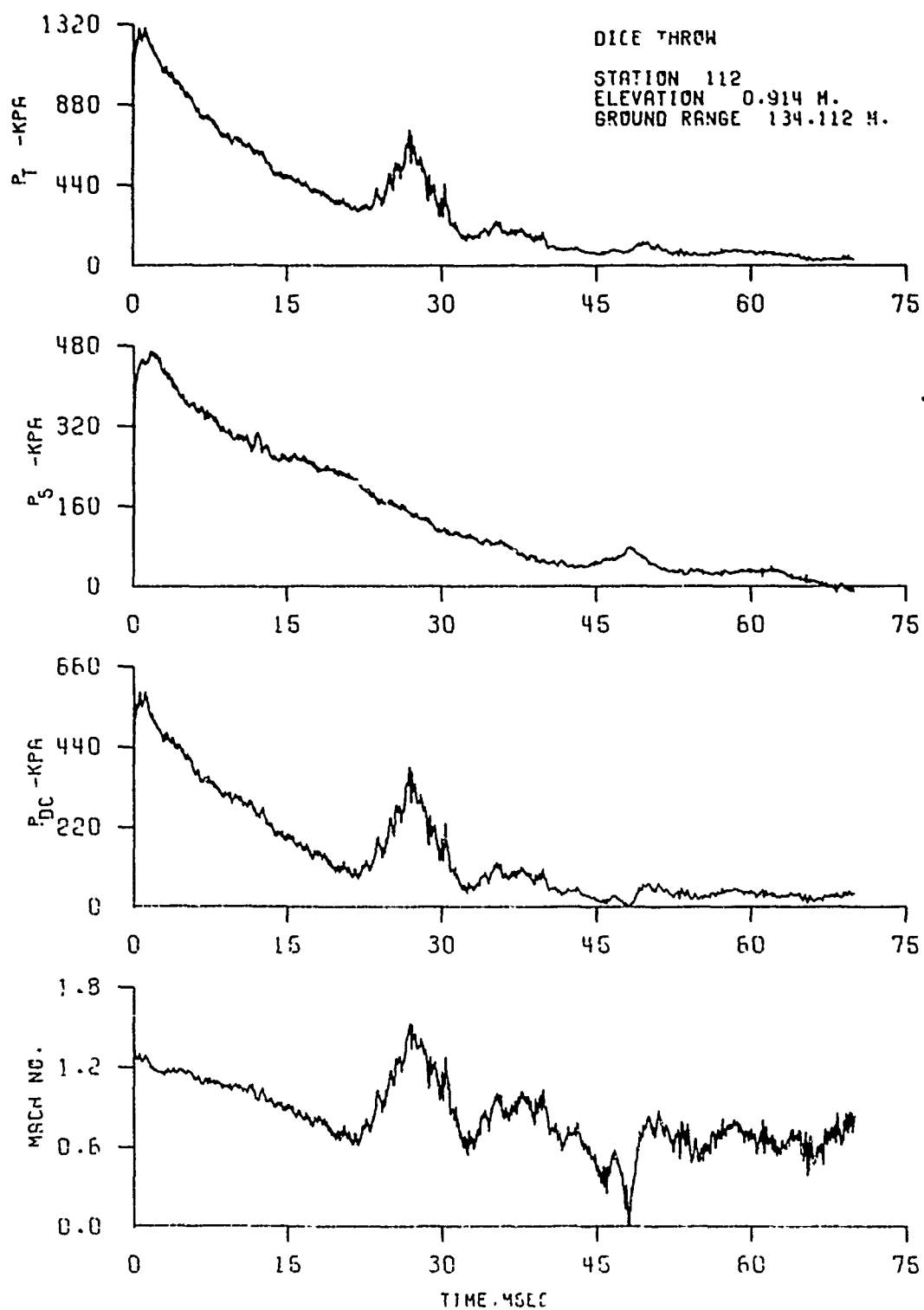


Figure A35. Dynamic pressure-time history - Station 112

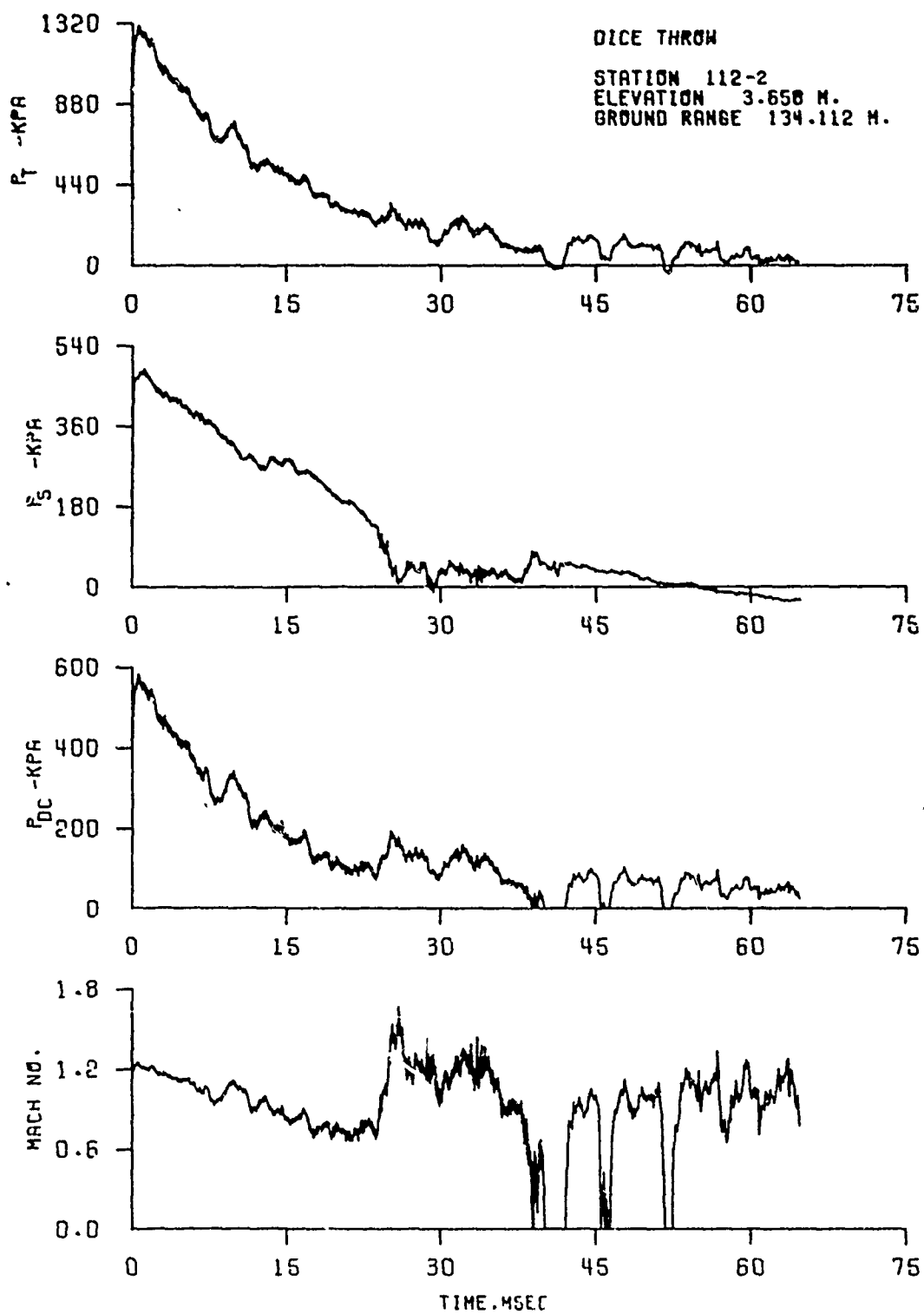


Figure A36. Dynamic pressure-time history - Station 112-2

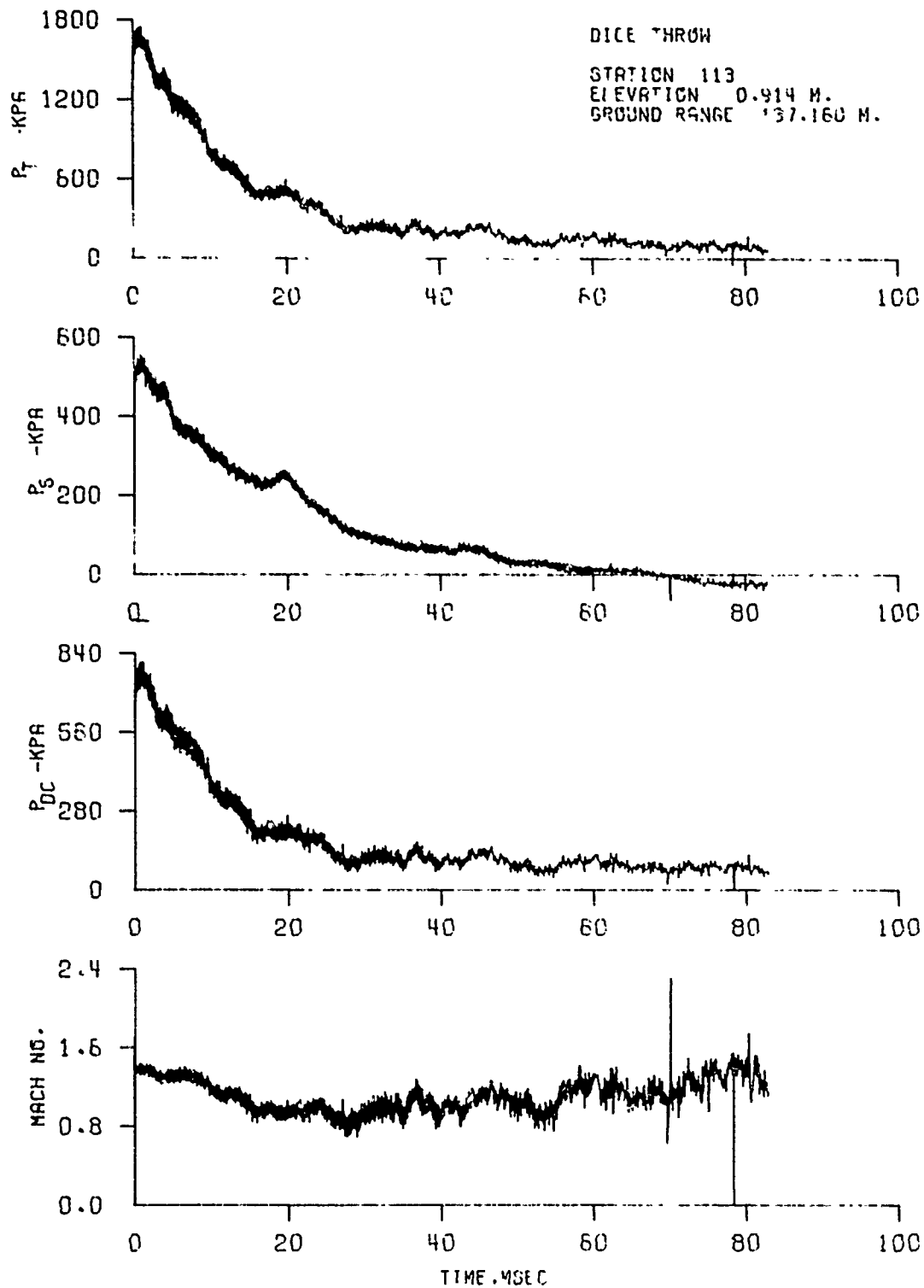


Figure A37. Dynamic pressure-time history - Station 113

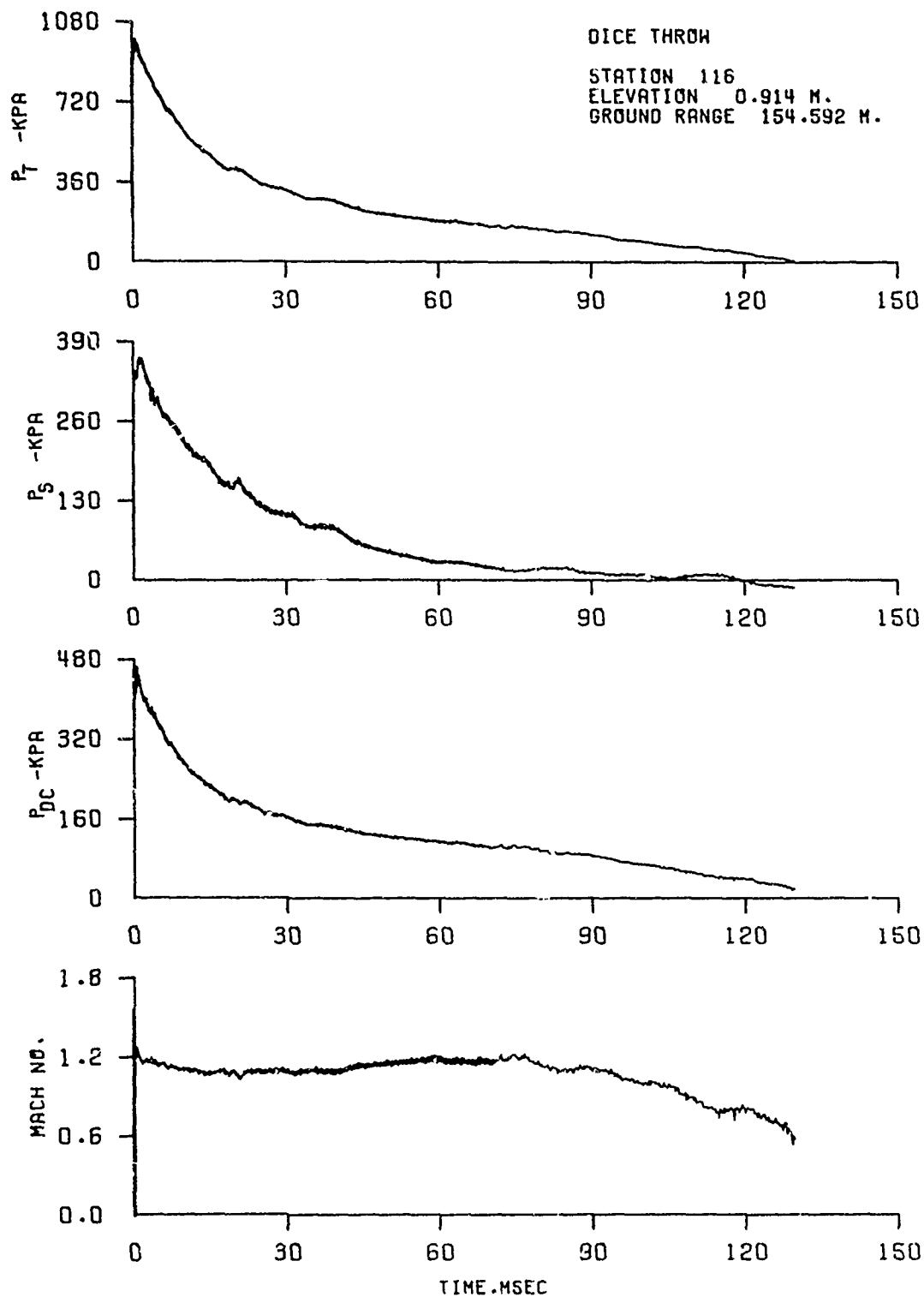


Figure A38. Dynamic pressure-time history - Station 116

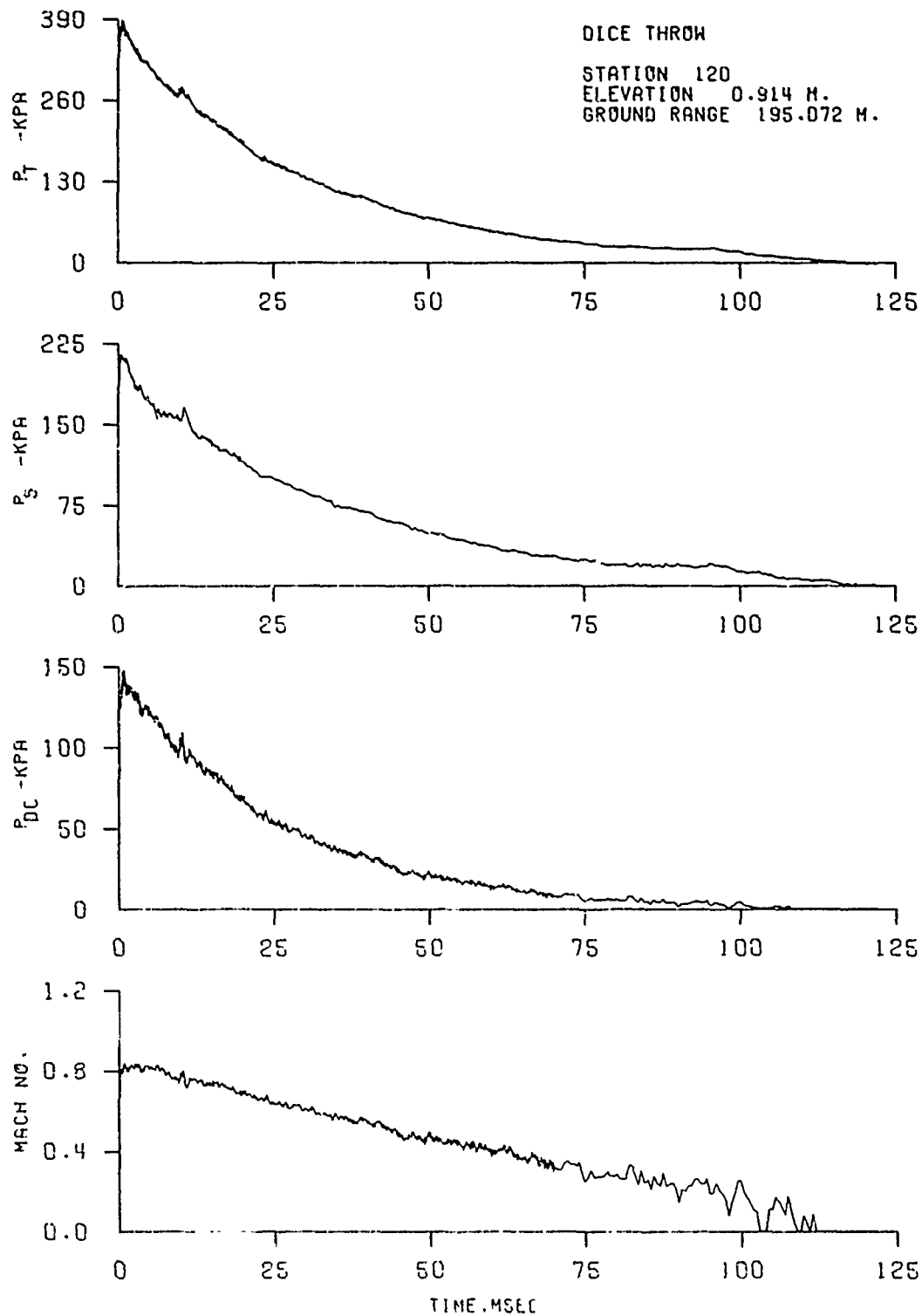


Figure A39. Dynamic pressure-time history - Station 120

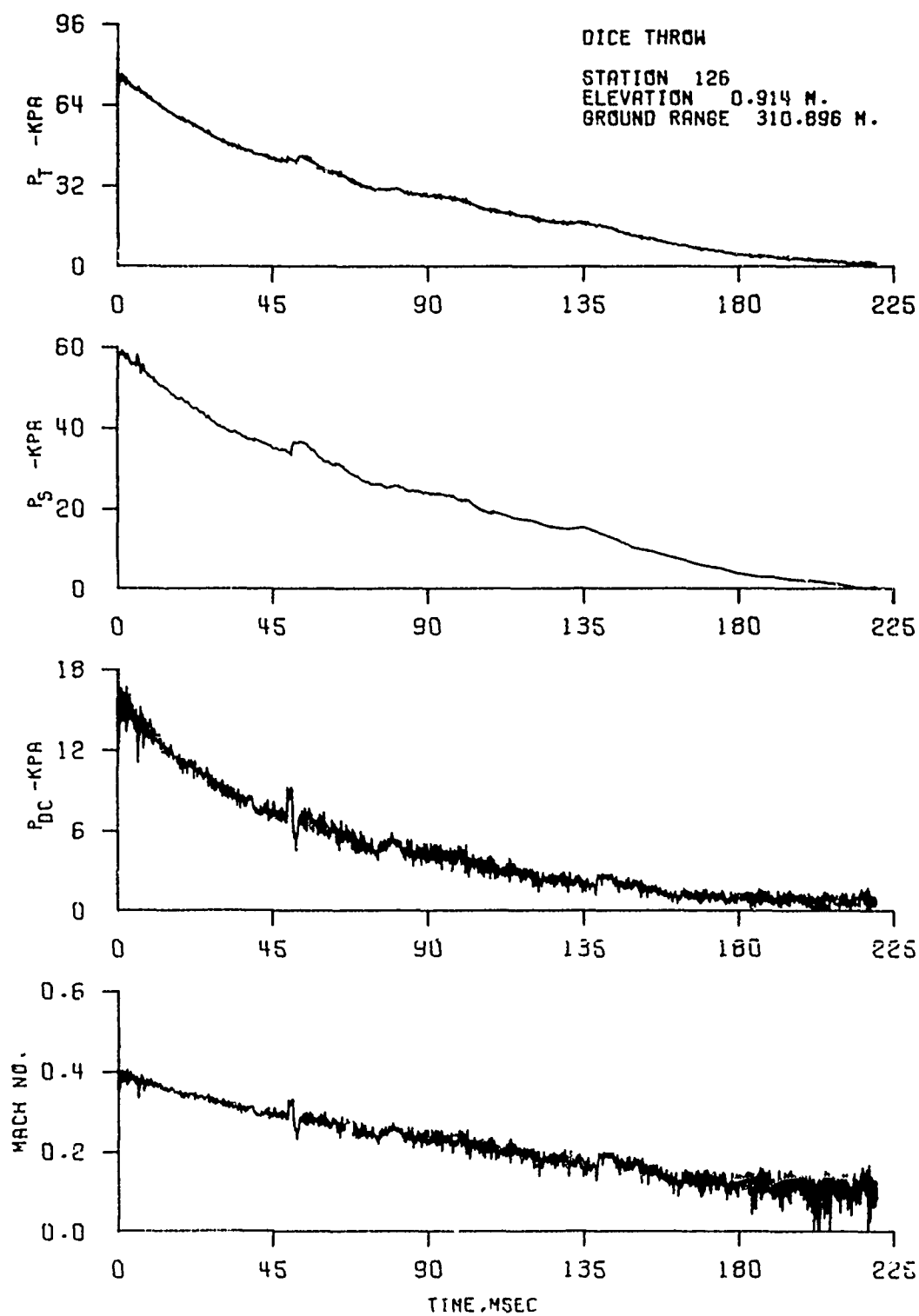


Figure A40. Dynamic pressure-time history - Station 126

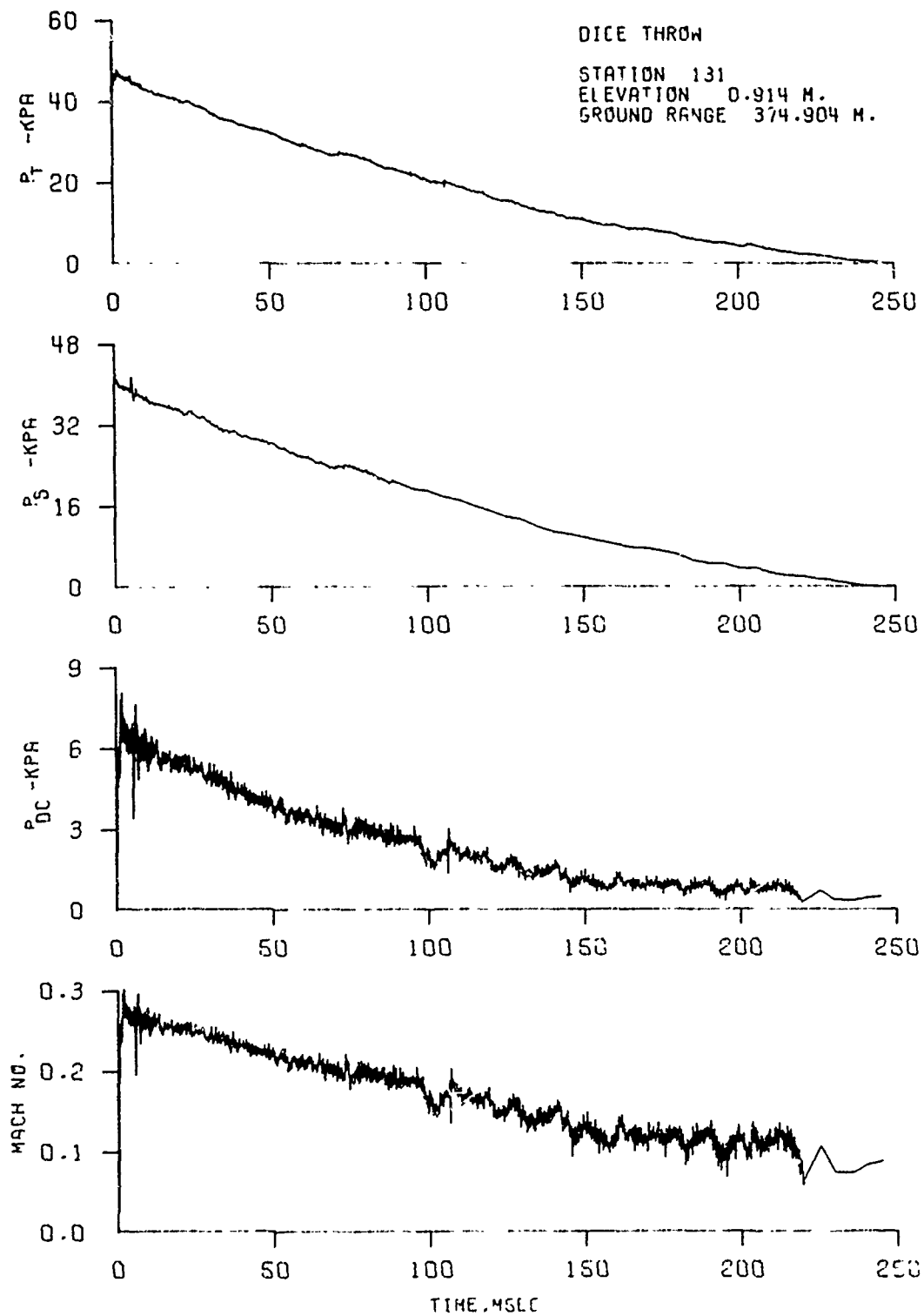


Figure A41. Dynamic pressure-time history - Station 131



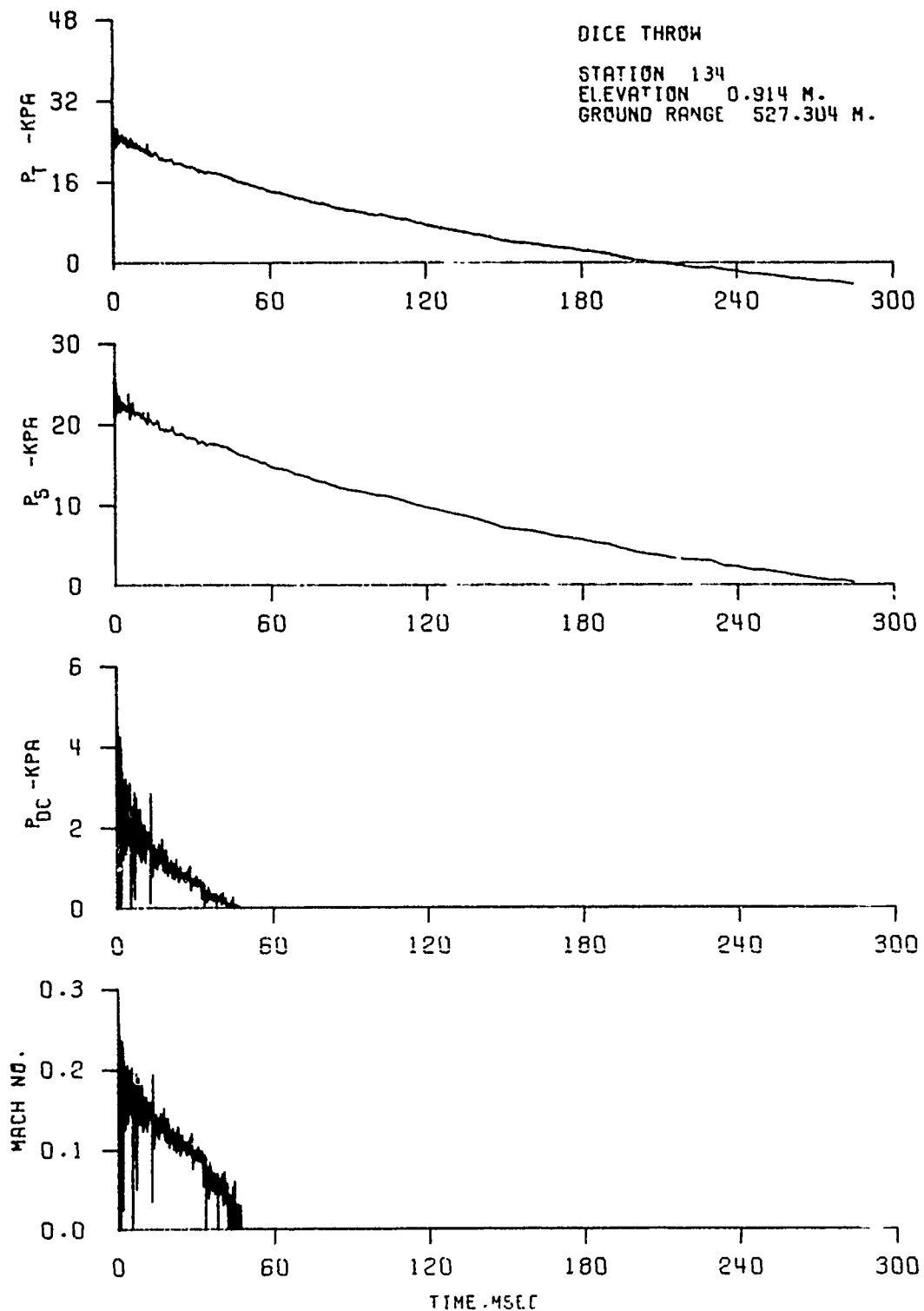


Figure A42. Dynamic pressure-time history - Station 134

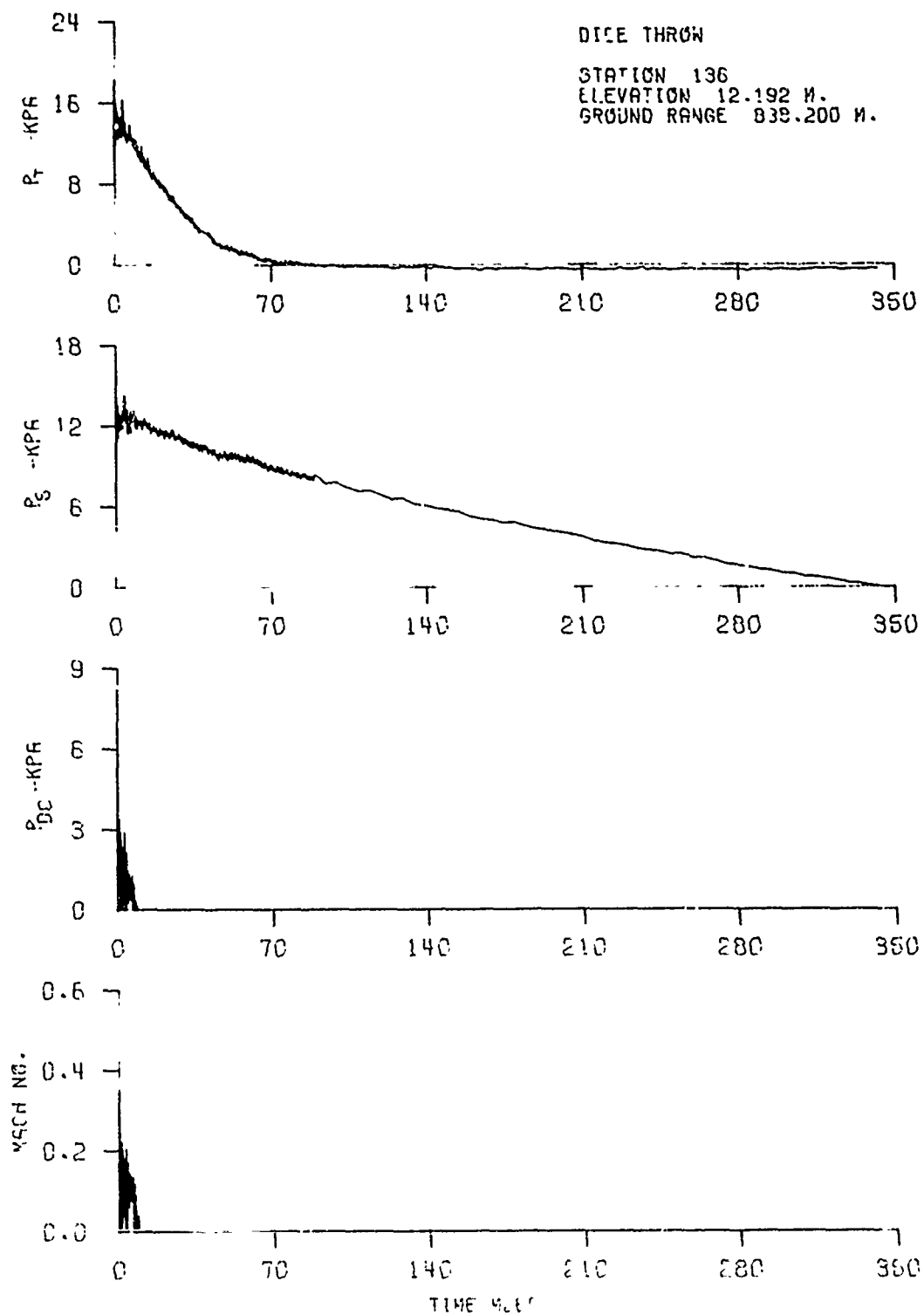


Figure A43. Dynamic pressure-time history - Station 136

## APPENDIX B

This appendix contains the time histories of the incident and dynamic pressures acquired along and adjacent to Blast Line 2. Included in this appendix are the data taken in the AFWL (Exp. 398) and BRL (Exp. 103) areas.

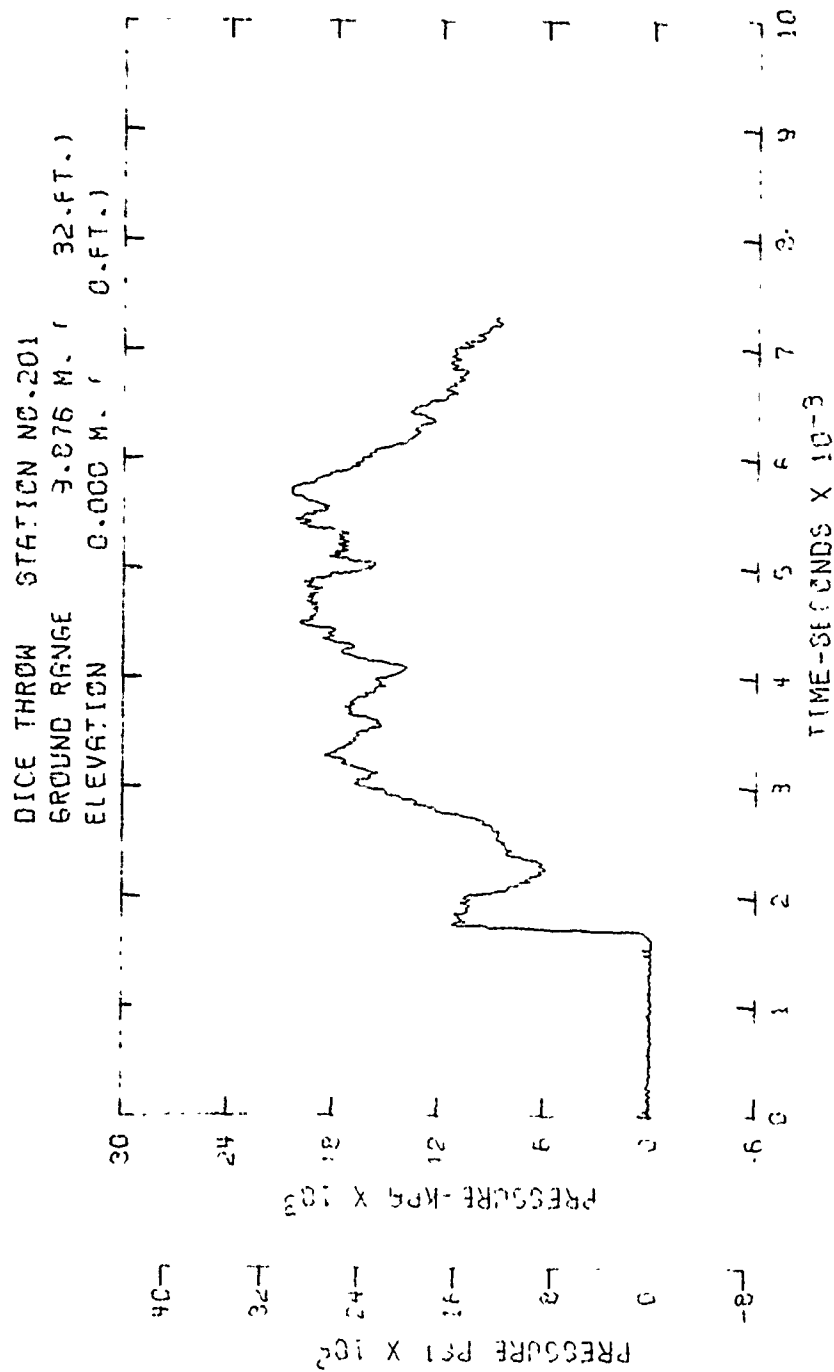


Figure B1. Incident pressure-time history - Station 201

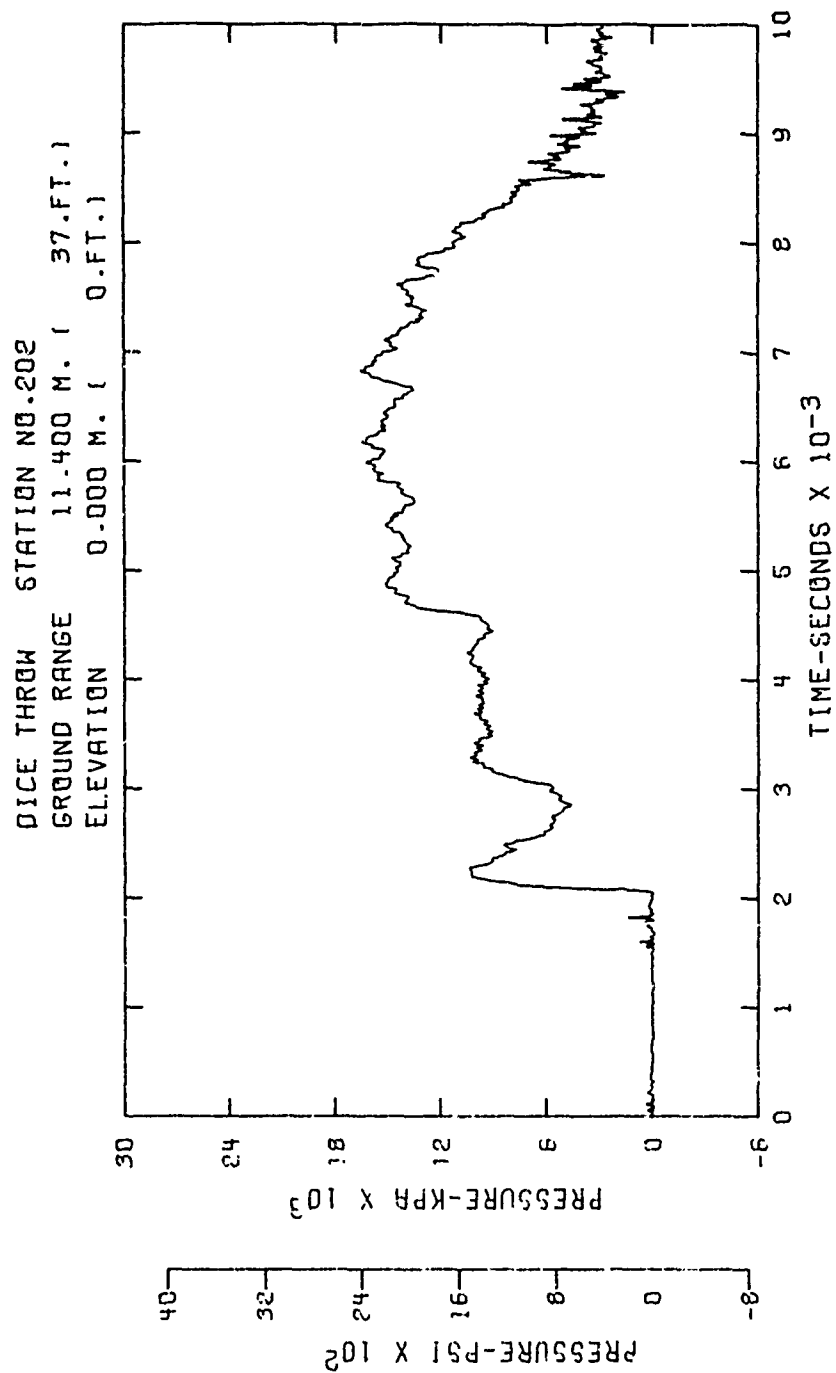


Figure B2. Incident pressure-time history - Station 202

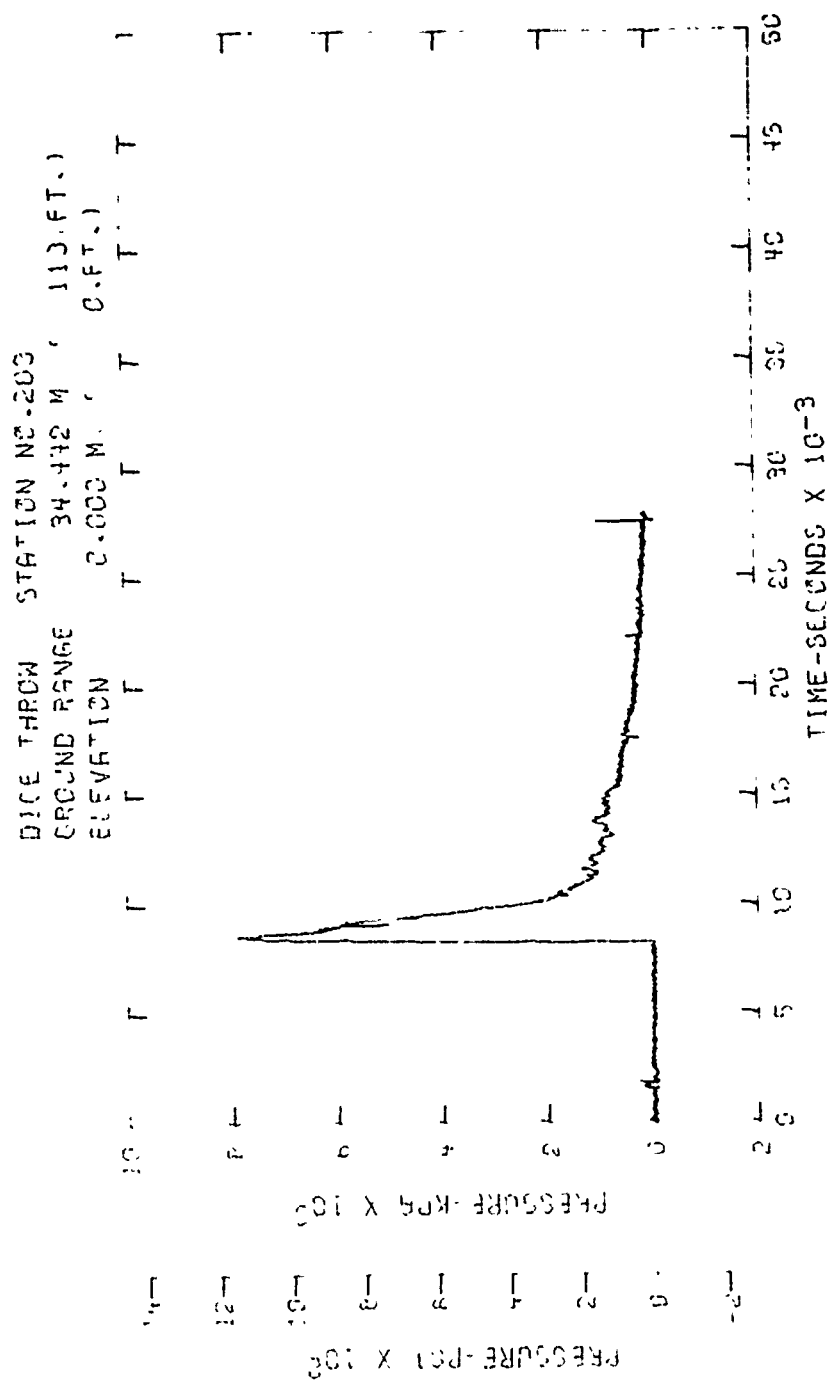


Figure B3. Incident pressure-time history - Station 203

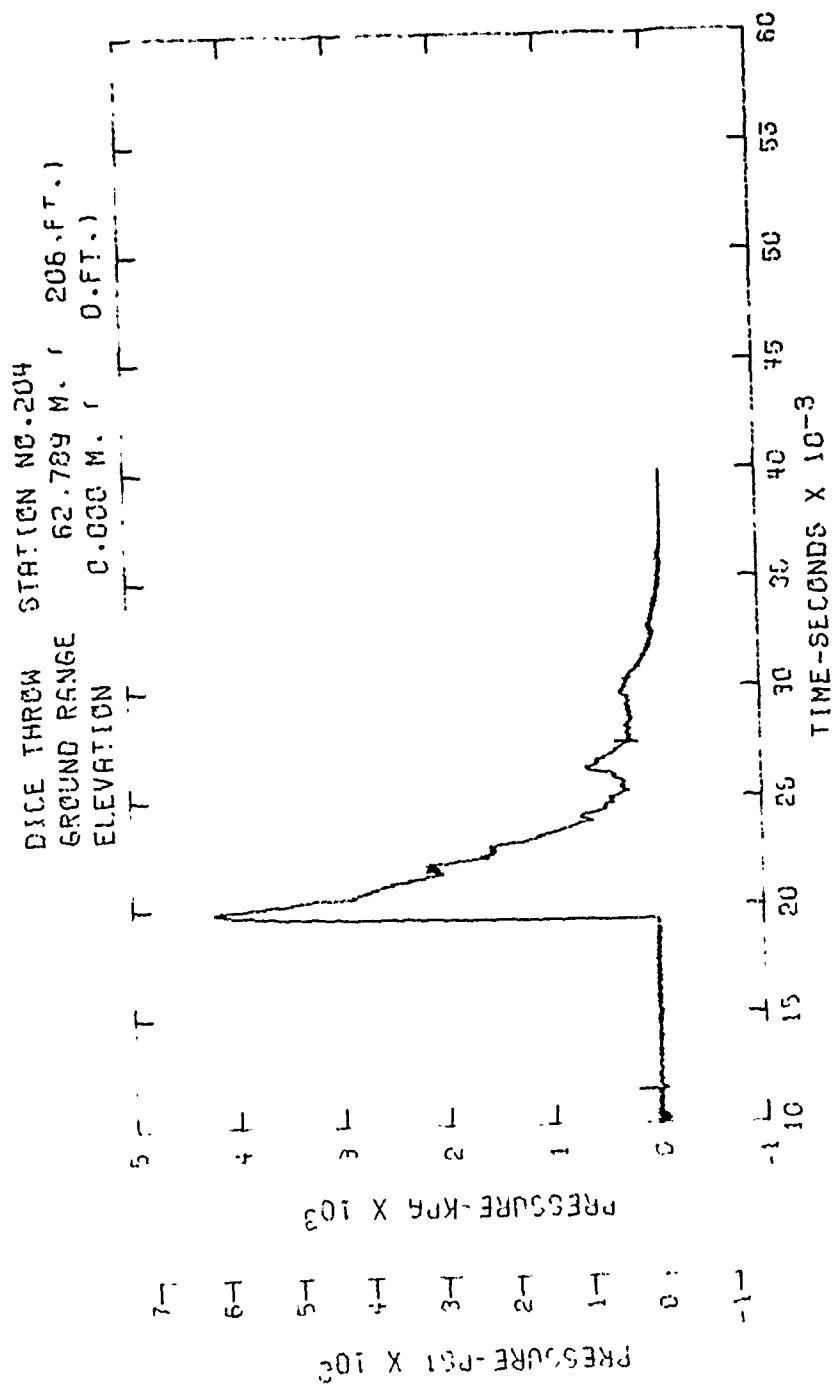


Figure B4. Incident pressure-time history - Station 204

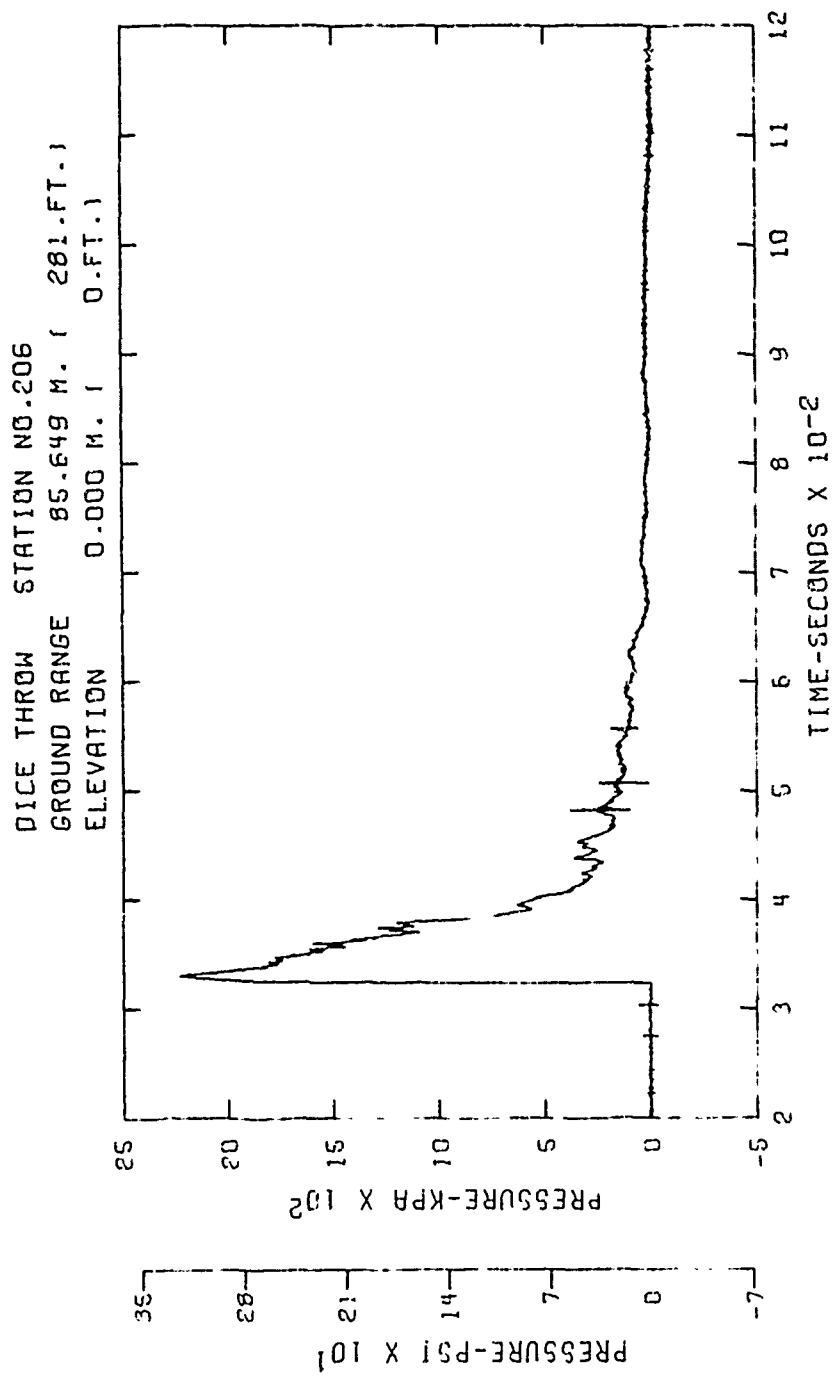


Figure B5. Incident pressure-time history - Station 206



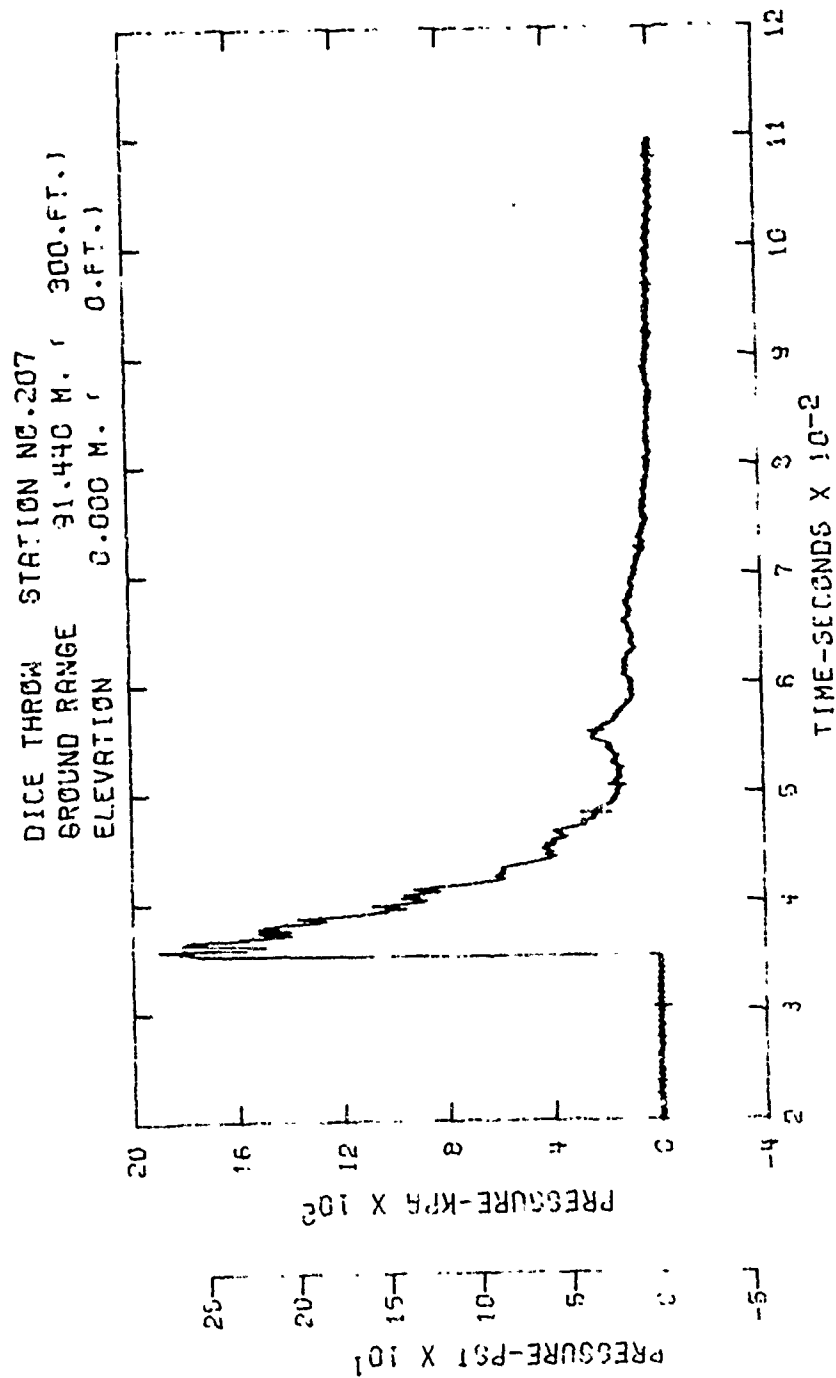


Figure B6. Incident pressure-time history - Station 207

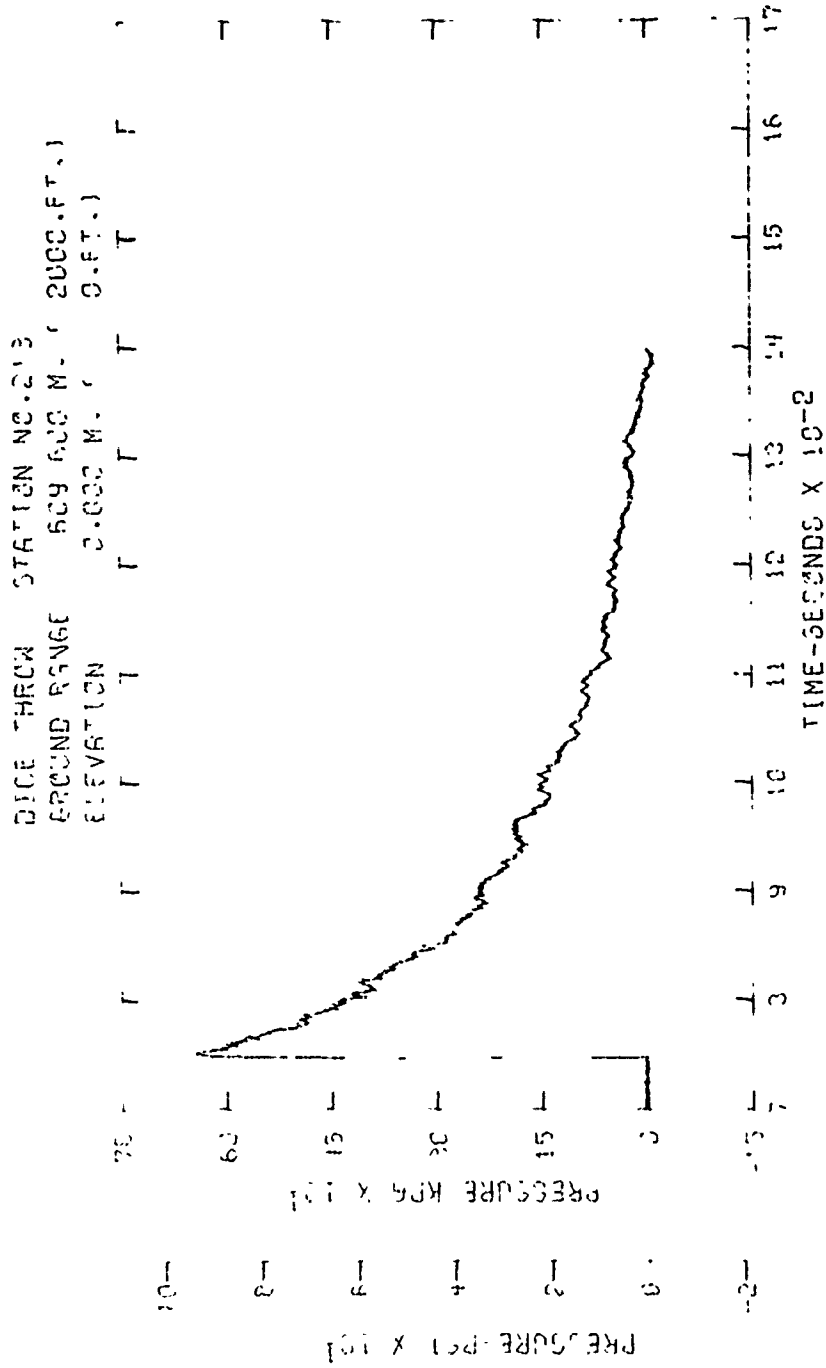


Figure B7. Incident pressure-time history - Station 213

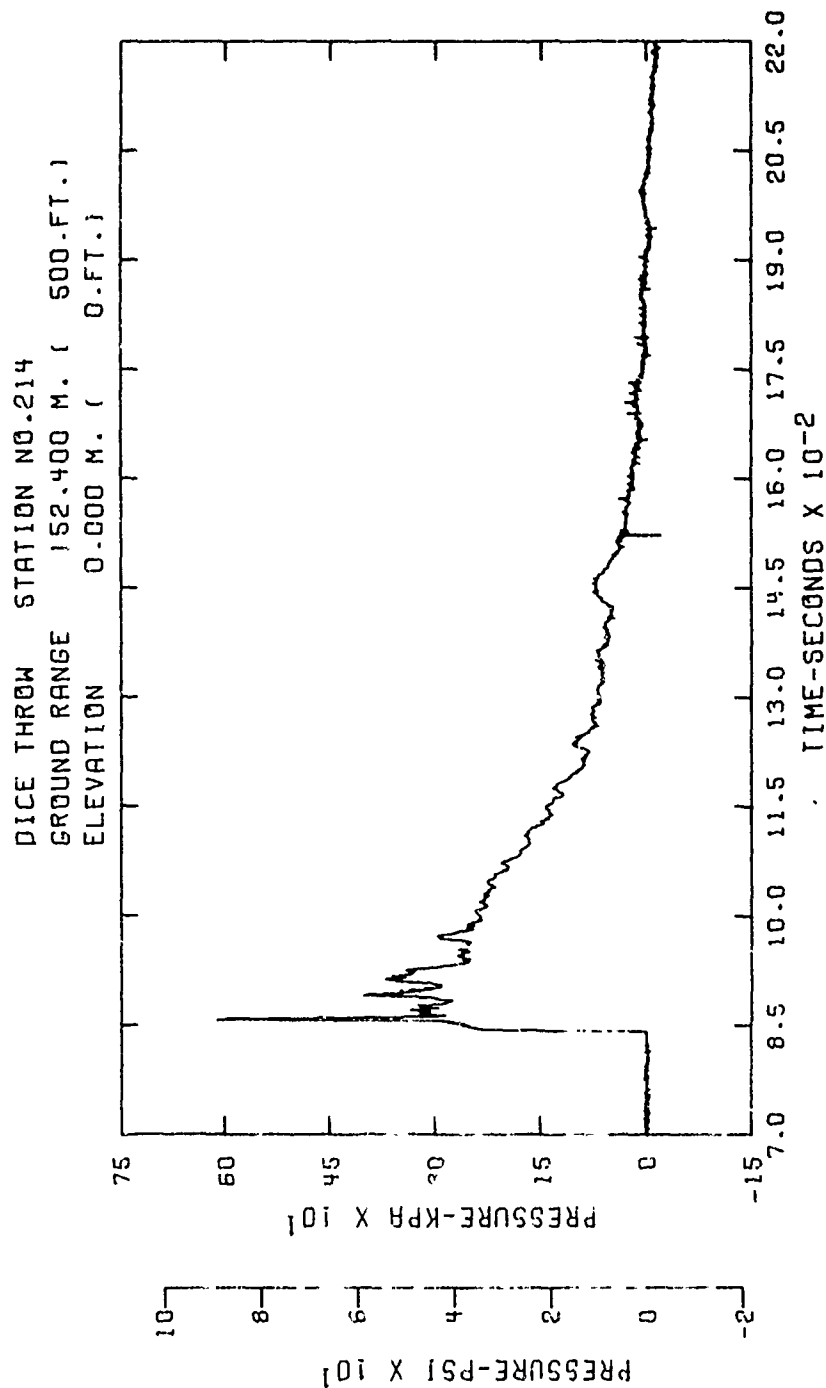


Figure B8. Incident pressure-time history - Station 214

DICE THROW STATION NO. 214-2  
 GROUND RANGE 152.400 M. ( 500.FT.)  
 ELEVATION 3.658 M. ( 12.FT.)

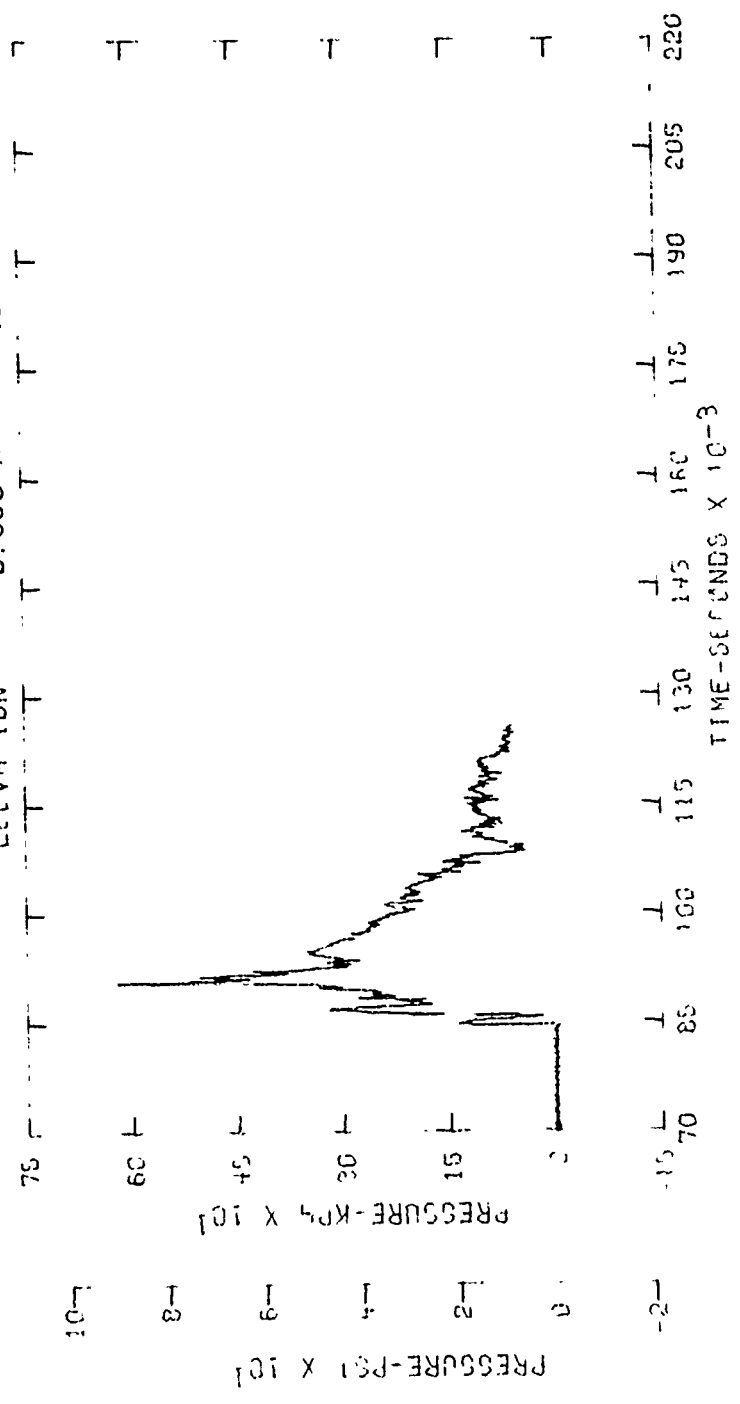


Figure B9. Incident pressure-time history - Station 214-2

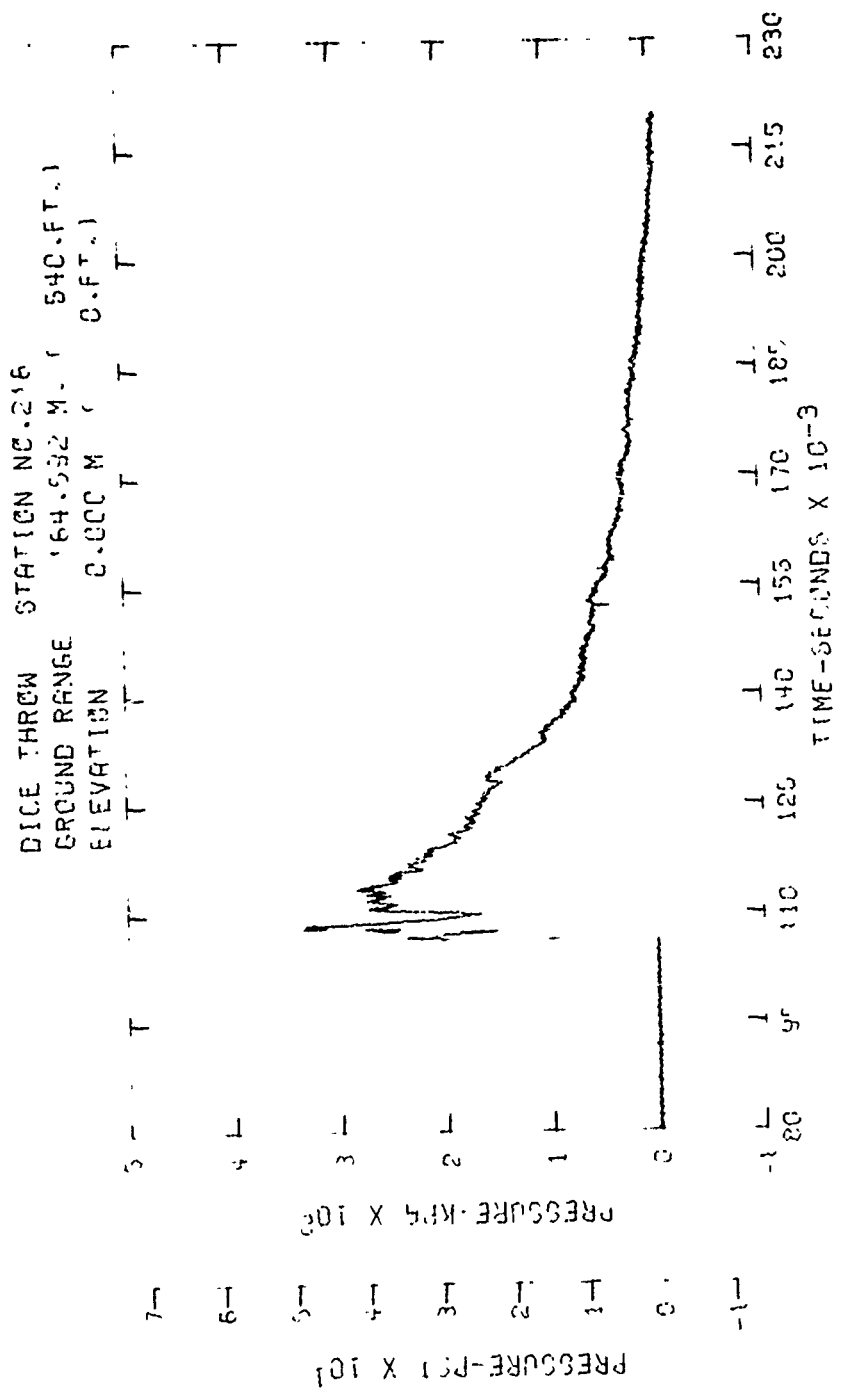


Figure B10. Incident pressure-time history - Station 216

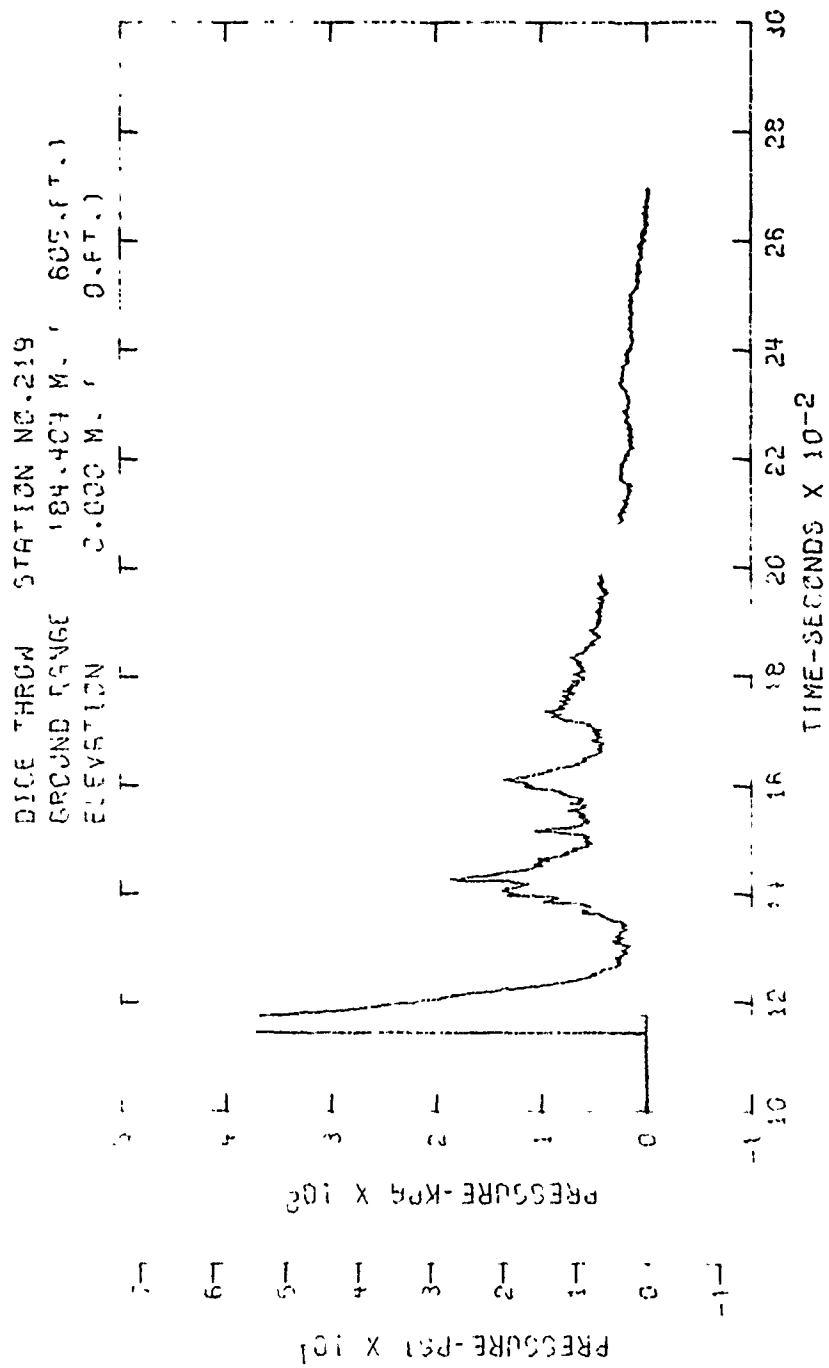


Figure B11. Incident pressure-time history - Station 219

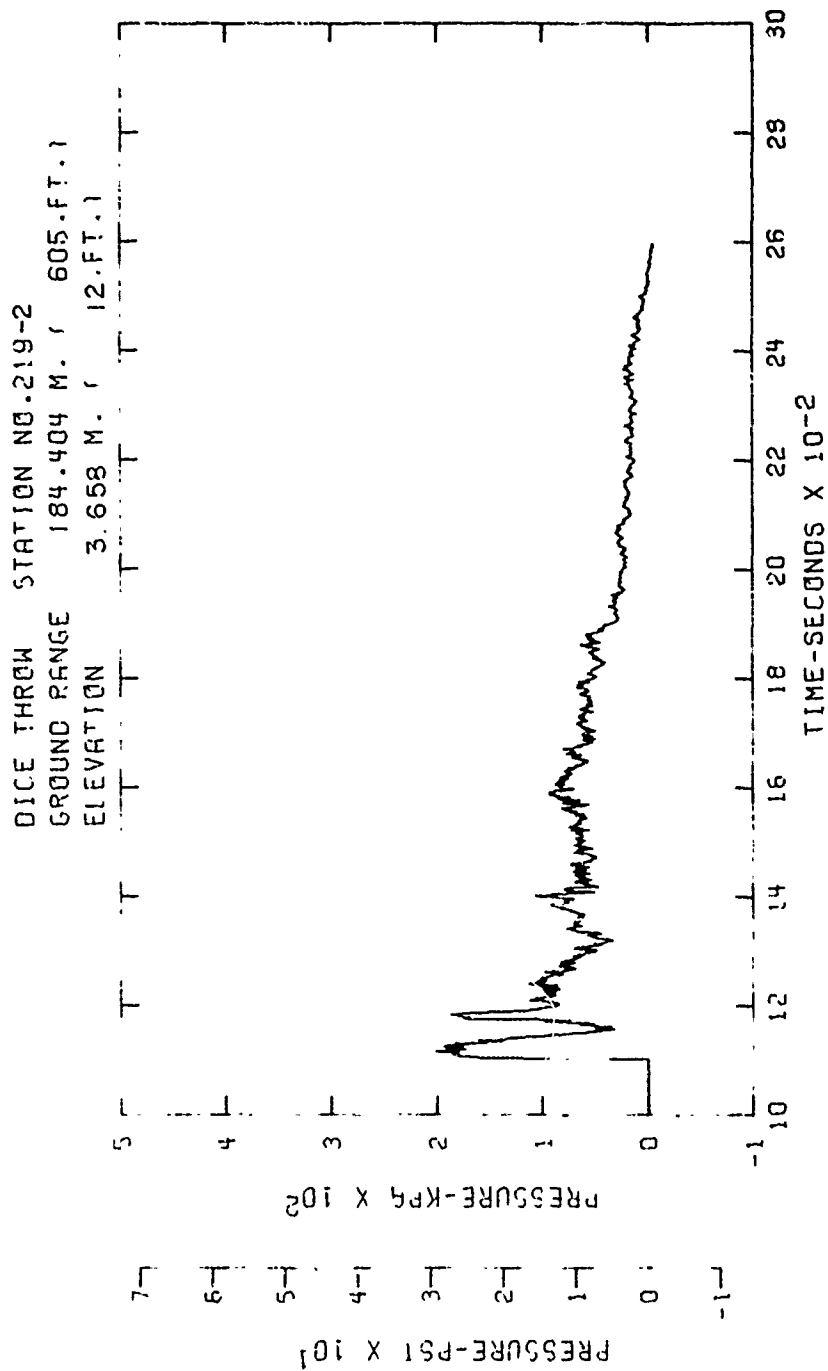


Figure B12. Incident pressure-time history - Station 219-2

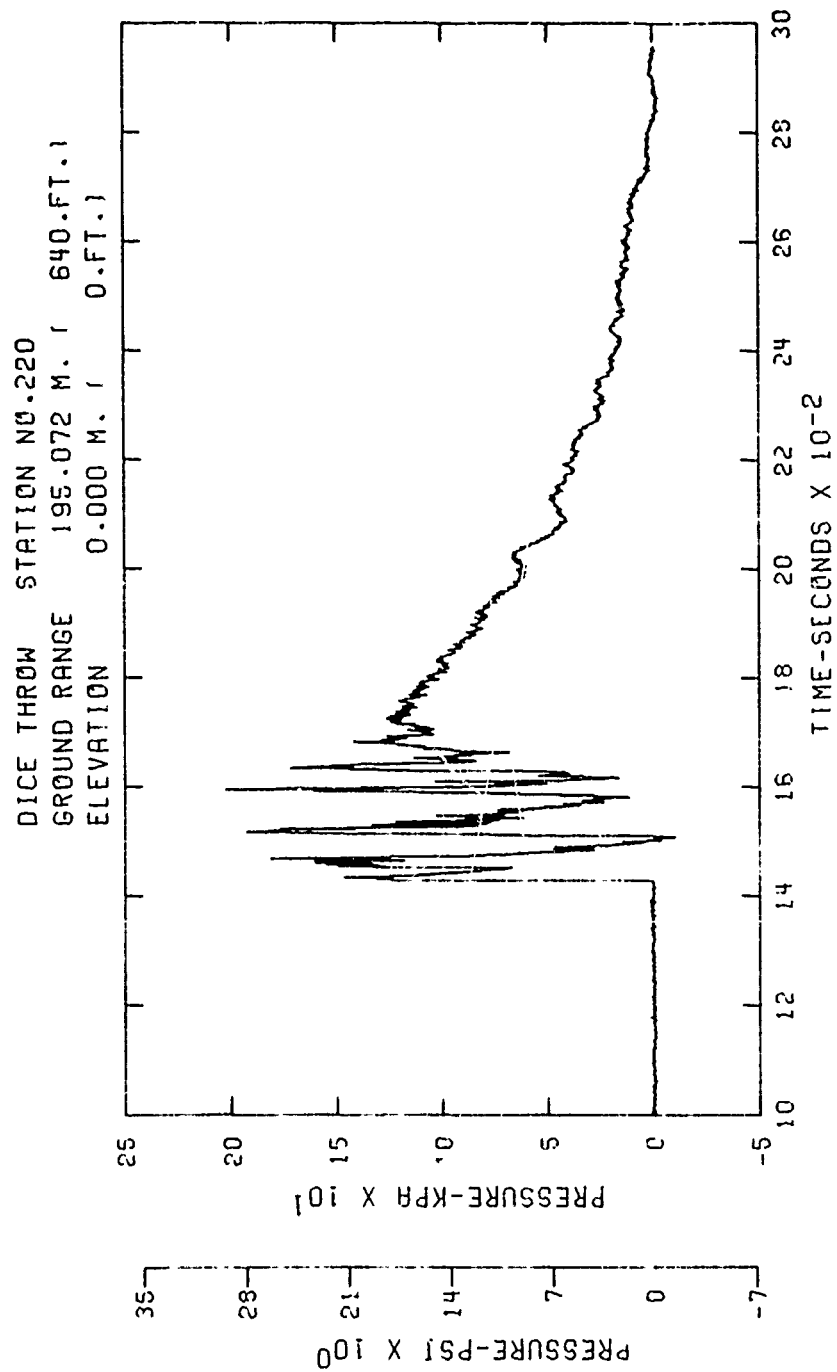


Figure B13. Incident pressure-time history - Station 220



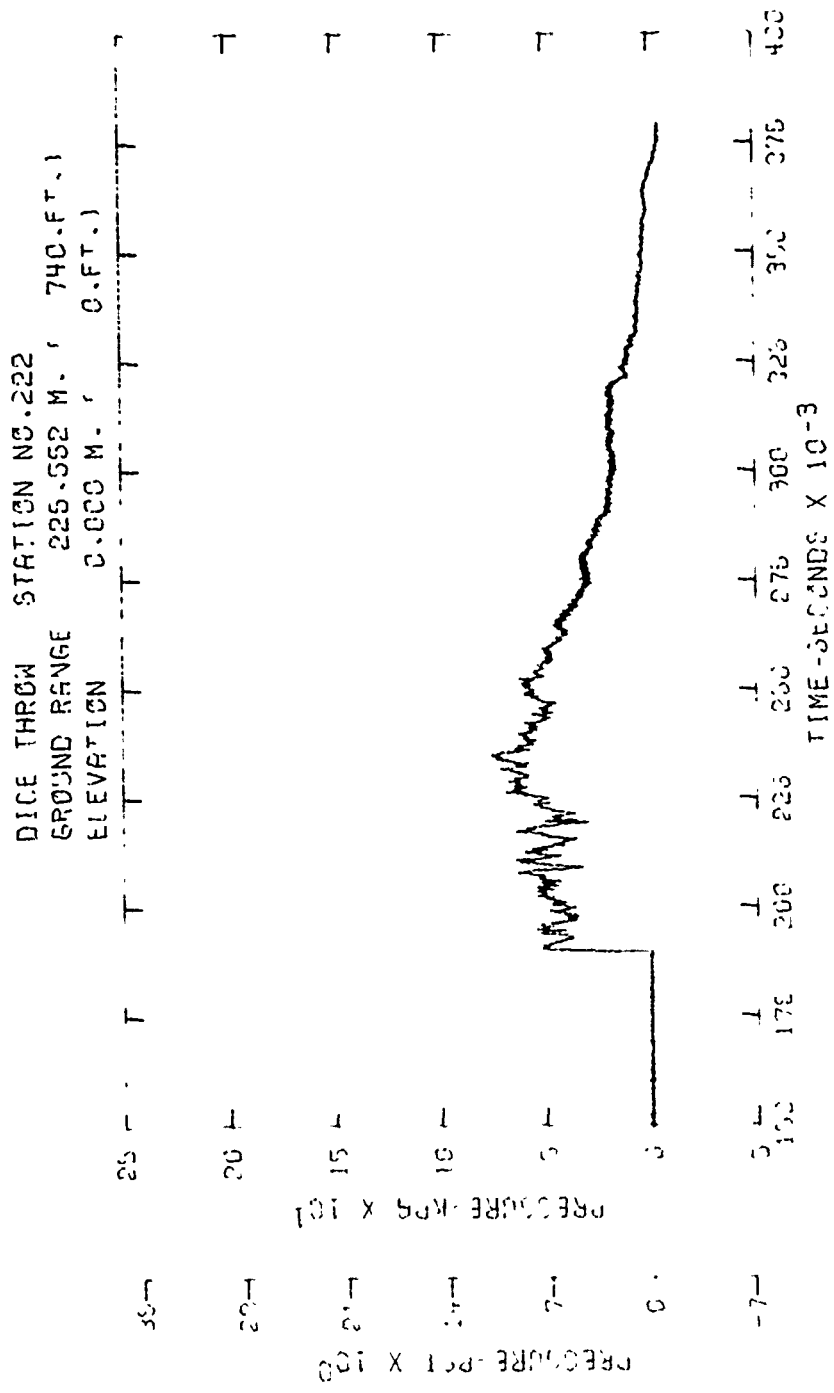


Figure B14. Incident pressure-time history - Station 222

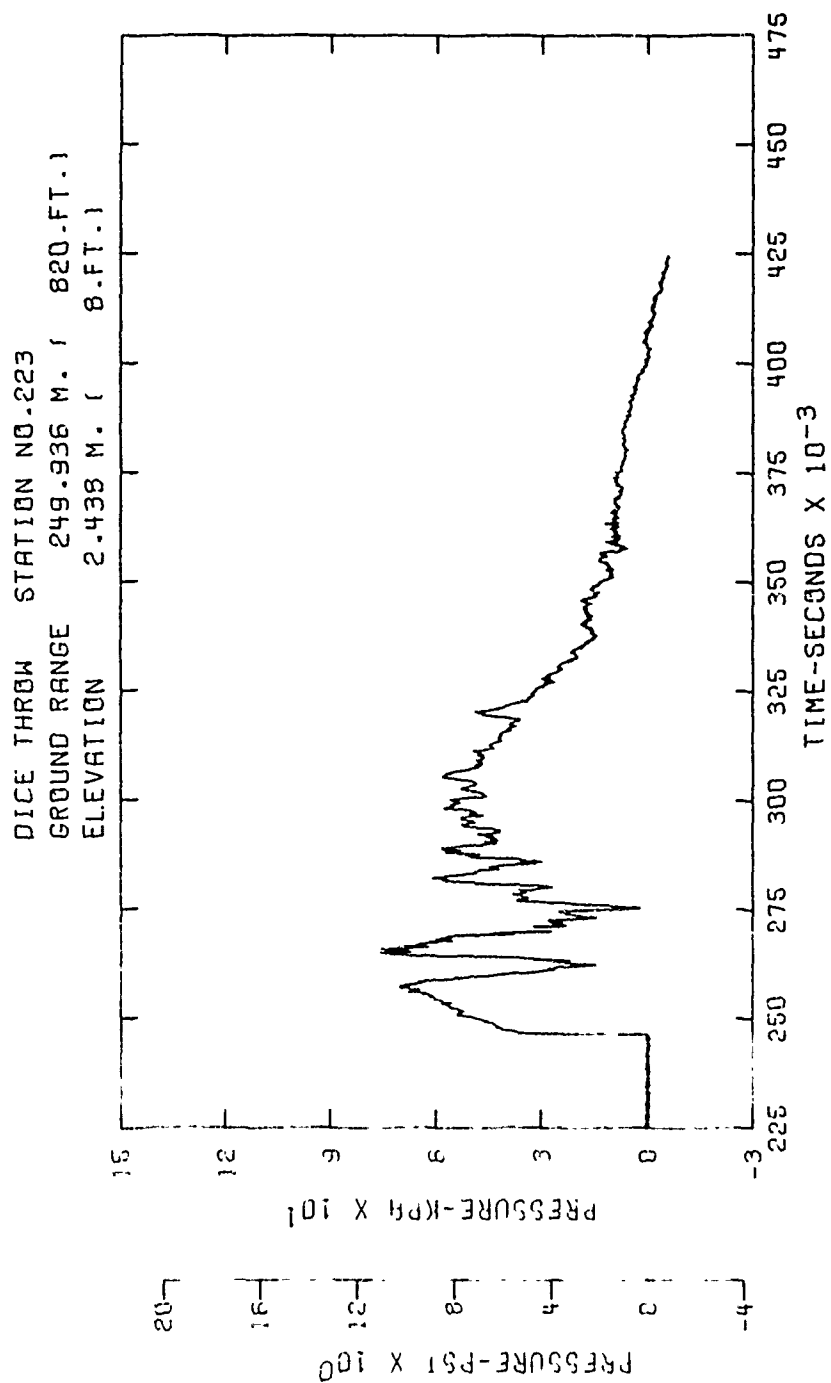


Figure B15. Incident pressure-time history - Station 223

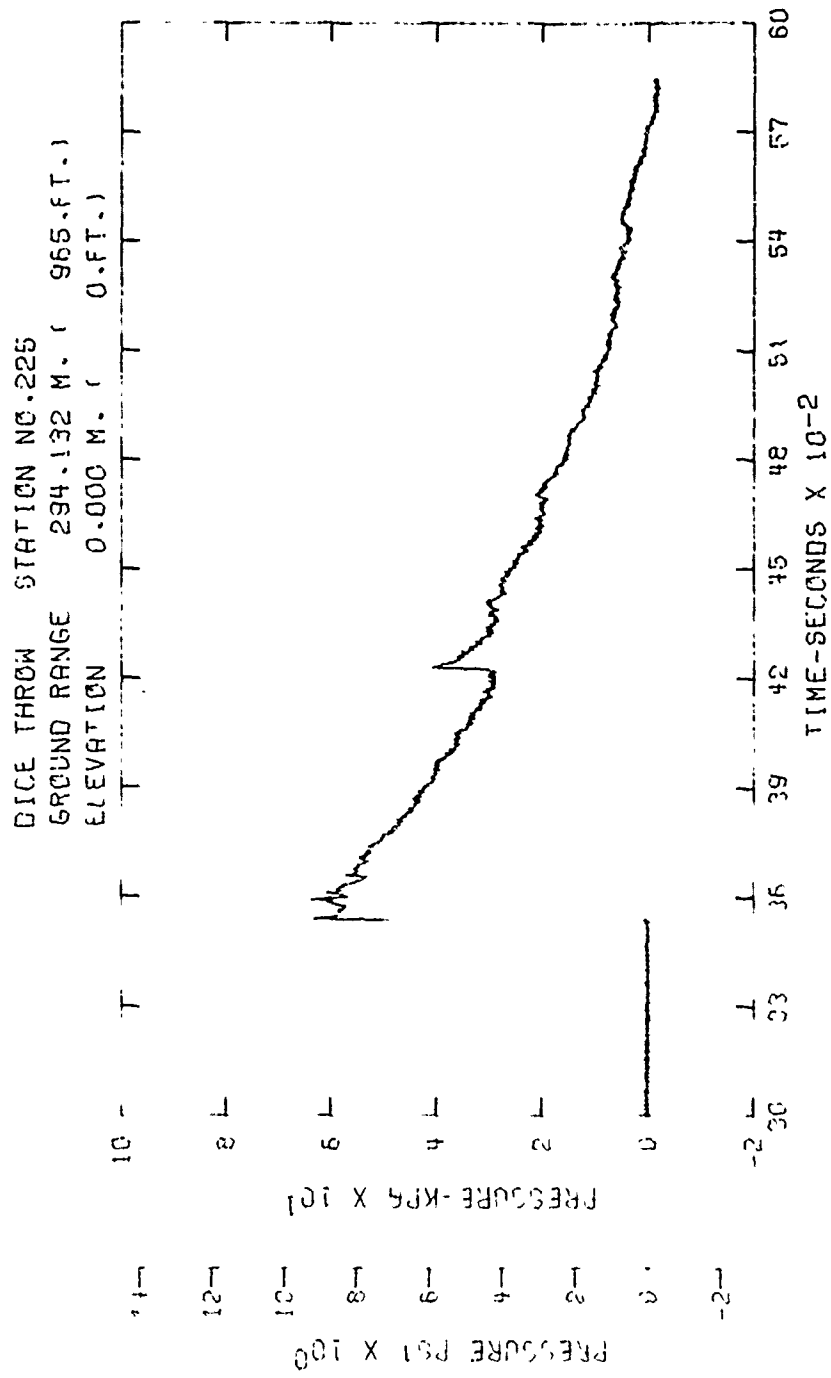


Figure B16. Incident pressure-time history - Station 225

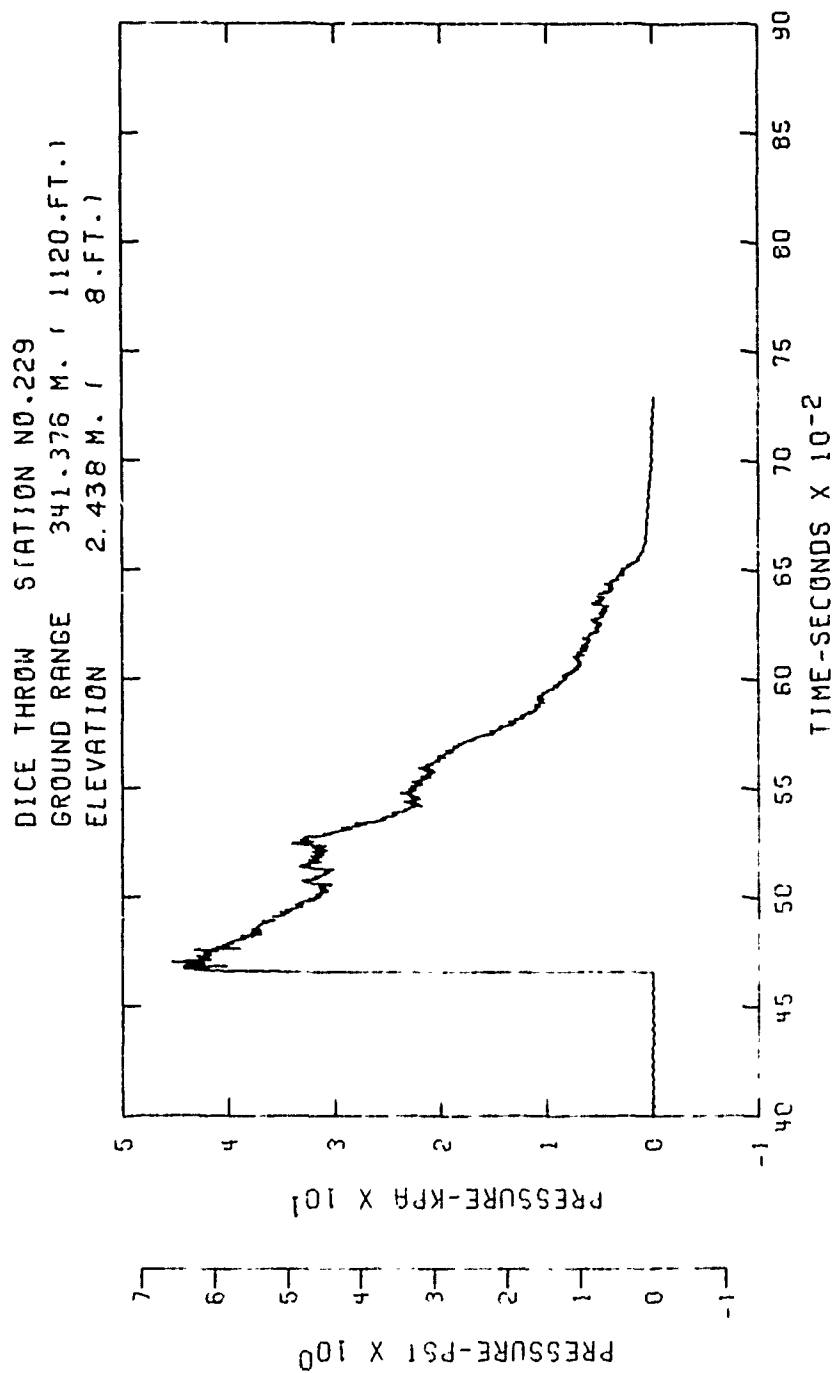


Figure B17. Incident pressure-time history - Station 229

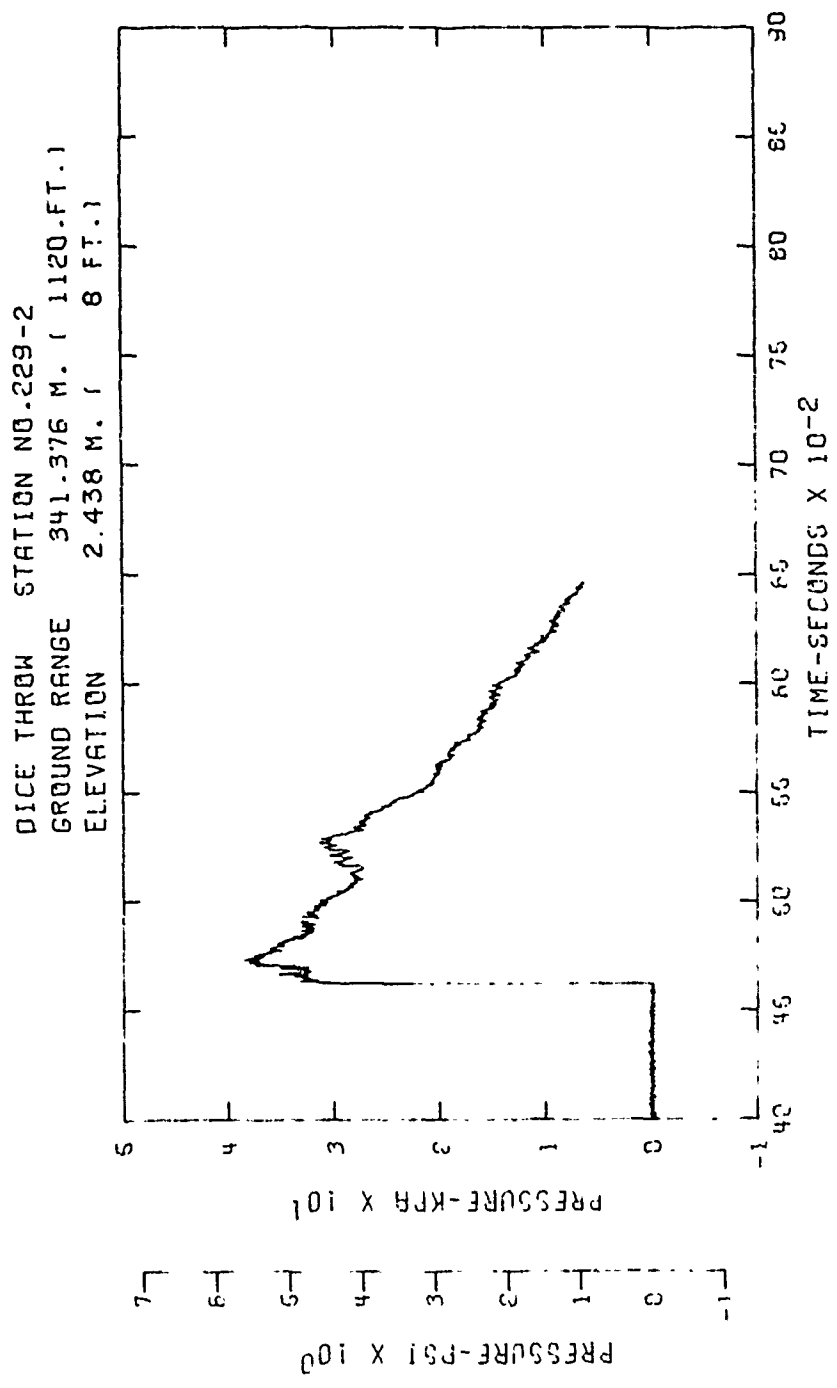


Figure B18. Incident pressure-time history - Station 229-2

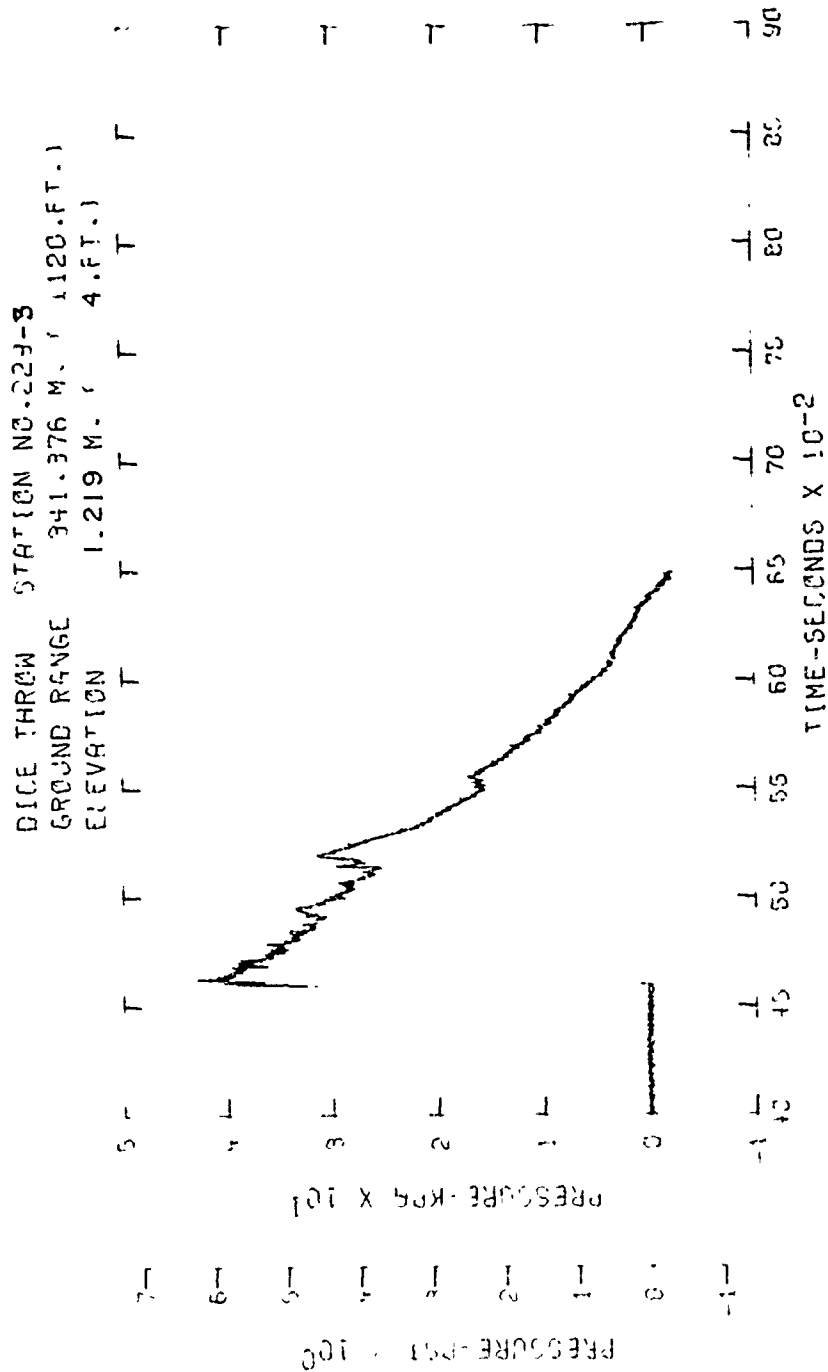


Figure B19. Incident pressure-time history - Station 229-3

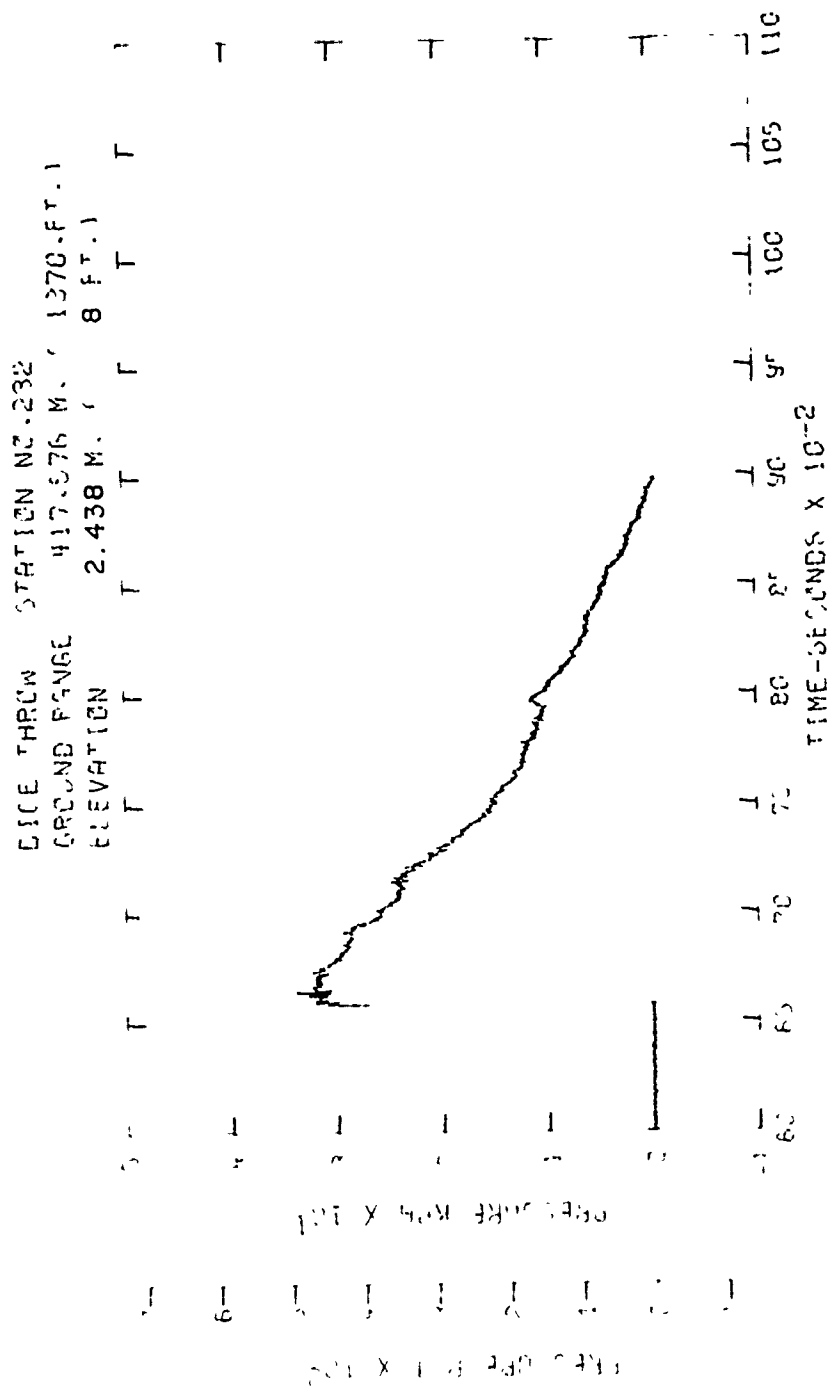


Figure B20. Incident pressure-time history - Station 232

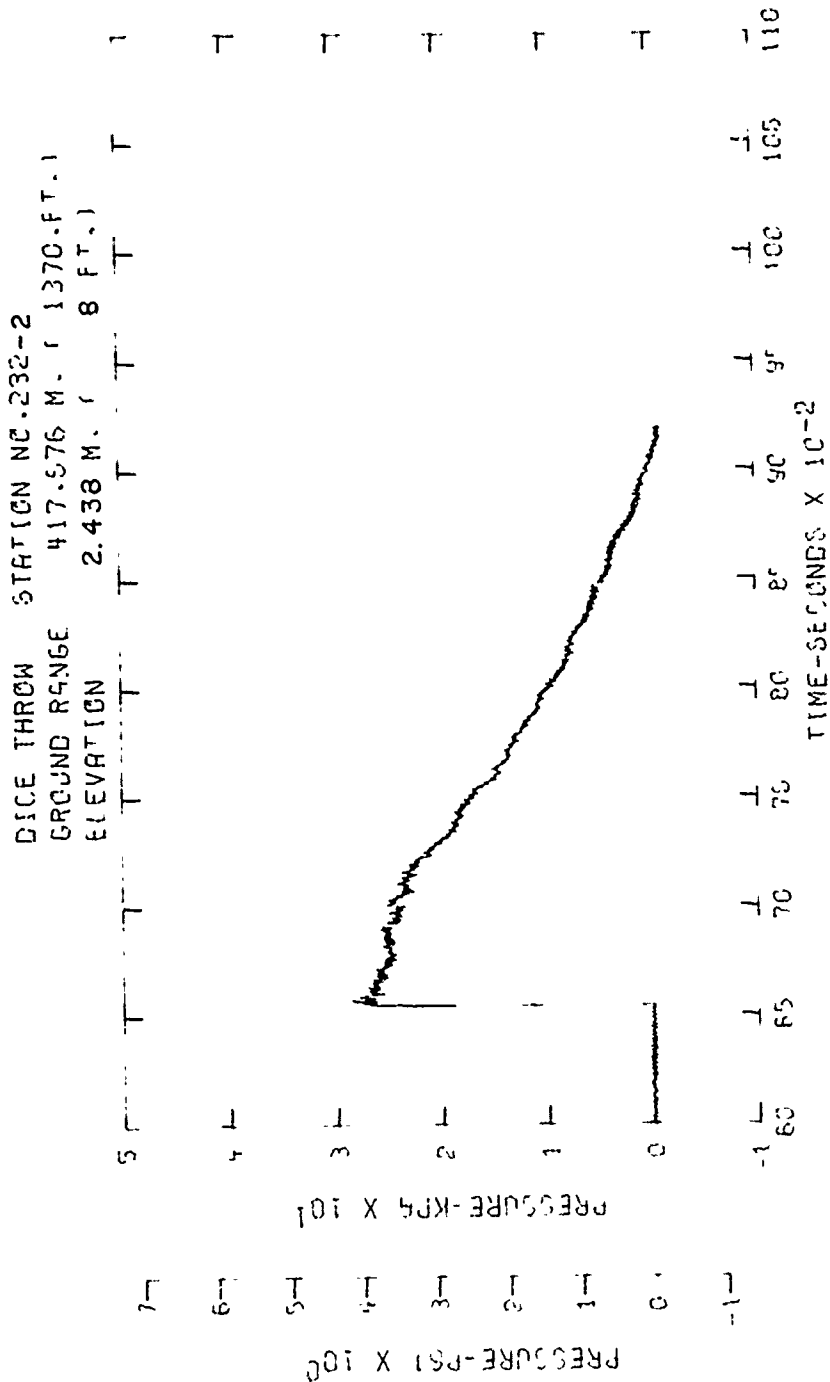


Figure B21. Incident pressure-time history - Station 232-2



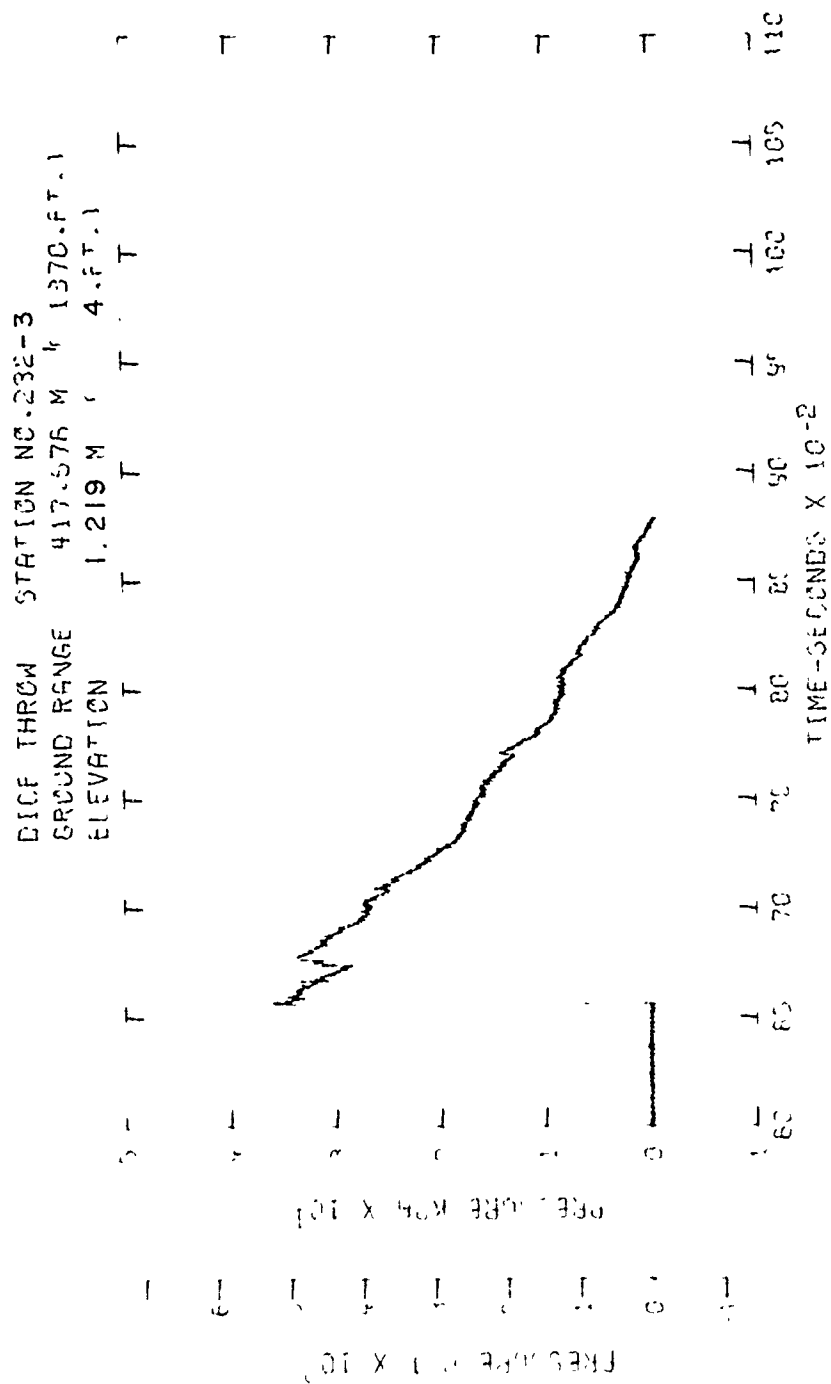


Figure B22. Incident pressure-time history - Station 232-3

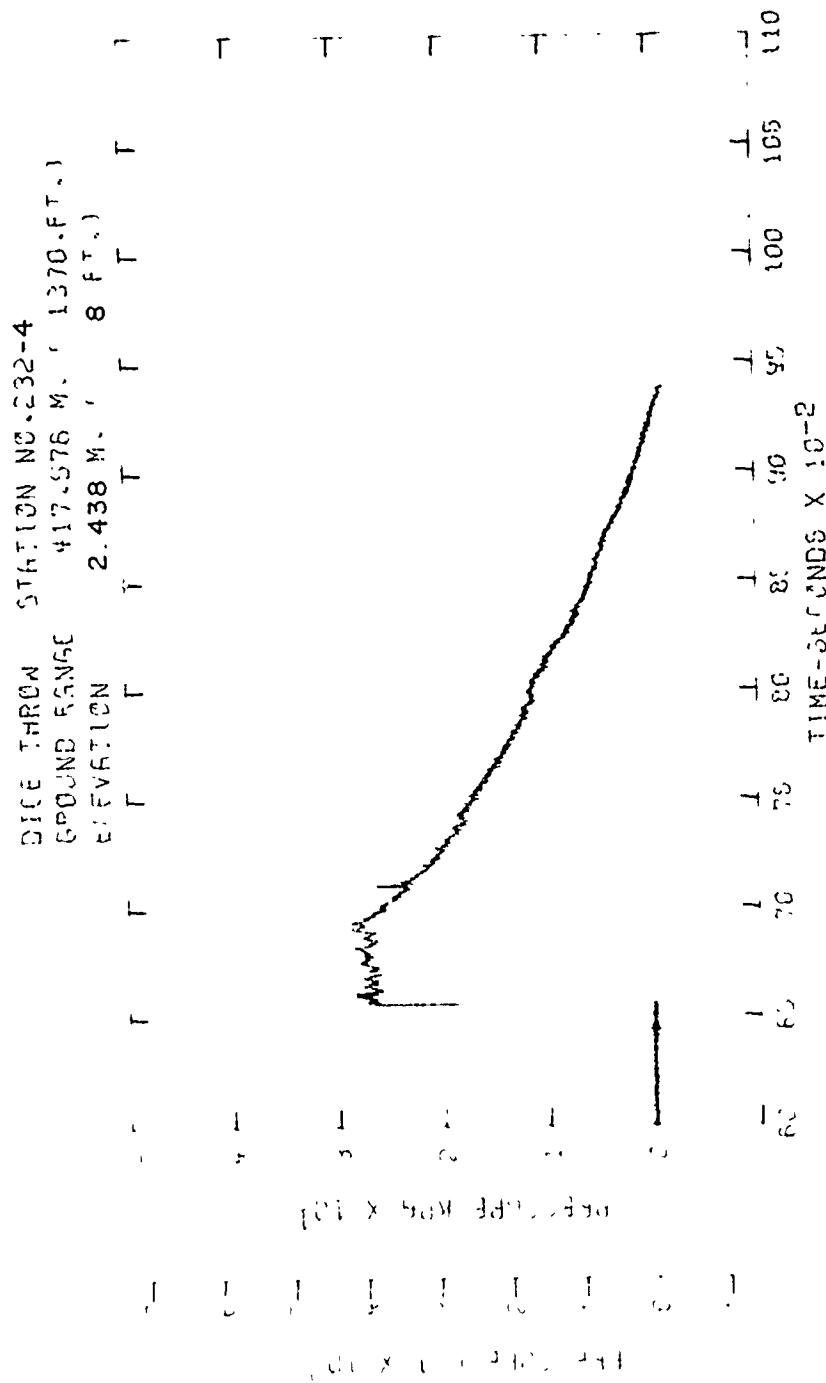


Figure B23. Incident pressure-time history - Station 232-4

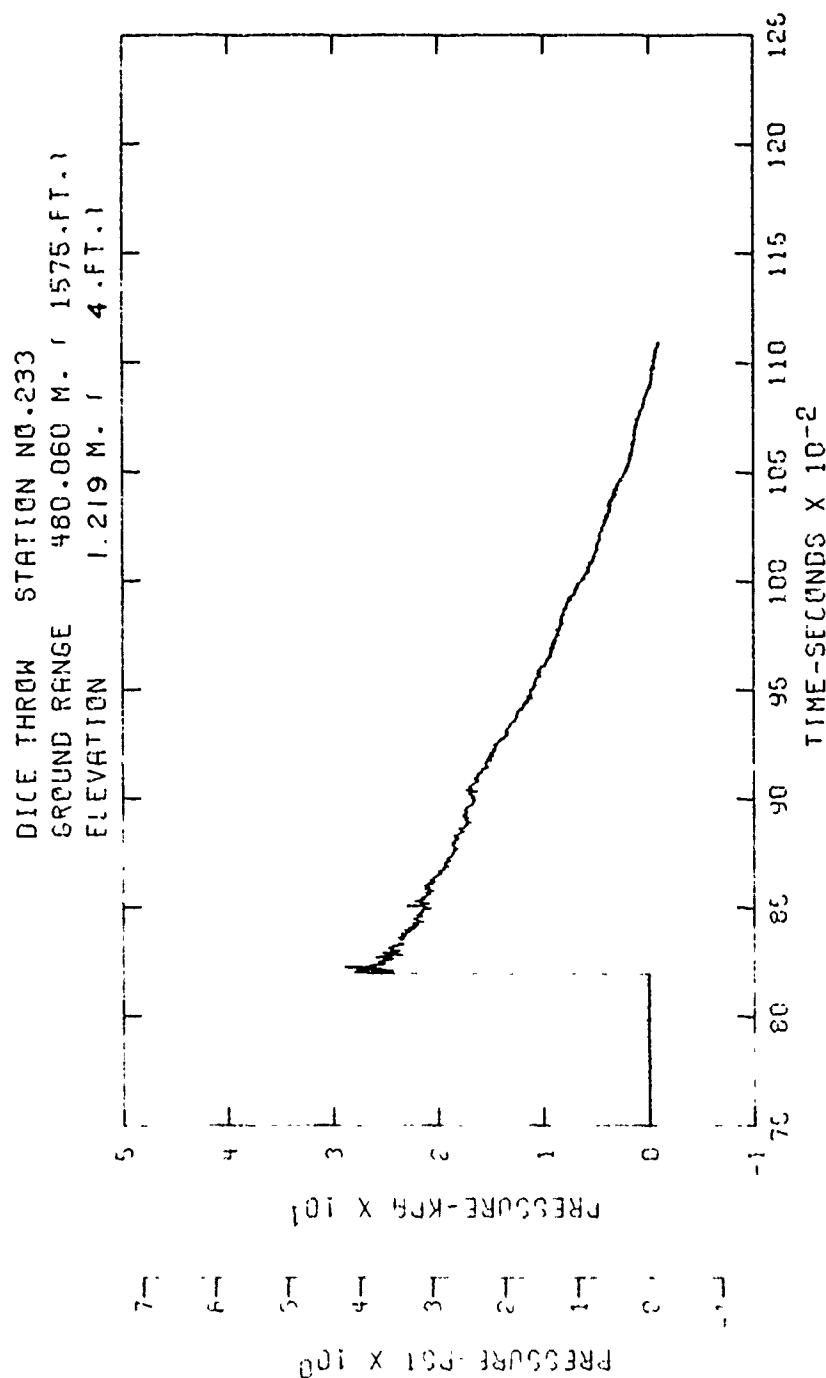


Figure B24. Incident pressure-time history - Station 233

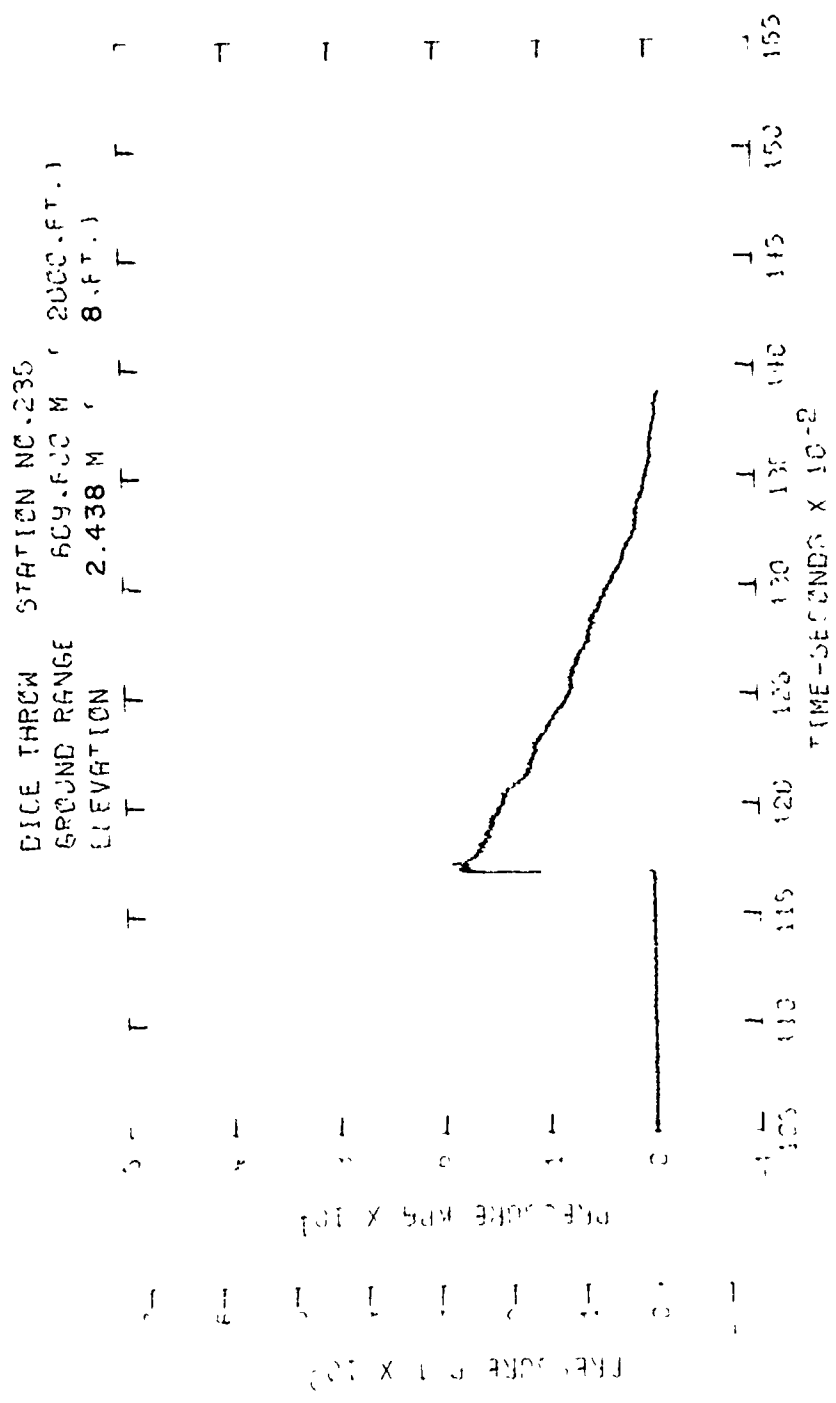


Figure B25. Incident pressure-time history - Station 235

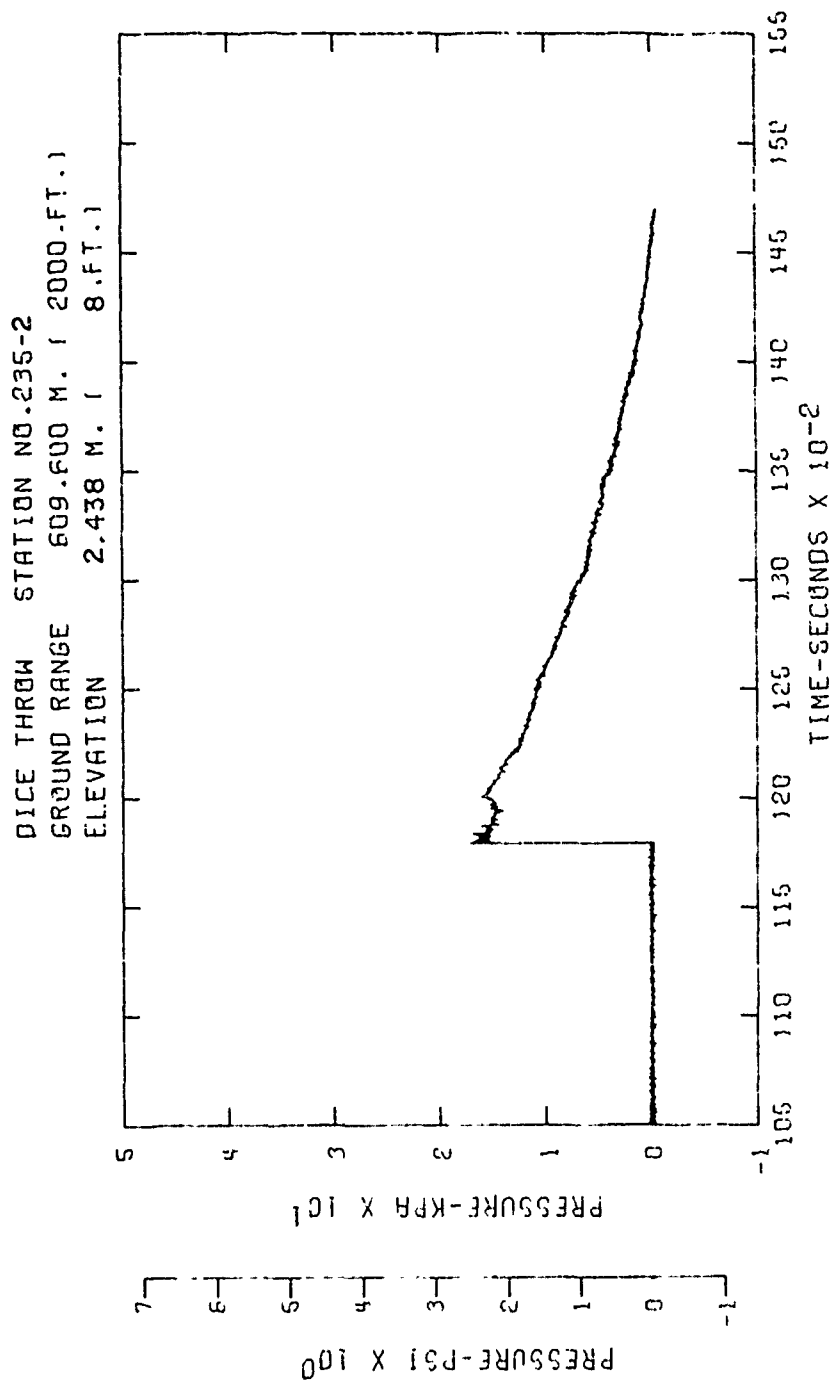


Figure B26. Incident pressure-time history - Station 235-2

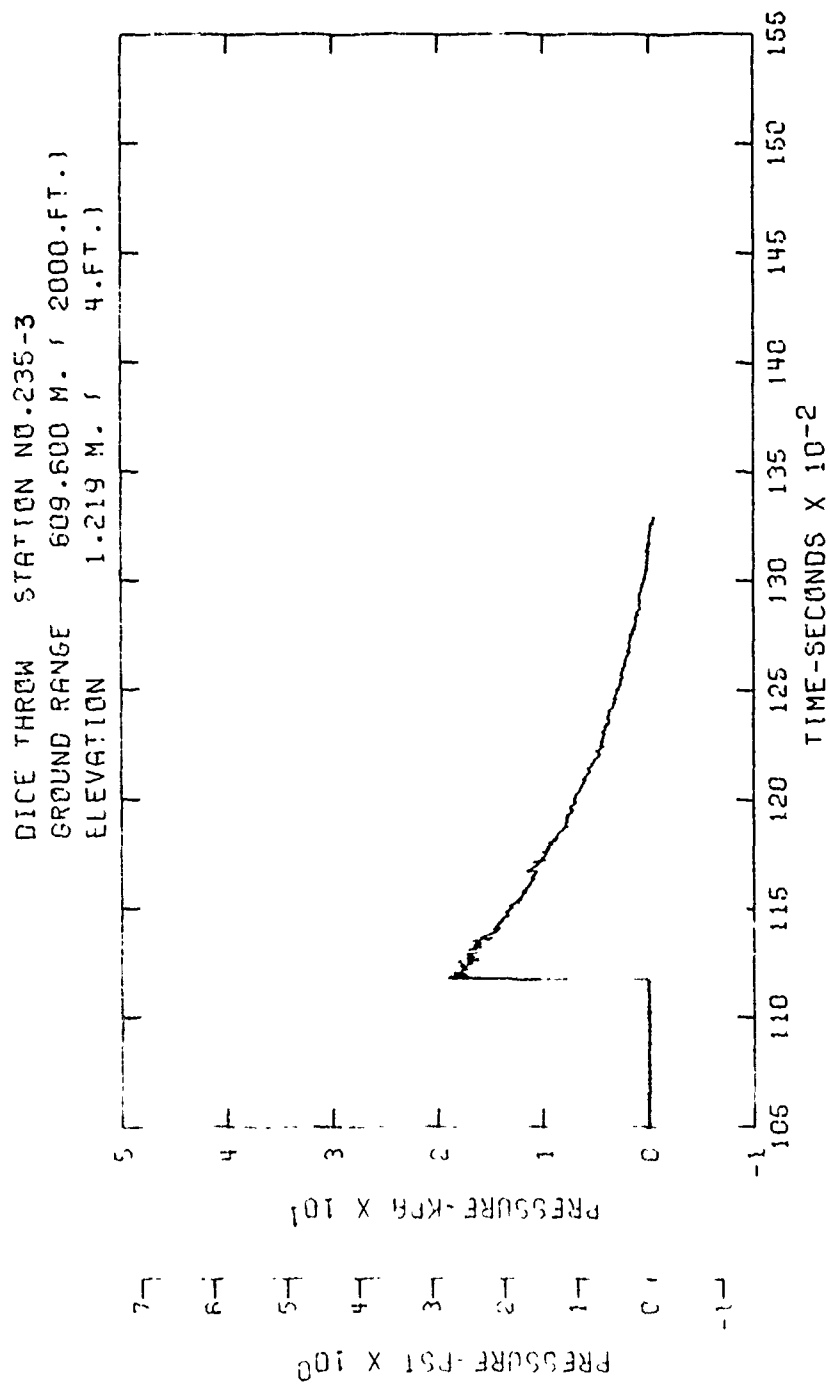


Figure B27. Incident pressure-time history - Station 235-3

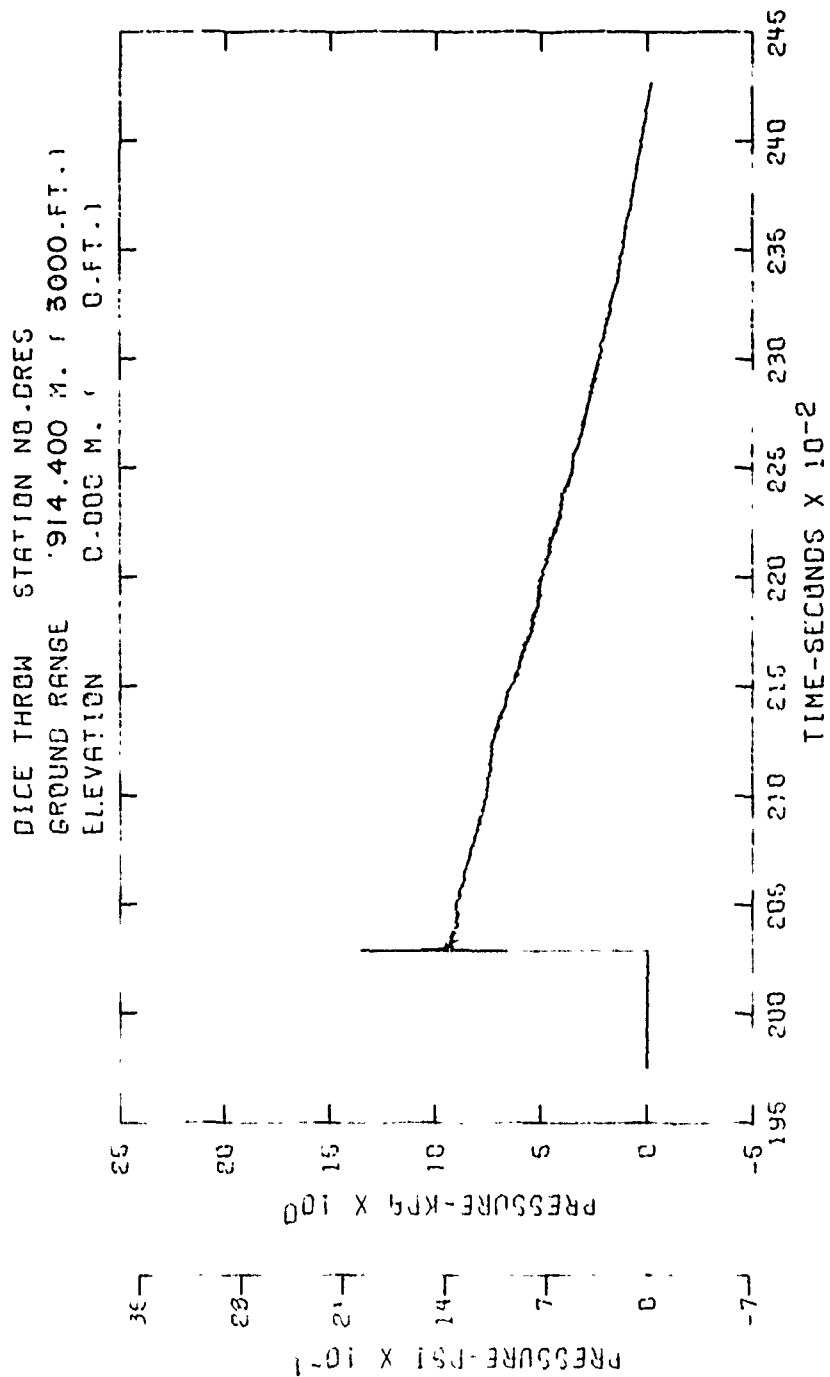


Figure B28. Incident pressure-time history - Station DRES

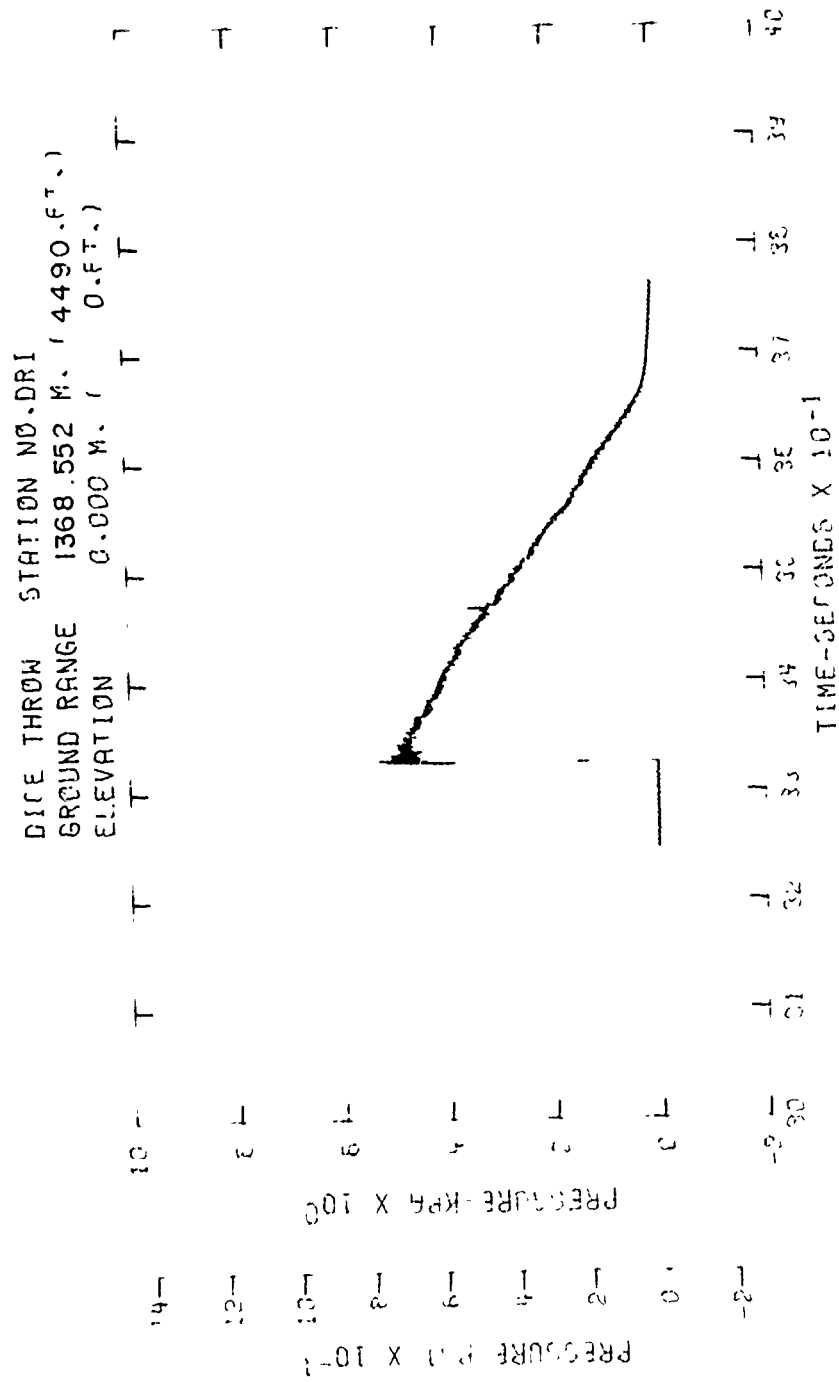


Figure B29. Incident pressure-time history - Station DRI



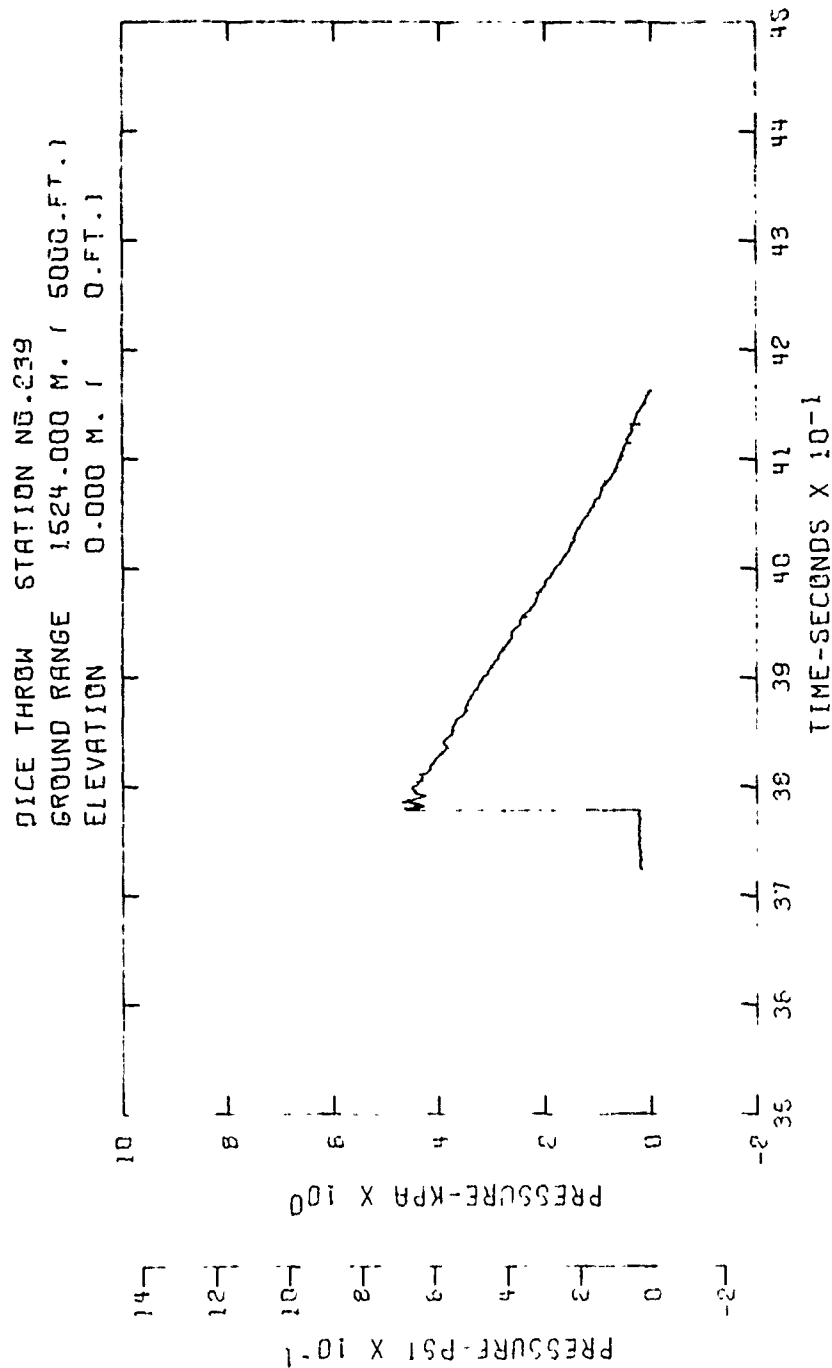


Figure B30. Incident pressure-time history - Station 239

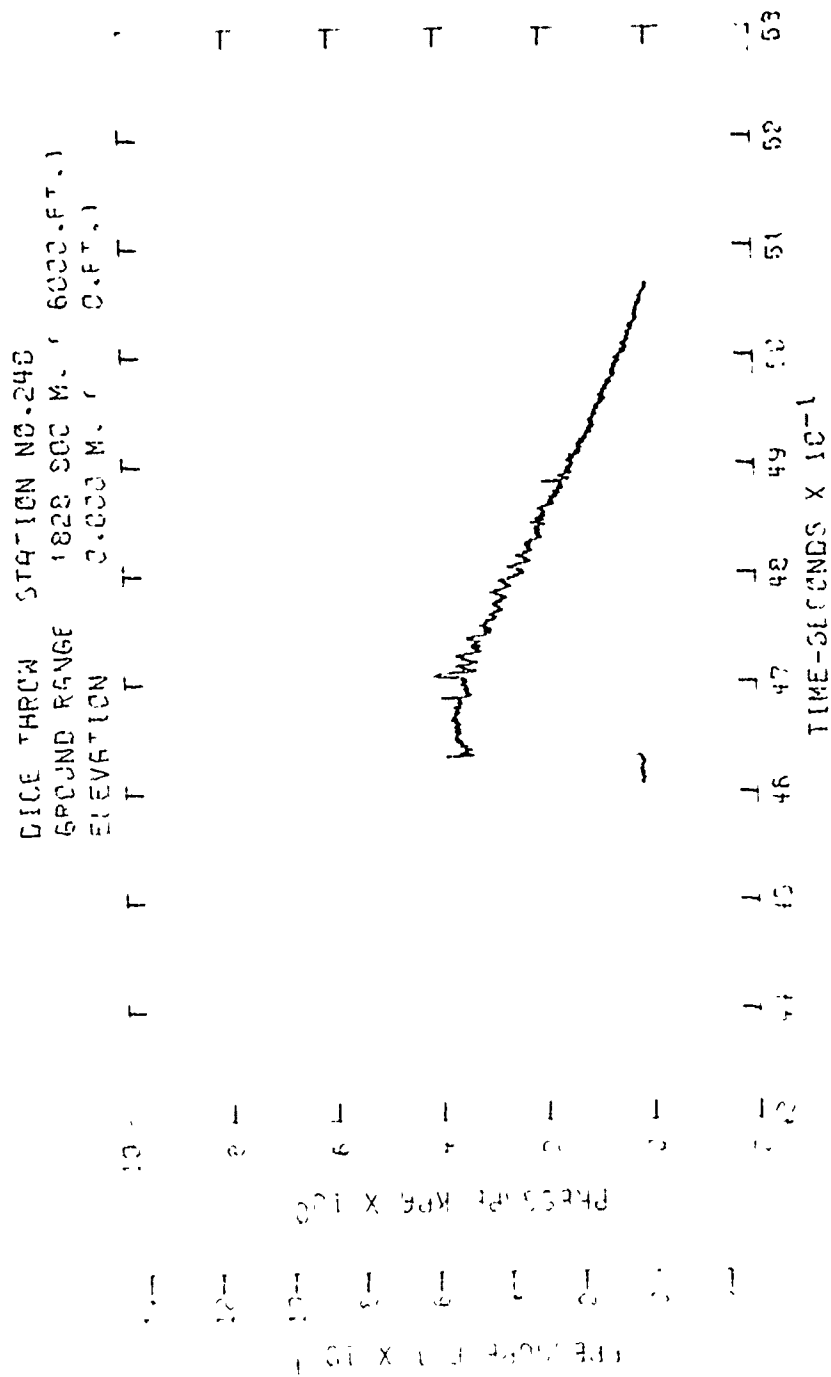


Figure B31. Incident pressure-time history - Station 240

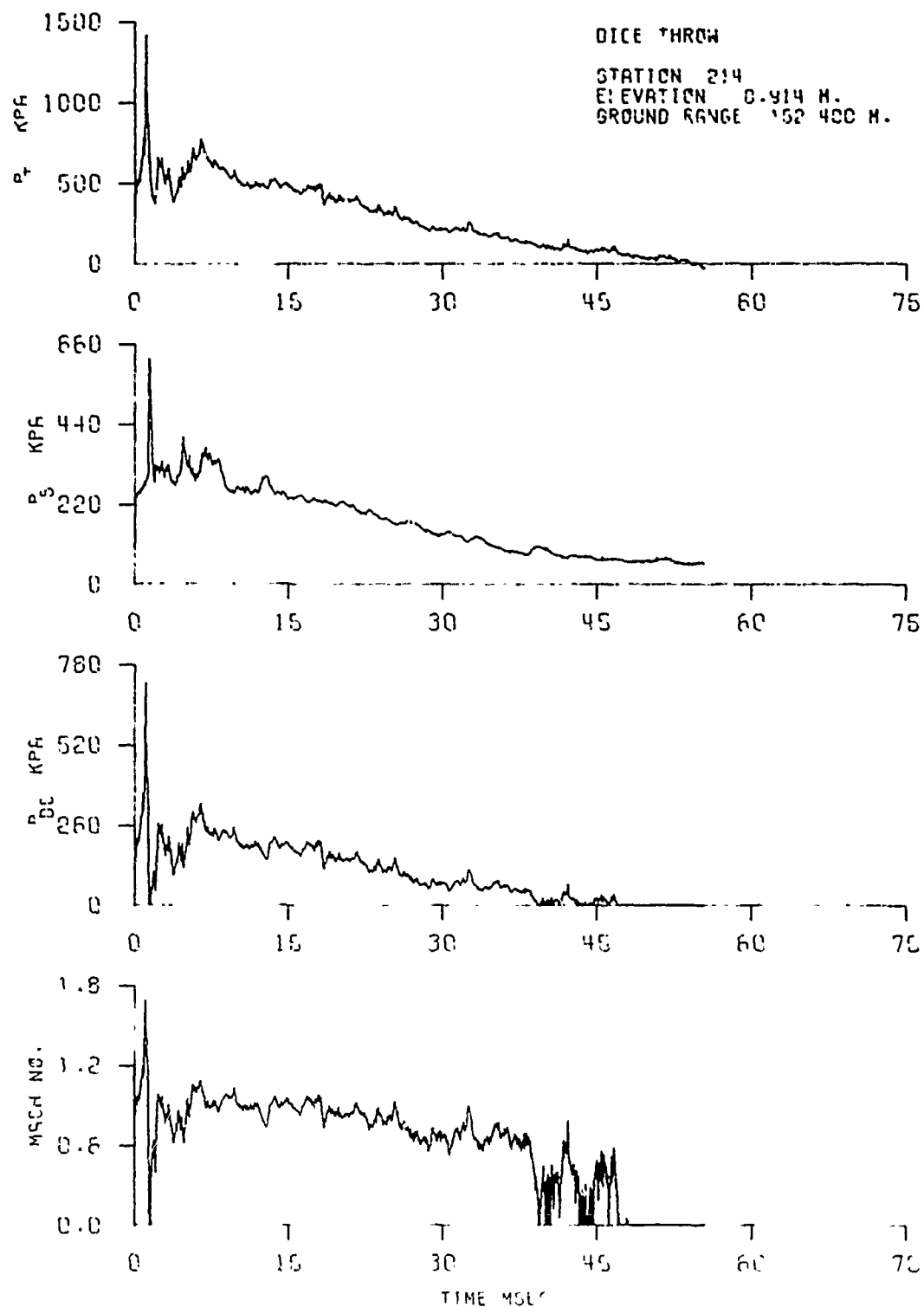


Figure B32. Dynamic pressure-time history - Station 214

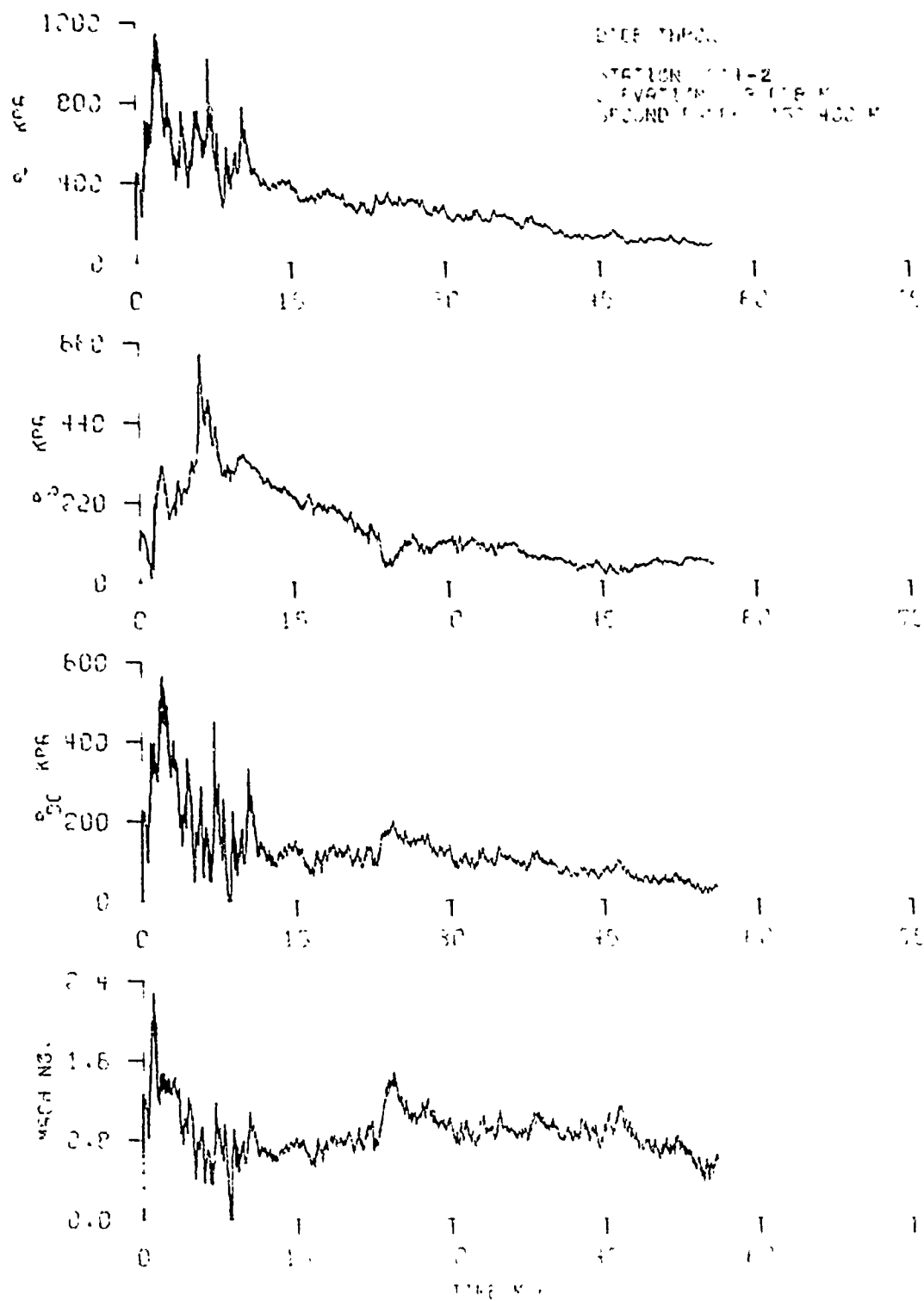


Figure B33. Dynamic pressure-time history - Station 214-2

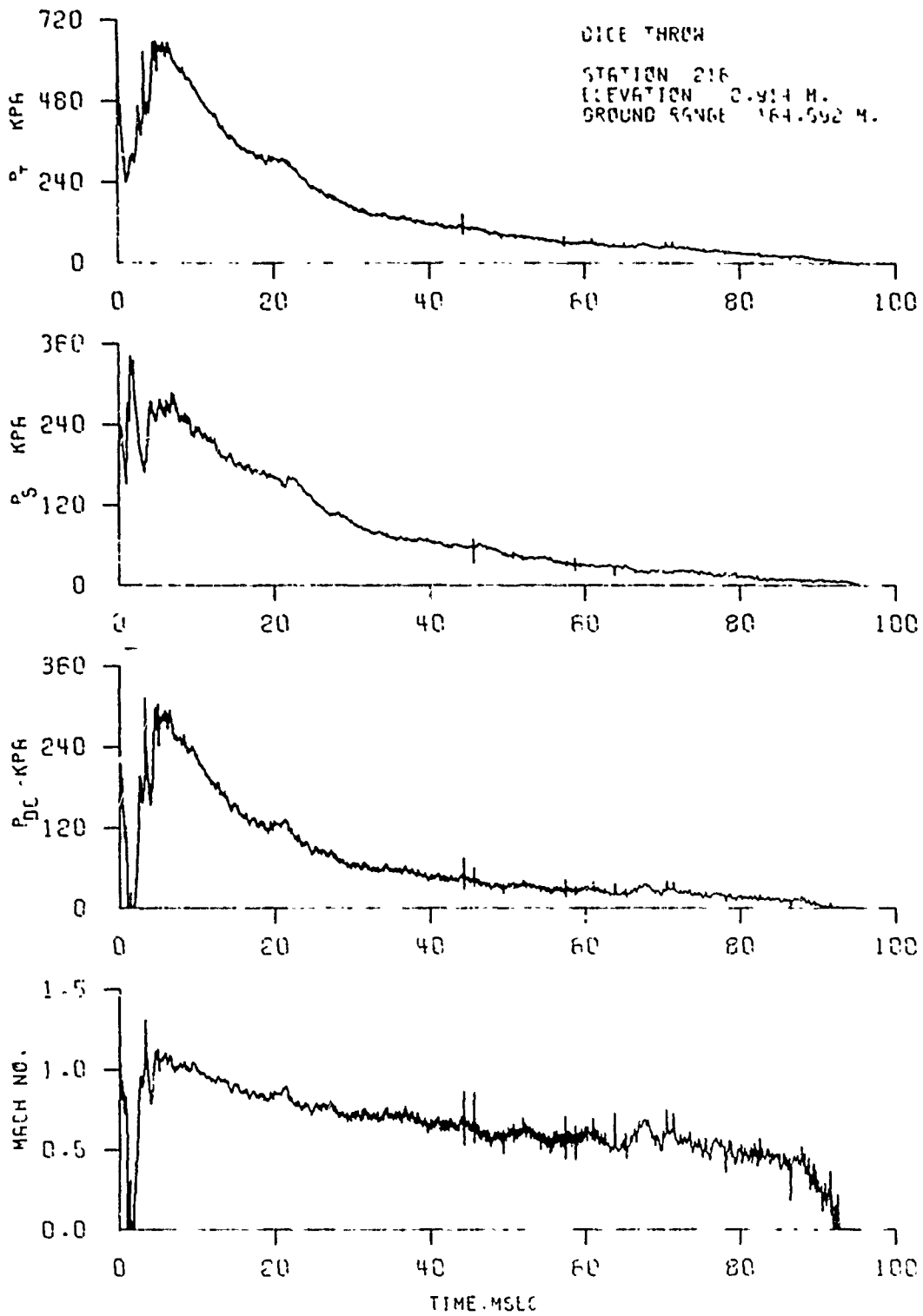


Figure B34. Dynamic pressure-time history - Station 216

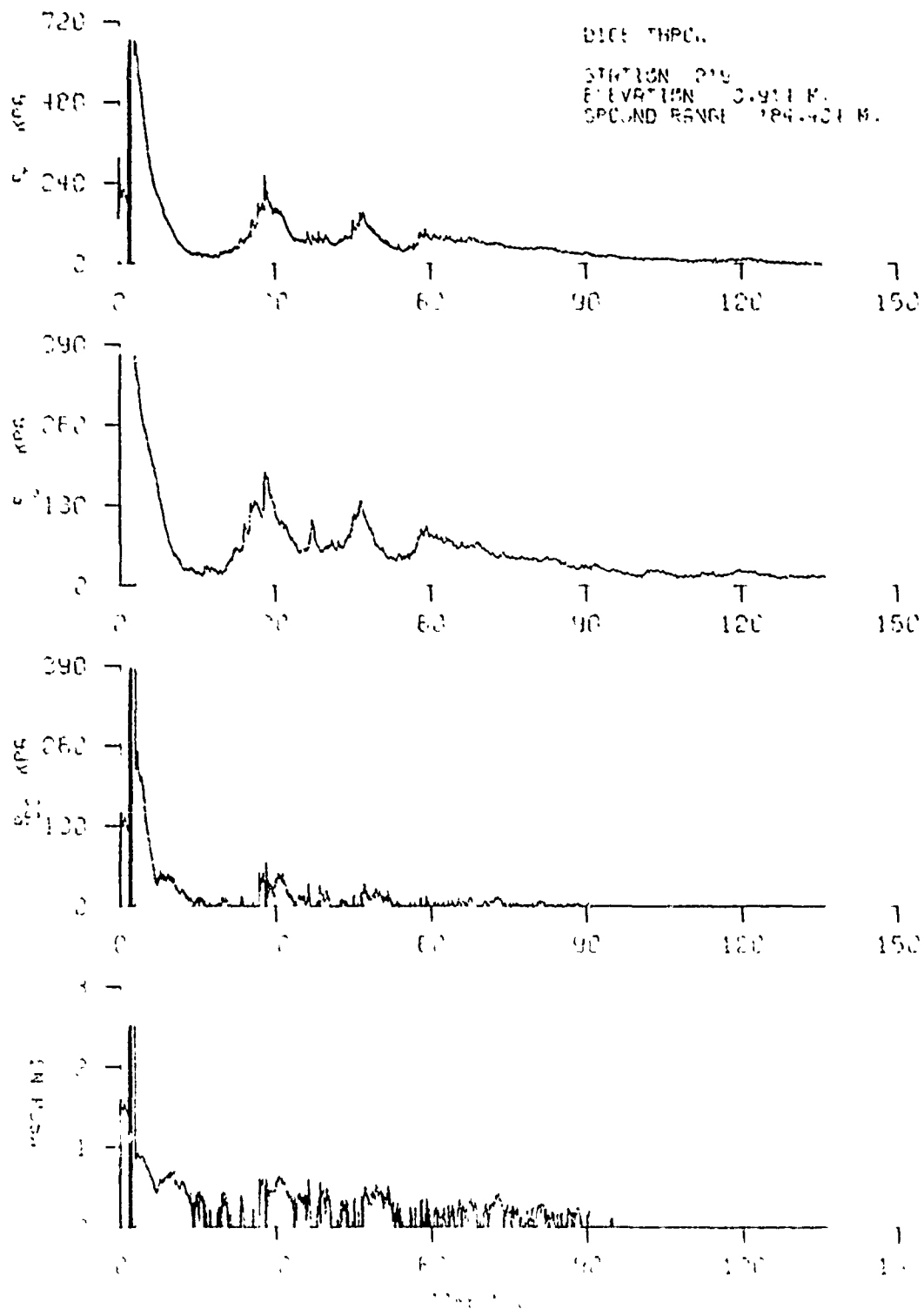


Figure B35. Dynamic pressure-time history - Station 219

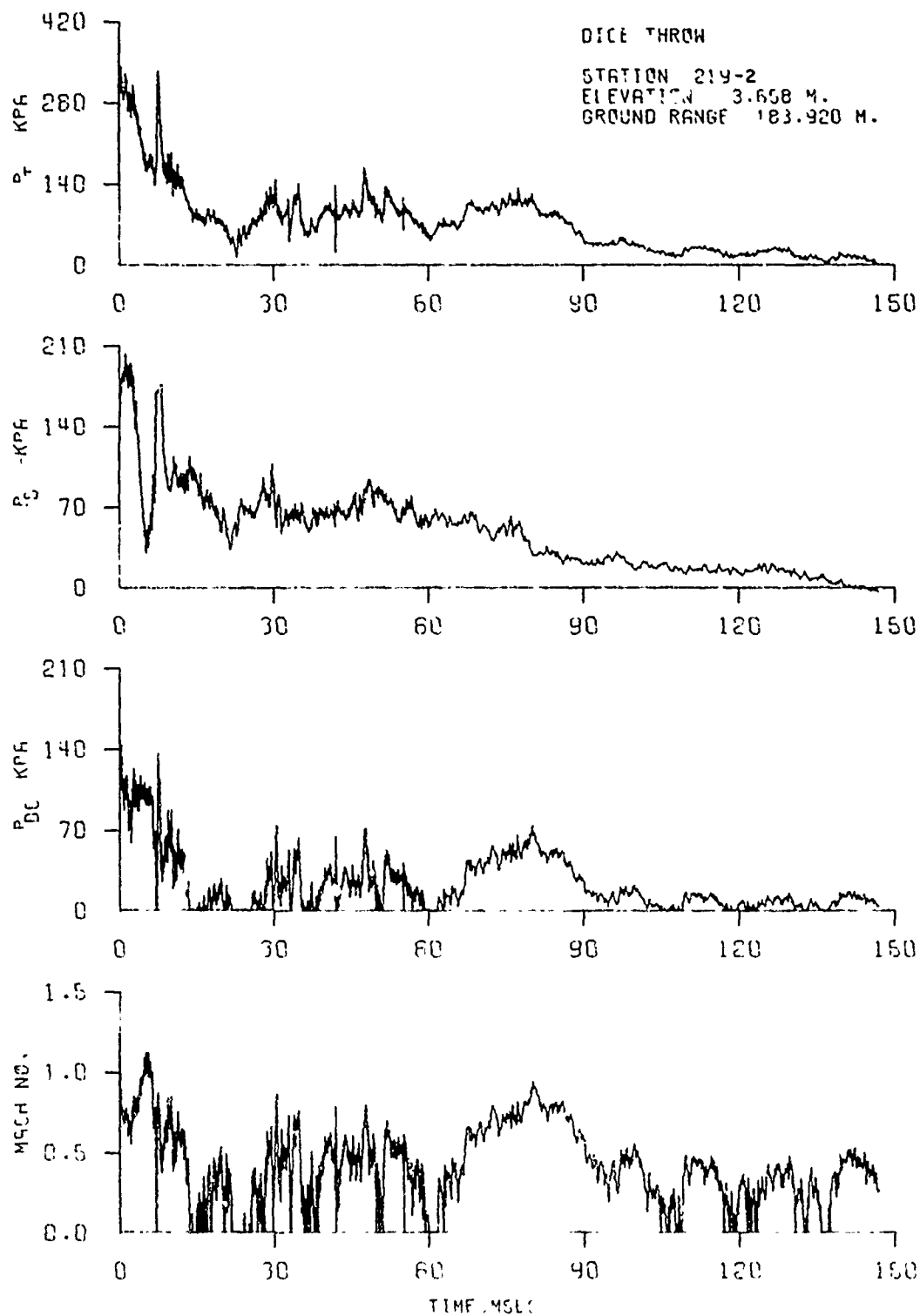


Figure B36. Dynamic pressure-time history - Station 219-2

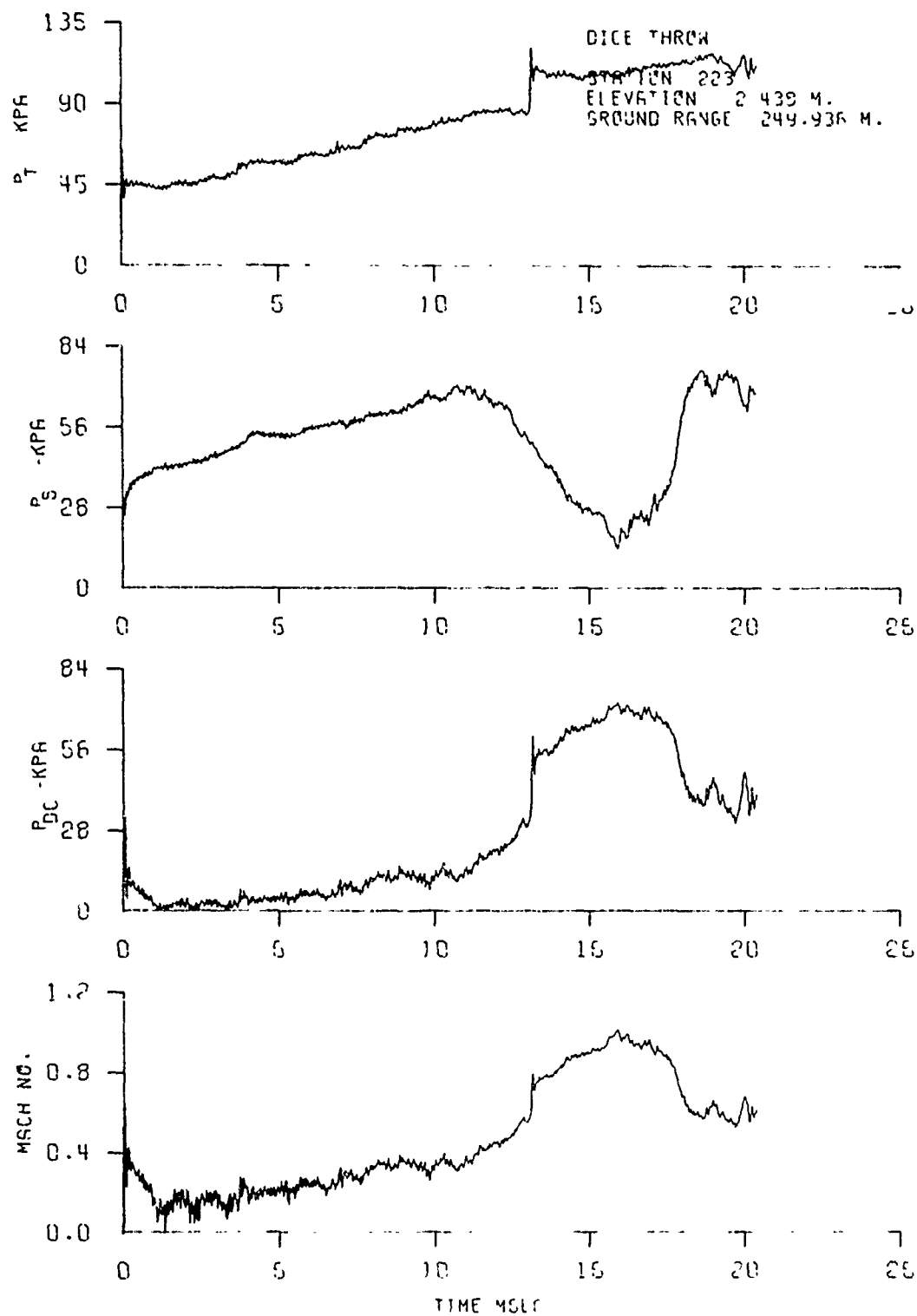


Figure B37. Dynamic pressure-time history - Station 223



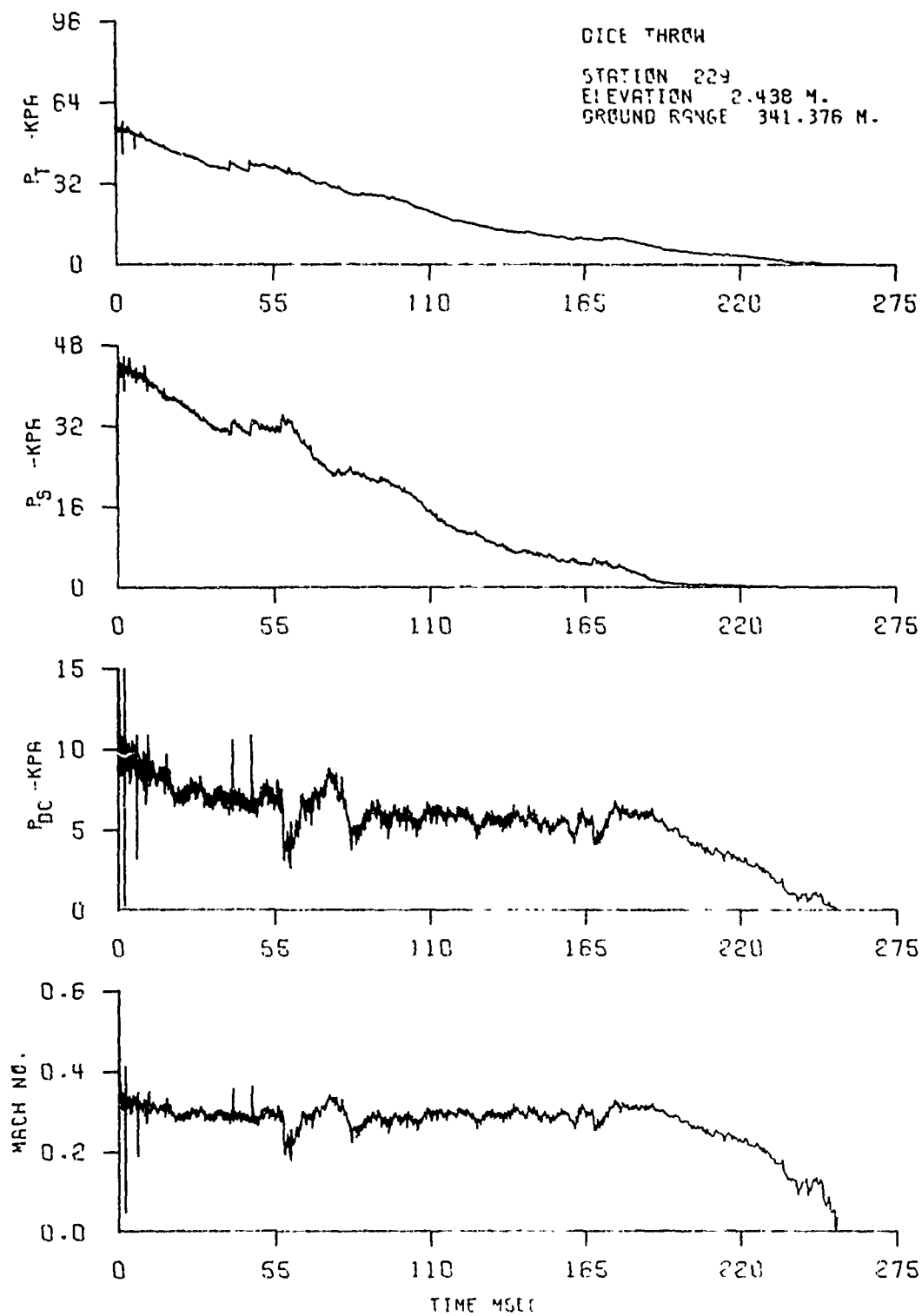


Figure B38. Dynamic pressure-time history - Station 229

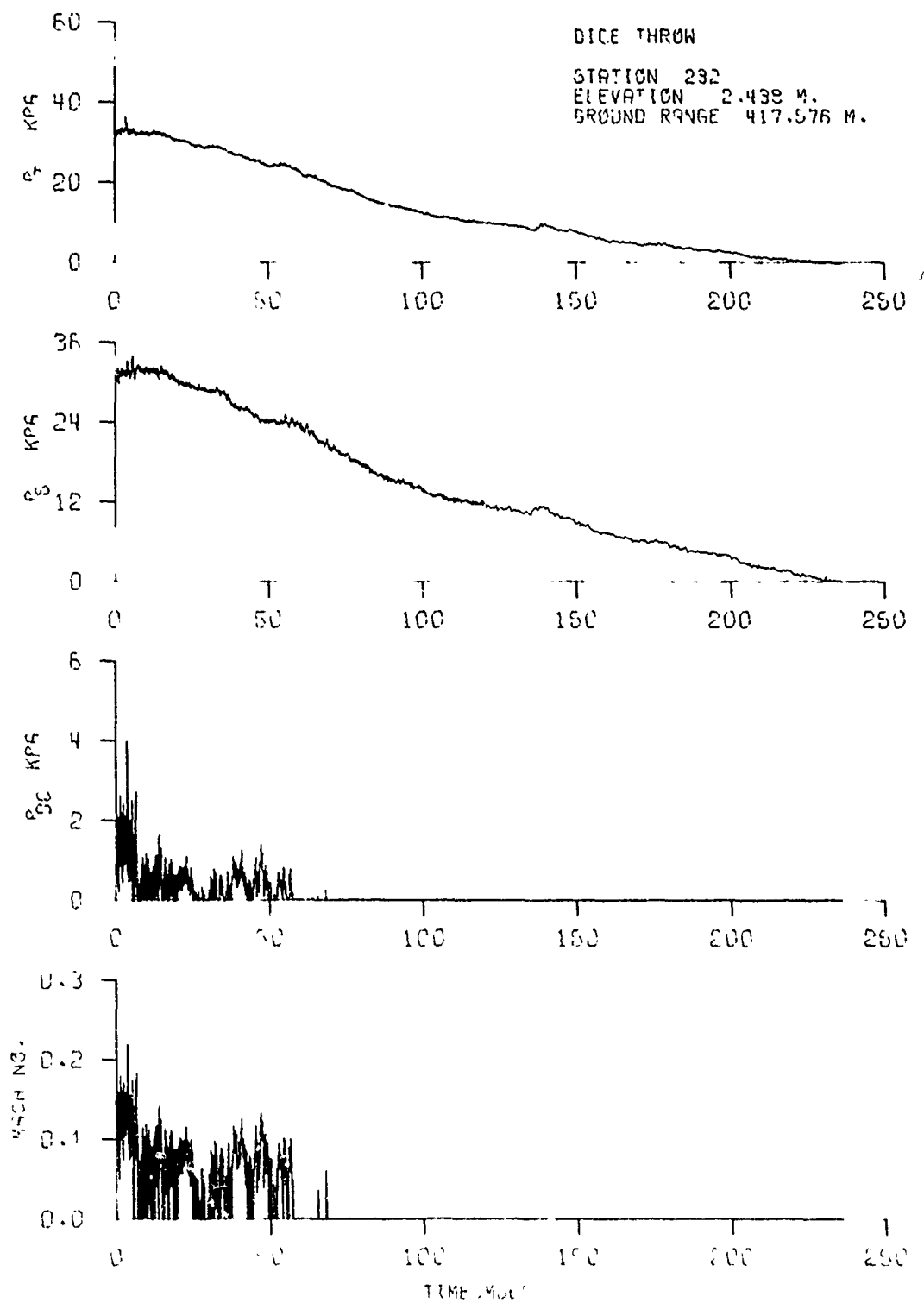


Figure B39. Dynamic pressure-time history - Station 229-2

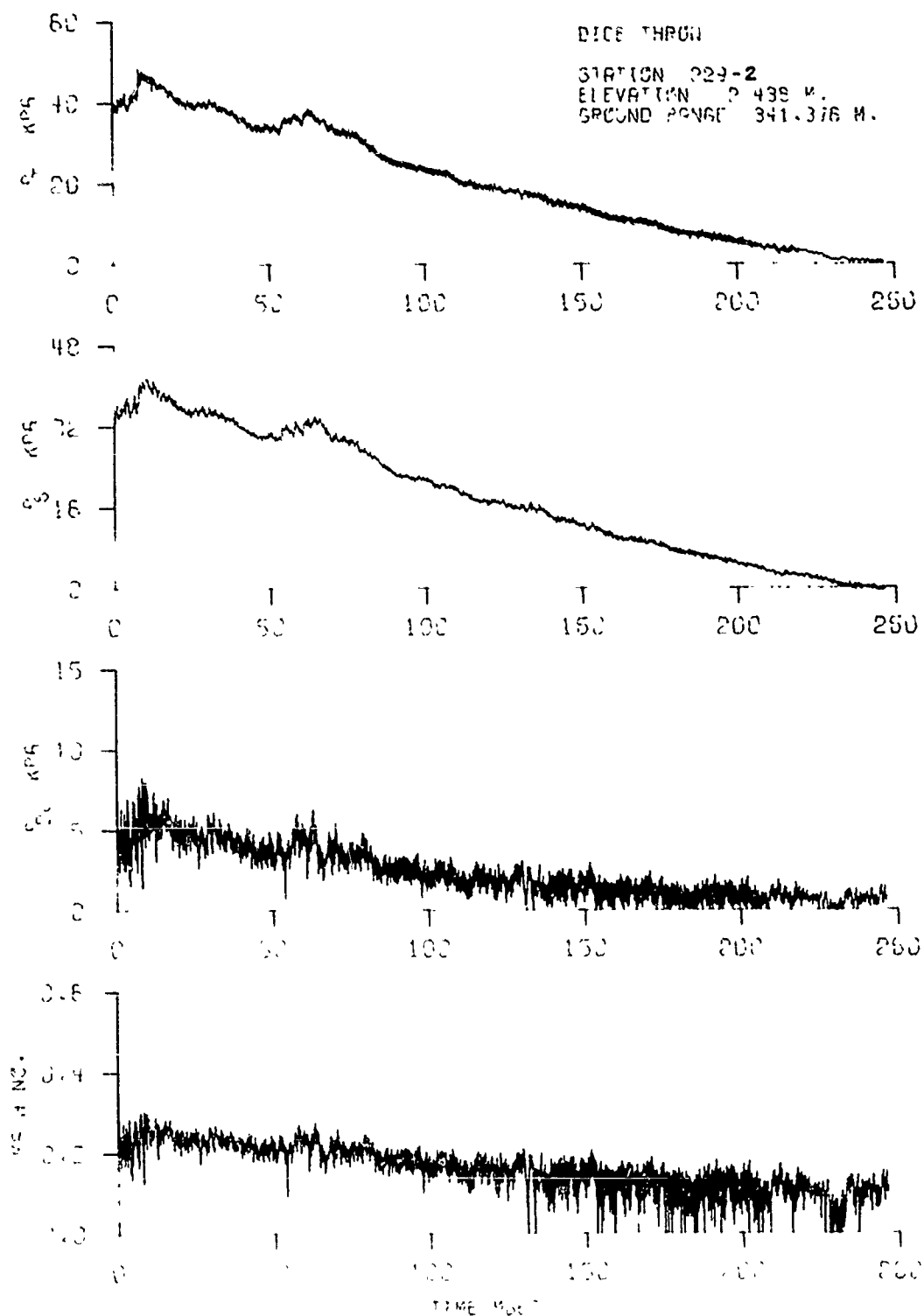


Figure B40. Dynamic pressure-time history - Station 232

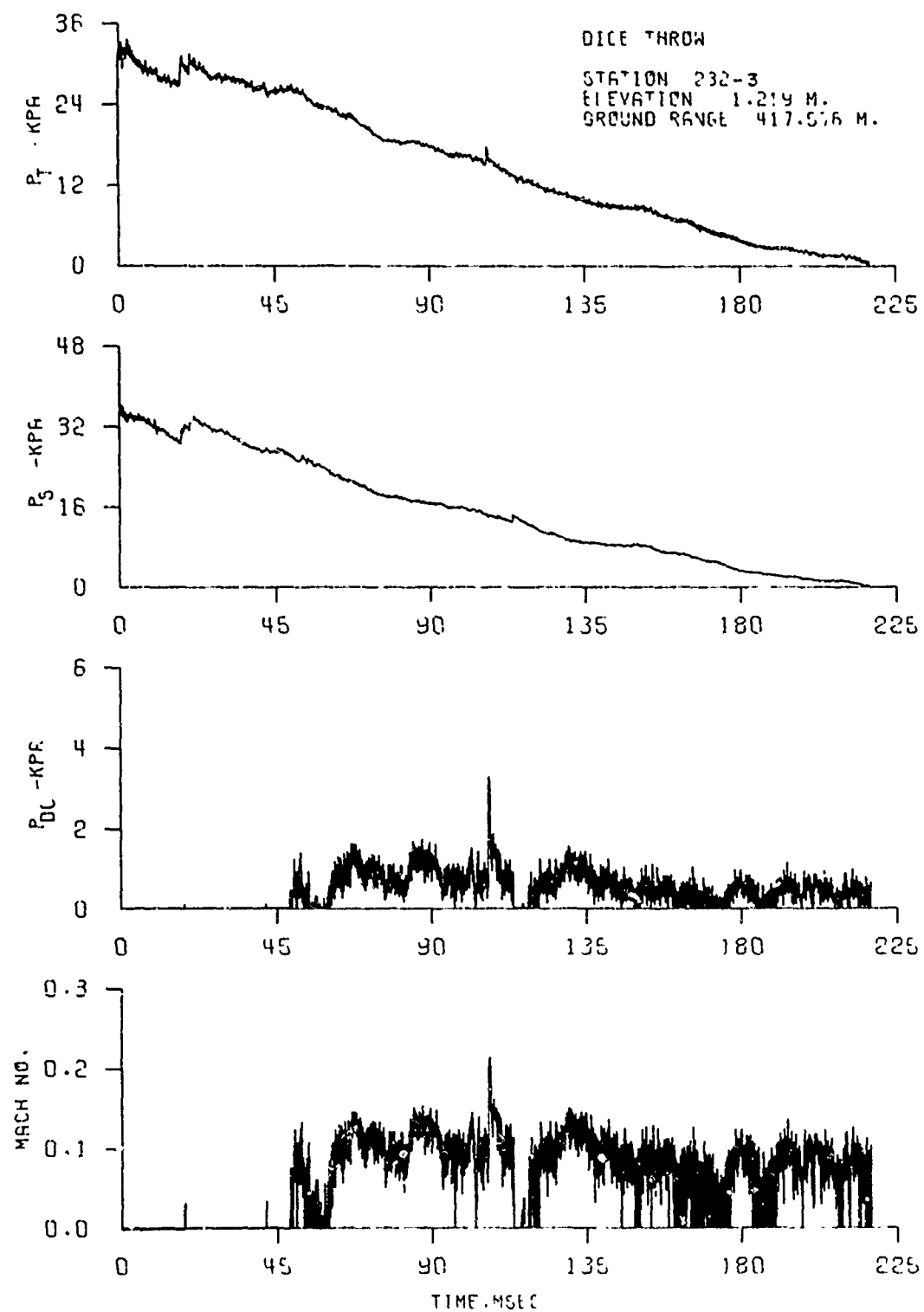


Figure B41. Dynamic pressure-time history - Station 232-3

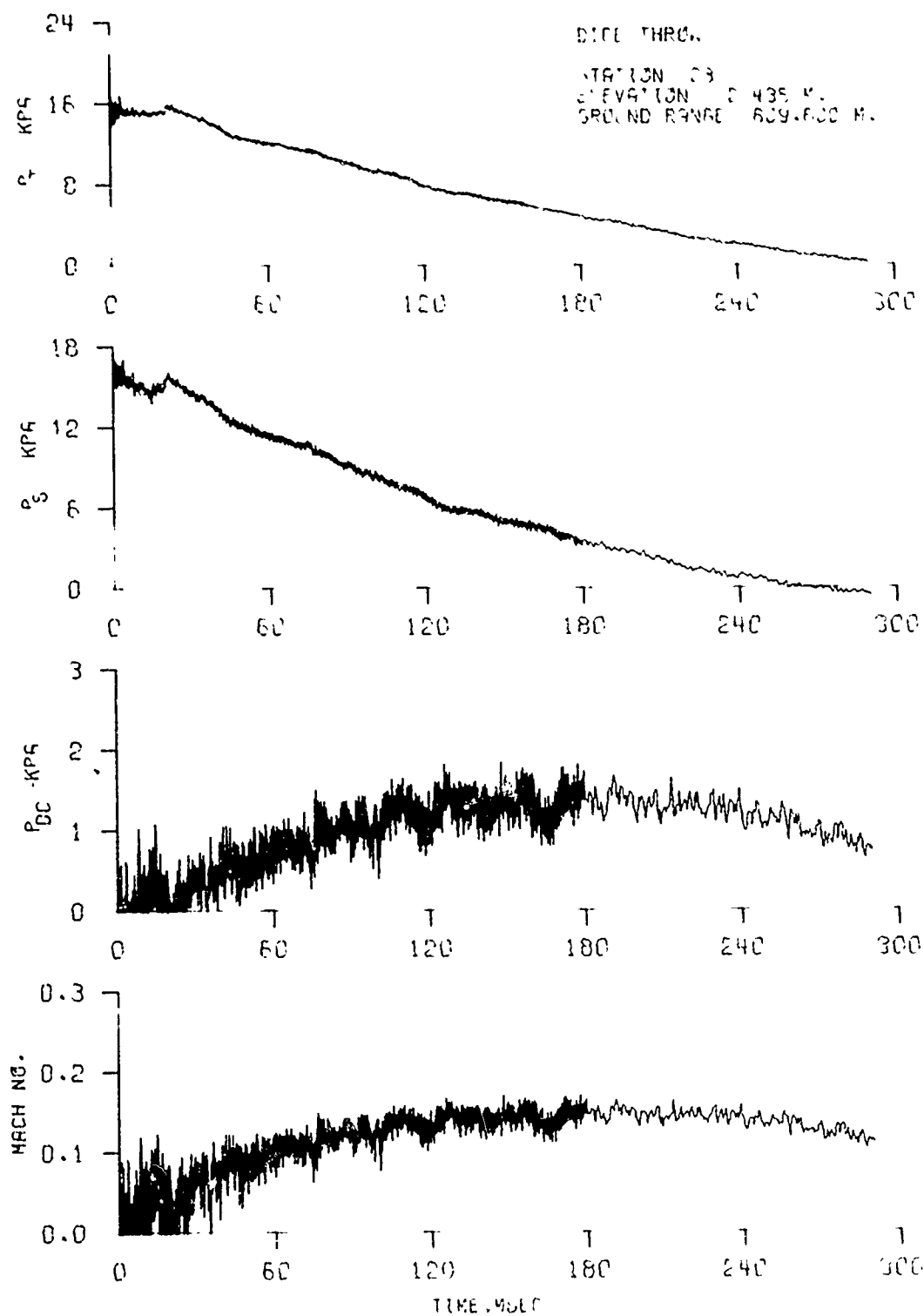


Figure B42. Dynamic pressure-time history - Station 235

## APPENDIX C

The incident and dynamic pressure-time histories recorded along Blast Line 3 and in the BRL (Exp. 034) area are contained in this appendix.

PRECEDING PAGE BLANK

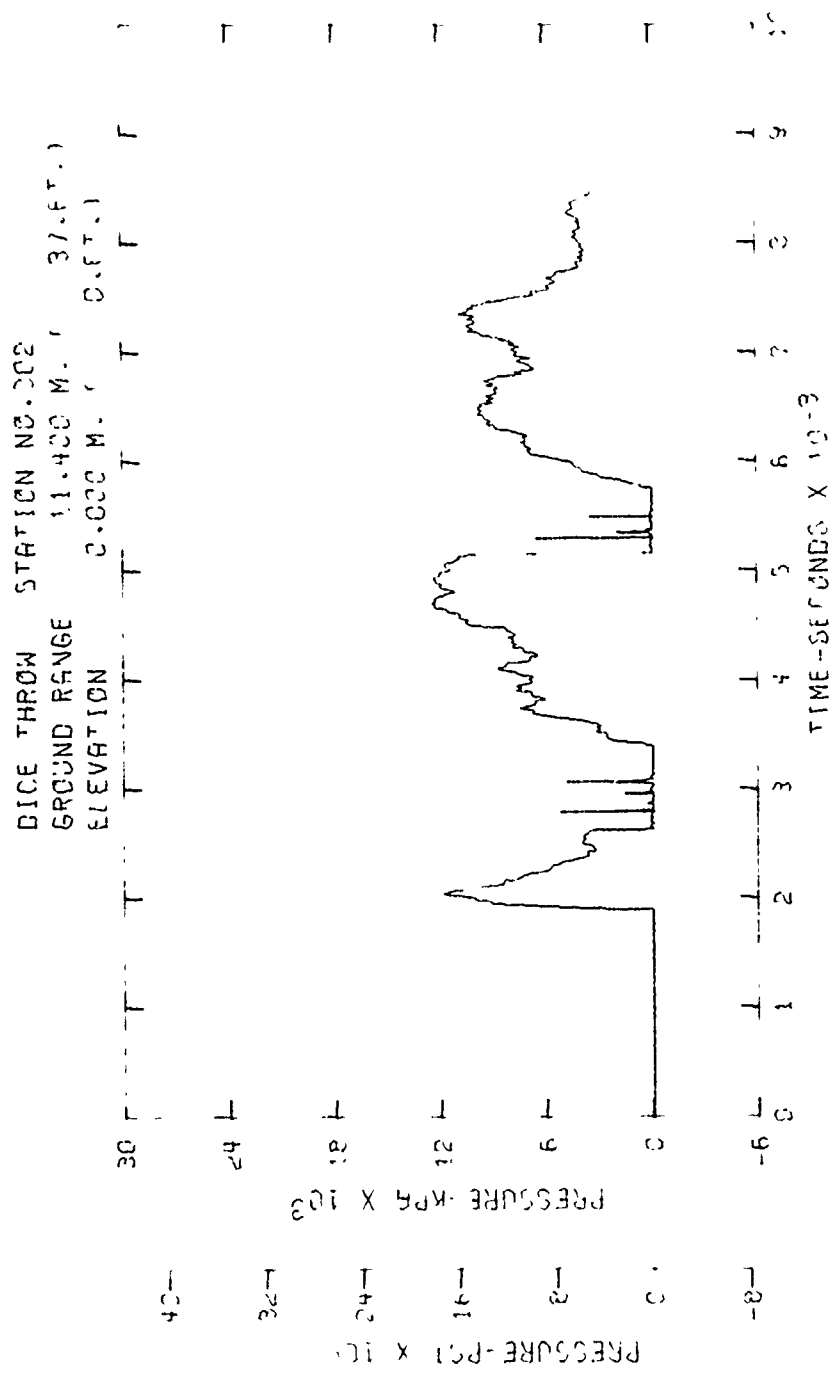


Figure C1. Incident pressure-time history - Station 302

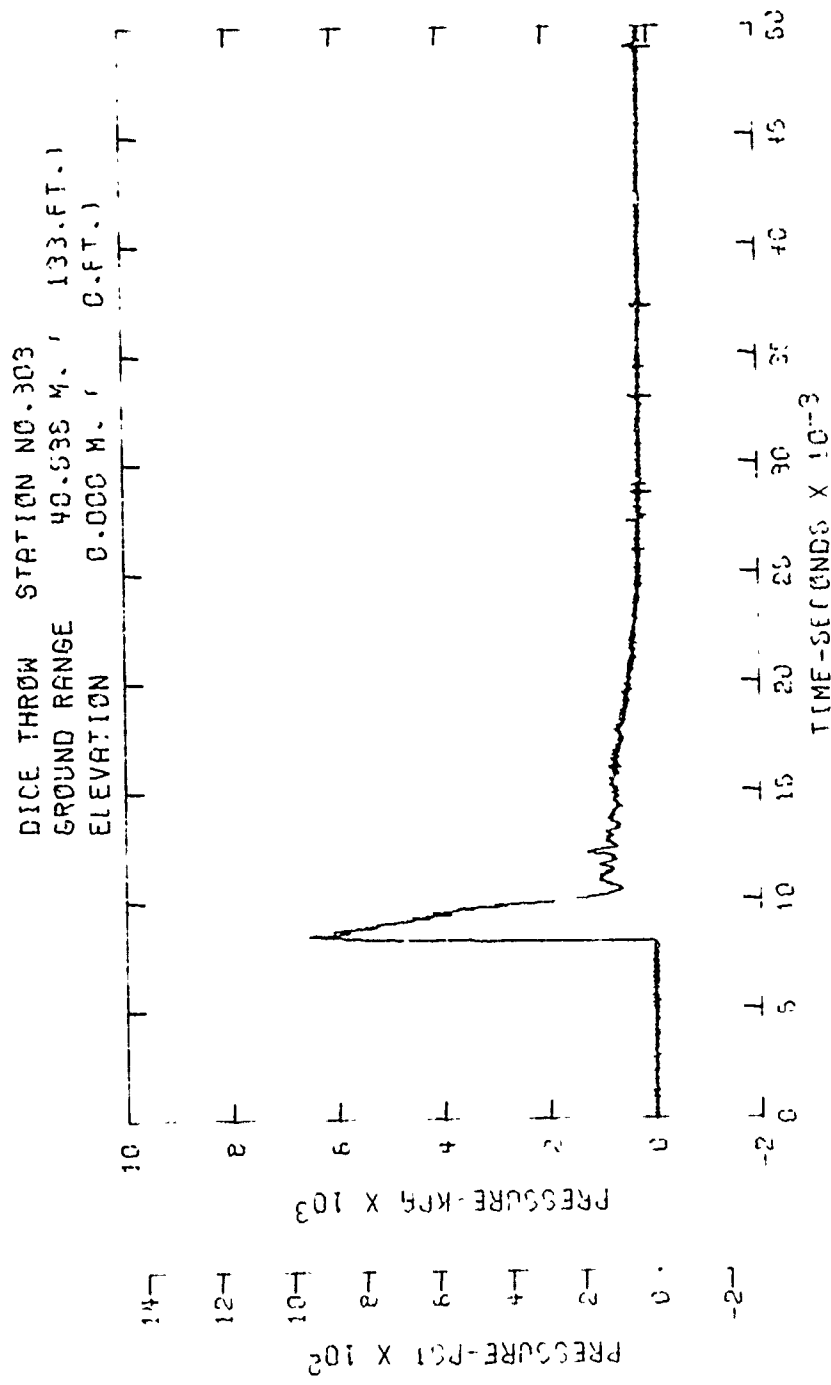


Figure C2. Incident pressure-time history - Station 303



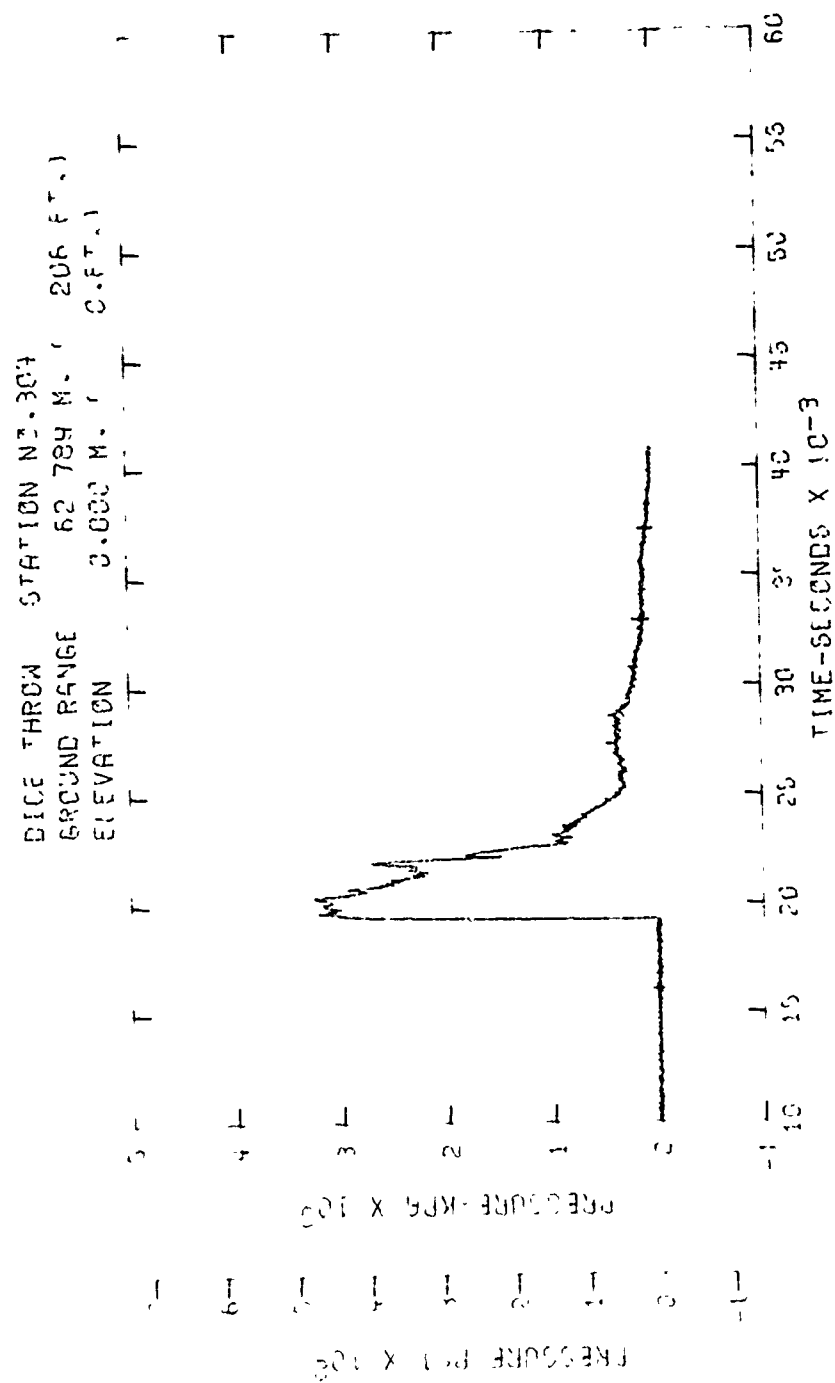


Figure C3. Incident pressure-time history - Station 304

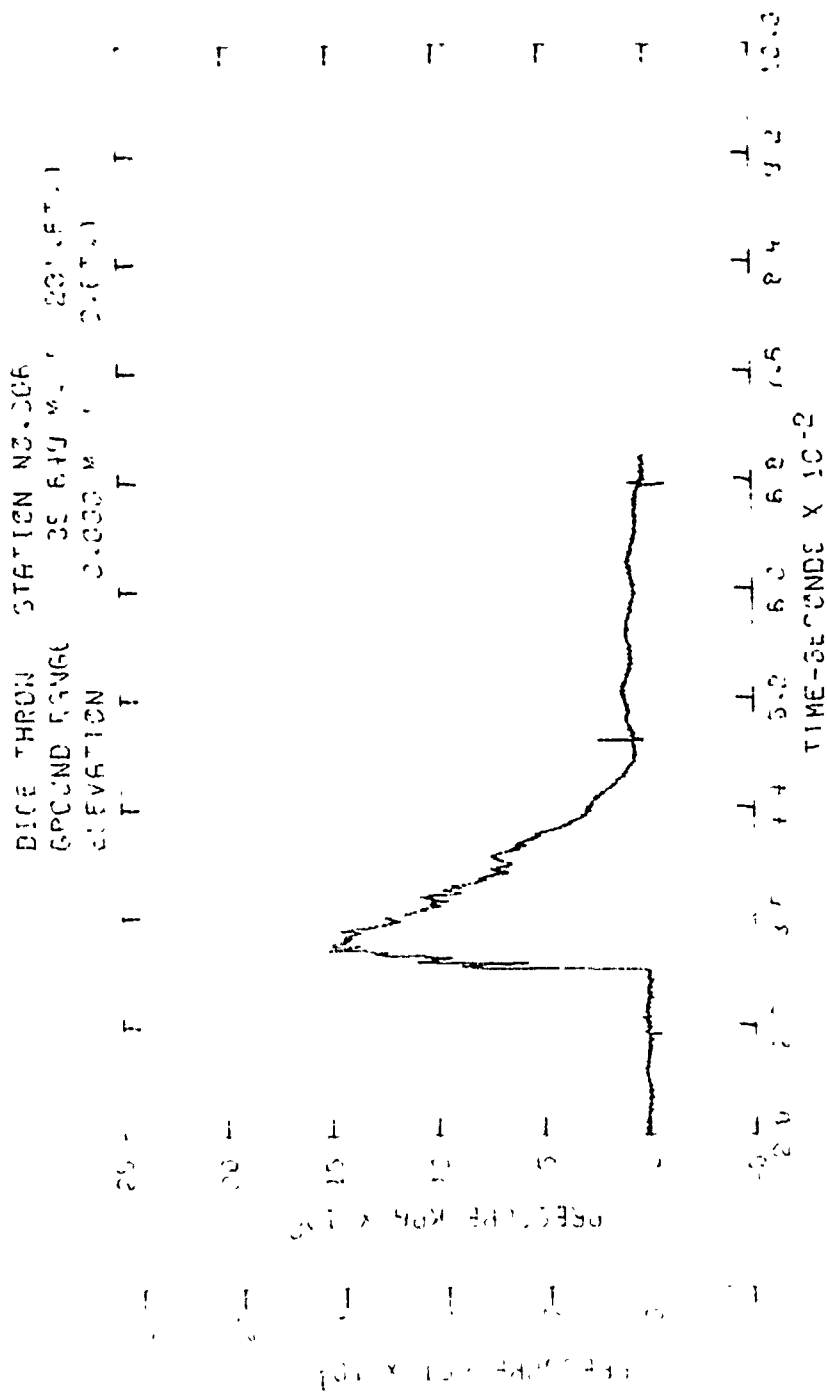


Figure C4. Incident pressure-time history - Station 306

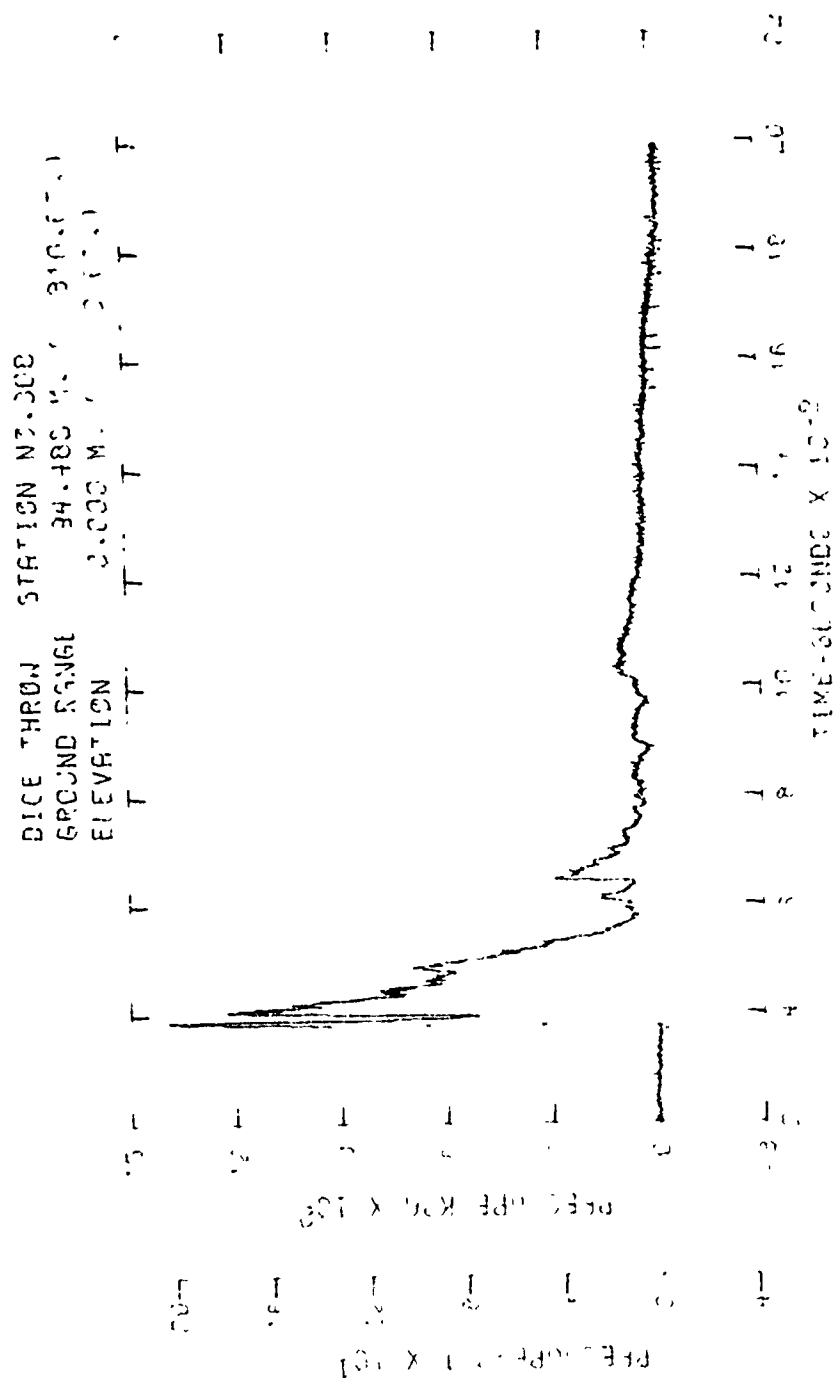


Figure C5. Incident pressure-time history - Station 308

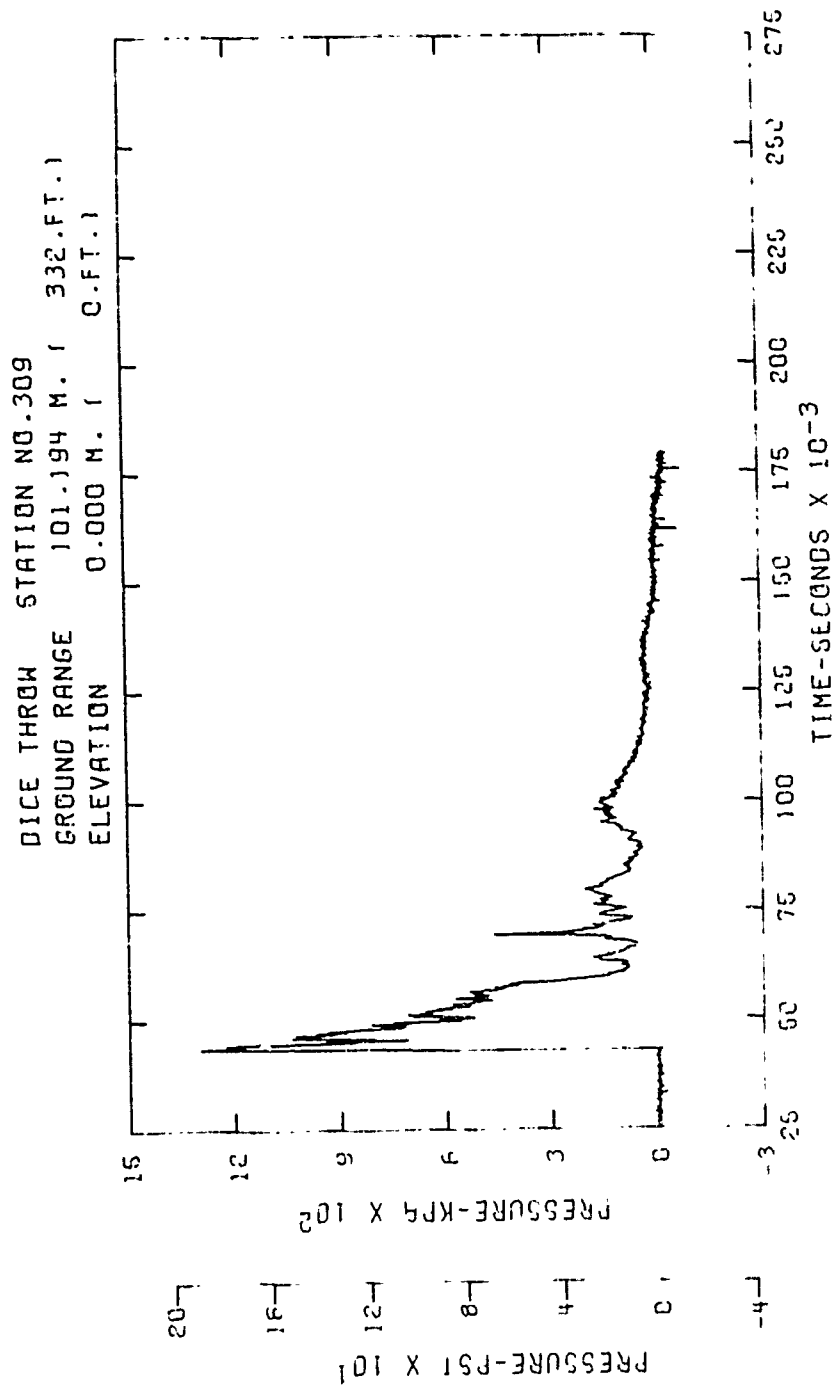


Figure C6. Incident pressure-time history - Station 309

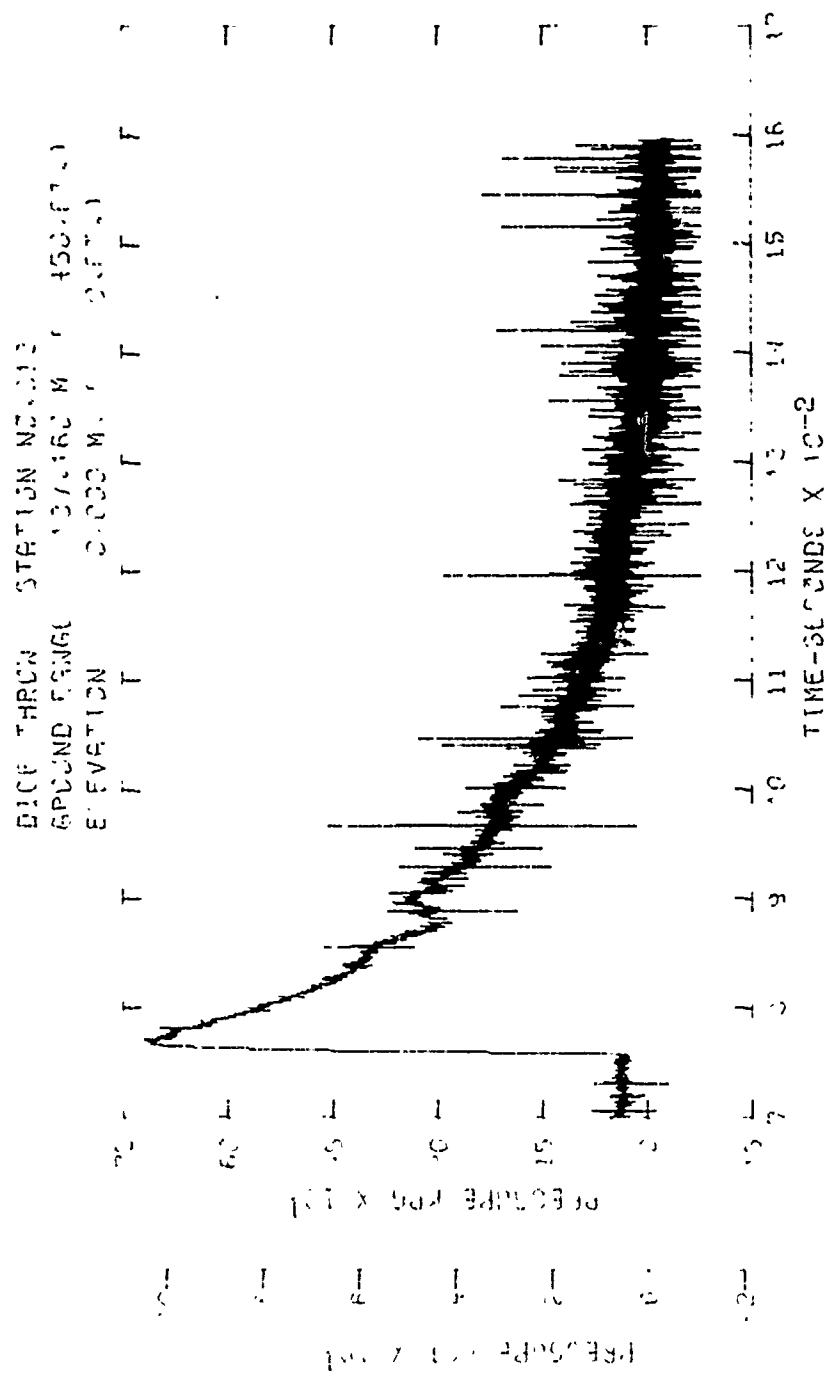


Figure C7. Incident pressure-time history - Station 313

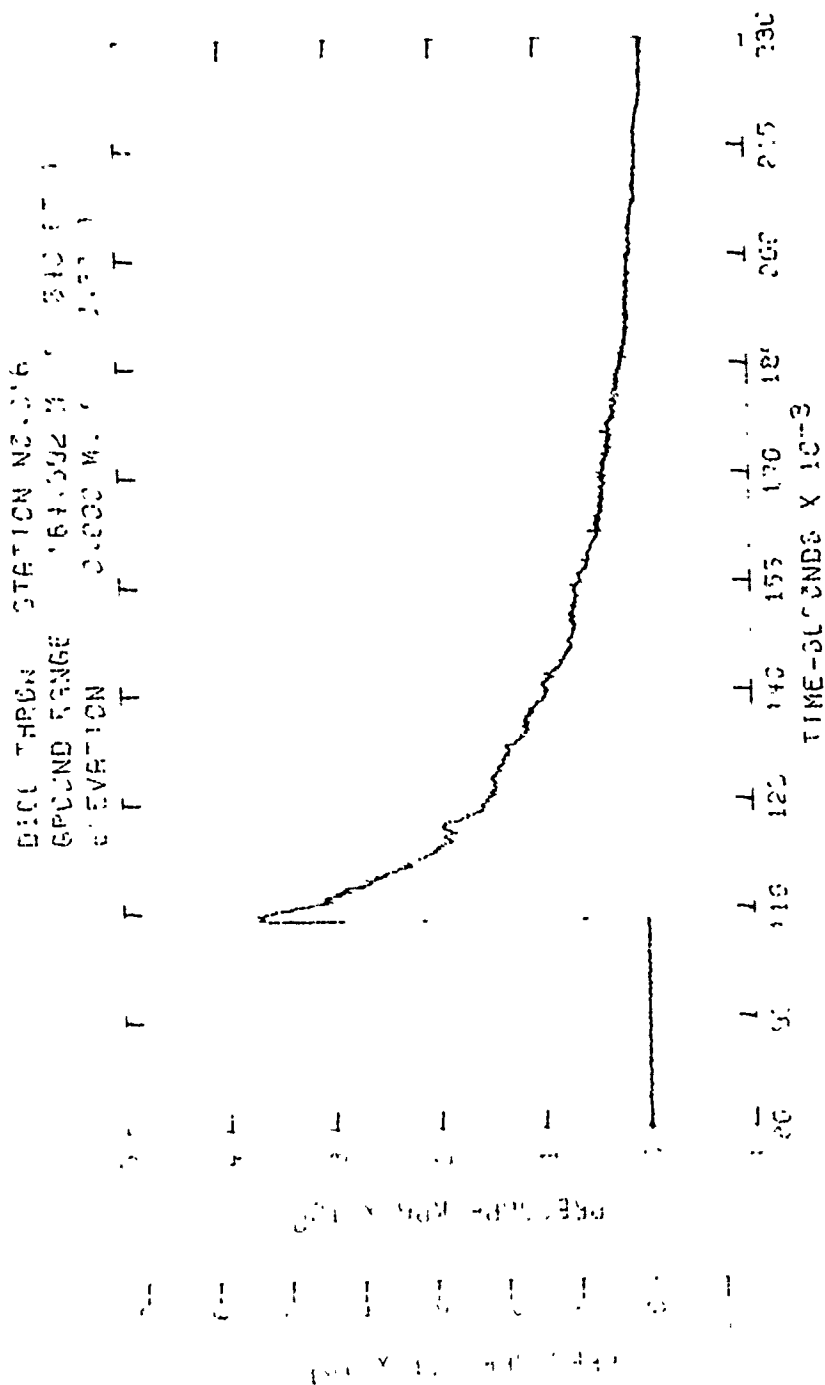


Figure.C8. Incident pressure-time history - Station 316

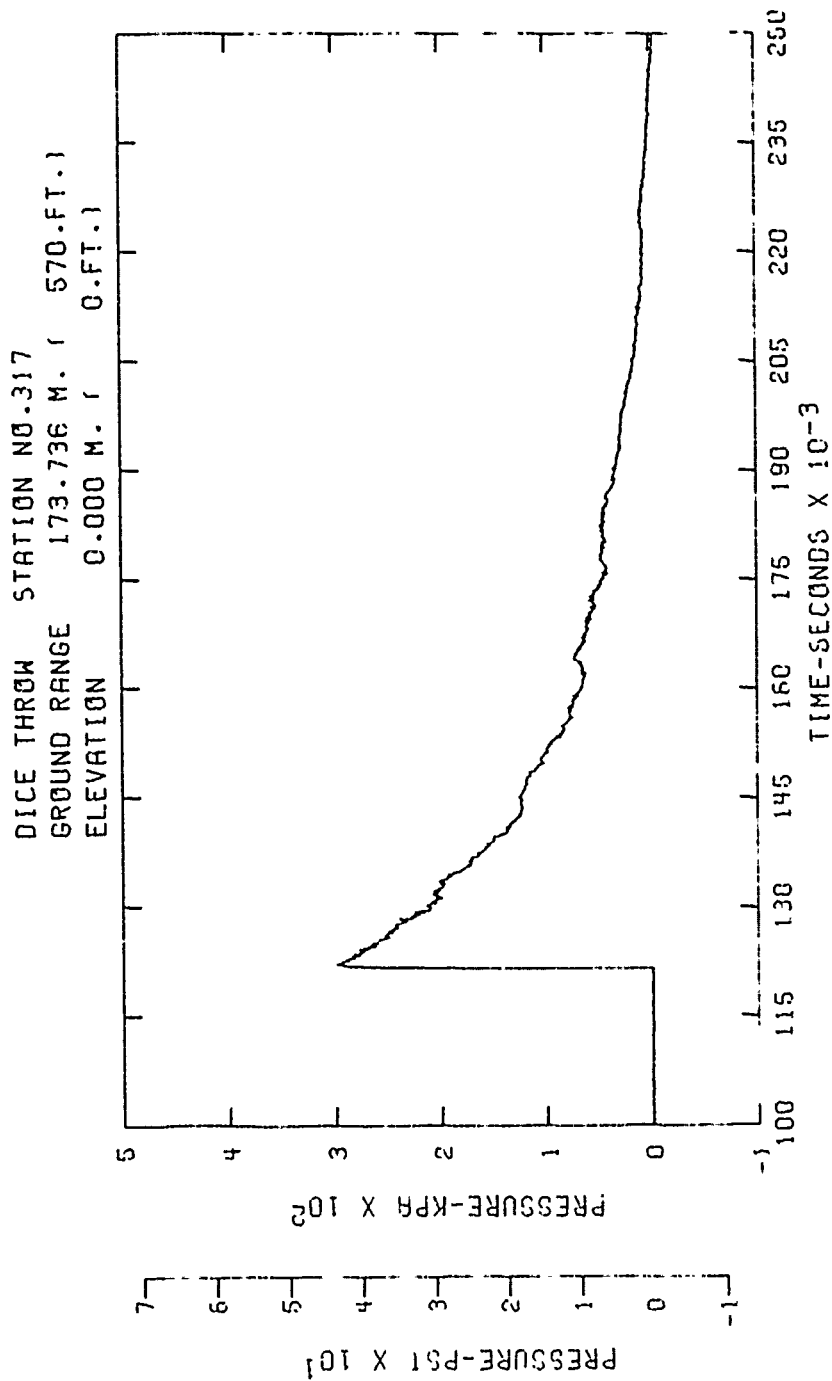


Figure C9. Incident pressure-time history - Station 317

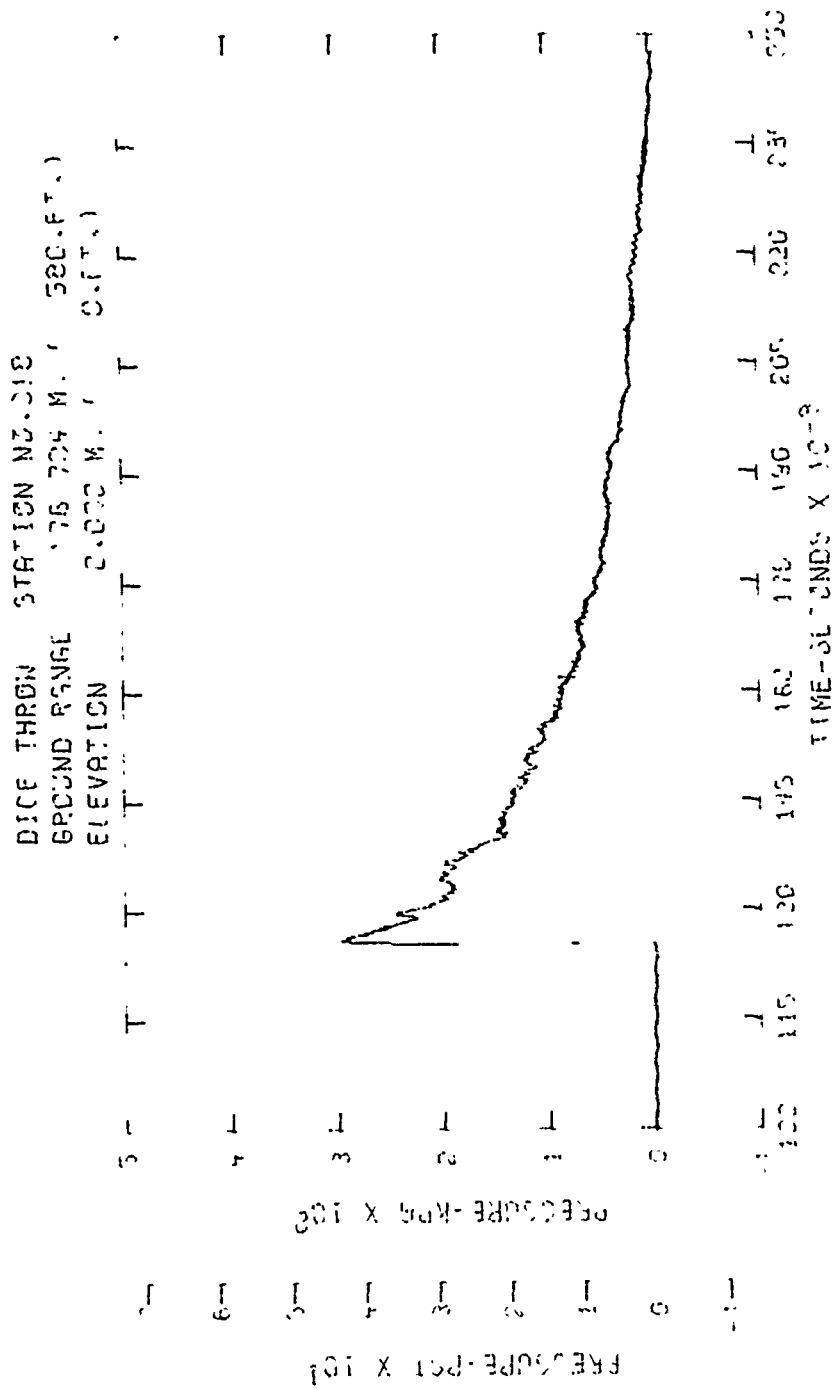


Figure C10. Incident pressure-time history - Station 318



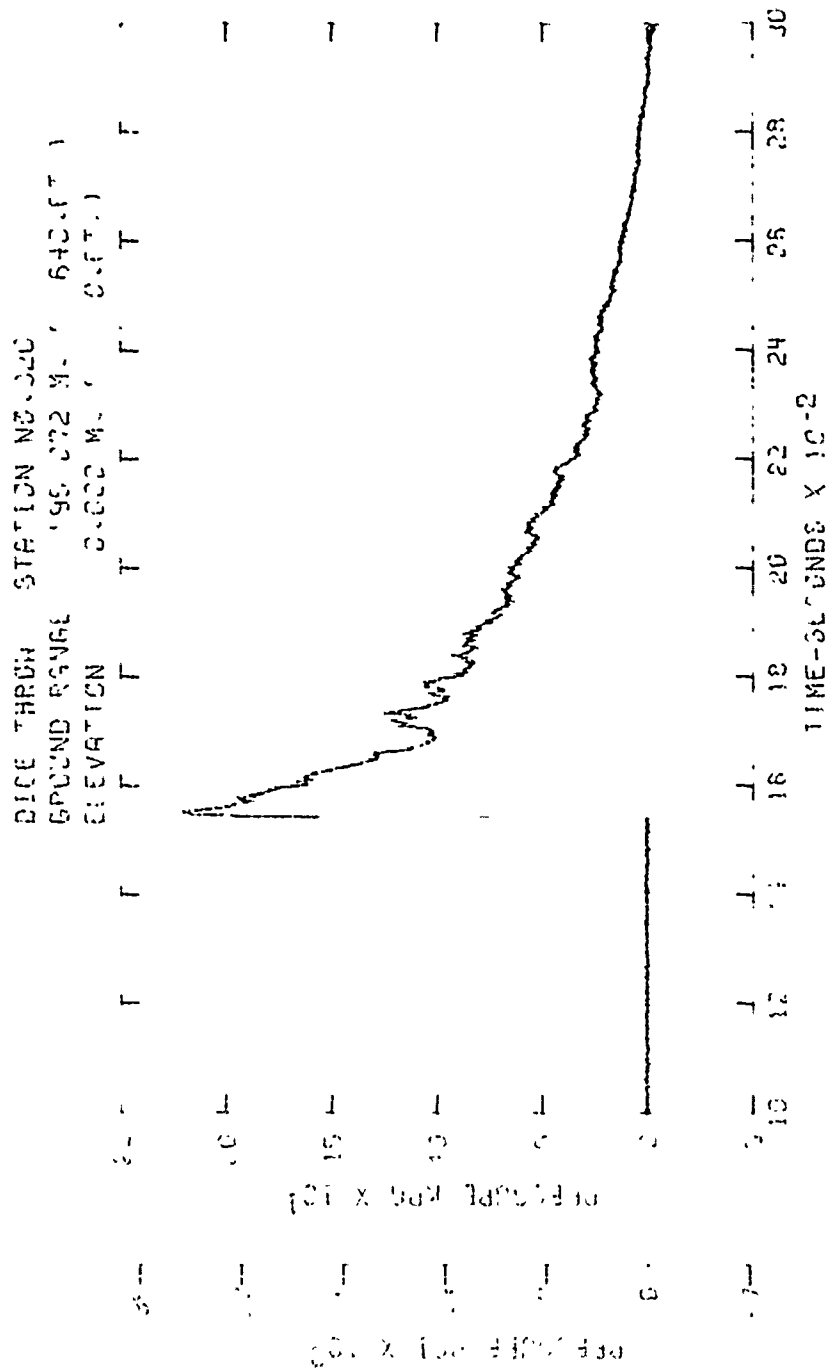


Figure C11. Incident pressure-time history - Station 320

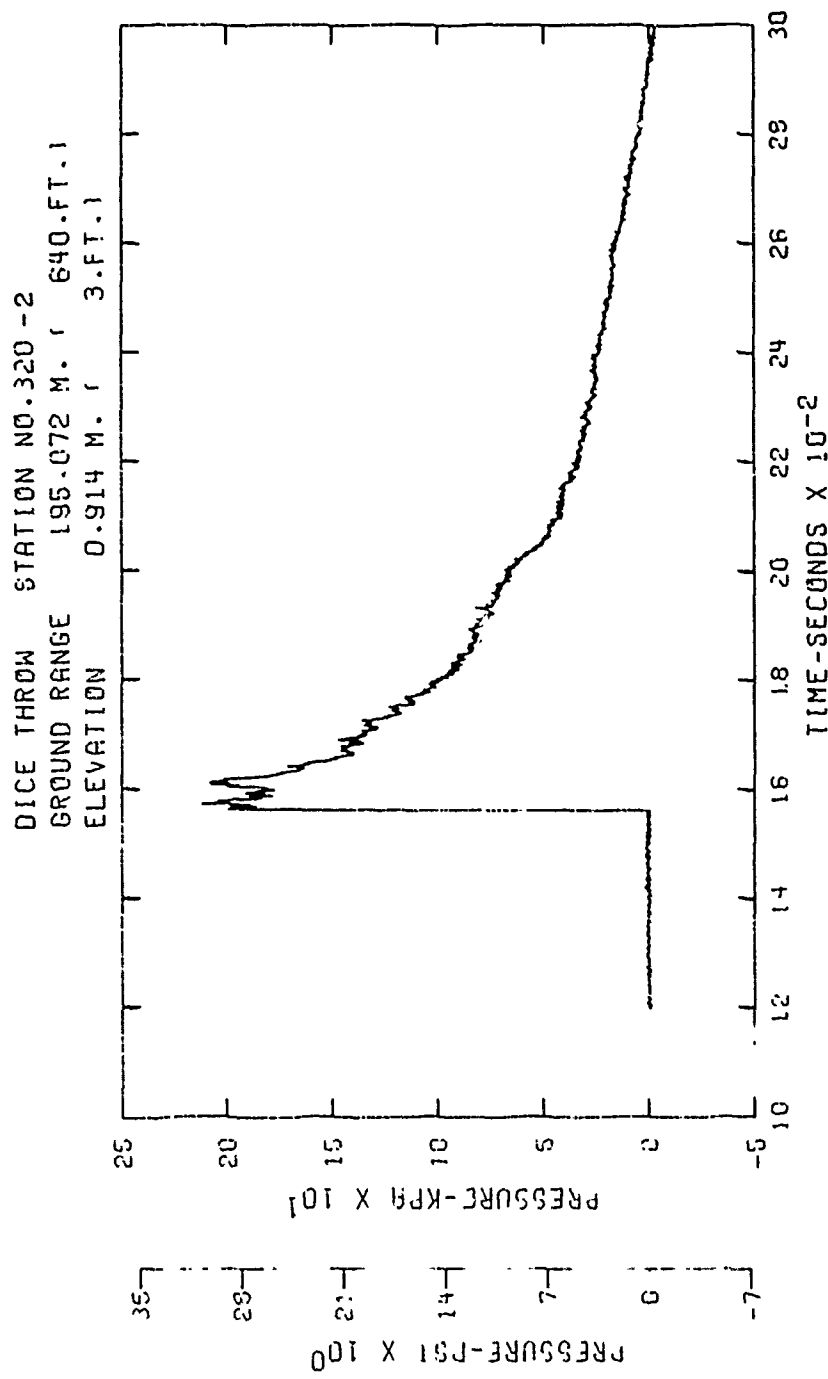


Figure C12. Incident pressure-time history - Station 320-2

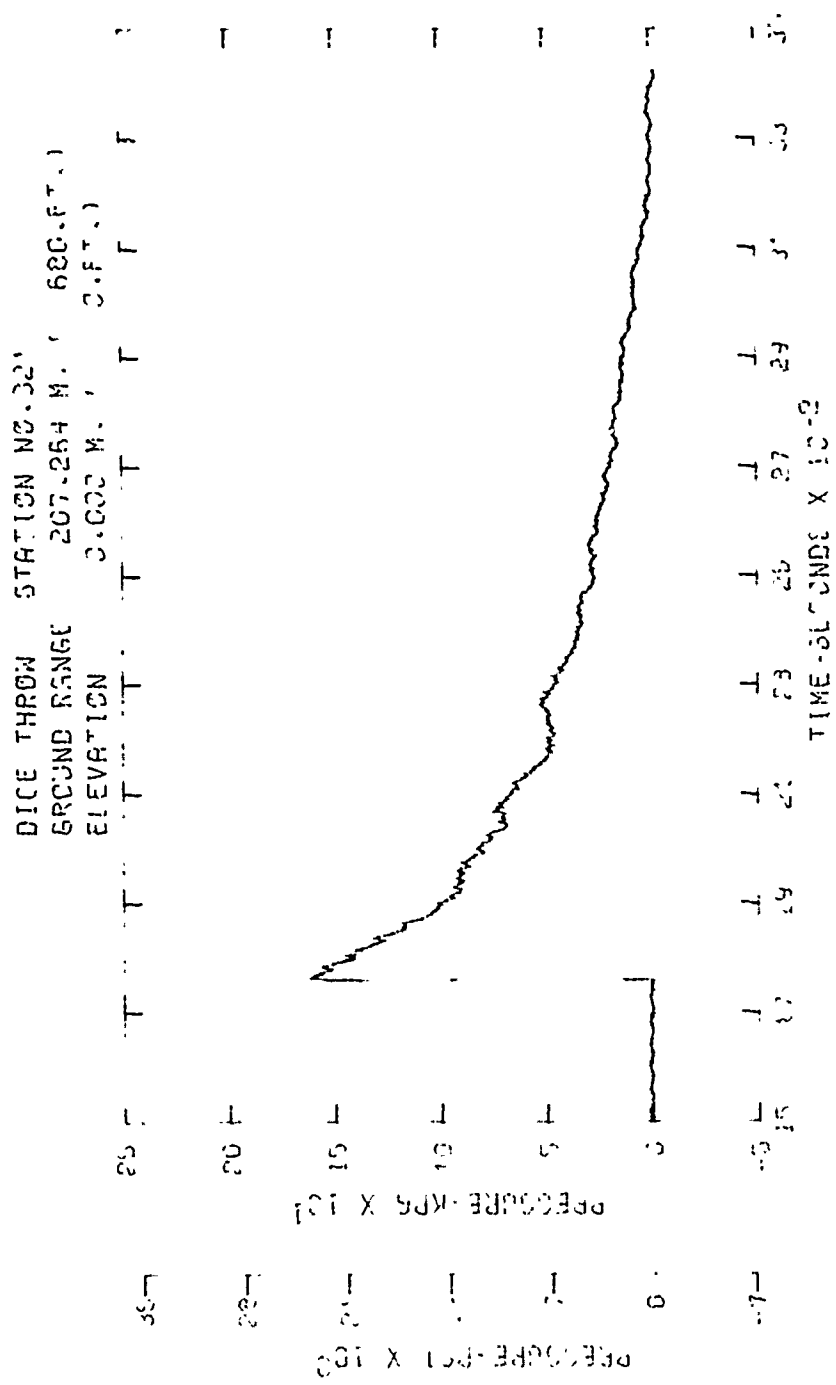


Figure C13. Incident pressure-time history - Station 321

DICE THROW STATION NO. 321-2  
 GROUND RANGE 207.264 M. ( 680-FT.)  
 ELEVATION 0.000 M. ( 0-FT.)

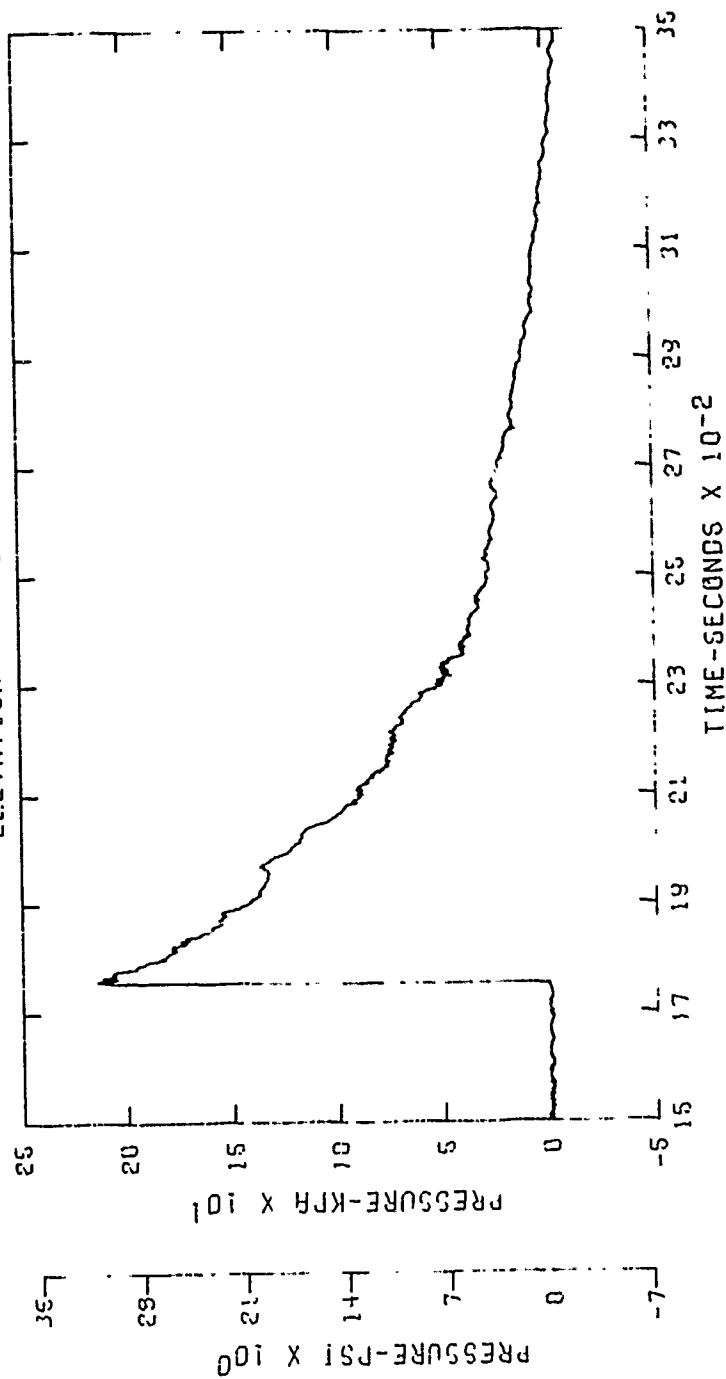


Figure C14. Incident pressure-time history - Station 321-2

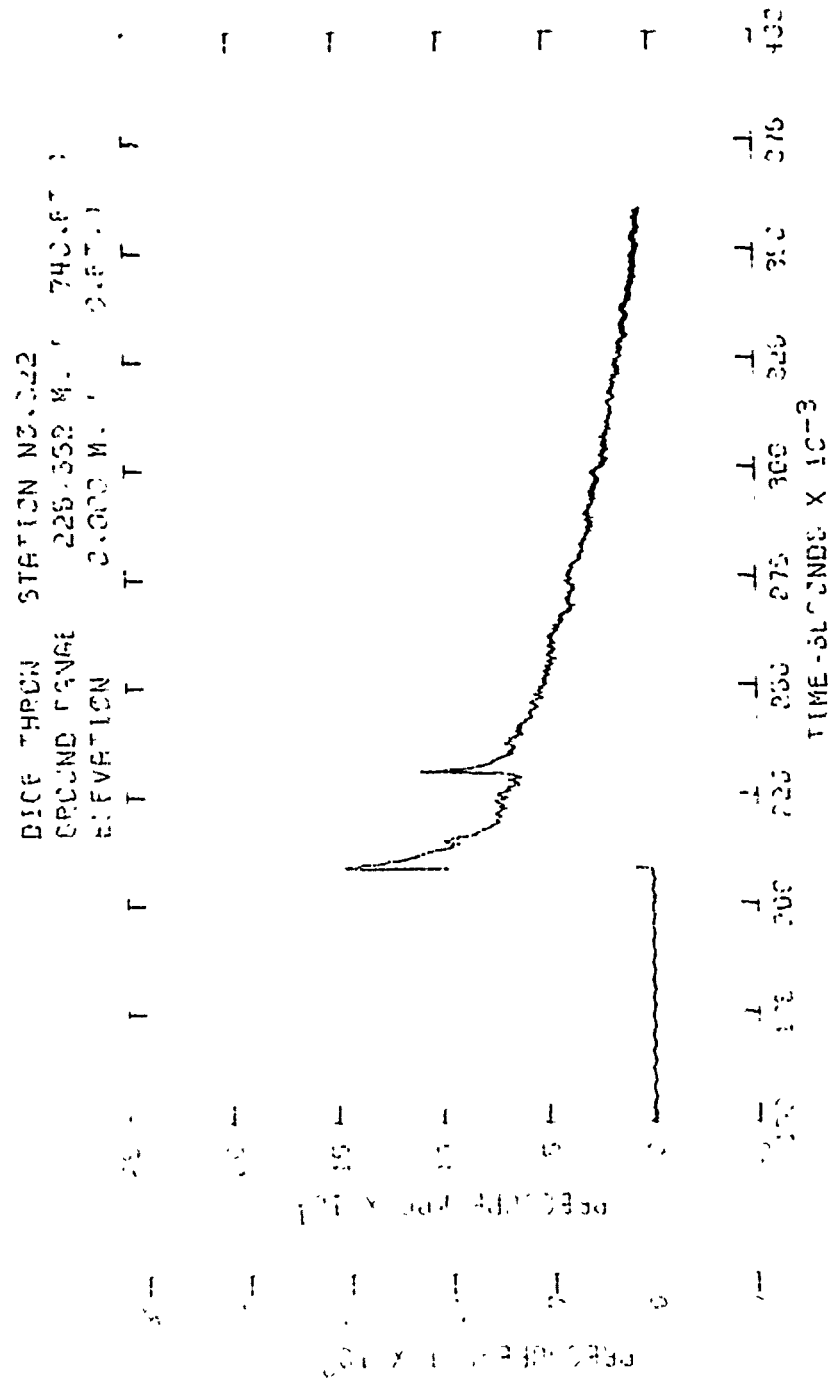


Figure C15. Incident pressure-time history - Station 322

DICE THROW STATION NO. 322-2  
 GROUND RANGE 225-552 M. ( 740.F.T.)  
 ELEVATION 0.914 M. ( 3.F.T.)

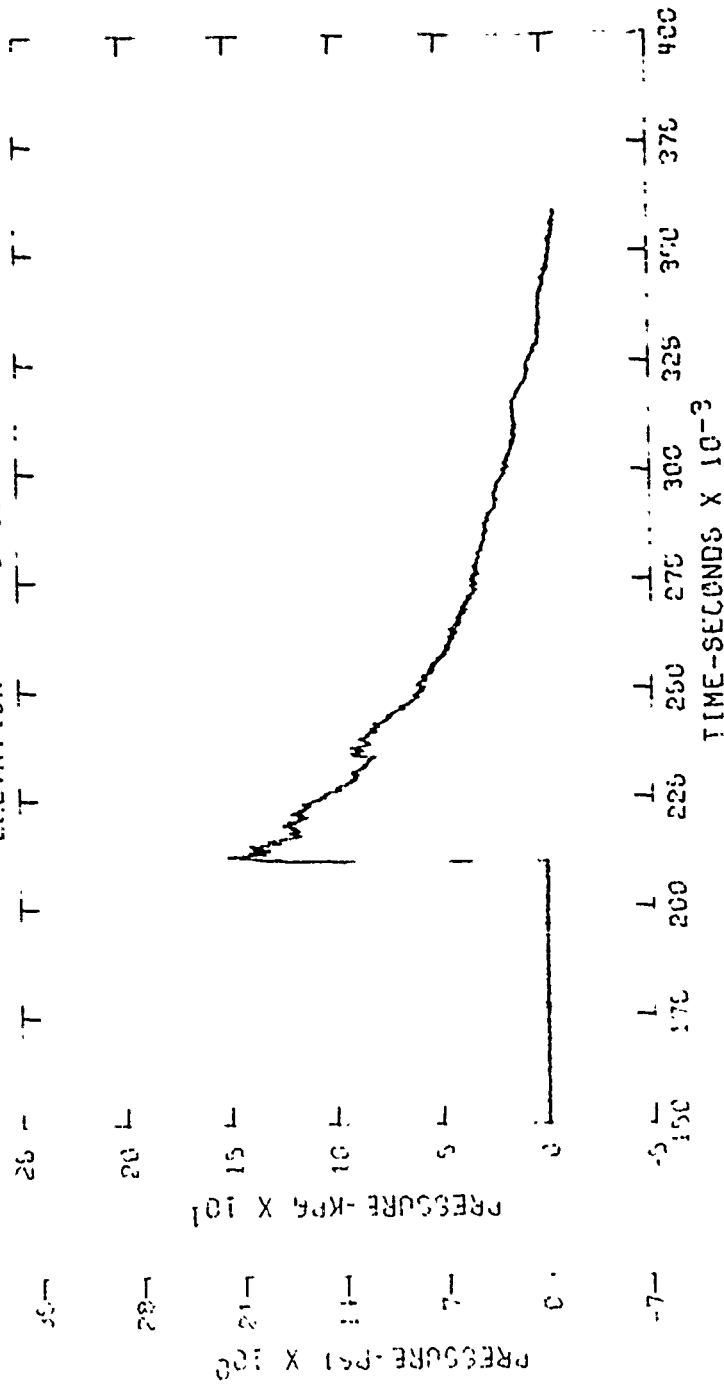


Figure C16. Incident pressure-time history - Station 322-2

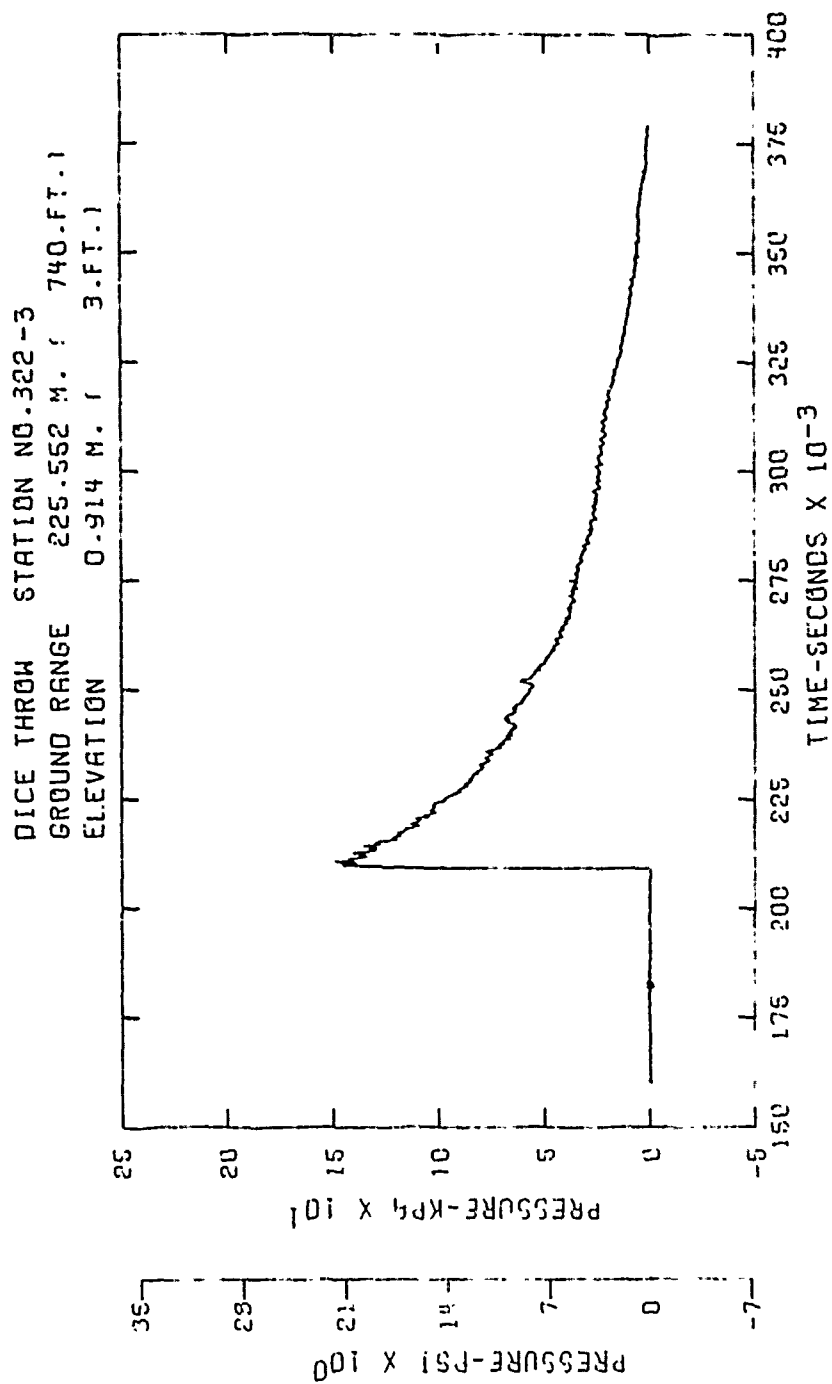


Figure C17. Incident pressure-time history - Station 322-3

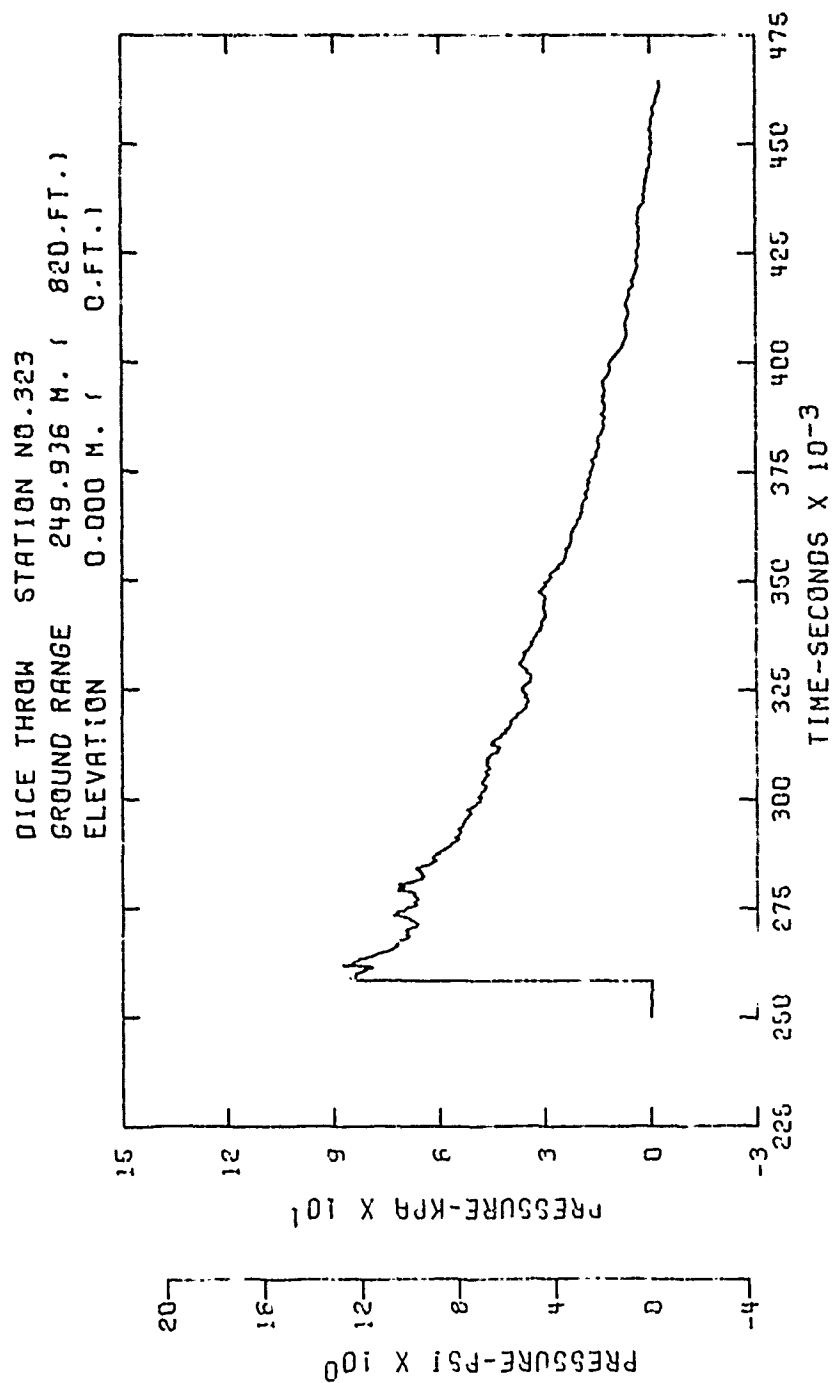


Figure C18. Incident pressure-time history - Station 323



DICE THROW STATION NO. 323-2  
 GROUND RANGE 249.436 M. ( 820.FT.)  
 ELEVATION 0.000 M. ( 0.FT.)

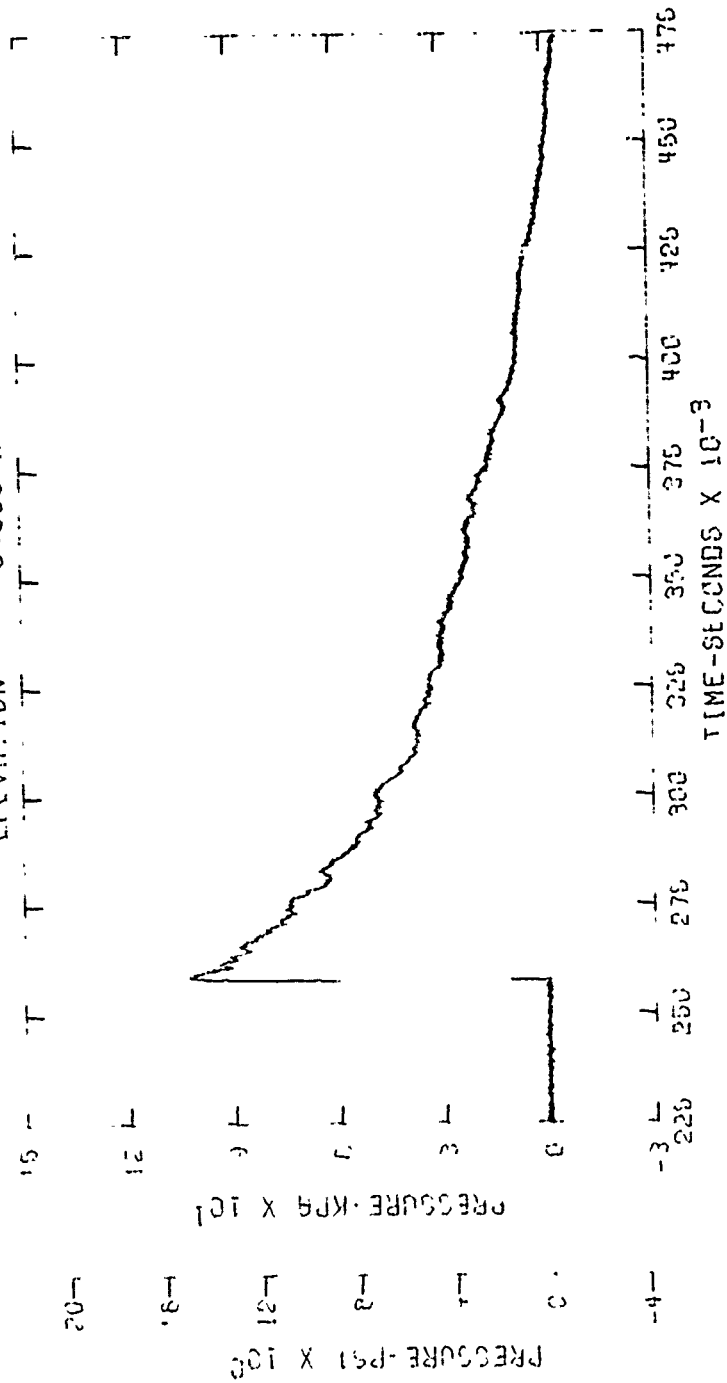


Figure C19. Incident pressure-time history - Station 323-2

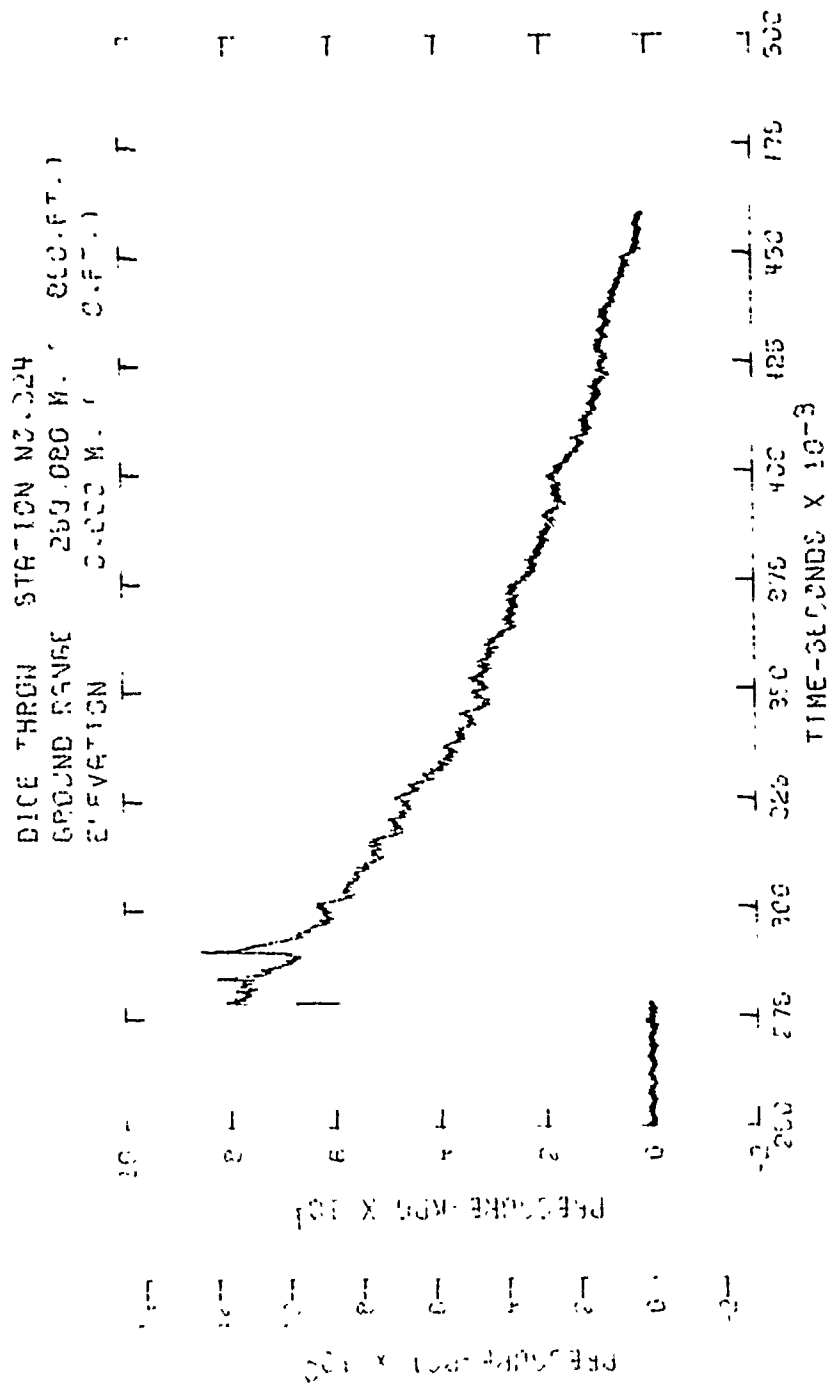


Figure C20. Incident pressure-time history - Station 324

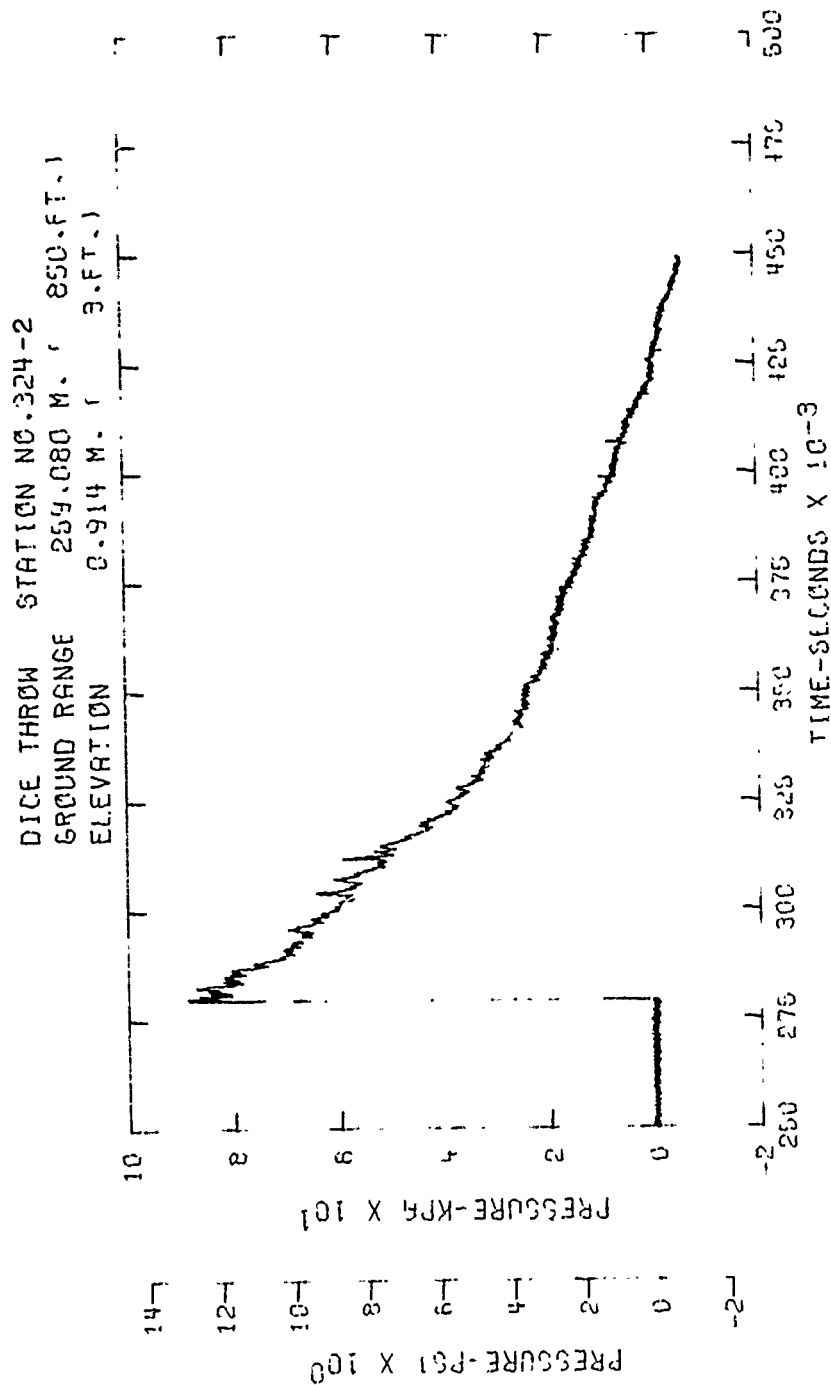


Figure C21. Incident pressure-time history - Station 324-2

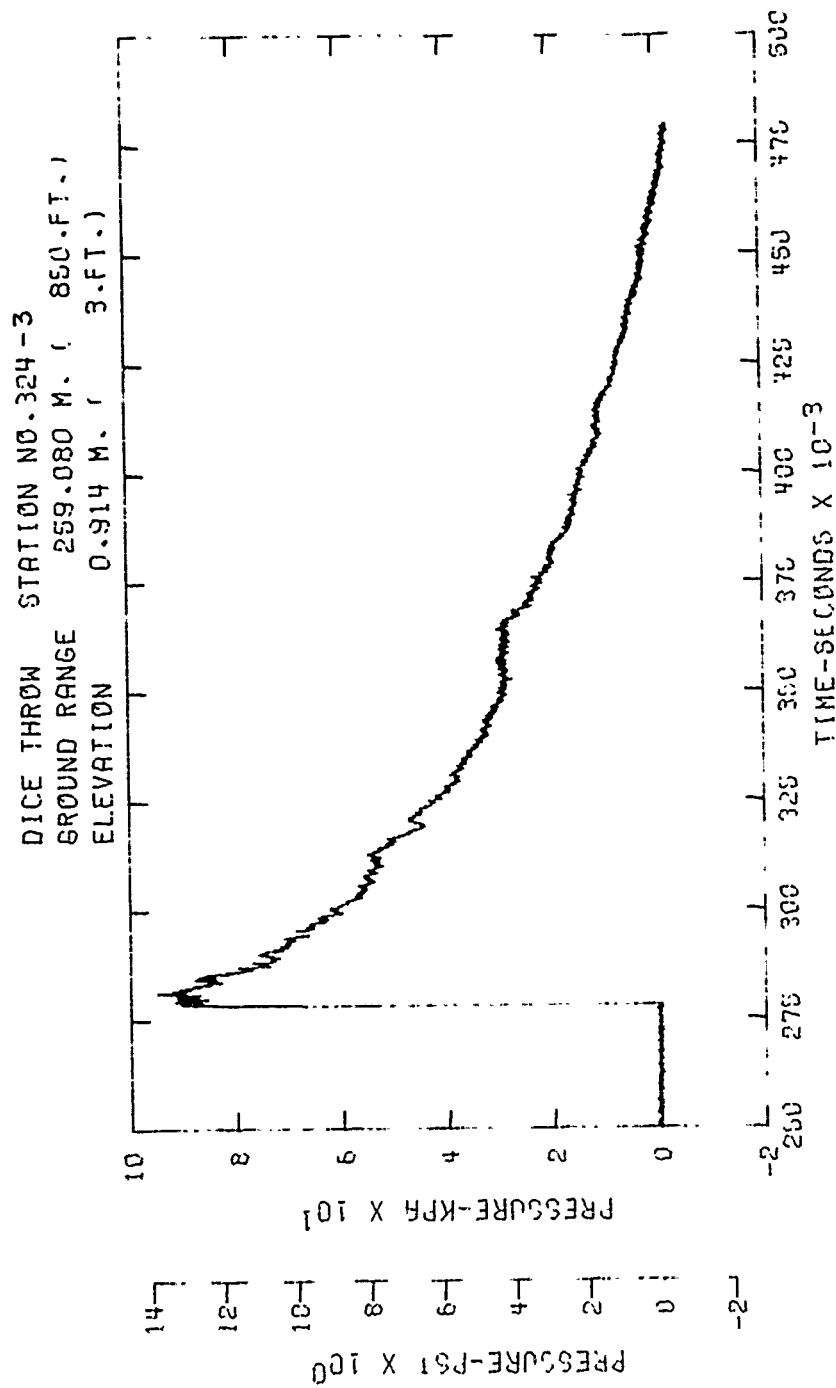


Figure C22. Incident pressure-time history - Station 324-3

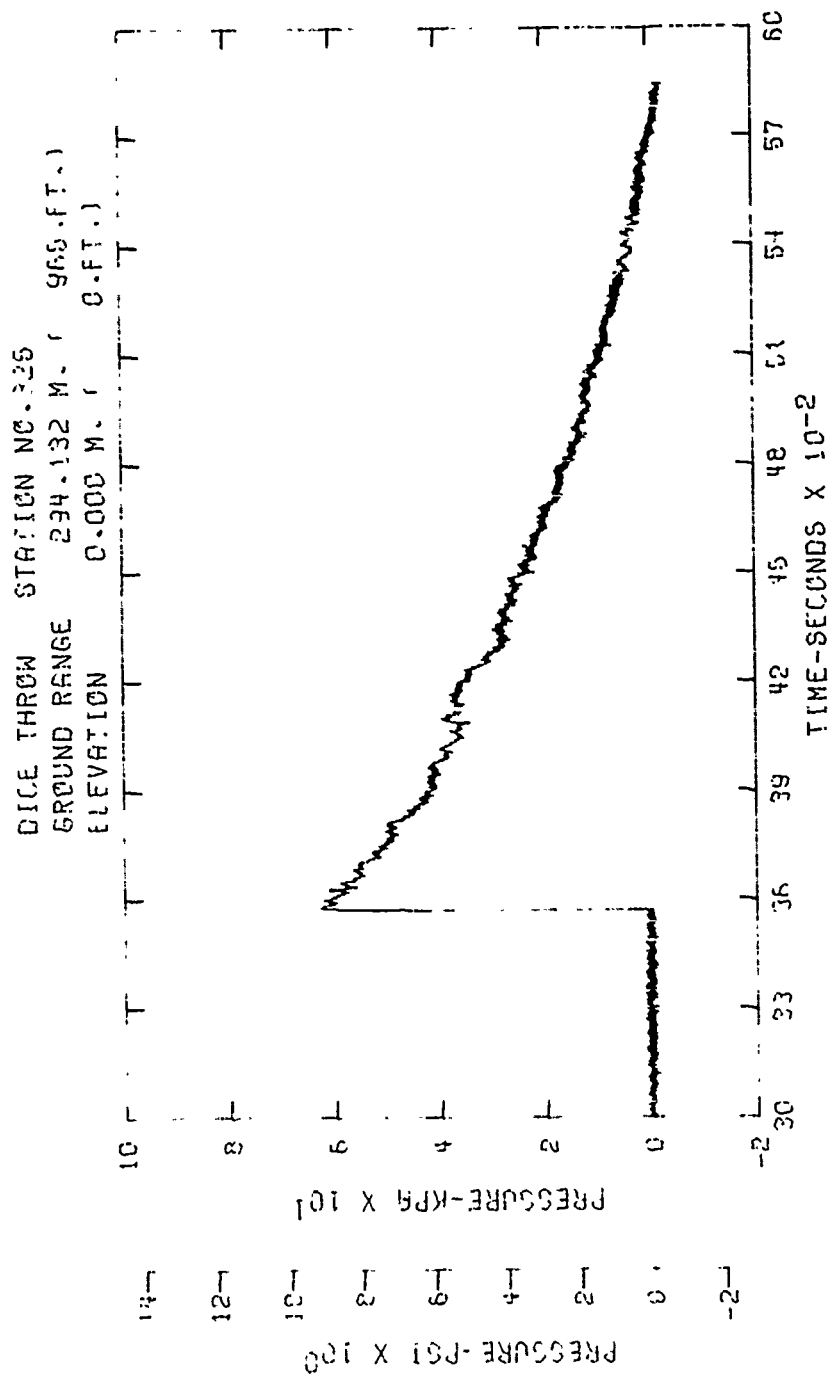


Figure C23. Incident pressure-time history - Station 325

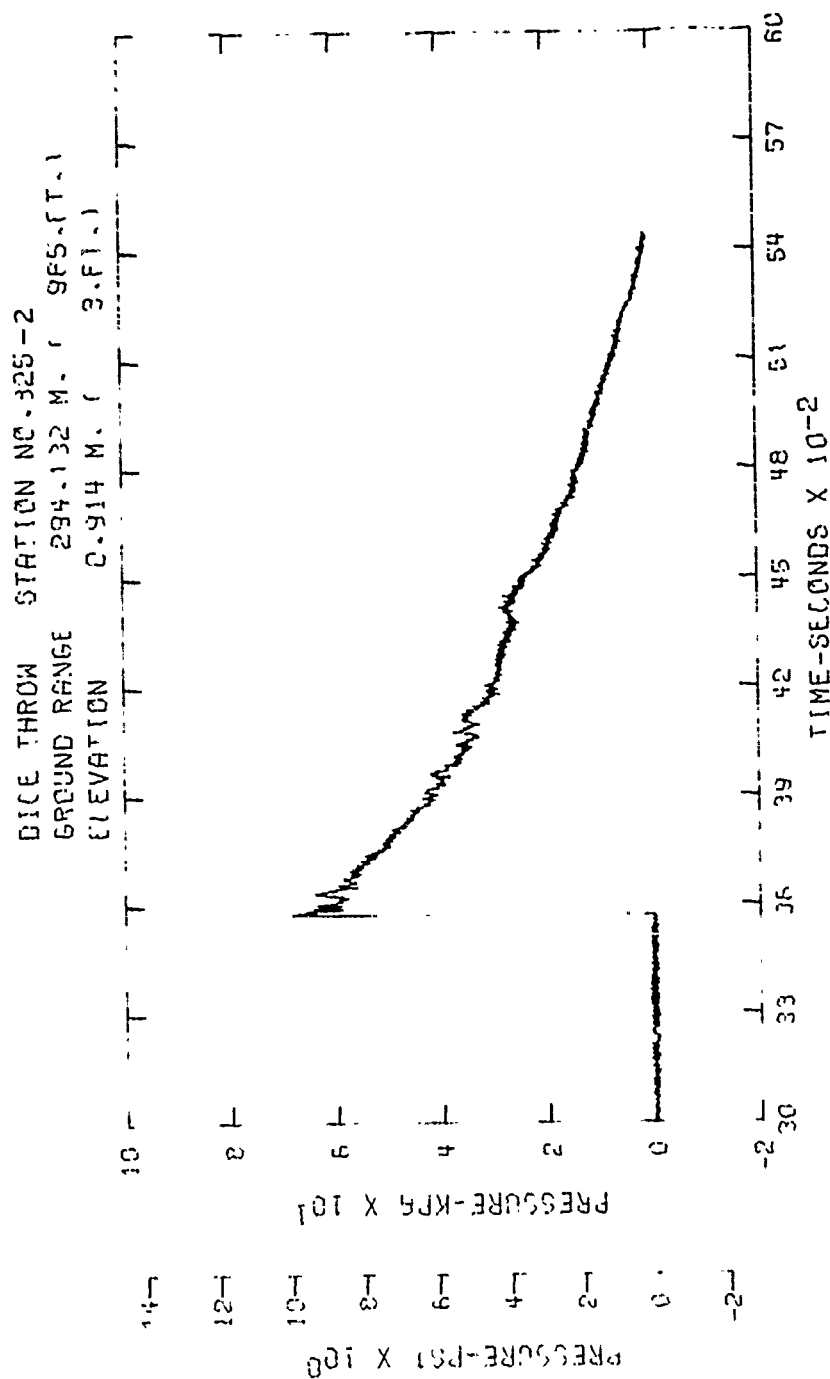


Figure C24. Incident pressure-time history - Station 325-2

DICE THROW STATION NO. 327  
 GROUND RANGE 320.040 M. ( 1050.FT.)  
 ELEVATION 0.000 M. ( 0.FT.)

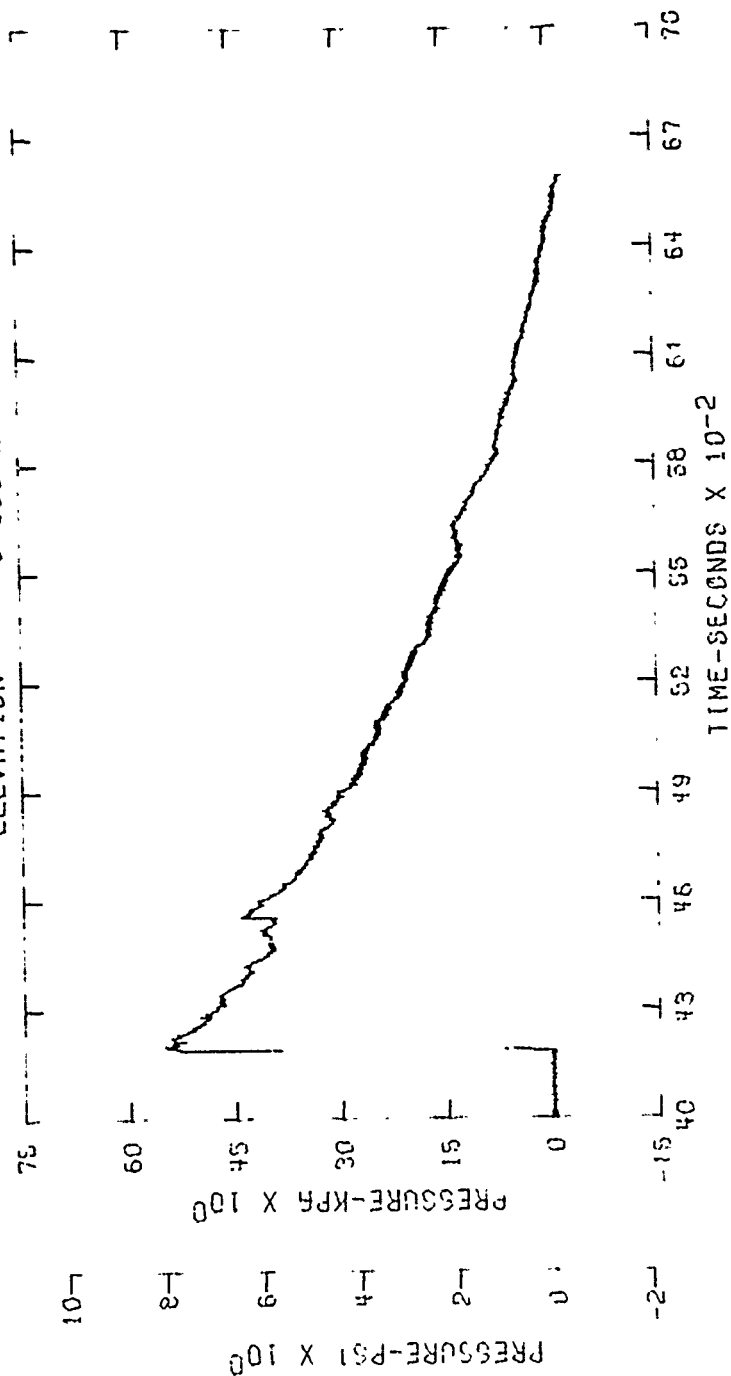


Figure C25. Incident pressure-time history - Station 327

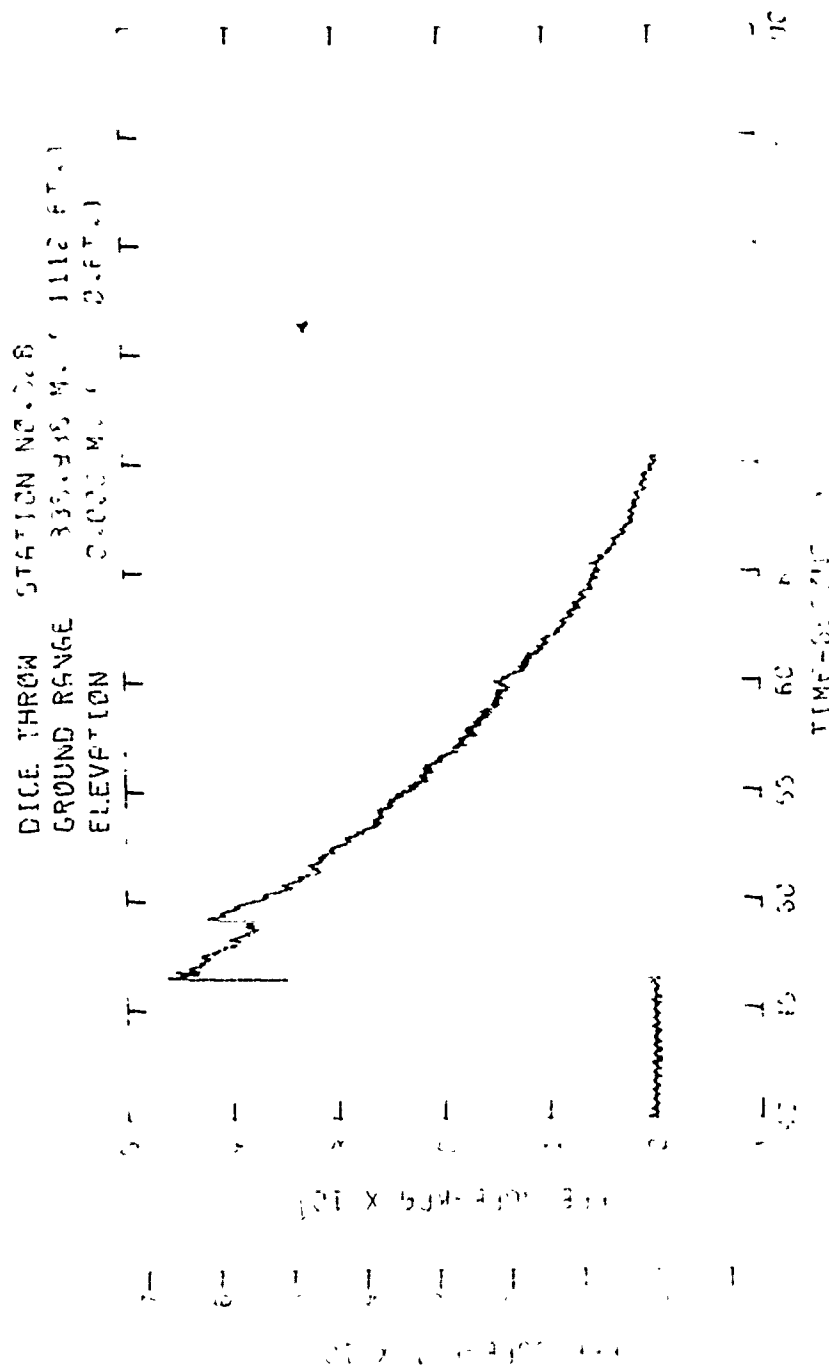


Figure C26. Incident pressure-time history - Station 328



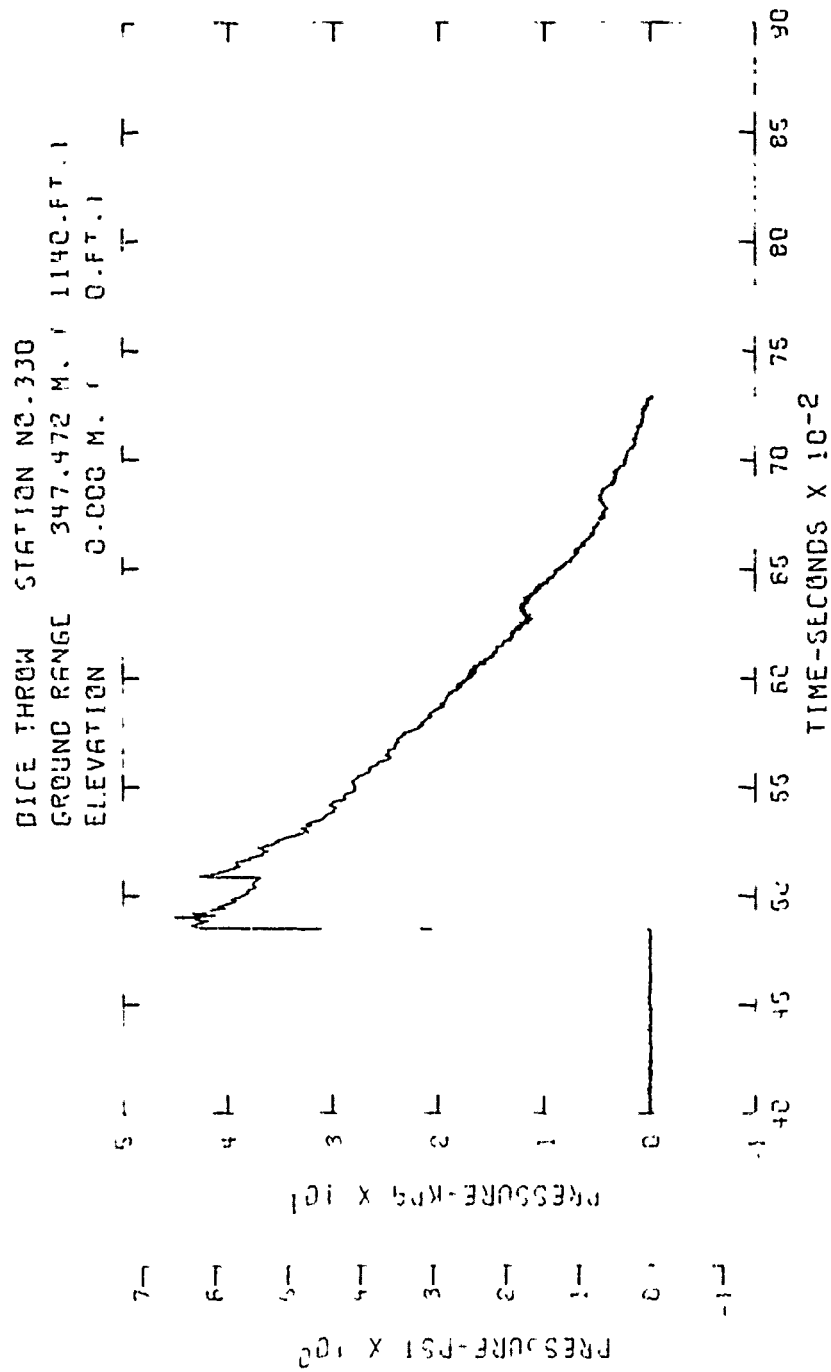


Figure C27. Incident pressure-time history - Station 330

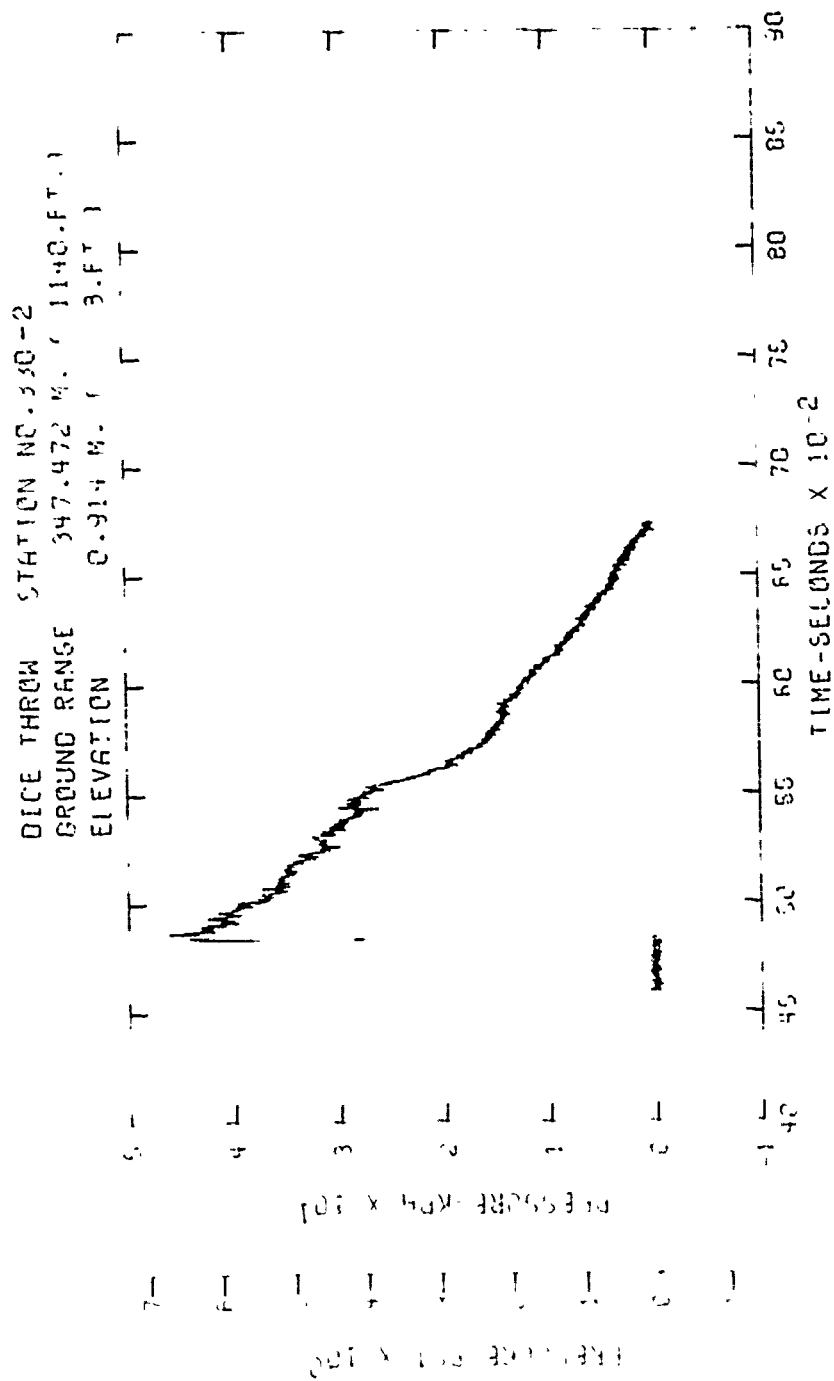


Figure C28. Incident pressure-time history - Station 330-2

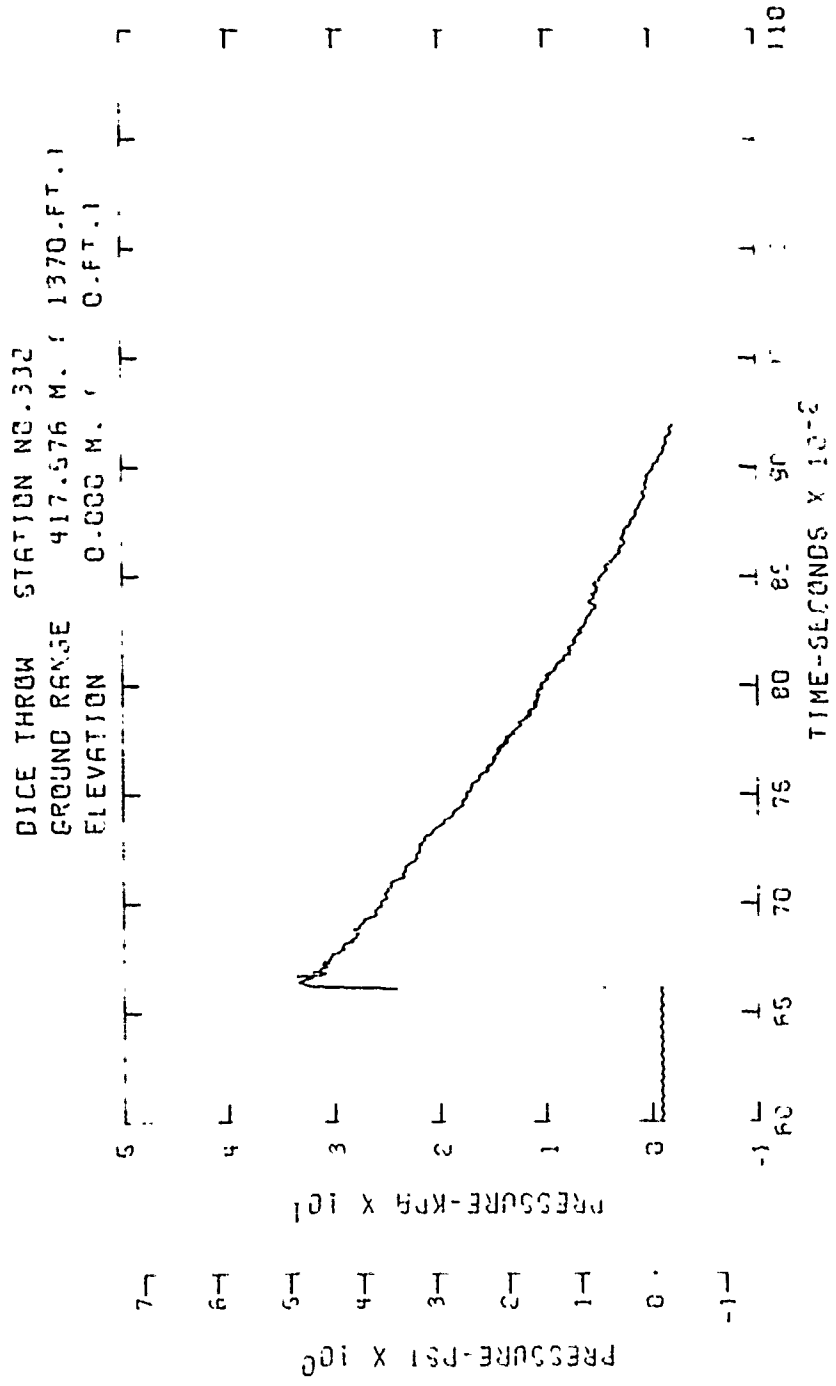


Figure C29. Incident pressure-time history - Station 332

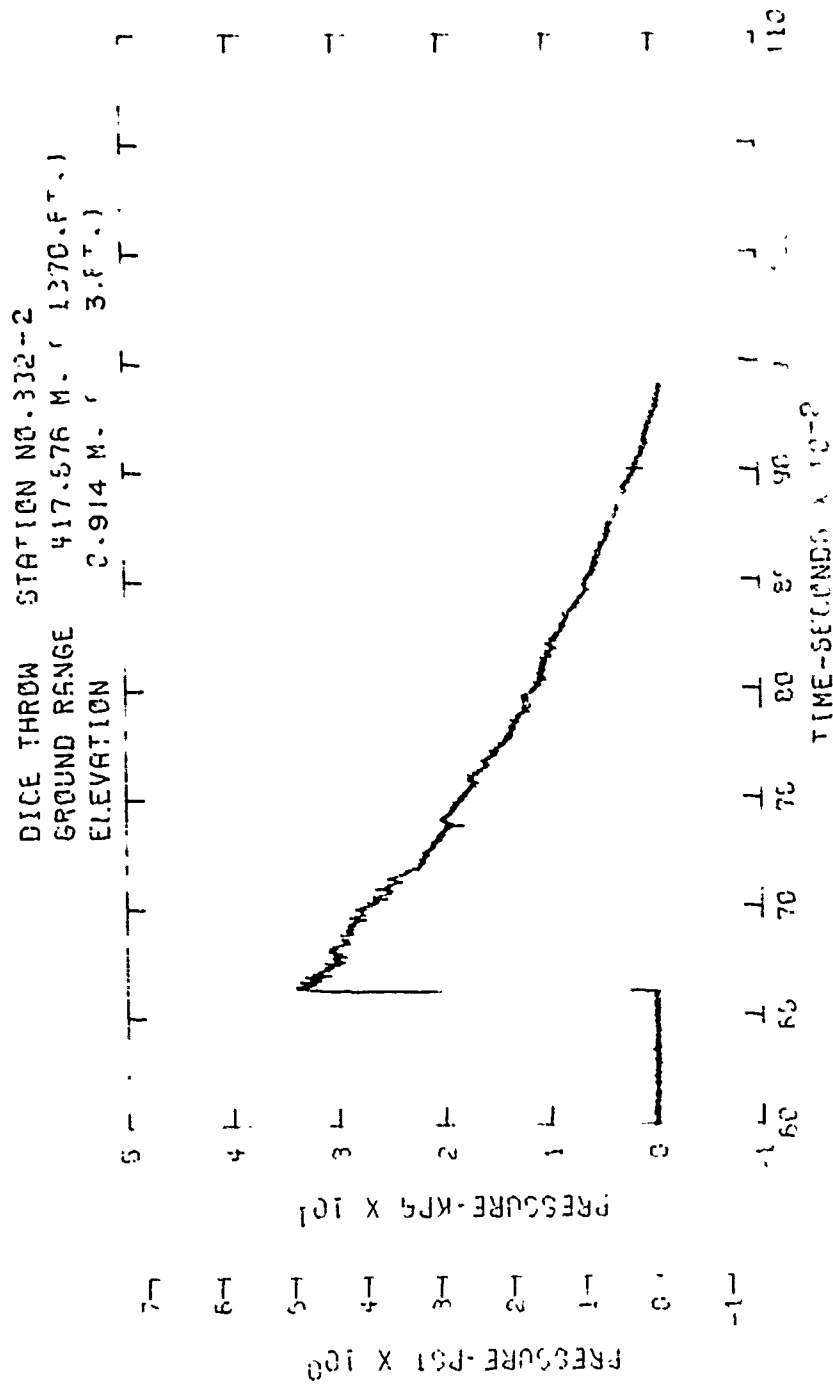


Figure C30. Incident pressure-time history - Station 332-2

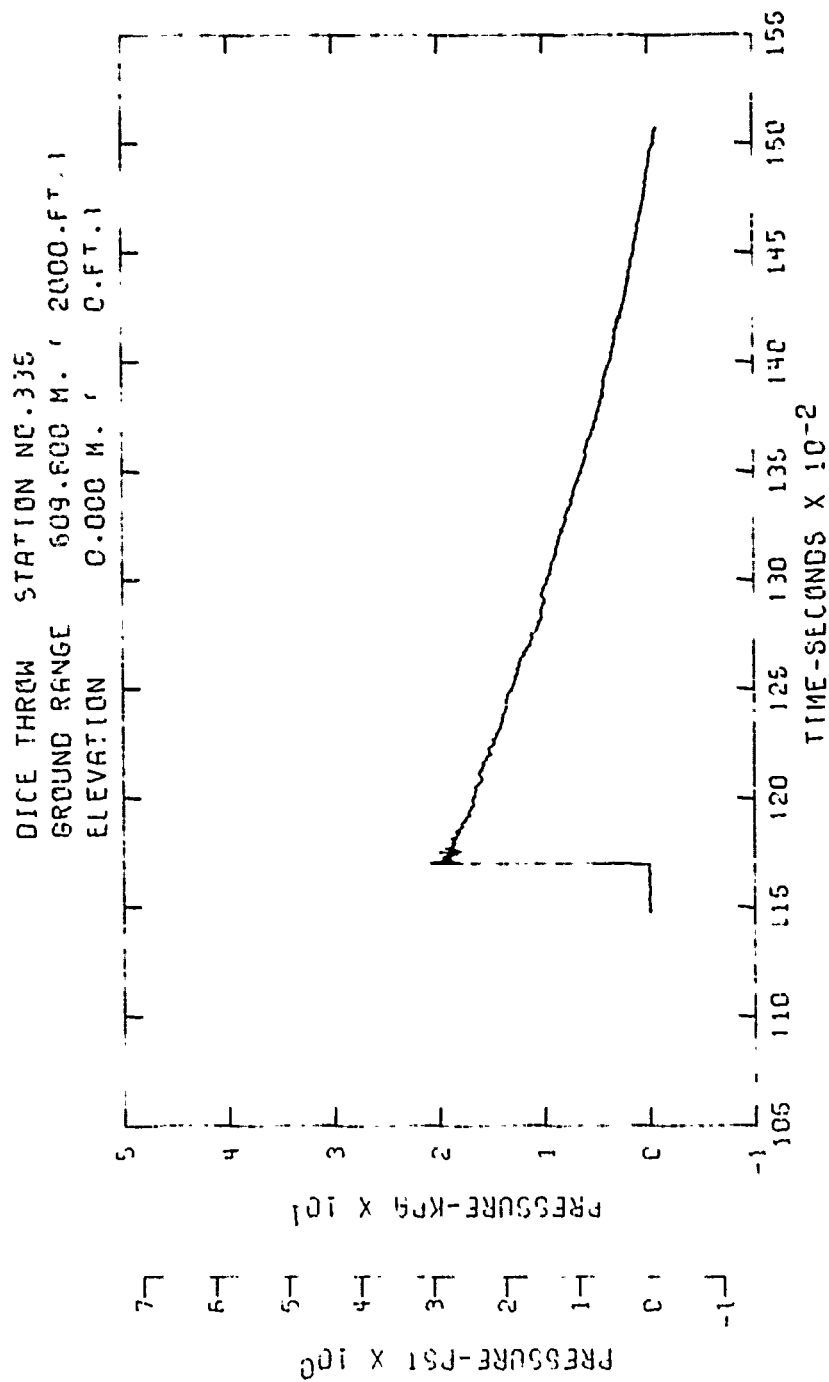


Figure C31. Incident pressure-time history - Station 335

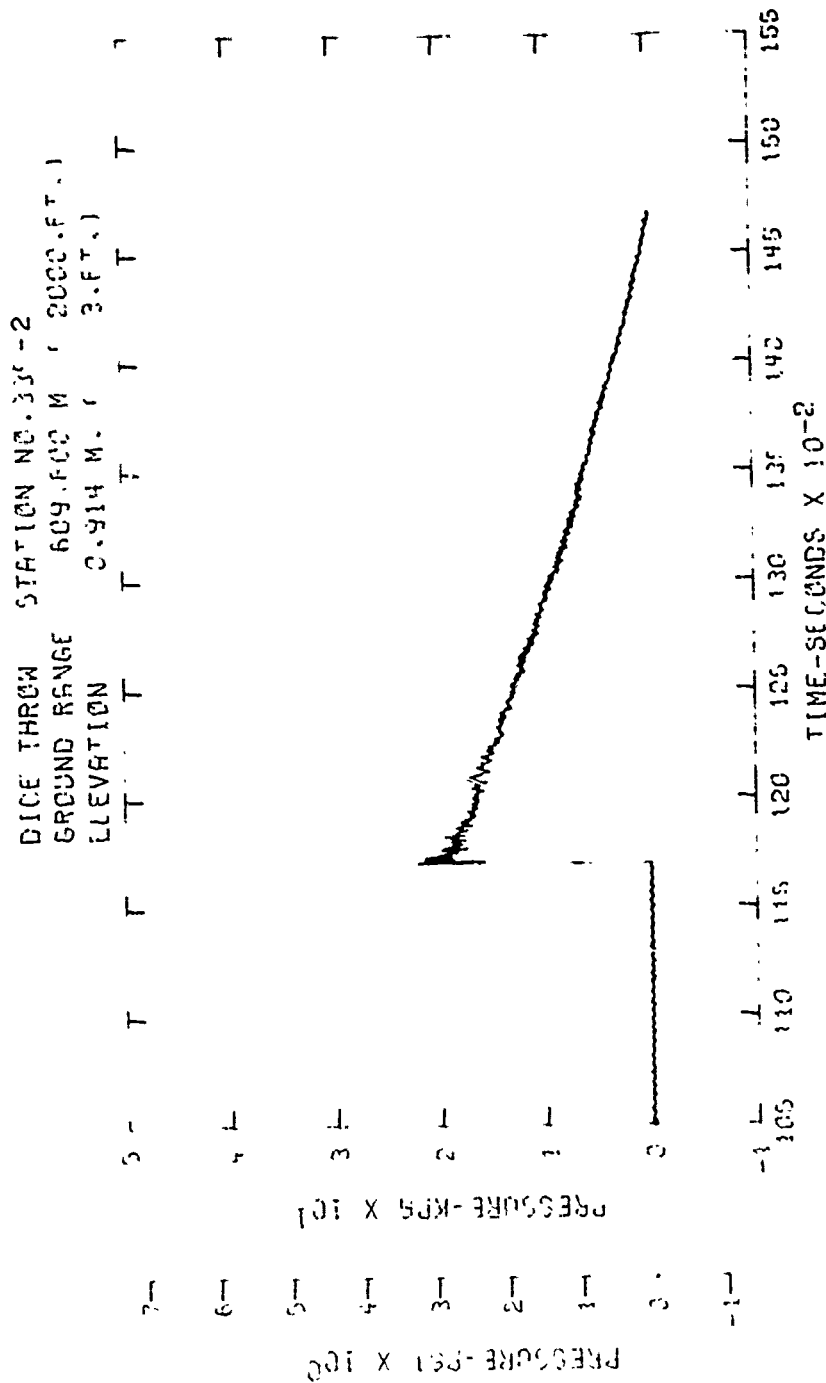


Figure C32. Incident pressure-time history - Station 335-2

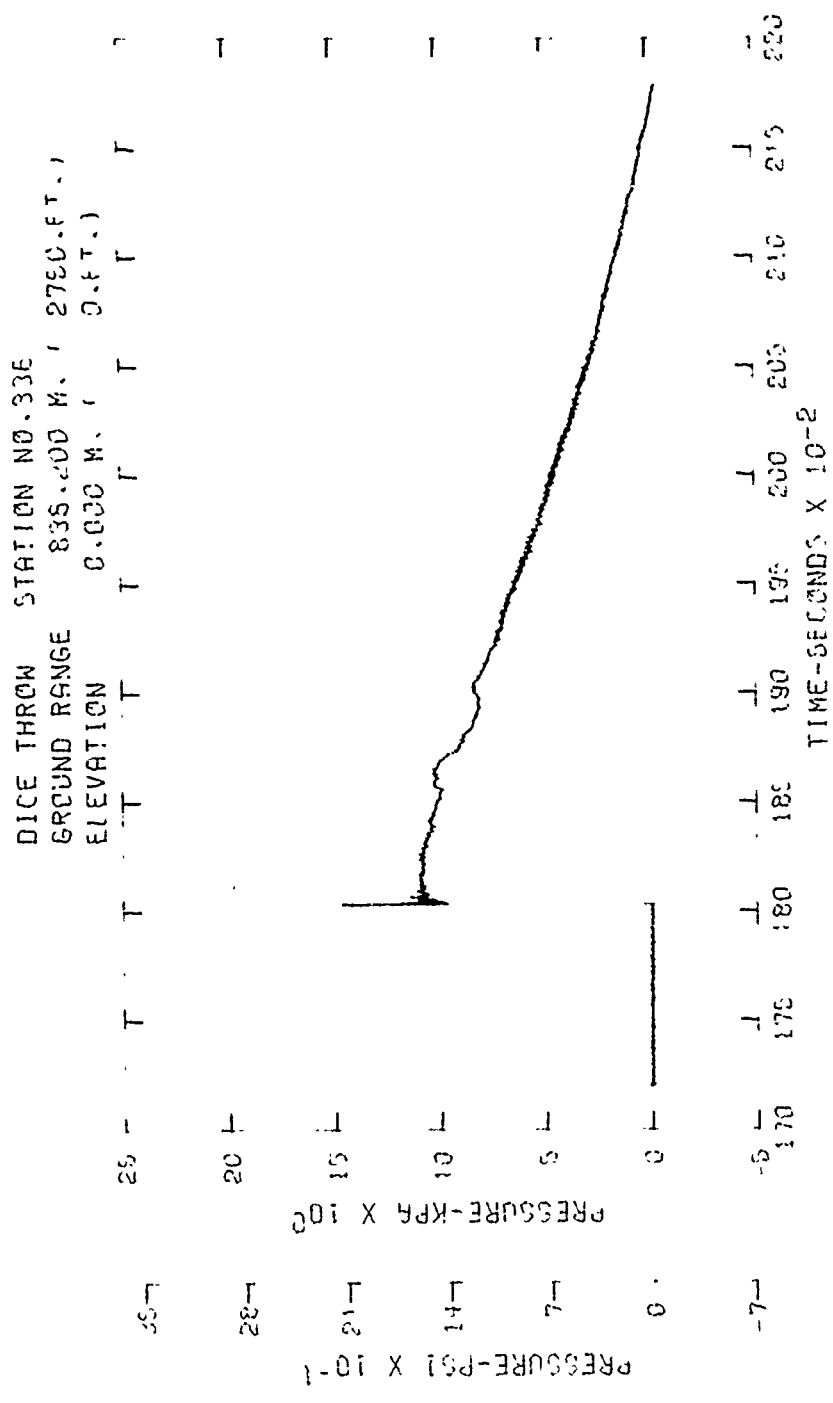


Figure C33. Incident pressure-time history - Station 336

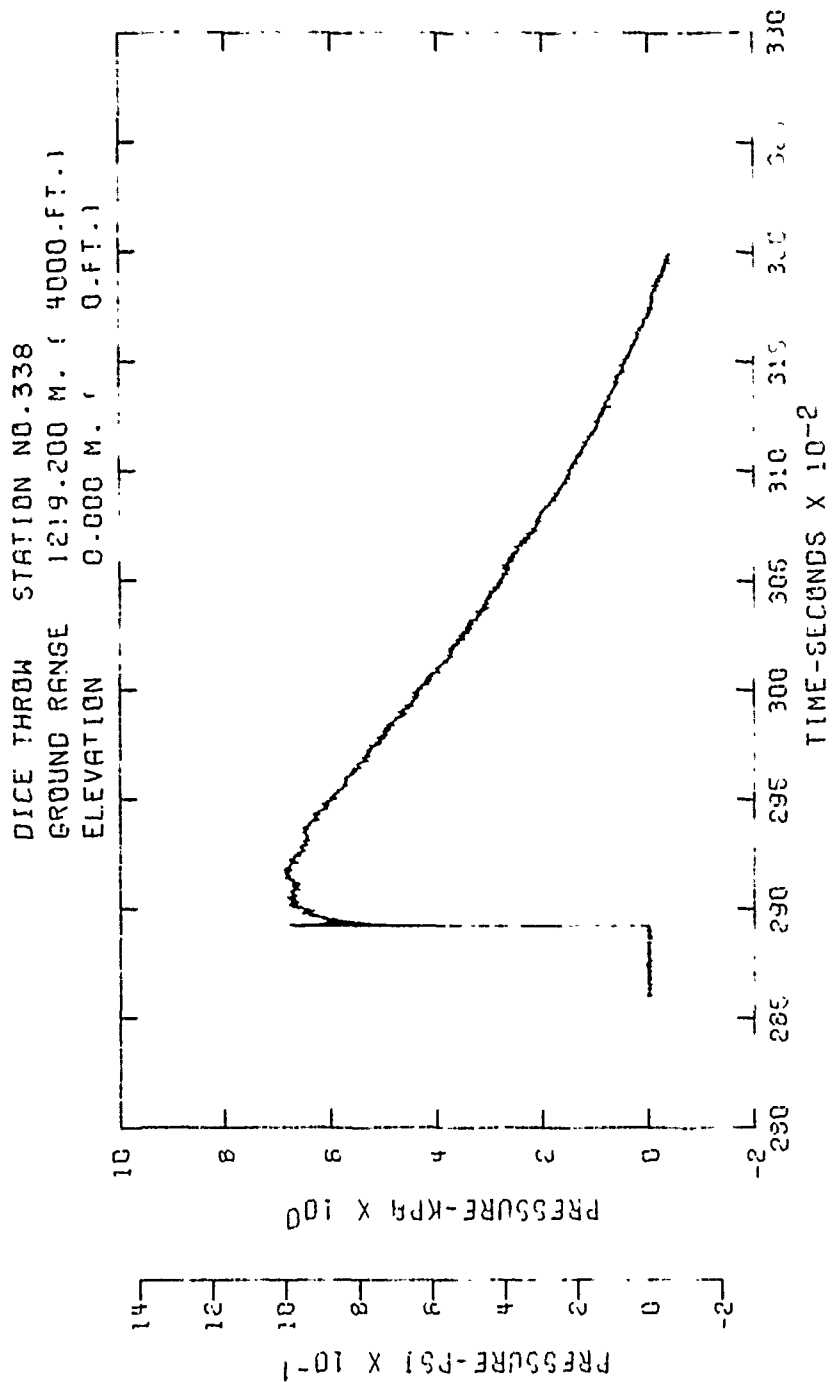


Figure C34. Incident pressure-time history - Station 338



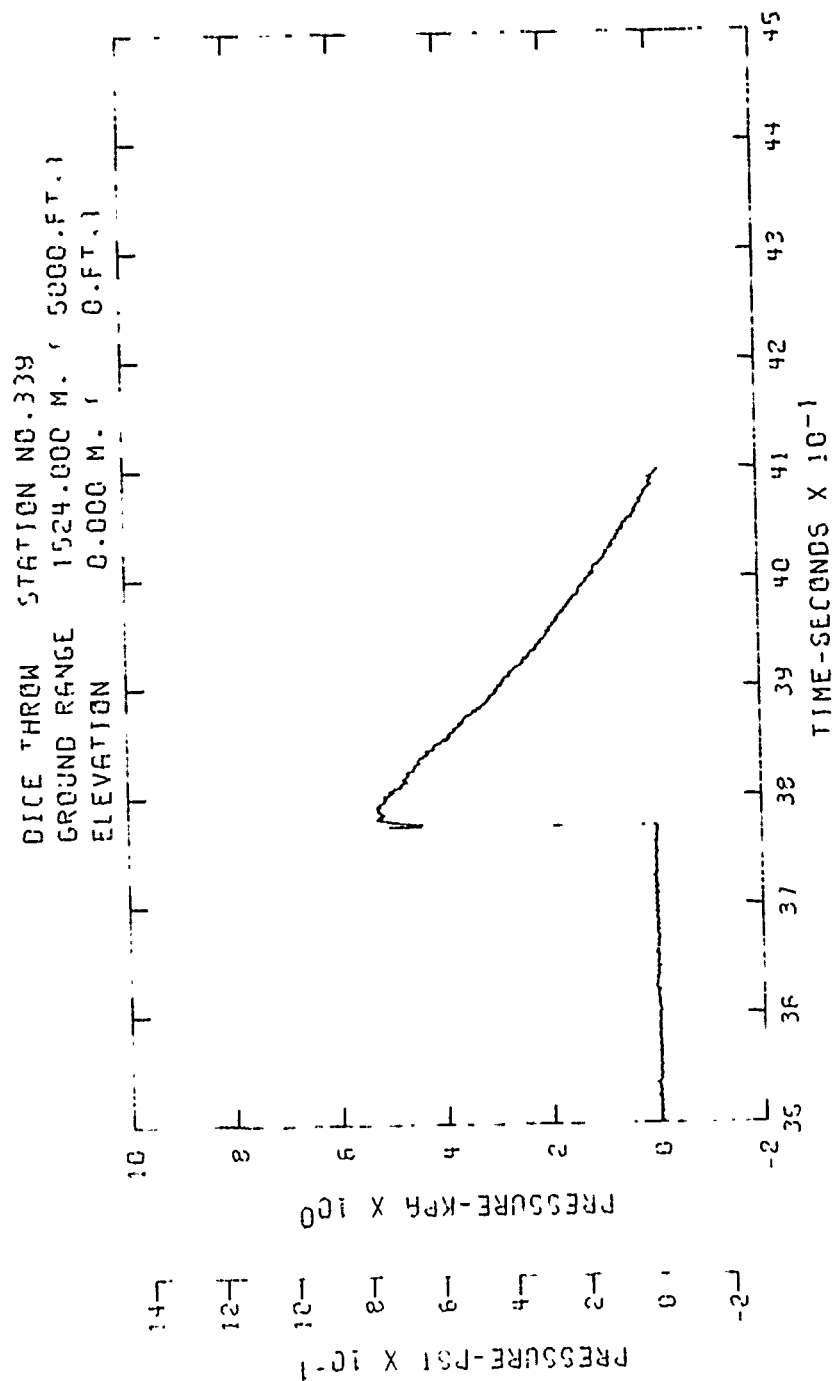


Figure C35. Incident pressure-time history - Station 339

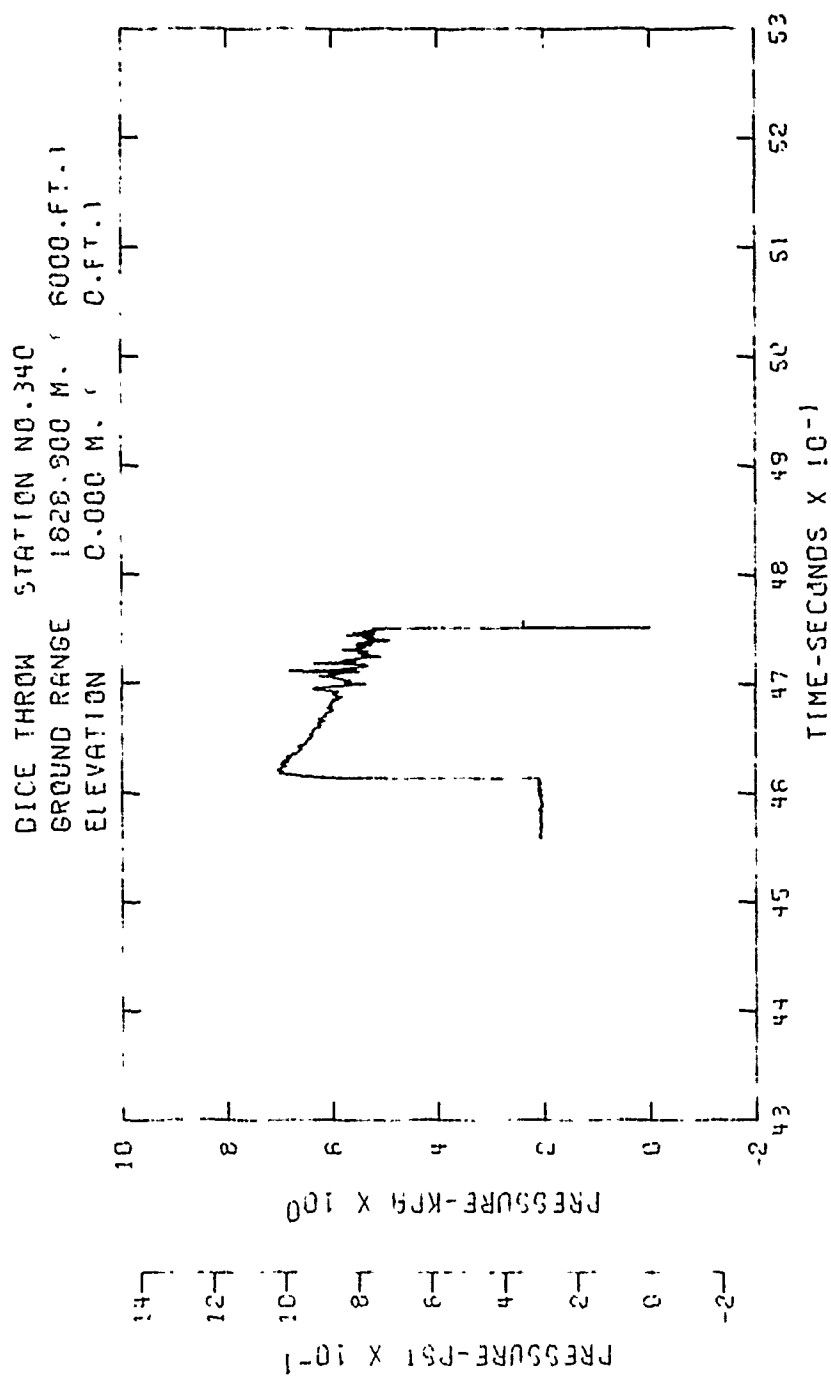


Figure C36. Incident pressure-time history - Station 340

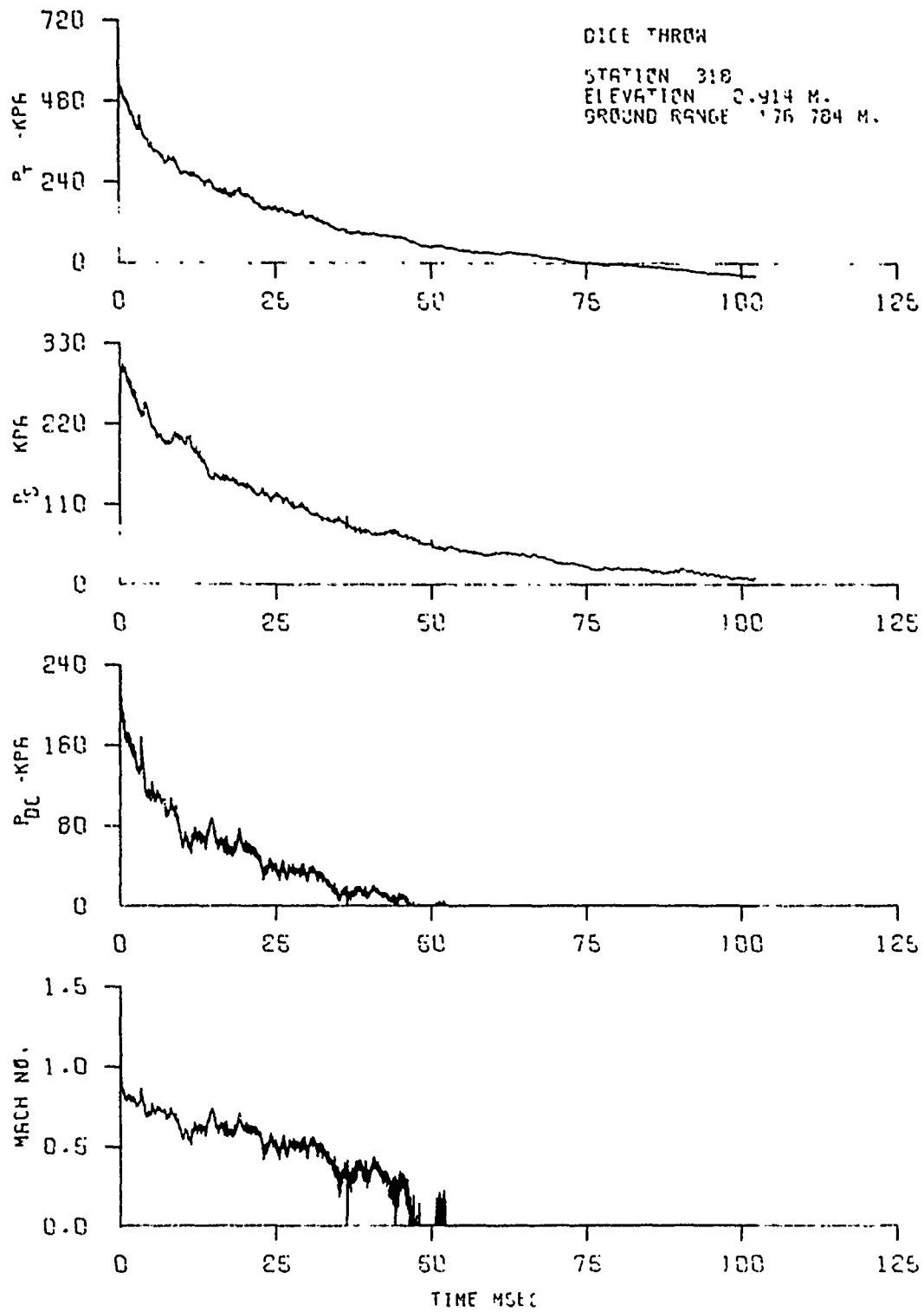


Figure C37. Dynamic pressure-time history - Station 318

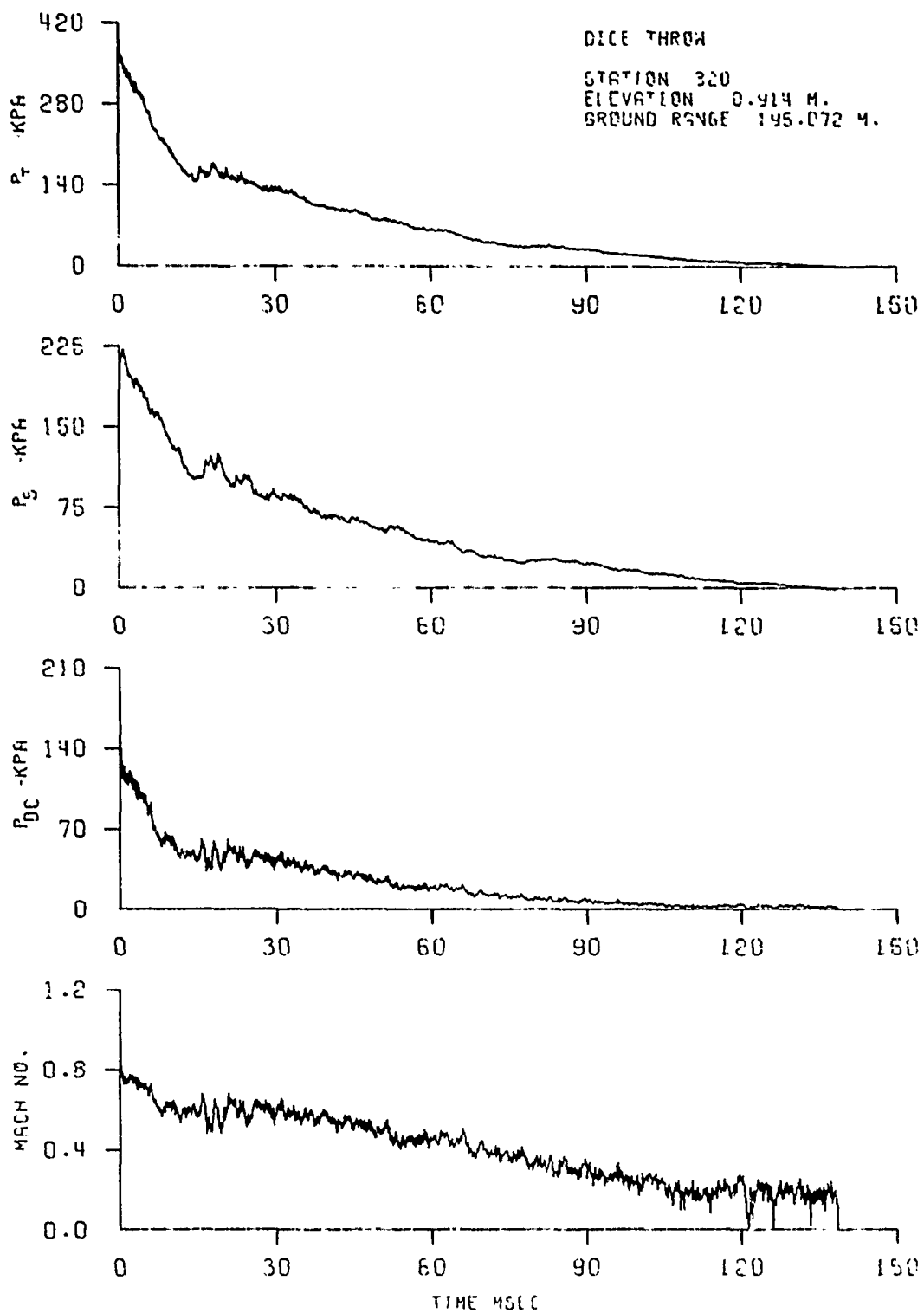


Figure C38. Dynamic pressure-time history - Station 320

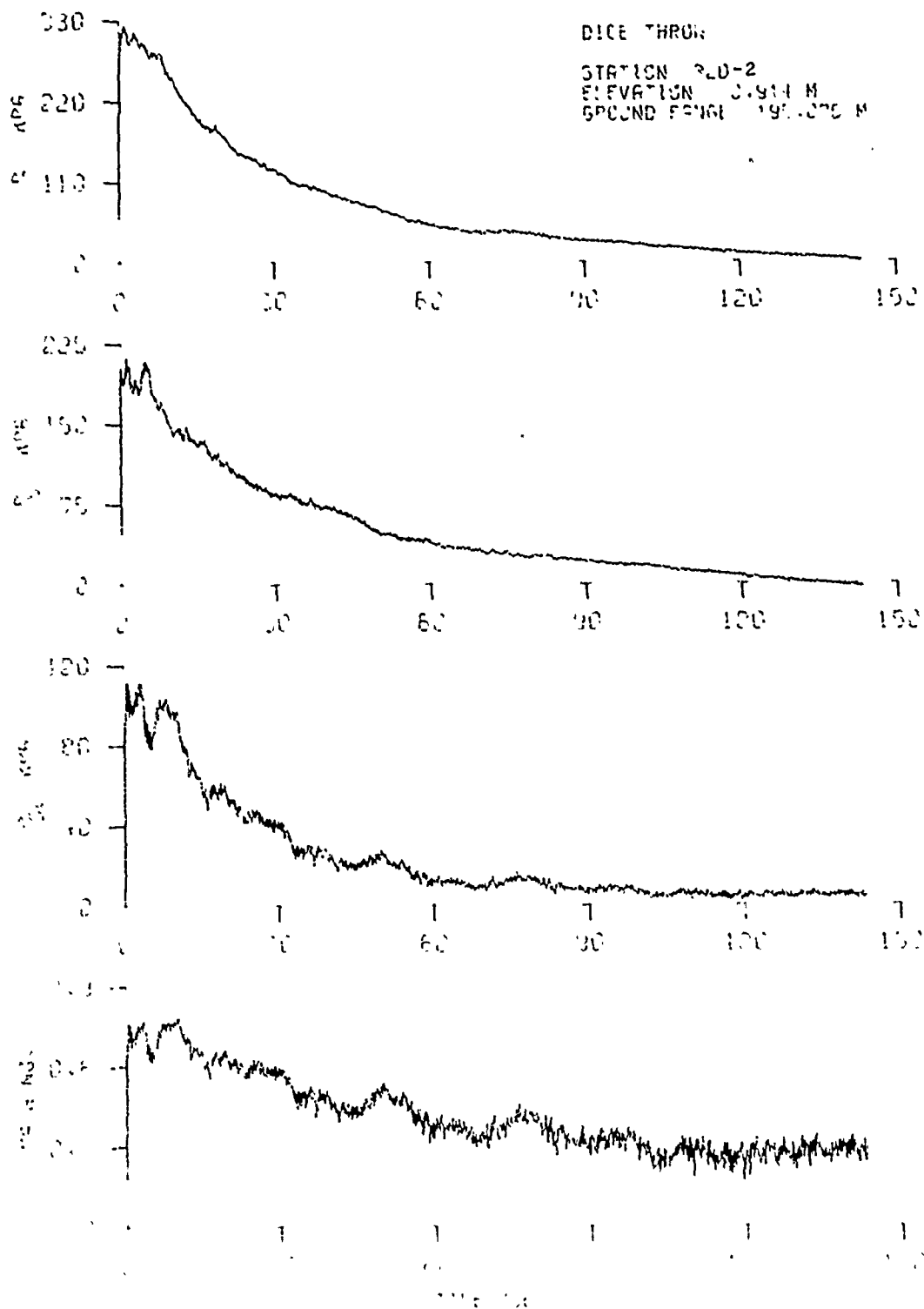


Figure C39. Dynamic pressure-time history - Station 320-2

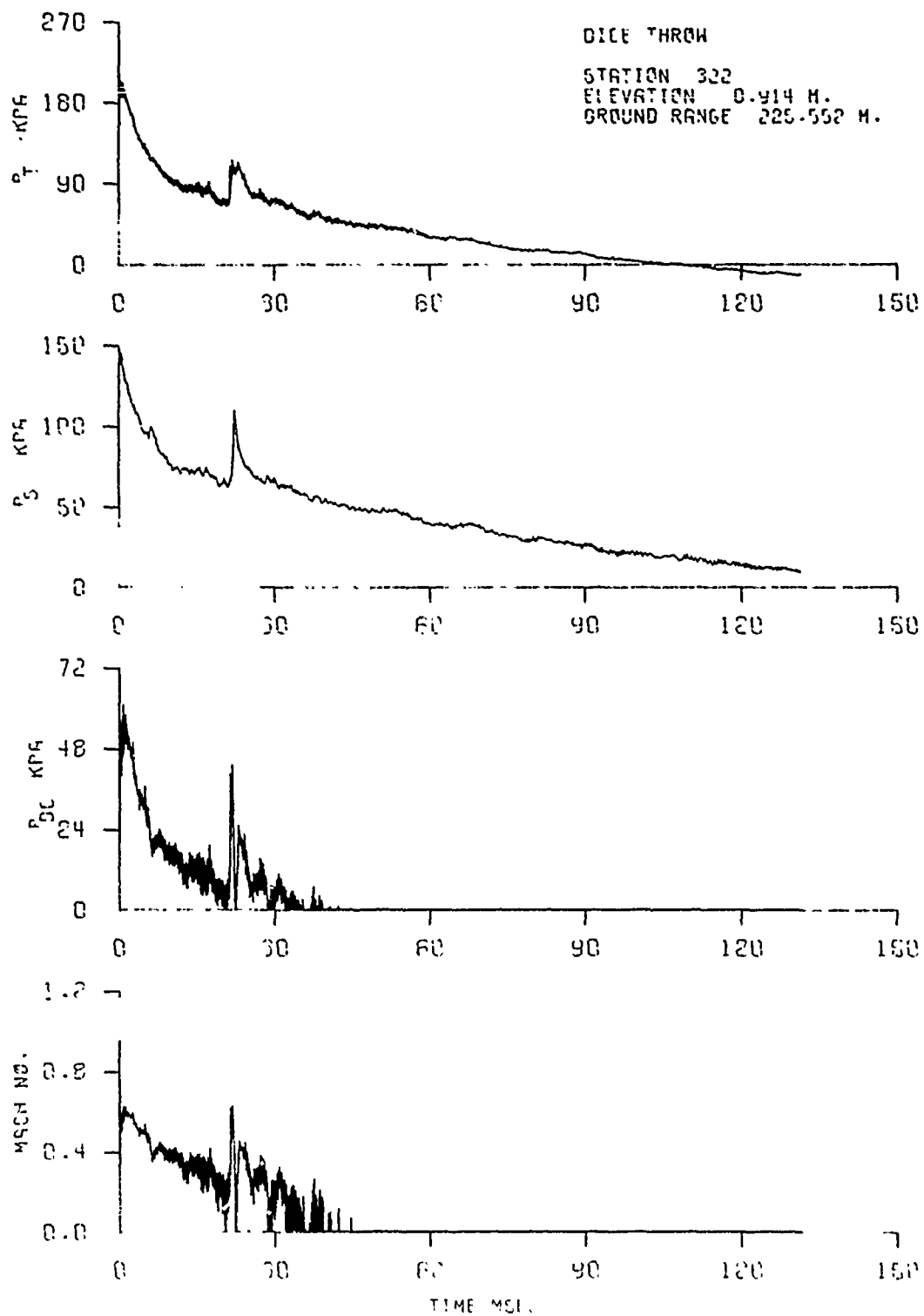


Figure C40. Dynamic pressure-time history - Station 322

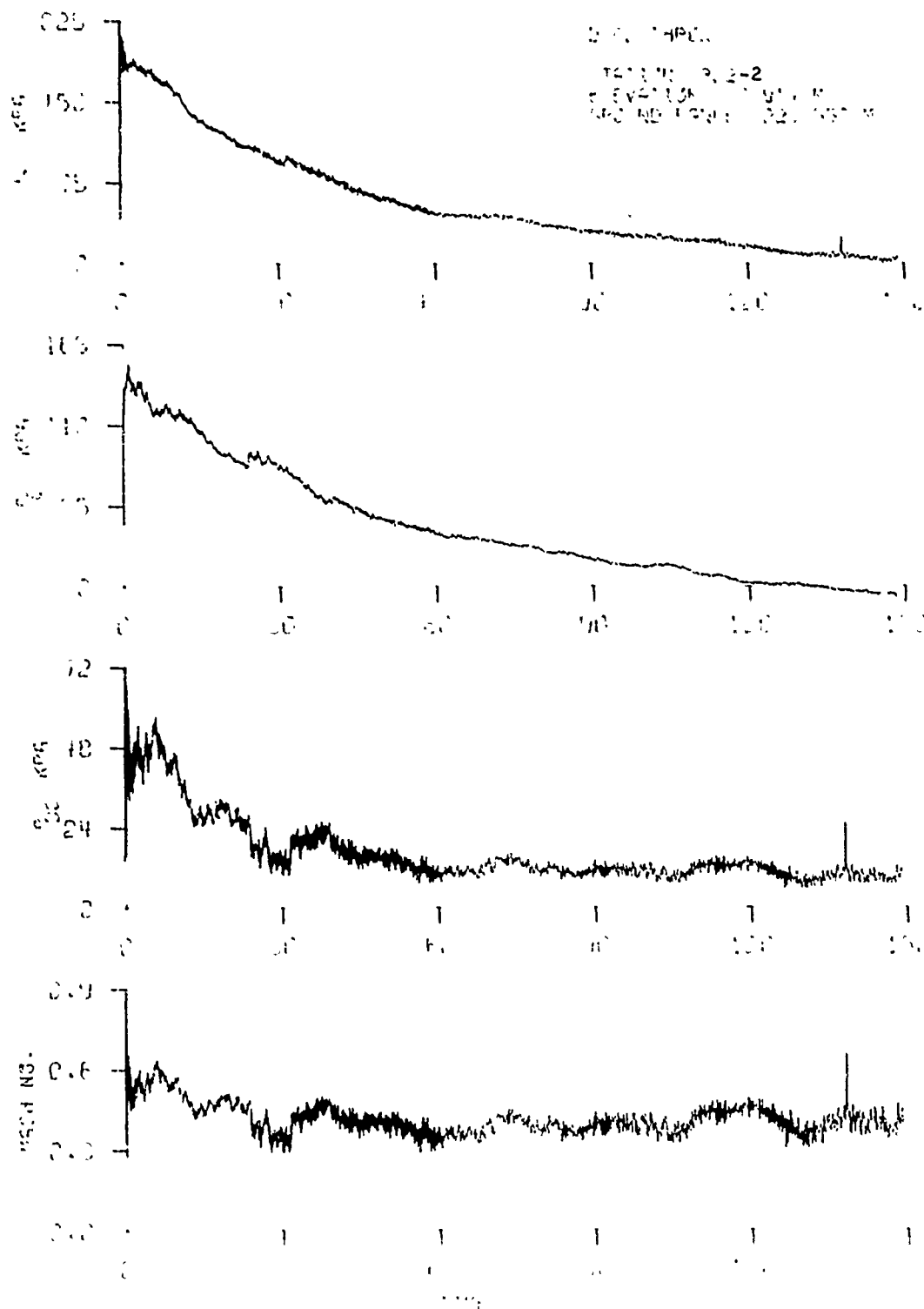


Figure C41. Dynamic pressure-time history - Station 322-2

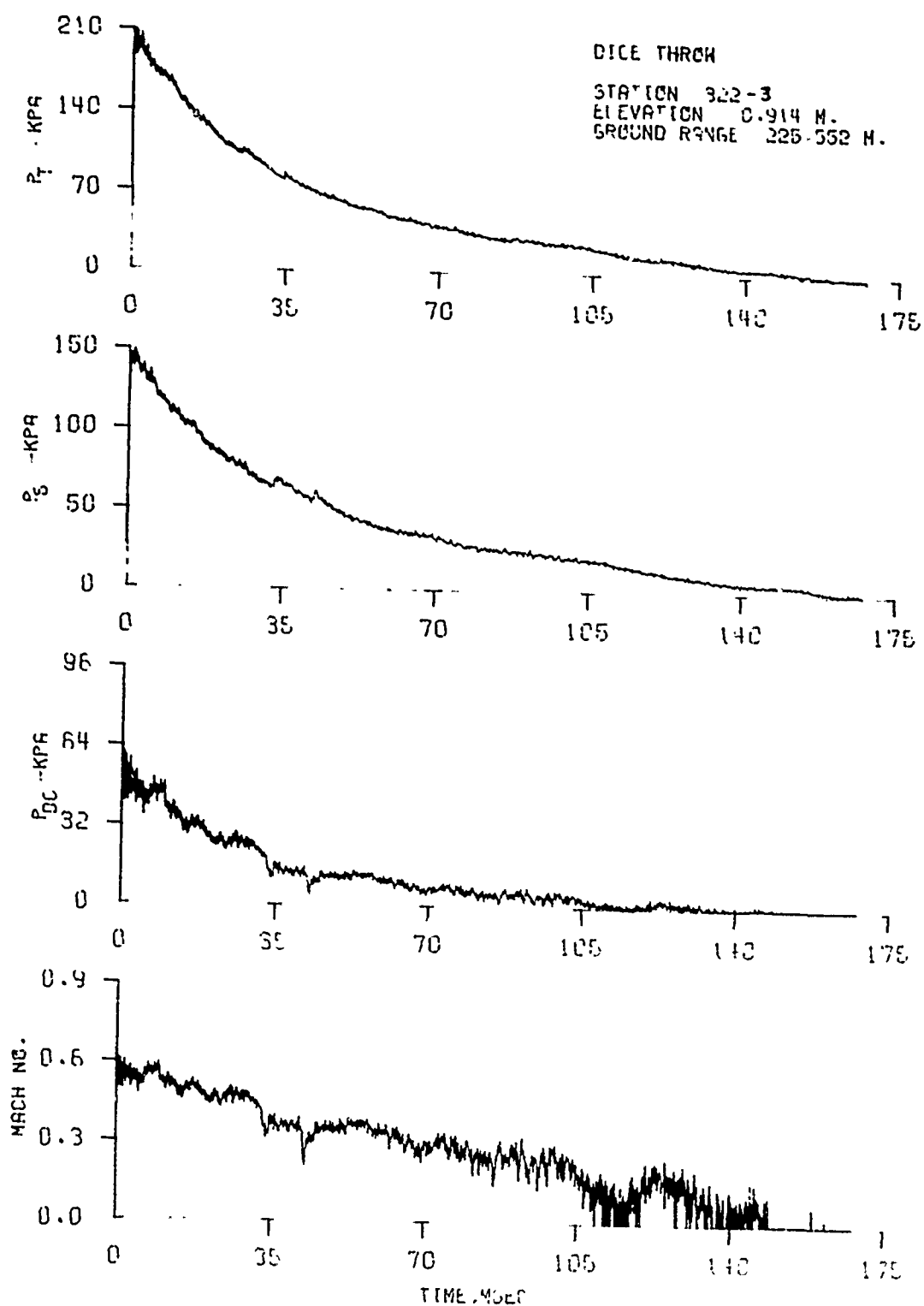


Figure C42. Dynamic pressure-time history - Station 322-3



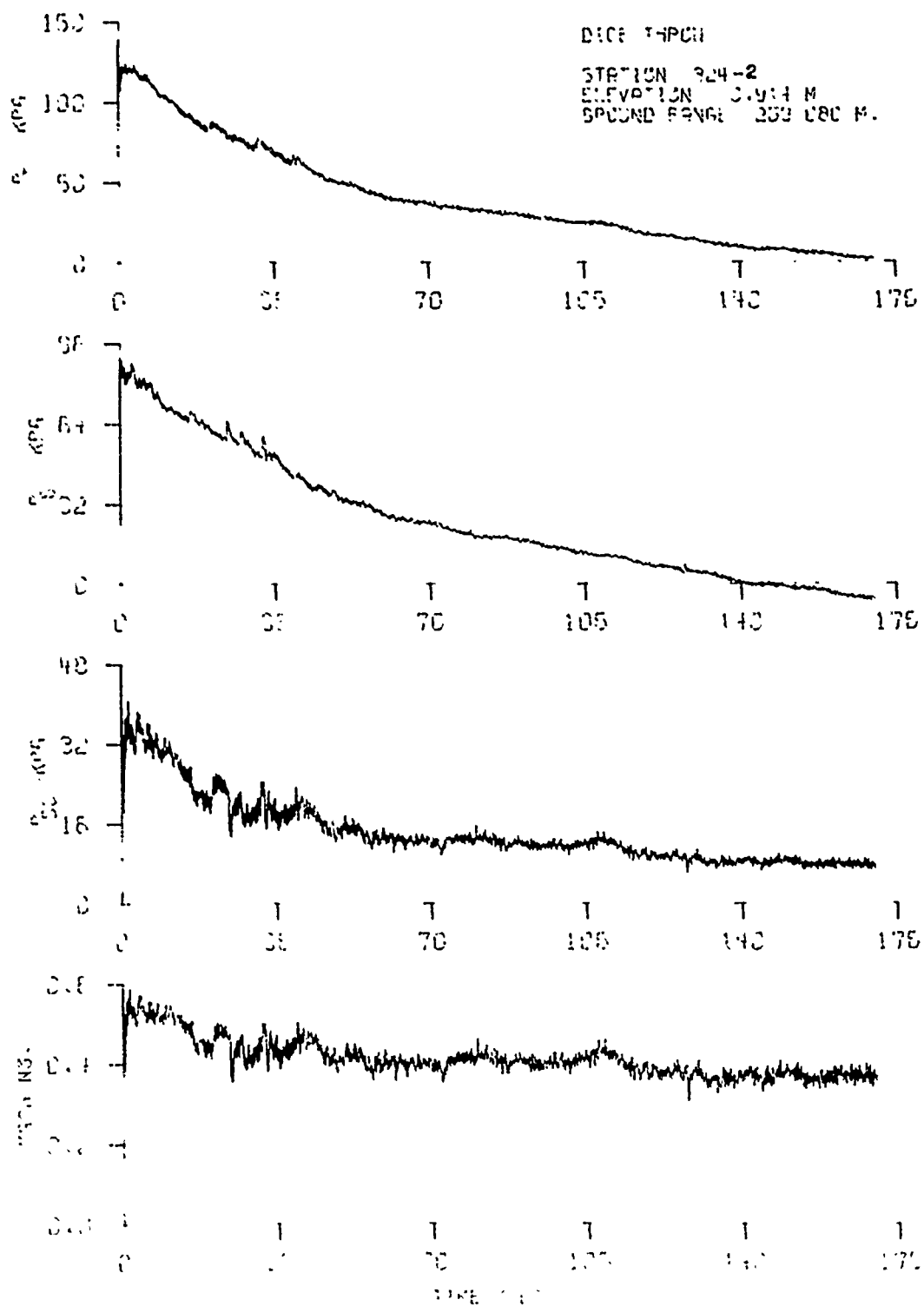


Figure C43. Dynamic pressure-time history - Station 324-2

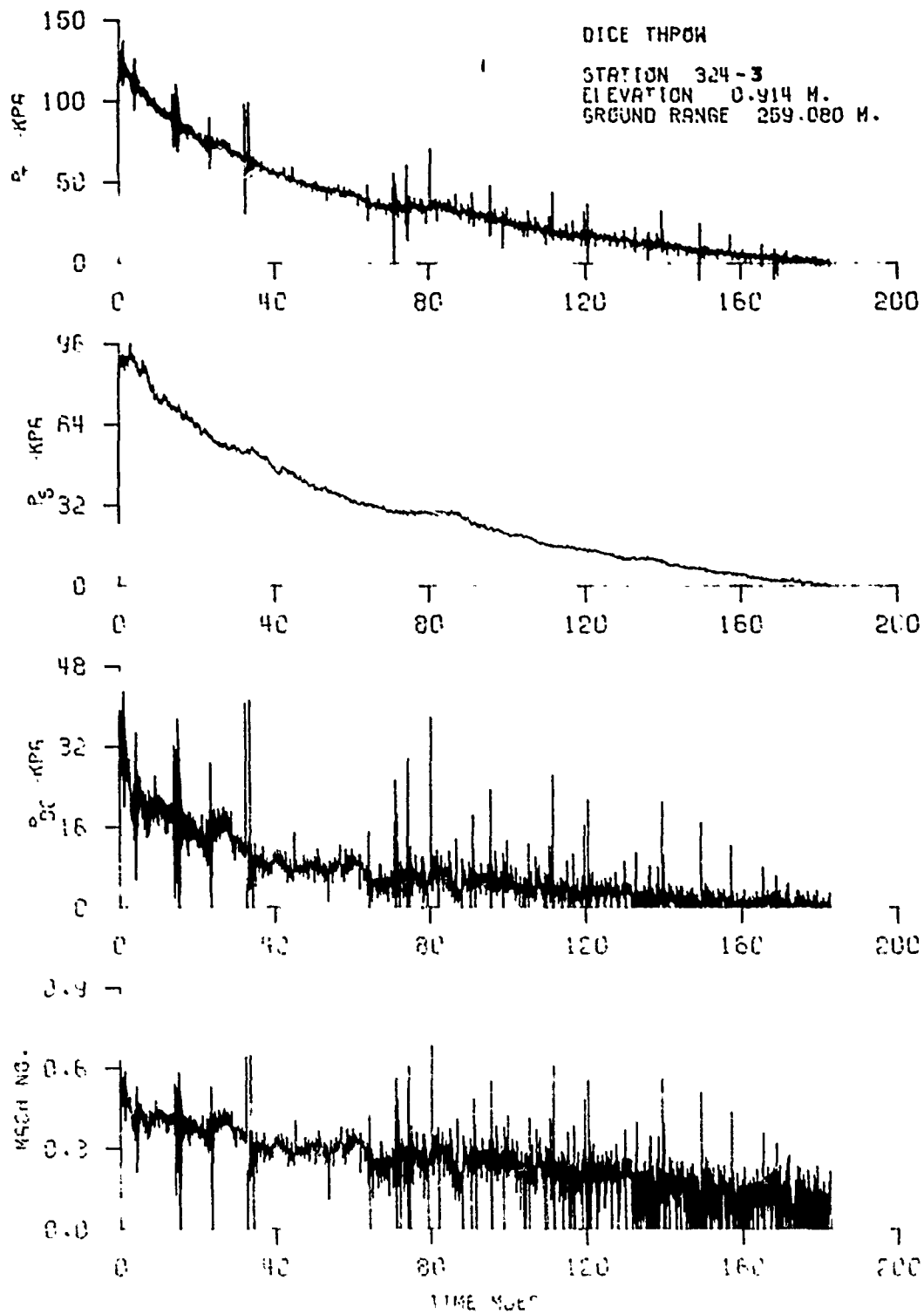


Figure C44. Dynamic pressure-time history - Station 324-3

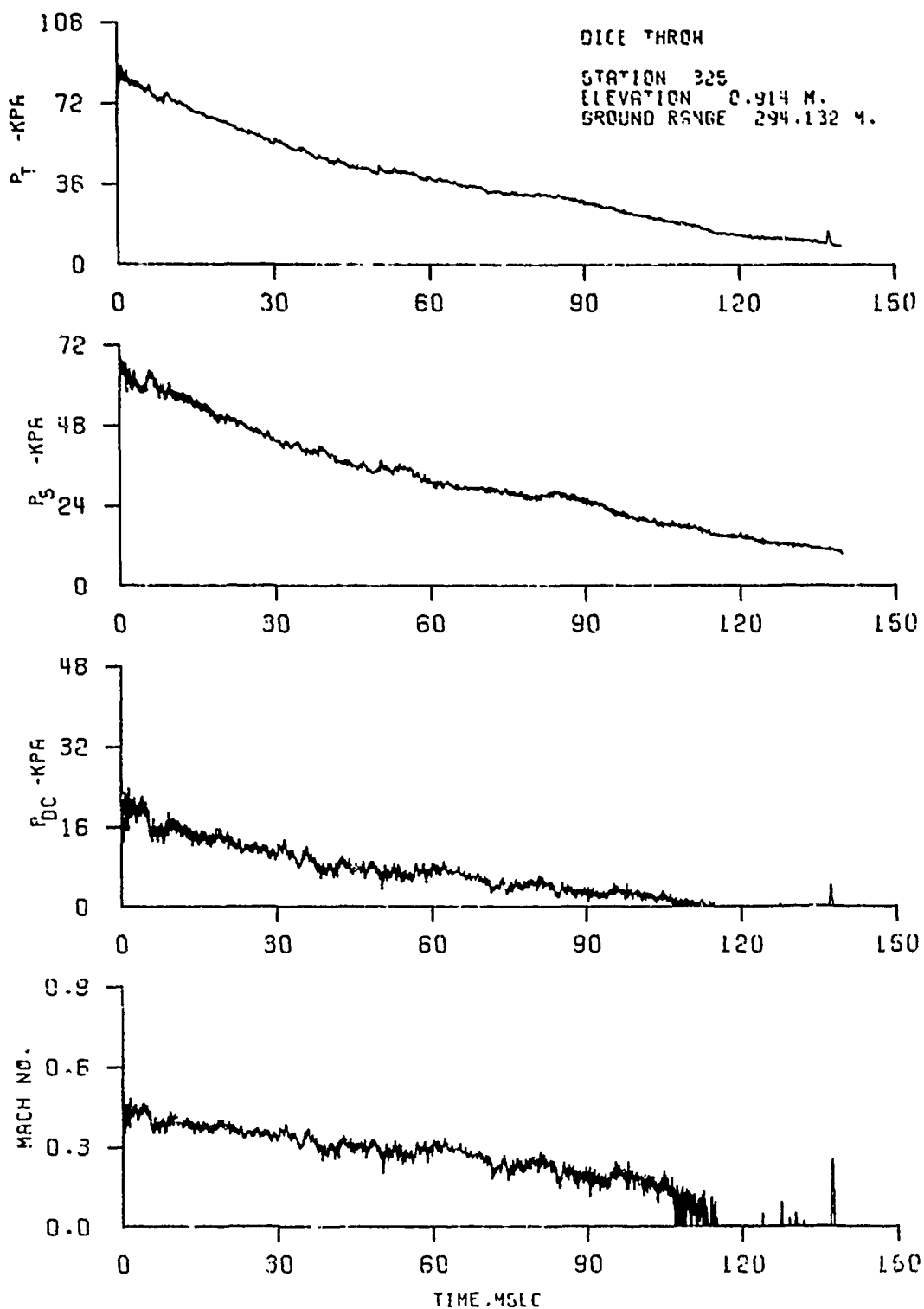


Figure C45. Dynamic pressure-time history - Station 325

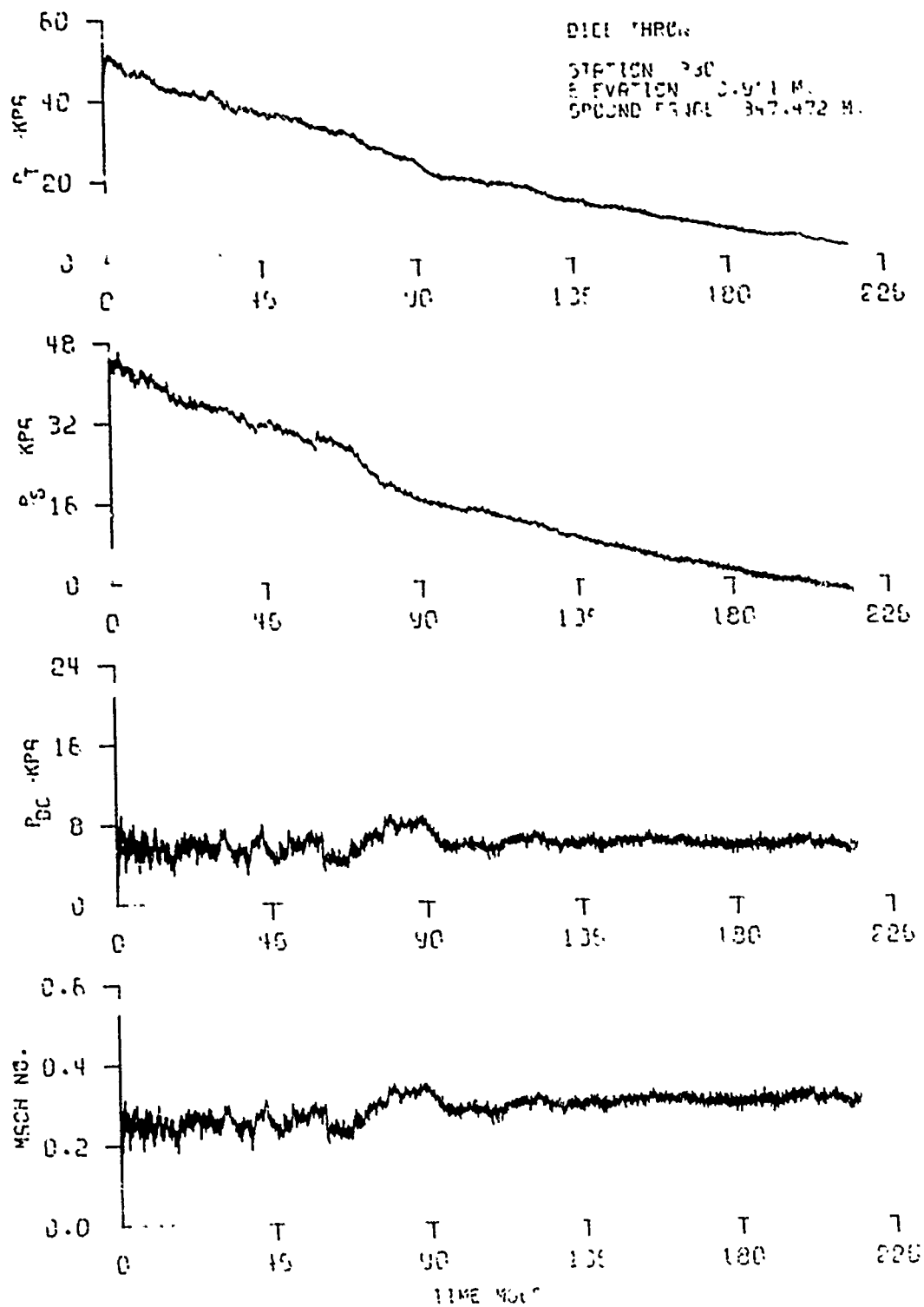


Figure C46. Dynamic pressure-time history - Station 330

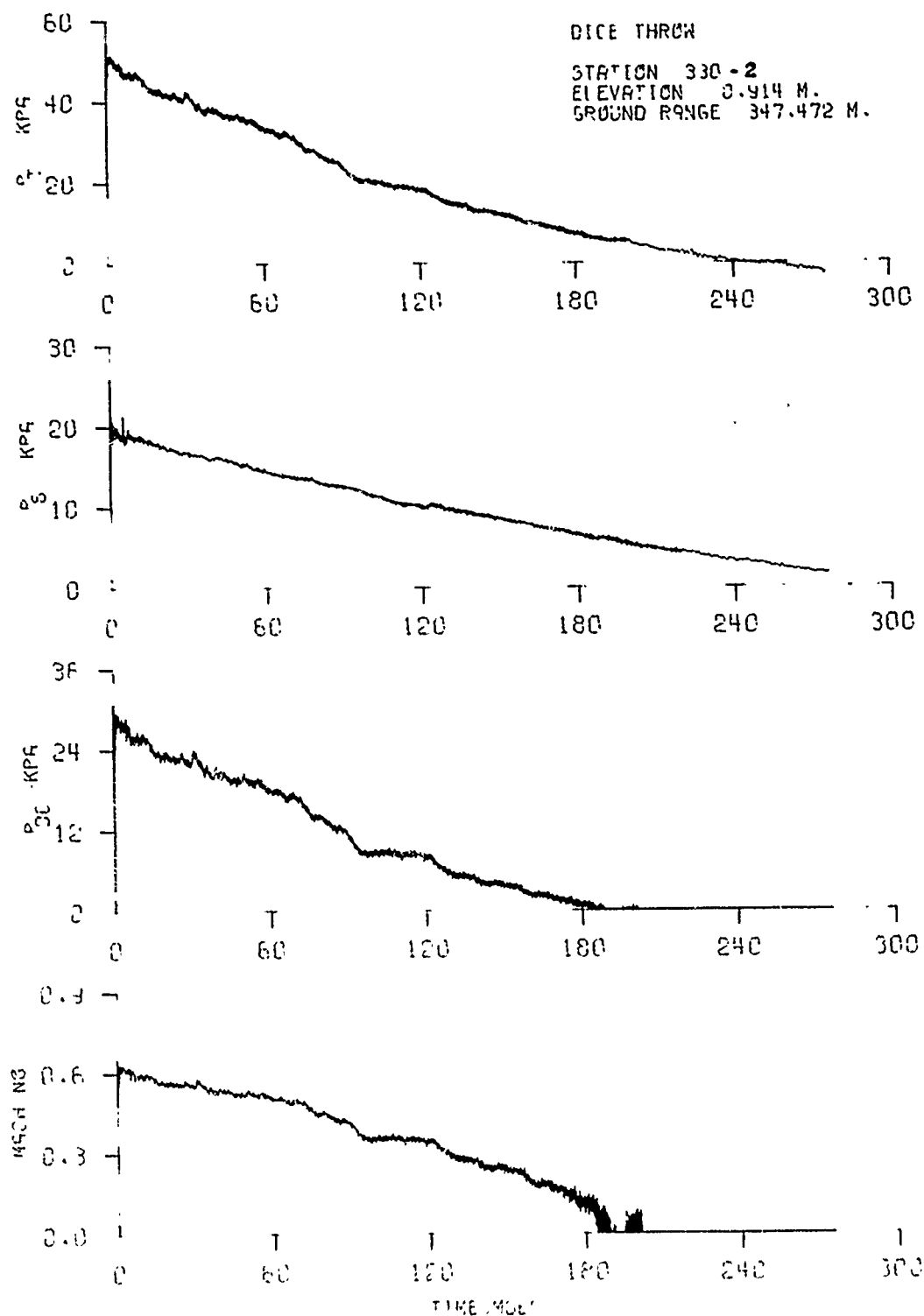


Figure C47. Dynamic pressure-time history - Station 330-2

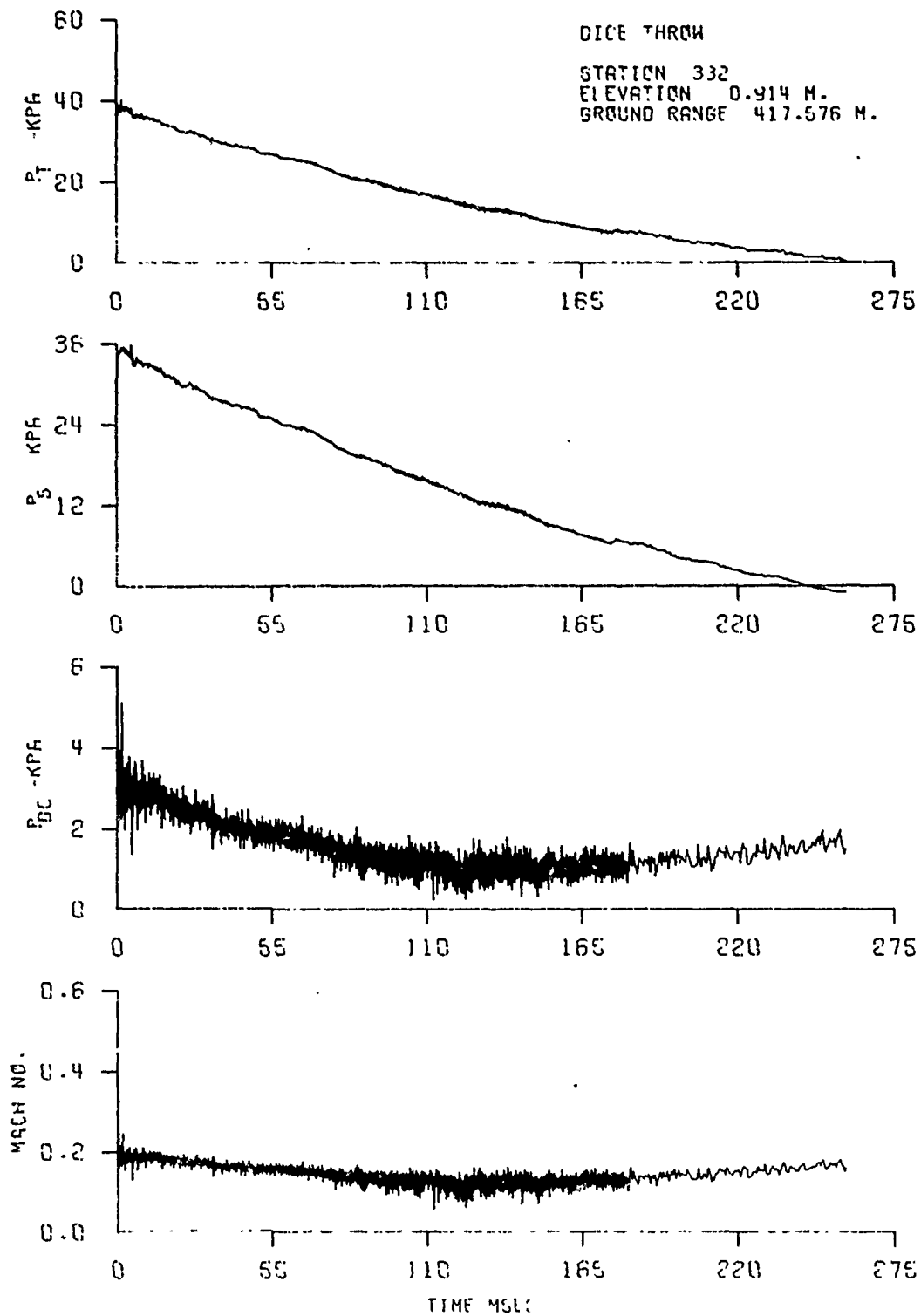


Figure C48. Dynamic pressure-time history - Station 332

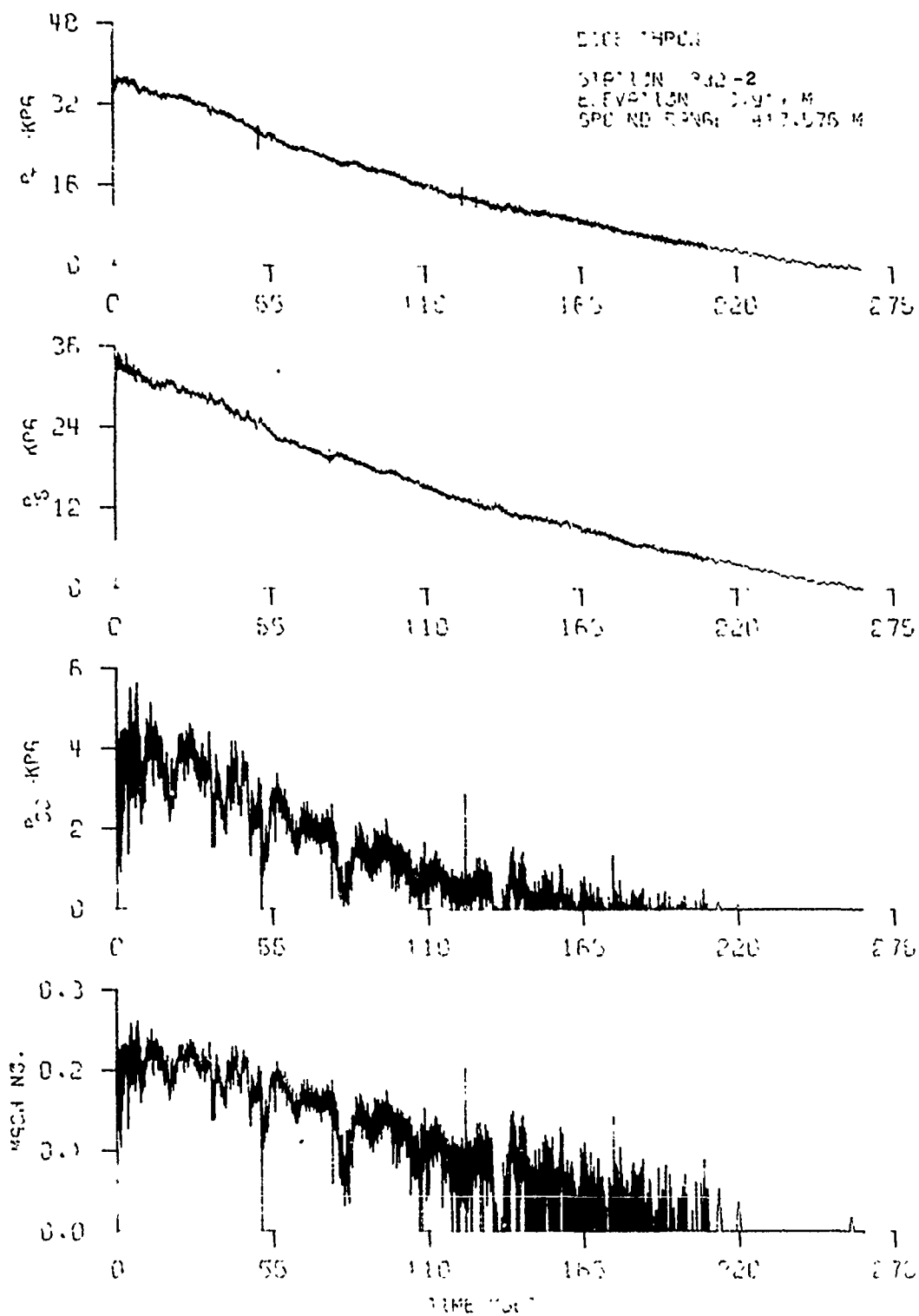


Figure C49. Dynamic pressure-time history - Station 332-2

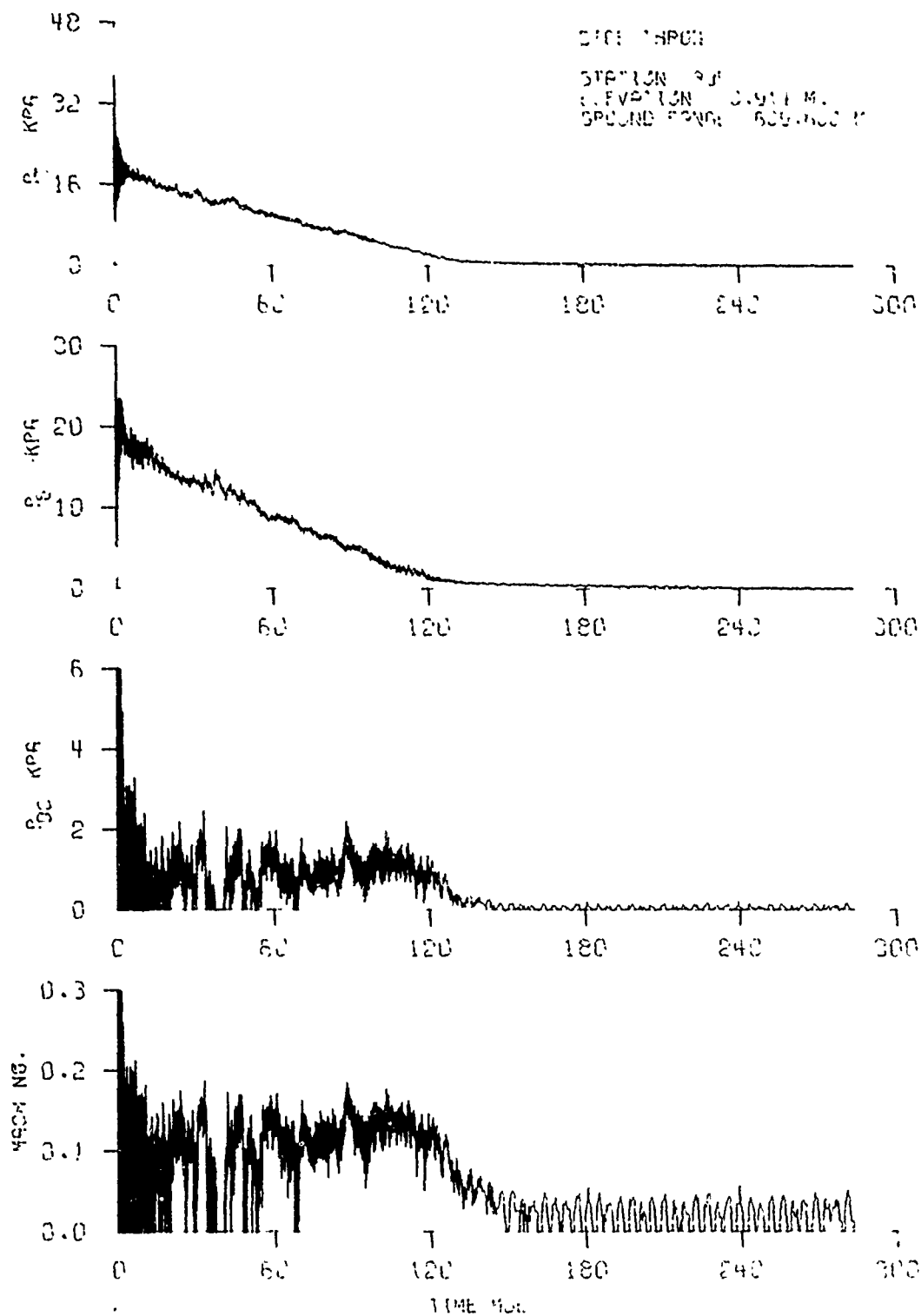


Figure C50. Dynamic pressure-time history - Station 335



**8. DICE THROW PROJECT OFFICER'S REPORT -  
THEORETICAL AIR BLAST CALCULATIONS**

**by**

**C.E. Needham**

**Air Force Weapons Laboratory**

## CONTENTS

- I. INTRODUCTION
- II. INITIAL CONDITIONS
- III. CALCULATION
- IV. RESULTS DATA COMPARISON
- V. CONCLUSIONS

## ABSTRACT

The theoretical calculation of air blast parameters for Project Dice Throw is described. This calculation provided prediction of the air blast environment from detonation to less than 10KPa. The calculation included the multiple detonation system, the initial expansion of the detonation products into the air, air shock formation and breakaway and late time propagation. Blast parameters were monitored as a function of time and space with special attention paid to the shock front in the 10 meters nearest the ground surface.

Comparisons between calculational results and experimental data are presented. Overall agreement is very good for a wide range of all parameters.

## SECTION I

### INTRODUCTION

Project Dice Throw called for the detonation of six hundred tons of Ammonium Nitrate/Fuel Oil (ANFO). The geometric configuration, detonation procedure and detonator placement were determined during Project Pre-Dice Throw (Ref 1). These determinations were made on the basis of a combined experimental and theoretical program. Consideration was given to air blast sensitive targets and to the ground motion experiments to provide an optimal charge design.

## SECTION II

### INITIAL CONDITIONS

A three material version of the AFWL HULL hydrodynamics computer code was used for the majority of this calculation. HULL uses a purely Eulerian representation of the fluid. For this problem a cylindrical coordinate system was chosen such that the axis of symmetry coincided with the vertical axis of the charge. A reflecting plane was placed at an altitude of 1442 m, which represented the ground at the White Sands test site, above the ground plane the calculational grid was established on a mesh of 180 radial by 140 axial zones. Each zone was 15 cm square, thus the overall mesh extended from 1442 m to 1463 m axially and from zero to 27 m in the radial direction.

In this mesh was placed the ANFO charge. The cylindrical section was 4.55 m in radius and 6.82 m in height. A hemispherical cap, 4.55 m in radius was placed on top of the cylinder for an overall height of 11.37 m. Seven detonators were symmetrically placed on the axis of the cylinder between the ground plane and 4.55 m. The detonators were centered at 1442, 1443.14, 1444.27, 1445.41, 1446.55, 1447.69, and 1448.82 m.

A 1962 U.S. standard tropical atmosphere was placed in the remainder of the grid. All velocities were zeroed.

### SECTION III

#### THE CALCULATION

Using the conditions described in the previous section the calculation was begun at a time of 1 sec. The propagation of the detonation from each detonator was calculated. The detonation fronts from adjacent detonators started interacting at just over 200 sec. The detonation rate increased in the regions of interaction causing transient peaks in pressure and velocity. By a time of 1.3 sec the transients had nearly damped out and the detonation front was near the surface of the charge. (Fig 1)

At a time of 2 msec the charge had expanded to approximately twice its original diameter. (Fig 2). The pressure in the detonation products (24 thousand atmosphere) is so great that the atmosphere surrounding the charge has essentially no effect. (Fig 3) The charge is in a free expansion phase.

By a time of 3 ms, the regions of cylindrical and spherical expansion can clearly be distinguished. A short transition region exists between 1448 and 1453 m altitudes. The expansion near the ground remains cylindrical and perpendicular to the ground.

At 6 ms the shock has expanded over 20 m from the charge surface near the ground but only 17 m in the vertical direction (Fig 5 & 6). There is a smooth transition between cylindrical and spherical regions. There is an indication of some instability at the surface of the detonation products.

The spherical region overexpands and a recovery shock forms in the vertical direction (Figure 7 & 8, 60 ms) at an altitude of about 1510 m. By 80 ms the downward moving shock has reached an altitude of 1485 m while no such shock exists in the radial direction. When the downward moving shock reaches 20 m above the ground (100 ms), a similar shock is starting to form at a radius of about 80 m near the ground. At this time the peak pressure at the shock front is down to 5.8 atm. It is this downward moving shock combined with the cylindrical expansion and lack of a corresponding shock in the radial direction which induces a counterclockwise rotation. The counterclockwise rotation delays the fireball rise, and spreads the detonation products near the ground. (Fig 9). The spread of detonation products further inhibits fireball rise. It is not until seven seconds that this shock-induced motion is overcome by the rising fireball.

The minor instabilities noticed at 8 ms fail to grow and play only a small part in the shock properties.

A horizontal direction, shock-following rezone was used in this calculation. Use of this rezone allows the shock to be defined in a region of the mesh which has fine resolution. This calculation retained 15 cm zone size in the shock region, throughout the calculations. The shock front resolution was accomplished at the expense of the fireball region. This is particularly evident in figure 7, at a time of 60 ms when the zones near the axis were over 5 meters in radial extent.

#### SECTION IV RESULTS

The output of the calculation has many forms. The primary data source is magnetic tape. All hydrodynamic parameters are written on tape at selected times during the calculation. This tape provides snapshots of any hydrodynamic parameter as a function of spatial coordinates. Histograms, contours and vector plots are made from this tape.

A second tape contains hydrodynamic parameters as a function time at selected points in space. It is this data which is used to produce waveforms of various parameters and calculate other quantities such as positive duration and impulse. This tape is analyzed to find peak overpressures, impulses, arrival times and many other parameters, which are then tabulated. Table I contains the tabulated data for the Dice Throw calculation. The column headings are:

STAT	-	station number
XCORD	-	radial coordinate in ft of the station
YCORD	-	height above ground in ft of the station
FT	-	arrival time of the shock in milliseconds
DP	-	peak overpressure in PSI
OPI	-	overpressure impulse in PSI-ms
HDPP	-	peak horizontal component of dynamic pressure in PSI
VDPP	-	peak vertical component of dynamic pressure in PSI
PPD	-	Overpressure positive phase in ms.
DPIH	-	vertical dynamic pressure impulse in PSI ms
DPIV	-	vertical dynamic pressure impulse in PSI ms

In addition to tabulations the various parameters may be plotted as a function of ground range for different heights above ground. If more



[illegible]

APPL FULI 000001 AMFJ, PR03=0001.007

STAT	ACORD (FI)	YCORD (FI)	AT (MS)	UP (PSI)	UPI (PSI.MS)
51	9.02E+02	1.01E+02	1.5E+00	1.177E+03	2.410E+03
52	9.02E+02	1.01E+02	1.3E+00	9.289E+02	1.026E+03
53	9.84E+02	1.03E+02	7.03E+00	1.217E+03	2.619E+03
54	9.04E+02	0.99E+02	7.00E+00	1.179E+03	2.050E+03
55	9.04E+02	1.01E+02	1.01E+00	1.085E+03	2.237E+03
56	9.04E+02	1.02E+02	0.1E+00	0.547E+02	1.754E+03
57	1.11E+02	1.03E+02	1.01E+00	9.01E+02	2.159E+03
58	1.11E+02	1.03E+02	0.1E+00	9.74E+02	1.128E+03
59	1.11E+02	1.03E+02	3.03E+00	9.273E+02	2.017E+03
60	1.11E+02	1.03E+02	0.94E+00	7.081E+02	1.047E+03
61	1.11E+02	1.03E+02	1.03E+00	0.12E+02	1.918E+03
62	1.01E+02	0.99E+02	1.01E+00	0.197E+02	1.927E+03
63	1.01E+02	1.01E+02	1.01E+00	1.11E+02	1.370E+03
64	1.01E+02	1.03E+02	1.01E+00	0.82E+02	1.00E+03
65	1.47E+02	1.03E+02	1.29E+00	7.59E+02	1.807E+03
66	1.47E+02	0.99E+00	1.29E+00	7.57E+02	1.849E+03
67	1.47E+02	1.01E+02	1.01E+00	0.07E+02	1.732E+03
68	1.47E+02	1.02E+02	1.00E+00	5.2E+02	1.061E+03
69	1.01E+02	1.03E+02	1.01E+00	0.30E+02	1.77E+03
70	1.01E+02	0.99E+00	1.01E+00	0.18E+02	1.783E+03
71	1.04E+02	1.03E+02	1.01E+00	0.13E+02	1.762E+03
72	1.01E+02	1.01E+02	1.01E+00	5.5E+02	1.008E+03
73	1.01E+02	1.03E+02	1.71E+02	3.1E+02	1.791E+03
74	1.03E+02	0.99E+00	1.01E+00	5.72E+02	1.782E+03
75	1.03E+02	1.01E+02	1.74E+02	5.0E+02	1.777E+03
76	1.83E+02	1.02E+02	1.73E+02	5.9E+02	1.094E+03
77	1.90E+02	1.03E+02	1.90E+02	5.13E+02	1.838E+03
78	1.90E+02	0.99E+00	1.90E+00	5.20E+02	1.840E+03
79	1.90E+02	1.01E+02	1.91E+02	5.11E+02	1.856E+03
80	1.90E+02	1.02E+02	2.0E+02	4.675E+02	1.732E+03
81	2.13E+02	1.03E+02	2.1E+02	4.35E+02	1.92E+03
82	2.13E+02	0.99E+00	2.1E+02	4.73E+02	1.337E+03
83	2.13E+02	1.01E+02	2.1E+02	4.077E+02	1.855E+03
84	2.13E+02	1.02E+02	2.27E+02	4.29E+02	1.70E+03
85	2.23E+02	1.03E+02	2.40E+02	4.347E+02	1.129E+03
86	2.23E+02	0.99E+00	2.40E+00	4.33E+02	2.004E+03
87	2.23E+02	1.01E+02	2.477E+02	4.26E+02	1.944E+03
88	2.23E+02	1.02E+02	2.529E+02	3.33E+02	1.828E+03
89	2.40E+02	1.03E+02	2.7E+02	3.95E+02	2.159E+03
90	2.40E+02	0.99E+00	2.70E+00	3.89E+02	2.128E+03
91	2.40E+02	1.01E+02	2.74E+02	3.82E+02	2.157E+03
92	2.40E+02	1.02E+02	2.74E+02	3.82E+02	1.874E+03
93	2.62E+02	1.03E+02	3.1E+02	3.40E+02	2.35E+03
94	2.62E+02	0.99E+00	3.17E+02	3.40E+02	2.321E+03
95	2.62E+02	1.01E+02	3.00E+02	3.42E+02	2.207E+03
96	2.62E+02	1.02E+02	3.01E+02	3.21E+02	1.911E+03
97	2.78E+02	1.03E+02	3.3E+02	3.88E+02	3.427E+03
98	2.78E+02	0.99E+00	3.31E+02	3.88E+02	3.349E+03
99	2.78E+02	1.01E+02	3.3E+02	3.047E+02	2.937E+03
100	2.78E+02	1.02E+02	3.37E+02	2.87E+02	1.939E+03

AFNL 7001 0.0000 ANFJ, PRJ3=0.000007

STAT	ACJRU (FI)	YJORD (FI)	AI (MS)	UP (PS1)	UPI (PS1,MS)
101	2.955E+02	2.955E+02	3.000E+00	2.745E+00	2.955E+00
102	2.955E+02	0.991E+00	3.000E+00	2.745E+00	2.955E+00
103	2.955E+02	2.955E+02	3.000E+00	2.745E+00	2.955E+00
104	2.955E+02	2.955E+01	3.000E+00	2.745E+00	2.955E+00
105	3.000E+02	2.955E+00	4.000E+00	2.745E+00	2.955E+00
106	3.231E+02	0.991E+00	4.320E+01	2.745E+00	2.955E+00
107	3.231E+02	2.955E+00	4.320E+00	2.745E+00	2.955E+00
108	3.231E+02	2.955E+01	4.320E+01	2.745E+00	2.955E+00
109	3.937E+02	2.955E+00	5.944E+01	2.745E+00	2.955E+00
110	3.937E+02	0.991E+00	5.944E+01	2.745E+00	2.955E+00
111	3.937E+02	2.955E+00	5.944E+01	2.745E+00	2.955E+00
112	3.937E+02	2.955E+01	5.944E+01	2.745E+00	2.955E+00
113	4.921E+02	2.955E+00	9.000E+00	0.000E+00	2.955E+00
114	4.921E+02	0.991E+00	9.000E+01	0.000E+00	2.955E+00
115	4.921E+02	2.955E+00	9.000E+01	0.000E+00	2.955E+00
116	4.921E+02	2.955E+01	9.000E+01	0.000E+00	2.955E+00
117	5.937E+02	2.955E+00	1.000E+00	0.000E+00	2.955E+00
118	5.937E+02	0.991E+00	1.000E+00	0.000E+00	2.955E+00
119	5.937E+02	2.955E+00	1.000E+00	0.000E+00	2.955E+00
120	5.937E+02	2.955E+01	1.000E+00	0.000E+00	2.955E+00
121	0.000E+02	2.955E+00	1.000E+00	2.745E+00	2.955E+00
122	0.000E+02	0.991E+00	1.000E+00	2.745E+00	2.955E+00
123	0.000E+02	2.955E+00	1.000E+00	2.745E+00	2.955E+00
124	0.000E+02	2.955E+01	1.000E+00	2.745E+00	2.955E+00
125	0.231E+02	2.955E+00	2.000E+00	1.470E+01	3.437E+00
126	0.231E+02	0.991E+00	2.000E+00	1.470E+01	3.437E+00
127	0.231E+02	2.955E+00	2.000E+00	1.470E+01	3.437E+00
128	0.231E+02	2.955E+01	2.000E+00	1.470E+01	3.437E+00
129	9.842E+02	2.955E+00	3.700E+00	9.220E+00	7.000E+00
130	9.842E+02	0.991E+00	3.700E+00	9.220E+00	7.000E+00
131	9.842E+02	2.955E+00	3.700E+00	9.220E+00	7.000E+00
132	9.842E+02	2.955E+01	3.700E+00	9.220E+00	7.000E+00
133	1.148E+03	2.955E+00	4.890E+00	0.951E+00	3.980E+00
134	1.148E+03	0.991E+00	4.890E+00	0.951E+00	3.980E+00
135	1.148E+03	2.955E+00	4.890E+00	0.951E+00	3.980E+00
136	1.148E+03	2.955E+01	4.890E+00	0.951E+00	3.980E+00
137	1.312E+03	2.955E+00	0.000E+00	5.420E+00	3.207E+00
138	1.312E+03	0.991E+00	0.000E+00	5.420E+00	3.207E+00
139	1.312E+03	2.955E+01	0.000E+00	5.420E+00	3.207E+00
140	1.312E+03	2.955E+00	0.000E+00	5.420E+00	3.207E+00
141	1.470E+03	2.955E+00	7.400E+00	4.439E+00	3.002E+00
142	1.470E+03	0.991E+00	7.400E+00	4.439E+00	3.002E+00
143	1.470E+03	2.955E+01	7.400E+00	4.439E+00	3.002E+00
144	1.470E+03	2.955E+00	7.400E+00	4.439E+00	3.002E+00
145	1.040E+03	2.955E+00	0.718E+02	3.092E+00	3.492E+00
146	1.040E+03	0.991E+00	0.718E+02	3.092E+00	3.492E+00
147	1.040E+03	2.955E+01	0.718E+02	3.092E+00	3.492E+00
148	1.040E+03	2.955E+00	0.718E+02	3.092E+00	3.492E+00
149	1.834E+03	2.955E+00	1.000E+00	3.128E+00	4.002E+00
150	1.834E+03	0.991E+00	1.000E+00	3.128E+00	4.002E+00

AFML 7001 POSITION ANFO, PRJB=0J02.007

STAF	XGJRU (FT)	YJRU (FT)	AI (MS)	UP (PSI)	UPI (PSI,MS)
102	1.834E+00	1.015E+00	1.115E+00	3.127E+00	1.051E+00
102	1.834E+00	1.023E+00	1.005E+00	3.128E+00	1.048E+00
103	1.838E+00	1.035E+00	1.175E+00	2.095E+00	3.409E+00
104	1.950E+00	0.991E+00	1.140E+00	2.094E+00	3.408E+00
105	1.953E+00	1.025E+00	1.145E+00	2.095E+00	3.408E+00
106	1.955E+00	1.025E+00	1.145E+00	2.095E+00	3.408E+00
107	0.	0.	0.	0.	0.
108	0.	0.	0.	0.	0.
109	0.	0.	0.	0.	0.
110	0.	0.	0.	0.	0.
111	0.	0.	0.	0.	0.
112	0.	0.	0.	0.	0.
113	0.	0.	0.	0.	0.
114	0.	0.	0.	0.	0.
115	0.	0.	0.	0.	0.
116	0.	0.	0.	0.	0.
117	0.	0.	0.	0.	0.
118	0.	0.	0.	0.	0.
119	0.	0.	0.	0.	0.
120	0.	0.	0.	0.	0.
121	0.	0.	0.	0.	0.
122	0.	0.	0.	0.	0.
123	0.	0.	0.	0.	0.
124	0.	0.	0.	0.	0.
125	0.	0.	0.	0.	0.
126	0.	0.	0.	0.	0.
127	0.	0.	0.	0.	0.
128	0.	0.	0.	0.	0.
129	0.	0.	0.	0.	0.
130	0.	0.	0.	0.	0.
131	0.	0.	0.	0.	0.
132	0.	0.	0.	0.	0.
133	0.	0.	0.	0.	0.
134	0.	0.	0.	0.	0.
135	9.842E+00	3.941E+00	3.711E+00	9.567E+00	1.003E+00
136	9.842E+00	3.952E+00	3.718E+00	9.543E+00	1.002E+00
137	1.024E+00	3.941E+00	4.035E+00	0.980E+00	3.982E+00
138	1.248E+00	3.952E+00	4.901E+00	0.975E+00	3.973E+00
139	1.011E+00	3.941E+00	0.100E+00	5.451E+00	3.102E+00
140	1.011E+00	3.952E+00	1.108E+00	5.445E+00	3.105E+00
141	1.470E+00	3.941E+00	7.411E+00	4.426E+00	3.008E+00
142	1.470E+00	3.952E+00	7.415E+00	4.427E+00	3.997E+00
143	1.950E+00	3.941E+00	1.145E+00	2.091E+00	3.400E+00
144	1.950E+00	3.952E+00	1.145E+00	2.087E+00	3.409E+00

ATHEL 7001 0.1000 ANFJ, P203=0000.000

STAL	MDPP (PS1)	VDP (PS1)	PPU (HS)	UPH (PS1.MS)	UPIV (PS1.MS)
1	1.0210E+0	0.	1.490E+01	1.490E+0	0.
2	1.0200E+0	0.800E+01	2.490E+01	1.490E+0	4.043E+02
3	1.0200E+0	0.400E+02	2.490E+01	1.490E+0	1.024E+03
4	1.0200E+0	2.100E+04	2.490E+01	1.490E+0	1.044E+04
5	1.0200E+0	0.	2.490E+01	1.490E+0	0.
6	1.0200E+0	0.400E+01	2.490E+01	1.490E+0	0.911E+02
7	1.0200E+0	0.000E+02	2.490E+01	1.490E+0	1.077E+03
8	1.0200E+0	0.000E+03	2.490E+01	1.490E+0	1.080E+04
9	1.0200E+0	0.	2.490E+01	1.490E+0	0.
10	1.0200E+0	1.400E+01	2.490E+01	1.490E+0	0.000E+02
11	1.0200E+0	0.000E+02	2.490E+01	1.490E+0	1.400E+03
12	1.0200E+0	1.040E+03	2.490E+01	1.490E+0	1.074E+04
13	1.0200E+0	0.	2.490E+01	1.490E+0	0.
14	1.0200E+0	0.400E+01	2.490E+01	1.490E+0	0.200E+02
15	1.0200E+0	1.000E+02	2.490E+01	1.490E+0	1.000E+03
16	1.0200E+0	1.000E+03	2.490E+01	1.490E+0	0.400E+04
17	1.0200E+0	0.	2.490E+01	1.490E+0	0.
18	1.0200E+0	0.000E+02	2.490E+01	1.490E+0	0.900E+02
19	1.0200E+0	1.700E+02	2.490E+01	1.490E+0	1.200E+03
20	1.0200E+0	0.000E+03	2.490E+01	1.490E+0	0.000E+04
21	1.0200E+0	0.	2.490E+01	1.490E+0	0.
22	1.0200E+0	4.000E+01	2.490E+01	1.490E+0	0.400E+02
23	1.0200E+0	1.000E+02	2.490E+01	1.490E+0	1.000E+03
24	1.0200E+0	0.000E+03	2.490E+01	1.490E+0	0.000E+04
25	1.0200E+0	0.	2.490E+01	1.490E+0	0.
26	1.0200E+0	0.400E+01	2.490E+01	1.490E+0	0.400E+02
27	1.0200E+0	0.800E+01	2.490E+01	1.490E+0	0.800E+02
28	1.0200E+0	0.000E+02	2.490E+01	1.490E+0	0.000E+03
29	1.0200E+0	0.	2.490E+01	1.490E+0	0.
30	1.0200E+0	0.000E+03	2.490E+01	1.490E+0	0.000E+04
31	1.0200E+0	1.000E+01	2.490E+01	1.490E+0	0.000E+02
32	1.0200E+0	1.000E+02	2.490E+01	1.490E+0	0.000E+03
33	1.0200E+0	0.	2.490E+01	1.490E+0	0.
34	1.0200E+0	0.000E+01	2.490E+01	1.490E+0	0.000E+02
35	1.0200E+0	0.000E+02	2.490E+01	1.490E+0	0.000E+03
36	1.0200E+0	0.000E+03	2.490E+01	1.490E+0	0.000E+04
37	1.0200E+0	0.	2.490E+01	1.490E+0	0.
38	1.0200E+0	1.000E+01	2.490E+01	1.490E+0	0.000E+02
39	1.0200E+0	1.000E+02	2.490E+01	1.490E+0	0.000E+03
40	1.0200E+0	0.	2.490E+01	1.490E+0	0.
41	1.0200E+0	0.000E+01	2.490E+01	1.490E+0	0.000E+02
42	1.0200E+0	0.000E+02	2.490E+01	1.490E+0	0.000E+03
43	1.0200E+0	0.000E+03	2.490E+01	1.490E+0	0.000E+04
44	1.0200E+0	0.	2.490E+01	1.490E+0	0.
45	1.0200E+0	0.000E+01	2.490E+01	1.490E+0	0.000E+02
46	1.0200E+0	0.000E+02	2.490E+01	1.490E+0	0.000E+03
47	1.0200E+0	0.000E+03	2.490E+01	1.490E+0	0.000E+04
48	1.0200E+0	0.	2.490E+01	1.490E+0	0.
49	1.0200E+0	0.000E+01	2.490E+01	1.490E+0	0.000E+02
50	1.0200E+0	0.000E+02	2.490E+01	1.490E+0	0.000E+03

4FWL 700 DIVISION ANF0, PR03=0 00001

STAT	ADPP (PSI)	VOPP (PSI)	PP0 (HS)	UPIH (PSI.MS)	UPIV (PSI.MS)
01	4.748E+03	3.030E+01	1.945E+01	0.228E+04	2.798E+02
02	3.022E+03	3.004E+02	1.890E+01	2.202E+04	8.044E+02
03	5.168E+03	0.	1.850E+01	3.288E+04	0.
04	4.342E+03	2.499E+01	1.858E+01	3.130E+04	7.378E+01
05	4.421E+03	1.07E+02	1.850E+01	2.788E+04	2.408E+02
06	3.487E+03	3.499E+02	1.855E+01	1.989E+04	7.225E+02
07	4.227E+03	0.	1.851E+01	2.534E+04	0.
08	4.192E+03	3.27E+01	1.852E+01	2.424E+04	6.048E+01
09	4.037E+03	1.039E+02	1.852E+01	2.224E+04	2.028E+02
00	3.211E+03	3.072E+02	1.559E+01	1.042E+04	3.001E+02
01	3.724E+03	0.	1.450E+01	1.973E+04	0.
02	3.765E+03	2.472E+01	1.444E+01	1.932E+04	4.348E+01
03	3.228E+03	9.472E+01	1.390E+01	1.810E+04	1.508E+02
04	2.827E+03	2.02E+02	1.318E+01	1.390E+04	4.024E+02
05	3.323E+03	0.	1.168E+01	1.538E+04	0.
06	3.248E+03	2.185E+01	1.172E+01	1.508E+04	3.304E+01
07	3.313E+03	7.340E+01	1.150E+01	1.503E+04	1.219E+02
08	1.380E+03	2.253E+02	1.074E+01	1.255E+04	3.840E+02
09	1.021E+03	0.	9.273E+00	1.321E+04	0.
10	2.712E+03	1.429E+01	9.313E+00	1.294E+04	2.420E+01
11	1.59E+03	5.593E+01	9.139E+00	1.257E+04	9.403E+01
12	1.934E+03	1.777E+02	8.198E+00	1.337E+04	3.113E+02
13	2.292E+03	0.	8.032E+00	1.125E+04	0.
14	2.257E+03	1.190E+01	8.042E+00	1.093E+04	2.122E+01
15	2.001E+03	4.130E+01	8.495E+00	1.073E+04	7.337E+01
16	1.550E+03	1.422E+02	8.175E+00	9.221E+03	2.511E+02
17	1.023E+03	0.	8.529E+00	9.745E+03	0.
18	1.724E+03	8.099E+00	8.600E+00	9.470E+03	1.278E+01
19	1.000E+03	3.189E+01	8.800E+00	9.224E+03	5.287E+01
20	1.214E+03	1.132E+02	7.185E+00	8.122E+03	1.995E+02
21	1.455E+03	0.	8.789E+00	8.540E+03	0.
22	1.509E+03	7.355E+00	8.777E+00	8.207E+03	1.315E+01
23	1.260E+03	2.871E+01	8.979E+00	8.104E+03	4.880E+01
24	3.112E+02	9.152E+01	8.952E+00	7.242E+03	1.720E+02
25	1.03E+03	0.	8.814E+00	7.030E+03	0.
26	1.010E+03	8.074E+00	8.827E+00	7.432E+03	1.368E+01
27	9.705E+02	2.200E+01	8.770E+00	7.381E+03	4.594E+01
28	8.210E+02	7.434E+01	1.270E+01	8.775E+03	1.505E+02
29	8.94E+02	0.	1.257E+01	8.872E+03	0.
30	8.815E+02	3.940E+00	1.240E+01	8.867E+03	1.041E+01
31	3.473E+02	1.909E+01	1.220E+01	8.938E+03	3.933E+01
32	7.351E+02	3.840E+01	1.898E+01	8.291E+03	-2.137E+02
33	7.007E+02	0.	2.078E+01	8.187E+03	0.
34	7.010E+02	-3.832E+00	2.081E+01	8.415E+03	-1.794E+01
35	7.350E+02	1.370E+01	1.904E+01	8.985E+03	-1.775E+02
36	8.404E+02	4.540E+01	2.977E+01	5.330E+03	-4.199E+02
37	8.286E+02	0.	1.117E+02	5.950E+03	0.
38	8.541E+02	-4.254E+00	1.021E+02	8.457E+03	-4.438E+01
39	8.325E+02	1.153E+01	1.021E+02	8.827E+03	-2.045E+02
100	5.576E+02	3.902E+01	3.522E+01	4.454E+03	-3.734E+02

STAI	NDPP (PSI)	VOPP (PSI)	PPU (MS)	UPLH (PSI,MS)	UPLV (PSI,MS)
1-1	5.057E+2	0.	9.642E+01	5.980E+03	0.
1-2	5.622E+2	2.370E+00	9.087E+01	5.581E+03	-2.580E+01
1-3	5.430E+2	1.011E+01	9.095E+01	0.237E+03	-9.387E+01
104	4.855E+02	3.107E+01	9.055E+01	3.408E+03	-1.738E+02
1-5	4.005E+2	0.	0.621E+01	5.034E+03	0.
107	4.157E+2	1.030E+00	8.025E+01	0.125E+03	1.175E+01
1-7	5.902E+2	5.541E+00	8.657E+01	5.270E+03	5.703E+01
108	5.030E+02	1.737E+01	3.007E+01	2.097E+03	1.217E+02
1-9	2.124E+2	0.	0.069E+01	5.907E+03	0.
110	2.117E+02	0.514E-01	3.055E+01	5.952E+03	1.277E+01
1-11	2.081E+2	2.240E+00	0.039E+01	5.455E+03	5.127E+01
112	1.934E+02	7.150E+00	8.525E+01	2.271E+03	1.013E+02
1-13	7.827E+01	0.	5.955E+01	1.902E+03	0.
114	7.812E+01	1.370E-01	8.902E+01	2.808E+03	5.039E+01
1-15	7.742E+01	4.591E-01	0.918E+01	1.019E+03	1.202E+01
116	7.479E+01	1.483E+00	8.822E+01	1.295E+03	4.204E+01
117	5.009E+01	0.	1.168E+02	9.240E+02	0.
118	5.509E+01	1.420E-02	1.187E+02	8.775E+02	8.807E-01
1-19	2.997E+01	7.012E-02	1.180E+02	7.975E+02	5.820E+00
120	2.957E+01	3.300E-01	1.181E+02	7.255E+02	1.177E+01
121	1.090E+01	0.	1.557E+02	0.138E+03	0.
122	1.050E+01	0.314E-03	2.557E+02	5.850E+02	4.058E-01
123	1.091E+01	3.417E-02	1.355E+02	5.433E+02	1.540E+00
124	1.074E+01	1.108E-01	1.351E+02	5.092E+02	4.557E+00
125	5.451E+00	0.	1.712E+02	2.717E+02	0.
126	5.453E+00	8.707E-04	1.712E+02	2.028E+02	5.403E-02
127	5.425E+00	4.717E-03	1.712E+02	2.550E+02	2.352E-01
128	5.454E+00	1.010E-02	1.712E+02	2.457E+02	0.650E-01
129	2.575E+00	0.	2.011E+02	1.403E+02	0.
130	2.575E+00	1.855E-04	2.011E+02	1.454E+02	1.523E-02
131	2.575E+00	9.957E-04	2.011E+02	1.392E+02	5.599E-02
132	2.575E+00	3.415E-03	2.125E+02	1.557E+02	1.412E-01
133	2.250E+00	0.	2.419E+02	8.957E+01	0.
134	1.290E+00	-5.051E-05	2.419E+02	8.866E+01	3.209E-03
135	1.297E+00	-5.318E-04	2.418E+02	3.754E+01	1.558E-02
136	1.298E+00	-1.215E-03	2.410E+02	8.013E+01	5.302E-02
137	8.105E-01	0.	2.582E+02	0.009E+01	0.
138	0.114E-01	-2.442E-05	2.582E+02	5.984E+01	1.441E-03
139	8.098E-01	-1.357E-04	2.561E+02	5.945E+01	7.852E-03
140	0.054E-01	-4.714E-04	2.580E+02	5.955E+01	2.700E-02
141	5.418E-01	0.	3.187E+02	4.505E+01	0.
142	5.427E-01	1.577E-05	3.187E+02	4.511E+01	7.952E-04
143	5.404E-01	5.858E-05	3.187E+02	4.291E+01	4.318E-03
144	5.421E-01	2.025E-04	3.185E+02	4.279E+01	1.458E-02
145	5.777E-01	0.	3.550E+02	5.225E+01	0.
146	5.777E-01	0.122E-00	3.550E+02	5.222E+01	4.522E-04
147	5.775E-01	3.300E-05	3.550E+02	5.211E+01	1.401E-03
148	5.775E-01	1.171E-04	3.549E+02	5.215E+01	5.470E-03
149	2.729E-01	0.	4.019E+02	2.417E+01	0.
150	1.728E-01	3.072E-00	4.019E+02	2.417E+01	2.640E-04

APAC 7001 POSITION AND PRESSURE DATA

STAT	UJPP (PSI)	VJPP (PSI)	PPU (MS)	UPIH (PSI,MS)	UPIV (PSI,MS)
101	2.727E-01	2.000E-00	4.000E+00	2.400E+01	2.407E-03
102	2.728E-01	2.000E-00	4.000E+00	2.410E+01	4.948E-03
103	2.730E-01	2.000E-00	2.000E+00	2.700E+01	0.000E+00
104	2.733E-01	2.000E-00	2.000E+00	2.700E+01	1.594E-04
105	2.734E-01	2.000E-00	2.000E+00	2.700E+01	0.673E-04
106	2.735E-01	4.401E-00	2.000E+00	2.700E+01	2.987E-03
107	0.000E+00	0.000E+00	0.000E+00	0.000E+00	0.000E+00
108	0.000E+00	0.000E+00	0.000E+00	0.000E+00	0.000E+00
109	0.000E+00	0.000E+00	0.000E+00	0.000E+00	0.000E+00
110	0.000E+00	0.000E+00	0.000E+00	0.000E+00	0.000E+00
111	0.000E+00	0.000E+00	0.000E+00	0.000E+00	0.000E+00
112	0.000E+00	0.000E+00	0.000E+00	0.000E+00	0.000E+00
113	0.000E+00	0.000E+00	0.000E+00	0.000E+00	0.000E+00
114	0.000E+00	0.000E+00	0.000E+00	0.000E+00	0.000E+00
115	0.000E+00	0.000E+00	0.000E+00	0.000E+00	0.000E+00
116	0.000E+00	0.000E+00	0.000E+00	0.000E+00	0.000E+00
117	0.000E+00	0.000E+00	0.000E+00	0.000E+00	0.000E+00
118	0.000E+00	0.000E+00	0.000E+00	0.000E+00	0.000E+00
119	0.000E+00	0.000E+00	0.000E+00	0.000E+00	0.000E+00
120	0.000E+00	0.000E+00	0.000E+00	0.000E+00	0.000E+00
121	0.000E+00	0.000E+00	0.000E+00	0.000E+00	0.000E+00
122	0.000E+00	0.000E+00	0.000E+00	0.000E+00	0.000E+00
123	0.000E+00	0.000E+00	0.000E+00	0.000E+00	0.000E+00
124	0.000E+00	0.000E+00	0.000E+00	0.000E+00	0.000E+00
125	0.000E+00	0.000E+00	0.000E+00	0.000E+00	0.000E+00
126	0.000E+00	0.000E+00	0.000E+00	0.000E+00	0.000E+00
127	0.000E+00	0.000E+00	0.000E+00	0.000E+00	0.000E+00
128	0.000E+00	0.000E+00	0.000E+00	0.000E+00	0.000E+00
129	0.000E+00	0.000E+00	0.000E+00	0.000E+00	0.000E+00
130	0.000E+00	0.000E+00	0.000E+00	0.000E+00	0.000E+00
131	0.000E+00	0.000E+00	0.000E+00	0.000E+00	0.000E+00
132	0.000E+00	0.000E+00	0.000E+00	0.000E+00	0.000E+00
133	0.000E+00	0.000E+00	0.000E+00	0.000E+00	0.000E+00
134	0.000E+00	0.000E+00	0.000E+00	0.000E+00	0.000E+00
135	2.074E+00	7.200E-03	2.119E+00	1.000E+00	2.909E-01
136	2.073E+00	1.404E-02	2.112E+00	1.020E+00	5.900E-01
137	2.099E+00	2.074E-03	2.400E+00	8.529E+00	1.149E-01
138	1.032E+00	2.270E-03	2.407E+00	8.481E+00	2.322E-01
139	8.091E-01	1.000E-03	2.078E+00	2.070E+00	5.779E-02
140	8.008E-01	1.901E-03	2.504E+00	2.844E+00	1.105E-01
141	2.090E-01	4.298E-04	0.180E+00	4.200E+00	3.173E-02
142	2.009E-01	8.723E-04	0.179E+00	4.254E+00	6.385E-02
143	2.008E-01	9.300E-05	2.000E+00	2.700E+00	0.000E-03
144	2.004E-01	1.890E-04	2.000E+00	2.700E+00	1.279E-02



detail is needed, copies of the tapes can be sent to individual users.

The Dice Throw Calculation required approximately 20 hours of 7600 time and followed the phenomenology from initiation ( 1 sec) to less than 2.5 PSI (1.2 seconds). The calculation was continued to late time under another project.

## SECTION V

### COMPARISON WITH EXPERIMENT

Experimental free field airblast data were collected by several agencies including BRL and the Canadian, Suffield Experimental Station. Published preliminary experimental data has been compared with the AFWL HULL Dice Throw calculated parameters. The vast majority of the experimental data was collected at or near ground level. The comparisons presented here are only for those data below five feet above the ground.

The most easily measured parameter is the arrival time. Figure 10 compares calculated and measured arrival. The inconsistencies in calculated parameters for distances less than 35 feet are a result of the free expansion phase, during which the shock is not well formed and is difficult to define numerically. Beyond 35 feet the agreement is excellent.

The peak overpressure (Fig 11) is the next easier measurement to make. The calculated curve indicates distinct changes in slope at several radii. These variations are associated with air shock separation from the detonation products, rarefaction waves and secondary shocks. Overall agreement between calculation and experiment is excellent.

The effects of detonation products are dramatically reflected in the overpressure impulse vs ground range (Fig 12). A sharp spike appears at a ground range of approximately 290 ft. Although the spike was not observed experimentally on Dice Throw, it has been observed on spherical TNT detonations including Mixed Company. For the TNT detonations the calculated spike is a factor of two larger than for Dice Throw. The smaller spike of Dice Throw is caused by a combination of the lower loading density for ANFO and the cylindrical charge geometry.

The positive phase duration (Fig 13) is a more difficult parameter to measure experimentally because a judgment must be made regarding the time at which the overpressure returns to ambient. This is affected by electronic and digitization noise, base line drift and the experience of the reader. Calculationally it is well defined when the shock is well defined. Thus inside of 35 feet the positive duration is somewhat questionable.

Beyond 200 feet agreement is very good. Experimental dynamic pressure data was not available for comparison in this paper.

#### Conclusior -

The Hull Code provides a powerful tool for the prediction of free air blast parameters for large scale detonations. A wide variety of parameters have been compared with experimental data and overall agreement is very good.

The Hull calculation was extended to extremely low overpressure using a linearized model for shock propagation. These results give good agreement with experiment but experimental data had large scatter.

It should be pointed out that the Dice Throw Calculation is the result of over a year's effort of preliminary calculations and experimental comparisons. This is the result of the cooperation of several agencies within the DOD and their contractors.

### References

1. Needham, C.E., Pre Dice Throw Project Officers Report on Theoretical Airblast Calculation.
2. Fry, M.A., et al., The Hull Hydrodynamics Computer Code  
AVWL TR 76-183. Air Force Weapons Lab, Kirtland AFB, NM, Sept 76.
3. Needham, C.E., Prairie Flat Air Blast Calculations  
AFWL TR-69-4. Air Force Weapons Lab, Kirtland AFB, NM, Feb 1969

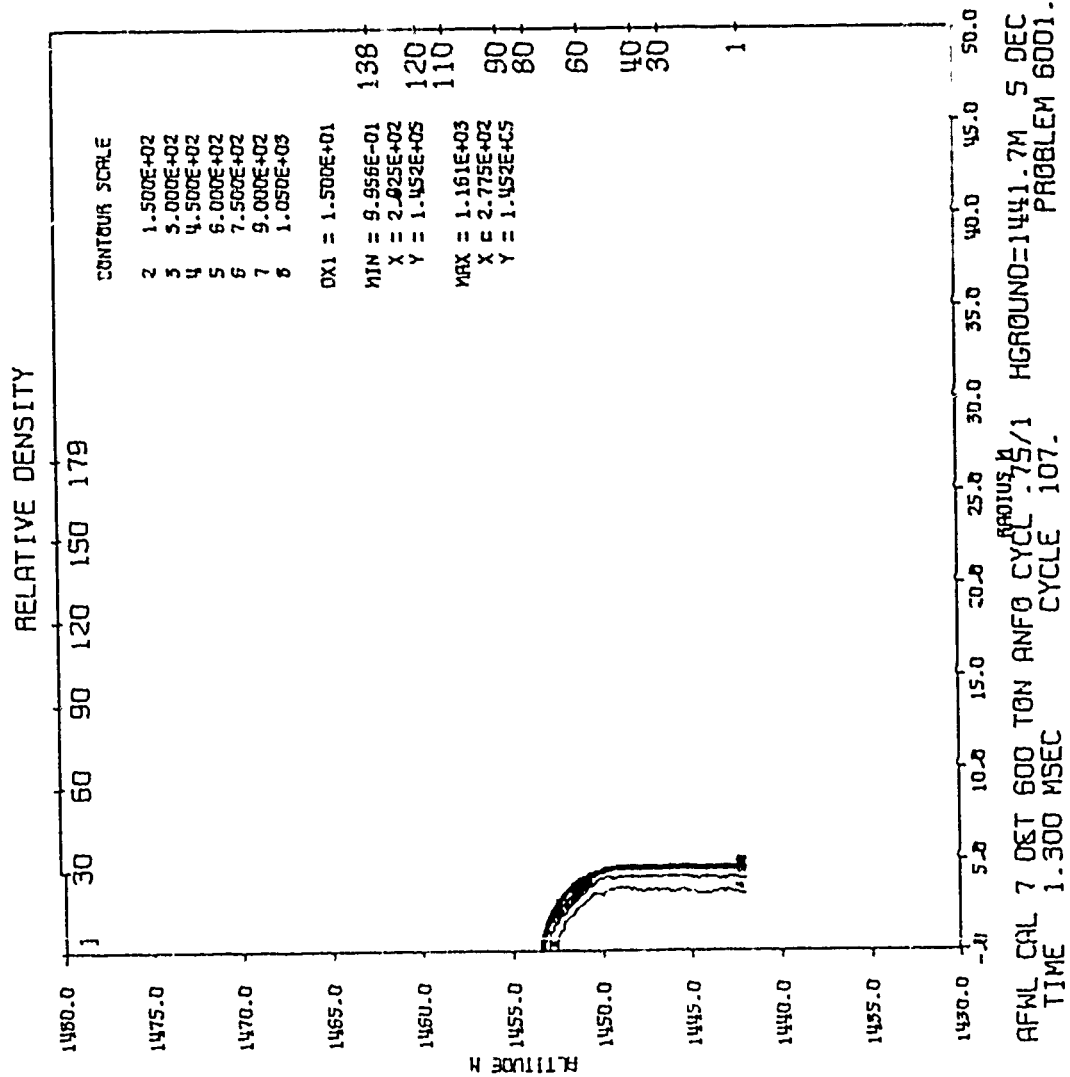


Figure 1

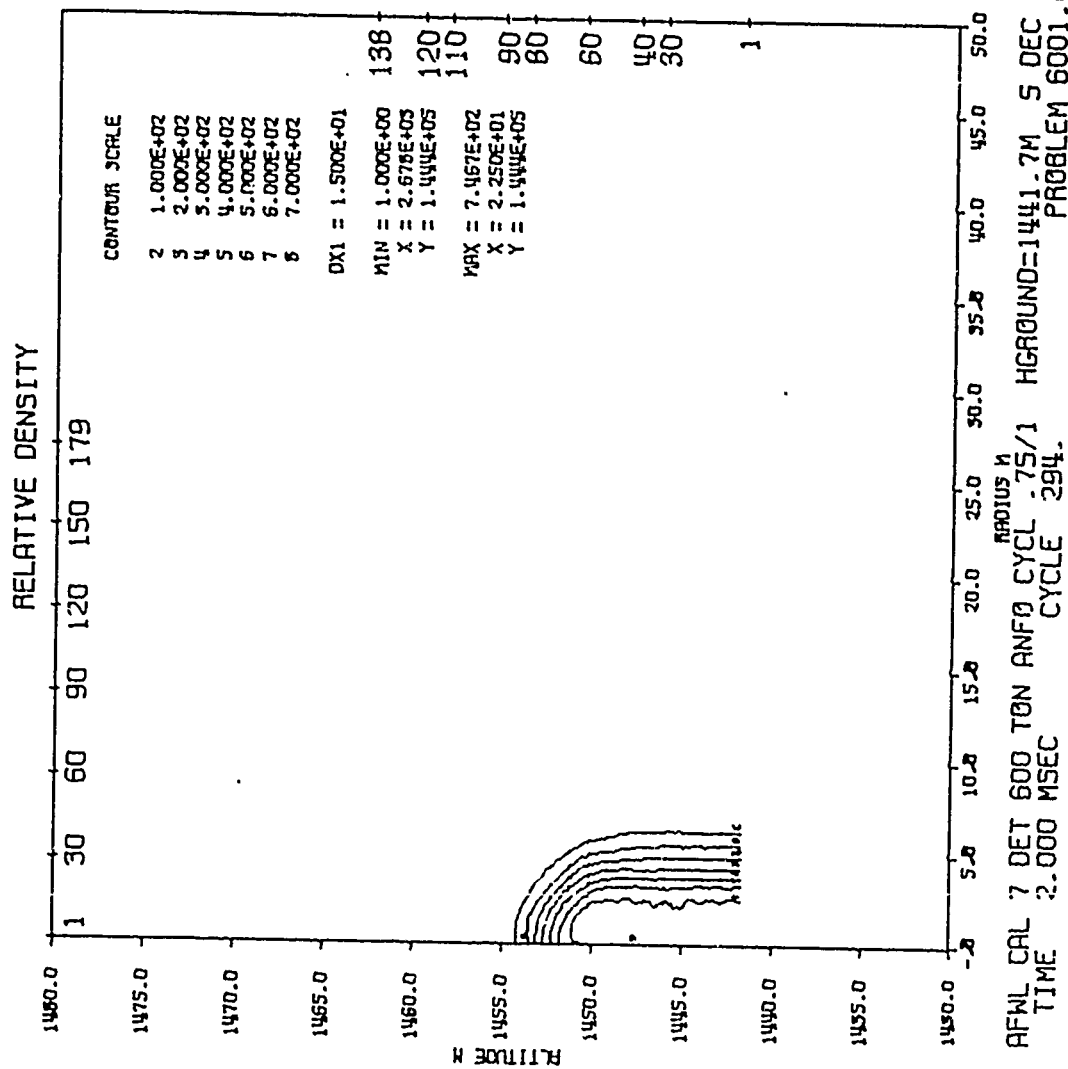


Figure 2

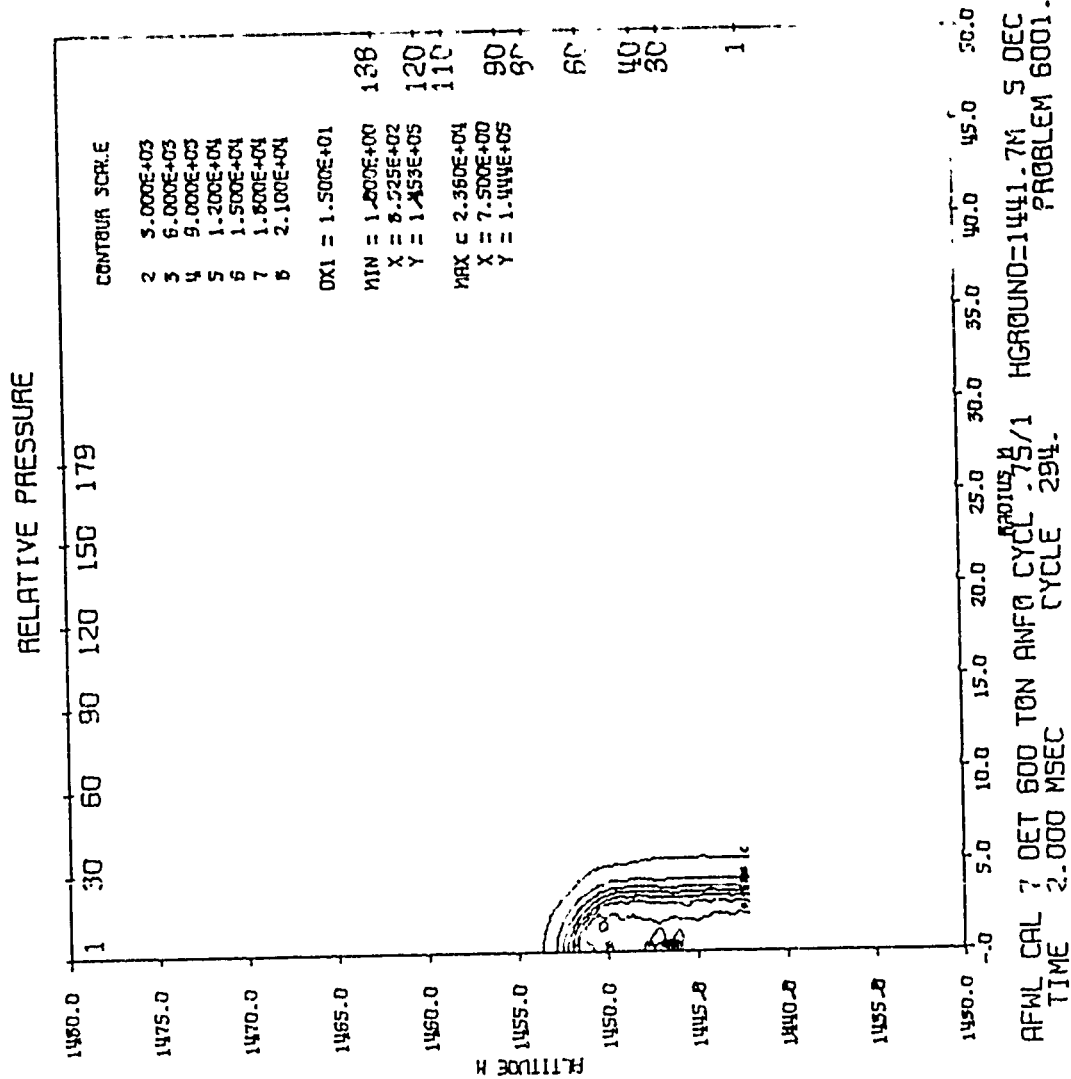


Figure 3



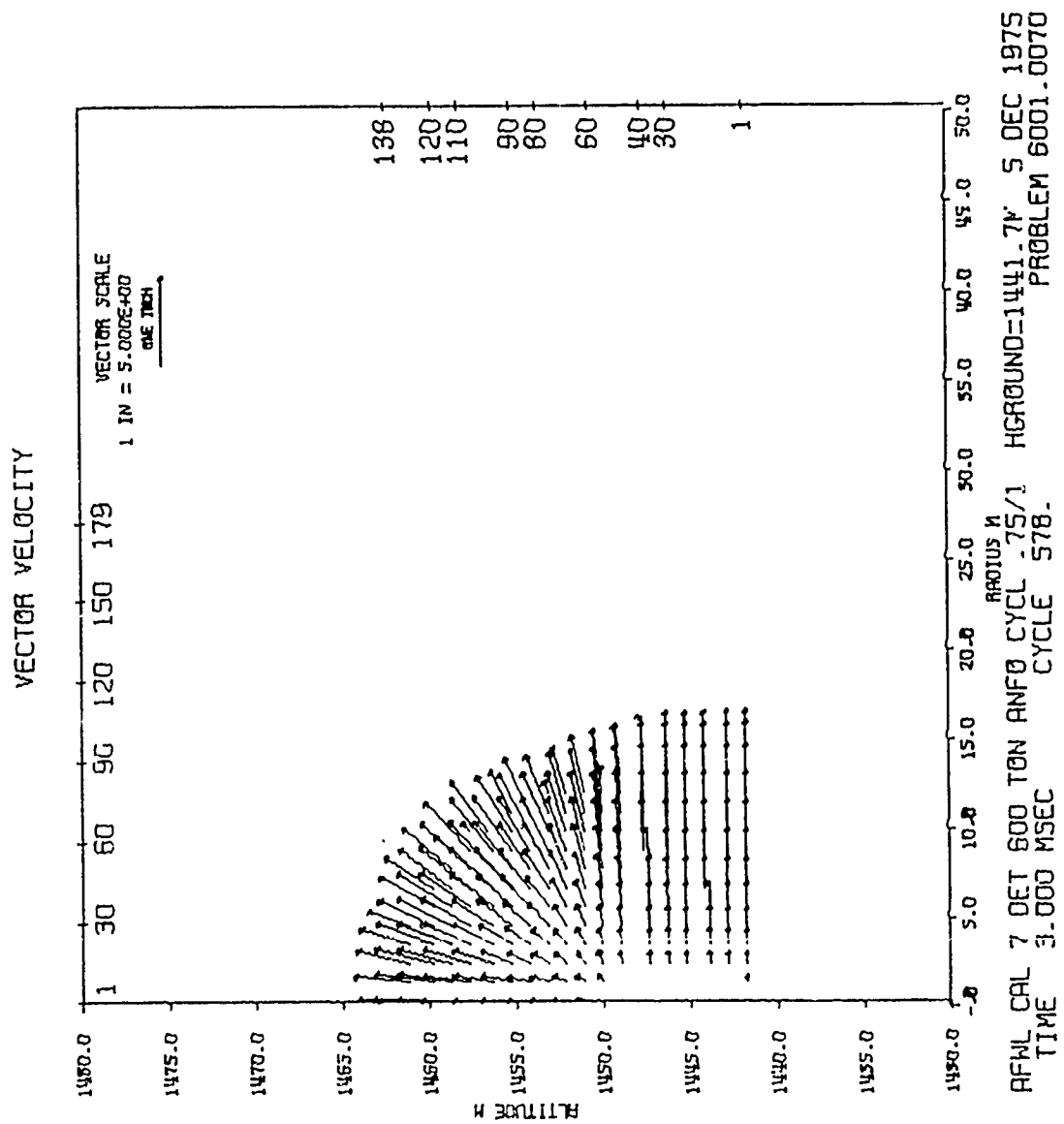


Figure 4

# KINETIC ENERGY

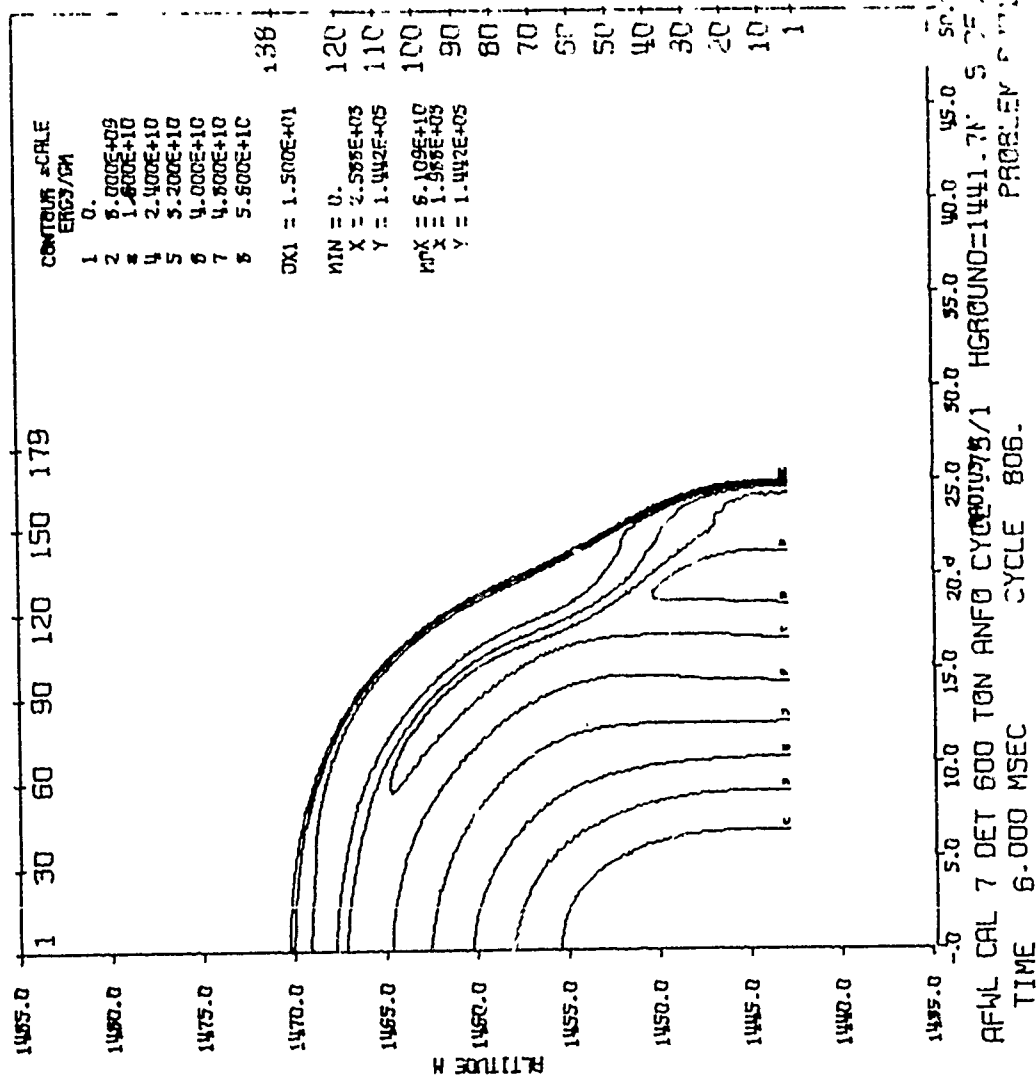


Figure 5

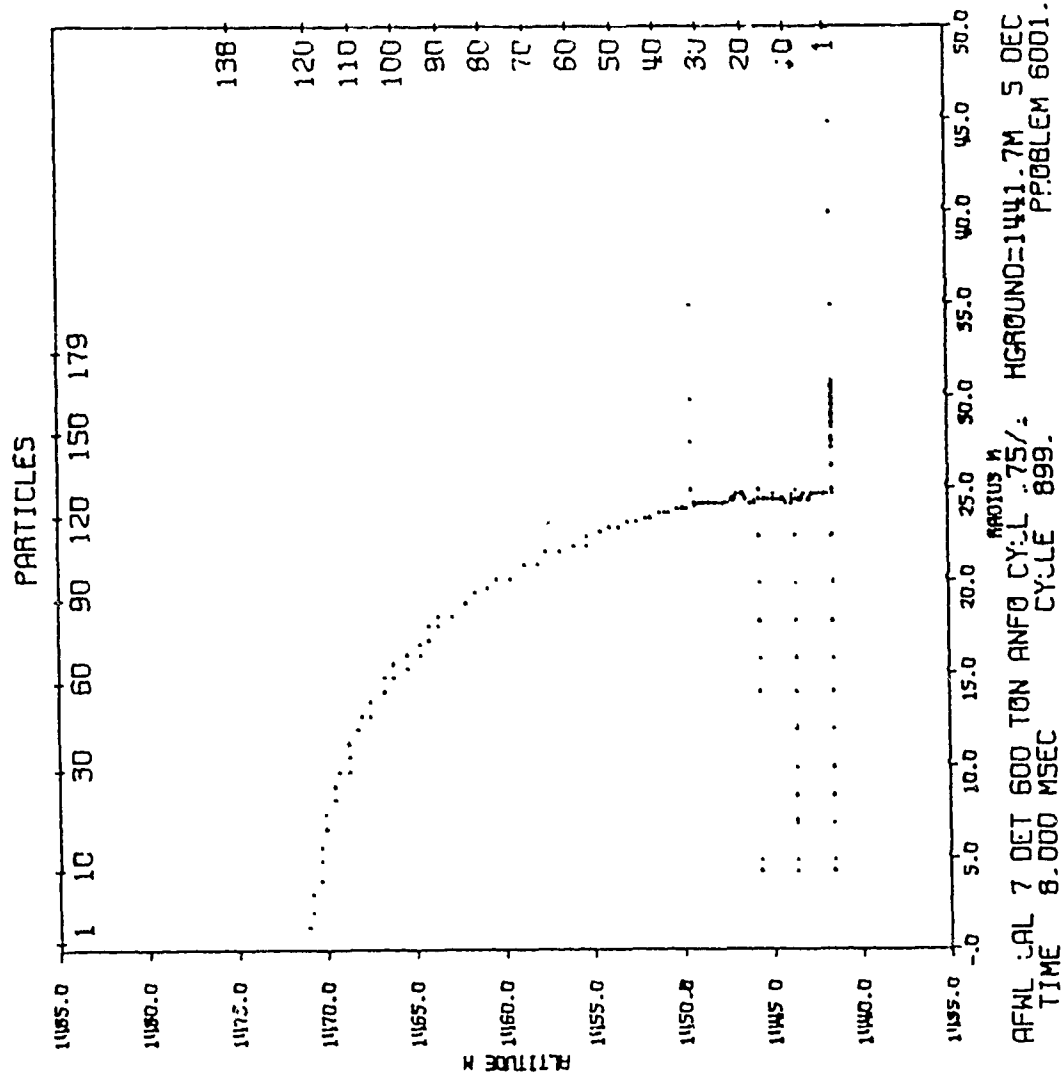


Figure 6

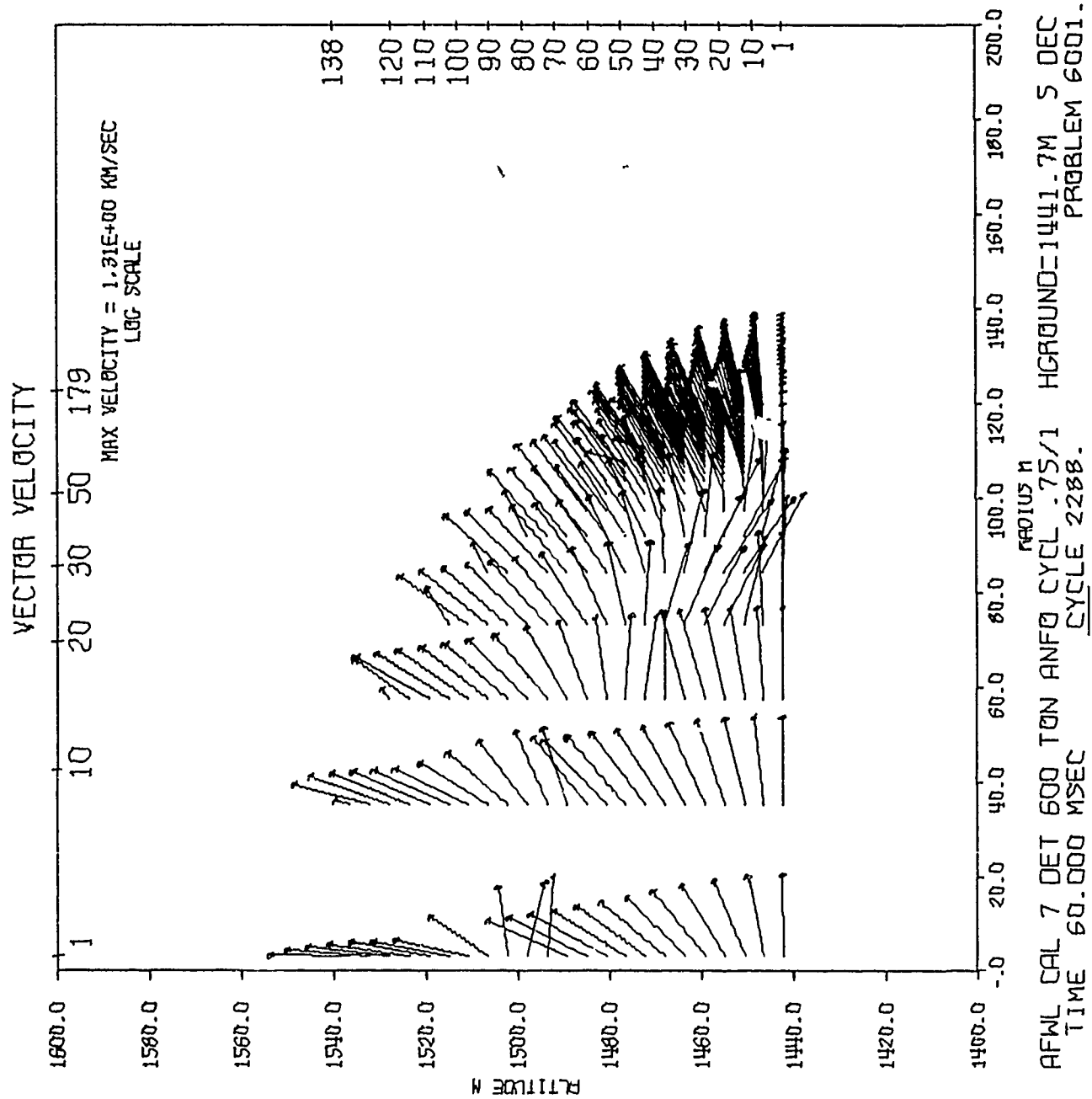


Figure 7

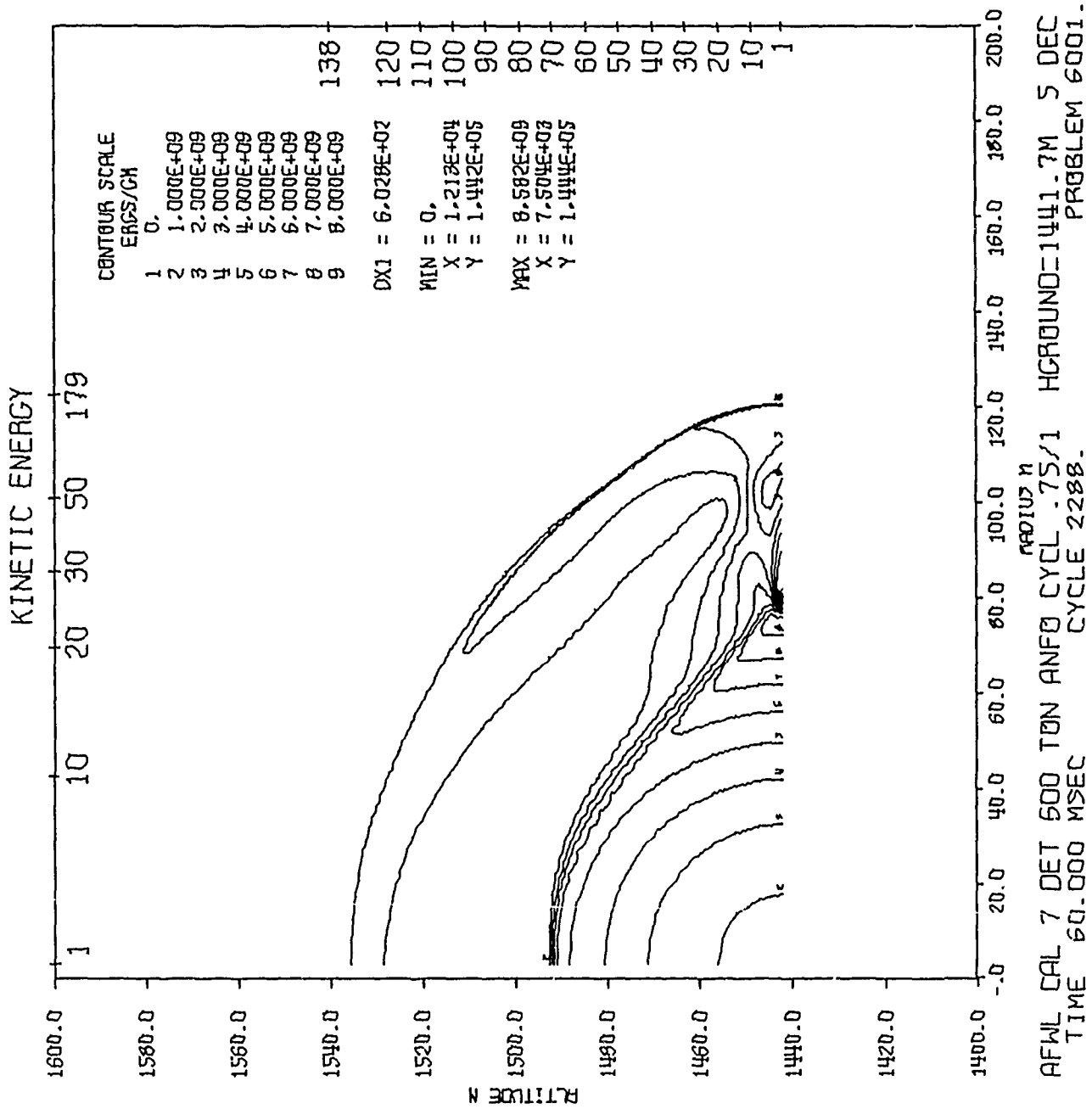


Figure 8

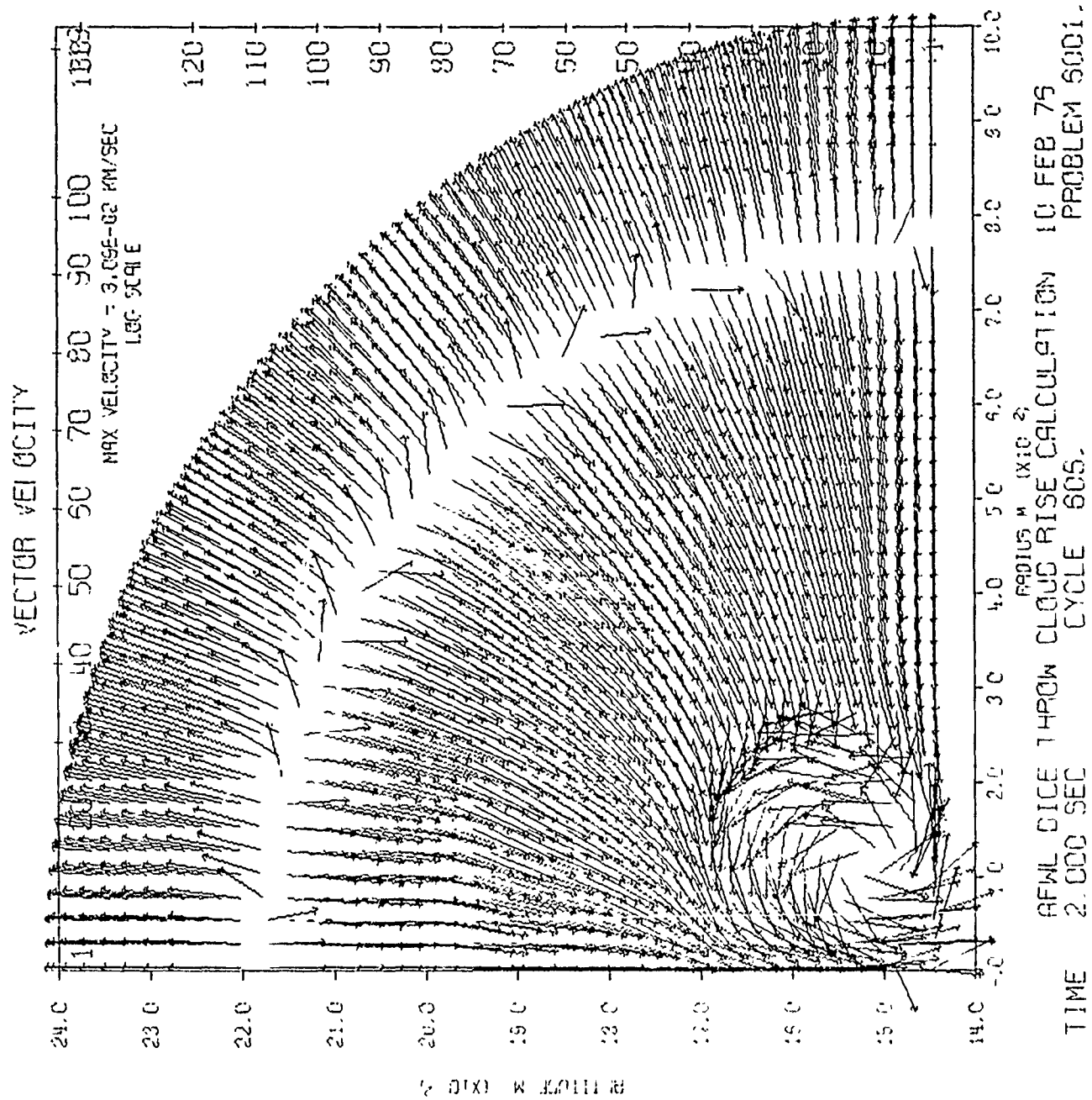


Figure 9

AFWL 7DET 600TON ANFO, PROB=6001.007  
ARRIVAL TIME VS RADIUS

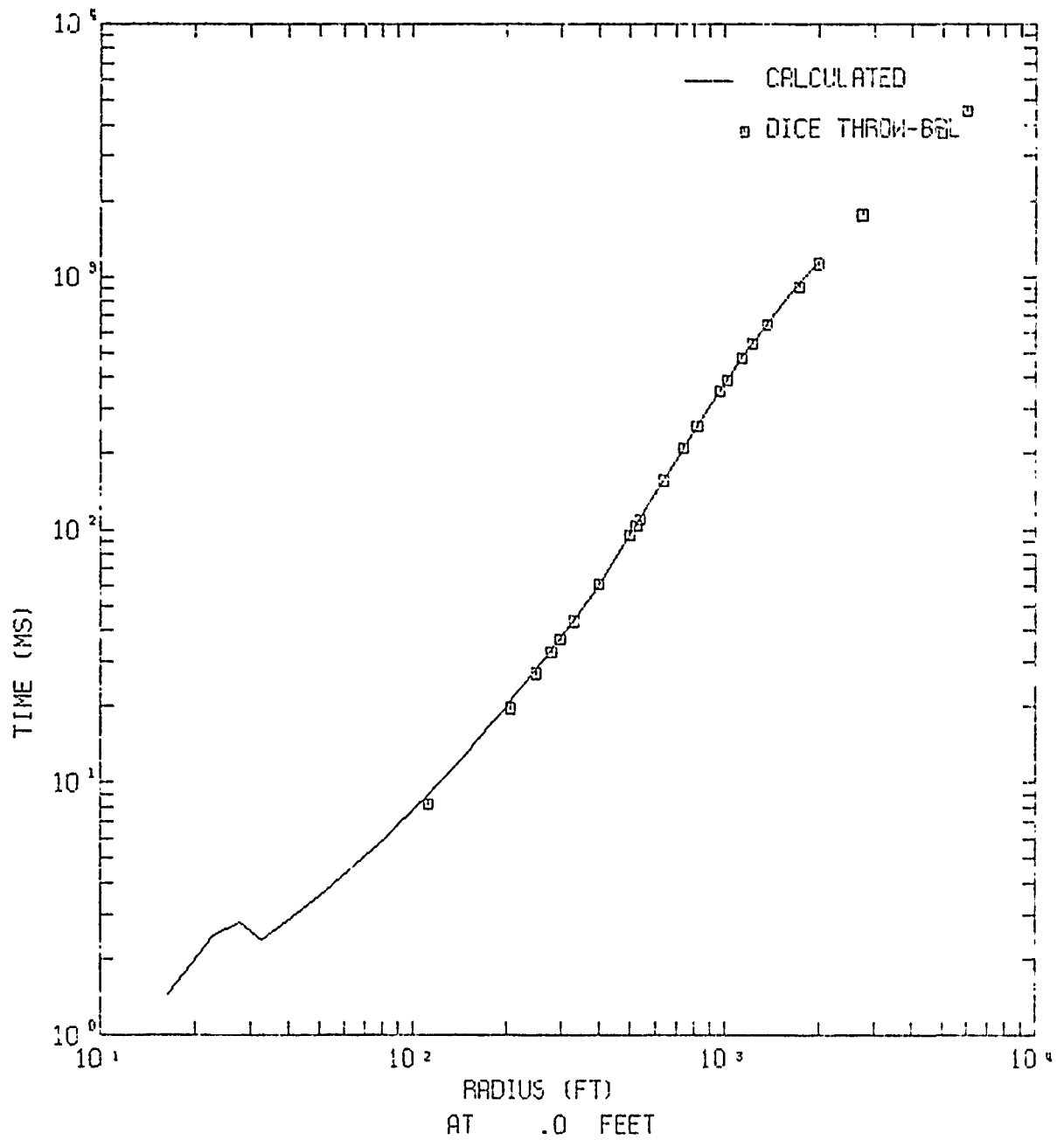


Figure 10

AFWL 70ET 6000N ANFO, PROB=6001.007  
OVERPRESSURE VS RADIUS

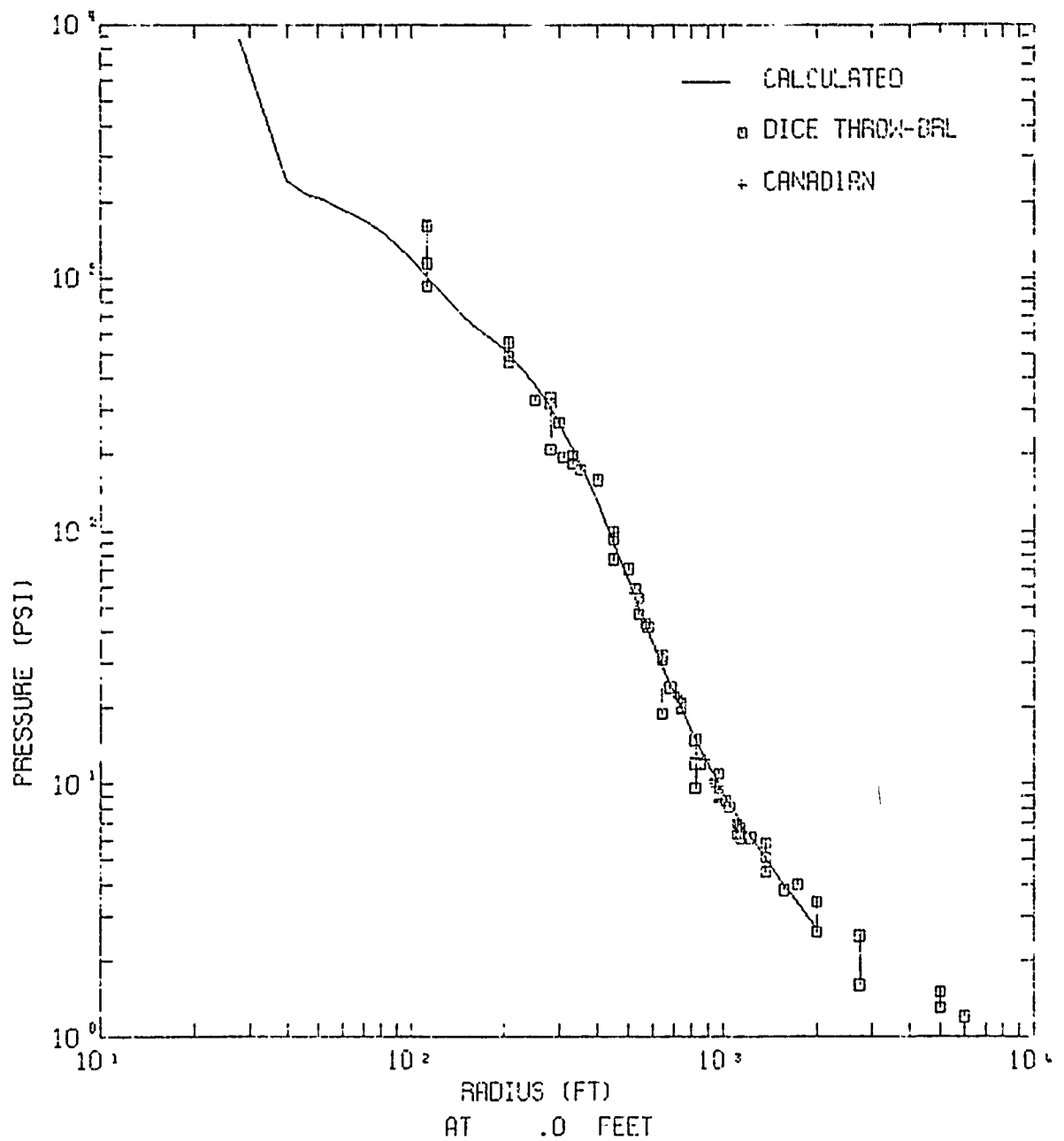


Figure 11



AFKL 7DET 600TON ANFO, PR3B=6001.007  
OVERPRESSURE IMPULSE VS RADIUS

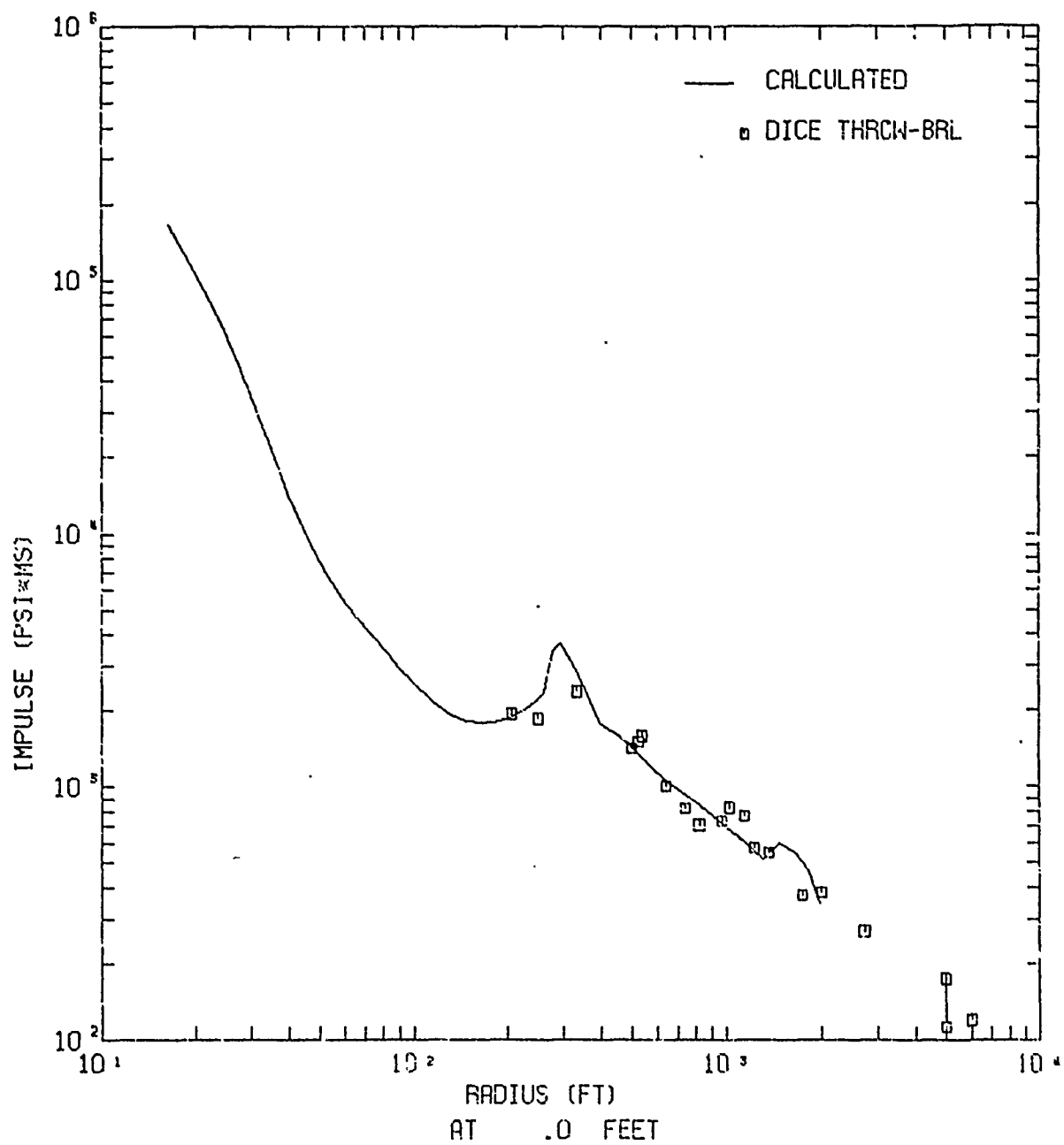


Figure 12

SFWL 7DET 500TCN ANFO.PP05=6001.007  
 POSITIVE PHASE DURATION VS RADIUS

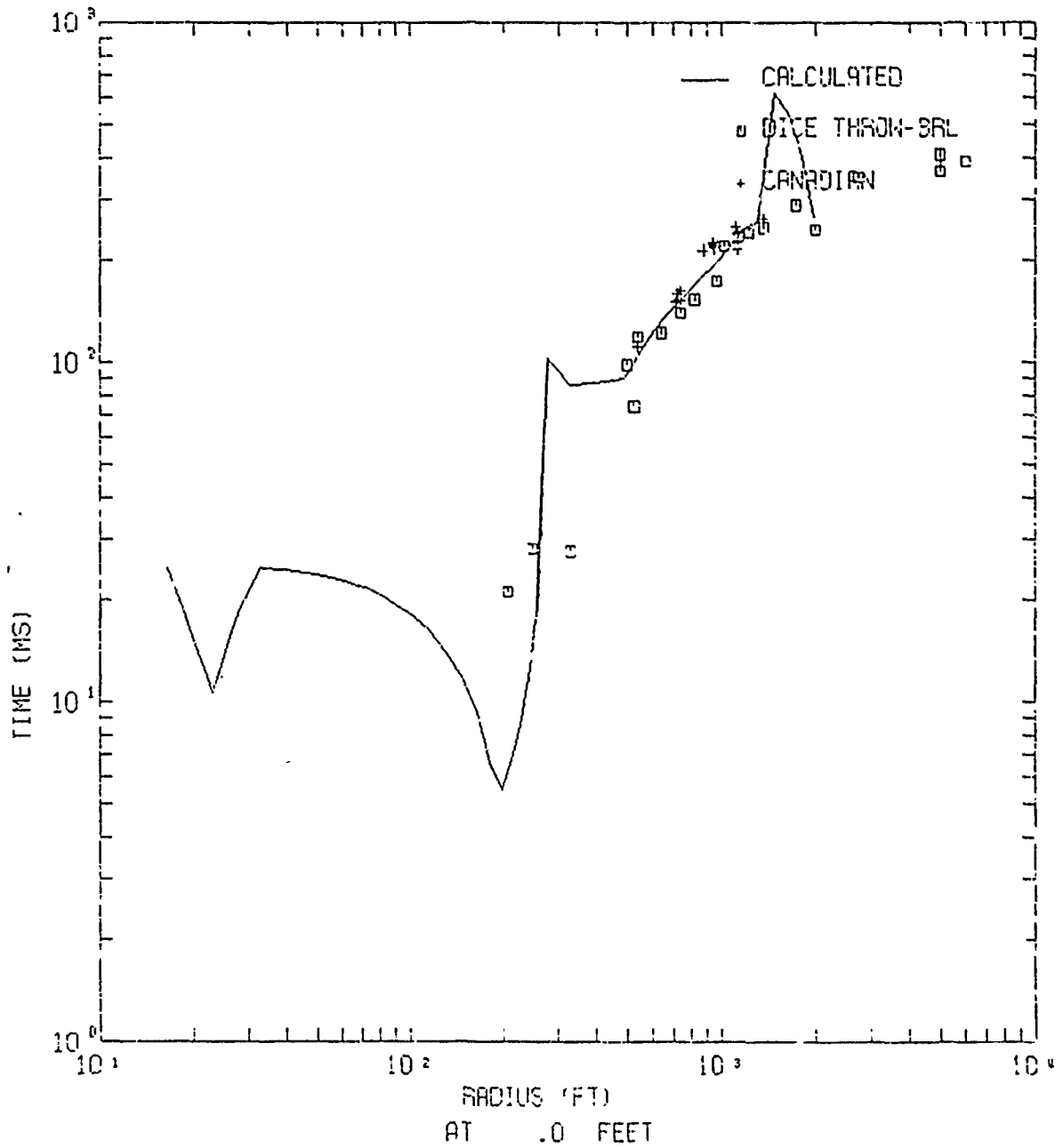


Figure 13

**9. BLAST EFFECTS ON HELICOPTER -  
EVENT DICE THROW**

**by**

**Robert Mayerhofer  
Ballistic Research Laboratory**

## ABSTRACT

Last year the BRL participated in the DNA sponsored 500 ton H.E. blast trial called Dice Throw with an experiment involving the vulnerability of an in-flight helicopter and helicopter windows. More specifically, the objectives of the experiment were: (1) to determine the structural response and rigid body motions of an in-flight helicopter subjected to blast loading and compare the resultant data with analytical predictions made by computer models, and (2) compare the response of recently developed transparent armor windows to the response of conventional Plexiglas windows. This report presents the results of that experiment and an overview of the current status of helicopter vulnerability to nuclear blast.

## PREFACE

This report is the final Project Officer's Report on Project 107, Event Dice Throw. The project was designed to extend the work of the drone helicopter experiments conducted under Project LN 114, Mixed Company, and Project MT 101, Pre-Mine Throw IV, and to investigate the response of a new type of ballistic transparent armor for helicopter windows. The details of the instrumentation calibration work, the computer code descriptions and the experimental/analytical correlations are not discussed here because these areas are comprehensively covered in the referenced documents. This report presents the results of the experiment and an overview of the current status of helicopter vulnerability to nuclear blast.

## TABLE OF CONTENTS

	<u>Page</u>
PREFACE -----	2
CHAPTER 1      INTRODUCTION -----	5
1.1    General -----	5
1.2    Objectives -----	5
1.3    Background -----	5
CHAPTER 2      PROCEDURE -----	8
2.1    Drone Helicopter -----	8
2.2    Static Helicopter -----	20
CHAPTER 3      PREDICTIONS -----	23
3.1    Drone Helicopter -----	23
3.2    Transparent Armor -----	24
CHAPTER 4      RESULTS -----	26
4.1    Drone Helicopter -----	26
4.2    Static Helicopter -----	38
CHAPTER 5      EXPERIMENTAL DATA AND ANALYTICAL PREDICTION CORRELATION -----	43
CHAPTER 6      CONCLUSIONS -----	51
REFERENCES -----	54
APPENDIX A      RAW DATA -----	55

## LIST OF ILLUSTRATIONS

<u>Figure</u>	<u>Page</u>
2.1 Test Layout - Drone Helicopter -----	9
2.2 UH-1 Helicopter Overall Dimensions -----	10
2.3 Flight Control Console Inside Main Bunker -----	11
2.4 Drone Helicopter on the Pad with the Main Control Bunker in the Background -----	12
2.5 Pilot's View of the Drone Helicopter in Flight -----	13
2.6 Location of Transparent Armor - Drone Helicopter -----	14
2.7 Strain Gage Locations on Rotor Blades -----	17
2.8 Strain Gage and Pressure Transducer Locations on Tail Boom and Fin -----	18
2.9 Free-Field Blast Gages -----	19
2.10 Test Layout - Static Helicopter -----	22
4.1 Typical Side-On Blast Damage -----	27
4.2 Popped Open Nose Compartment Door -----	28
4.3 Forward Fuselage Blast Side Damage -----	29
4.4 Cargo Door Blast Side Damage -----	30
4.5 Aft Fuselage Blast Side Damage -----	31
4.6 Tail Boom Blast Side Skin Damage -----	33
4.7 Tail Boom Interior Damage Viewing Forward -----	34
4.8 Tail Boom Interior Damage Viewing Aft -----	35
4.9 Engine Cowling Damage Side Opposite Blast -----	36
4.10 Fuselage Damage on Side Opposite Blast -----	37
4.11 Damage to Plexiglas Window Side - Static Helicopter -----	39
4.12 Damage to Transparent Armor Side - Static Helicopter -----	40
4.13 Transparent Armor Broken from Slide Channel in Front Door -----	41
4.14 View from Pilot's Seat Through Shattered Transparent Armor Windshield -----	42
5.1 Extreme Values of Flapwise Bending Moments for <u>Tail Rotor Blades</u> - Experimental/Analytical Comparison -----	44
5.2 Extreme Values of Flapwise Bending Moments for <u>Main Rotor Blades</u> - Experimental/Analytical Comparison -----	45
5.3 Time Vs. <u>Yaw Deviation</u> - Experimental/Analytical Comparison -----	46
5.4 Time Vs. <u>Yaw Rate</u> - Experimental/Analytical Comparison -----	47
5.5 Peak Total <u>Fin</u> Lateral Bending Moments - Experimental/Analytical Comparison -----	49
5.6 Peak Total <u>Tail Boom</u> Lateral Bending Moments - Experimental/ Analytical Comparison -----	50
A.1 Raw Data -----	58
thru	
A.43	100

## LIST OF TABLES

<u>Table</u>		
2.1 Instrumentation List -----		16
2.2 UH-1 Transparent Armor/Plexiglas Comparison -----		21
6.1 Approach to Determining Helicopter Nuclear Blast Vulnerability-----		53
A.1 Raw Data Identification -----		56

## CHAPTER 1

### INTRODUCTION

#### 1.1 GENERAL

This report presents the results of the Ballistic Research Laboratory (BRL) drone helicopter experiment, Project 107, Event Dice Throw. In order to maintain a reasonable report size and to avoid repetition of material presented in other reports, much of the details of the analytical and experimental correlations and computer code descriptions have been deleted and only an overview of the project results are presented. The digitized raw data is presented in Appendix A. For a comprehensive description of all other aspects of the experiment, the referenced documents should be used.

#### 1.2 OBJECTIVES

The objectives of this experiment were: (1) to determine the structural response and rigid body motions of an in-flight helicopter subjected to blast loading and to compare the resultant data with predictions made by several of the currently most prominent computer codes in use and (2) to compare the response of newly developed transparent armor for helicopter windows to the response of the conventional Plexiglas windows.

#### 1.3 BACKGROUND

The BRL became actively involved with aircraft vulnerability to nuclear blast by participating in the 500 ton HE blast trial entitled Dial Pack, that was conducted in July 1970 at the Suffield Experimental Station, Canada (Reference 1). The BRL experiment, Project LN 111, consisted of subjecting four different types of aircraft (two fixed wing and two helicopters) in parked configurations, side-on to the blast at various overpressure levels, to obtain damage data and to determine if the prediction methodology in use at BRL at that time was valid. The results indicated that the methodology was reasonably accurate when applied to some of the aircraft and that modification was required for application to others. In general, the methodology was acceptable for predicting gross structural damage to most kinds of parked aircraft but could not be used with a high level of confidence for predicting detailed damage or damage under in-flight conditions. In addition to the data obtained on airframe structural damage, the experiment revealed the potential threat of Plexiglas window breakup for increasing the vulnerability of the aircraft through incapacitation of the pilot and crew due to Plexiglas fragment injury. The results of Project LN 111



were the impetus for the conception of the drone helicopter experiment, Project LN 114, Mixed Company.

The Mixed Company, 500 ton TNT, blast trial was conducted in November 1972 at Grand Junction, Colorado. The BRL's drone helicopter experiment, Project LN 114, was proposed for this event because of the need to expand the studies of structural response and rigid body motions of in-flight aircraft, and to validate several of the existing computer models used for predicting the responses. Project LN 114 was designed to obtain response data by using a fully instrumented drone helicopter in a hover configuration and exposing it to a blast overpressure of 1.3 psi. The Bell Helicopter Company (BHC) was contracted to design, fabricate and operate the autopilot system for the drone helicopter and to install instrumentation, operate recording equipment and reduce the resultant data. Kaman Avidyne, under contract to DNA, was to make pretest predictions of rigid body motions, compare resultant data with the predictions, and critique the methodology used.

Project LN 114 was basically unsuccessful because of autopilot system problems on the morning of the shot day. The helicopter could not be flown as a drone and was required to remain on the test pad as a static target. The resultant damage was minor and about 50 percent of the data sought was collected. Although the dynamic conditions were not achieved, Kaman Avidyne was able to apply the structural response data to the verification of several computer models. The results of that work indicated that more and better quality data was needed for a proper evaluation (Reference 2).

The 100 ton nitromethane blast trial, Pre-Mine Throw IV, that was conducted in November 1973 at the Nevada Test Station, Nevada provided the opportunity to retest the drone helicopter experiment at a minimum of cost and time. The damaged helicopter from Mixed Company was repaired; personnel from the USA Air Mobility R&D Laboratory (AMRDL) at Fort Eustis, Virginia, accepted the tasks previously contracted to BHC; the high speed motion picture coverage was provided by the Denver Research Institute (under contract), and a new set of pretest predictions were made by Kaman Avidyne. About 5 days before the shot day the container for the nitromethane burst under water test loadings and all projects were terminated until a new container could be designed and fabricated.

The retest of Pre-Mine Throw IV finally took place August 1974 at NTS as originally planned. After some technical problems on the shot-day, the drone helicopter was successfully flown and landed, 95 percent of the data required was

obtained, and Kaman Avidyne was able to conduct an analysis of the data and show the correlation between the experimental data and the pretest predictions (Reference 3). The helicopter survived a 1.3 psi overpressure environment with no critical structural damage (broken Plexiglas windows and a crushed cargo door) and a minor amount of rigid body motion (3 degrees of Yaw). The data analysis by Kaman Avidyne showed that there was good correlation between the experimental data and the predictions for rigid body motions, rotor blade flap and bending moments; and tail boom and fin bending; however, there was poor correlation for the bulkhead and panel strains. For a general overview of Projects LN 114 and MT 101 refer to the Project Officer's Report (Reference 4).

In order to increase the confidence level in the prediction methodologies, to obtain more data for those responses that correlated poorly, and to better establish the threshold for a helicopter "kill," Project 107 was proposed for Event Dice Throw. In most respects, Project 107 was a retest of Project MT 101 (Pre-Mine Throw IV) except that the overpressure level for exposure was increased to 1.8 psi, the drone was fitted with a newly developed transparent armor, instrumentation was improved, and a static helicopter was added as a transparent armor target at the 3.5 psi level. All of the organizations previously involved with Project MT 101 were again employed to work on Project 107 in the same capacity as before. In addition, the Bell Helicopter Company was contracted to AMRDL to provide a technical representative to support the operation of the autopilot system. Each Army Project Officer was required to provide, for publication, pretest analyses of the predicted response of the primary target equipment of the experiments. The pretest analysis of the drone helicopter was conducted by Kaman Avidyne (Reference 5) and will be summarized later in this report.

On shot day, October 6, 1976, the drone helicopter was once again successfully flown during the blast, landed safely, and the required data recorded. The transparent armor results have provided considerable insight into the Plexiglas window breakup problem and have shown that a component designed specifically to reduce the vulnerability of the helicopter to conventional projectiles can also reduce the vulnerability of the helicopter to nuclear blast.

## CHAPTER 2

### PROCEDURE

#### 2.1 DRONE HELICOPTER

2.1.1 Test Layout. The general layout of the drone helicopter test is shown in Figure 2.1. The drone helicopter, a UH-1B (Figure 2.2) was positioned to fly side-on to the blast wave propagation in a hover mode at an altitude of 60 ft and a side-on overpressure level of 1.8 psi (2750 ft from GZ). For safety purposes the helicopter was tethered to a ground anchor by a 230 ft long steel cable, leaving 170 ft of slack cable for recovery maneuvering after the blast event.

The take-off landing pad was a 200 x 200 ft macadam surface 2 inches thick. This pad provided a clear level area for helicopter operations and ground handling, and minimized the dust and debris from the rotor blade downwash.

The autopilot system was mounted onboard the helicopter and was "hard wired" to the main control bunker where the pilot and flight control console were housed (Figure 2.3). The main control bunker was located 500 ft from the helicopter tether point and to the rear of the helicopter (Figure 2.4); this was as close a simulation of the pilot's normal cockpit position as possible. The distance selected was a compromise between safety in the event of an aircraft crash, and acceptable limits for remote control and visual observation. The pilot viewed the helicopter through a 4 inch thick Plexiglas window (Figure 2.5) and maintained flight position visually, by the instruments of the flight control console, and by voice communication with two observers located in the bunker annex.

The bunker annex was a 6 x 6 ft cubicle located in a three-quarter forward position with respect to the helicopter and was also 500 ft from the center of the pad. By viewing the helicopter from the two bunker positions, the pilot was better able to maintain the desired hover position over the center of the pad.

The helicopter was fitted with two components not previously tested in the series of drone helicopter experiments: (1) an anthropomorphic dummy, fully dressed in the standard flight uniform, with a pressure transducer and 4 fixed-level accelerometers mounted in the chest cavity; and (2) transparent armor mounted in the front windshield and both front doors (Figure 2.6). The Lovelace Foundation, with the exception of the pressure transducer, instrumented and conducted the testing of the anthropomorphic dummy and will publish a report covering the results. The transparent armor was provided by the Army Materials and Mechanics Research Center

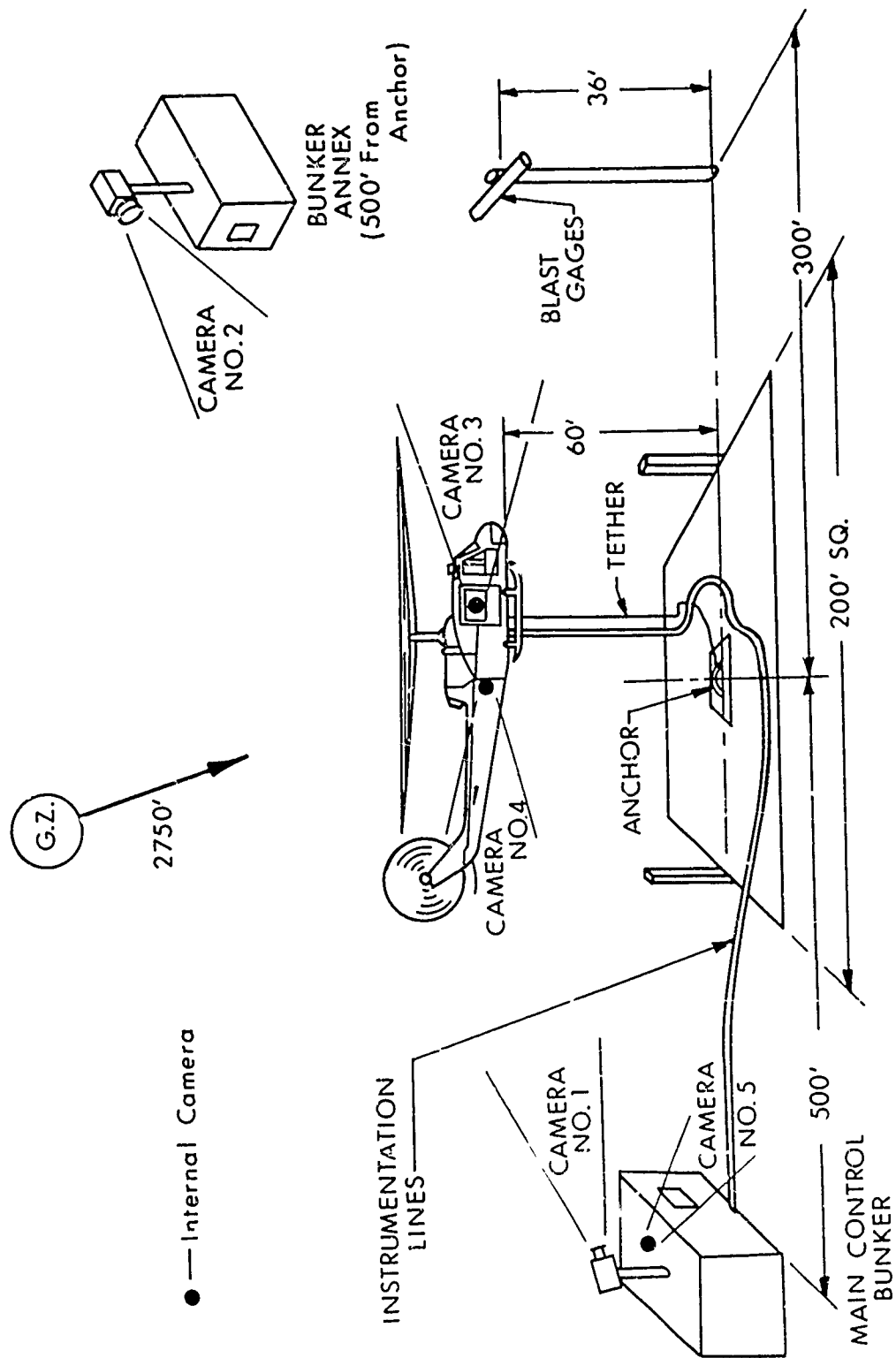


Figure 2.1. Test Layout - Drone Helicopter

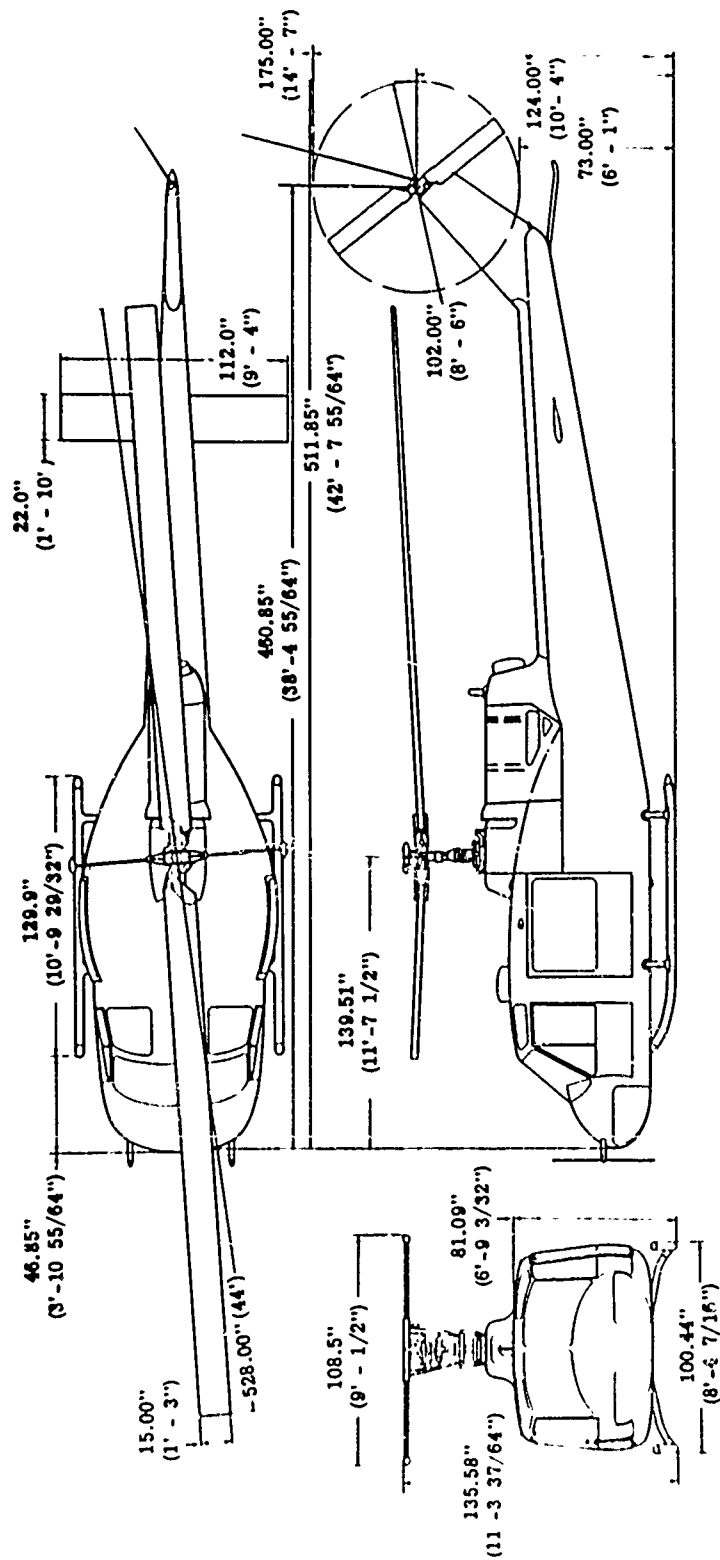


Figure 2.2. UH-1 Helicopter Overall Dimensions



Figure 2.3. Flight Control Console Inside Main Bunker

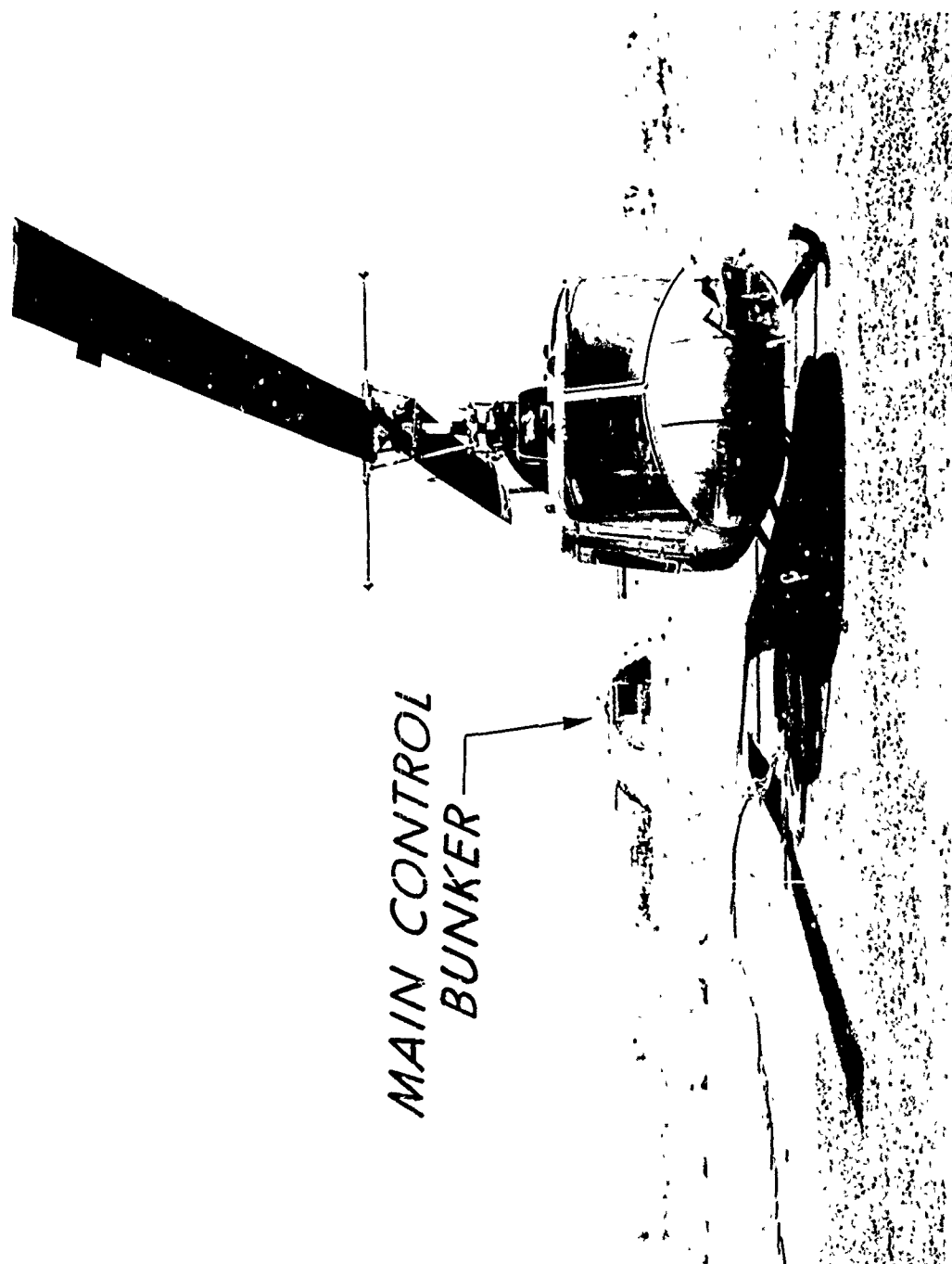


Figure 2.4. Drone Helicopter on the Pad with the Main Control Bunker in the Background



Figure 2.5. Pilot's View of the Drone Helicopter in Flight



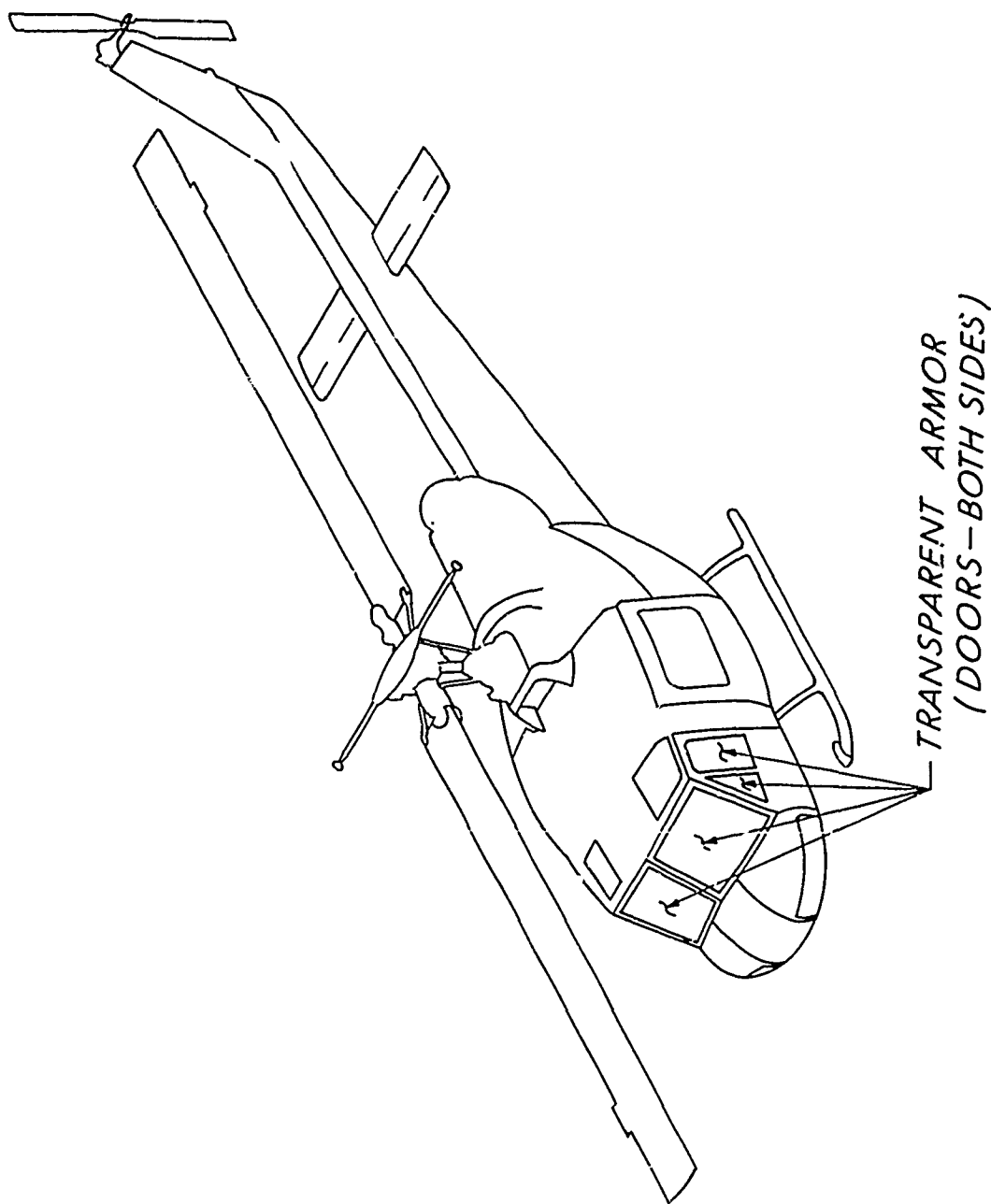


Figure 2.6. Location of Transparent Armor - Drone Helicopter

(AMMRC). One AMMRC representative and two prime contractor (Goodyear Aerospace Corp.) representatives were present during the event to comment on the transparent armor response.

2.1.2 Instrumentation. All helicopter instrumentation was "hard wired" between the helicopter and the recording equipment in the main control bunker. Data were recorded on four VR-3300 CEC 14 channel magnetic tape recorders and one Honeywell 8 channel oscillograph recorder. Each magnetic tape recorder was used for 11 channels of instrumentation data, one channel of reference timing, one channel of (detonation zero marking)/(IRIG-B timing), and one spare channel. Eight channels of the oscillograph recorder were used for quick-look playback of the magnetic tape in the field and also to record the flight control console stick positions and to make redundant recordings of the helicopters control stick positions.

The instrumentation consisted of a variety of sensors and components: pressure transducers, strain gages, linear and geared potentiometers, rate gyros and attitude control system, and a radar altimeter. The 52 channels of magnetic tape recorder instrumentation are listed in Table 2.1. The strain gage locations for the main and tail rotor blades and the tail boom are shown in Figures 2.7 and 2.8 respectively. In addition to the pressure transducers located in the anthropomorphic dummy, the tail boom, and the tail boom fin, a pressure transducer was mounted inside the cabin/cargo compartment facing the cargo door window to measure the increase in pressure level after the window was blown out.

Free-field blast measurements were made at a position 300 ft forward of the helicopter and at the same ground range as the helicopter. Blast gages were on a pole at a height of approximately 36 ft (Figure 2.9).

The high speed motion picture photography consisted of four 16 mm movie cameras with 400 ft magazines of color film and operated at 400 frames per second. Camera locations are shown in Figure 2.1. Camera 1 viewed the helicopter much the same as the pilot in the bunker, Camera 2 was positioned atop the annex bunker, Camera 3 was pedestal mounted inside the helicopter behind and between the front seats to view the instrument panel and windshield, and Camera 4 was mounted inside the tail boom viewing aft. Camera 5 was a 16 mm movie camera operated at 24 frames per second that was positioned inside the bunker to view the pilot's reactions during the blast event and the electrical meters on the autopilot instrument panel.

2.1.3 Transparent Armor. The transparent armor that was installed in the drone helicopter was a high-performance glass/plastic composite armor that provides

Table 2.1. Instrumentation List

<u>RESPONSE</u>	<u>MEASUREMENT</u>
Main Rotor Blade Bending	6 (4 + 2)
Tail Rotor Blade Bending	6 (4 + 2)
Tail Boom Bending	2
Tail Boom Stringer & Longeron Bending	2
Tail Boom Panel Strain	7
Tail Boom Fin Bending	<u>2</u>
TOTAL STRUCTURAL RESPONSE	25
Roll, Pitch, & Yaw Rates	3
Roll, Pitch, & Yaw Attitudes	3
Altitude	<u>1</u>
TOTAL RIGID BODY RESPONSE	7
Main & Tail Rotor Blade Flap Angle	2
Main & Tail Rotor Blade Azimuth	2
Cockpit Control Positions	4
Tail Boom, Fin, Cabin, Dummy Pressure	4
100 Hz, IR1G-B, FIDU	<u>8</u>
TOTAL SUPPORT DATA	20

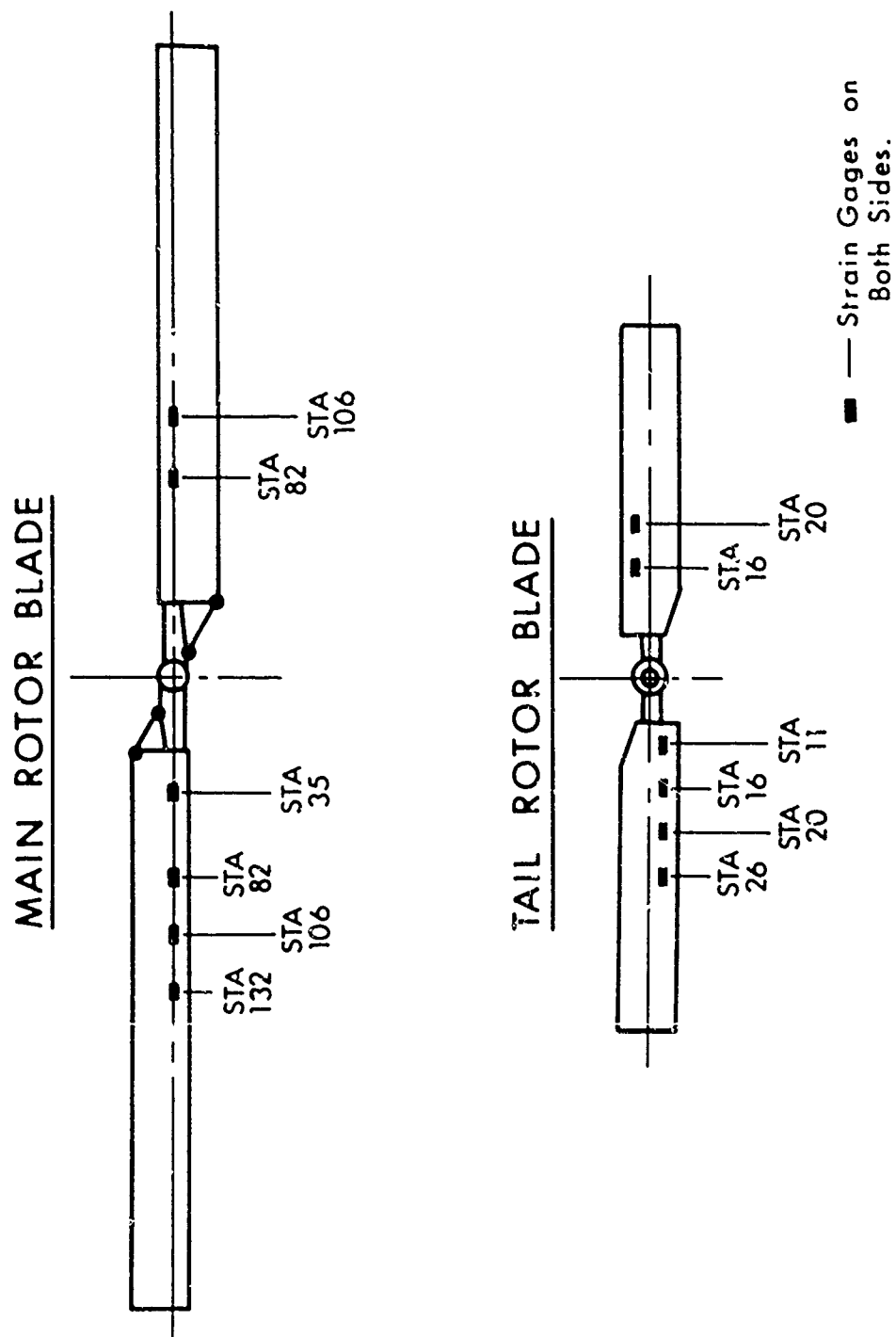


Figure 2.7. Strain Gage Locations on Rotor Blades

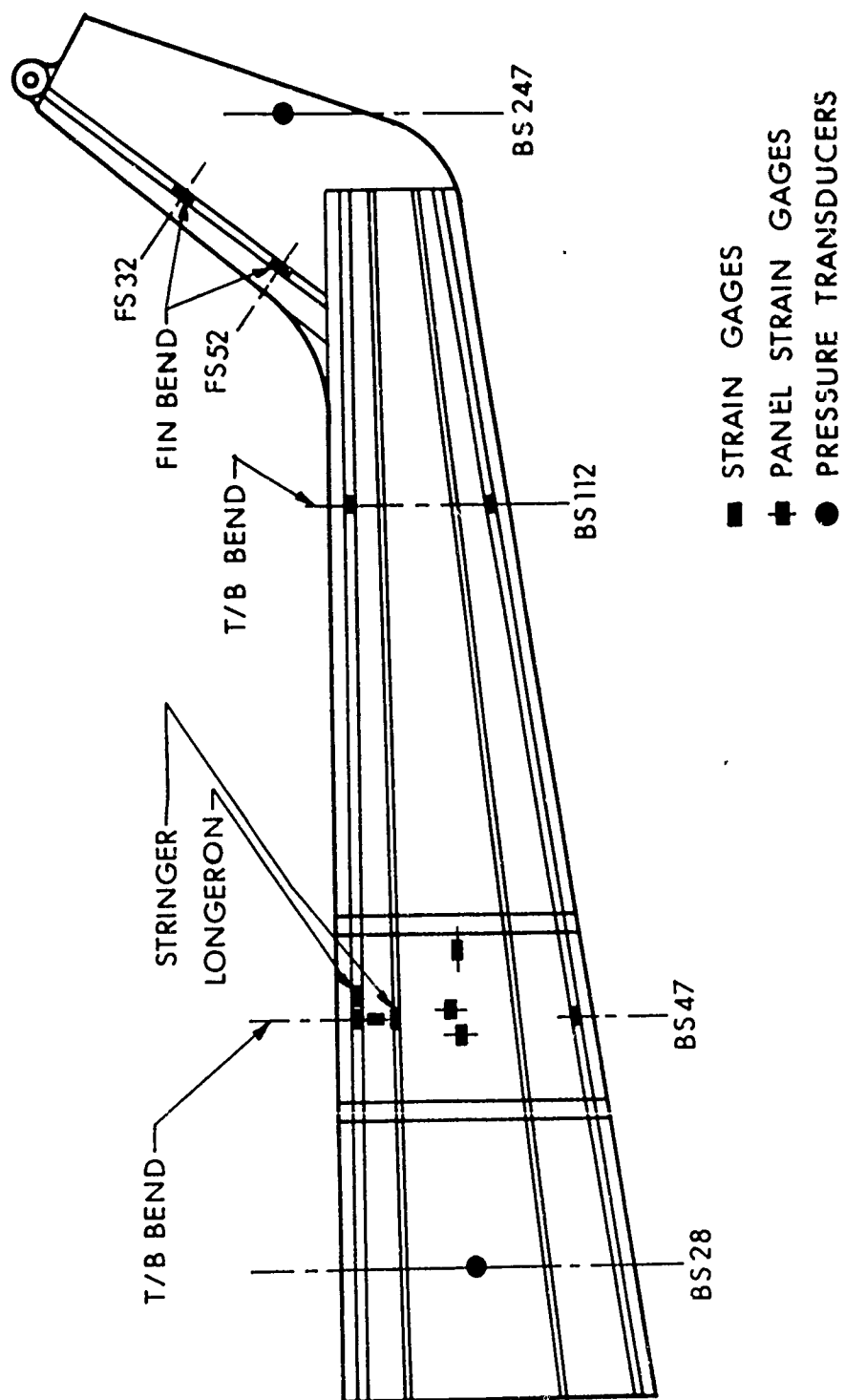


Figure 2.8. Strain Gage and Pressure Transducer Locations on Tail Boom and Fin

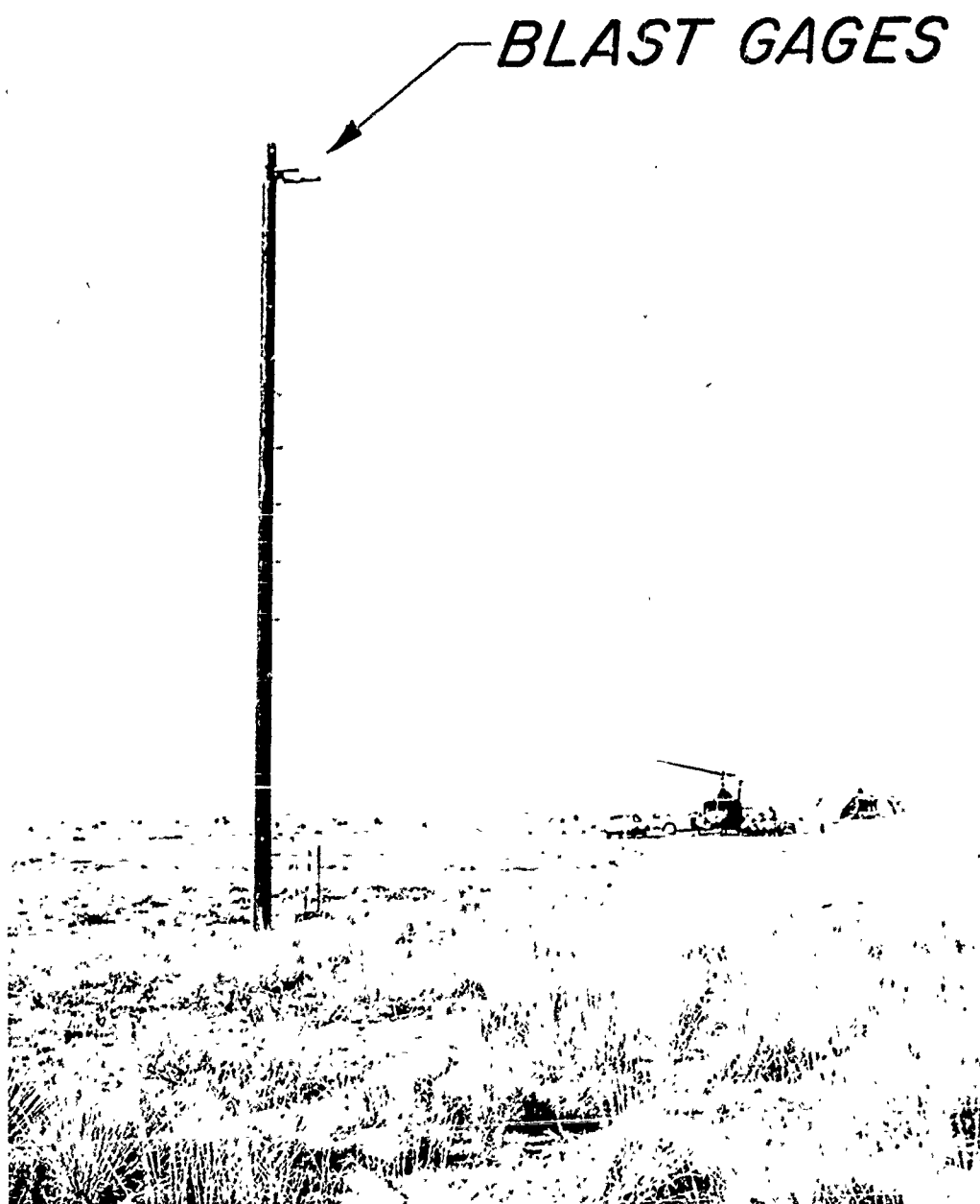


Figure 2.9. Free-Field Blast Gages

ballistic protection from fragments and projectiles at an areal density and thickness significantly lower than prior state-of-the-art laminated glass armor. The glass/plastic composite armor also eliminates the backside spalling of injurious particles upon ballistic impact. The performance of this armor has been known for some time, but until the Goodyear contract with AMMRC (Jan 1973) no attempt had been made to design and install the new armor on an actual aircraft. Some of the major considerations in the development of the armor were: retrofitting armor to existing mountings, limiting weight increase, fabricating contoured glass and plastic, and maintaining optical specifications. After subjecting the transparent armor to a series of ballistic, environment, and flight tests, it was concluded that the armor has application to current helicopters and should be the basis for transparent armor design in the next generation aircraft.

The transparent armor kit for installation in the UH-1 helicopter consisted of contoured armor for the windshield and flat plate armor for the front doors and the lower forward area inside the cockpit. Contoured armor could not be provided for the chin bubble because of the fabrication problems associated with severe curvatures. Because the internal armor provides no blast protection after the conventional Plexiglas window has been blown out, it was not installed in the drone helicopter.

For a general description of the transparent armor and for a comparison of thicknesses with conventional UH-1 Plexiglas windows, see Table 2.2. Notice from Table 2.2 that the transparent armor is 3.5 times thicker than the thickest Plexiglas (windshield). The total armor kit installation, including internal armor, increases the helicopter weight by 193 pounds. More detailed information can be obtained from AMMRC and Reference 6.

## 2.2 STATIC HELICOPTER

2.2.1 Test Layout. A UH-1 helicopter hulk (without tail boom or rotor blades) was used as a static target at the 3.5 psi overpressure level (1730 ft from GZ) to test the same kind of transparent armor used in the drone helicopter but at a higher overpressure level and face-on to the blast. The general layout is shown in Figure 2.10. Transparent armor was installed only on the right half of the windshield and in the right front door for a direct comparison with the conventional Plexiglas windows on the left side. The helicopter hulk was staked to the ground to minimize translation.

2.2.2 Instrumentation. The instrumentation consisted of two 16 mm high speed motion picture cameras with 400 ft magazines of color film and operated at 400 frames per second. The approximate locations are shown in Figure 2.10.

Table 2.2. UH-1 Transparent Armor/Plexiglas Comparison

<u>TRANSPARENT ARMOR</u>	<u>THICKNESS (in.)</u>
Soda-lime annealed plate glass	.250
Polyvinyl butyral (PVB) interlayer	.060
Soda-lime annealed plate glass	.125
Code F4X-1 cast-in-place (CIP) Goodyear proprietary interlayer	.100
Polycarbonate (ultraviolet stabilized) with Code 701 Goodyear proprietary abrasion- resistant coating	.125
	<hr/>
TOTAL	.660
 <u>CONVENTIONAL PLEXIGLAS**</u>	
*Windshield	.188
*Front Door	.148
*Front Door Triangle	.076
Cargo Door	.136
Chin Bubble	.119
Overhead Window	.080

\*Transparent Armor Available

\*\*Nonstretched Acrylic



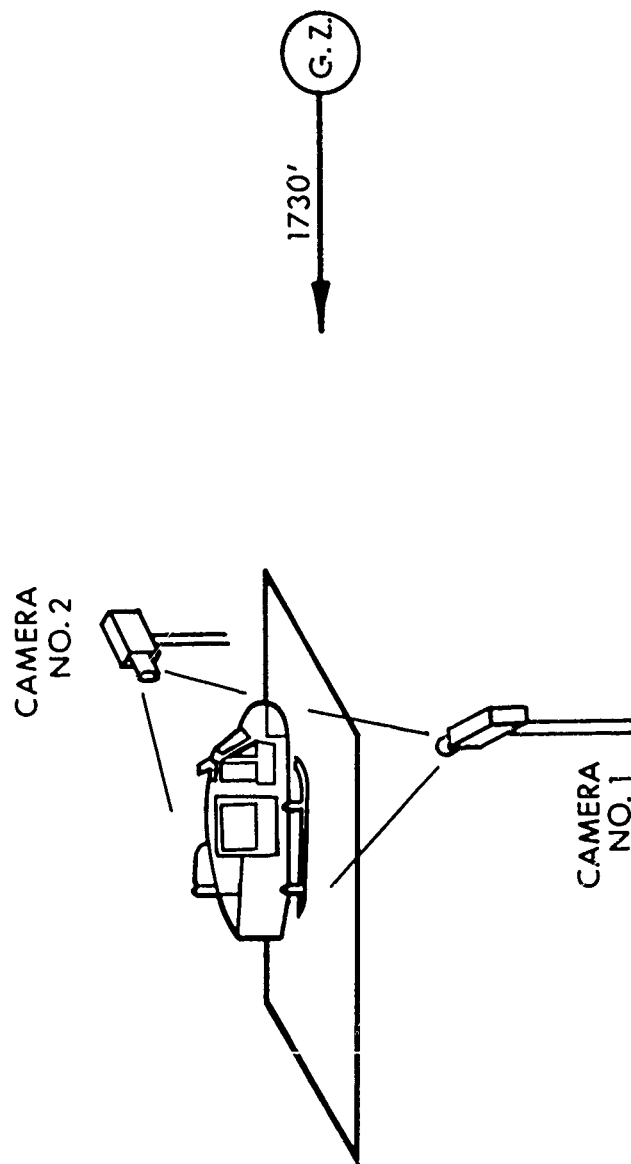


Figure 2.10. Test Layout - Static Helicopter

## CHAPTER 3

### PREDICTIONS

#### 3.1 DRONE HELICOPTER

The pretest analysis for the blast response of the drone helicopter was performed by Kaman Avidyne under contract to the BRL and was published several months before Event Dice Throw (Reference 5). The primary responses predicted were: (1) main and tail rotor bending moments, (2) fin and tail boom bending moments, (3) helicopter rigid body motions, and (4) autopilot control commands. The same analytical techniques used for the Pre Mine Throw IV test (Reference 3) were used for this test with one exception. Here, the fin and tail boom bending moments were estimated by a more comprehensive dynamic analysis involving the first three natural frequencies and mode shapes of the fin-tail boom combination instead of the single degree-of-freedom analysis previously used. No predictions were calculated for the stringer, longeron and panel strains because of the poor correlation of predicted strains and experimental measurements for Pre Mine Throw IV. With little or no development in the NASTRAN and NOVA codes used since that time, there was no increased confidence that the predictions would be any better for this test. In an effort to conserve time and costs, it was decided that the experimental strain data for the stringer, longeron, and panels would be utilized only in the post test data correlation where an analysis may have more significance.

With the exception of the fin and tail boom bending moments, which were solved by a series of complex equations, the primary computer code used to make the predictions was the HELP code with options MODEOP = 1 and MODEOP = 4. The details will not be discussed in this report because they are well documented in Reference 7. Similarly, the results of the pretest analyses are not presented in detail; instead, a summary of the responses predicted by Kaman Avidyne are presented below:

1. The maximum rigid body motions predicted for an 1.8 psi environment were:

Altitude (up, down)	- 4 ft, 7 ft
Roll (right, left)	- 1.5°, 2.0°
Pitch (down)	- 2.2°
Yaw (tail right)	- 7.5°
Roll Rate	- 5.5°/s
Pitch Rate	- 2.2°/s
Yaw Rate	- 18°/s

2. All maximum rigid body motions predicted (Item 1 above) were within acceptable limits as specified by the manufacturer and were predicted not to be a "kill" threat to the helicopter.

3. The maximum incremental control inputs (in terms of percent of full throw) required from the autopilot for recovery from the rigid body motions incurred at the 1.8 psi level were: Collective - 4 percent, Pedal - 28 percent, Lateral Cyclic - 7 percent, and Fore and Aft Cyclic - 3 percent. These values including time requirements were well within the capability of the autopilot system used and, therefore, complete recovery would have been expected.

4. Main rotor blade bending moments were well within the yield allowables specified by BHC.

5. Tail rotor blade bending moments approached the safe limits of the yield allowable bending moments. The tail rotor blade was considered a susceptible and critical component to being damaged.

6. The fin and tail boom bending moments far exceeded the yield allowable bending moments specified by BHC and failure of either or both component(s) was predicted. Confidence in the prediction was low because the same prediction was made for the Pre Mine Throw IV drone helicopter and no damage occurred to the fin or tail boom at the lesser yield and overpressure level. Based on the correlation of experimental data and predictions from Pre Mine Throw IV, the analysis used, predicts reasonably well. Therefore, the allowable bending moments specified appeared to be quite conservative.

Between the time of the publication of Reference 5 and the post test analysis of the data, some new information was acquired on the autopilot system and the allowable bending moments. This new information was incorporated in the post test analysis and will be discussed later.

### 3.2 TRANSPARENT ARMOR

No analytical predictions were made for the transparent armor because the time required to determine the physical and mechanical properties of the armor and run the computer model for a curved panel of composite material did not concur with the pre-test schedule. For the drone helicopter experiment, the overpressure level selected for exposure was determined from the predicted responses of other components and not the windows; therefore, a prediction was not required. It was known, however, from previous tests that at 1.8 psi overpressure the transparent armor in the front doors

would be in a blast environment that would blow out conventional Plexiglas windows; on that basis some comparison could be made. Likewise, for the static helicopter, the blast environment for this experiment was based on the results of previous work (Reference 8). The face-on orientation was selected because it allowed the transparent armor to be tested in the most severe environment within the limits of airframe structural survivability. Incipient breakage of conventional Plexiglas for the face-on orientation of a UH-1 helicopter windshield occurs at about 2.3 psi and sure-breakage at 3.5 psi. In addition, at the 3.5 psi level, the tail boom will sustain structural damage. Therefore, the 3.5 psi overpressure level with a face-on orientation seemed the most desirable to determine if the transparent armor and mountings can survive where Plexiglas windows cannot and how the hardness of the armor compared to the hardness of the helicopter structure.

## CHAPTER 4

### RESULTS

#### 4.1 DRONE HELICOPTER

On the morning of the shot, the helicopter was lifted-off without incident and was stabilized at the approximate altitude (66 ft) and azimuth over the take-off/landing pad. Surface wind velocity was rather high at times and the helicopter was trimmed with a roll attitude to the left side (towards GZ). In general, there were more pre-blast helicopter motions than in the previous tests, which may account for some of the data correlation problems discussed later.

The rigid body motions of the helicopter after the shock wave impact were greater in comparison to previous testing as would be expected. The most noticeable motions were in the lateral translation and yaw (5.8 deg - approx three times more than in Pre Mine Throw IV). The Altitude varied from a 1 ft rise during the first second to a 12 ft descent during the next 4.5 seconds. The total Pitch variation (up and down) was less than 7 degrees over a 10 second period and Roll varied approximately 1 degree over a 3 second period. All of the motions were readily handled by the autopilot and the pilot.

A post test visual examination of the resultant structural damage was typical of damage sustained in the previous tests (Figure 4.1):

##### Blast Side

1. The nose compartment door popped open (Figure 4.2), and as seen from Camera 3 (viewing through the windshield), was only a momentary obstruction of the pilots view.

2. The left front door was flattened slightly, the pillar between that door and the cargo door was buckled at the top, and the overhead window was blown out (Figure 4.3).

3. The cargo door was crushed and the window blown out (Figure 4.4).

4. The area near the top and aft of the cargo door was flattened, the engine cowling was slightly buckled, and the fiberglass equipment compartment doors had been deflected sufficiently to impact on the equipment in the compartments before popping back to the original configuration (Figure 4.5).

5. The tail boom sustained the most severe damage of all the structural components. The bending loads induced were sufficient to cause a noticeable opening

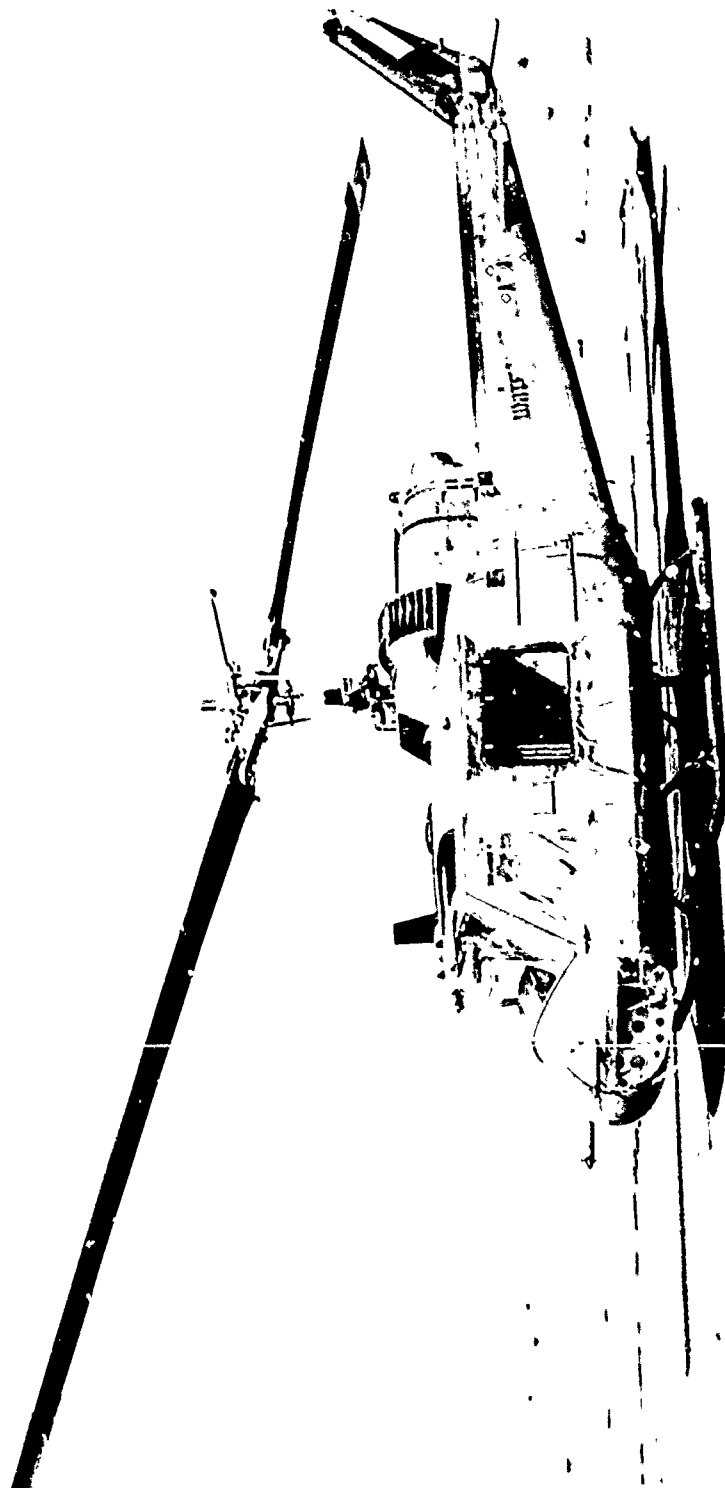


Figure 4.1. Typical Side-On Blast Damage



Figure 4.2. Popped Open Nose Compartment Door

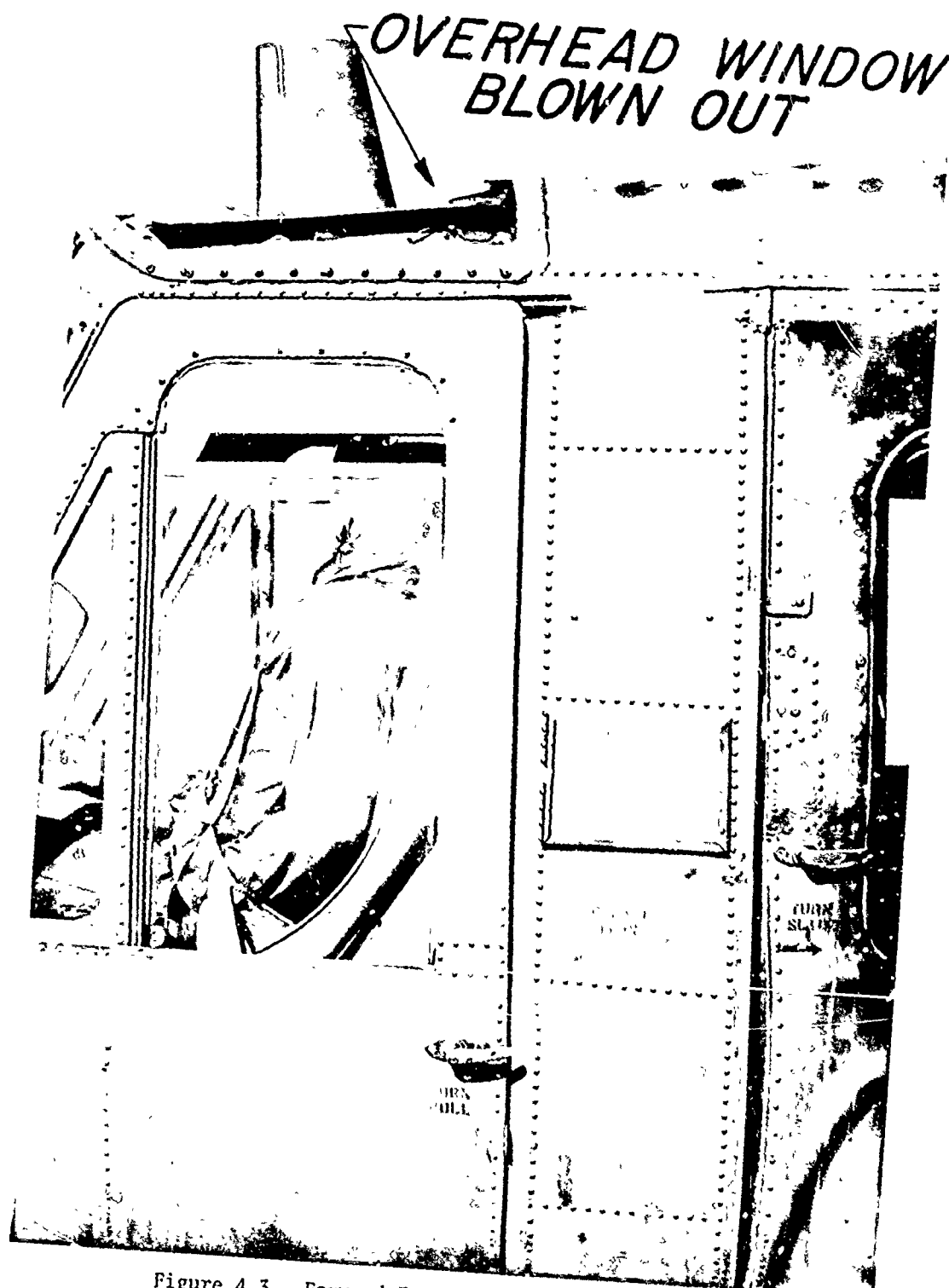


Figure 4.3. Forward Fuselage Blast Side Damage



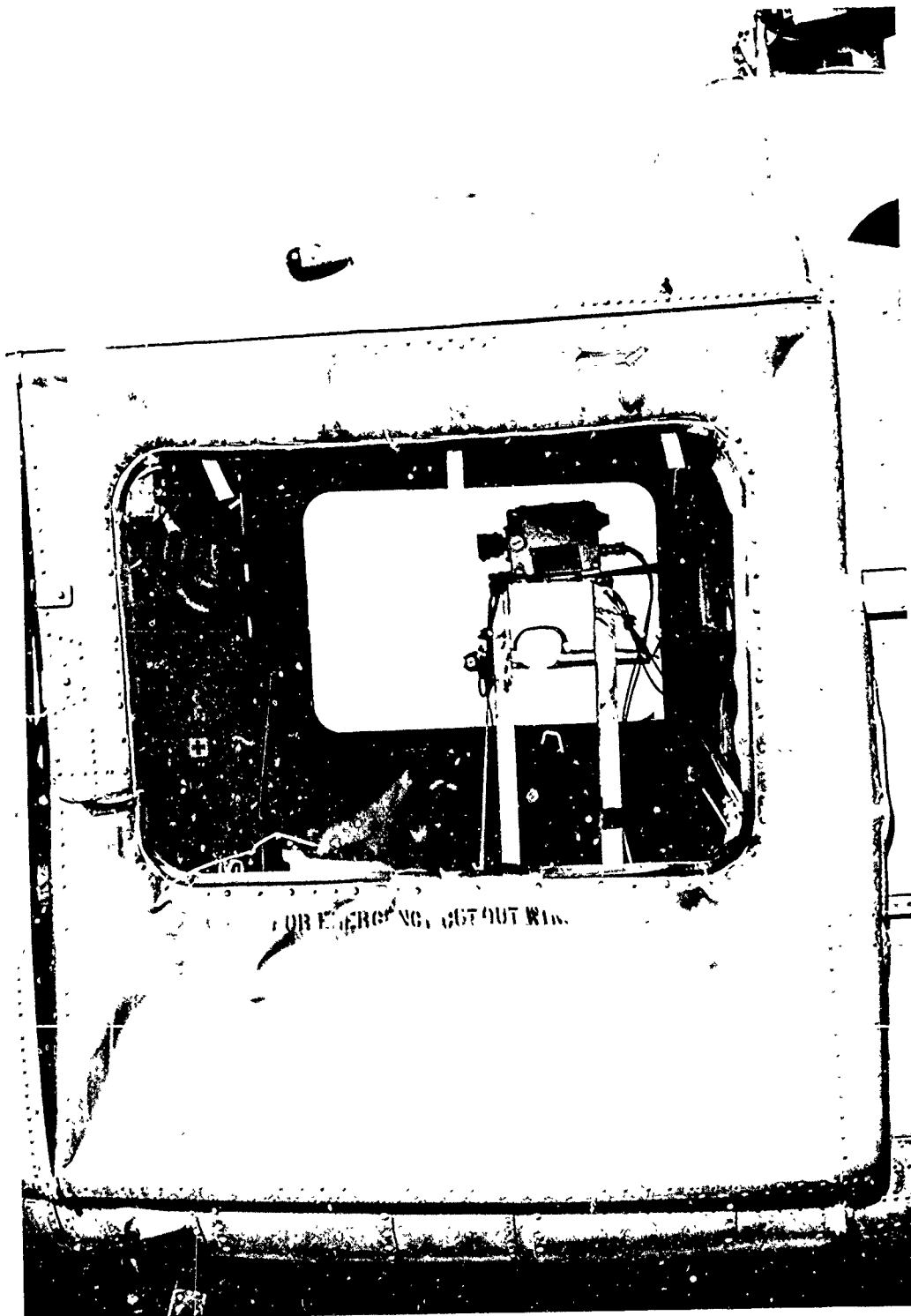


Figure 4.4. Cargo Door Blast Side Damage

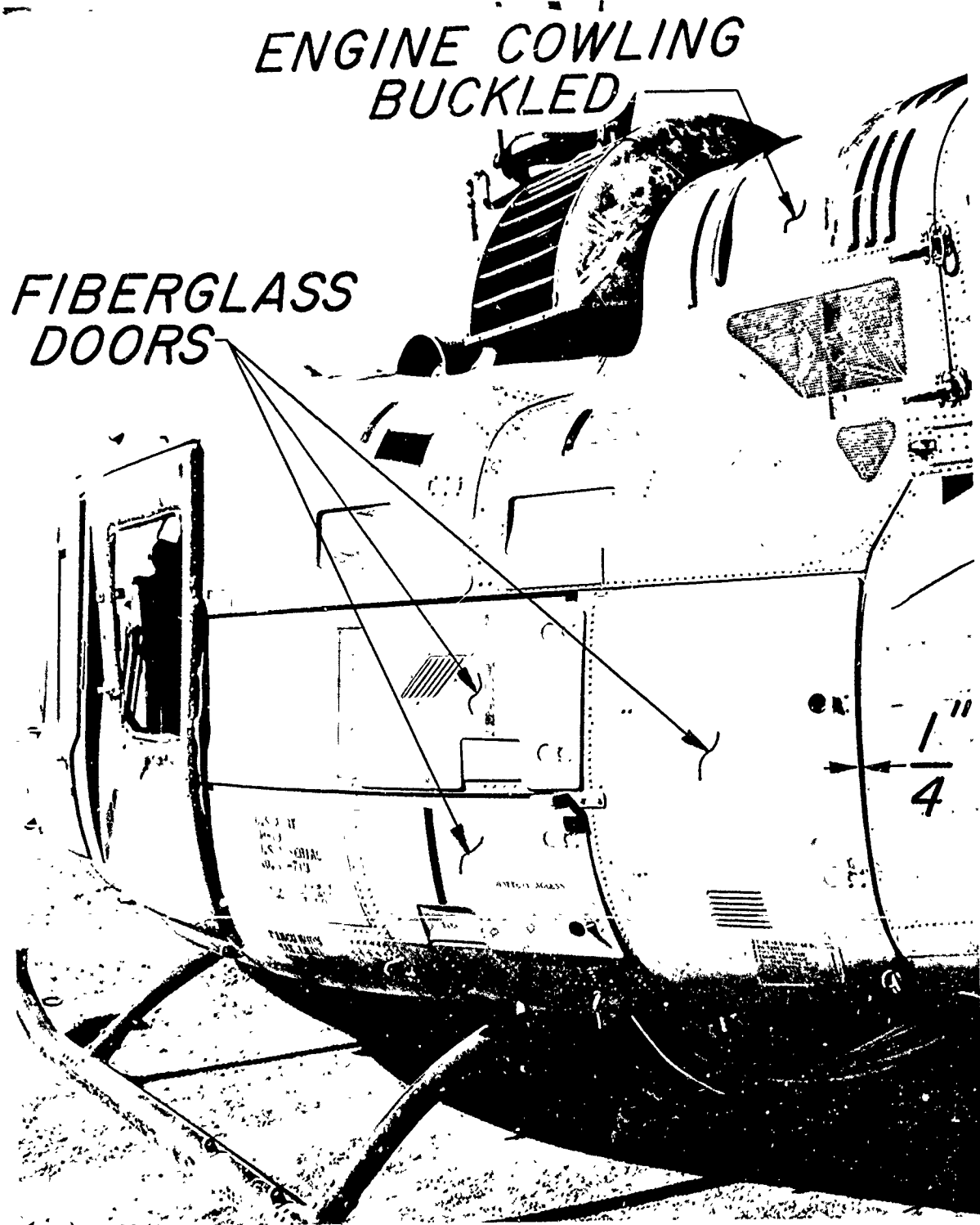


Figure 4.5. Aft Fuselage Blast Side Damage

(approximately 1/4 in.) between the tail boom and the fuselage (Figure 4.5). The skin panels between the third and sixth frame (BS 38.6 - BS 101.4) were wrinkled (Figure 4.6). An inspection of the interior revealed that in the same area of skin wrinkling, four frames had undergone some minor buckling (Figures 4.7 and 4.8).

#### Side Opposite the Blast

1. The engine cowling was broken loose from the top hinge (Figure 4.9)
2. The cargo door was slightly wrinkled under the window, the window was broken (from blast and/or from Plexiglas fragments from the blast side window), and the hatch behind the door was permanently deformed (Figure 4.10).

None of the transparent armor was damaged. The pilot had been instructed to continue to fly the helicopter for 2-3 minutes after the blast arrival to simulate the time required to land a damaged helicopter flying at combat altitudes at the time damage occurred. The helicopter appeared to have good flight capability, but the post shot assessment of the tail boom damage indicated that severe maneuvering could result in tail boom failure.

Immediately after the shock wave impact, two yellow warning lights on the helicopter instrument panel were illuminated. One of the lights, the Master Caution Indicator, when illuminated is "aviation yellow" and the pilot is alerted to check the Caution Panel for the fault condition. Because the Caution Panel located in the console between the seats was not in full view of the onboard camera, the system that malfunctioned was not identifiable. Because the light blinked several times rather than remain continuous, and because there was no obvious system failure, the light being illuminated was associated with the buckling of the fiberglass door covering the battery compartment (discussed earlier under Blast Side damage Item 4). The door has an electrical switch attached to it to indicate through the Master Caution Indicator that the Auxiliary Power Unit has been removed and the door closed. The other illuminated light has not been positively identified because of under exposed photography; however, it is thought to be the Engine Inlet Air Warning light. This light would normally alert the pilot to a clogged filter and a heavy concentration of dust or sand in the area of operation, but because the light works in conjunction with a differential pressure switch, the blast pressure may have triggered the light. The warning light illumination was discovered after the technical movie film had been processed; after that time the helicopter had not been readily available for a rerun. Despite the lack of confirmation on what caused the warning lights to be illuminated, the helicopter seems to have suffered no consequences from the event.

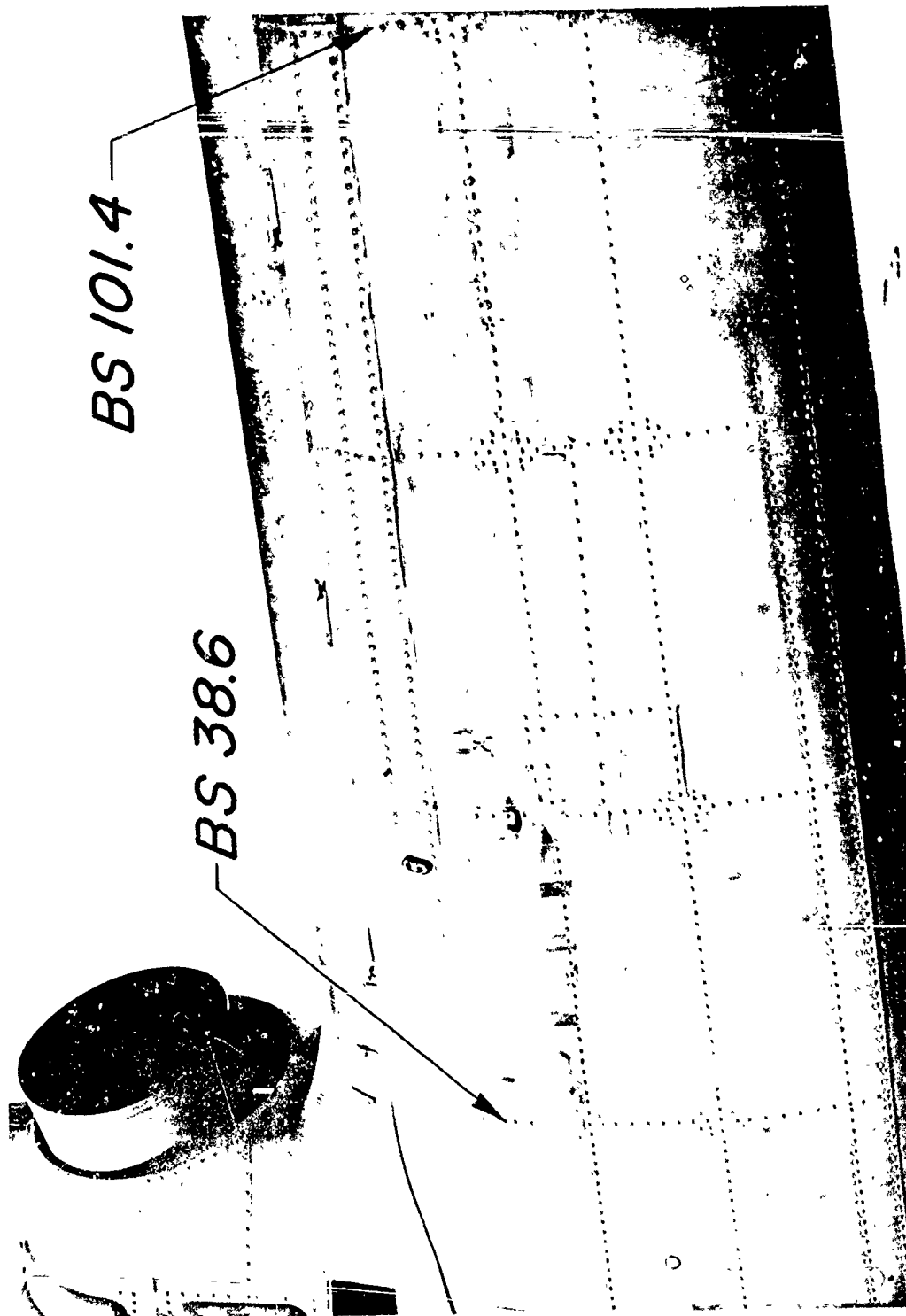


Figure 4.6. Tail Boom Blast Side Skin Damage

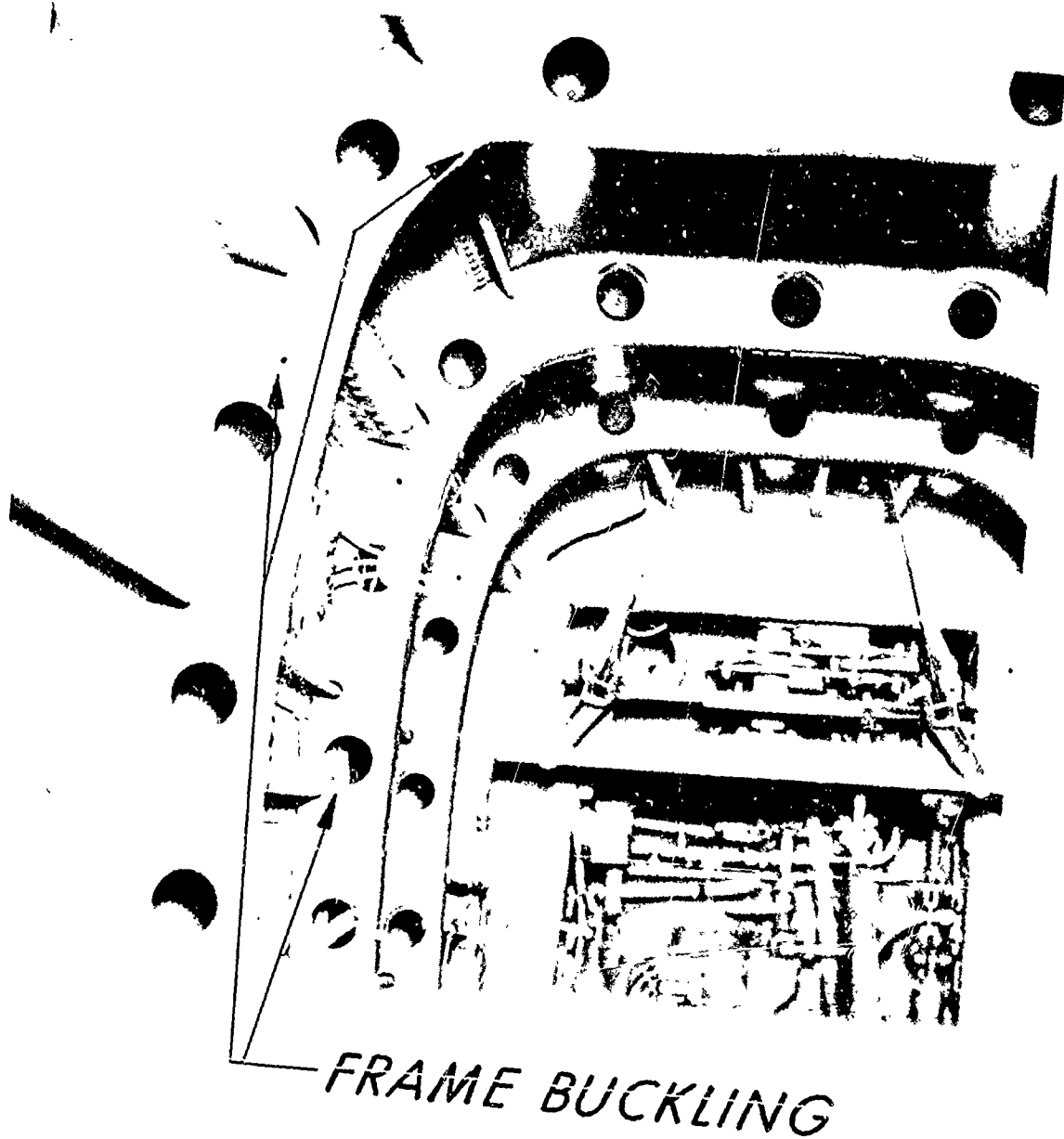


Figure 4.7. Tail Boom Interior Damage Viewing Forward

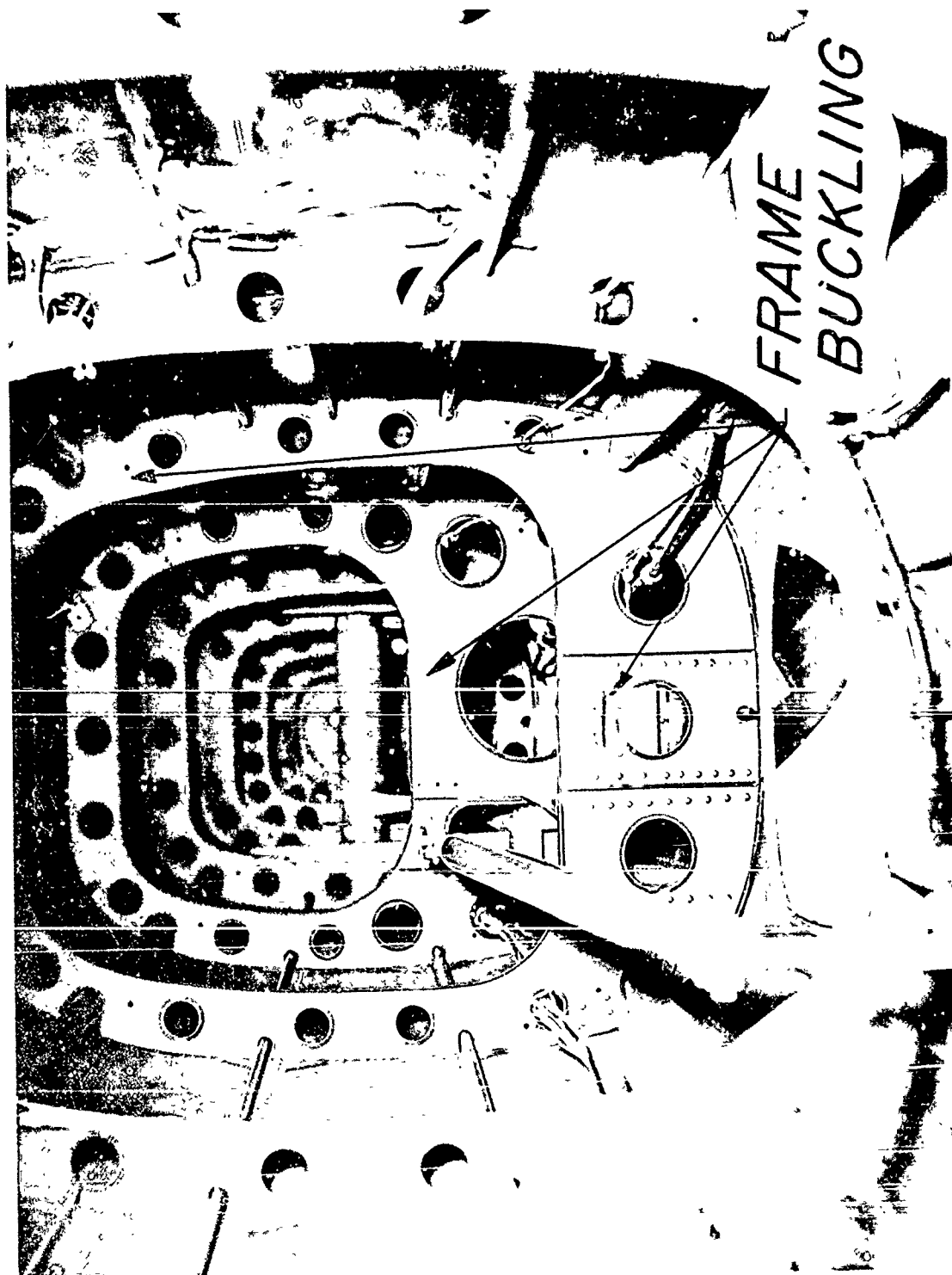


Figure 4.8. Tail Boom Interior Damage Viewing Aft

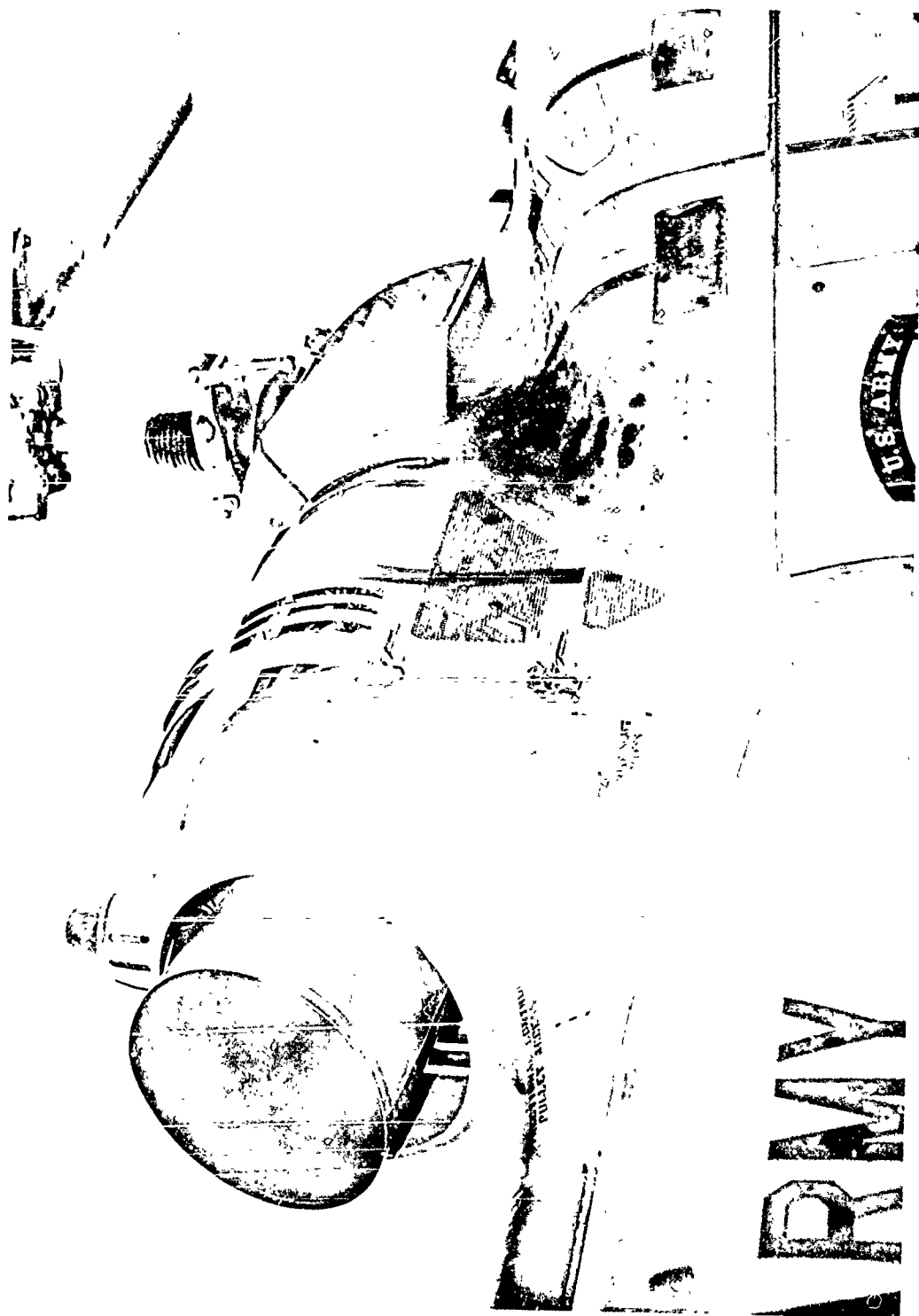


Figure 4.9. Engine Cowling Damage Side Opposite Blast

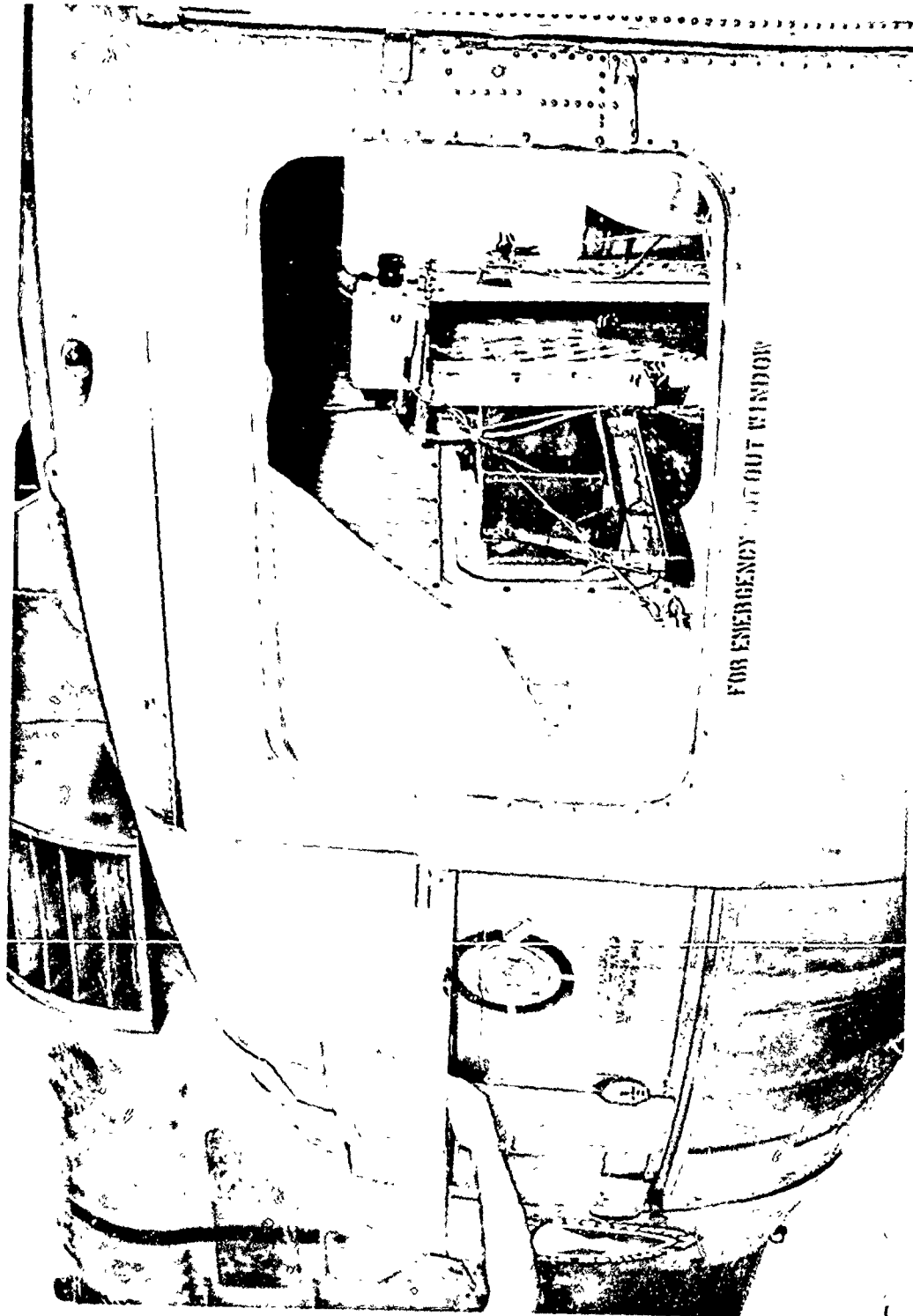


Figure 4.10. Fuselage Damage on Side Opposite Blast



The anthropomorphic dummy appeared to have survived the blast rather well. There were five major impacts on the helmet from Plexiglas fragments from the broken overhead window and the accelerometers indicated that the dummy did not experience as much as 10 g's. In addition, the maximum velocity and displacement of the dummy were well below the level for causing serious injury. The pressure transducer in the chest cavity failed to produce a measurement; however, the cabin/cargo pressure transducer recorded a maximum overpressure of 2.0 psi. (Figure A.43). Further description of the anthropomorphic dummy results will be presented by the Lovelace Foundation.

#### 4.2 STATIC HELICOPTER

All of the conventional Plexiglas windows with the exception of the small triangular window in the left front door were blown out as expected (Figure 4.11). The transparent armor in the windshield and right front door, except for the small triangular window, were badly shattered (Figure 4.12). The shattering was limited to the outer two glass laminations. The inner layer of polycarbonate and the special interlayers between the laminations retained the shattered glass and prevented internal spall fragments from being generated. The door window could have caused a serious problem by being blown into the cockpit area because the glass edge and the retaining slide channel both failed. But, because the window extended below the door sill it was restrained (Figure 4.13). The remaining visibility through the shattered windows appeared adequate to safely land the helicopter (Figure 4.14).

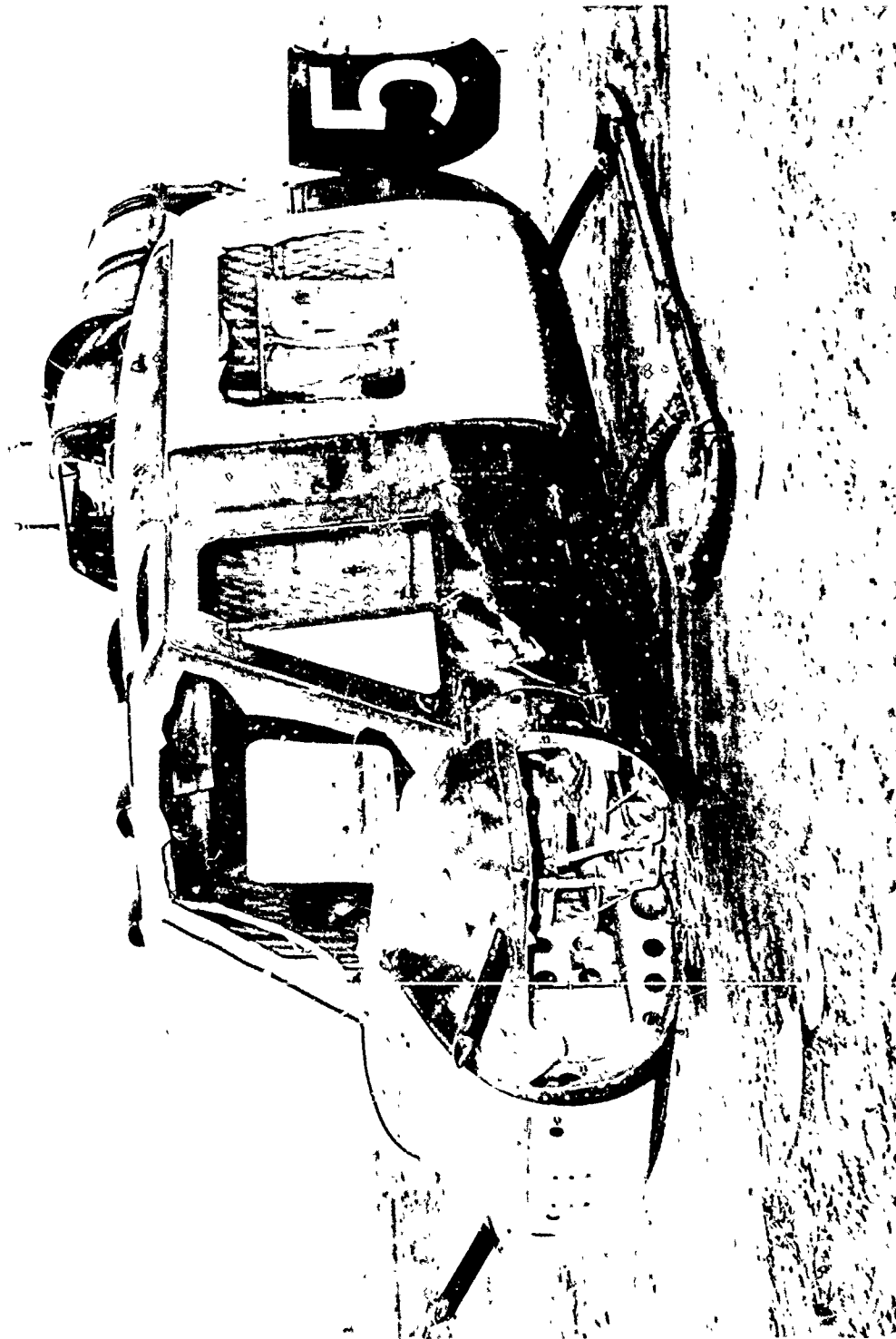


Figure 4.11. Damage to Plexiglas Window Side - Static Helicopter

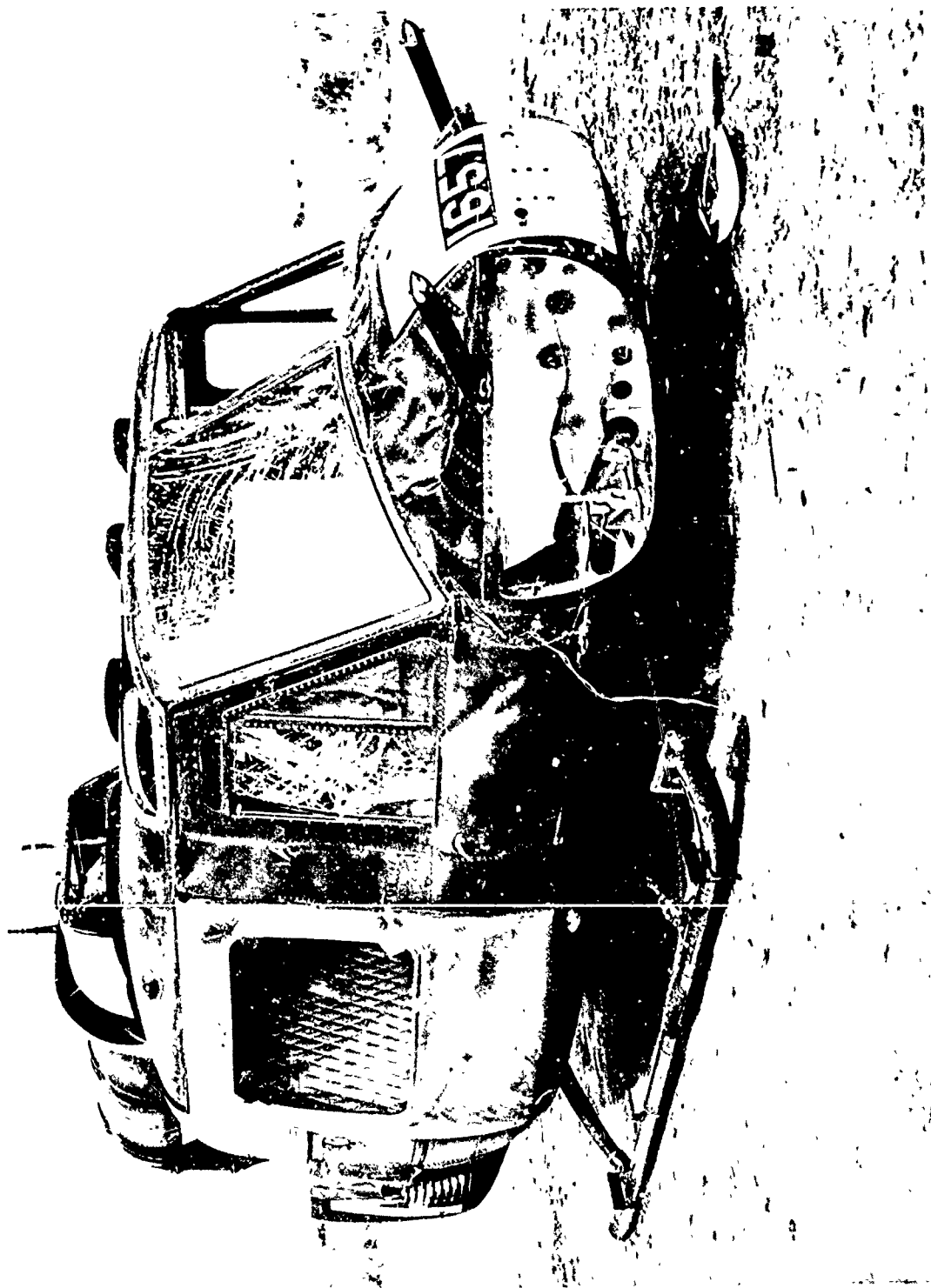


Figure 4.12. Damage to Transparent Armor Side - Static Helicopter

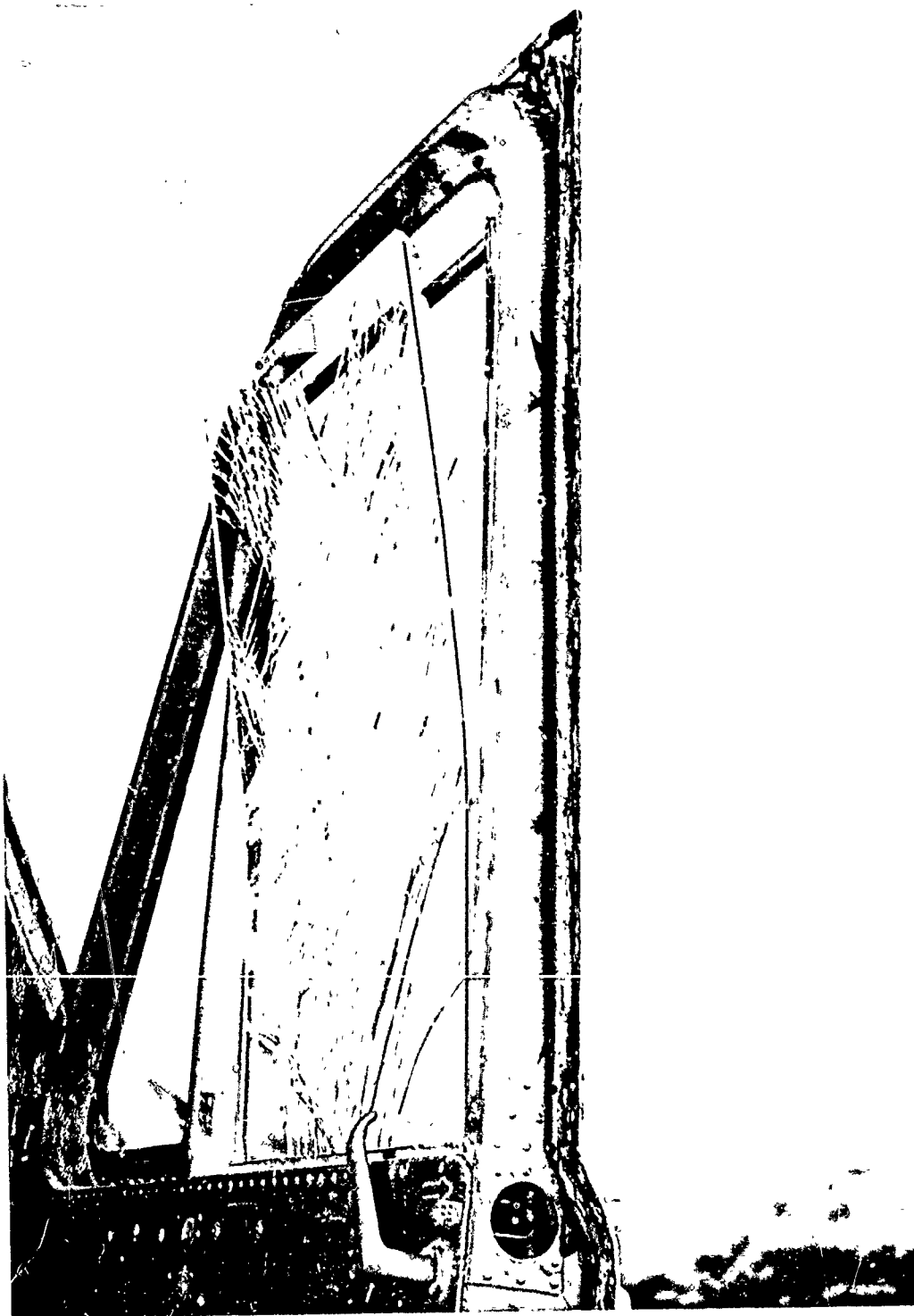


Figure 4.13. Transparent Armor Broken from  
Slide Channel in Front Door

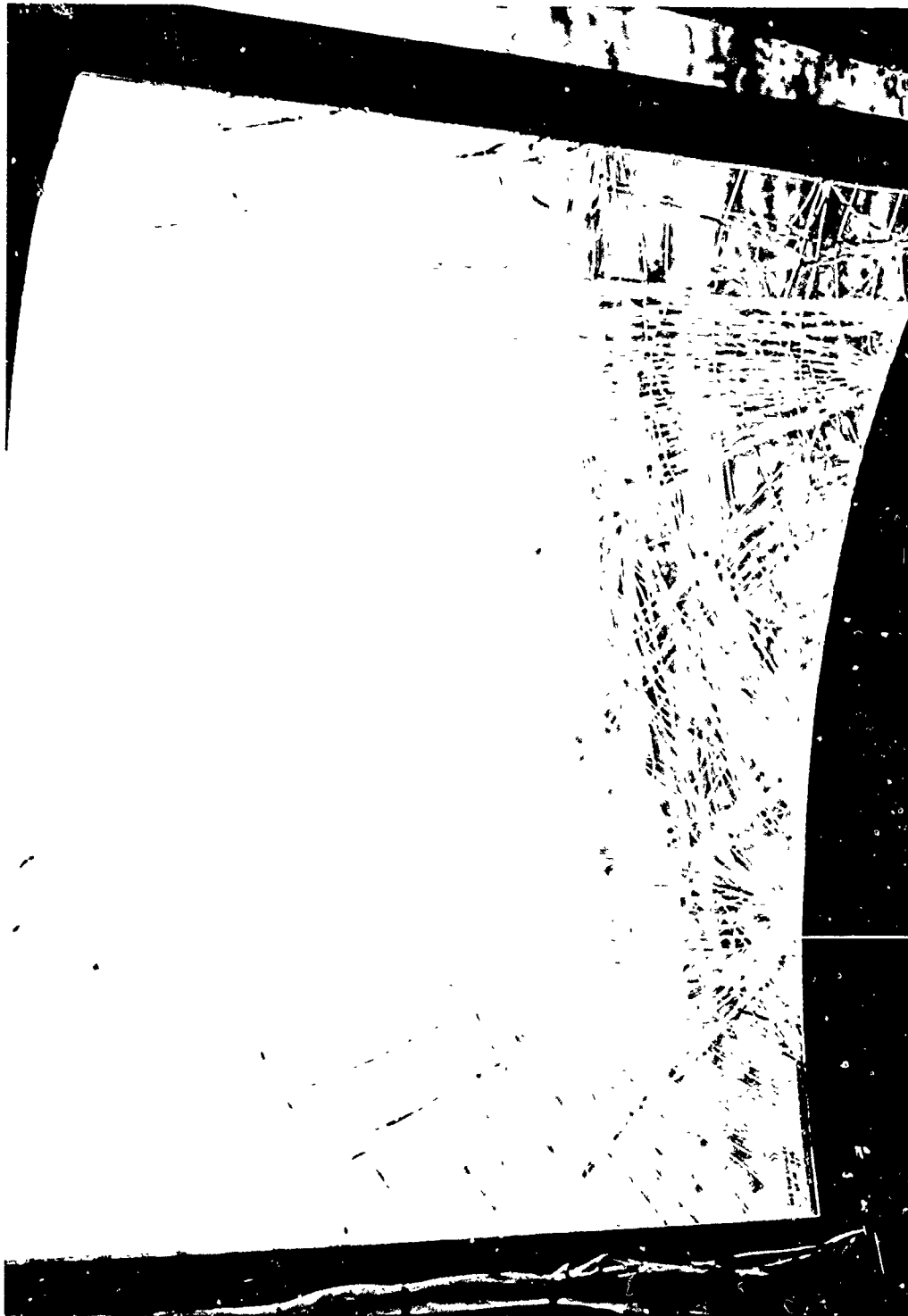


Figure 4.14. View from Pilot's Seat Through Shattered  
Transparent Armor Windshield

CHAPTER 5  
EXPERIMENTAL DATA AND ANALYTICAL  
PREDICTION CORRELATION

The responsibility for the correlation of the experiment data and the analytical predictions was tasked to Kaman Avidyne under contract to BRL. The results of that work have been presented in a comprehensive report currently under publication (Reference 9) and will not be repeated here. Only a summary of that work with certain details pertaining to critical predictions follow:

1. The tail rotor blade peak bending moments correlated well with the predicted bending moments and were close to the allowables (Figure 5.1).
2. The main rotor blade peak bending moments correlated not quite as well as the tail rotor bending moments and were far below the yield allowables as might be expected (Figure 5.2).
3. For both rotor blades, the pre-blast bending moment variations and flapping angles were much higher than predicted. The probable cause was tail boom and fin interference effects.
4. The resultant rigid body motions were affected by large pre-blast helicopter motions and sizeable remote control inputs. The present computer code cannot handle these kinds of inputs without extensive code modification.
5. The altitude was predicted to increase by 4 ft followed by a descent of 7 ft. The drone actually lost 12 ft altitude; the difference is attributed to inadvertent remote collective input as observed from the data.
6. With a compensation factor of 2.1 for the calibration of the Yaw rate channel, the experimental-analytical correlation for Yaw deviation and Yaw rate appears quite good for the first 0.7 seconds (Figures 5.3 and 5.4). Thereafter remote pedal inputs affect the correlation.
7. There are inconsistencies in and between the Roll and Pitch channels and the cause cannot be determined.
8. A Pitch deviation of 1.5 degrees down was predicted during the first 1.2 seconds and experimentally the drop was 1.2 degrees for the same period. The prediction of 1.5 degrees was a correction of the 2.2 degrees shown in Chapter 3 because of different trim conditions for the actual experiment.

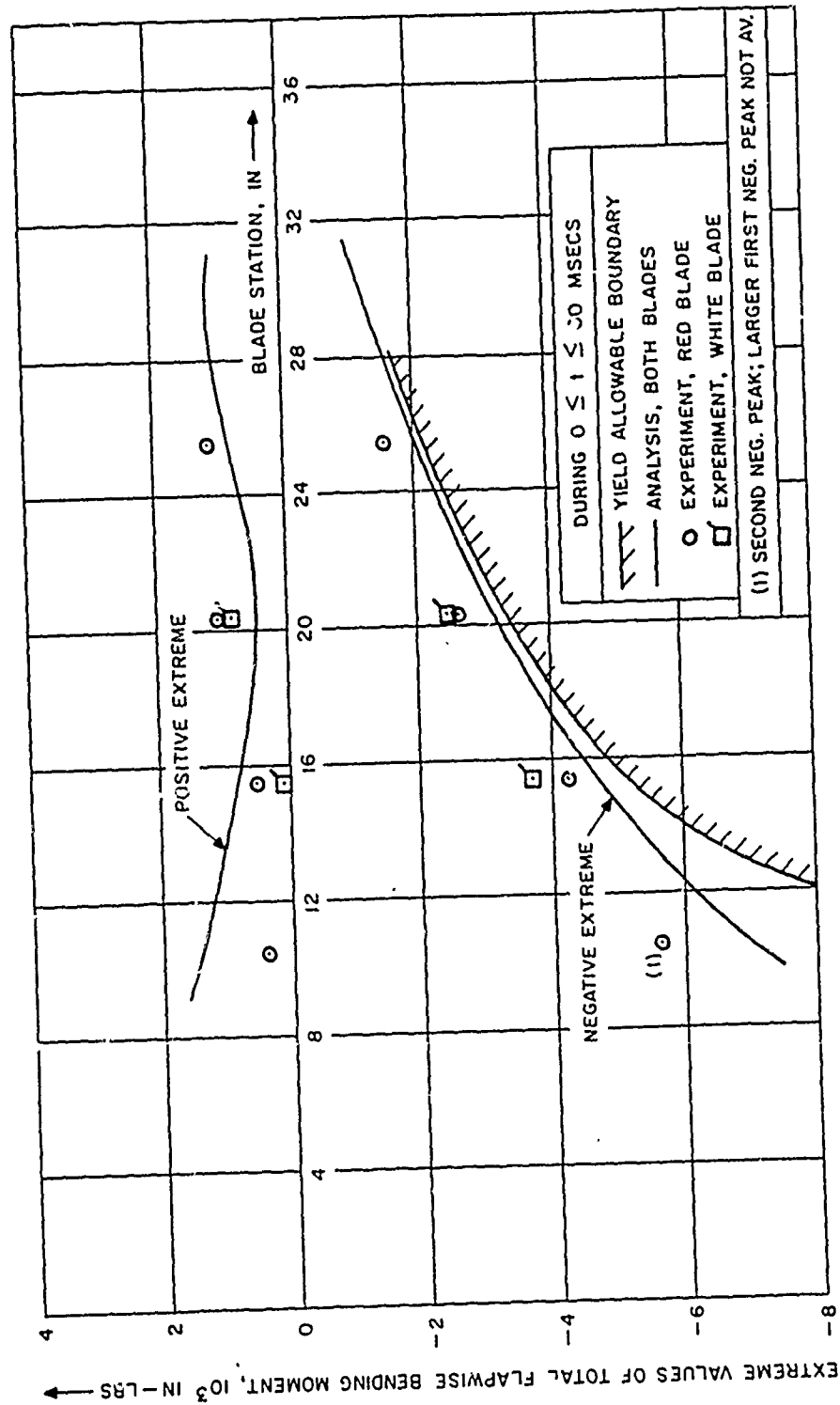


Figure 5.1. Extreme Values of Flapwise Bending Moments for Tail Rotor Blades - Experimental/Analytical Comparison

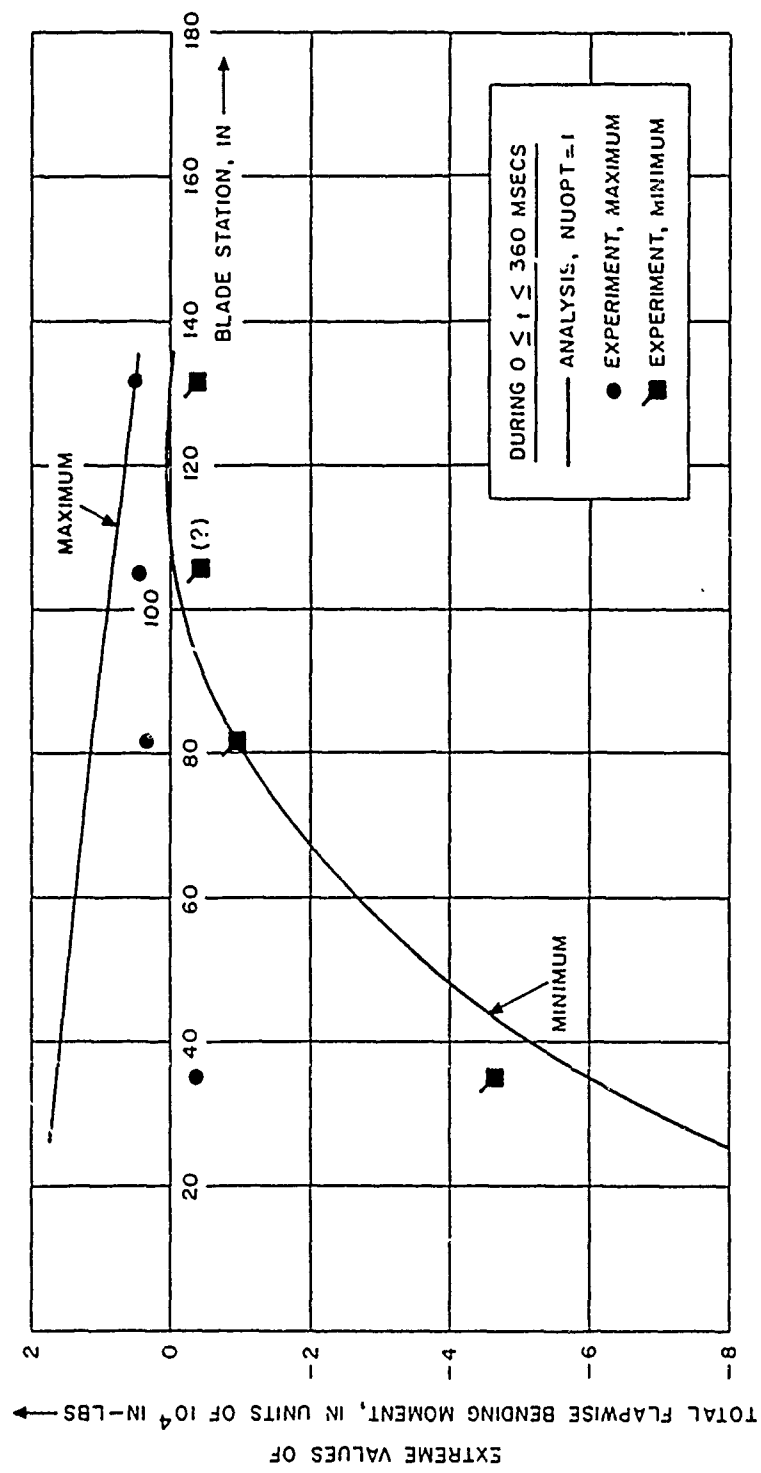


Figure 5.2. Extreme Values of Flapwise Bending Moments for Main Rotor Blade - Experimental/Analytical Comparison



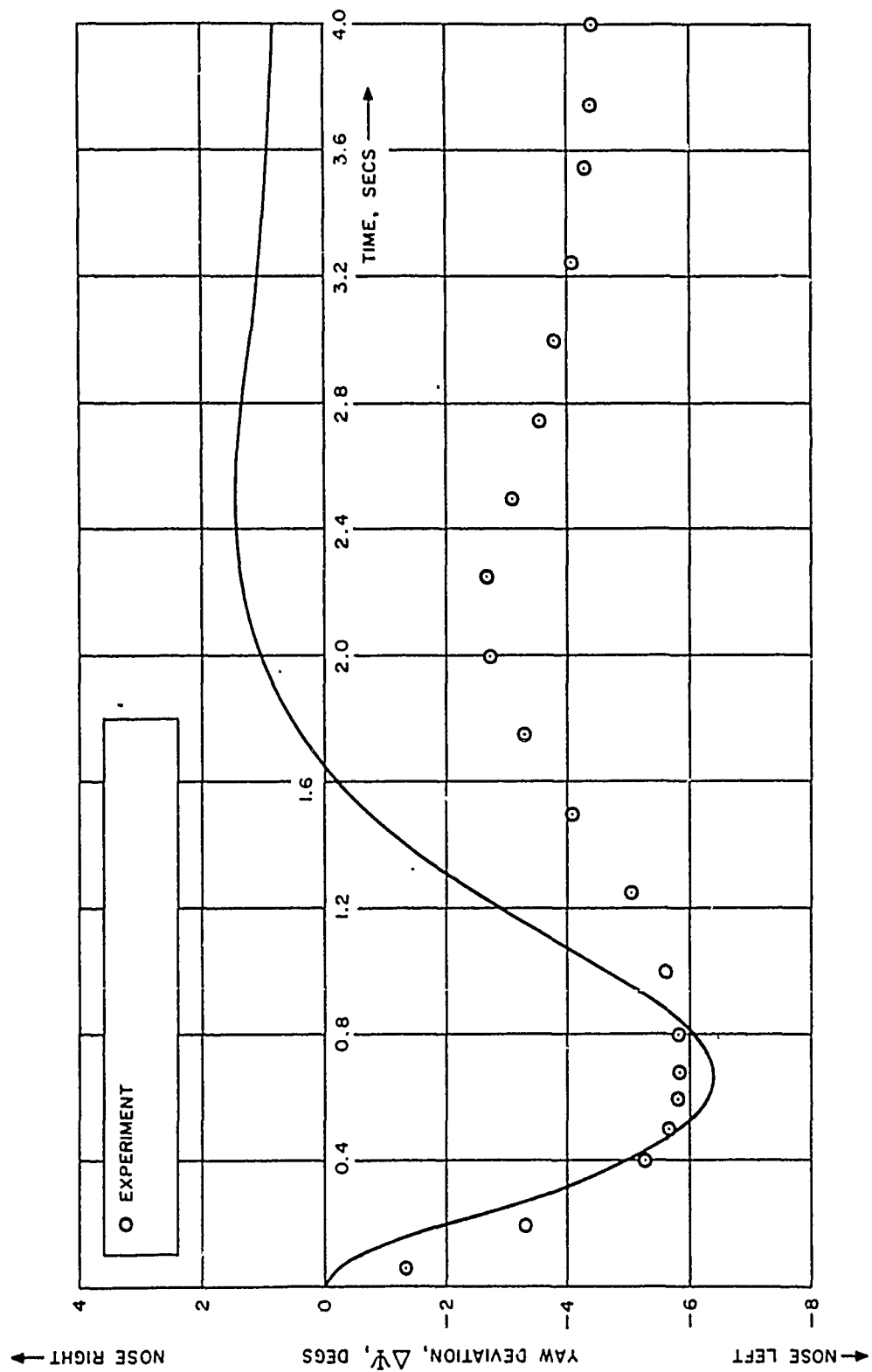


Figure 5.3. Time Vs. Yaw Deviation - Experimental/Analytical Comparison

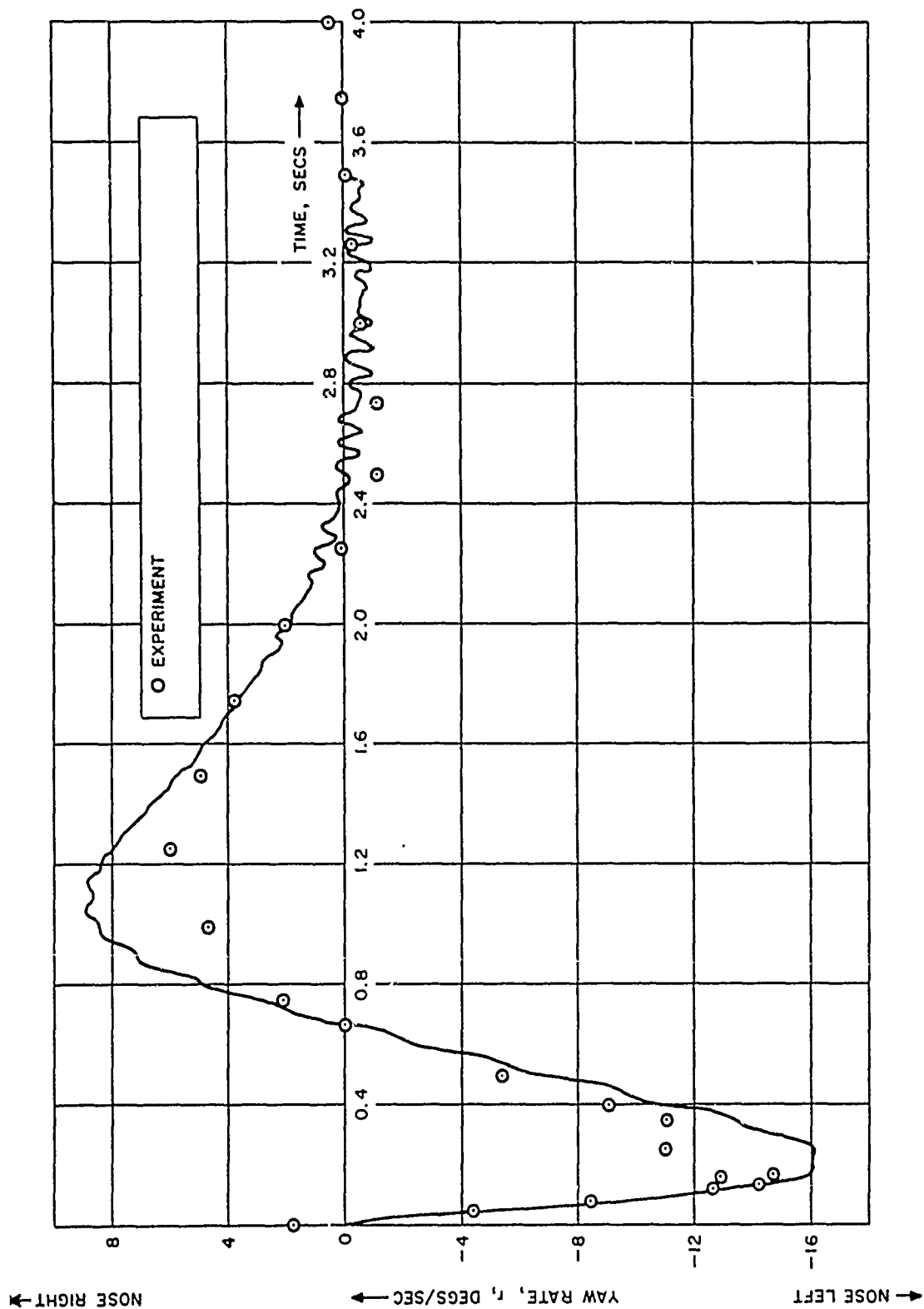


Figure 5.4. Time Vs. Yaw Rate - Experimental/Analytical Comparison

9. The Pitch rate, Roll deviation, and Roll rate have poor experimental-analytical correlation.

10. The peak fin lateral bending moments were underestimated by analysis, by about 20 percent at STA 32 and 8 percent at STA 52 (Figure 5.5). This correlation could be improved by using the MODEOP = 4 option of the HELP code which includes the high-frequency components of the tail rotor force resulting from the flexible motions of the rotor blades.

11. The tail boom bending moment correlation was good except for BS 112 after blast impact (Figure 5.6). The analysis overpredicts slightly but the experimental results and the predictions indicate that the tail boom bending moments reached levels just below the failure boundary. The original predictions (Chapter 3) strongly indicated failure of the tail boom and/or the fin; however, at the time those predictions were made the allowable bending moments were approximately half as large as later established. The consequences are that the damage is slightly less than that planned for in the experiment.

12. The NOVA-2 code was used to analyze the panel, stringer and longeron strains; once again as in Mixed Company and Pre Mine Throw IV, the correlation was poor. The panel responses are too sensitive to curvature, edge conditions, and sensor locations to be determine accurately by a field test like Dice Throw. In addition, NOVA-2 does not handle the coupling between structural members.

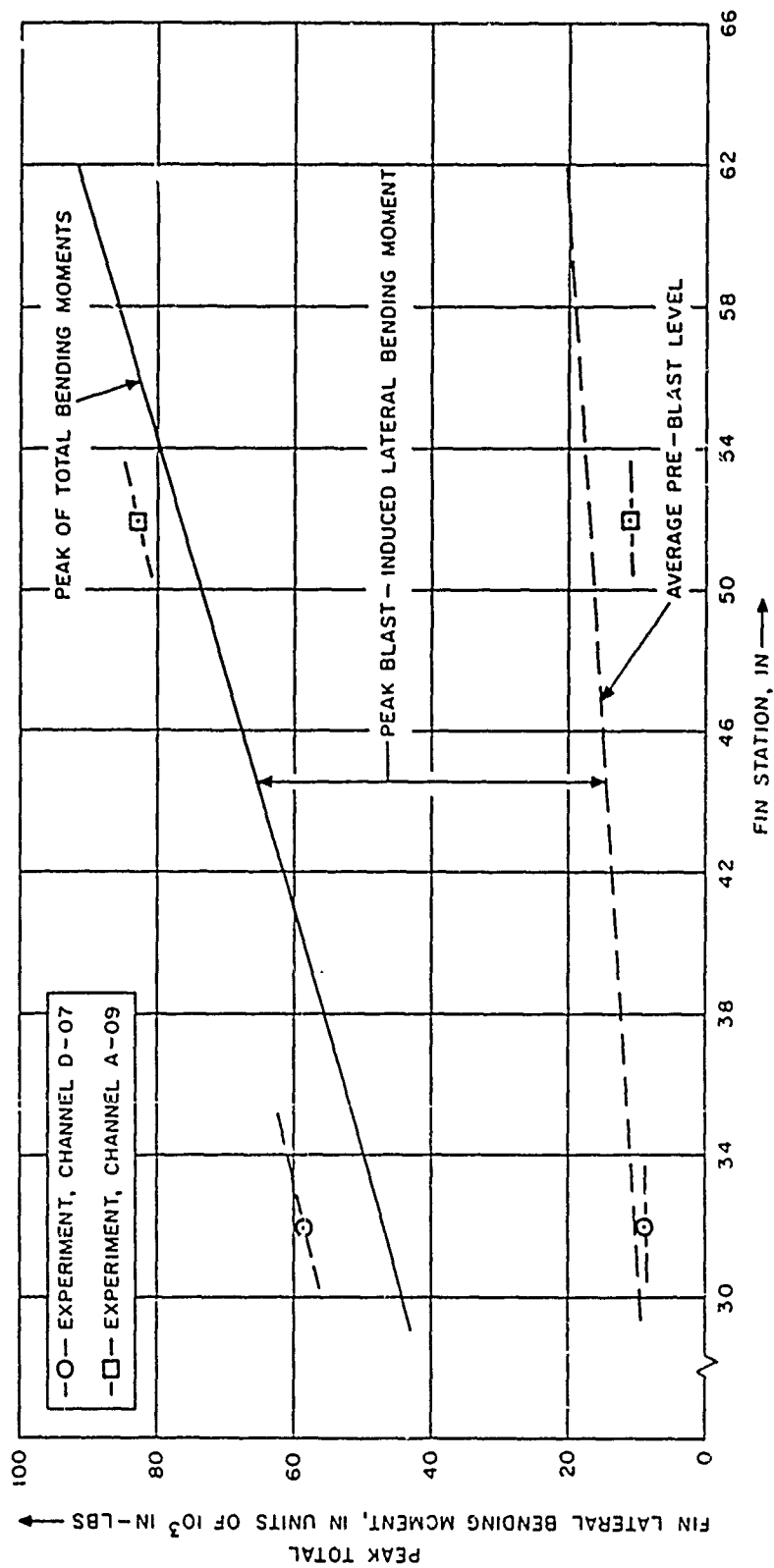


Figure 5.5. Peak Total Fin Lateral Bending Moments - Experimental/Analytical Comparison

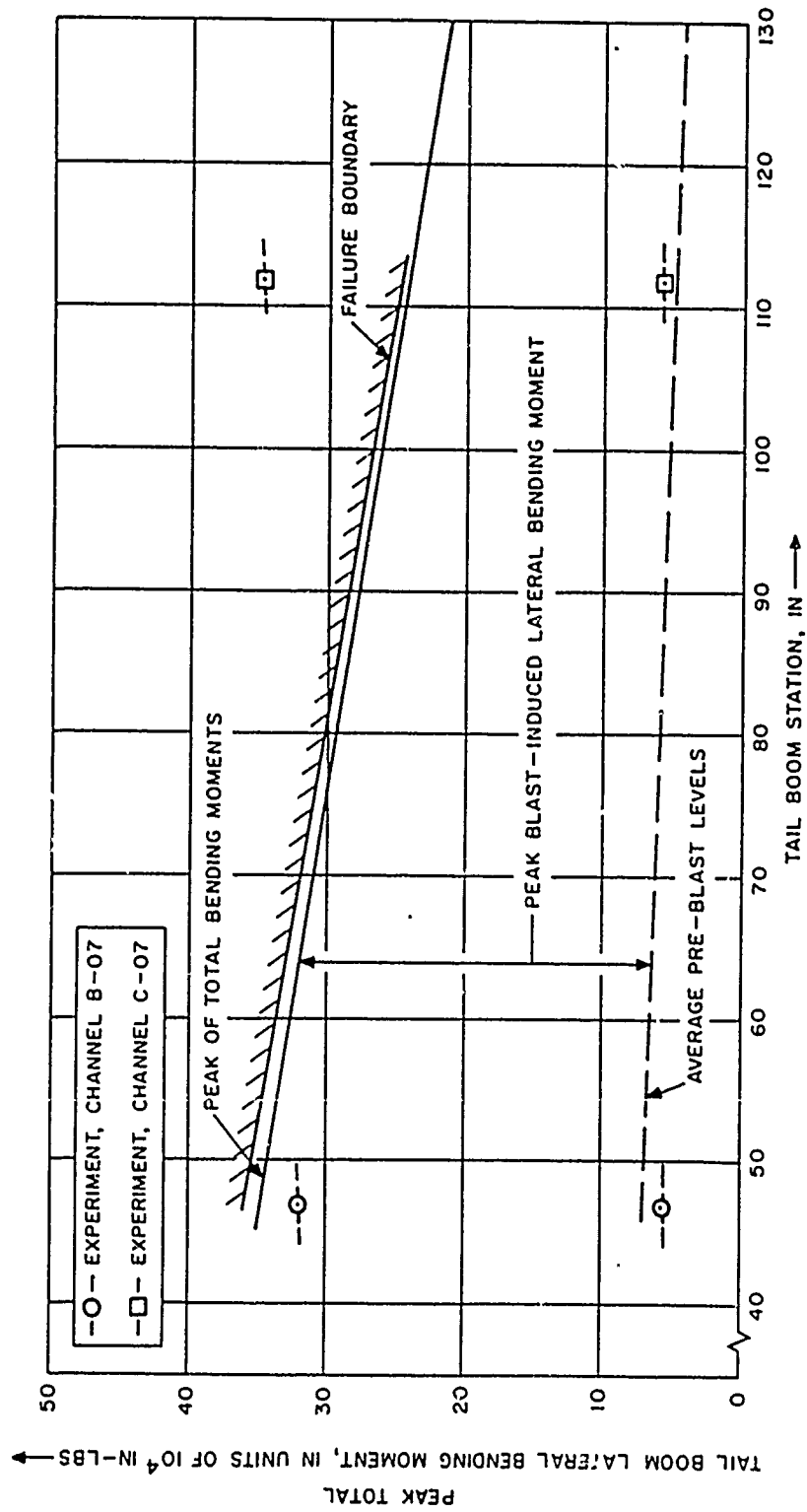


Figure 5.6. Peak Total Tail Boom Lateral Bending Moments - Experimental/Analytical Comparison

## CHAPTER 6

### CONCLUSIONS

To date, there have been four large scale blast trials in which UH-1 helicopters have been subjected as structural response targets:

1. Dial Pack - 500 tons TNT  
Parked, Side-On, 2.3 psi, probable "Kill" under flight conditions  
(Reference 1)
2. Mixed Company - 500 tons TNT
  - a. Parked, Side-On, 1.3 psi, "No Kill" (Reference 4)
  - b. Parked, Side-On, 1.3 psi, "No Kill" (Reference 10)
  - c. Parked, Nose-On, 3.5 psi, probable "Kill" under flight conditions  
(Reference 8)
  - d. Parked, Nose-On, 5.0 psi, "Kill" (Reference 10)
3. Pre-Mine Throw IV - 100 tons Nitromethane  
In-Flight, Side-On, 1.3 psi- "No Kill" (Reference 4)
4. Dice Throw - 600 tons ANFO  
In-Flight, Side-On, 1.8 psi, "No Kill"\*

All of the pressures indicated above are side-on overpressures at the target range. From the experiments thus far completed, it appears that the UH-1 helicopter, in an in-flight hover side-on orientation, can be "killed" from a 500 ton explosive charge at a side-on overpressure level of 2.0 psi. This estimate is based primarily on visual observations and subjective assessments of the gross structural damage. For the case stated, the estimate is reliable; however, future vulnerability studies will certainly involve other yields, helicopters, orientations, flight conditions, etc. For some of those studies, the problem will demand an analytical solution. The Mixed Company, Pre-Mine Throw IV, and Dice Throw events were designed to verify the capability of several of the most prominent computer codes available (HELP, NOVA, NASTRAN, DNA 2048, etc.) that can be applied to the problem of predicting the rigid body motions and structural responses of helicopters. The results of these tests have indicated the following:

1. Good reliability in the predictions of blade flap, blade bending moments, altitude, attitudes, attitude rates, and control positions using the HELP code.

---

\*Tests reported herein.

2. DNA 2048 produces good predictions for some fin bending and tail bending locations but not all. A reasonable prediction can be made by using a simple analytical formulation with loading functions calculated from HELP. A more comprehensive dynamic analysis was tried for Dice Throw and it also produced good predictions.

3. NASTRAN and NOVA, for most cases, have not predicted panel, stringer, longeron, and frame strains with any degree of reliability.

In general, the Dice Throw experimental-analytical correlations were not as good as the correlations from the Pre-Mine Throw IV experiment. Much of the difference was attributed to the large amounts of pre-blast remote control inputs and helicopter motions, and apparent calibration problems. Nevertheless, the results followed the trends established from Pre-Mine Throw IV.

The transparent armor results have shown that a transparent armor designed to stop a conventional ballistic threat can also survive in a 500 ton H.E. environment near the threshold for a structural kill of the tail boom and not present the hazard of Plexiglas fragments. By changing the design of the sliding window mounting in the front door, additional hardness can be obtained.

As a result of all the experimental work conducted on helicopters in the large scale blast tests and the methodology development that has occurred over the years, the question must be asked, "What is the present capability for analyzing the vulnerability of a helicopter to a nuclear blast?" In response, Table 6.1 is presented as the author's assessment. From Table 6.1, the indications are that experimental data and empirical formulations are preferred to analytical computer codes for predicting structural crushing and window breakup, and that additional work in the development of a more applicable structural response code may be desirable. It also implies that a vulnerability analysis can be conducted with reasonable confidence without further study; however, it must be remembered that the helicopter thus far used as the experimental specimen has been the UH-1 helicopter. If a vulnerability analysis were required for a heavy-lift helicopter or a twin rotor helicopter, or a stubbed wing attack helicopter, then perhaps Table 6.1 would reflect a different status. In any event, substantial development in the capability to predict helicopter response to blast has evolved as a result of the efforts described herein.

Table 6.1. Approach to Determining Helicopter Nuclear Blast Vulnerability

DET LOCATION	ROTOR BLADES		TAIL BOOM			RIGID BODY RESPONSE	WINDOWS
	MAIN	TAIL	BENDING	CRUSHING	TORSION		
FORWARD	NC	NC	NC	NC	NC	NC	E
AFT	NC	NC	NC	NC	NC	A	NC
SIDE (1) TAIL ROTOR	NC	A	A	E	A	A	E
SIDE (2)	NC	A	A	E	A	A	E
TOP	A	NC	NC	NC	NC	NC	E
BOTTOM	A	NC	NC	NC	NC	NC	NC

NC - (Not Critical): Methodology may or may not be available, but response of the component will be insignificant compared to other critical components

A - (Analytical): Analysis by existing computer programs if the time and funds allow; otherwise based on experimental data.

E - (Experimental): Analysis based primarily on existing experimental data because analytical techniques lack confidence.



## REFERENCES

1. R. Mayerhofer, "Response to Blast of Parked Aircraft (Event Dial Pack)," Ballistic Research Laboratory Memorandum Report No. 2267, January 1973, (Confidential).
2. G. Zartarian and K. Wetmore, "Correlation Study of the UH-1B Helicopter Blast Test Results from the Mixed Company Event," Kaman Avidyne Report No. TR-99, September 1973.
3. G. Zartarian, E. Cole, and M. Ayvazian, "Correlation Study of the UH-1B Helicopter Blast Test Results from the Pre-Mine Throw IV Event," Kaman Avidyne Report No. TR-116 or Defense Nuclear Agency Report No. DNA 3704F, March 1975.
4. R. Mayerhofer, "Mixed Company/Pre-Mine Throw IV Event, Blast Effects on In-Flight Helicopters," Defense Nuclear Agency Report No. POR , May 1977.
5. G. Zartarian, "Pre-Test Analysis for the Blast Response of the UH-1B Helicopter, Project No. 107," No Report Number, Under Dice Throw Cover, August 1976. Produced under BRL Contract No. DAAD05-76-C-0772.
6. W. McDonald and R. Huyett, "Window Contoured Glass/Plastic Transparent Armor for the UH-1D Helicopter," Goodyear Aerospace Report No. GERA-2074 or Army Materials and Mechanics Research Center Report No. AMMRC CTR 75-12, May 1975.
7. Zartarian, Thompson, and Hobbs, "Analysis of Helicopter Response to Nuclear Blast," Kaman Avidyne Report Numbers TR-72(R), Vols I, II, III, November 1972 or Defense Nuclear Agency Report Numbers DNA 2910F-1, DNA 2910F-2, and DNA 2910F-3.
8. E. Fletcher, D. Richmond, R. Jones, and W. Jackson, "Blast Effects on Helicopter Plexiglas Windows," Ballistic Research Laboratory Contract Report No. 142, March 1974, (Confidential) or Defense Nuclear Agency Report No. POR 6631 (FOUO).
9. G. Zartarian, E. Cole, and W. Lee, "Correlation Study of the UH-1B Helicopter Blast Test Results from the Dice Throw Event," Kaman Avidyne Report No. KA-TR-138, May 1977.
10. R. Schumacher, "Blast Response of Helicopters Parked in Revetments (Event Mixed Company), Ballistic Research Laboratory Memorandum Report No. 2516, August 1975, or Defense Nuclear Agency Report No. POR 6607, May 1975.

## APPENDIX A

### RAW DATA

#### EXTRACTED FROM REFERENCE 9

Included in this Appendix are the digitized raw data plots of the drone helicopter instrumentation. For identification and location of data, use Table A.1. Channel D-09 was considered "lost"; Channels A-08, B-08, C-08, and D-08 were 100 KHz reference timing channels; Channels A-13, B-13, C-13, and D-13 were IR1G-B/FIDU; and A-14, B-14, C-14, and D-14 were spare channels. The eight channels of oscillograph records were not reproducible for this report because the recording traces had deteriorated (normal); draftsman's reproductions appear in Reference 9.

Table A.1 Raw Data Identification

<u>CHANNEL</u>	<u>COMPONENT</u>	<u>STA LOCATION</u>	<u>MEASUREMENT</u>
A-01	Main Rotor	35.0 Red	Bending
B-01	Main Rotor	82.0 Red	Bending
C-01	Main Rotor	105.6 Red	Bending
D-01	Main Rotor	132.0 Red	Bending
A-02	Main Rotor	82.0 White	Bending
B-02	Main Rotor	105.6 White	Bending
C-02	Main Rotor		Flap Angle
D-02	Main Rotor		Azimuth
A-03	Tail Rotor	10.5 Red	Bending
B-03	Tail Rotor	15.5 Red	Bending
C-03	Tail Rotor	20.4 Red	Bending
D-03	Tail Rotor	25.5 Red	Bending
A-04	Tail Rotor	15.5 White	Bending
B-04	Tail Rotor	20.4 White	Bending
C-04	Tail Rotor		Flap Angle
D-04	Tail Rotor		Azimuth
A-05	Tail Boom Panel	49.0 Top Inside	Strain
B-05	Tail Boom Panel	49.0 Top Outside	Strain
C-05	Tail Boom Panel	49.0 Center Inside	Strain
D-05	Tail Boom Panel	49.0 Center Outside	Strain
A-06	Tail Boom Panel	58.0 Aft Inside	Strain
B-06	Tail Boom Panel	58.0 Aft Outside	Strain
C-06	Tail Boom Panel	49.0 Center Horiz.	Strain
D-06	Longeron	49.0 Center Horiz.	Strain

Table A.1 Raw Data Identification (Cont'd)

<u>CHANNEL</u>	<u>COMPONENT</u>	<u>STA LOCATION</u>	<u>MEASUREMENT</u>
A-07	Stringer	49.0	Strain
B-07	Tail Boom	47.0	Bending
C-07	Tail Boom	112.0	Bending
D-07	Fin	35.0	Bending
A-09	Fin	55.0	Bending
B-09	Tail Boom	28.0	Pressure
C-09	Fin	37.0	Pressure
D-09	Dummy	Crew Seat	Pressure
A-10	Rigid Body	Gyro	Pitch Attitude
B-10	Rigid Body	Gyro	Roll Attitude
C-10	Rigid Body	Gyro	Yaw Attitude
D-10	Rigid Body	Gyro	Pitch Rate
A-11	Rigid Body	Gyro	Roll Rate
B-11	Rigid Body	Gyro	Yaw Rate
C-11	Rigid Body	Radar	Altitude
D-11	Controls	Stick	Position-Lateral
A-12	Controls	Stick	Position Fore/Aft
B-12	Controls	Stick	Position Collective
C-12	Controls	Stick	Position Pedal
D-12	Cabin/Cargo	Camera Stand	Pressure

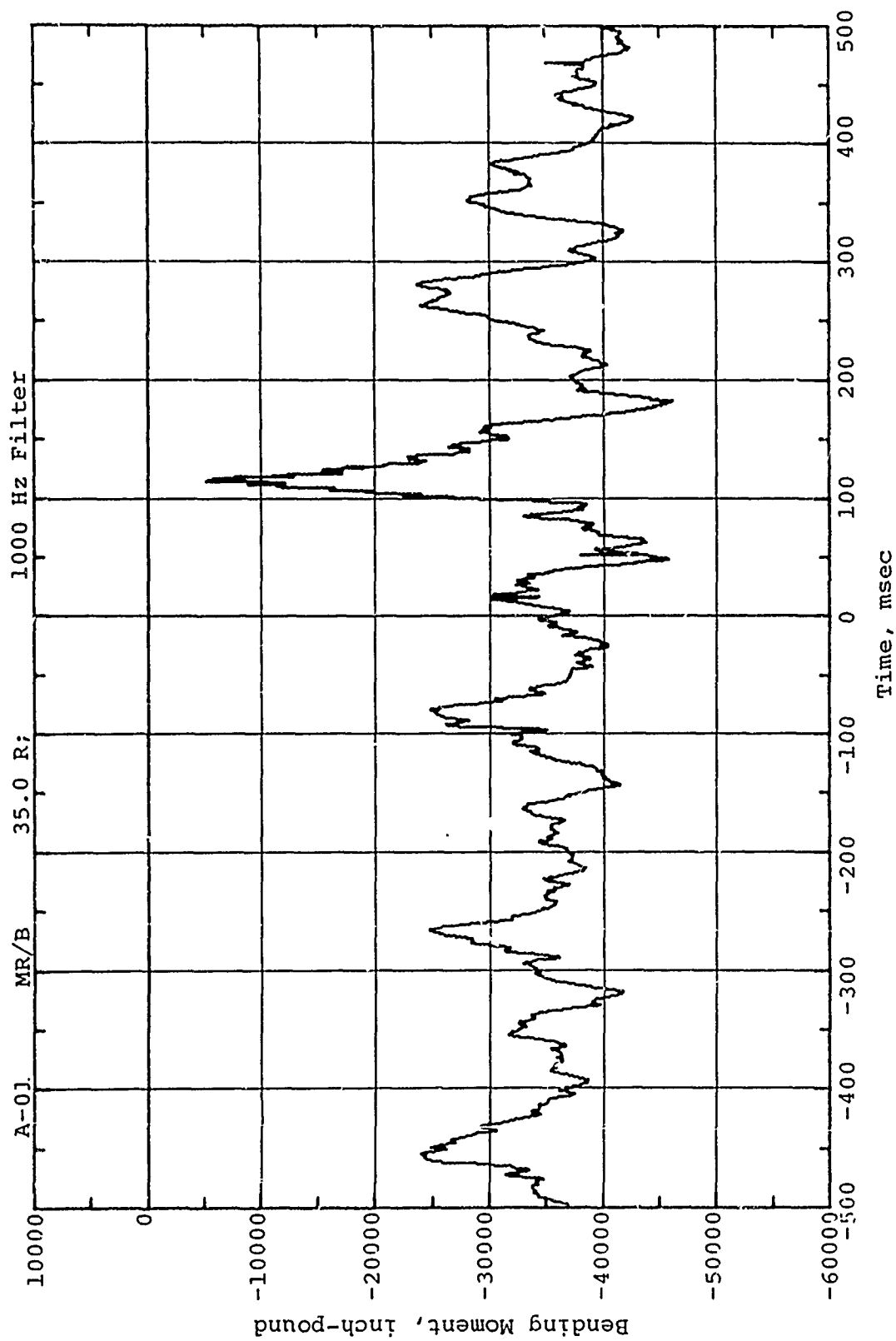


Figure A.1 Time-Variation of Total Flapwise Bending Moment.  
Main Rotor Red Blade Station 35. Channel A-01

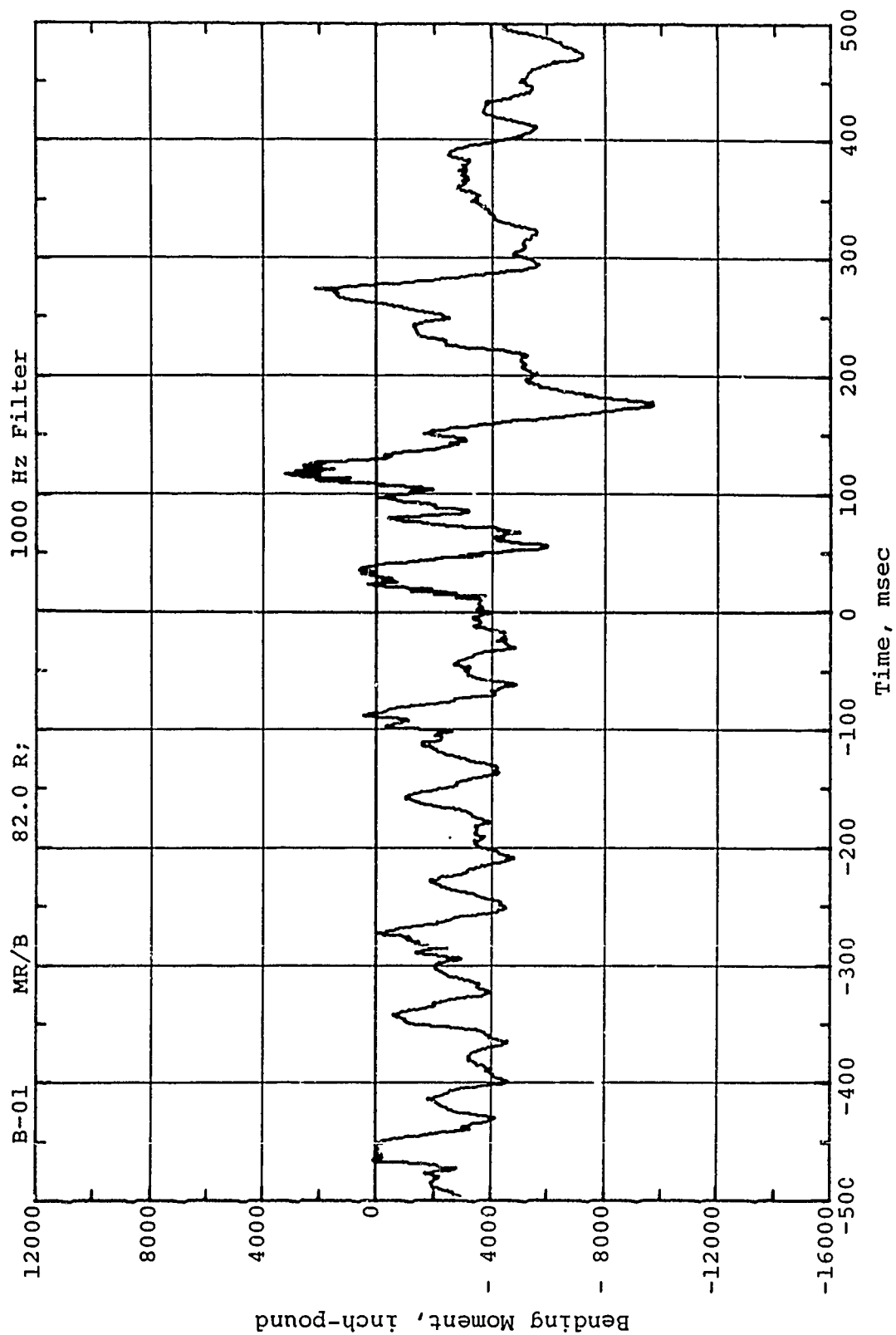


Figure A.2 Time-Variation of Total Flapwise Bending Moment.  
Main Rotor Red Blade Station 82. Channel B-01

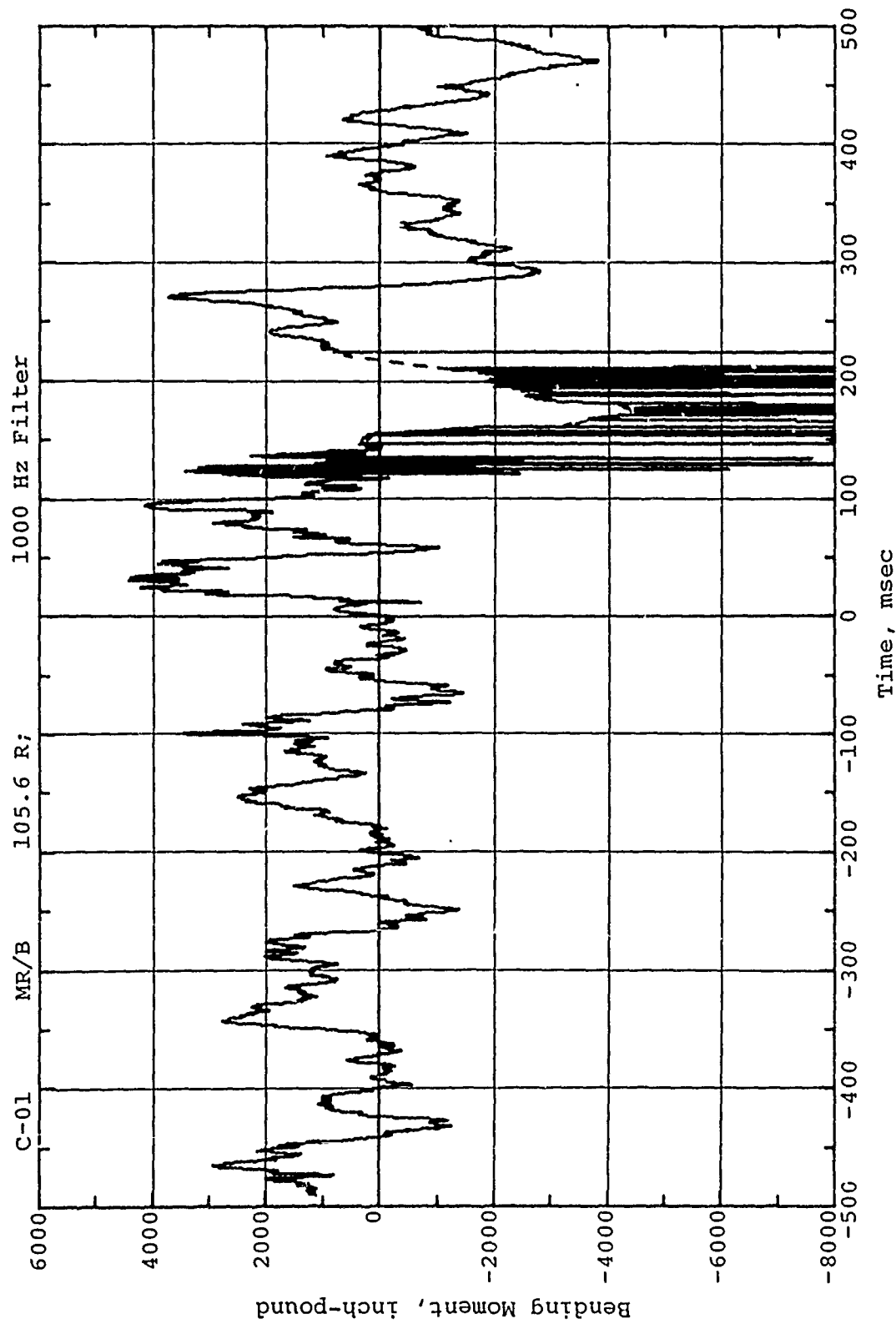


Figure A.3 . Time-Variation of Total Flapwise Bending Moment.  
Main Rotor Red Blade Station 105.6. Channel C-01

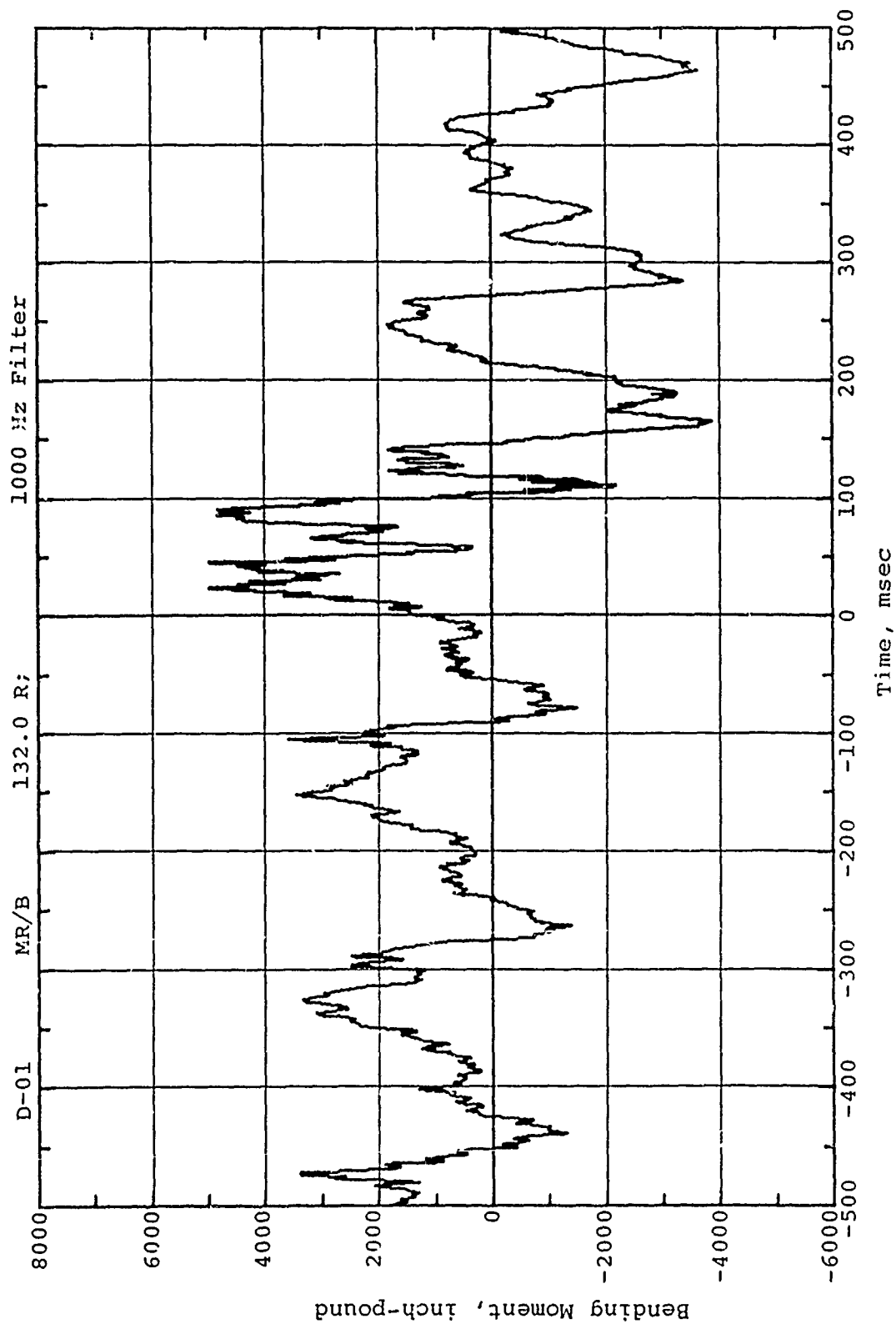


Figure A.4 Time-Variation of Total Flapwise Bending Moment.  
Main Rotor Red Blade Station 132. Channel D-01



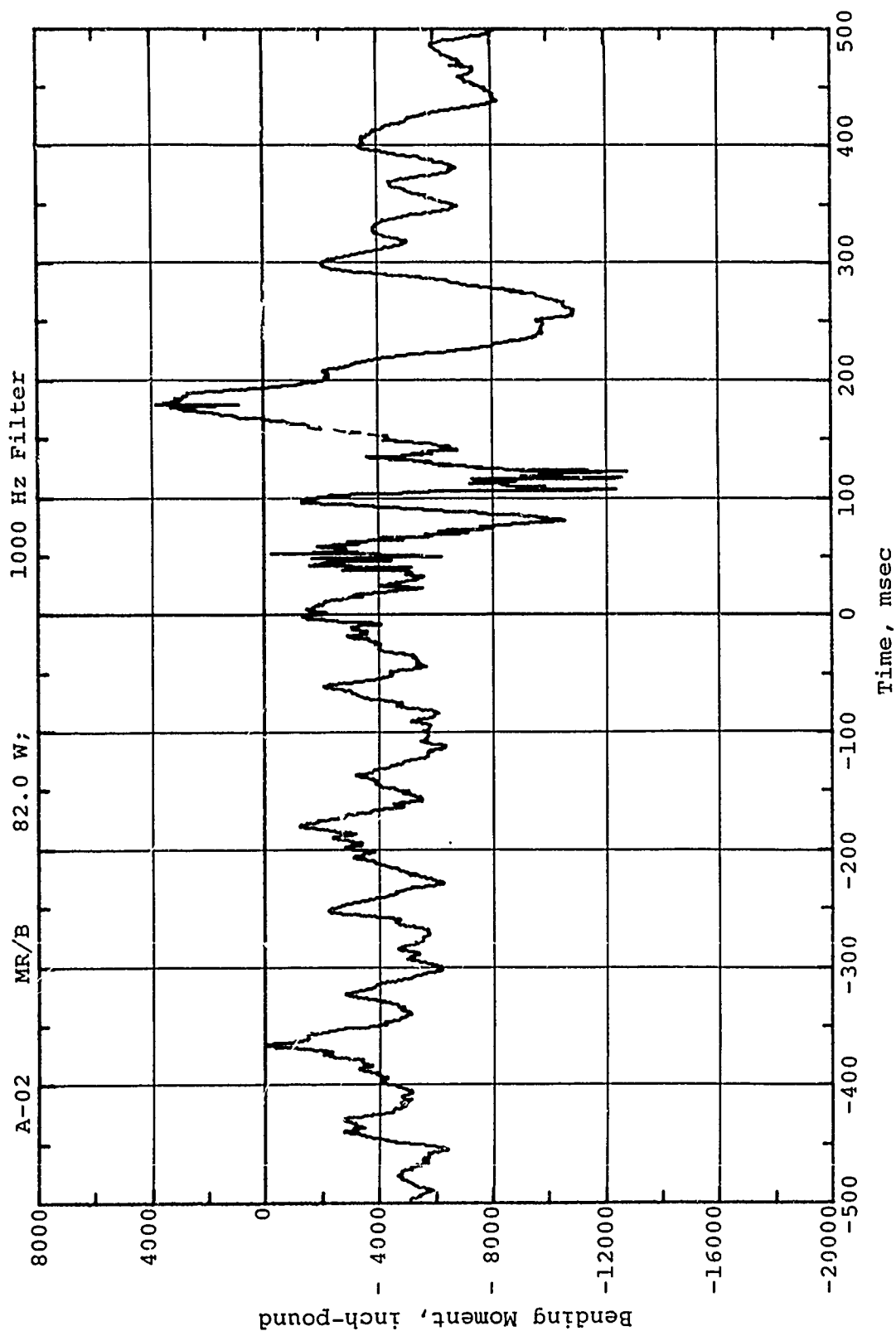


Figure A.5 Time-Variation of Total Flapwise Bending Moment.  
Main Rotor White Blade Station 82. Channel A-02

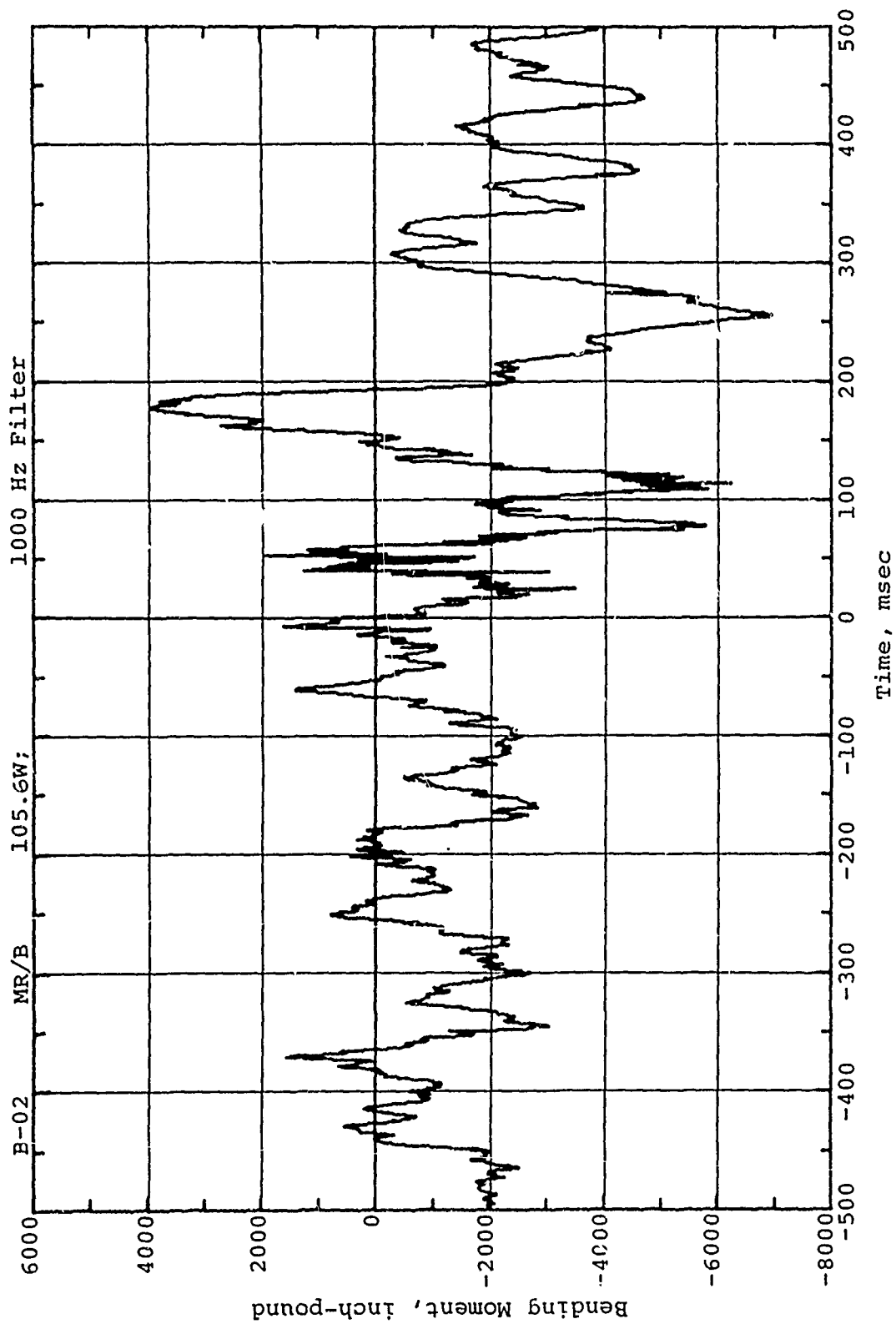


Figure A.6 Time-Variation of Total Flapwise Bending Moment.  
Main Rotor White Blade Station 105.6. Channel B-02

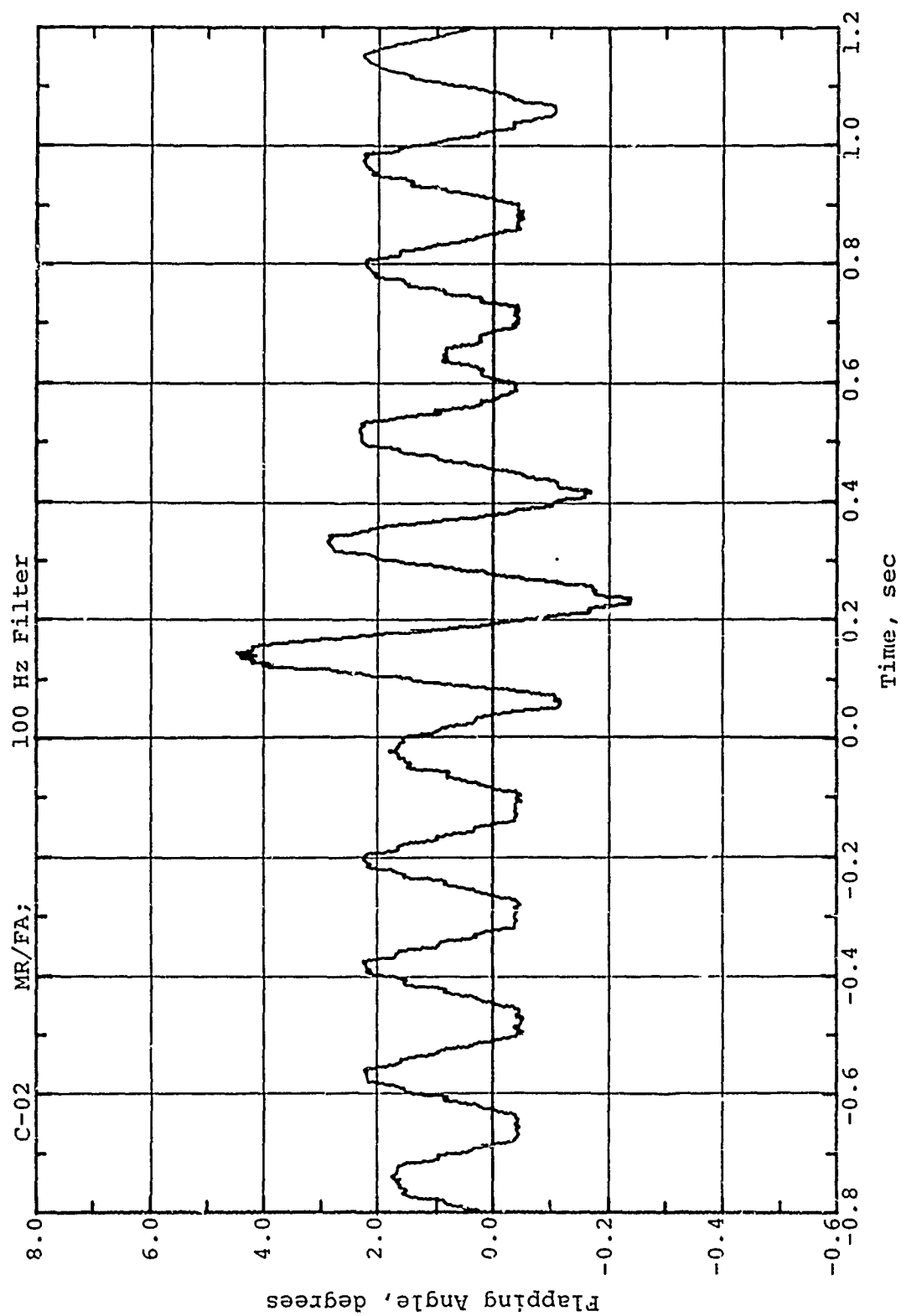


Figure A.7 Time-Variation of Main Rotor Red Blade Flapping Angle.  
Channel C-02

30-1 15 KHZ

DO2MR/AZ

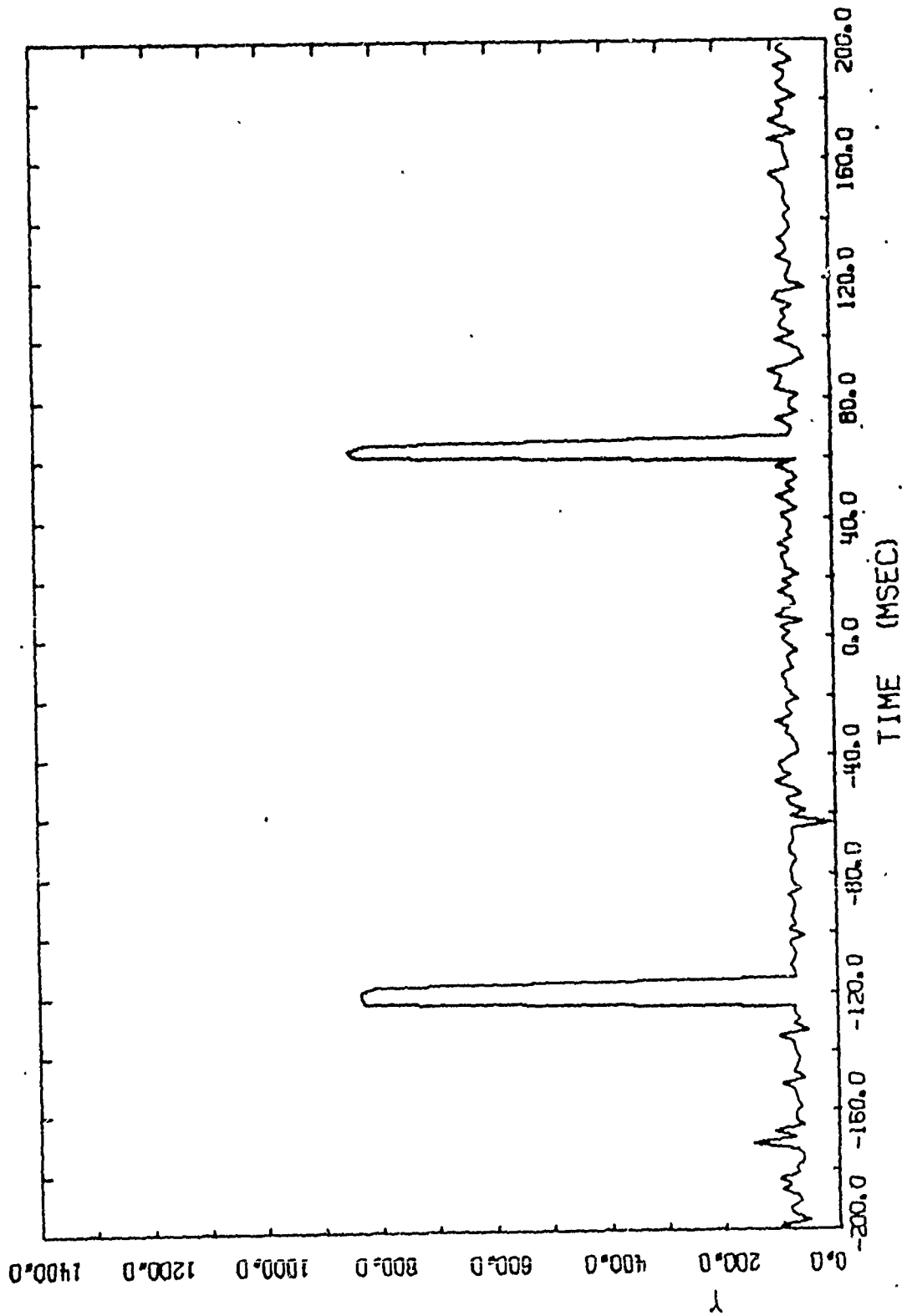


Figure A.8 Main Rotor Blade Azimuth

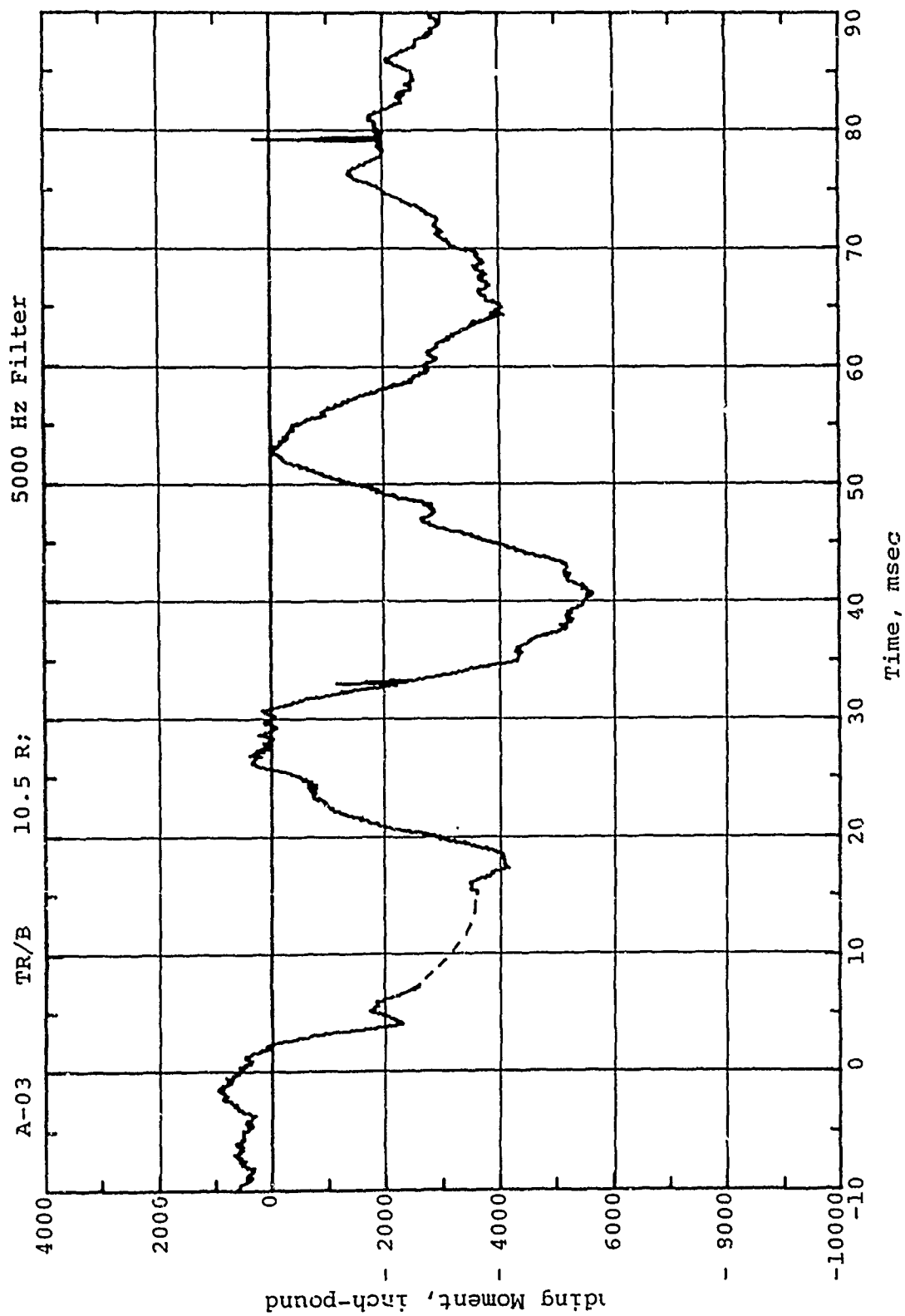


Figure A.9 Time-Variation of Total Flapwise Bending Moment At Tail Rotor Red Blade Station 10.5. Channel A-03

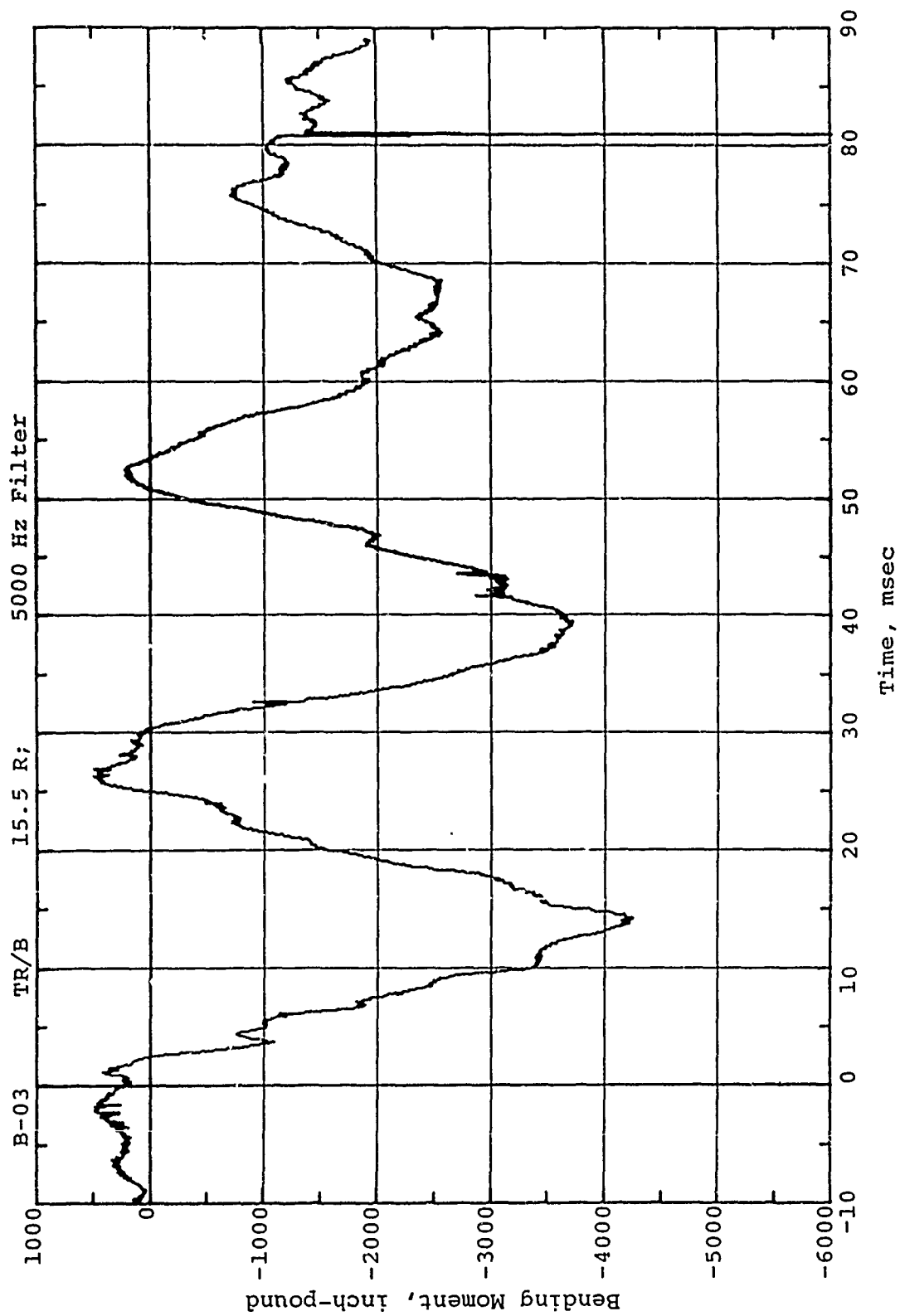


Figure A.10 Time-Variation of Total Flapwise Bending Moment At Tail Rotor Red Blade Station 15.5. Channel B-03

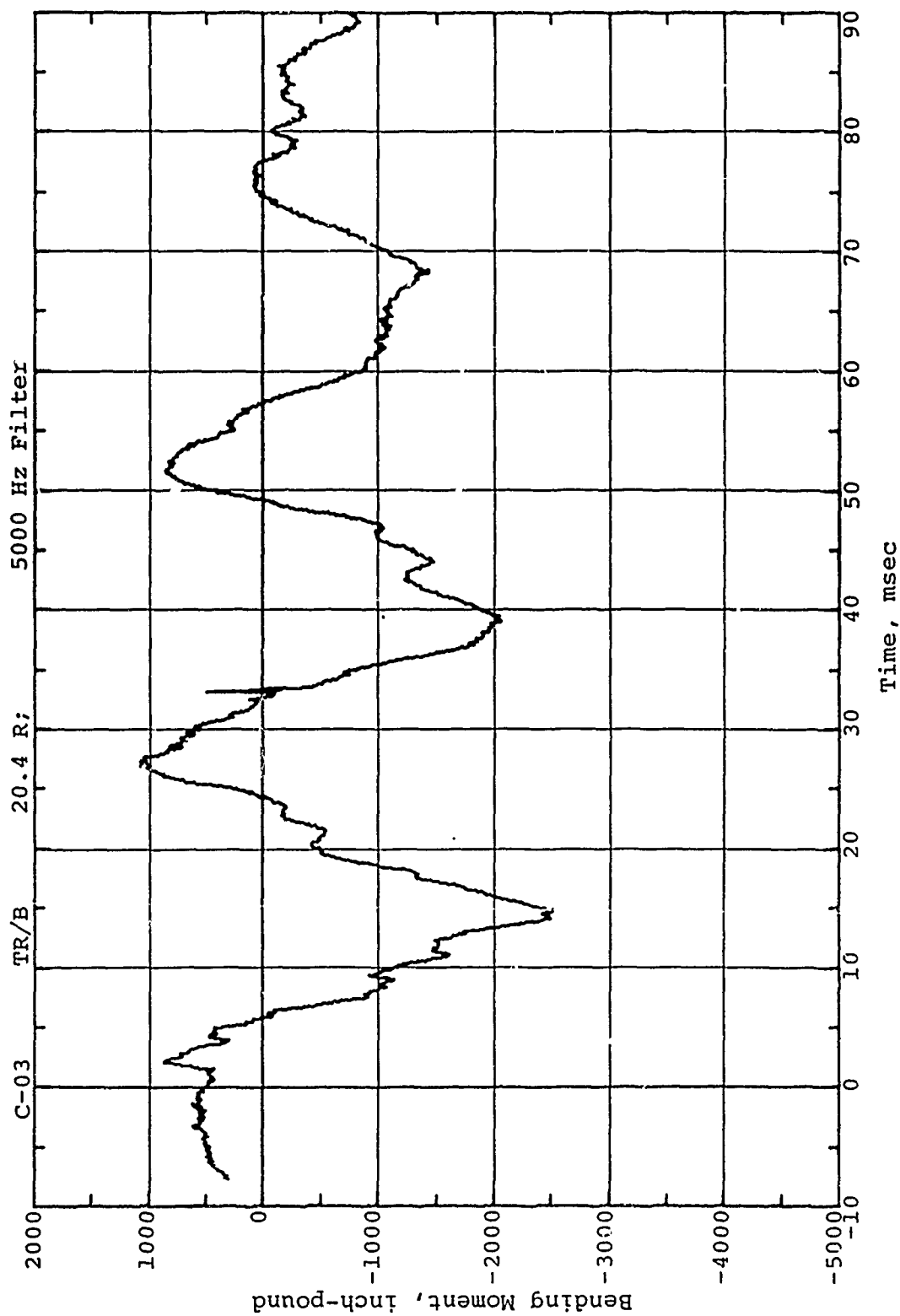


Figure A.11 Time-Variation of Total Flapwise Bending Moment At  
Tail Rotor Red Blade Station 20.4. Channel C-03

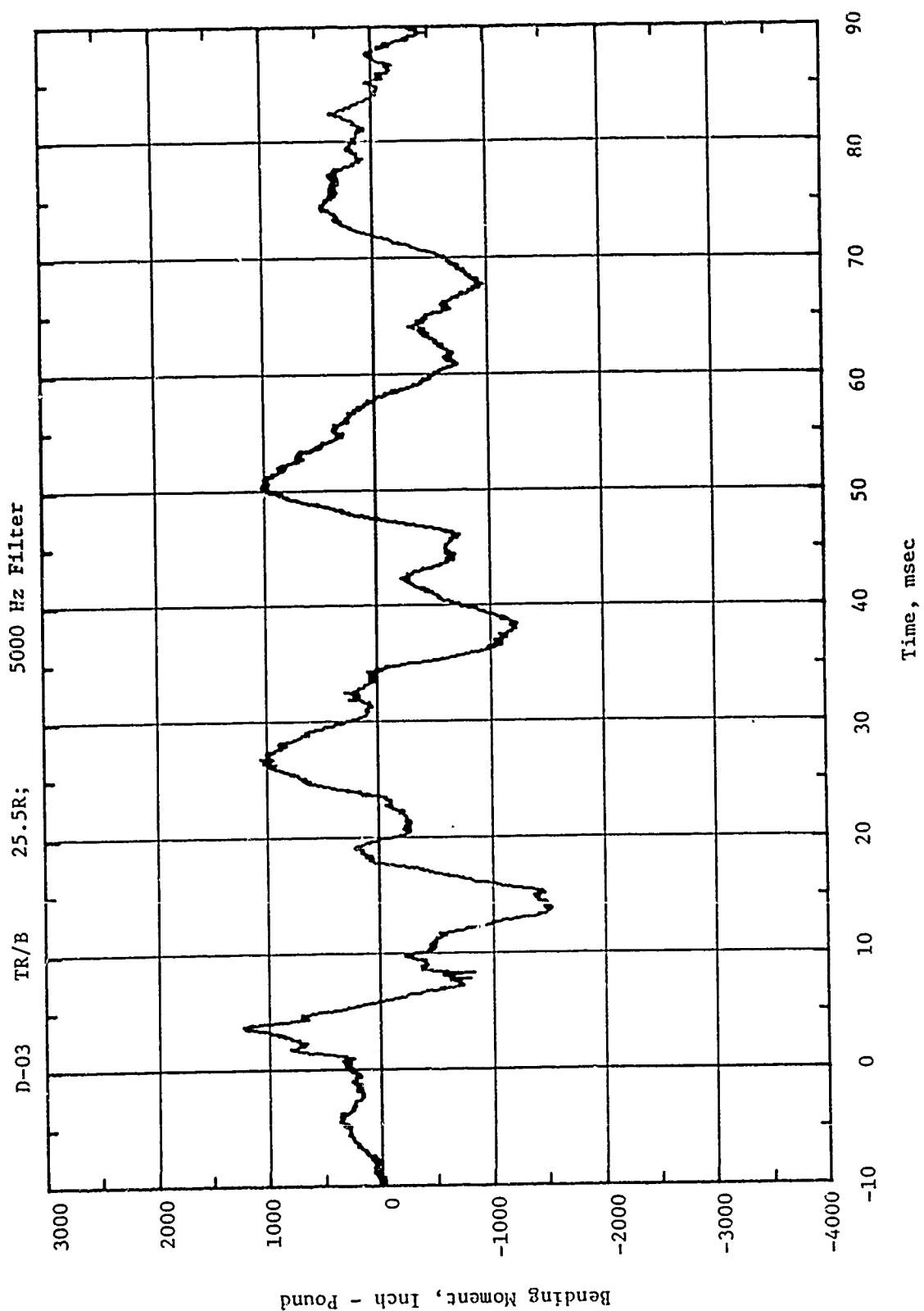


Figure A.12 Time-Variation of Total Flapwise Bending Moment At  
Tail Rotor Red Blade Station 25.5. Channel D-03



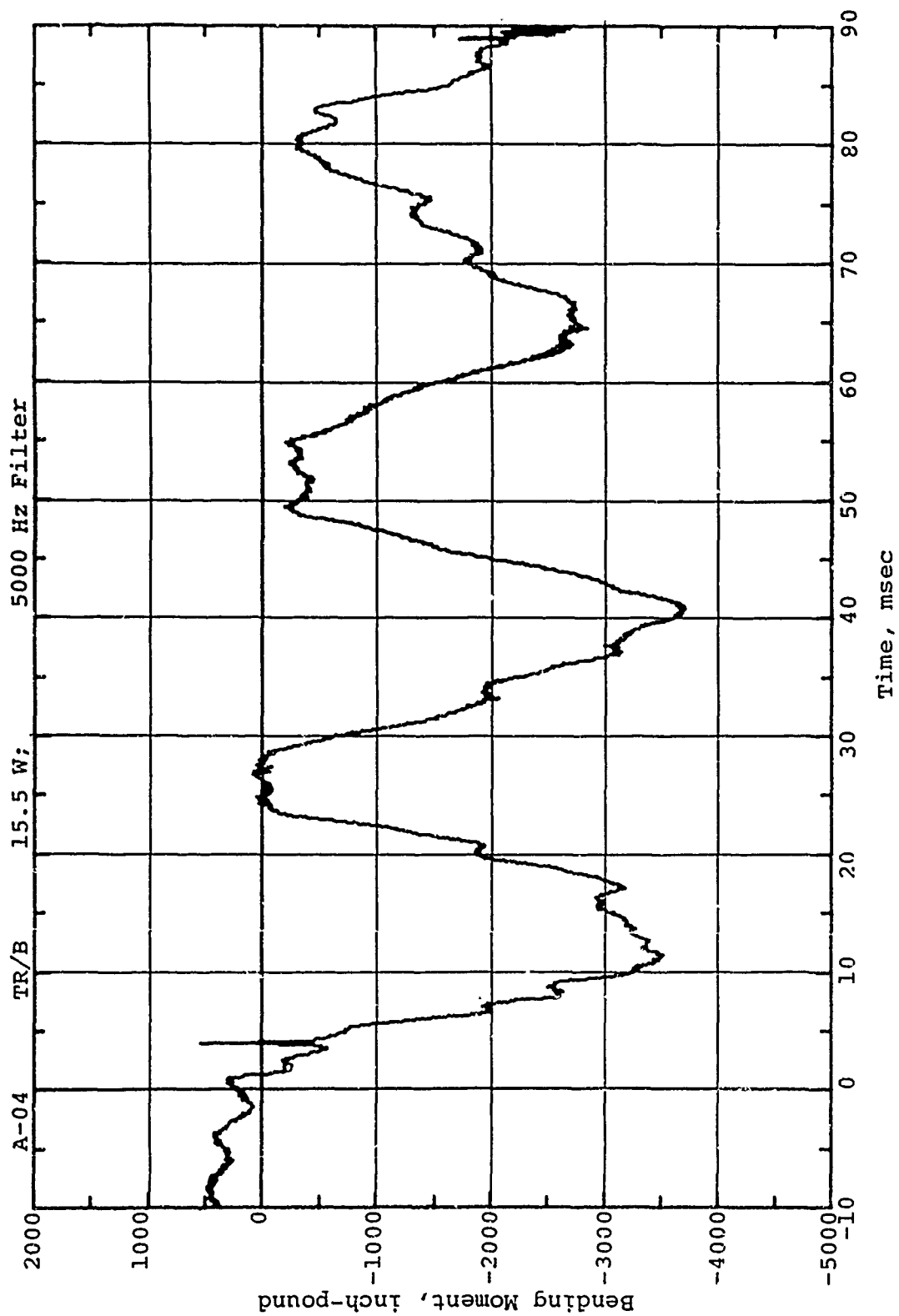


Figure A.13 Time-Variation of Total Flapwise Bending Moment At  
Tail Rotor White Blade Station 15.5. Channel A-04

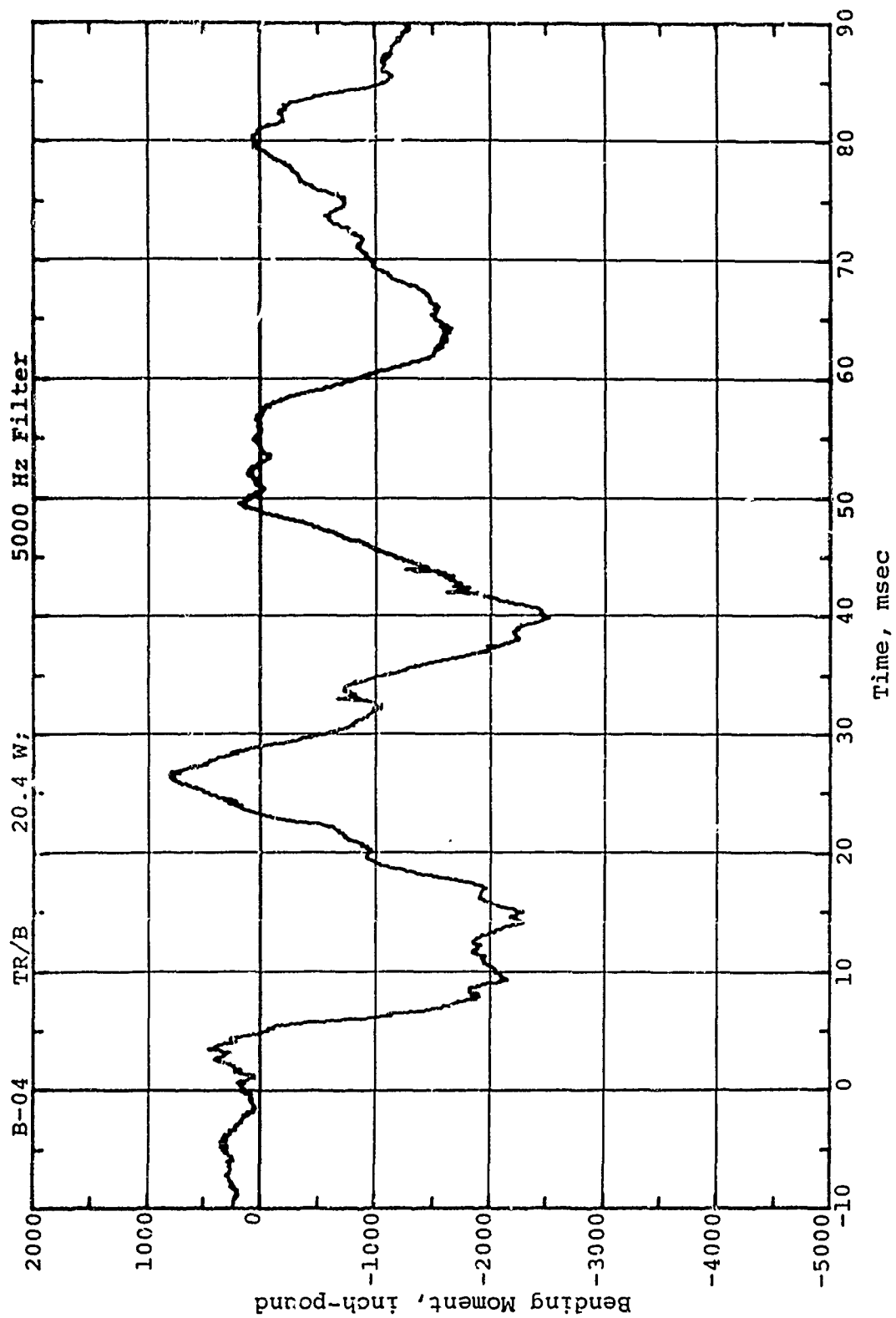


Figure A.14 Time-Variation of Total Flapwise Bending Moment At Tail Rotor White Blade Station 20.4. Channel B-04

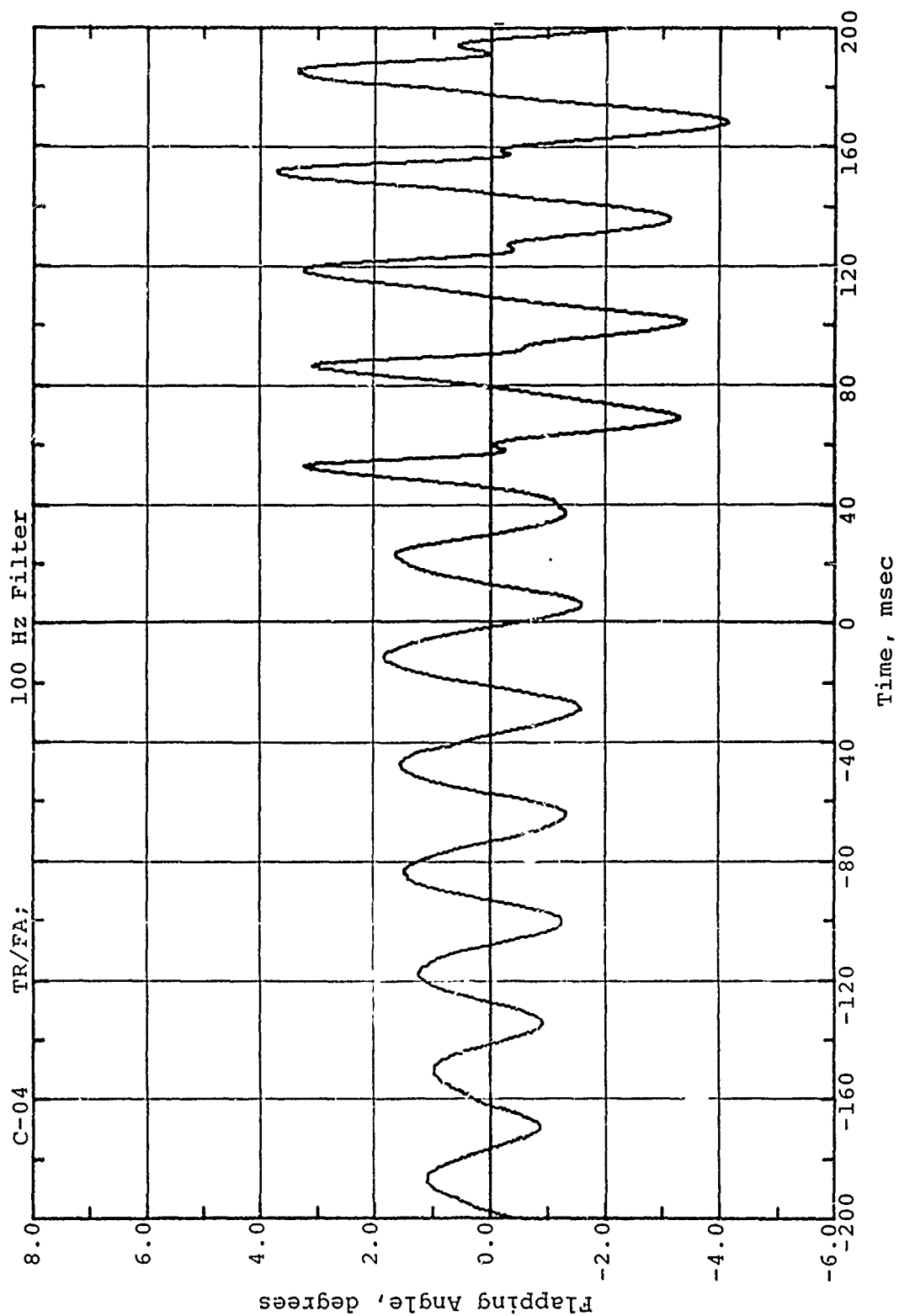


Figure A.15 Time-Variation of Tail Rotor Red Blade Flapping Angle.  
Channel C-04

20-3 15 KHZ  
D04TR/AZ

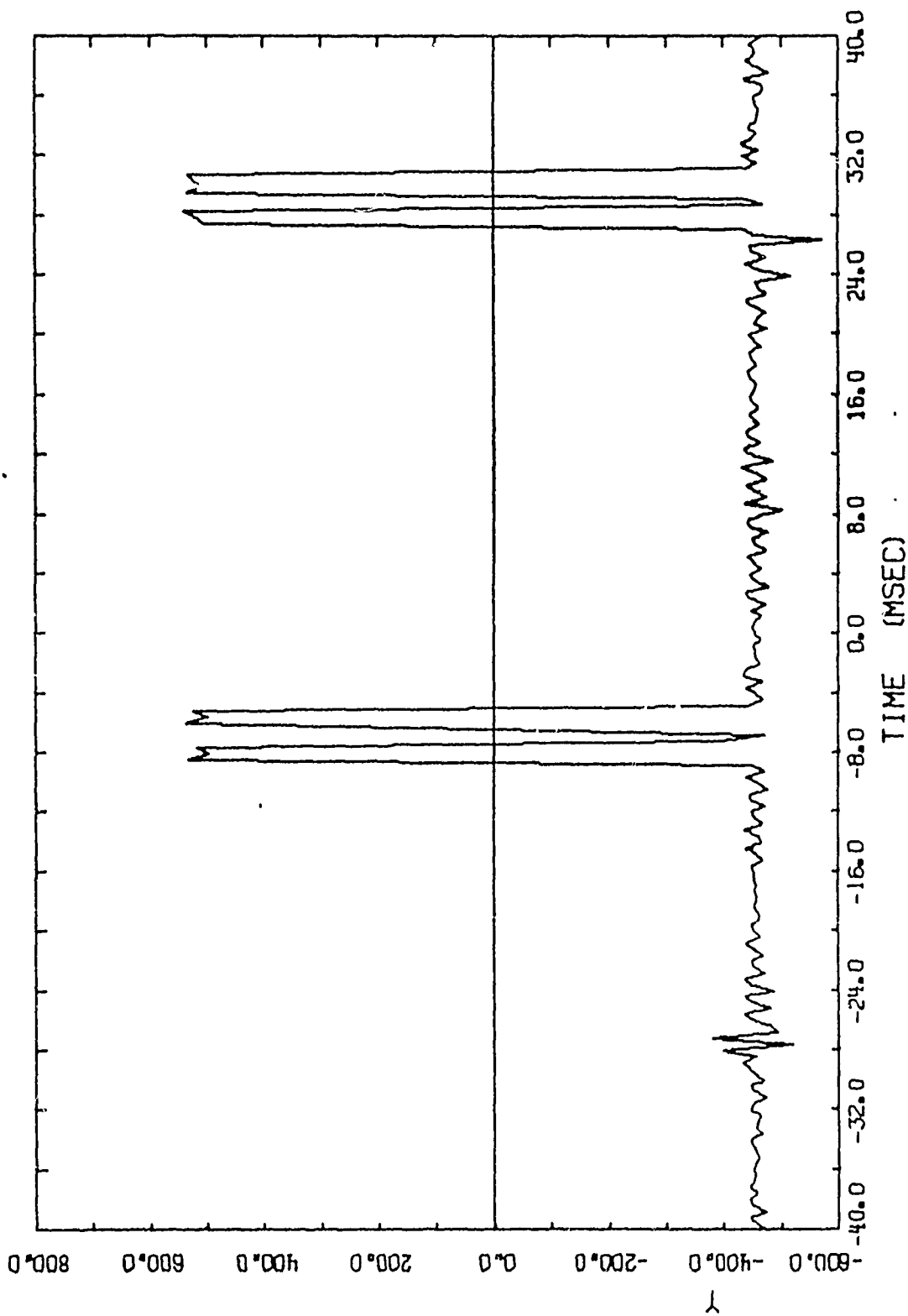


Figure A.16 Tail Rotor Blade Azimuth

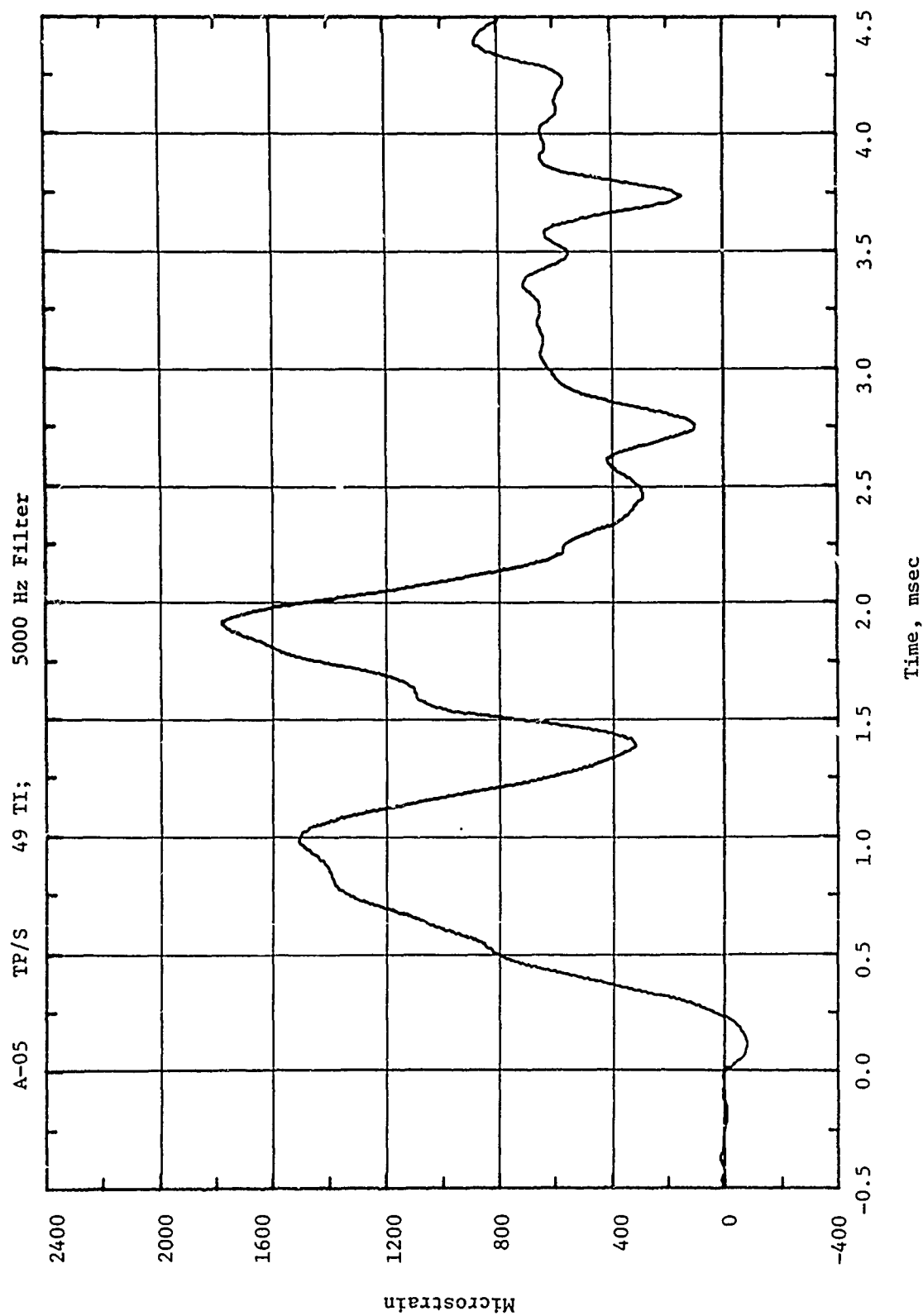


Figure A.17 Time-Variation of Panel Circumferential Strain at Inner Surface Point Near Longeron and on Centerline. Channel A-05

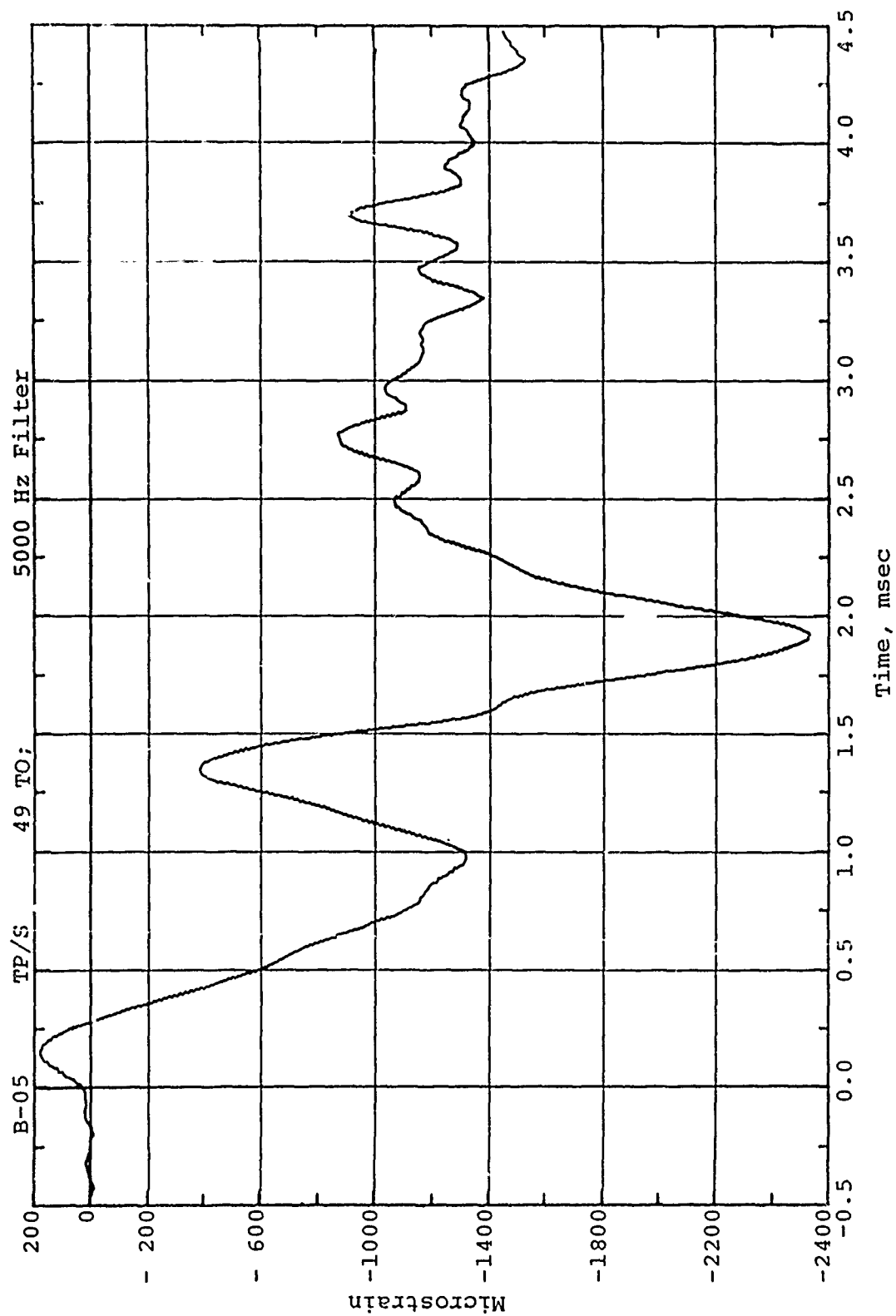


Figure A.18 Time-Variation of Panel Circumferential Strain at Outer Surface  
Point Near Longeron and on Centerline. Channel B-05

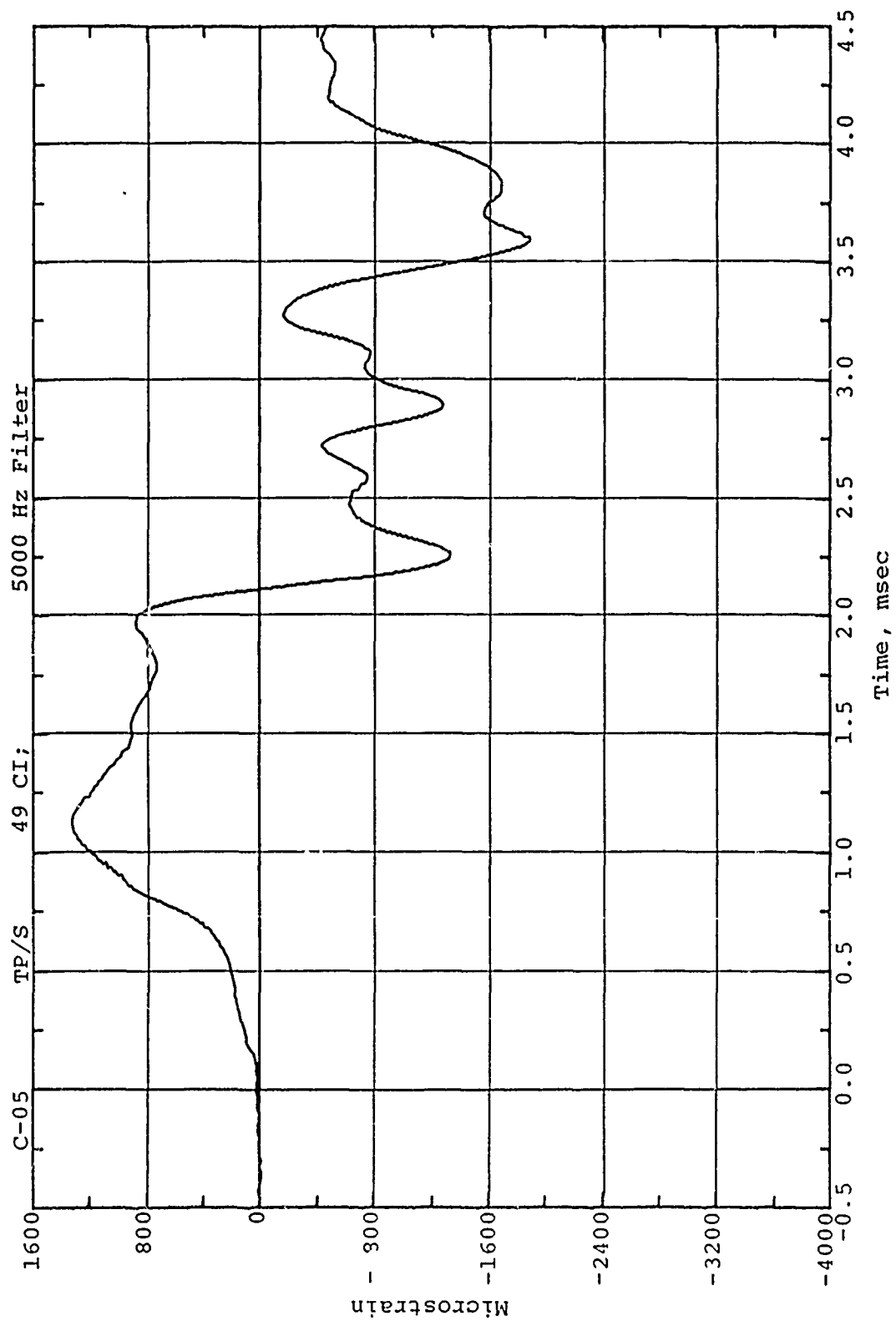


Figure A.19 Time-Variation of Panel Circumferential Strain at Inner Surface Center Point. Channel C-05

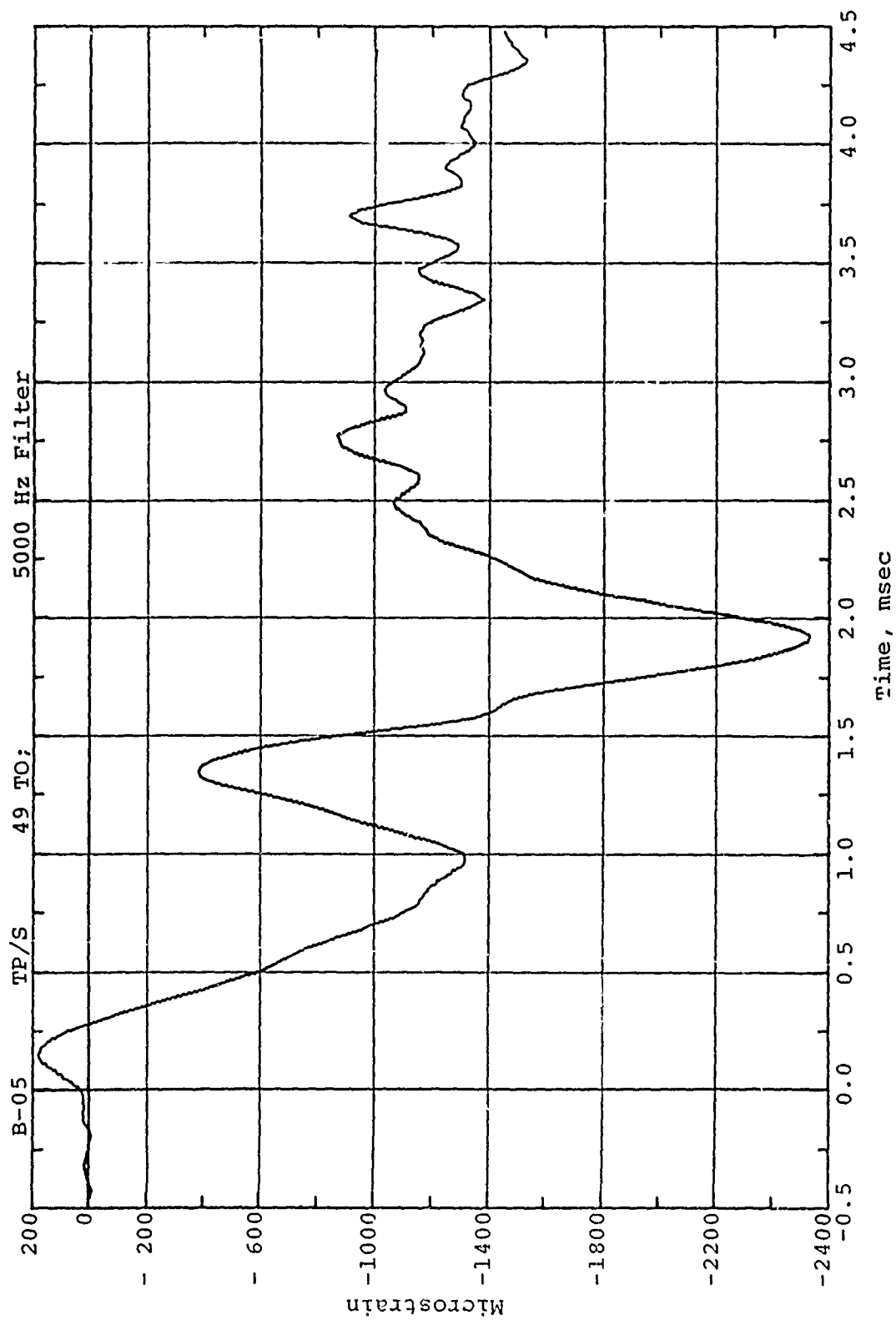


Figure A.13 Time-Variation of Panel Circumferential Strain at Outer Surface  
Point Near Longer on and on Centerline. Channel B-05



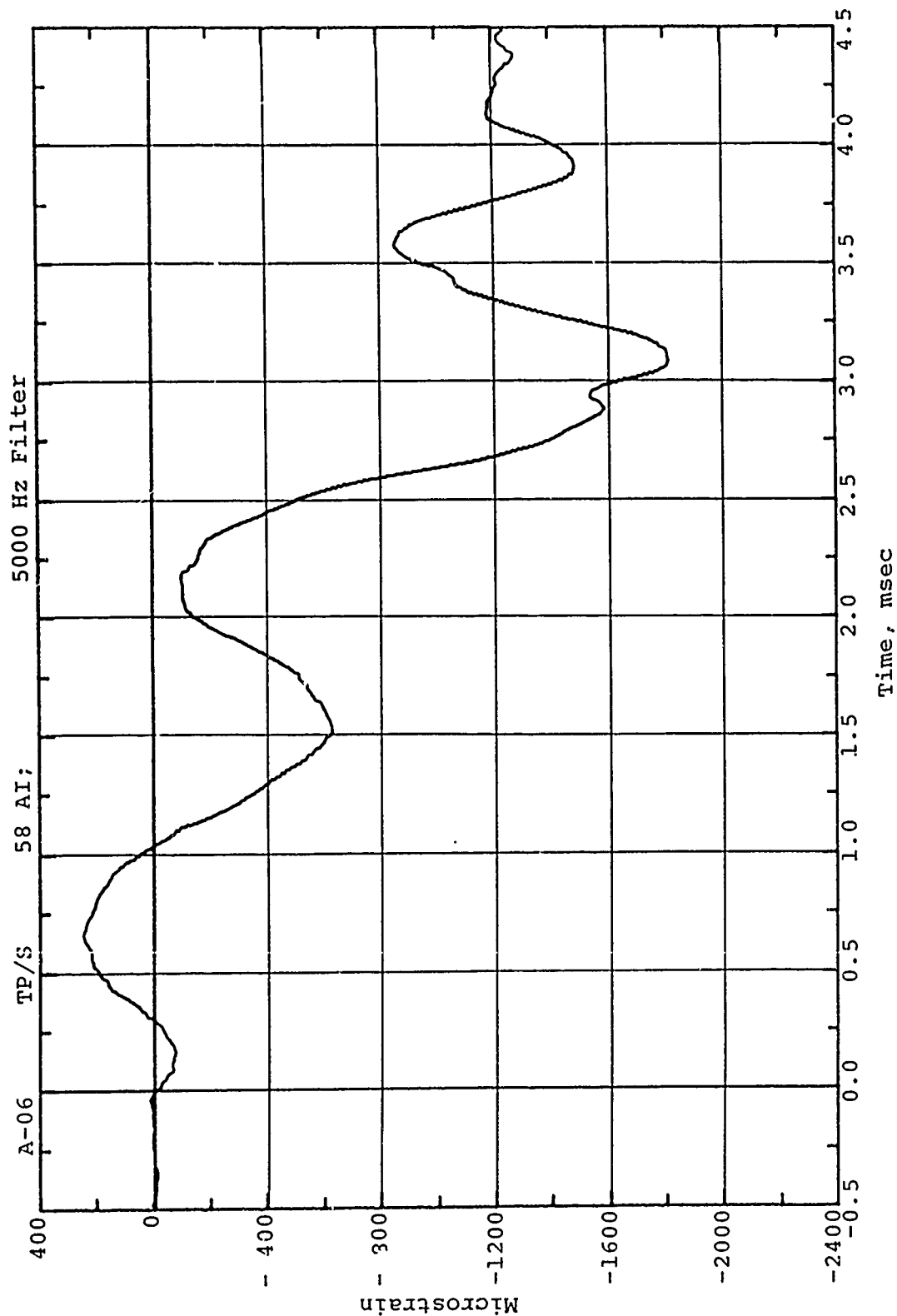


Figure A.21 Time-Variation of Panel Longitudinal Strain at Inner Surface Point Near Bulkhead and on Centerline. Channel A-06

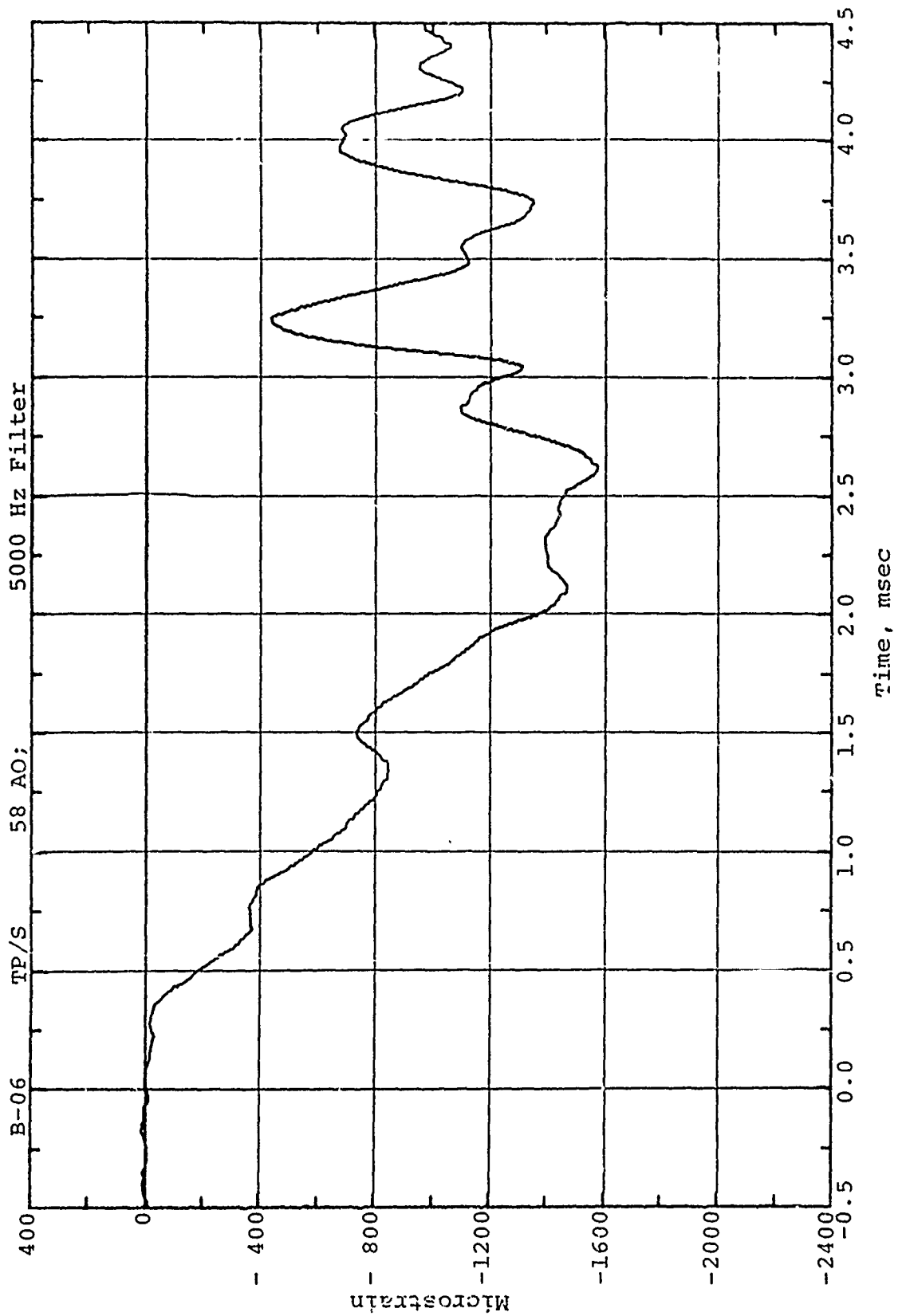


Figure A.22 Time-Variation of Panel Longitudinal Strain at  
Outer Surface Point Near Bulkhead and on  
Centerline. Channel B-06

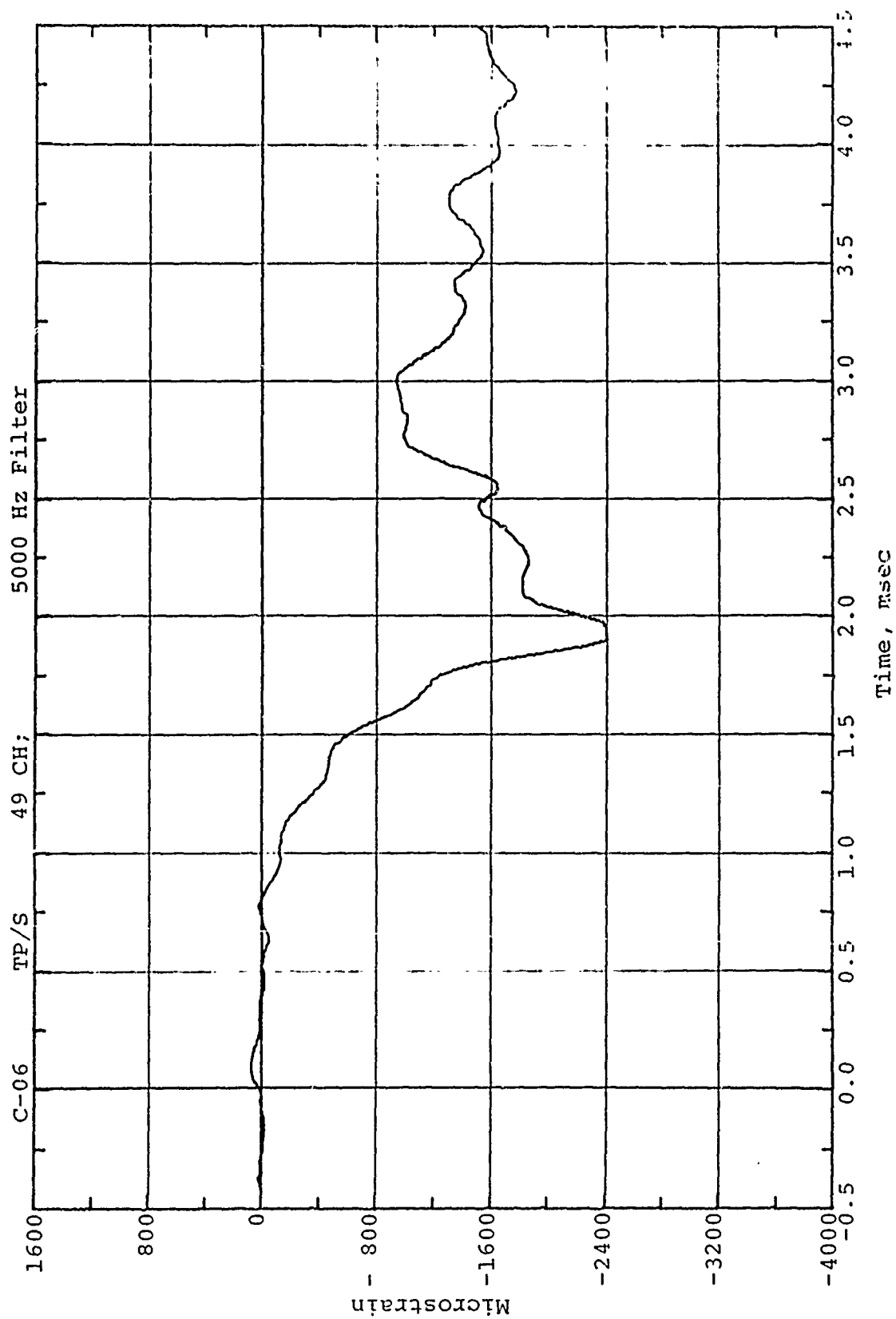


Figure A.23 Time-Variation of Panel Longitudinal Strain at Inner Surface Near Center Point. Channel C-06

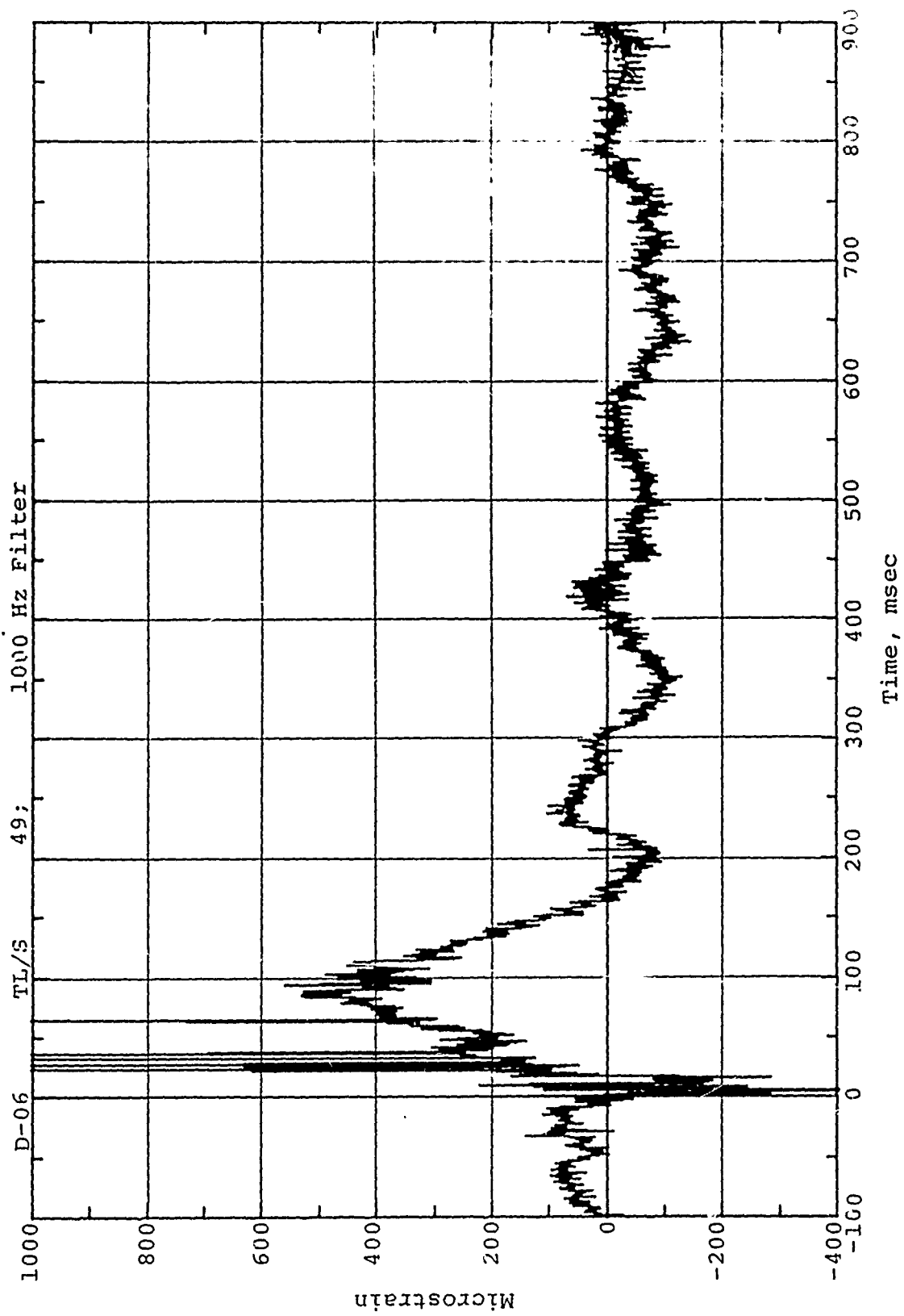


Figure A.24 Time-Variation of Longeron Extensional Strain  
at Its Mid-Span Station. Channel D-06

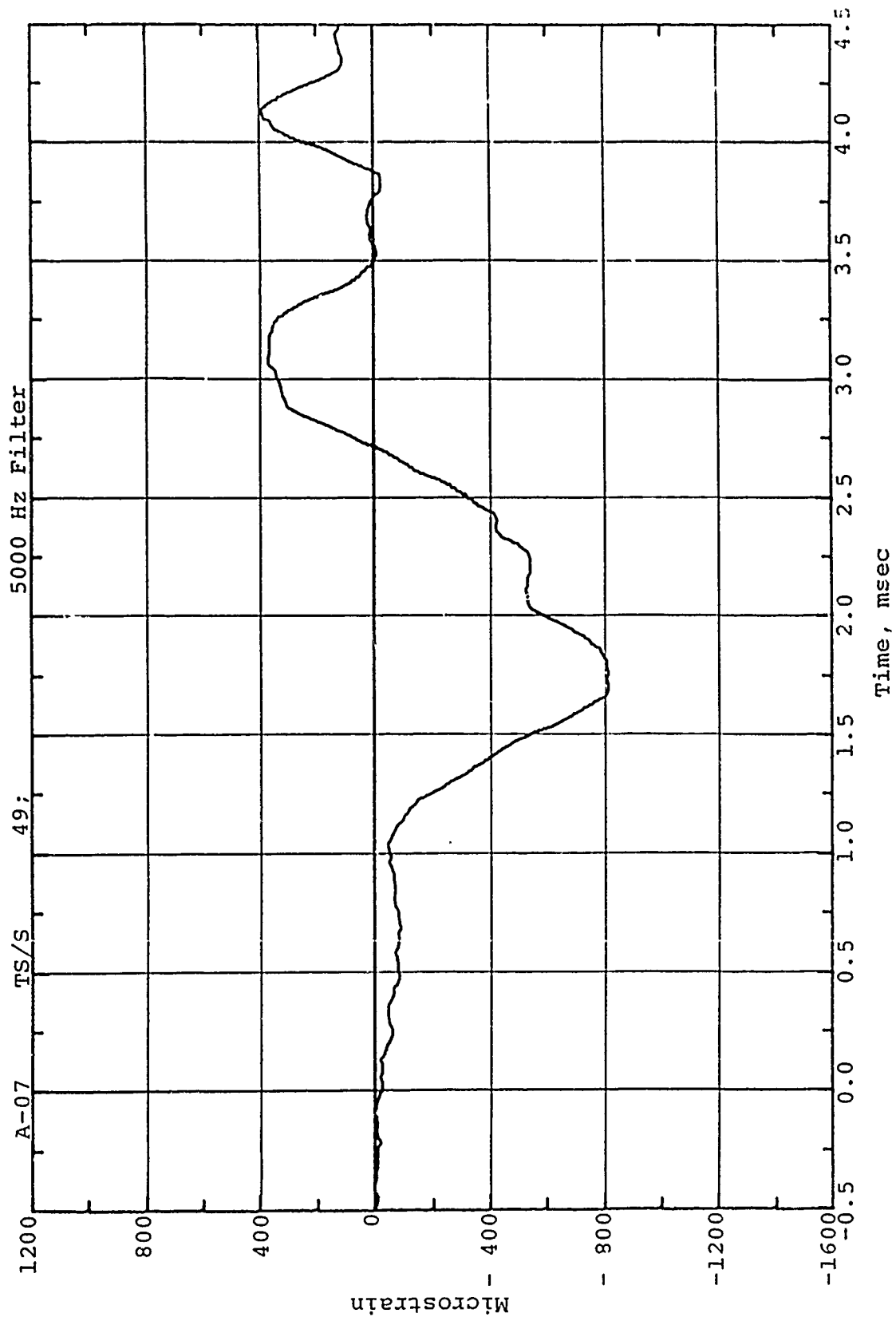


Figure A.25 Time-Variation of Stringer Extensional Strain at Its Mid-Span Station. Channel A-07

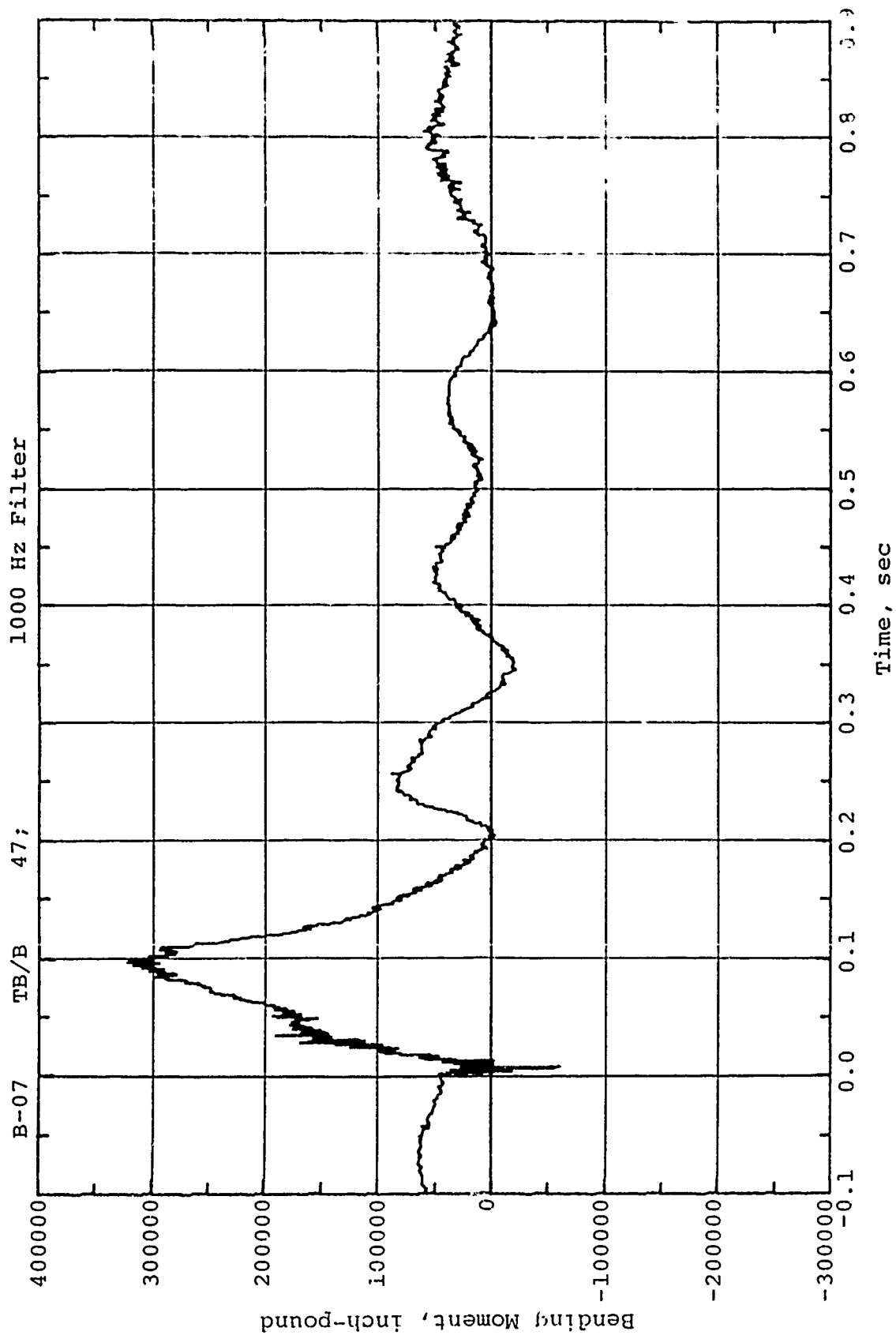


Figure A.26 Time-Variation of Total Tail Boom Lateral Bending Moment.  
Tail Boom Station 47. Channel B-07

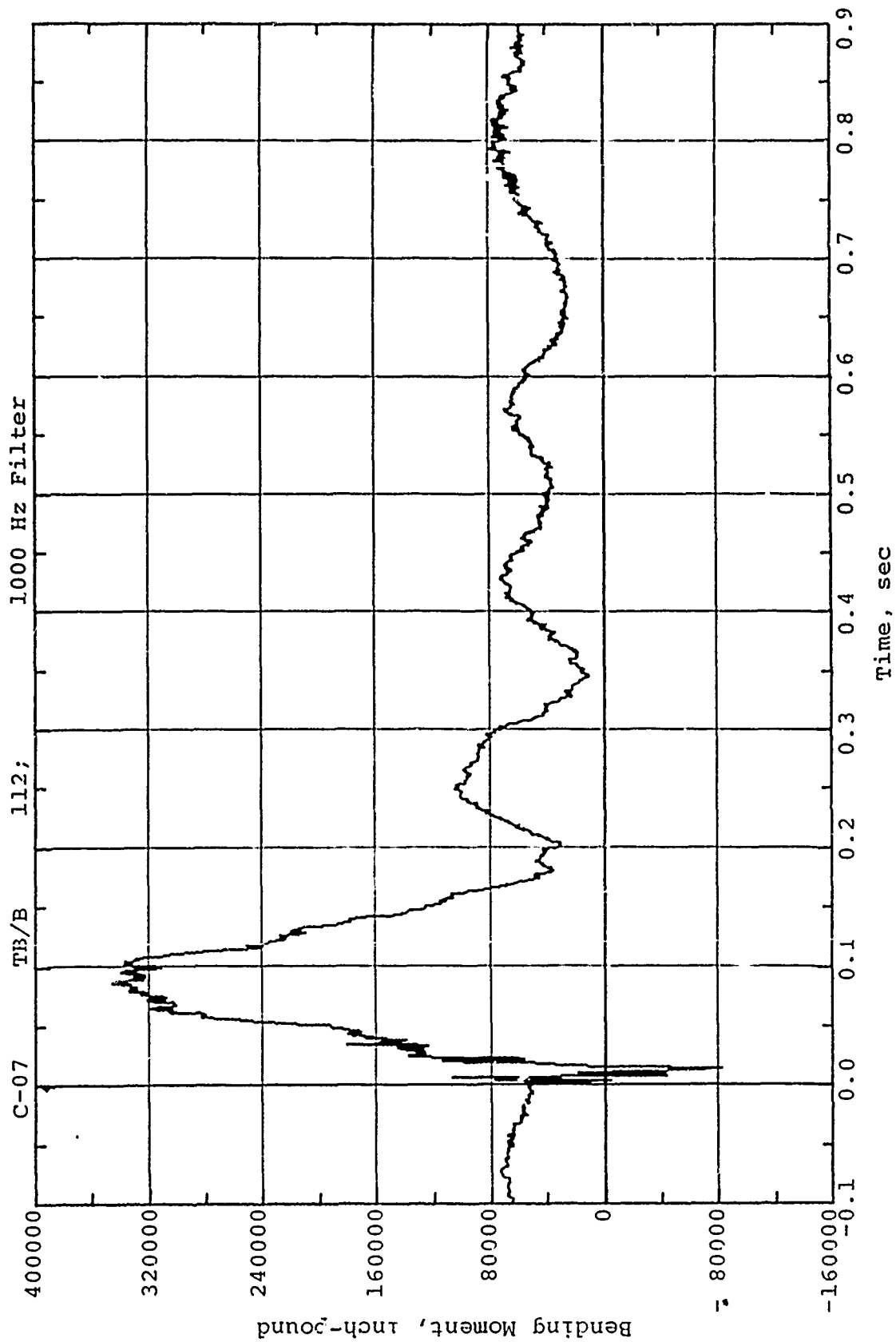


Figure A.27 Time-Variation of Total Tail Boom Lateral Bending Moment.  
Tail Boom Station 112. Channel C-07

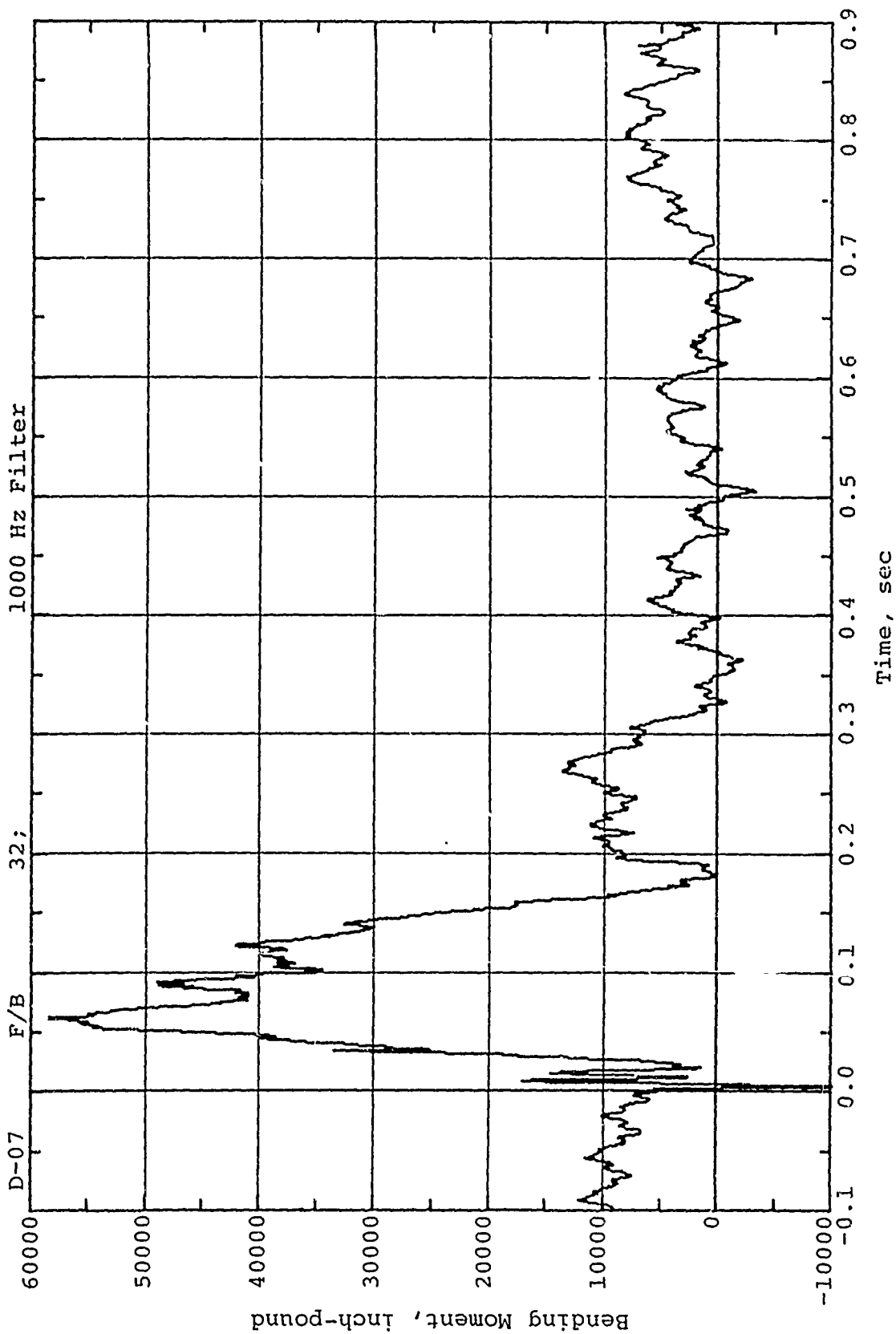


Figure A.28 Time-Variation of Total Fin Lateral Bending Moment.  
Fin Station 32. Channel D-07



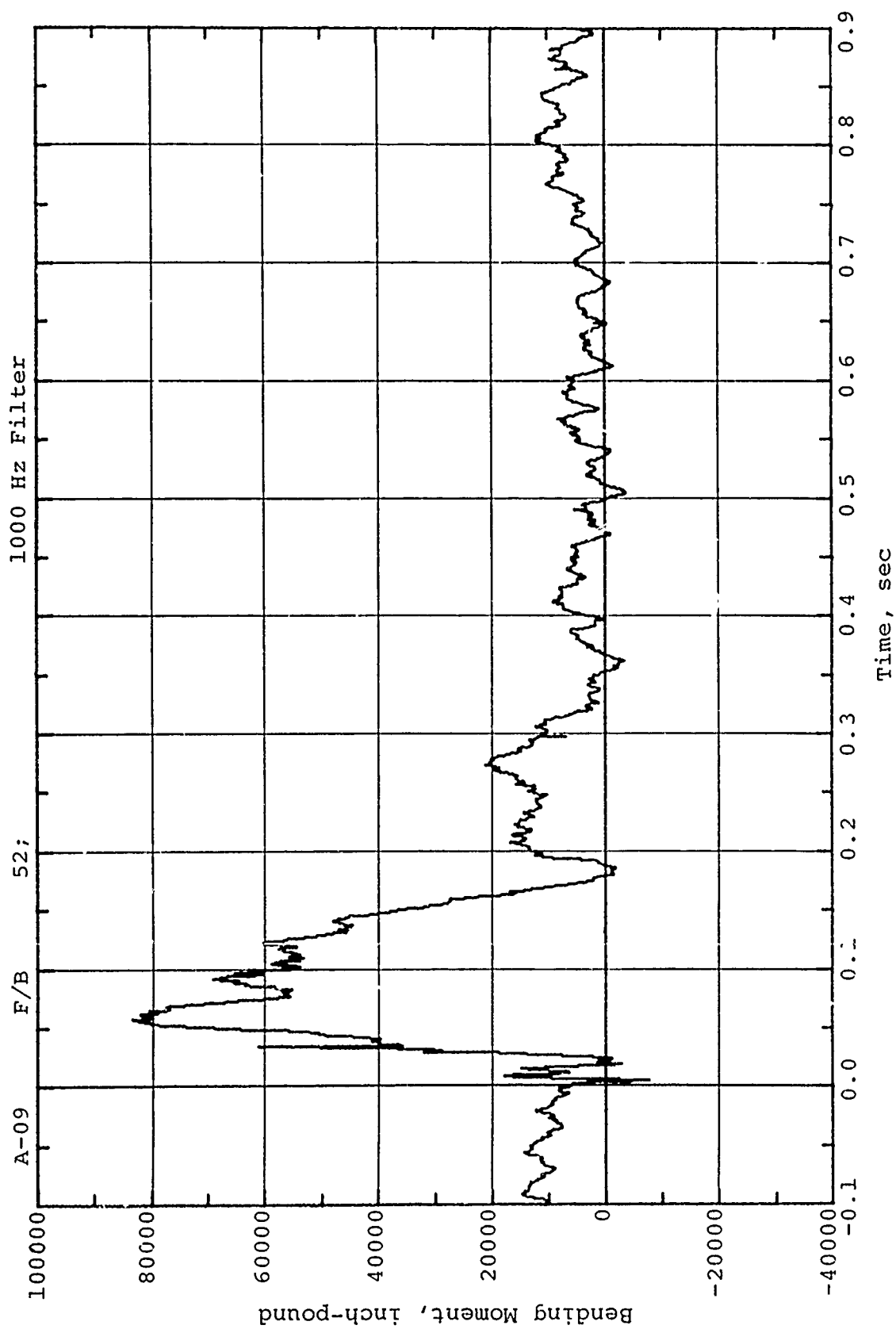


Figure A.29 Time-Variation of Total Fin Lateral Bending Moment.  
Fin Station 52. Channel A-09

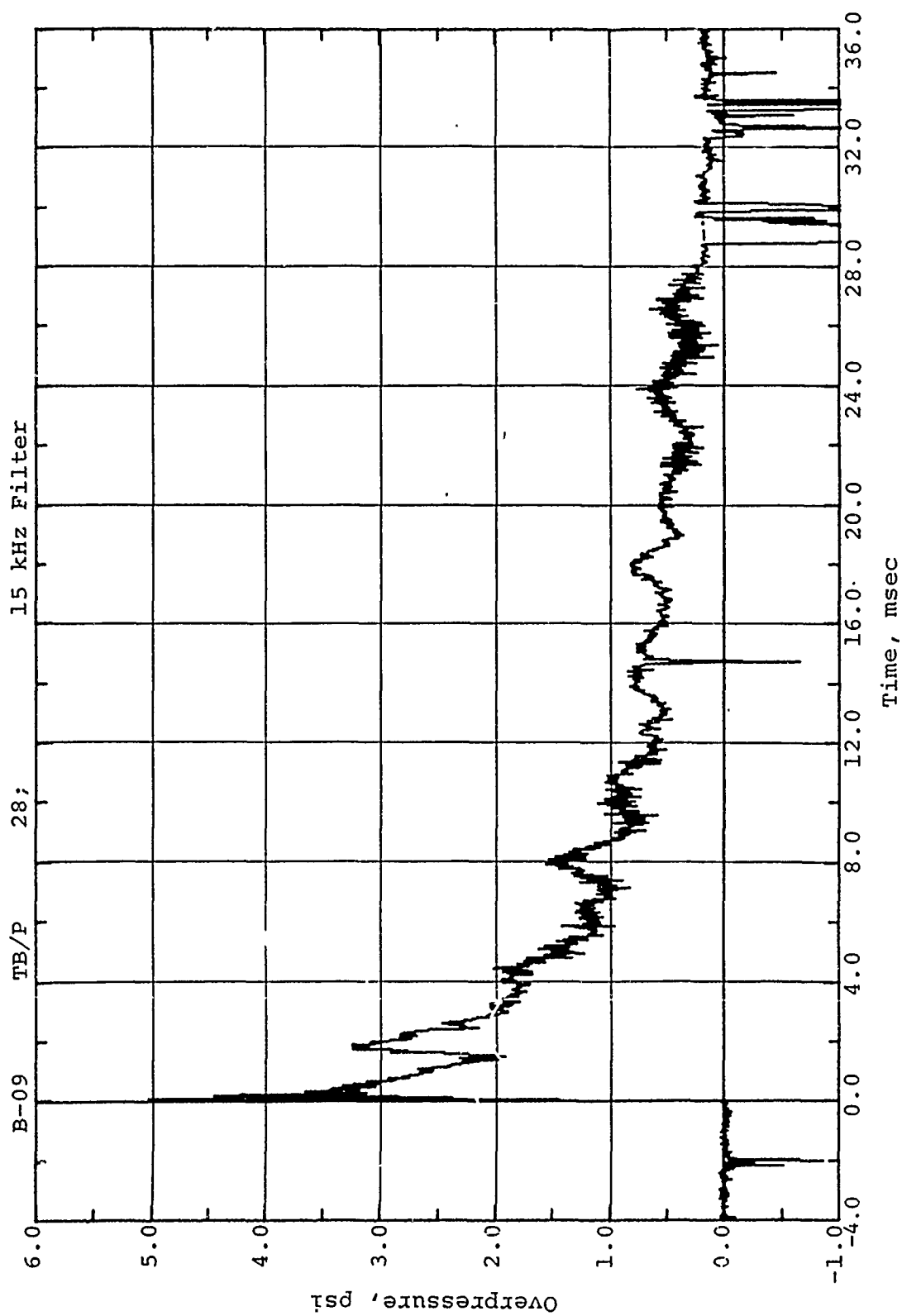


Figure A.30 Time-Variation of Overpressure Differential at Center of Panel.  
Tail Boom Station 28. Unfiltered

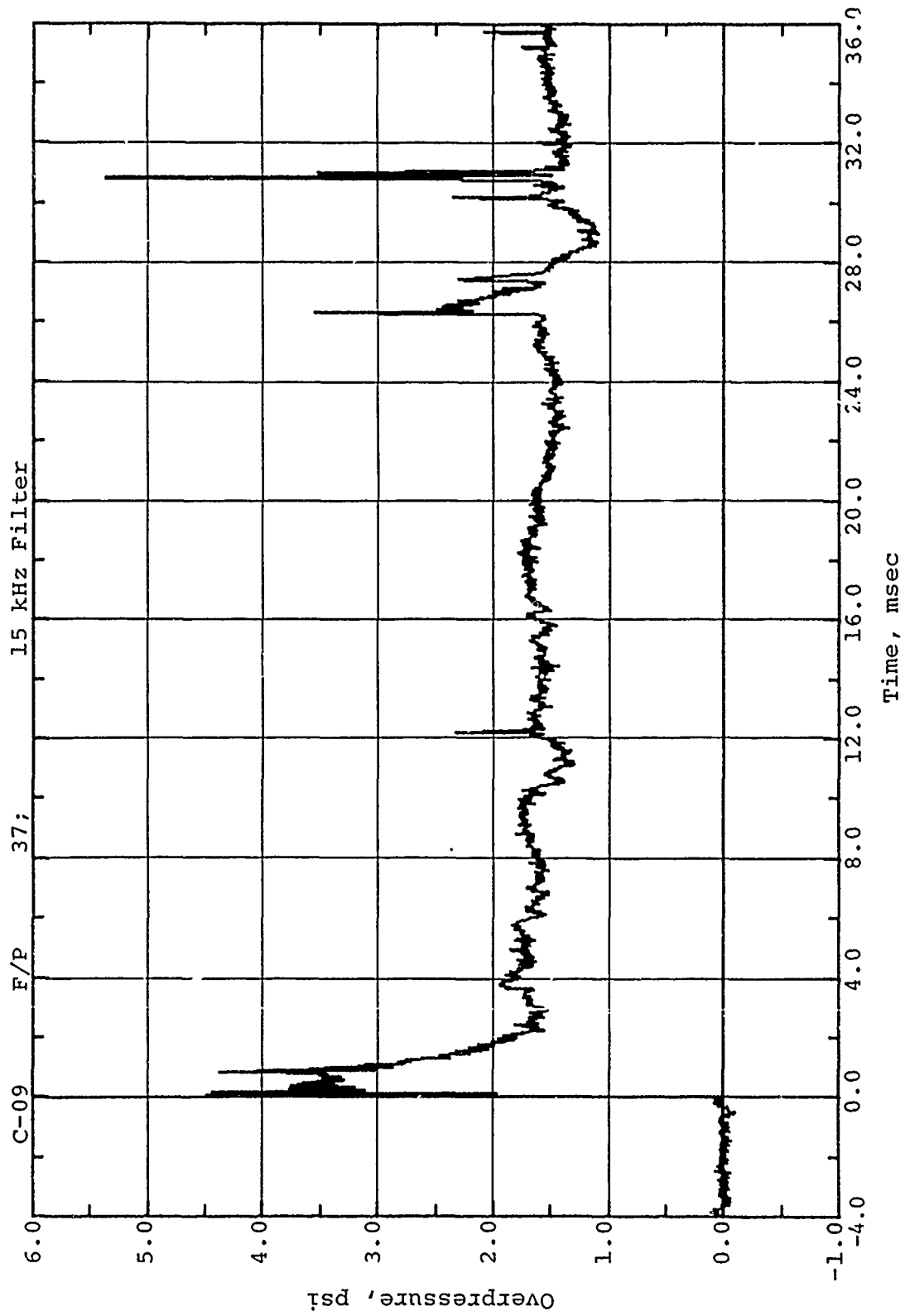


Figure A.31 Time-Variation of Overpressure at Fin Station 37.  
Unfiltered

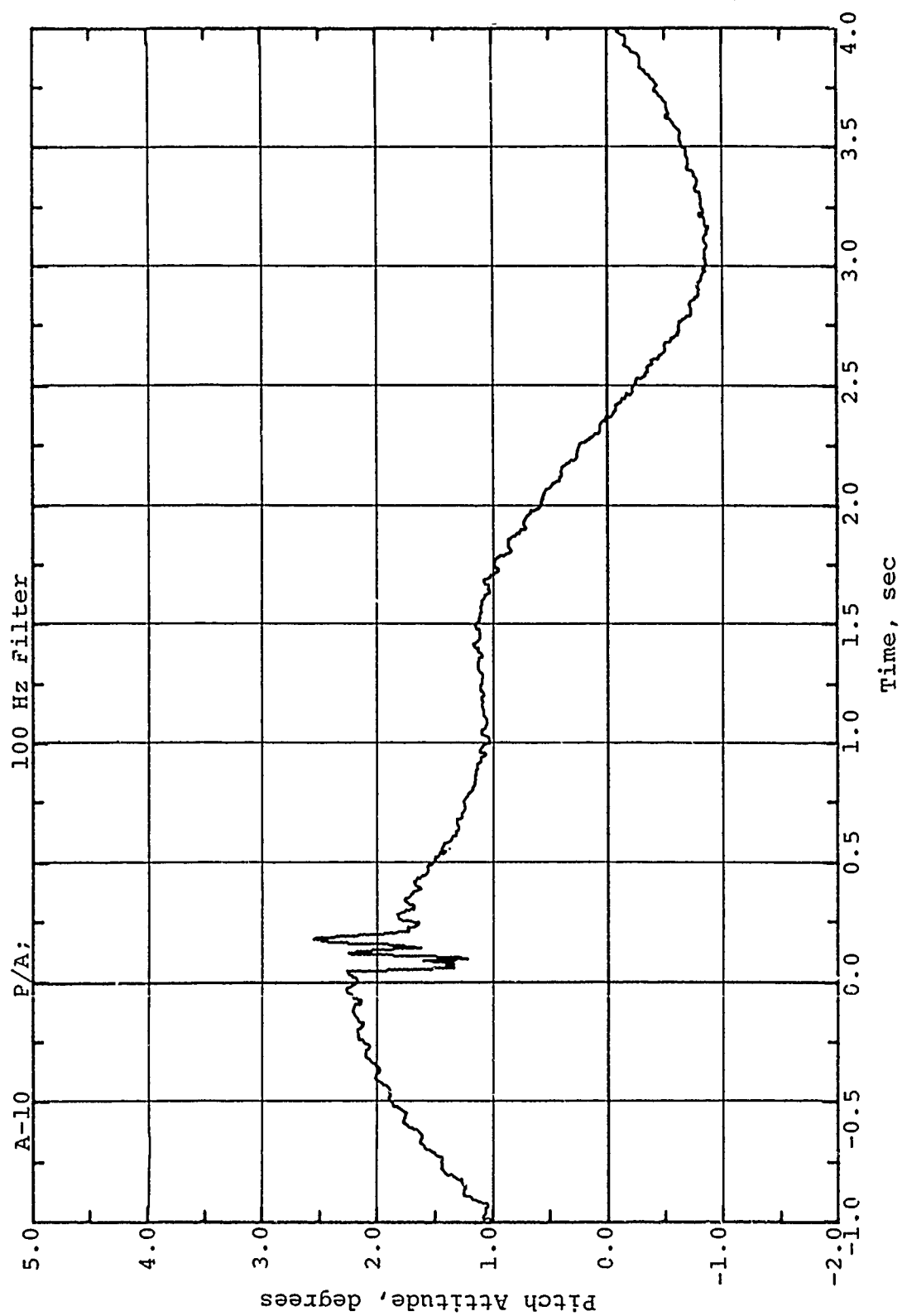


Figure A.32 Time-Variation of Pitch Attitude.  
Channel A-10

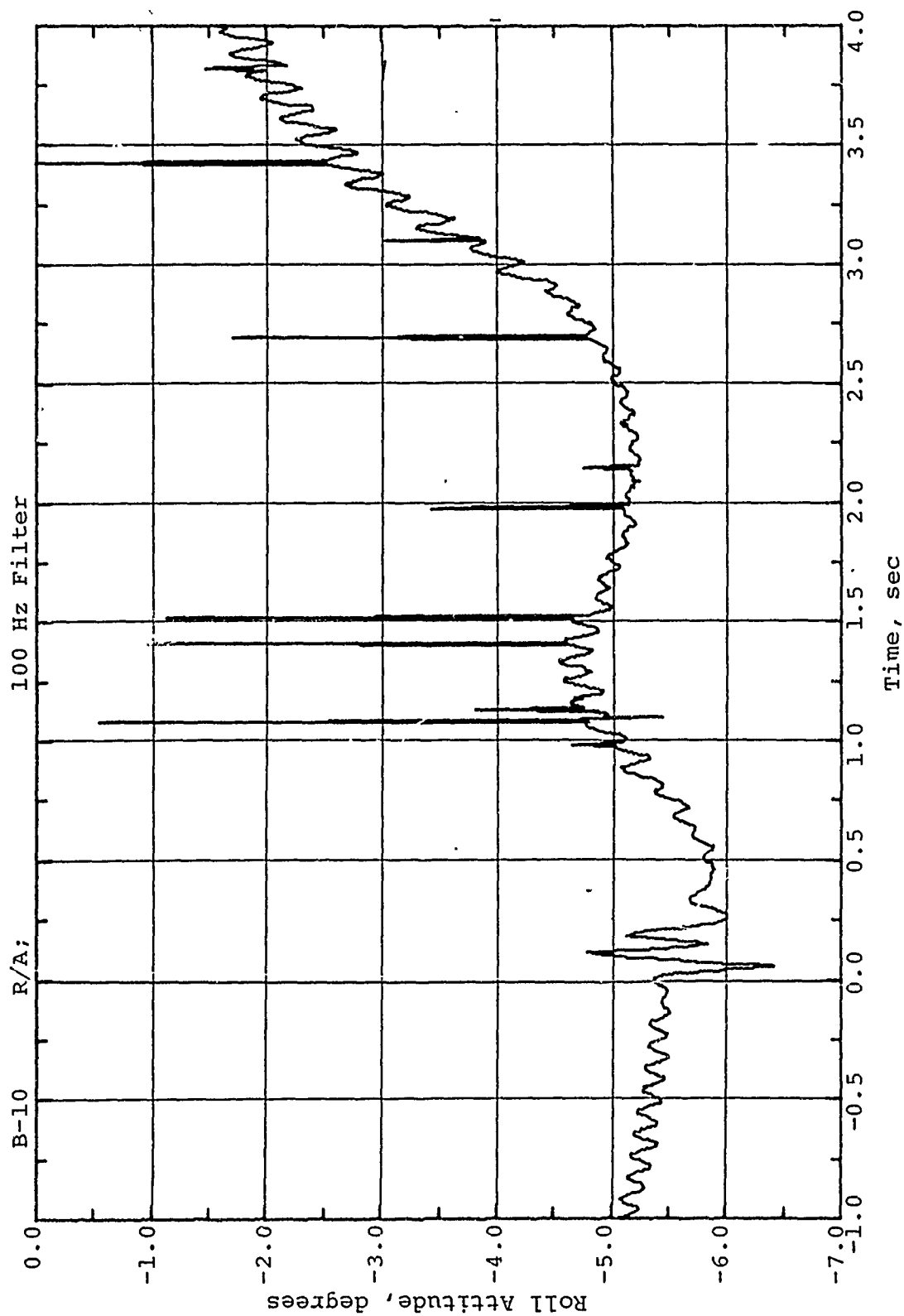


Figure A.33 Time-Variation of Roll Attitude.  
Channel B-10

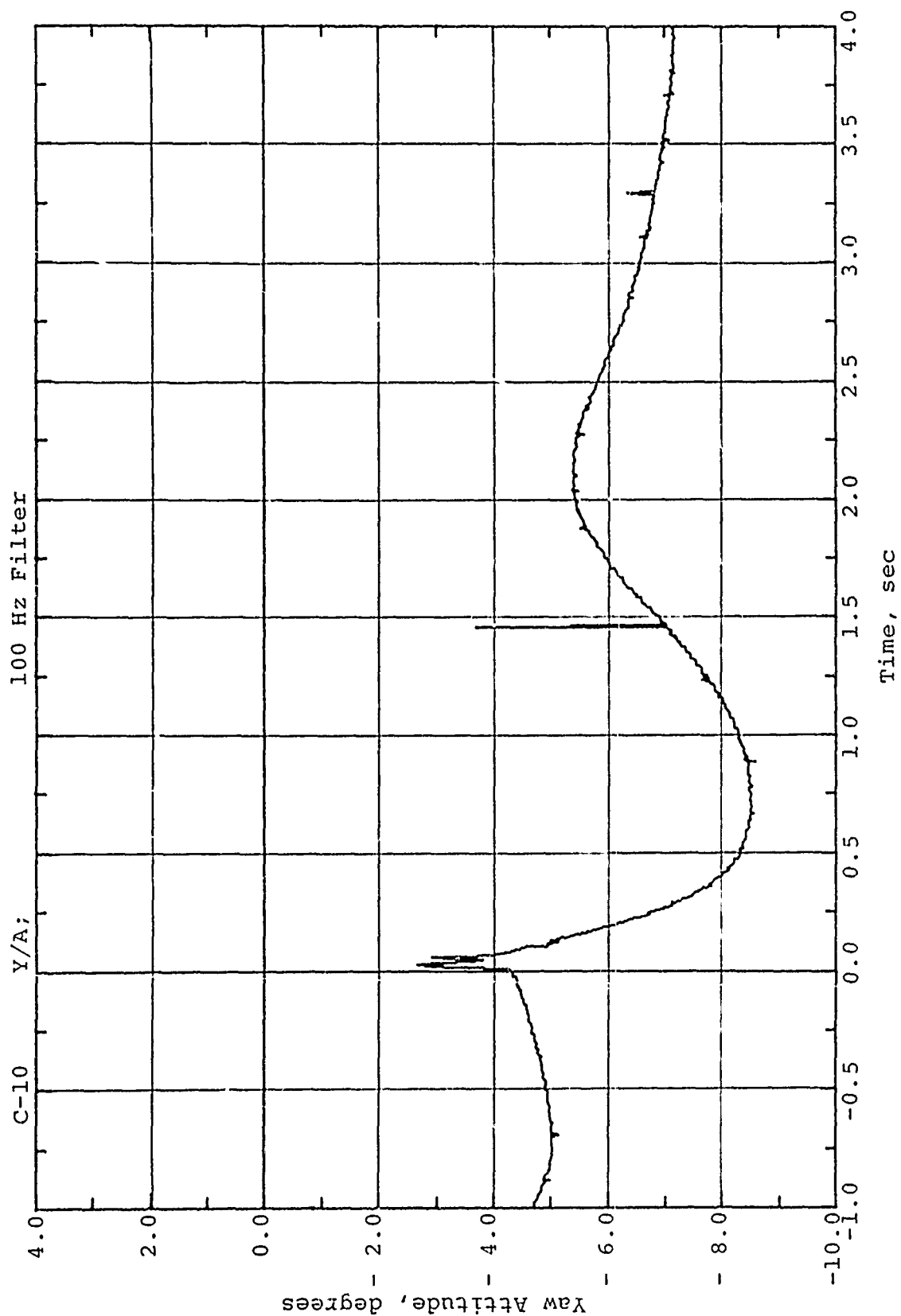


Figure A.34 Time-Variation of Yaw Attitude. Channel C-10

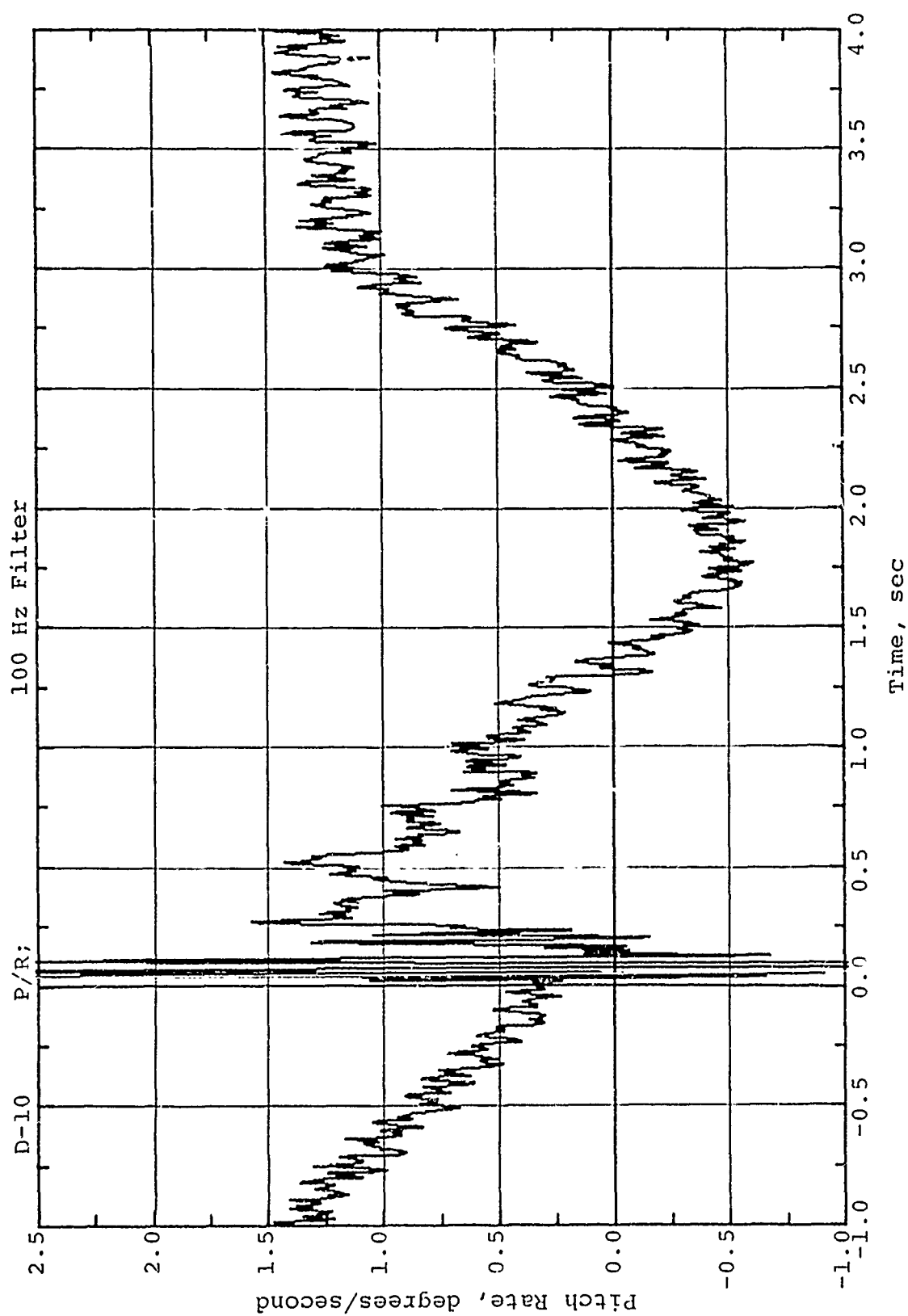


Figure A.35 Time-Variation of Pitch Rate.  
Channel D-10

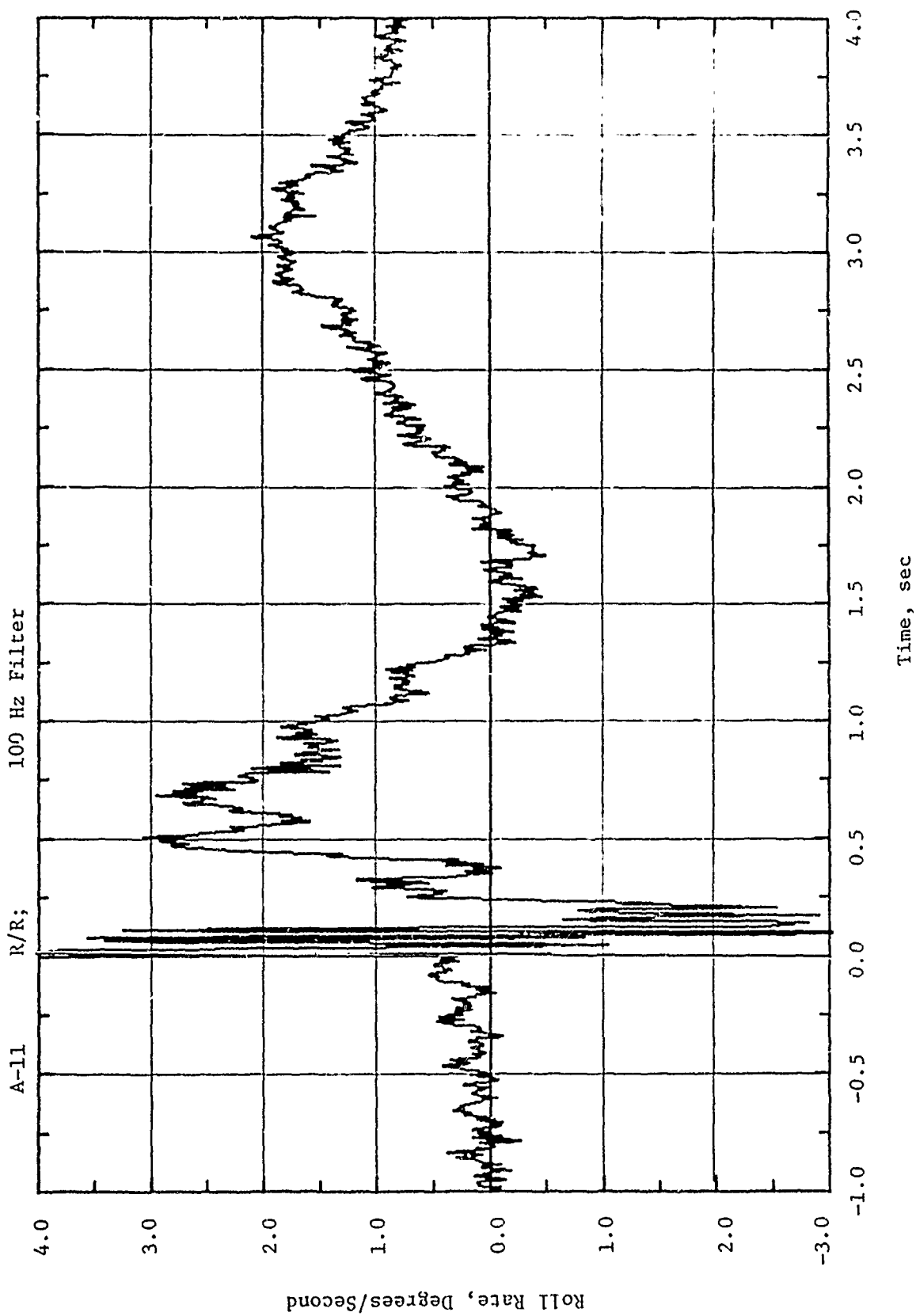


Figure A.56 Time-Variation of Roll Rate.  
Channel A-11



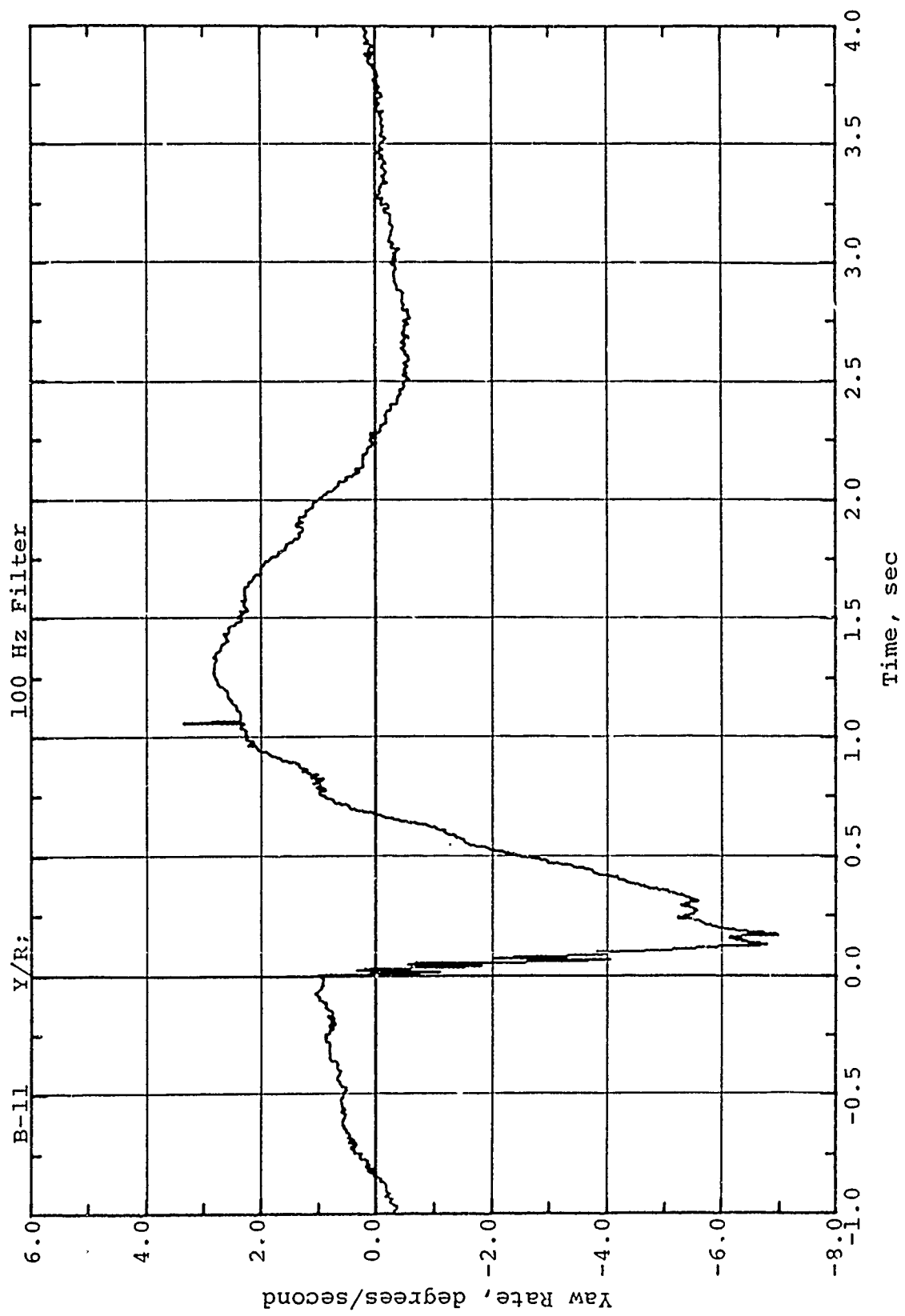


Figure A.37 Time-Variation of Yaw Rate. Channel B-11

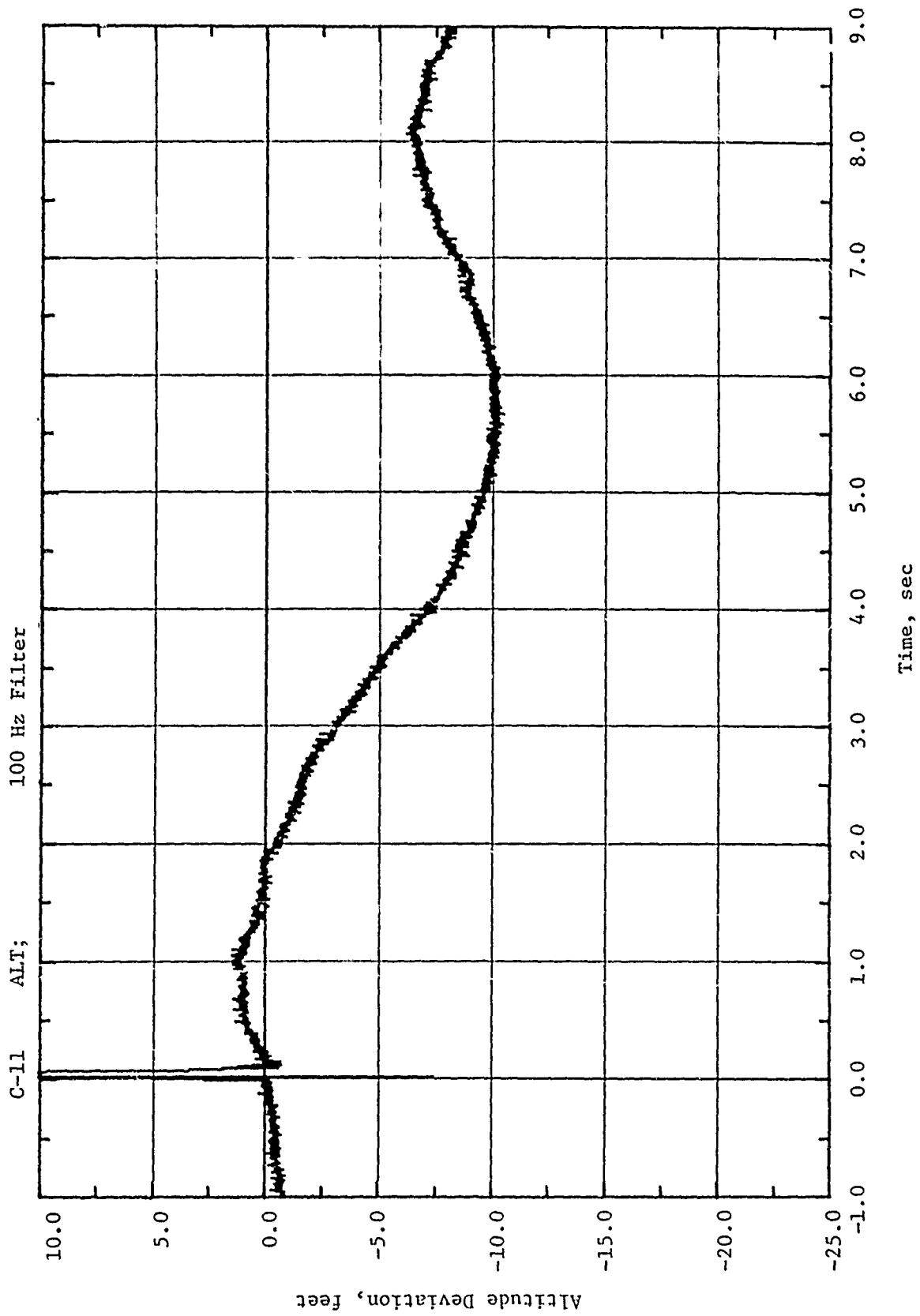


Figure A.38 Time-Variation of Altitude Deviation. Channel C-11

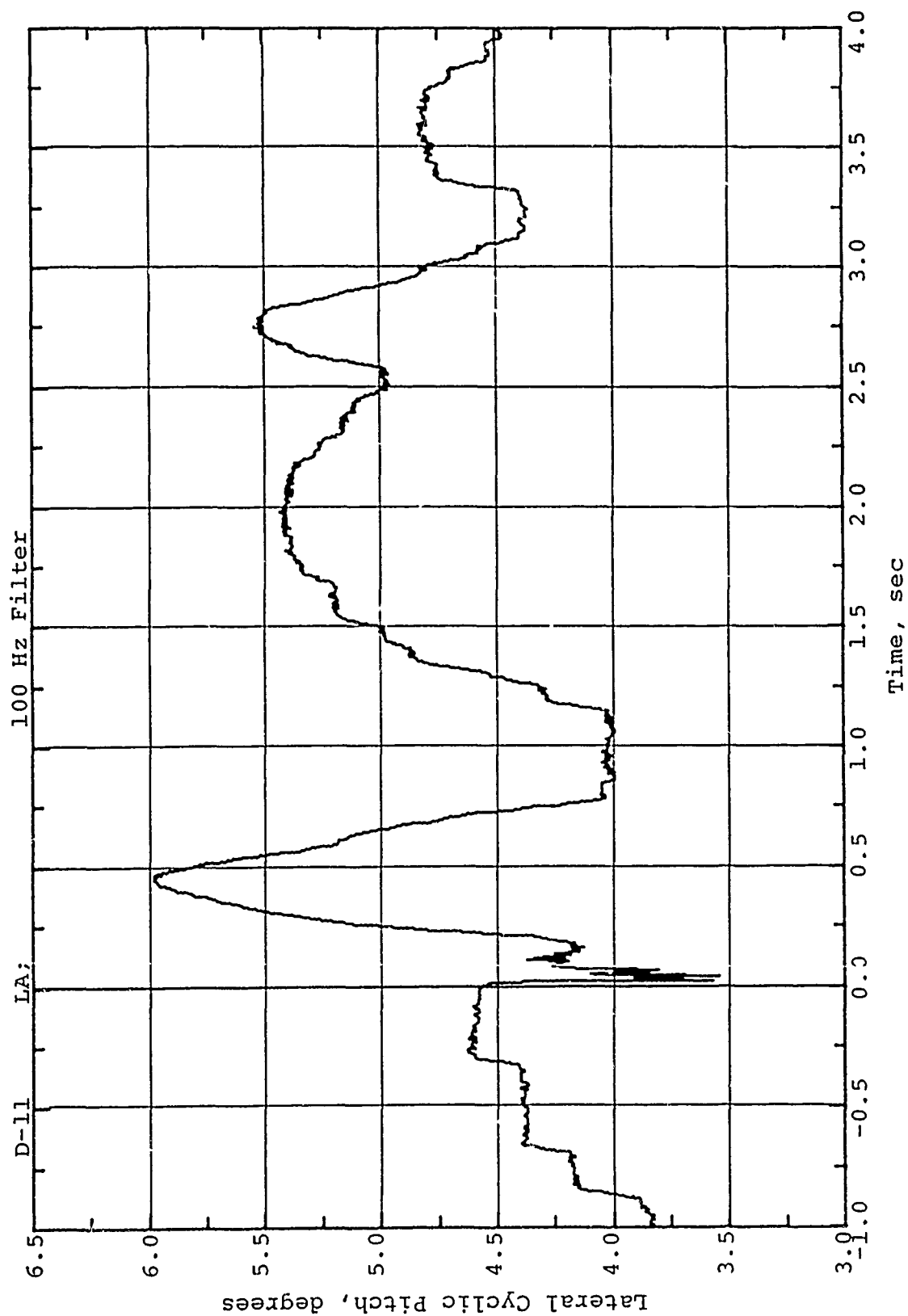


Figure A.39 Time-Variation of Aircraft Lateral Stick Deflection Interpreted as Time-Variation of Main Rotor Lateral Cyclic Pitch Angle. Channel D-11

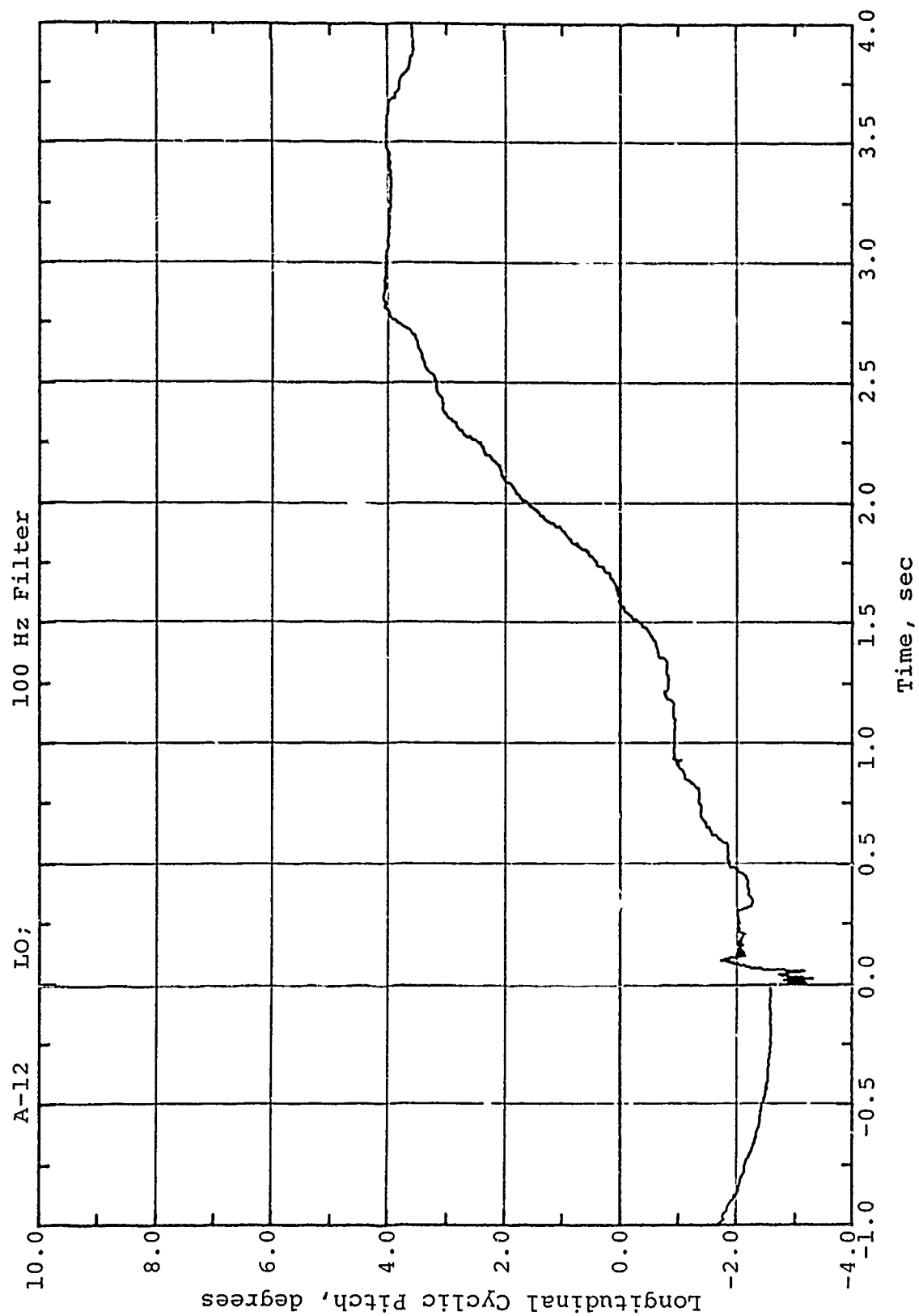


Figure A.40 Time-Variation of Aircraft Fore-and-Aft Stick Deflection  
Interpreted as Time-Variation of Main Rotor Longitudinal  
Cyclic Pitch Angle. Channel A-12

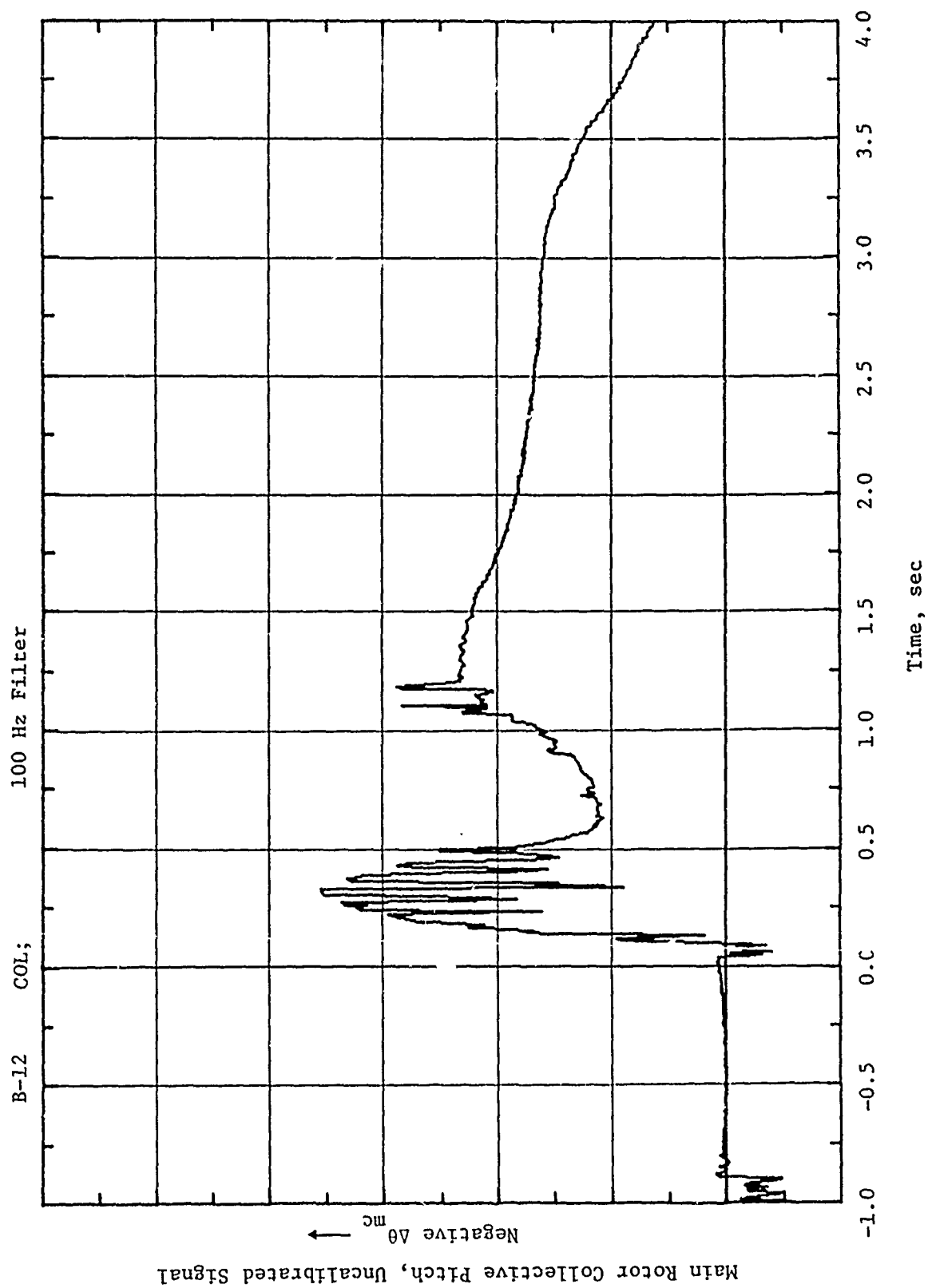


Figure A.41 Time-Variation of Aircraft Collective Stick Deflection Interpreted as Time-Variation of Main Rotor Collective Pitch Angle. Channel B-12. (Valid Calibration Data Not Available.)

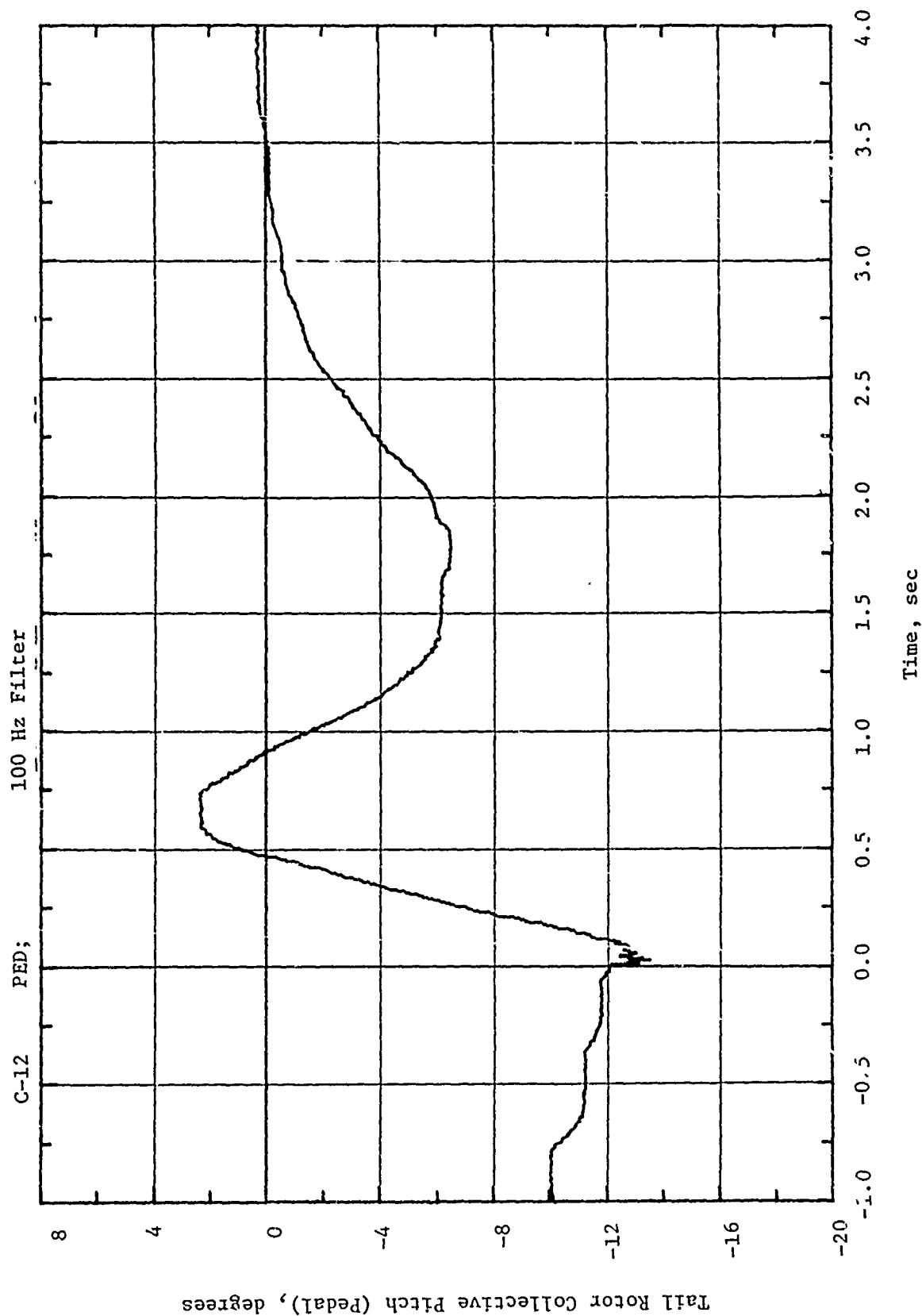


Figure A.42 Time-Variation of Aircraft Pedal Deflection Interpreted  
As Time-Variation of Tail Rotor Collective Pitch Angle.  
Channel C-12

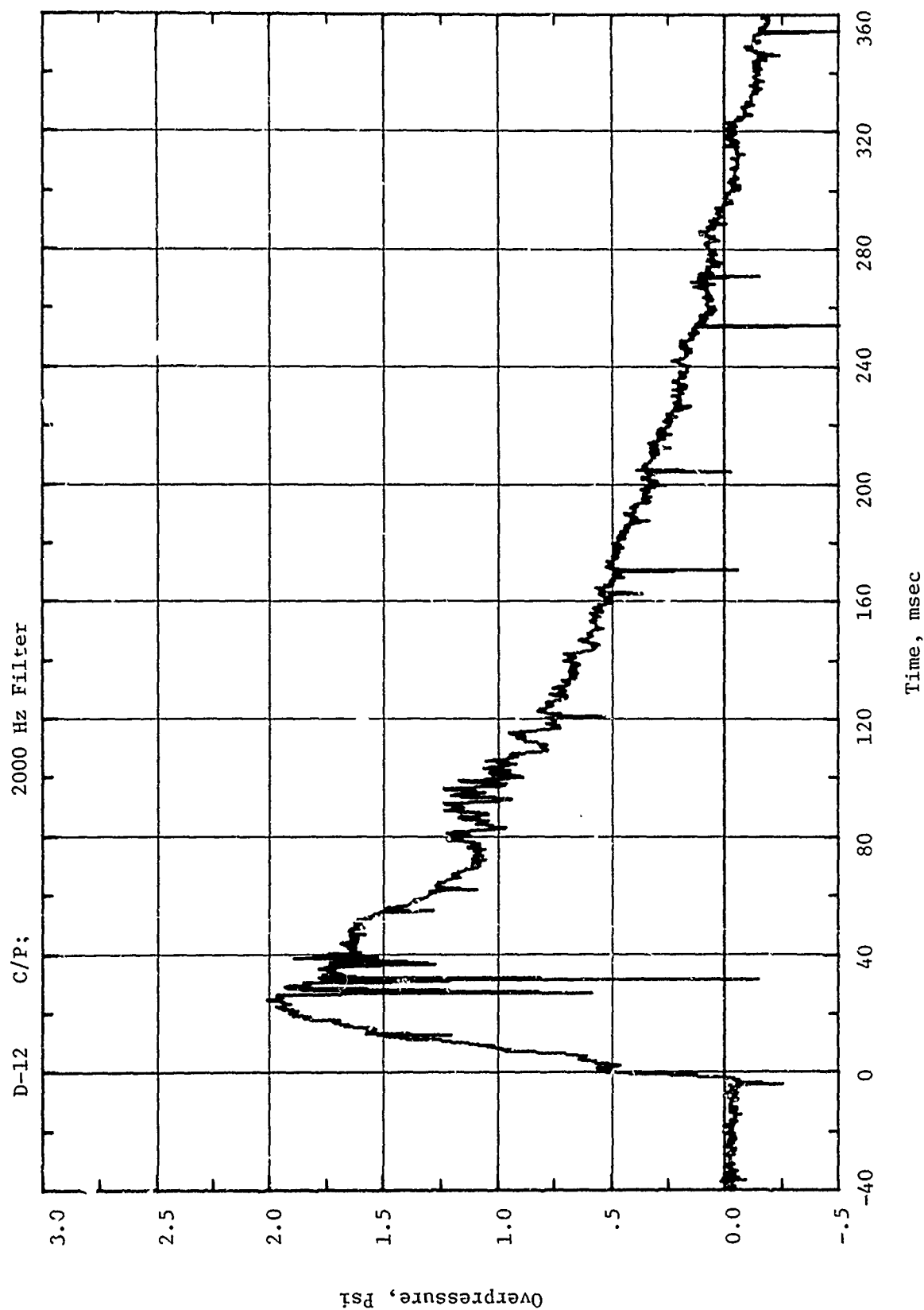


Figure A.43 Time-Variation of Overpressure at Camera Stand in Cabin.  
Long Duration Trace.

**10. EVENT DICE THROW MOBILITY EXPERIMENTS**

by

**C.E. Green**

**U.S. Army Engineer Waterways Experiment Station**



## ABSTRACT

Event DICE THROW, a 2.5-TJ (600-ton) charge of ammonium nitrate-fuel oil (ANFO), was detonated on 6 October 1976 at the Giant Patriot Site on the White Sands Missile Range in New Mexico. The soil is predominantly loose silty sand with random lenses of hard silty clay. Mobility experiments were conducted to determine the degree to which the crater and its associated ejecta field constituted a physical barrier to the movement of military vehicles. Four terrain units in the crater and ejecta area were delineated as significant to ground mobility and described in terms of soil strength, soil moisture content, surface configuration, ejecta depth, and areal extent. The test vehicles, i.e. an M60A1 tank, an M551 Sheridan tank, an M577A1 command post carrier, an M109 self-propelled howitzer, an M35A2C 2-1/2-ton cargo truck, and an M715 1-1/4-ton cargo truck, could operate with ease in all the terrain units except the crater wall. The crater wall was too steep for the vehicles to make a safe entry into the crater; therefore, a D7F bulldozer was used for 10 minutes to make an entrance lane into the crater. By entering the crater by way of the entrance lane the M577A1 and the M109 were able to exit the crater by way of the crater wall. The M60A1 was not tested on the crater wall due to the mechanical condition of its track system. No engineering effort (bulldozing) was done to ensure passage of all the test vehicles across the crater due to the short time the test vehicles were available and the unavailability of a bulldozer operator. The total time required by a D7F bulldozer to make the crater passable for all the test vehicles, except the M109 and M577A1, was estimated to be 20 minutes. Degradation in terms of drawbar-pull coefficient and speed increased for all the vehicles tested in each terrain unit from the original surface to ground zero (GZ). The degraded area per gigajoules (0.24 ton) of explosive was  $0.73 \text{ m}^2$  ( $7.85 \text{ ft}^2$ ), which indicates that large-scale surface explosives in this type of material (silty sand) are not an efficient means of creating barriers to military vehicles. The effective no-go width for the crater was 48 metres (160 feet). Comparison of measured values and values predicted by AMM-74X (Army Mobility Model) for four vehicle performance parameters revealed that the overall accuracy of the predictions for go-no go, drawbar pull, motion resistance, and speed was acceptable in every case.

EVENT DICE THROW  
Mobility Experiments

CHAPTER 1  
INTRODUCTION

DICE THROW was the name given to the 2.5-TJ (600-ton) charge of ammonium nitrate-fuel oil (ANFO), which was detonated on 6 October 1976 at the Giant Patriot Site on the White Sands Missile Range in New Mexico.

The possibility of creating barriers to vehicular mobility with surface or near-surface explosives such as the atomic demolition munition (ADM) has been a subject of military interest for several years. A number of questions need to be answered, the most important of which concerns the actual mobility restriction for a combat vehicle attempting to traverse a crater field. Once a sufficient number of tests have been conducted with tactical vehicles in a variety of sizes and shapes of craters formed in consolidated and unconsolidated sediments, pertinent relations will be established between craters and vehicle characteristics for estimating tactical vehicle performance and engineering effort requirements. The results will be incorporated in field manuals for use by troops in the theater of operations.

OBJECTIVE AND SCOPE

The objective of the mobility experiments was to determine the degree to which a crater formed in a layered natural unconsolidated material by a large surface explosion constitutes a physical barrier to the movement of military vehicles (tanks, armored personnel carriers, and cargo carriers).

The study was limited to: describing the craters for ground mobility purposes; conducting tests with six vehicles (M60A1 tank, M551 Sheridan tank, M577A1 command post carrier, M109 self-propelled howitzer, M35A2C 2-1/2-ton cargo truck, and M715 1-1/4-ton cargo truck) to

determine the degradation of vehicle performance as the vehicle traveled from the natural, undisturbed terrain across the crater; and comparing measured performance parameters with those predicted with the Army Mobility Model (AMM-74X) (Reference 1). Also, if the crater was impassable, the amount of engineering effort required to construct a passable route for the vehicles under consideration was to be determined.

## CHAPTER 2

### TEST PROGRAM

#### 2.1 LOCATION AND DESCRIPTION OF TEST SITE

The DICE THROW test site was the Giant Patriot Site at White Sands Missile Range (WSMR) in New Mexico. This site is located 13 miles southeast of the Stallion Range Center in the northern portion of WSMR. The site is at an elevation of 4729.46 feet above sea level in the northern portion of the Jornada del Muerto Basin. The soil is predominantly loose silty sand with random lenses of hard silty clay. The topography of the area is level and the nearest mountains are approximately 8 miles to the east.

The apparent crater formed was symmetrical and circular in shape. Generally, the cratered area was available for vehicle tests, except for the northern 1/4 section which was used for other experiments.

At the time of the mobility tests, the surface of the area beyond the ejecta was fairly smooth, with a sparse grass cover. The surface in the ejecta area was composed predominantly of loose, sandy material (silty sand) sprinkled with clods of the same material. These clods were small, scattered, and golf-ball size near the outer edge of the ejecta of the crater, increasing near the crest to baseball size.

The steepest parts of the crater slopes were smooth; the more gentle portions near the bottoms of the slopes contained clods of the same size as on the outer edge.

#### 2.2 VEHICLES TESTED

Six vehicles were furnished by Fort Bliss, Texas, for use in the program. An M60A1 tank (Figure 2.1), an M551 Sheridan tank (Figure 2.2), an M577A1 command post carrier (Figure 2.3), an M109 self-propelled howitzer (Figure 2.4), an M35A2C 2-1/2-ton cargo truck (Figure 2.5), and an M715 1/4-ton cargo truck (Figure 2.6) were used as test vehicles.

The weight of each of the test vehicles is shown in the following tabulation.

<u>Vehicle</u>	<u>Vehicle Weight, kg (lbs)</u>
M60A1	45,359 (100,000)
M551	16,329 ( 36,000)
M577A1	9,979 ( 22,000)
M109	20,412 ( 45,000)
M35A2C	6,350 ( 14,000)
M715	2,721 ( 6,000)

### 2.3 TESTS CONDUCTED

Self-propelled and speed tests were conducted with the six test vehicles. Also drawbar-pull (DBP) and motion resistance (MR) tests were conducted with the M577A1, the M35A2C, and the M715. The areas in which specific types of tests were conducted are shown in Figure 2.7 and discussed in subsequent paragraphs. The procedures used in these tests are discussed in the following paragraphs.

2.3.1 Self-Propelled Tests. The vehicles were positioned near the outer edge of the ejecta and driven at a slow speed in a straight line toward the center of the crater to determine the terrain units that they could negotiate. Prior to the start of a test, the appropriate terrain data were measured (see section 2.4) along the intended paths of the vehicles. The terrain and vehicle data were examined to identify the terrain units (see section 3.1) in which the vehicle(s) would definitely not go or would experience a marginal go. If an obvious no-go condition was indicated because of terrain conditions or for safety reasons, i.e. traveling down steep slopes, a bulldozer was used to do the minimum amount of work required to make the particular terrain unit passable. The time spent bulldozing was recorded as the time required to make the craters negotiable for the test vehicles. If a marginal go or definite go condition was indicated, a test was conducted. If it was estimated that a vehicle could negotiate all crater terrain units, the course was laid out such that the vehicle had to negotiate the steepest wall available while exiting the crater.

2.3.2 Drawbar-Pull Tests. Vehicle tests were conducted to determine the maximum DBP each vehicle could achieve in each terrain unit large enough to conduct such tests. These data were compared with DBP data obtained on the original surface, i.e. the area beyond the ejecta, to determine the amount of performance degradation caused by the ejecta on the surface. DBP and slip were measured in each of the terrain units where area was available and go conditions were established. DBP was measured by a load cell attached to a 21-metre- (70-ft) long cable extending from the rear of the test vehicle to the front of the load vehicle. Slip was computed from measured distance traveled by the vehicle and by the traction elements. The test vehicle pulled the load vehicle at a steady speed of approximately 3.2 km (2 miles) per hr and the load vehicle driver increased the load in several stages (by applying brakes gradually) from no load-no slip to high load-high slip or stall out. A continuous record of DBP and of the distances the test vehicle and the wheel or track traveled was obtained. As the record was being made, it was observed by the test engineer for any irregularities. Measurements were made in this manner until sufficient data had been obtained to plot a DBP-slip curve.

Following the above procedures, DBP and slip were measured with the M577A1, the M715, and the M35A2C on short segments of nearly level terrain in Terrain Units 1 and 2 (paragraphs 3.1.1 and 3.1.2) of the crater. No DBP tests were conducted in Terrain Units 3, 4, and 5 due to a lack of area in Terrain Units 3 and 5 and due to a no-go condition in Terrain Unit 4.

2.3.3 Motion Resistance (MR) Tests. Towed MR tests were conducted using the same instrumentation as was used in the DBP tests. With the test vehicle's transmission disengaged, the force required to tow the vehicle at a speed of approximately 3.2 km (2 miles) per hr was measured and recorded. These tests were conducted adjacent to the DBP tests.

2.3.4 Speed Tests. Straight-line test courses 76 and 91 metres (250 to 300 ft) in length were laid out in Terrain Units 1 and 2 of the crater. A vehicle was positioned at the beginning of the test course

and allowed to accelerate until a maximum speed was achieved. The time required for the vehicle to traverse the last 30.5 metres (100 ft) of the test course was recorded, and the maximum average speed was calculated from distance traveled and time elapsed.

#### 2.4 TERRAIN DATA OBTAINED

Terrain data were taken to describe the crater for mobility purposes and to relate vehicle performance to specific terrain attributes. Data for description purposes were taken along a line drawn through the center of the crater. A schematic of the terrain units of the crater is shown in plan view along with a profile sketch in Figure 2.8. Surface composition (type of material, strength, moisture content, and density) and surface geometry data were measured for each terrain unit. The same terrain data were measured in each of the areas selected for vehicle tests. The locations of areas in which data were measured are shown in Figure 2.7.

2.4.1 Surface Geometry. Elevation profiles were measured along and perpendicular to crater radii by standard surveying techniques to characterize the craters. Microprofiles were taken roughly parallel to the crater walls in Terrain Units 2 and 3 and along various test courses. The approximate locations of these profiles are given in Figure 2.7.

A U. S. Army Engineer Waterways Experiment Station (WES) cone penetrometer was used to obtain an index of the shearing resistance of the soil from the surface to the 30-inch depth or to a lesser depth if the capacity of the instrument was exceeded. Moisture content and density measurements were made, and bulk samples were collected for laboratory identification of soil type.

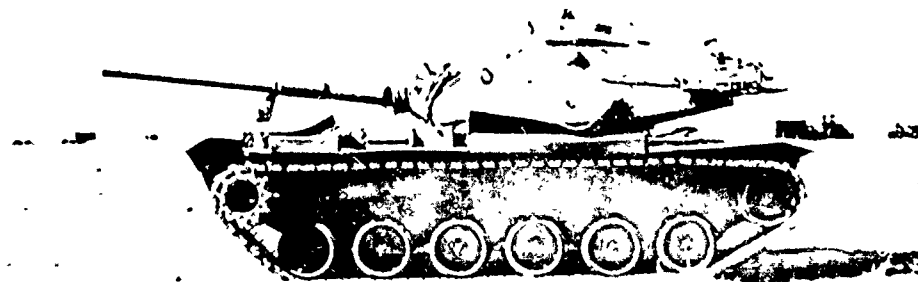


Figure 2.1 M60A1 tank



Figure 2.2 M551 Sheridan tank

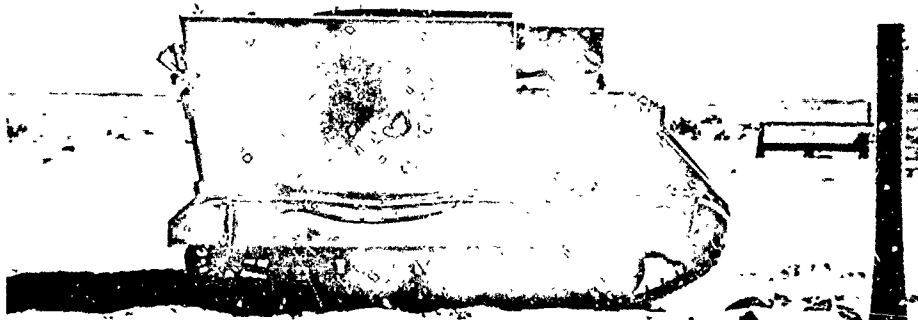


Figure 2.3 M557A1 command post carrier



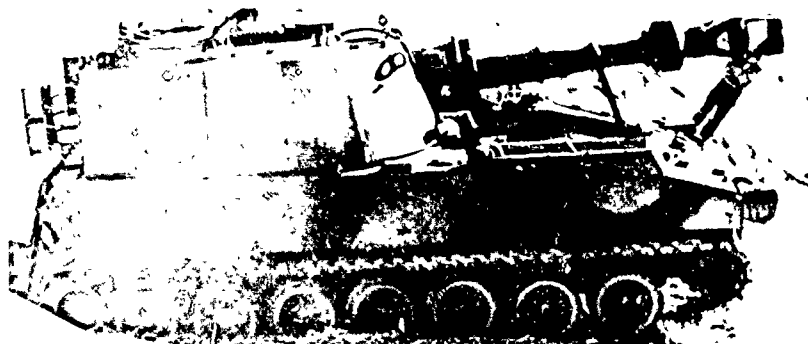


Figure 2.4 M109 self-propelled howitzer

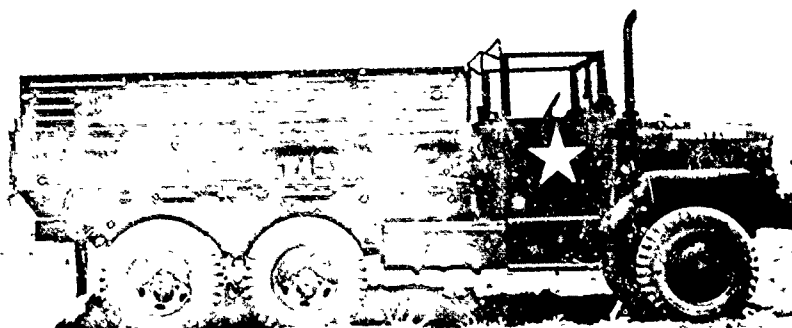


Figure 2.5 M35A2C, 2-1/2-ton cargo truck

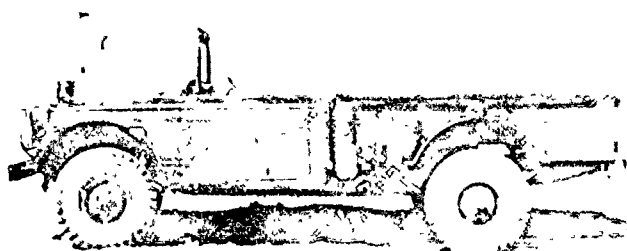
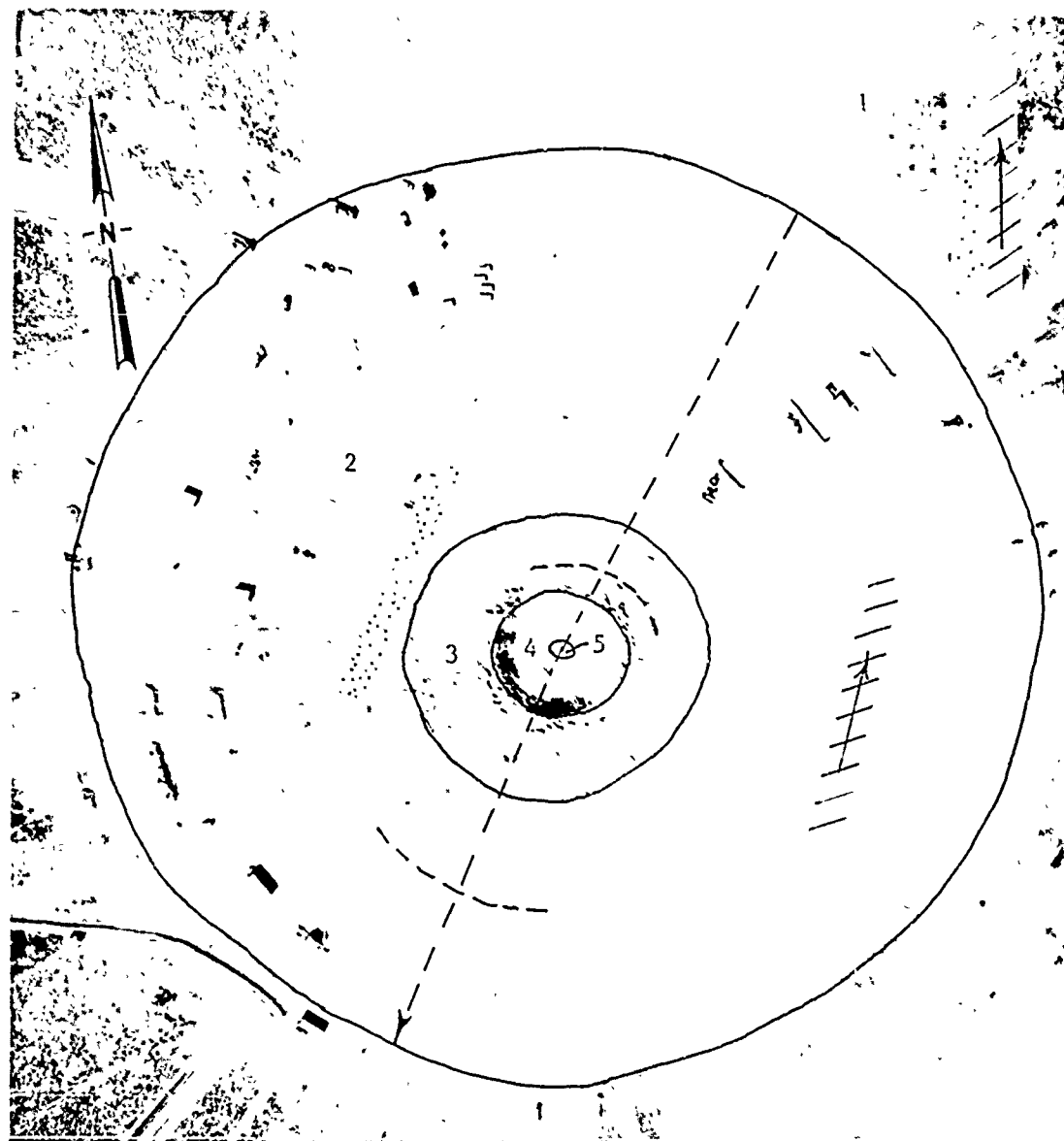


Figure 2.6 M715, 1-1/4-ton cargo truck



#### LEGEND

No.	Terrain Unit Description
1	Original Surface
2	Outer Lip
3	Inner Lip
4	Crater Wall
5	Crater Floor

Straight dashed line indicates approximate locations of elevation profiles and self-propelled (SP) vehicle tests. Arrow indicates direction of SP tests. Curved dashed lines indicate locations of microprofiles.

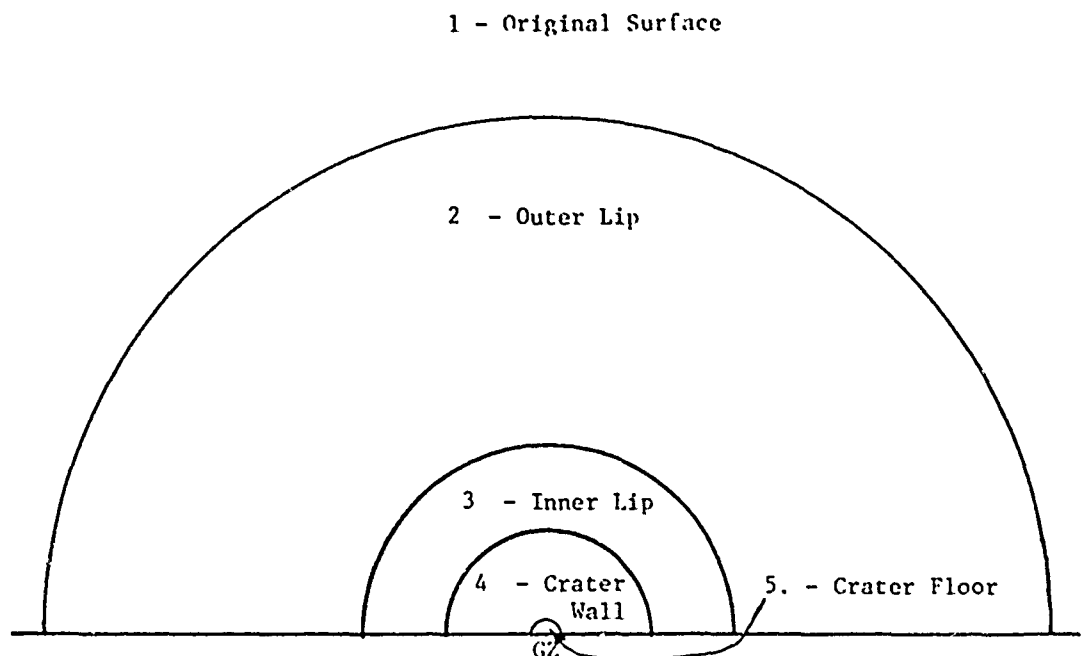


- DBP and MR test areas



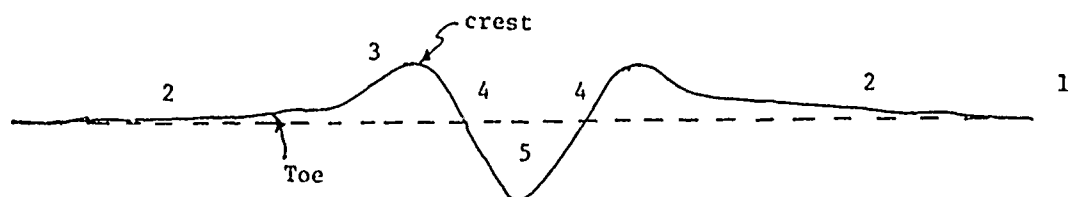
- Speed test areas

Figure 2.7 Aerial Photograph of DICE THROW Crater with the Five Terrain Units Identified



Average Distance from GZ to Outer Edge of Terrain Unit					Average Distance from GZ to Outer Edge of Terrain Unit				
2		3	4	5	5	4	3		2
m		m	m	m	m	m	m		m
(ft)		(ft)	(ft)	(ft)	(ft)	(ft)	(ft)		(ft)
122		48	24	3	3	24	48		122
(400)		(155)	(80)	(10)	(10)	(80)	(155)		(400)

a. Plan View



b. Profile Sketch

Figure 2.8. Schematic of Terrain Units for DICE THROW Crater

## CHAPTER 3

### TEST RESULTS AND ANALYSES

The results of this investigation are discussed in four sections: Description of the Crater for Mobility Purposes, Performance Degradation, Prediction of Vehicle Performance, and Comparison of Measured and Predicted Performance.

#### 3.1 DESCRIPTION OF THE CRATER FOR MOBILITY PURPOSES

The crater, associated ejecta, and natural terrain areas were divided into five terrain units offering various degrees of impedance to vehicle mobility as a result of difference in soil strength, slope, and surface geometry. Surface composition data taken along a line through the center of the crater and in the test areas were identified as to the terrain unit and averaged. These data are shown in Table 3.1. The surface geometry data, microprofiles, and profiles were taken in the terrain units that exhibited significant irregular surfaces. The microprofile data for Terrain Units 2 and 3 were used to determine surface roughness. The profile data shown graphically in Figure 3.1 were taken along a radius in Terrain Unit 4 (crater wall) that had the maximum slope in the area available for testing. The following sections present a brief discussion of the data shown in the tables and figures identified above.

3.1.1 Terrain Unit 1 (original surface). The area past the limit of the ejecta field of each crater was identified as the original surface (Terrain Unit 1). These areas were level, firm, and almost smooth, with a sparse cover of grass about 203 mm (8 in.) tall. Table 3.1 shows that the average soil strength was greatest in these areas and the slope was the least.

3.1.2 Terrain Unit 2 (outer lip). The area of continuous shallow ejecta extending from the natural terrain to the foot of the outer slope was identified as the outer lip (Terrain Unit 2). The distance from GZ

to the outer and inner boundaries of this area varied along different radii of the crater. In this terrain unit, the original surface was covered with ejecta ranging from individual grain particles to clods several inches in size. The average soil strength in the 0- to 152.4-mm (0- to 6-in.) layer was lower in Terrain Unit 2 than in Terrain Unit 1 as a result of a 100- to 180-mm- (4- to 7-in.-) thick layer of soft ejecta. The soil was relatively dry, and the ejecta clods disintegrated when pressure was applied. The depth of the ejecta gradually increased from the outer edge of the ejecta toward GZ, resulting in a slight average slope of 3 percent.

3.1.3 Terrain Unit 3 (inner lip). The area of continuous ejecta extending from the foot of the outer slope to the crest was identified as the inner lip (Terrain Unit 3). The distances from GZ to the outer and inner boundaries of this area varied along different radii of the crater. The ejecta depth averaged more than 610 mm (24 in.) in this terrain unit, resulting in a lower average soil strength than in Terrain Units 1 and 2, as can be seen in Table 3.1. The surface of the inner lip was relatively rough because of undulating ejecta or the presence of clods.

3.1.4 Terrain Unit 4 (crater wall). The sloping sides of the craters extending from the lip crest to the toe of the slope at the edge of the crater floor were identified as the crater wall (Terrain Unit 4). The distances from GZ to the outer and inner boundaries of this area varied along different radii of the crater. The loose, dry material on the slopes was greater than 610 mm (24 in.) deep, and the average soil strength was similar to that in Terrain Unit 3. The overall slope of the crater walls varied in magnitude at the upper and lower ends and along different crater radii. The minimum and maximum slope was 50 and 56 percent, respectively. An elevation profile of the crater wall of maximum slope of the crater is given in Figure 3.1.

3.1.5 Terrain Unit 5 (crater floor). The area extending from the toe of the slope of the crater wall to GZ was identified as the crater floor (Terrain Unit 5). The outer boundaries of this area varied along

different radii of the crater. The average soil strength was higher in this terrain than any other terrain unit except Terrain Unit 1 (Table 3.1).

### 3.2 PERFORMANCE DEGRADATION

3.2.1 Measured Performance Data. Four first-pass vehicle performance parameters commonly measured, shown in Table 3.2, are go-no go, DBP, MR, and speed. Of these performance parameters, only DBP and speed were considered in the analysis of degradation of vehicle performance of the various terrain units; however, all vehicle performance parameters measured in the crater and ejecta areas are given in Table 3.2. Results of the self-propelled (go-no go) tests and DBP tests are discussed in the following paragraphs.

1. Self-propelled tests. All the test vehicles could operate with ease in Terrain Units 1, 2, 3, and 5; however, none of the vehicles could make a safe entry into the crater because of the steep slopes (50 percent). A D7F bulldozer was used for 10 minutes to do the minimum amount of work required for the vehicles to make a safe entry into the crater. The slope of the crater wall after bulldozing was 30 percent. The vehicles then entered the crater, crossed the crater floor, and attempted to exit by way of the crater wall. A summary of these test results are shown in the following tabulation:

<u>Vehicle</u>	<u>Performance</u>	<u>No. of Attempts</u>
M60A1 tank	not tested	0
M551	no go	5
M577A1	go <sup>a</sup>	3
M109	go	3
M35A2C	no go	6
M715	no go	6

<sup>a</sup> Go after entrance lane was constructed.

The M60A1 tank was not tested in Terrain Units 4 or 5 due to the mechanical condition of its track system. Several attempts were made before two of the vehicles (M577A1 and M109) could negotiate Terrain

Unit 4. On the fifth attempt to exit the crater the M551 threw a track. All the vehicles tested were able to climb onto the crater wall (Terrain Unit 4); however, only the M577A1 and the M109 were able to negotiate the wall. The other vehicles were turned around on the crater floor and driven out the crater by way of the entrance lane. No additional engineering effort (bulldozing) was done to insure passage of all the test vehicles across the crater due to the short time the test vehicles were available and the unavailability of a bulldozer operator. The test engineer estimated that it would take approximately the same amount of time (10 min.) to make an exit lane as it did the entrance lane. The total time required by a D7F bulldozer to make the crater passable for all the test vehicles except the M109 and M577A1 was estimated to be 20 min.

2. Drawbar-pull tests. DBP, in terms of DBP coefficient (DBP/W, where W is the vehicle weight), was plotted versus wheel or track slip for each test and curves of best visual fit were drawn through the data points (Figure 3.2).

DBP/W is a performance parameter often used in evaluating the traction capabilities of vehicles. The maximum DBP/W occurs, on occasions, at or near 100 percent slip in these tests. At 100 percent slip, maximum DBP/W is not a meaningful parameter because no useful work can be done when a vehicle is not moving forward. A more meaningful performance parameter is the optimum DBP/W value, which is the value of DBP/W when the vehicle's work output coefficient (WOC) is at a maximum (Reference 2). WOC is an arbitrary index of efficiency defined as the ratio of work output to work input, where work output is DBP times the distance the vehicle travels (S) in the time interval (t), and work input is the weight of the vehicle (W) times the distance the wheel or tracks travel (L) in the same time interval (t), or

$$WOC = \frac{DBP \left( \frac{S}{t} \right)}{W \left( \frac{L}{t} \right)} \quad (1)$$

Since

$$\text{Slip} = 1 - \frac{S/t}{L/t}$$

or

$$\frac{S/t}{L/t} = 1 - \text{slip}$$

then

$$\text{WOC} = \frac{\text{DBP}}{W} (1 - \text{slip})$$

An example of the determination of optimum DBP/W at maximum WOC for each test vehicle in Terrain Unit 1 of the crater is shown in Figure 3.3. Figure 3.3 shows that the optimum slip was 20 percent for the M715 and 18 percent for the M35A2C and the M577A1; the optimum DBP coefficients for the three vehicles in Terrain Unit 1 of the crater were 0.52, 0.43, and 0.59, respectively. Past studies at WES have shown that optimum DBP generally occurs at or near 20 percent slip, as was found in the tests in this program.

3.2.2 Degradation of Vehicle Performance. The effectiveness of the craters as barriers to mobility is shown as the degradation of speed and DBP. Degradation is expressed in percent and is obtained from the following expression:

$$\text{Percent degradation} = \left(1 - \frac{T}{N}\right) \times 100 \quad (2)$$

where

T = performance in a terrain unit

N = performance in natural terrain unit

Degradation in performance in each of the terrain units tested is shown in Table 3.3.

As previously mentioned, the six test vehicles could operate with ease in Terrain Units 2, 3, and 5 of the crater but at some degradation (cost) in performance. None of the test vehicles could enter the crater without engineering effort because of the steep slopes (50 percent) on the crater walls (Terrain Unit 4). Although the vehicles could operate with ease on Terrain Units 3 and 5, DBP and speed tests were not



conducted because the areas were too small. DBP tests were not conducted with the M60A1, the M551, and the M109 due to the short time the vehicles were available for testing or to the mechanical conditions of their track system.

The degradation in speed for the track vehicles (M60A1, M551, M577A1, and M109) varied from 16 percent for the M109 to 37 percent for the M577A1. The degradation in optimum DBP coefficient in Terrain Unit 2 for the M577A1 was 8 percent. The degradation in speed of the wheeled vehicles (the M35A2C and the M715) was somewhat higher than the degradation in optimum DBP coefficient. It may be noted that the degradation in optimum DBP coefficient of the M577A1 was about half that of the M35A2C and the M715. This is a result of the configuration of the traction elements (wheels versus tracks) of the vehicles and the surface of the terrain units. Even though the clods in the ejecta generally deformed under traffic, the front wheels of the wheeled vehicles had to climb a slope at each clod, whereas the track of the M577A1 spanned several clods.

3.2.3 Areal Effectiveness. Using the dimensions given in Figure 2.8, the areas occupied by Terrain Units 2 through 5, inclusive, are shown in the following tabulation along with the speed degradation in percent.

No.	Terrain Unit Description	Area m <sup>2</sup> (ft <sup>2</sup> )	Speed Degradation, pct					
			M60A1	M551	M577A1	M109	M35A2C	M715
2	Outer Lip	39,686 (426,962)	14	19	37	10	16	19
3	Inner Lip	5,144 ( 55,342)	NM*	NM	NM	NM	NM	NM
4	Crater Wall	1,839 ( 19,782)	100	100	100	100	100	100
5	Crater Floor	29 ( 314)	NM	NM	NM	NM	NM	NM
	Total	46,698 (502,400)						

\* NM = not measured.

The areal extent of 100 percent degradation, i.e. complete barrier to mobility, was approximately  $1,839 \text{ m}^2$  ( $19,782 \text{ ft}^2$ ) for all the test vehicles. The degraded area per gigajoules (0.24 ton) of explosive was  $0.73 \text{ m}^2$  ( $7.85 \text{ ft}^2$ ), which indicates that large-scale surface explosives in this type of material (silty sand) are not an efficient means of creating barriers to the movement of military vehicles.

In a combat situation, the major concern may be the width of the no-go area rather than the areal effectiveness, for example, how wide a pass could be blocked with a particular charge. Using the dimensions shown in Figure 2.8 the effective no-go width was approximately 48 metres (160 ft), which indicates that a similar charge in the same soil conditions would be effective in combat conditions for creating obstacles in this width range.

Although the results discussed in the previous paragraphs are, as would be expected, for craters in this type of material, it is cautioned that this single crater cannot be considered definitive of all craters formed in unconsolidated materials in which the explosive material varied in amount and depth of charge.

### 3.3 PREDICTION OF VEHICLE PERFORMANCE

Vehicle performance was predicted for the terrain units identified for ground mobility purposes in the DICE THROW crater, using AMM-74X (Reference 1). The basic premises of AMM-74X (Reference 3) are given in the following paragraphs.

The performance of a vehicle at any moment is the result of a complex interplay among many different characteristics of the vehicle, numerous features of the particular terrain in which it is operating, its immediate past operating history, and elections and constraints imposed on the driver. AMM-74X postulates that the maximum practical speed of a sound vehicle at any moment, including zero (no go), is an appropriate measure of its mobility at that time and place. Accordingly, each of the many system parameters potentially involved must be quantified in engineering terms that will permit calculation of probable

vehicle speed as limited by one or more of the number of possible specific terrain-vehicle-driver interactions. The following tabulation outlines off-road system attributes considered in AMM-74X.

Terrain	Vehicle	Driver
Surface material	Geometry	Reaction time
Type	Mechanical	Recognition distance
Strength	components	V-ride limit
	Inertial	Vertical acceleration limit
Surface geometry	components	
Slope		
Discrete obstacles		
Roughness		
Vegetation	Geometry	Reaction time
Stem size and spacing	Mechanical	Recognition distance
Visibility	components	V-ride limit
	Inertial	Vertical acceleration limit
Hydrologic geometry <sup>a</sup>	components	
Stream cross section		
Water velocity and depth		

<sup>a</sup> These terrain attributes are necessary for linear features such as streams. In this study, linear features were not considered.

The endless variability of real terrain can be represented by a mosaic of pieces, each of which, to some feasible resolution, can be considered uniform in terms of measureable factors affecting vehicle responses. Such a subclass of terrain is called a terrain unit. An areal terrain unit is currently characterized by the 13 measurements listed below:

1. Surface factors

- (1) Type
- (2) Strength in cone index or rating cone index
- (3) Slope, percent
- (4) Roughness, root mean square (rms) elevation<sup>b</sup> in inches.

<sup>b</sup> A measure of the rms of the deviations of the terrain elevations from the mean:

$$rms = \sqrt{\frac{\sum_{j=1}^N (x_j - \bar{x})^2}{N}}$$

where

N = number of elevation points

x<sub>j</sub> = terrain elevation

$\bar{x}$  = mean value of terrain elevation in a given profile

## 2. Obstacle factors

- (5) Approach angle, degrees
- (6) Height, mm (in.)
- (7) Base width, mm (in.)
- (8) Length, m (ft)
- (9) Spacing, m (ft)
- (10) Type

## 3. Vegetation factors

- (11) Stem diameter, mm (in.)
- (12) Stem spacing, m (ft)
- (13) Visibility, m (ft)

Maximum practical speeds for a vehicle in each areal unit within an area, calculated from validated engineering relations, can be combined by suitable procedures to predict the performance of the vehicle along any given path in the real terrain and/or to accumulate a statistical representation of vehicle performance in the area as a whole.

### 3.4 COMPARISON OF MEASURED AND PREDICTED PERFORMANCE

The vehicle performance parameters measured and predicted in the DICE LOW crater and ejecta areas are given in Table 3.2. Plots comparing measured and predicted DBP/W and MR/W are shown in Figure 3.4 and those comparing measuring and predicted speeds are shown in Figure 3.5.

Table 3.2 shows that the performance of the vehicles in terms of go-no go was predicted correctly in every case. Table 3.2 and Figure 3.4 show that the predicted values of DBP/W in most cases was slightly higher than the measured values. All predicted values for DBP/W and MR/W were well within the acceptable limits of prediction accuracy as the model now stands. Table 3.2 and Figure 3.5 show that the variation in measured and predicted values of speed were somewhat larger than for the other parameters. The relative deviations of the predicted values for each terrain unit are shown in Table 3.4.

The mean absolute deviation shown in Table 3.4 varied from a minimum of 0.2 kilometre (0.1 mile) per hour to a maximum of 6.1 kilometres (3.8 miles) per hour from the predicted to the measured values indicating that the average absolute deviations were relatively small from the standpoint of vehicle speed. The overall average relative deviation for all vehicles tested was 6.8 percent. Based on average relative deviation, the M60A1 presented the best prediction accuracy (1.5 percent), and the M715 presented the worst prediction accuracy (14.5 percent). This is a result of the configuration of the traction elements of the vehicles and the surface of the terrain unit. Even though the clods in the various terrain units deformed under traffic, the wheeled vehicles were confronted with individual clods, whereas the tracked vehicles spanned several clods. The average relative deviations indicated good correlation between model-predicted speeds and field-measured speeds for all the test vehicles. The relative deviations of the predicted values from the measured values increased from the original surface to GZ in every case. This was expected, since AMM-74X is set up to evaluate natural terrain such as the original surface. The average deviations in the cratered areas were well within the acceptable limits of prediction accuracy as the model now stands.

TABLE 3.1 SURFACE COMPOSITION DATA FOR DICE THROW CRATER

No.	Terrain Unit Description	Average Depth of Ejecta mm (in.)	Cone Index		Moisture Content						Surface Geometry				
			0 to 152 mm (0 to 6 in.)	152 to 305 mm (6 to 12 in.)	Percent Dry Weight						Average Slope %	rms in.			
					Dry Density										
					0 to 152 mm (0 to 6 in.) kg/m <sup>3</sup> (lb/ft <sup>3</sup> )	152 to 305 mm (6 to 12 in.) kg/m <sup>3</sup> (lb/ft <sup>3</sup> )	0 to 25.4 mm (0 to 1 in.)	25.4 to 152 mm (6 to 6 in.)	152 to 305 mm (6 to 12 in.)	305 to 610 mm (12 to 24 in.)					
1	Original Surface	NA <sup>a</sup>	321	584	1.0	3.2	2.6			1.35	84.2	1.36	84.8	1.6	0.85
2	Outer Lip	102 (4)	57	159	1.3	3.0	4.4			1.39	86.9	1.41	88.2	3.0	1.61
3	Inner Lip	610 (>24)	34	49	0.5	1.7	4.8			1.41	87.9	1.41	87.8	13.7	2.84
4	Crater Wall	610 (>24)	27	51	11.4	20.6	20.2			1.15	71.8	1.21	75.4	53.0	NA
5	Crater Floor	NA	166	175	12.4	17.2	24.9			1.33	82.8	1.28	80.0	4.5	NA

<sup>a</sup> NA means not applicable.

TABLE 3.2 MEASURED AND PREDICTED VEHICLE PERFORMANCE IN THE DIRT THROW CRATER

No.	Terrain Unit Description	Performance Parameter				Speed	
		Go/No Go		Optimum		Motion	
		Measured	Predicted	Drawbar Full/Weight % Measured	Predicted	Resistance/Height Measured	Predicted
<u>M60A1 tank</u>							
1	Original Surface	Go	Go	NM <sup>a</sup>	NP <sup>b</sup>	NM	NP
2	Outer Lip	Go	Go	NM	NP	NM	NP
3	Inner Lip	Go	Go	NM	NP	NM	NP
4	Crater Wall	NM	Go	NM	NP	NM	NP
5	Crater Floor	NM	Go	NM	NP	NM	NP
<u>M551 Sheridan tank</u>							
1	Original Surface	Go	Go	NM	NP	23.8 (14.8)	24.2 (15.0)
2	Outer Lip	Go	Go	NM	NP	19.3 (12.0)	18.5 (11.5)
3	Inner Lip	Go	Go	NM	NP	NM	NP
4	Crater Wall	No Go	No Go	NM	NP	NAC	NP
5	Crater Floor	Go	Go	NM	NP	NM	NP
<u>M577A1 command post carrier</u>							
1	Original Surface	Go	Go	0.59	0.6 <sup>c</sup>	0.08	0.06
2	Outer Lip	Go	Go	0.54	0.58	0.14	0.13
3	Inner Lip	Go	Go	NM	NP	NM	NP
4	Crater Wall	Go	Go	NM	NP	NM	NP
5	Crater Floor	Go	Go	NM	NP	NM	NP
<u>M109 self-propelled howitzer</u>							
1	Original Surface	Go	Go	NM	NP	NM	NP
2	Outer Lip	Go	Go	NM	NP	NM	NP
3	Inner Lip	Go	Go	NM	NP	NM	NP
4	Crater Wall	Go	Go	NM	NP	NM	NP
5	Crater Floor	Go	Go	NM	NP	NM	NP
(Continued)							
1	Original Surface	Go	Go	24.8 (15.4)	25.8 (16.0)	NM	NP
2	Outer Lip	Go	Go	22.2 (13.8)	19.0 (11.8)	NM	NP
3	Inner Lip	Go	Go	NM	NP	NM	NP
4	Crater Wall	Go	Go	NM	NP	NM	NP
5	Crater Floor	Go	Go	NM	NP	NM	NP

a NM means not measured.

b NP means not predicted.

c NA means not applicable.

(Sheet 1 of 2)

TABLE 3.2 (CONCLUDED)

No.	Terrain Unit Description	Performance Parameter									
		Go-No Go		Optimum Drawbar Pull/Weight		Yotion Resistance/Height		Speed			
		Measured	Predicted	Measured	Predicted	Measured	Predicted	Measured	Predicted	Measured	Predicted
<u>M35A2C, 2-1/2-Ton Cargo Truck</u>											
1	Original Surface	Go	Go	0.43	0.46	0.08	0.05	25.7 (16.0)	26.6 (16.5)		
2	Outer Lip	Go	Go	0.37	0.38	0.14	0.12	21.7 (13.5)	19.8 (12.3)		
3	Inner Lip	Go	Go	NM	NP	NM	NP	NM	NP		
4	Crater Wall	No Go	No Go	NM	NP	NM	NP	NA	NP		
5	Crater Floor	Go	Go	NM	NP	NM	NP	NM	NP		
<u>M715, 1-1/4-Ton Cargo Truck</u>											
1	Original Surface	Go	Go	0.52	0.54	0.10	0.07	36.5 (22.7)	39.3 (24.4)		
2	Outer Lip	Go	Go	0.45	0.49	0.16	0.13	29.6 (18.4)	23.5 (14.6)		
3	Inner Lip	Go	Go	NM	NP	NM	NP	NM	NP		
4	Crater Wall	No Go	No Go	NM	NP	NM	NP	NA	NP		
5	Crater Floor	Go	Go	NM	NP	NM	NP	NM	NP		



TABLE 3.3 DEGRADATION OF VEHICLE PERFORMANCE

No.	Terrain Unit Description	Speed		Speed Degradation pct	Optimum Drawbar Pull/Weight	Drawbar-Pull Degradation pct
		km/hr	(mph)			
<u>M60 Tank</u>						
1	Original Surface	22.2	(13.8)	0	NM <sup>a</sup>	NM
2	Outer Lip	19.0	(11.8)	14	NM	NM
3	Inner Lip	NM	NM	NM <sup>b</sup>	NM	NM
4	Crater Wall	NM	NM	100	NM	100
5	Crater Floor	NM	NM	NM	NM	NM
<u>M551 Sheridan Tank</u>						
1	Original Surface	23.8	(14.8)	0	NM	NM
2	Outer Lip	19.3	(12.0)	19	NM	NM
3	Inner Lip	NM	NM	NM	NM	NM
4	Crater Wall	NM	NM	100	NM	100
5	Crater Floor	NM	NM	NM	NM	NM
<u>M577A1 Command Post Carriers</u>						
1	Original Surface	29.5	(18.3)	0	0.59	0
2	Outer Lip	18.5	(11.5)	37	0.54	8
3	Inner Lip	NM	NM	NM	NM	NM
4	Crater Wall	NM	NM	100	NM	100
5	Crater Floor	NM	NM	NM	NM	NM
<u>M109 Self-Propelled Howitzer</u>						
1	Original Surface	24.8	(15.4)	0	NM	NM
2	Outer Lip	22.2	(13.8)	10	NM	NM
3	Inner Lip	NM	NM	NM	NM	NM
4	Crater Wall	NM	NM	100	NM	100
5	Crater Floor	NM	NM	NM	NM	NM

<sup>a</sup> Not measured - either due to no-gc condition or lack of test area.

<sup>b</sup> None of the vehicles were able to make a safe entry into the crater due to steep slopes.

TABLE 3.3 (CONCLUDED)

No.	Terrain Unit Description	Speed		Speed Degradation pct	Optimum Drawbar Pull/Weight	Drawbar-Pull Degradation pct
		km/hr	(mph)			
<u>M35A2C, 2-1/2-Ton Cargo Truck</u>						
1	Original Surface	25.7	(16.0)	0	0.43	0
2	Outer Lip	21.7	(13.5)	16	0.37	14
3	Inner Lip	NM	NM	NM	NM	NM
4	Crater Wall	NM	NM	100	NM	100
5	Crater Floor	NM	NM	NM	NM	NM
<u>M715, 1-1/4-Ton Cargo Truck</u>						
1	Original Surface	36.5	(22.7)	0	0.52	0
2	Outer Lip	29.6	(18.4)	19	0.45	13
3	Inner Lip	NM	NM	NM	NM	NM
4	Crater Wall	NM	NM	100	NM	100
5	Crater Floor	NM	NM	NM	NM	NM

TABLE 3.4 NUMERICAL EVALUATION PARAMETERS

Terrain Unit <sup>a</sup>		Mean Absolute Deviation		Relative Deviation
No.	Description	km/hr	(mph)	pct
<u>M60A1 Tank</u>				
1	Original Surface	0.2	(0.1)	1
2	Outer Lip	0.3	(0.2)	<u>2</u>
				Average 1.5
<u>M551 Sheridan Tank</u>				
1	Original Surface	0.4	(0.2)	2
2	Outer Lip	0.8	(0.5)	<u>5</u>
				Average 3
<u>M577A1 Command Post Carrier</u>				
1	Original Surface	0.6	(0.4)	2
2	Outer Lip	1.9	(1.2)	<u>10</u>
				Average 6
<u>M109 Self-Propelled Howitzer</u>				
1	Original Surface	1.0	(0.6)	4
2	Outer Lip	3.2	(2.0)	<u>14</u>
				Average 9
<u>M35A2C, 2-1/2-Ton Cargo Truck</u>				
1	Original Surface	0.9	(0.5)	4
2	Outer Lip	1.9	(1.3)	<u>9</u>
				Average 6.5
<u>M715, 1-1/4-Ton Cargo Truck</u>				
1	Original Surface	2.8	(1.7)	8
2	Outer Lip	6.1	(3.8)	<u>21</u>
				Average 14.5

<sup>a</sup>Only the terrain units where speed tests were conducted are shown.

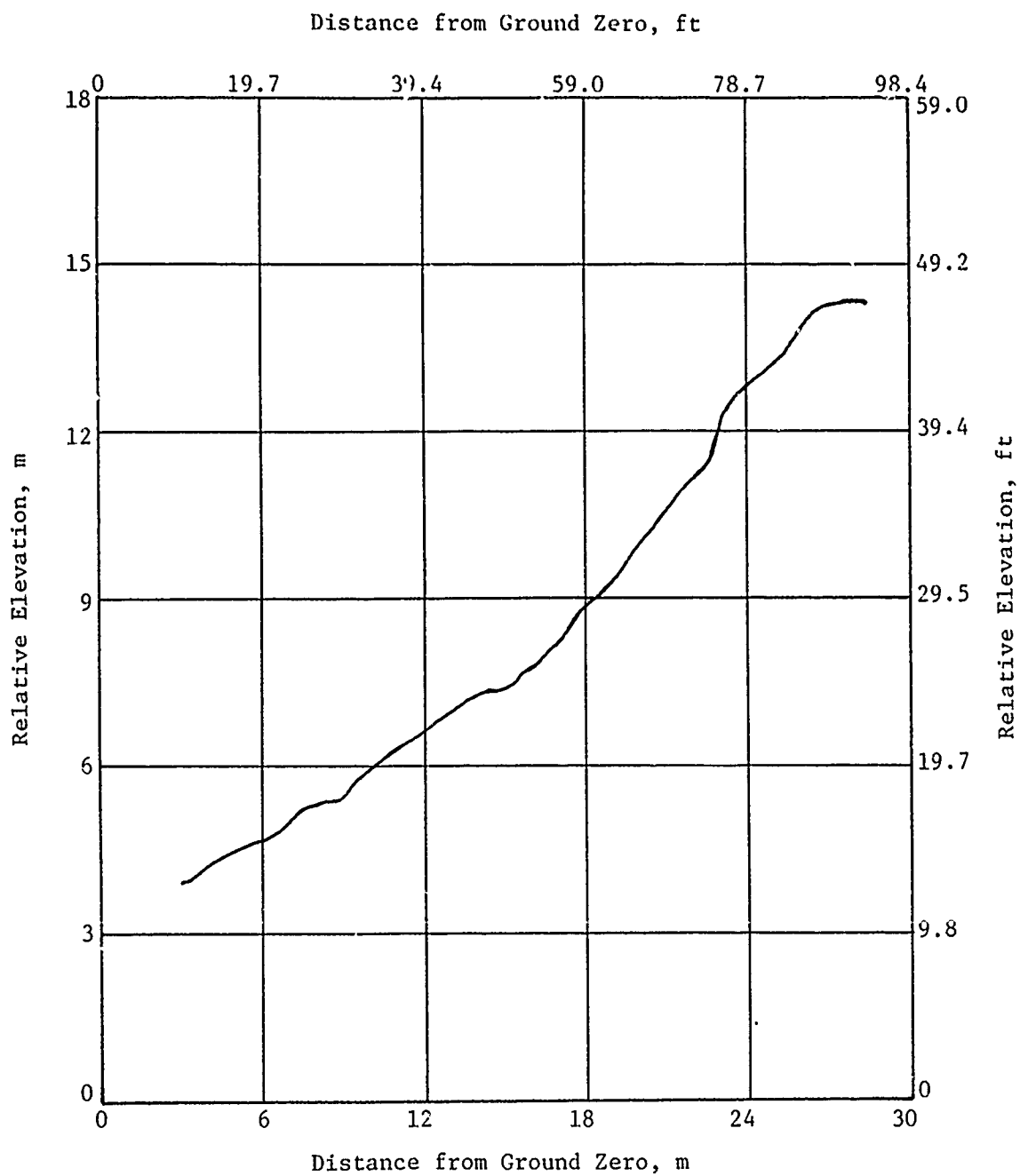


Figure 3.1 Elevation Profile of Terrain Unit 4,  
Crater Wall of Maximum Slope

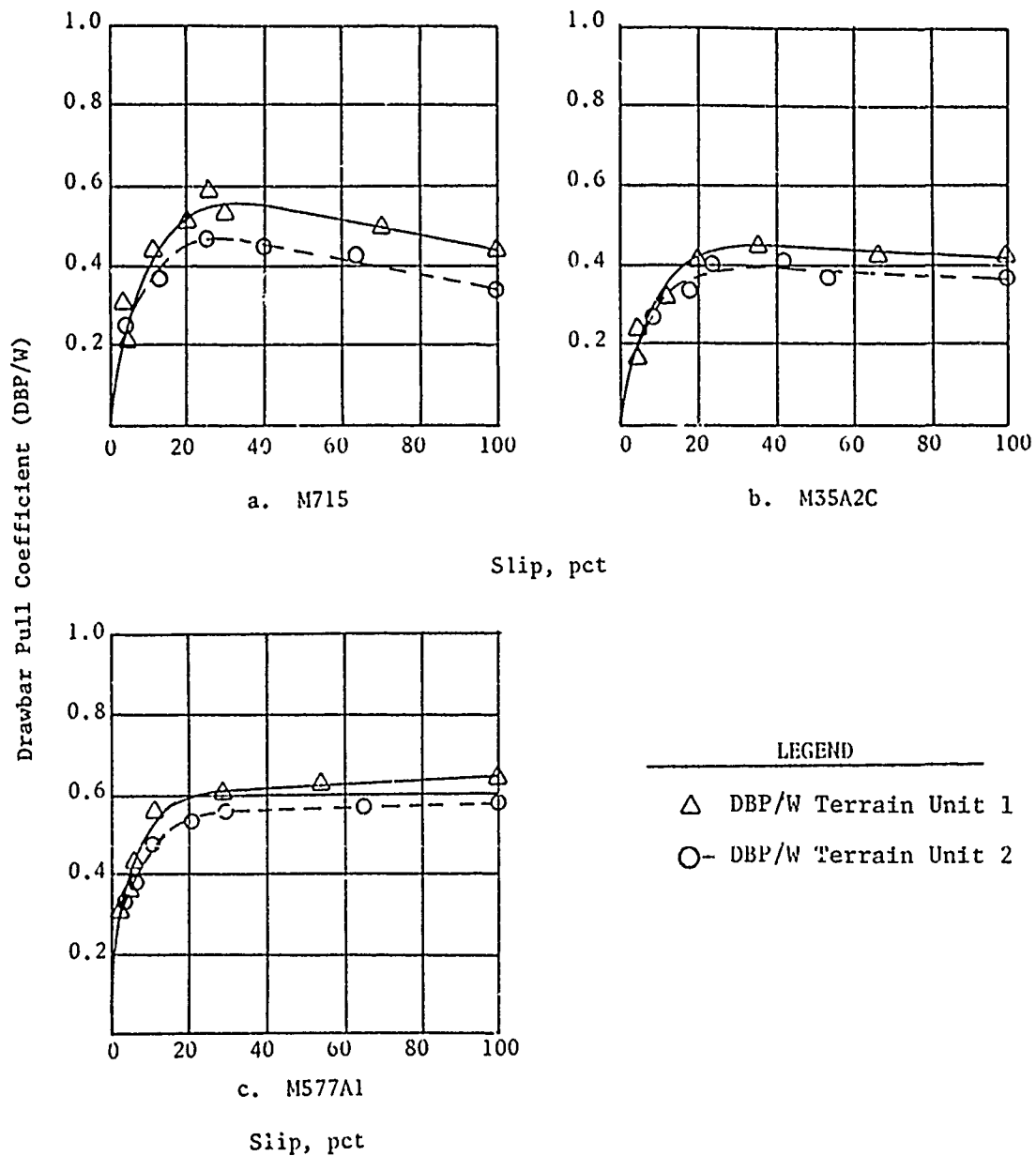
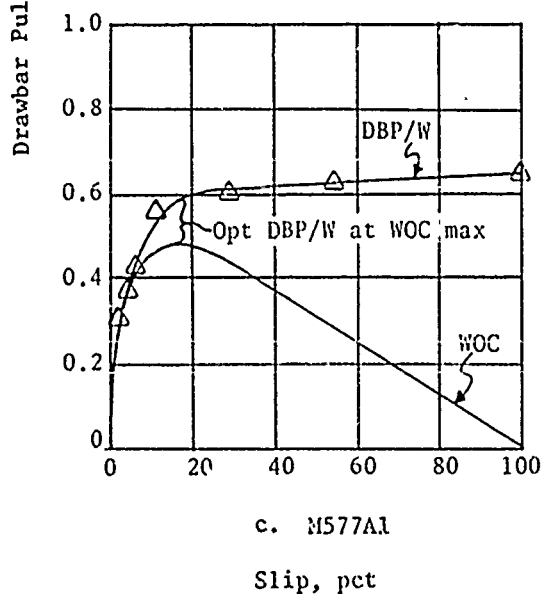
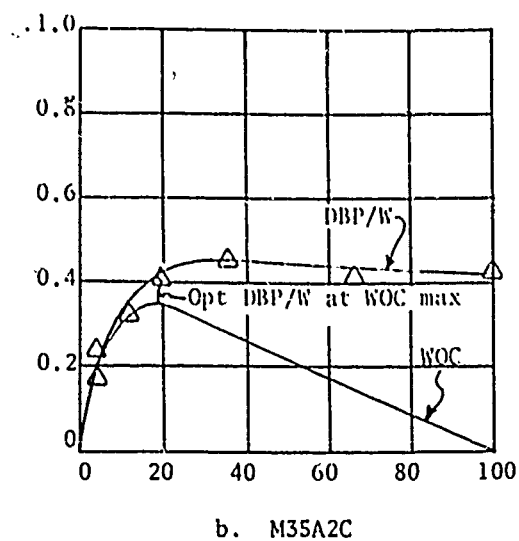
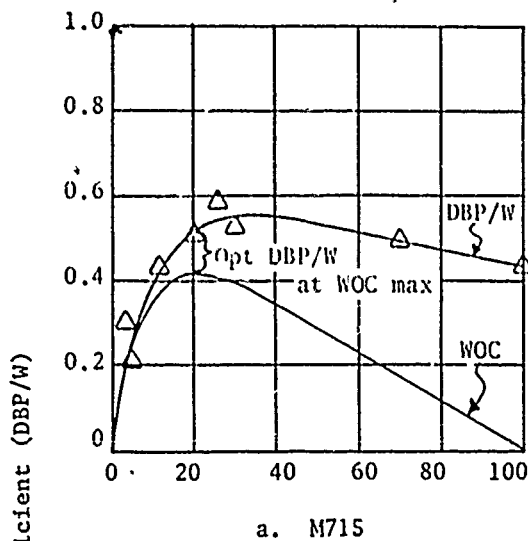


Figure 3.2 Drawbar-Pull Coefficient (DBP/W) versus Slip



NOTE: Triangles indicate measured data.

Figure 3.3 Determination of Optimum DBP Coefficient (DBP/W) for Three of the Test Vehicles in Terrain Unit 1

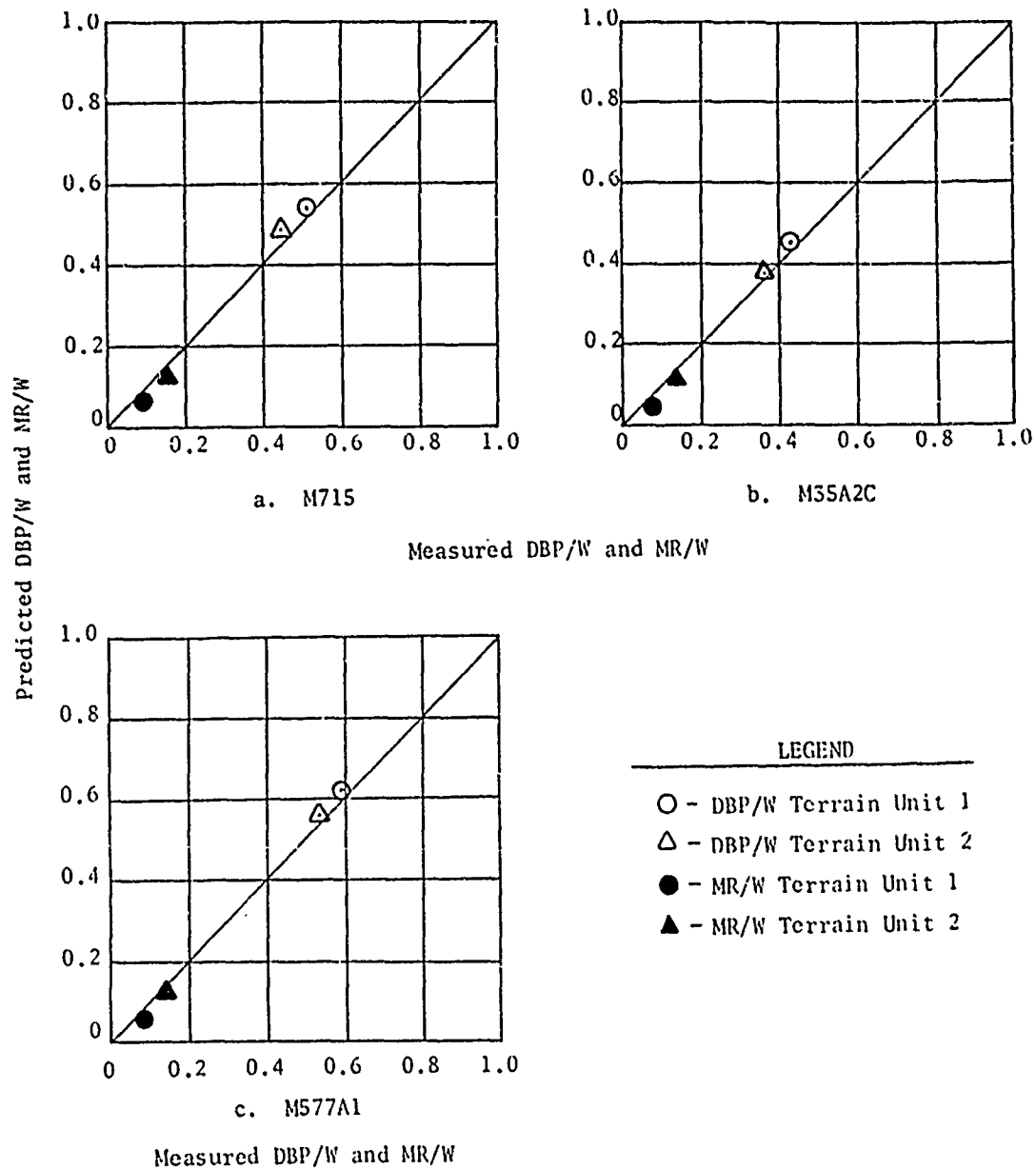
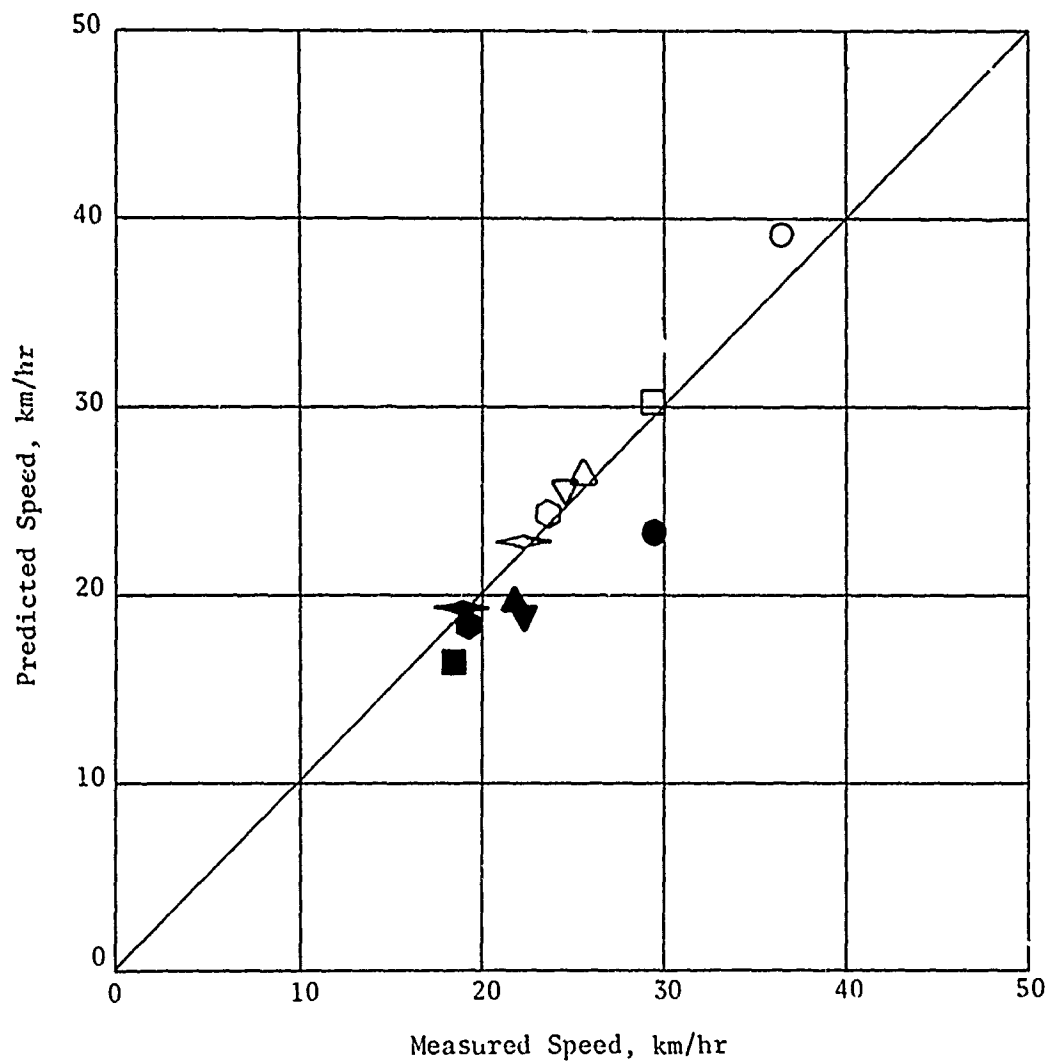


Figure 3.4 Comparison of Measured and Predicted DBP/W and MR/W for Three of the Test Vehicles



LEGEND			LEGEND		
Symbol	Vehicle	Terrain Unit	Symbol	Vehicle	Terrain Unit
○	M715	1	□	M577A1	1
●	M715	2	■	M577A1	2
△	M35A2C	1	▽	M109	1
▲	M35A2C	2	▼	M109	2
◊	M551	1	◇	M60A1	1
◐	M551	2	◑	M60A1	2

Figure 3.5 Comparison of Measured and Predicted Speeds



## CHAPTER 4

### CONCLUSIONS AND RECOMMENDATIONS

#### 4.1 CONCLUSIONS

The DICE THROW crater and associated ejecta areas comprised four terrain units (2 through 5), each of which was significant to vehicle ground mobility based on soil strength, soil moisture content, ejecta depth, and surface configuration.

The test vehicles, i.e. the M60A1 tank, the M551 Sheridan tank, the M577A1 command post carrier, the M109 self-propelled howitzer, the M35A2C 2-1/2-ton cargo truck, and the M715 1-1/4-ton cargo truck, could operate with ease in all terrain units except the crater wall.

The test vehicles were unable to make a safe entry into the crater due to the steep slope (50 percent) of the crater wall (Terrain Unit 4). A D7F bulldozer required 10 minutes to make an entrance lane. The M109 and M577A1 were the only test vehicles that could exit the crater by way of the crater wall. The total engineering effort (time required by a D7F bulldozer) to make the crater passable for all the test vehicles was estimated to be 20 minutes.

The DICE THROW crater was effective as a complete barrier to the mobility of the vehicles tested.

Degradation of vehicle performance in Terrain Units 2 through 5, in terms of DBP/W, ranged from 8 percent for the M577A1 for the outer lip (Terrain Unit 2) to 100 percent for all the test vehicles on the crater wall (Terrain Unit 4). Degradation in terms of speed ranged from 10 percent for the M109 on the outer lip (Terrain Unit 2) to 100 percent for all the test vehicles on the crater wall (Terrain Unit 4). The area of 100 percent performance degradation was  $1,839 \text{ m}^2$  ( $19,782 \text{ ft}^2$ ) for all test vehicles.

The degraded area per gigajoules (0.24 ton) of explosive was  $0.73 \text{ m}^2$  ( $7.85 \text{ ft}^2$ ), which indicates that large-scale surface explosives in this type of material (silty sand) are not an efficient means of creating barriers to the movement of military vehicles.

The effective no-go width for the crater was 48 metres (160 feet), which indicates that a similar charge in the same soil conditions would be effective in combat conditions for creating obstacles in this width range.

Comparison of measured values and values predicted by AMM-74X (Army Mobility Model) for four vehicle performance parameters revealed that the overall accuracy of the predictions for go-no go, DBP, MR, and speed were acceptable in every case.

#### 4.2 RECOMMENDATIONS

It is recommended that investigations be continued in a range of consolidated and unconsolidated layered materials to increase the catalog of cratered terrain information for ground mobility purposes. These investigations should also include vehicle tests to collect data for refining techniques for predicting vehicle performance in crater ejecta. These techniques should include a simple and rapid solution to be incorporated into field manuals for predicting performance in cratered terrain that will evaluate all terrain factors of significance to mobility.

The potential of small row charges or multiple detonations as a barrier to mobility should also be investigated.

The scope of future projects should be extended to include a barrier-counter barrier analysis, i.e. for both offensive and defensive military operations.

It is further recommended that in all future test programs the amount of construction effort required to remove ejecta and to bypass, bridge, or fill craters to make them passable for ground vehicles be determined.

It is also recommended that in all future projects involving surface or subsurface explosives, the craters be characterized for mobility purposes so that vehicle performance can be predicted.

Finally, sufficient data need to be gathered such that an analysis can be performed to compare obstacle effectiveness against mobility caused by cratering various geologic media (e.g., hard and soft rock and wet and dry soils of significantly different mineralogy).

## REFERENCES

1. Nuttall, C. J. and Randolph, D. D., "Mobility Analyses of Standard- and High-Mobility Tactical Support Vehicles (HIMO Study)," Technical Report M-76-3, Feb 1976, U. S. Army Engineer Waterways Experiment Station, CE, Vicksburg, Miss.
2. Blackmon, C. A. and Rula, A. A., "Event Dial Pack; Project LN309, Effectiveness of Craters as Barriers to Mobility," Miscellaneous Paper M-70-4, March 1971; U. S. Army Engineer Waterways Experiment Station, CE, Vicksburg, Miss.
3. U. S. Army Tank-Automotive Command; "The AMC-71 Mobility Model," Technical Report No. 11789 (LL143), July 1973, Warren, Mich.

BEST AVAILABLE COPY

## DISTRIBUTION LIST

### DEPARTMENT OF DEFENSE

Director  
Defense Advanced Research Project Agency  
ATTN: Strategic Tech Office  
ATTN: NMRO  
ATTN: Technical Library

Director  
Defense Communications Agency  
ATTN: NMCSG Code 310

Defense Documentation Center  
Cameron Station  
12 ATTN: IC

Director  
Defense Intelligence Agency  
ATTN: DI-IC Nuc Eng Branch  
ATTN: DI-2 Wpns & Sys Div  
ATTN: DI-7D

Director  
Defense Nuclear Agency  
ATTN: DBST  
ATTN: TISI Archives  
3 cy ATTN: TITL Technical Library  
ATTN: STSP  
ATTN: SPAS  
ATTN: Maj. William A. Alter  
ATTN: Maj. L. Neal Gunby  
ATTN: Tom Kennedy  
ATTN: Maj. Edmund Mueller  
ATTN: LTC Edwin T. Still  
ATTN: SPSS  
ATTN: SPTD

Director  
Defense Research & Engineering  
ATTN: SGSS (OS)  
ATTN: AD/ET J. Persh

Commander  
Field Command  
Defense Nuclear Agency  
ATTN: FCTMD  
ATTN: FCTMOT  
ATTN: FCTMOF  
ATTN: FCPR  
ATTN: FCT  
ATTN: Capt. V.A. Alvarez  
ATTN: Capt. R.G. DeRaad  
ATTN: Noel Gantick  
ATTN: Lt. C. Klirmek  
ATTN: LCDR J.D. Strode  
ATTN: Maj. R.I. Bestgen

Director  
Joint Staff Jgt Planning Staff JUS  
ATTN: JLDN-2  
ATTN: JPIM  
ATTN: JPTP

Chief  
Livermore Division Field Command DVA  
Lawrence Livermore Laboratory  
ATTN: LCPRL

Explosive Safety Board  
ATTN: Dr. Thomas Zaker

The Pentagon  
ATTN: 1-5 Plans & Pol Planning & Prgm Div  
ATTN: 1-5 Plans & Policy Nuc Div

Studies Analysis and Gaming Agency  
Joint Chiefs of Staff  
ATTN: SOLB

Director  
Defense Civil Preparedness Agency  
ATTN: Michael A. Pachuta

Director  
National Security Agency  
ATTN: Edward Butala (NS11)  
ATTN: William DeBoy (NS11)

Commander  
902 Military Intelligence Group  
ATTN: Col. Hassel L. Parker

### DEPARTMENT OF THE ARMY

Director  
BMD Advanced Tech Center  
ATTN: ATC-T Melvin T. Capps  
ATTN: Marcus Whitfield

Program Manager  
BMD Program Office  
ATTN: DACS-BMT John Shea  
ATTN: DACS-BM2  
ATTN: DACS-BM2-D Julian Davidson  
ATTN: DACS-BMT Clifford I. McLain

Commander  
BMD System Command  
ATTN: BDMSC-TEN Noah J. Hurst

Deputy Chief of Staff for Rsch Dev & Acq  
Department of the Army  
ATTN: Technical Library

# BEST AVAILABLE COPY

## DEPARTMENT OF THE ARMY, continued

Deputy Chief of Staff for Operations & Plans  
Department of the Army  
ATTN: Director of Nuclear Plans & Policy

Commander  
U.S. Army Electronics Command  
ATTN: Robert Frieberg

Commander  
SOC USAOCCS  
ATTN: Capt. Alexander I. Wojcicki

Commander  
Harry Diamond Laboratories  
ATTN: DRXDO-RBH James H. Gwaltney  
ATTN: DRXDO-TF Robert B. Oswald, Jr.  
ATTN: DRXDO-11, Technical Library  
ATTN: DRXDO-NP  
ATTN: L. Belliveau  
ATTN: W. Vault

Commander  
Picatinny Arsenal  
ATTN: Al Ioeb  
ATTN: SARPA-ND-C-T Donald Miller  
ATTN: SARPA-FR-E Louis Avrami  
ATTN: SHUPA-MD Henry Opat

Director  
TRASANA  
ATTN: R.L. Dekinder, Jr.

Commander  
White Sands Missile Range  
ATTN: Richard Dysart  
ATTN: Dale W. Green

Director  
U.S. Army Ballistic Research Labs  
ATTN: J.H. Defer, DRDAR-BLE  
ATTN: DRXBR-A, Julius J. Meszaros  
ATTN: DRXRD-BVL, William J. Schuman, Jr.  
ATTN: Richard Vitali  
ATTN: DRXBR-TB, J.T. Frasier  
ATTN: Robert F. Eichelberger  
ATTN: Technical Library, Edward Bailey  
ATTN: W.D. Allison  
ATTN: N. Ithridge  
ATTN: Col. R. Gomez  
ATTN: A. Gupta  
ATTN: J. Jacobson  
ATTN: V. King  
ATTN: C. Kingery  
ATTN: R. Mayerhofer  
ATTN: R. Pearson  
ATTN: R.L. Peterson  
ATTN: F. Quigley  
ATTN: R.J. Raley  
ATTN: R.L. Reiser  
ATTN: I. Roecker  
ATTN: D.L. Rigotti  
ATTN: R. Schumacher  
ATTN: R. Shultor  
ATTN: F. Sullivan  
ATTN: W. Taylor  
ATTN: G. Teel  
ATTN: G. Watson  
ATTN: M. Wheeler

Director  
U.S. Army Engineer Waterways Experiment Station  
ATTN: Technical Library  
ATTN: James Ballard  
ATTN: Jimmy P. Balsara  
ATTN: William Flathau  
ATTN: William L. Huff  
ATTN: Adam A. Rula  
ATTN: James Watt  
ATTN: LTC Ronald R. Kaufmann

Commander  
U.S. Army Materiel & Mechanics Research Center  
ATTN: DRAMR-III, John F. Dignam

Commander  
U.S. Army Materiel Development & Readiness CMD  
ATTN: DRCDL-D, Lawrence Flvnn  
ATTN: Technical Library

Commander  
U.S. Army Missile Command  
ATTN: DRSMI-XS, Chief Scientist  
ATTN: DRS-RAP, W.B. Thomas  
ATTN: DRSMI-RRR, Bud Gibson

Commander  
U.S. Army Nuclear Agency  
ATTN: MONA-SA  
ATTN: MONA-1E  
ATTN: CDC-NVA  
ATTN: ATCA-NAW  
ATTN: Maj. John Uecke  
ATTN: Maj. Alan Lind

U.S. Army Satellite Communications Agency  
ATTN: Eugene Caulifield

Commander  
U.S. Army Armament R&D Command  
ATTN: Alvin Flugel (DRDAR-LCW)  
ATTN: Martin A. Riccio (DRDAR-LCS-W)  
ATTN: Daniel Waxler (DRDAR-LCS-W)

## DEPARTMENT OF THE NAVY

Chief of Naval Material  
ATTN: MAT 0323, Irving Jaffe

Chief of Naval Operations  
ATTN: Code 604C3, Robert Pracesi  
ATTN: Code 604C4, Robert A. Blaise  
ATTN: OP 62  
ATTN: OP 981

Chief of Naval Research  
ATTN: Technical Library

Director  
Naval Research Laboratory  
ATTN: Code 2600, Technical Library  
ATTN: Code 7770, Gerald Cooperstein  
ATTN: Code 5180, Mario A. Persechino

Commander  
Naval Sea Systems Command  
ATTN: 0533A, Marilyn A. Kinna

DEPARTMENT OF THE NAVY, continued

Officer-in-Charge  
Civil Engineering Laboratory  
Naval Construction Battalion  
ATTN: Technical Library

Officer-in-Charge  
Naval Surface Weapons Center  
ATTN: Code 4A07, Carson Lyons  
ATTN: Code 4R10, Joseph Petes  
ATTN: Code 4A50, Navy Nuclear Programs Office  
ATTN: Michael Swisdak  
ATTN: Phillip Peckham

Commanding Officer  
Naval Weapons Evaluation Facility  
ATTN: Lawrence R. Oliver  
ATTN: Peter Hughes  
ATTN: Rudolf Friedberg

Director  
Strategic Systems Project Office  
ATTN: ASP-272

Commander  
Naval Facilities Engineering Command Headquarters  
ATTN: Technical Library

Naval Sea Support Center  
Fleet Support Office  
ATTN: LCDR L.W. Edgerton

DEPARTMENT OF THE AIR FORCE

Commandant  
AF Flight Dynamics Laboratory, AFSC  
ATTN: FAX

AF Geophysics Laboratory, AFSC  
ATTN: Chan Touart

AF Materials Laboratory, AFSC  
ATTN: LPH Gordon Griffith  
ATTN: MBL George L. Schmitt  
ATTN: MBL Donald L. Schmidt  
ATTN: MAS  
ATTN: T. Nicholas  
ATTN: LTM

AF Rocket Propulsion Laboratory, AFSC  
ATTN: RTSN G.A. Beale

AF Weapons Laboratory, AFSC  
ATTN: DYS  
ATTN: Al Sharp  
ATTN: SAB  
ATTN: DYT  
ATTN: DYU  
ATTN: Dr. Minge  
ATTN: SUL  
ATTN: Lt. Joel C. Bradshaw  
ATTN: Susan Check  
ATTN: Steve Melzer  
ATTN: Charles Needham  
ATTN: Maynard A. Plamondon  
ATTN: LTC James Warren  
ATTN: Harry Webster  
ATTN: NTO  
ATTN: Technical Review

Air Force Institute of Technology, AFIT  
ATTN: Library, AFIT

Headquarters  
Air Force Systems Command  
ATTN: AR10  
ATTN: S0SS

Commander  
Arnold Engineering Development Center  
ATTN: AOA

Commander  
ASD  
Key ATTN: FWS D. Ward

Commander  
Foreign Technology Division, AFSC  
ATTN: TOPFN  
ATTN: PDBG  
ATTN: TDI BD, J. D. Pumphrey

HQ USAF/RD  
ATTN: RDQSM  
ATTN: RD  
ATTN: RIQ  
ATTN: RQPM

HQ USAF/XO  
ATTN: X00SS

SAMSO/DY  
ATTN: DYS

SAMSO/MN  
ATTN: MNH  
ATTN: MNR  
ATTN: Capt. Thomas Edwards

SAMSO/RS  
ATTN: RST  
ATTN: RSS  
ATTN: RSSI

Commander in Chief  
Strategic Air Command  
ATTN: XOBM  
ATTN: XPQM  
ATTN: Maj. Ronald W. Bashant  
ATTN: XPIS  
ATTN: D0XI

U.S. ENERGY RESEARCH & DEVELOPMENT ADMINISTRATION

Division of Military Application  
ATTN: Doc Con for Res & Dev. Branch

University of California  
Lawrence Livermore Laboratory  
ATTN: G. Stahle, L-21  
ATTN: C. Joseph Taylor, L-9  
ATTN: Joseph B. Knox, L-216  
ATTN: Joseph L. Keller Jr., L-125  
ATTN: Bernard Hayes

U.S. ENERGY R&D ADP., continued

Los Alamos Scientific Laboratory

ATTN: Doc. Control for Robert Skaggs  
ATTN: Doc. Control for R. Dingus  
ATTN: Doc. Control for John McQueen  
ATTN: Doc. Control for E.W. Taylor  
ATTN: Doc. Control for R.S. Thurston

Sandia Laboratories

Livermore Laboratory

ATTN: Doc. Control for Technical Library  
ATTN: Doc. Control for G.E. Norris, JESSIE

Santa Fe Laboratories

ATTN: Doc. Control for Thomas B. Cook  
ATTN: Doc. Control for E.R. Borden  
ATTN: Doc. Control for Albert Chabot  
ATTN: Doc. Control for M. Cowan  
ATTN: Doc. Control for Jack Reed  
ATTN: Doc. Control for Norman Breazeal  
ATTN: Doc. Control for Technical Library

Director

Oak Ridge National Laboratory

ATTN: Dr. C. Kearny, Bldg. 1500n

DEPARTMENT OF DEFENSE CONTRACTORS

Aeroc Corporation

ATTN: J. Huntington  
ATTN: J. Courtney  
ATTN: C. Nardo  
ATTN: R. Riddal

Aerospace Corporation

ATTN: W. Barry  
ATTN: R. Mortensen  
ATTN: Richard Crolius, A2-RM1027  
ATTN: H. Blaes  
ATTN: W. Mann  
ATTN: Robert L. Strickler  
ATTN: J. McClelland

Analytic Services, Inc.

ATTN: Jack Selig

AWO Research & Systems Group

ATTN: John Gilmore, J400  
ATTN: Document Control  
ATTN: John E. Stevens, J100  
ATTN: William Broding  
ATTN: George Weber, J230

Battelle Memorial Institute

ATTN: Technical Library  
ATTN: E. Unger  
ATTN: Merwyn R. Vanderlind

Boeing Company, The

ATTN: Edwin York  
ATTN: Robert Holmes  
ATTN: Robert Davidahl  
ATTN: Brian Tempieri  
ATTN: Jay C. Ivy  
ATTN: Roland Carlson

Boeing Wichita Company

ATTN: E. Skaney

Brown Engineering Company, Inc.

ATTN: Ronald Patrick

California Research & Technology, Inc.

ATTN: Ken Kreyenhagen

Chrysler Defense Division

ATTN: R.E. Smith

Calspan Corporation

ATTN: M.S. Holden

Dayton, University of

Industrial Security Super KL-505

ATTN: Hallock L. Swift  
ATTN: D. Gerdman

Denver, University of

Colorado Seminary, Denver Research Institute

ATTN: John Wisotski  
ATTN: Larry L. Brown

Effects Technology, Inc.

ATTN: Richard Parisse  
ATTN: Robert Wengler

EG&G, Inc.

Special Projects Div.

ATTN: Robert Ward

Electronichimical Systems of New Mexico, Inc.

ATTN: R.C. Shunk

Ford Aerospace & Communications Operations

ATTN: P. Spangler

General Electric Company

Space Division

ATTN: A. Martellucci  
ATTN: Phillip Cline  
ATTN: G. Harrison  
ATTN: Daniel Edelman  
ATTN: Carl Anderson

General Electric Company

HMPD-Center for Advanced Studies

ATTN: DASIAC

General Electric Company

HMPD-Center for Advanced Studies-Albuquerque

ATTN: Gerald Perry

General Electric Company

HMPD-Center for Advanced Studies-Bel Air

ATTN: E.J. Bryant

General Research Corporation

P.O. Box 558

ATTN: E. Stathacopoulos

Institute for Defense Analyses

ATTN: Doc. Bengston  
ATTN: HQ Librarian

Ion Physics Corporation

ATTN: Robert D. Evans



# BEST AVAILABLE COPY

## DEPT. OF DEFENSE CONTRACTORS, continued

### Kaman Avidyne

#### Division of Kaman Sciences Corp.

ATTN: I.S. Criscione  
ATTN: Ray Reutimick  
ATTN: Norman P. Hobbs

### Kaman Sciences Corporation

ATTN: Donald C. Sachs  
ATTN: Thomas Meagher  
ATTN: John R. Hoffman  
ATTN: Frank H. Shelton  
ATTN: John Keith

### Ken O'Brien & Associates

ATTN: Richard Cronk

### Lockheed Missiles & Space Co., Inc. - Sunnyvale

ATTN: R. Walz, Dept. 81-14

### Lockheed Missiles & Space Co., Inc. - El Segundo

ATTN: T.R. Fortune

### Lockheed Missiles & Space Co., Inc. - Palo Alto

ATTN: F.G. Borgardt

### Lovelace Foundation for Medical Education and Research

ATTN: D.R. Richmond  
ATTN: R.O. Clark  
ATTN: E.R. Fletcher

### Martin Marietta Aerospace Orlando Division

ATTN: William A. Gray, MP-61  
ATTN: Laird Kinnaird  
ATTN: Gene Aiello  
ATTN: James M. Potts, MP-61

### McDonnell Douglas Corporation

ATTN: L.A. Fitzgerald  
ATTN: R.J. Reck  
ATTN: H. Hurwitz  
ATTN: H.M. Berkowitz  
ATTN: J.F. Garibotti  
ATTN: L. Cohen

### National Academy of Sciences

#### ATTN: National Materials Advisory Board

ATTN: Donald G. Groves

### New Mexico, University of

#### Civil Engineering Research Facility

ATTN: Glen Jones  
ATTN: Golden Lane  
ATTN: Stephen Pickett

### Northrop Corporation

ATTN: Don Hicks

### Pacific-Sierra Research Corp.

ATTN: Gary Lang

### Physics International Company

ATTN: Doc Control for James Shea  
ATTN: Doc Control for Technical Library

### Prototype Development Associates, Inc.

ATTN: John McDonald  
ATTN: John Slaughter

### R&D Associates

ATTN: F.A. Field  
ATTN: Cyrus P. Knowles  
ATTN: Paul Rausch  
ATTN: Jerry Carpenter  
ATTN: Harold L. Brode  
ATTN: William R. Graham, Jr.  
ATTN: Edward Chapyak  
ATTN: Henry Cooper  
ATTN: Albert L. Latter

### RCA Corporation

ATTN: E. Van Keuren, Bldg. 13-5-2

### RAND Corporation, The

ATTN: J.J. Mate

### Raytheon Company

ATTN: Library

### Science Applications, Inc. - La Jolla

ATTN: Olan Nance  
ATTN: W. Yengst  
ATTN: John Warner  
ATTN: Dwane Hove  
ATTN: G. Ray

### Science Applications, Inc. - El Segundo

ATTN: Carl Swain  
ATTN: Lyle Dunbar  
ATTN: G. Burghart

### Science Applications, Inc. - McLean

ATTN: William R. Seebaugh  
ATTN: William M. Layson  
ATTN: Michael McDonnell

### Southern Research Institute

ATTN: C.D. Pears

### SRI International

ATTN: Philip J. Dolan  
ATTN: D. L. Huestis  
ATTN: George R. Abrahamson  
ATTN: Herbert I. Lindberg  
ATTN: Donald Curran  
ATTN: Carl Wiehle  
ATTN: Alan A. Burns

### Systems, Science and Software, Inc.

ATTN: G. A. Gurtman  
ATTN: Russell I. Duff

### Terra Tek, Inc.

ATTN: Sidney Green

### TRW Defense & Space Systems Group - Redondo Beach

ATTN: Peter Brandt, L-2006  
ATTN: Peter K. D., R1/2170  
ATTN: R.A. Plebuch, R1/2078  
ATTN: Thomas G. Williams  
ATTN: D.H. Baer, R1-2136  
ATTN: I. L. Alber, R1-1008  
ATTN: W.W. Wood

DEPT. OF DEFENSE CONTRACTORS, continued

TRW Defense & Space Systems Group - San Bernardino  
ATTN: William Polich  
ATTN: E.Y. Wong, 527/712  
ATTN: L. Berger  
ATTN: Earl M. Allen, 520/141  
ATTN: V. Blankenship

Admiralty Surface Weapons Establishment  
Ministry of Defence  
United Kingdom  
ATTN: W.D. Delany

British Embassy  
Washington, DC  
ATTN: ACOW

FOREIGN

Embassy of Australia  
Washington, DC  
ATTN: Office of the Defence Science Attache

Royal Fortification Administration  
Stockholm, Sweden  
ATTN: Dr. Eddy Abrahamsson  
ATTN: Brig. Gen. Gunnar Noren

National Defense Research Institute  
Stockholm, Sweden  
ATTN: H. Axelsson

Defence Research Establishment Suffield  
Raiston, Alberta, Canada  
ATTN: Clayton Coffey  
ATTN: Allan W.M. Gibb  
ATTN: G.A. Grant  
ATTN: R.M. Heggie

Infrastructure Staff  
Federal Republic of Germany  
ATTN: Col. Rottgerkamp  
ATTN: LTC Hermann Pahl  
ATTN: Eberhard Bachmann

Ernst-Mach Institute  
Federal Republic of Germany  
ATTN: Dr. Heintz Reichenbach  
ATTN: Gerhard Gurke

Office of Test & Development  
Norwegian Defence Construction Service  
Oslo, Norway  
ATTN: Arne Skjeltop

National Defence HQ  
Directorate of Maritime Activities and Research  
Quebec, Canada  
ATTN: Ole R. Bezemer

Technologisch Laboratorium (TNO)  
Rijswijk, Netherlands  
ATTN: H.J. Pasman

Federal Ministry of Defense  
Federal Republic of Germany  
ATTN: LTC D. Bruegmann  
ATTN: R. Schilling  
ATTN: E. F. Hentschel

Military Attache Staff  
Embassy of the Federal Republic of Germany  
ATTN: Col. Rudolf Erlemann

Federal Republic of Germany Liaison Office  
Alexandria, VA  
ATTN: Herman Pfrengle

BEST AVAILABLE COPY